SORPTION AND TRANSPORT PROCESSES IN RELATION TO SOIL STRUCTURE, WATER RETENTION, SOLUTE MOBILITY AND WATER UPTAKE BY PLANT ROOTS

by

L. A. G. AYLMORE B.Sc., Ph.D. (The University of Adelaide)

Selected Research Publications

Submitted to The University of Adelaide

for the

DEGREE OF DOCTOR OF SCIENCE

VOLUME 1 Nos. 1 - 50

April, 2002

CONTENTS

SUMMARY

The research described in this submission has provided a number of major advances in knowledge and practical outcomes including in particular:

1. The detailed description of the microporous structure of clay mineral systems by gas and vapour sorption leading to the recognition of quasi-crystals and clay domains as the assemblages of primary particles which constitute the operational elements in determining soil physical behaviour.

2. An enhanced understanding of electro-kinetic phenomena and the effects of ions on water structure and movement near the charged surfaces of clay particles.

3. A comprehensive analysis and theoretical description of the mechanisms involved in solute transport in soils including in particular, the effects of competitive adsorption between species and time dependency of sorption.

4. The detailed elucidation of the factors determining the persistence and mobility of pesticides in the soil profile and their potential for groundwater pollution leading to the development of a practical management model.

5. The adaption of computer assisted tomography applied to the attenuation of X- and gamma radiation (CAT Scanning), to the non-destructive *in situ* measurement of soil water content and structural changes and in particular to water uptake by plant roots. Coupled with the innovative use of ion specific microelectrodes, these studies provided the first detailed measurements of the temporal and spatial distribution of soil water and solute contents close to single plant roots.

6. The development of the Modulus of Rupture – Exchangeable Sodium Percentage (MOR – ESP) approach as a practical method for evaluating the structural status of soils and the influence of management practices. The method allows separate quantitative assessment of the roles of dispersive and non-dispersive mechanisms in contributing to structural instability in hard setting soils.

RESEARCH ACTIVITIES AND THEIR SIGNIFICANCE

The research activities presented herein cover a broad spectrum from fundamental studies of the surface physical chemistry and mechanisms involved in determining the behaviour of clay mineral, soil and plant systems to the resolution of more directly applied and practical problems dependent upon these processes and of concern to the agricultural, mining and environmental communities. These include studies of sorption, swelling and ionic transport in clay mineral systems; soil structure development, stabilization and amelioration; soil-plant-water relations; and water and solute transport in soil profiles with particular reference to the mobility of fertilizer constituents and pesticides.

The quality of these research activities and their significance is attested to by the substantial and continuing support they have received from research funding bodies such as the Australian Research Grants Scheme (more recently the Australian Research Council) from which continuous and frequently multiple Large Grants support was obtained from 1970 to 2002, the Australian Water Research Advisory Council, Land and Water Resources Research and Development Corporation, the Wheat Industry Research Committee of Western Australia, the Wheat Industry Research Council, the Reserve Bank (Rural Credits Development Fund), National Soil Conservation Program, Grains Research and Development Corporation, and numerous mining and other industry sources. My appointment to a Personal Chair in Soil Science in the University of Western Australia in 1990 and the award of the prestigious J.A. Prescott Medal by the Soil Science Society of Australia in 1995, were both based on recognition of the outstanding quality of the research activities outlined herein. In 1986 I was elected as a Fellow of the Royal Australian Chemical Institute.

These studies have involved collaboration with a large number of post-graduate students, research fellows and other colleagues. In addition they have frequently attracted extended visits from senior scientists from interstate and overseas. In relation to these studies I have, as indicated in the following text and publication list, been invited to present keynote papers at a number of national and international workshops and conferences and to write reviews, on a range of topics including soil structure, soil salinity, soil water repellency, pesticide transport and the application of computer assisted tomography to soil-plant-water relations. Many of the publications have been cited in subsequent text books and two have been awarded Publication Medals by the Australian Society of Soil Science.

The main areas of research, their significance and the contributions made, are outlined below. These are described in sequence from the more fundamental to more applied considerations. Relevant publications are indicated by number on the attached list. As a result of these activities I have achieved an international reputation in several areas. I believe the high degree of innovation achieved in each area is a significant feature of the research described.

1. SORPTION STUDIES IN POROUS CLAY MINERAL AND SOIL MATERIALS

Studies of the sorption of both polar and non-polar sorbates in porous materials are of considerable technical and academic interest. The sorptive properties of the layer lattice alumino-silicate clay minerals and sesquioxides are of

particular importance in agriculture and soil engineering as well as in their numerous industrial applications. These surfaces are responsible for the retention of water and plant nutrients and the clay-water interaction determines to a large extent the mechanical consistence, swelling and other physical properties of the soil. In addition, the nature of the pore space controls the transport of soil water and solutes and in particular the diffusion of nutrient ions to the plant root. In modern soil physics much of the emphasis which was at one time laid upon particle size measurement of soils has been transferred, with profit, to pore size distribution. However, the detailed elucidation of pore size distributions and pore geometries has been a major unsolved problem in the many disciplines concerned with porous materials.

1.1 Surface Area and Pore Structure

My contributions in this area have been concerned with:
(a) The validity and limitations of methods of specific surface area determination based on the interpretation of gas sorption isotherms on these materials; (b) The detailed elucidation of pore size distributions and pore geometries by analysis of liquid filling and emptying during complete adsorption-desorption isotherms to saturation; (c) The origins of the irreversible processes responsible for hysteresis in these systems and the question of the applicability of thermodynamic derivatives (such as the Kelvin Equation) to such isotherms; and (d) The mechanisms of hydration and swelling during the absorption of water and solutes by homo-ionic clays.

In the initial part of this work detailed studies of the sorption of a number of non-polar gases, commonly used in specific surface area and pore structure measurements were carried out on a number of clay mineral, sesquioxide and soil systems (10, 17, 18, 20,25, 26, 30). Analysis of sorption isotherms using the Brunauer, Emmett and Teller (B.E.T.) (1938) theory, the Kelvin equation (modified to take into account the contribution to sorption of physically adsorbed layers) and the more recently developed V-n approach, provided considerable insight into both the porous structure of these materials and the variation in apparent cross-sectional area for the sorbed gases with surface structure, exchangeable cation and microporosity of the materials. The clay matrix was shown to exhibit varying degrees of parallel orientation of the clay crystals (termed "domains") depending on crystal size and pretreatment (10,20). While specific surface areas obtained from argon adsorption at 78 K proved slightly less susceptible to change in exchangeable cation on the clay than corresponding measurements using nitrogen gas at 78 K, carbon dioxide sorption at 195 K was markedly affected by the nature of the exchangeable cation, increasing significantly in the order $La^{+++} < Ca^{++} < Na^{+} < Cs^{+}$ (26). From studies of argon, nitrogen and carbon dioxide sorption on goethite, hematite and gibbsite samples, it was concluded that enhanced sorption of the more energetic carbon dioxide into microporous regions of the oxides, inaccessible to nitrogen and argon, occurred in a fashion similar to that observed with carbon dioxide sorption into coal and charcoal materials. In addition, carbon dioxide sorption on kaolinite clays appeared to be severely inhibited by the surface structure of this mineral (17, 18, 26).

There had been considerable controversy surrounding the question of the possible penetration of gases into the interlamellar regions of the montmorillonite

(smectite) clay mineral matrix (Thomas and Bohor, Clays and Clay Miner., 16: 83, 1968; Knudsen and McAtee, Clays and Clay Miner., 22:59, 1974; Fripiat et al., Clays and Clay Miner., 22: 23, 1974). My studies included detailed analyses of nitrogen adsorption at 78 K and carbon dioxide sorption at 195 K on homoionic Li^+, Na^+, Cs^+, Ca^{++}, La^{+++} and hexane diammonium saturated montmorillonites by means of V-n plots. The nitrogen plots indicated that most of the surface area lies in pores of less than some 10 A equivalent plate separation (17, 18). Variations between cations were attributed to real differences in the porous matrix formed on drying rather than to differences in the degree of entry of gas into regions of oriented clay lamellae termed "quasi-crystals" (20). While the initial sorption of carbon dioxide was clearly influenced by the solvation properties of the cations, in the same order as previously observed on the non-expanding illite and kaolinte clays, the subsequent reversibility of the isotherms and linearity of the V-n plots indicated that for all but the largest cations, the same sorption process occurred essentially only on surfaces external to the quasi-crystalline regions (17, 18, 20).

Pore size distributions were calculated for a variety of compacted clay mineral systems by application of the Kelvin equation to complete adsorption-desorption isotherms for nitrogen to saturation at 78 K. These were compared with information on pore size distribution inferred from the corresponding V-n plots for the same data. A particularly significant feature of the information obtained was the evidence in support of the "open-pore" theory of the origin of hysteresis in gas sorption isotherms for materials containing slit-shaped pores such as are formed between plate-shaped clay mineral crystals (25). The validity of such assumptions is of importance in the application of thermodynamic derivatives to sorption isotherms and had been the subject of some dispute in the previous literature (Kington and Smith, Trans. Farad. Soc. 60. 705, 1964). The range of linearity of the V-n plots for nitrogen sorption on clay minerals indicated that adsorption in the slit-shaped pores within these systems takes place largely by the formation of physically adsorbed multilayers on the surfaces. With the filling of the pores, desorption is then governed by the curvature of the semi-cylindrical meniscus formed. Hysteresis in such systems thus results at least partly from a delay in the formation of a meniscus during the adsorption process in accord with the "open-pore" theory (25). This result was in marked contrast to that obtained for a system containing predominantly cylindrical pores (i.e, Vycor porous glass) for which low temperature high precision calorimetric studies demonstrated that neither the adsorption nor the desorption isotherms for argon sorption were thermodynamically reversible (22).

A combination of nitrogen gas sorption and mercury injection techniques was used to extend the studies of pore structure to examine the variation in pore structure of various clay mixtures common in soils (e.g. kaolinite-illite) as the proportions were varied (23, 24). These demonstrated that the pore size distributions of the mixtures were characteristic of neither of the components but showed a progressive reduction in pore size as the concentration of the finer illite increased. Application of similar techniques to investigate the pore structure of natural soil aggregates demonstrated that the wide disparity in the physical properties of plastic, sub-plastic and super-plastic soils of similar particle size distribution, could not be attributed to variations in pore structure within the 10 nm-50 μm range (27, 32).

1.2 Hydration and Swelling of Clay Mineral Systems

Detailed pore size distribution determinations obtained by application of the Kelvin equation to complete adsorption-desorption isotherms to saturation at 78 K, also formed the basis for a comprehensive study of the mechanisms of hydration and swelling during the adsorption of water and electrolytes by homoionic clay mineral systems (1, 2, 3, 4, 9, 16). A major objective of this work was to evaluate the applicability of the Gouy-Chapman diffuse double layer theory of ionic distributions at charged surfaces (Verwey and Overbeek, "Theory of stability of lyophobic colloids, Elsevier, 1949) to the swelling and flocculation of these colloidal materials. This work involved the development of a number of novel techniques for measuring the macroscopic swelling of a clay matrix with increasing water free energy and the interpretation of these results in terms of specific surface area and pore structure, the nature of the cations associated with the clay surface and electrolyte concentration. Contrary to current opinion at that time (e.g. Bolt, Geotechnique, 6, 86, 1956: Warkentin et al., Proc. Soil Sci Soc. Amer. 21, 495, 1957), it was demonstrated that while in some circumstances, diffuse double layer concepts gave a satisfactory description of the swelling behaviour of clays saturated with monovalent cations, they were completely inadequate to describe the restricted swelling of clays saturated with polyvalent cations. This was attributed to the presence of larger electrostatic attractive forces within regions of parallel orientation of clay crystals which were termed "domains" (2. 20). The presence of these regions was demonstrated by the pore size distribution studies and electron microscopic investigations. The initial work in this area (publications Nos. 1 to 4) was undertaken for the Ph.D. degree. These and subsequent studies have been cited in numerous colloid and soil science, clay mineral and related texts (e.g. "Soil and Water - Physical Principles and Processes" by Daniel Hillel, Academic Press, 1971; "Agricultural Physics" by C.W. Rose, Pergamon Press, 1966; "Clay in Engineering Geology" by Jack E. Gilliott, Elsevier Publ. Co., 1968; "Fabric and Mineral Analysis of Soils" by Roy Brewer, Wiley, N.Y., 1964; "Introduction to Clay Colloid Chemistry" by H. Van Olphen, Interscience, N.Y., 1963: "Soil Conditions and Plant Growth" by E.W. Russell, Longmans, 1973, 1989, and "Introduction to Principles and Practice of Soil Science" by R.W. White, 1979). These seminal studies have led to the now generally accepted concepts of quasi-crystals and domains as the assemblages of primary particles (crystals) which constitute the operational elements in determining soil physical behaviour. It can be fairly argued that this synthesis provided one of the major advances in soil physics during the twentieth century.

2. WATER AND SOLUTE MOVEMENT IN CLAYS AND SOILS

2.1 Water and Ionic Flow Through Compacted Clay Membranes

Compacted clay mineral systems are ideal for investigating the behaviour of ions in proximity to charged surfaces and in particular the influence of ionic distributions and water structure on the transport of water and ions through charged porous membranes. An understanding of these factors is essential in many agricultural, industrial and medical applications, such as the uptake of nutrients by plants, solution mining technology and desalination, as well as processes of importance in reverse osmosis, electro-dialysis and membrane technology in general. Studies of the pressure induced flow of solutions of various monovalent,

divalent and trivalent cations at various concentrations through highly compacted clay membranes were thus a logical and important extension to my previous research on clay-water interactions. In this respect the previous studies of pore structures in clay mineral systems were again very relevant in the interpretation of extensive measurements of the flows of water, chloride and sulphate solutions of various concentrations under high pressure (30 - 100 MPa) through compacted and constrained homoionic illite, montmorillonite and kaolinite cores (19, 31, 36).

These experiments demonstrated that three- to fourfold changes in permeability of the rigid clay membrane could occur depending on the nature and concentration of the exchangeable cation concerned. At the lower electrolyte concentrations permeability increased in the order $Na^+ < Ca^{++} < Ba^{++} < La^{+++} < Cs^+$ at a given concentration. In addition the permeability increased linearly with flow pressure to an extent ranging from some 15% for the Na^+ systems to 97% for the 3.0M $LaCl_3$ system over the pressure range examined. It was concluded that while significant variations in permeability could result from the electrokinetic effects arising in these systems, these were far outweighed by the effects of the size, charge, and concentration of the cations on the viscosity of coerced water layers in proximity to the clay surfaces. At high cationic concentrations the disruption of the coerced water layers resulted in rapid increases in permeability with increasing flow pressure (31). Maximum salt-sieving coefficients were measured at the lowest flow pressures used (approximately 3 MPa) and salt sieving decreased rapidly with increasing flow pressure (36). Over the range of flow pressures used it was concluded that convective flow overcomes the effects of diffusion which at lower flow pressures may partially compensate for the discrimination in transport between water and anions resulting from the excess negative potential in the pore spaces. Surprisingly the rapid decrease in salt sieving with increasing flow pressure did not appear to be accompanied by any major alteration in the integrity of the double-layer distribution. The maximum salt-sieving coefficients agreed well with the maximum salt rejections predicted by electrokinetic theory and were also in good agreement with measured osmotic efficiency coefficients. Wall potentials calculated from the streaming potential-pressure gradients agreed well with the outer Stern layer potentials calculated using simple diffuse-double-layer theory. This extension of structural research to flow studies in compacted clay media provided an enlarged view of electrokinetic phenomena and the effects of ions on the water structure near to the charged surfaces of clay particles. In view of the significance of these factors in other areas of surface and colloid chemistry this work has widespread implications.

2.2 Description and Prediction of Solute Movement in Soils

The ability to accurately predict the concentration distributions with time, of both reactive and non-reactive solutes in porous media such as soils, is of considerable importance in a number of disciplines, and in particular in relation to the efficiency of fertilizer usage, the control of agricultural chemicals and other contaminants as a means of maintaining groundwater quality, and in understanding the development and reclamation of saline and alkaline soils. The amount expended each year on chemical fertilizers is considerable and small increases in efficiency in the use of these fertilizers can lead to an appreciable saving for the individual farmer and on national fertilizer expenditures. Nutrient leaching represents not only a loss

to agriculture, and hence a cost to production, but also results in eutrophication when nutrients are transported to wetlands and streams. There is increasing concern with respect to the pollution of groundwaters arising from the continued and escalating application of herbicides and pesticides and a need for definitive data on which to base both safety and legislative recommendations. Furthermore, the rapid increase in the areas of previously-arable land in Australia, which have become salt affected following clearing for agricultural purposes, and the associated salinization of streams and water reservoirs, are major problems urgently requiring a physical understanding and quantitative description. I believe the following studies, bringing together existing knowledge on flow through porous materials, hydrodynamic dispersion of solutes and the distribution of solutes (including fertilizer ions and pesticide molecules) in soil profiles, provided a timely and influential contribution not only to soil science but also to environmental science, particularly in relation to water quality.

2.3 Computer Simulation of Solute Movement

An understanding and the control of the above processes depends largely on the ability to quantitatively describe the mechanisms involved in determining solute movement through soil profiles. This ability required solutions of the combined diffusive-dispersive-adsorptive-convective mass balance equations describing flow under the appropriate boundary conditions (34, 35, 37, 38, 39, 40 42, 43, 44, 45, 47, 64, 72). It also required knowledge of the magnitudes and spatial variability of the soil characteristics controlling the relevant processes. These processes include the physical and chemical aspects of the solute-soil interactions (i.e. adsorption and desorption, ion exchange, dissolution, precipitation, degradation etc.) (11, 21, 51, 58, 62, 63, 64, 66, 67) as well as molecular diffusion, hydrodynamic dispersion and convective flow.

Until the 1970s there had been little success in satisfactorily modelling solute movement in realistic situations because of the difficulty in coping, by analytical means, with the complicated non-linear partial differential equations which arise (13). These difficulties result not only from the complexity and variability of the interactions between solutes and soils but in particular the dynamic nature of the adsorption-desorption processes (34, 35), competition between different adsorbing species and soil structural effects on water and solute movement (37, 43, 44, 45). Consequently analytical approaches had in the past invariably necessitated a number of frequently unrealistic simplifying assumptions (such as linear adsorption isotherms, constant convective flow velocities and instantaneous equilibria) to provide mathematical solutions, which in turn have proved of severely limited applicability.

Fortunately the increasing accessibility of computers greatly facilitated the use of numerical methods for modeling the various processes involved. Using these techniques I have, in collaboration with my students, developed and evaluated sub-models to simulate the effects of many of the mechanisms which influence solute movement in both homogeneous and aggregated soils (34, 35, 37, 38, 39, 40 42, 43, 44, 45, 47, 72). This approach is of particular value in that it not only enables the accurate prediction of solute distributions with time, but also facilitates the interpretation of measured solute distributions in terms of the specific mechanisms involved. For example, of particular significance in this respect is that the movement

of water in field soils rarely, if ever, occurs continuously or at uniform velocity for any length of time. Thus a satisfactory model must be able to handle the "go-stop" and transient nature of water movement in soils, particularly where adsorption dynamics and intra-aggregate diffusion are concerned (35). This aspect had previously been largely ignored. Application of this concept has led to the development of a valuable methodology for investigating the dynamics of the sorption process occurring during solute transport which has been utilized by subsequent workers (e.g. Gerritse, 1989, Aust. J. Soil Res. 27: 55-66; Brusseau et al. 1989, J. Contam. Hydrol. V.4: 223-240, also 79, 80, 82). Similarly the transport of chemicals in solution through soils invariably involves competition for adsorption sites between two or more adsorbing species with sometimes drastic effects on the displacement of the less strongly sorbed species (37, 38, 39, 40, 42, 43, 44, 45). For example, it was demonstrated that as a result of such competition, far higher concentrations of less preferred species can be found in outflows than those initially present at the input stage (34, 37). These studies have contributed significantly to a unified treatment involving mathematical models, and the sophisticated treatment of adsorption and competition at surfaces and their effects on solute transport.

2.4 Pesticide Reactions and Mobility in Soil

The massive and increasing use of pesticides in horticulture and to a lesser extent in agriculture in general, is of particular concern. Although many pesticides considered hazardous for human or ecotoxic reasons are freely available, there has been very little real control on the intensity and frequency of their use. This is largely because of the lack of definitive information under Australian conditions as to the extent to which particular pesticides are retained in the soil, degrade under soil conditions and consequently, the rapidity with which they are transported by water movement through the soil profile to groundwater supplies.

In the first stage of these studies adsorption-desorption isotherms for a representative range of pesticides were examined using both batch and flow techniques, to establish the dynamics of their interactions with soils of various textures and composition (notably organic matter and sesquioxide contents), and their transport coefficients under a variety of soil conditions (pH, salinity, presence of organic co-solvent and competitive adsorption by other inorganic species (58, 62). The extent and mechanism of retention of the pesticides in soil was shown to be directly related to their chemical nature (i.e. whether ionic or non-ionic, basic or acidic). In general, adsorption of the pesticides examined followed the order paraquat > diquat > linuron > fenamiphos > simazine in all soils. Sorption data for fenamiphos, linuron and simazine could be fitted to a Freundlich type equation while that for diquat more closely fitted the Langmuir equation. Adsorption was found to be better correlated with organic matter than other soil properties and decreased with increasing pH for all pesticides except diquat (58, 62).

Desorption by a consecutive method showed hysteresis to occur with all pesticide-soil combinations examined and the magnitude of the hysteresis was unaffected by changes in soil to solution ratio (62). Using a dilution method, experimental procedures such as centrifugation and shaking were shown to only slightly affect desorption hysteresis. However hysteresis decreased markedly with increasing proportion of an organic solvent (methanol) in the soil solution and was negligible in the presence of 50% methanol. This indicates that under waste disposal

sites where the soil solution may commonly contain organic co-solvents, the mobility of pesticides could be much higher than would be expected from adsorption from aqueous solutions. Adsorption of the herbicides, linuron and simazine, in the presence of low methanol concentrations followed the solvophobic theory, which describes the adsorption of hydrophobic organic compounds in soils. Values of the Freundlich adsorption coefficient for aqueous solutions, of the two herbicides extrapolated from adsorption data for the methanol/water mixtures, showed close agreement with those obtained experimentally. Hence adsorption in aqueous solutions for pesticides of low aqueous solubility can be predicted reasonably accurately on this basis. However at methanol concentrations above some 2% a progressive decrease in adsorption was observed (66, 67).

Increasing background salt concentration markedly decreased the adsorption of diquat and paraquat, but only slightly altered the adsorption of other pesticides. Hysteresis observed after desorption in $CaCl_2$ solution, decreased with increasing methanol content for both herbicides. The decrease in hysteresis was ascribed to the swelling of the organic matter and the accompanying increased accessibility to solutes. These studies showed that the presence of organic solvents significantly affected not only the adsorption but also the desorption of herbicides in soils (66, 67). Although pesticides such as diquat and paraquat are generally considered to be essentially irreversibly retained by soil, it is significant that in these studies some 60% of adsorbed diquat could be released to solution from a sandy soil by extraction with 0.05 M $CaCl_2$. The effects of such factors on adsorption-desorption equilibria undoubtedly have significant consequences with respect to their mobility under field conditions (80, 82).

2.5 Time Dependency of Sorption

Under normal circumstances the transport of a specific pesticide is determined largely by the influence of water movement through the soil profile on the chromatographic adsorption-desorption phenomena. In these dynamic conditions the mobility of any species was shown to be markedly different from that anticipated simply on the basis of equilibrium adsorption kinetics (34, 35). The kinetics of pesticide sorption in soil had received relatively little experimental attention, and most sorption studies on pesticides in soil had dealt with equilibrium aspects (Rao and Jessup, Amer. Soc. Agron. and Soil Sci. Spec. Publ. No. 11, 1983; Yaron et al., Adv. Soil Sci. 3, 121, 1985). In particular, desorption kinetics had been very poorly understood. Furthermore, much previous work had been limited to the measurement of sorption equilibrium by batch methods involving shaking or stirring of soil suspensions. Consequently studies of pesticide sorption by batch methods have frequently indicated that the major fraction of pesticide sorption in soil is essentially instantaneous. However, it was demonstrated from breakthrough curves involving flow in soil columns, that the sorption process is almost invariably time dependent under flow conditions (35, 75, 76). The effects of such sorption dynamics may arise both from structural limitations on diffusion into micropores as well as from the kinetics of the sorption process itself. The assumption that an instantaneous reaction occurs, could clearly lead to serious underestimation of potential leaching and transport of a pesticide to groundwater (76). My earlier studies (34, 35) had illustrated that flow equilibration techniques provide a much more informative assessment of such characteristics since they take into account the effects of the many rate processes which must be involved. Using a flow technique a decrease in

the rate of adsorption with time to constant value was observed for all the pesticides studied (51). The flow technique and a batch method gave comparable adsorption results for similar equilibration times. Extrapolation of the results from the column experiments showed that considerable deviation from equilibrium in the adsorption of pesticides can occur under field conditions. More recent studies have confirmed the time-dependency of sorption in the field (Pignatello, SSSA Spec. Publ. 22, 1990; Brusseau et al. Environ. Sci. Technol. 25, 134, 1991). Furthermore use of a predictive model demonstrated that with decreasing organic matter with depth in a sandy soil profile, significant amounts of various pesticides could potentially reach groundwaters (63, 67). Flow techniques such as that subsequently developed in this work (75, 76, 77) are clearly preferable over batch techniques (Sparks, Adv. Agron. 38, 231, 1985) for estimating relevant parameters because these are realistic and suitable for modelling transport of pesticides in soil profiles.

2.6 Pesticide Degradation

Soil organic matter and soil water content have been shown to play significant roles in controlling biodegradation and hence the groundwater pollution potential, of a number of commonly used pesticides (84, 87, 91, 96, 105). In a series of field and laboratory studies the degradation behaviour of a range of commonly used pesticides was investigated with depth in the soil profile and under varying conditions of soil organic matter and water contents (87, 91, 96, 105). The pesticides studied included chlorpyriphos, chlorthal dimethyl, fenamiphos, linuron, metalaxyl, metribuzin, prometryne, propyzamide and simazine. Soil samples were from surface (0-25cm) and sub-surface (25-50cm) zones of sandy soils from horticultural research stations at Medina and Mandurah in Western Australia, each with differing soil physical properties and organic matter contents. A range of soil physical, chemical and biological properties including soil microbial biomass and soil respiration rate, were simultaneously measured on the samples. Measurements obtained principally allowed comparison of residual soil pesticide concentrations with soil organic matter, soil water potential and soil respiration rate over time.

In the laboratory, soil samples treated with pesticides (chlorpyriphos, chlorthal dimethyl, fenamiphos, linuron, metalaxyl, metribuzin, prometryne and propyzamide) were incubated for up to 190 days in a batchwise arrangement with periodic monitoring and sampling and the results compared with those measured under field conditions (96). Field degradation rates were also simulated on the basis of degradation rates measured in the laboratory, taking into account the effects of temporal variations in field moisture and temperature. These initial incubation studies showed that the pesticides had widely different degradation rates in both surface and subsoils, with half lives ranging from 23 to 142 days. Many of these half lives differed significantly from those reported in the literature illustrating the effects of differences in soil and environmental conditions. Four of the pesticides - fenamiphos, metalaxyl, metribuzin and prometryne, had half lives in the subsoil from two to more than four times those in the surface soil as could be expected from the decrease in organic matter and hence microbial activity with depth. However the reverse was observed for chlorpyriphos, chlorthal dimethyl, linuron and propyzamide. Such results contradict the usual assumption in modeling studies that degradation rates invariably decrease with soil depth. It was postulated that the non-uniform changes in degradation rates with soil depth were caused by interactive

effects of changes in soil microbial activities and in organic matter content (and thus pesticide sorption) in the different soil layers.

In a subsequent laboratory study on a sandy soil from Mandurah, Western Australia (105), degradation for four pesticides (simazine, metribuzin, fenamiphos and metalaxyl) was examined in both surface and subsoil horizons maintained at differing soil water potentials of –5kPa and –100kPa. Residual pesticide breakdown often followed first order degradation behaviour, while in some cases, conditions apparently conducive to pesticide breakdown were not realized, for example for simazine, fenamiphos and metalaxyl in the sub-soils (for these, reliable half-lives could not be estimated). Soil respiration rate and residual pesticide concentrations over the incubation generally related well to one another, indicating a dependence of pesticide degradation on microbial activity. Soil microbial biomass (in comparison to controls) was unaltered in all soil samples as a consequence of the presence of pesticides. Soil microbial biomass and respiration rates were in general lower in the subsurface compared to the surface, although in many cases respiration rates were comparable at both depths, albeit at low absolute values.

For all the pesticides, the surface treatments containing the highest organic matter and moisture contents produced the greatest rate of degradation, and all could be fitted to a first order degradation approach (R^2 of 0.67 to 0.96). Metribuzin demonstrated the most consistent degradation behaviour with depth, while fenamiphos was the least consistent. For metribuzin, good first order degradation fits (R^2 0.88-0.96) applied to all treatments, giving half-lives between 145 and 222 days. This suggests an abiotic degradation mechanism, since there was no significant difference in the rate of degradation with different treatments. In the case of fenamiphos, the only soil conditions which clearly demonstrated degradation were the high organic matter/high moisture treatment (first order fit R^2 0.96, $t_{1/2}$ 35 days), although accumulation of fenamiphos metabolites (sulfoxide and sulfone) were detected in all treatments (105). Simazine and metalaxyl demonstrated intermediate consistency in degradation behaviour compared to metribuzin and fenamiphos. Degradation rates generally decreased with decreasing soil moisture content over the potential range studied.

The transformation/degradation of fenamiphos under controlled conditions was studied in detail in the Medina surface and subsurface soils (91). In the surface soil, fenamiphos was rapidly oxidized to its sulfoxide analogue. Further oxidation to the sulfone was very slow, resulting in the accumulation of fenamiphos sulfoxide. Little accumulation of fenamiphos sulfone occurred during the study period (139 days) The time taken for 50% loss of the total residue of fenamiphos (fenamiphos + sulfoxide + sulfone) was found to be be approximately 50 days in the surface soil and about 140 days in the subsurface soil. Simulations showed that the rate of transformation of fenamiphos to sulfoxide in the surface soil was 100 times faster than that of fenamiphos sulfoxide to sulfone. In the subsurface soil, the difference between the two oxidation steps was much smaller (four fold). The observed differences in transformation behaviour are undoubtedly associated with the differences in the microbial biomass and the organic matter contents of the soils. This slower transformation in the subsurface soils can have major implications on its potential for groundwater contamination in vulnerable areas, such as the Swan Coastal Plain of Western Australia.

2.7 Predicting Pesticide Groundwater Pollution Potential

The results obtained in these studies illustrate the complexity and variability associated with pesticide degradation in the soil profile. Furthermore, given the extreme complexity and spatial variability in texture and structure in soil profiles, in addition to variations in the magnitude and timing of recharge, initial and transient water contents etc., it was concluded that a practical management model for pesticide leaching based on detailed mechanistic representation of all physical processes appears neither feasible nor likely to be user friendly in terms of input parameter requirements.

With this in mind a simple management model (PESTSCRN) incorporating soil and pesticide parameters was developed to assess the groundwater contamination potential of pesticides (88). The model was based on linear, equilibrium, and reversible sorption, first order degradation and steady piston flow, and allowed the unsaturated soil zone to be divided into a number of layers of different thickness and properties. The model was designed to screen out or identify those pesticides which have a high probability for causing groundwater contamination in a region (e.g. a catchment, a farm or a particular cropping area), so that more detailed studies can be focused on these pesticides. It was intended that the model be simple and easy to use, versatile in its applications and limited in its data requirements. The leaching depths predicted by this model for nine common pesticides generally agreed with the mean leaching depths measured in a field study on the sandy Medina soil, with those predicted by the more complex CALF (Nicholls et al., Pesticide Science 12, 484, 1982) and were statistically related to those simulated by the LEACHM model (Hutson and Wagenet, Version 3, Cornell University, N.Y. 1992). The values of leaching depth predicted by LEACHM were found to be much higher than those by PESTSCRN and CALF.

The model was extended (PESTSCRN 2) to take into account the often significant spatial variability in soil and pesticide properties, such as organic matter content, bulk density, moisture content, sorption characteristics and degradation half-lives using Monte Carlo simulations (92). For each input parameter, 500 random data were generated from normal distributions that characterized the variability of the parameters. The fate of 29 pesticides were assessed using soil and environmental conditions of the Swan Coastal Plain of Western Australia. The predicted pesticide residue fractions were shown to be described by β distributions, and the corresponding travel times by normal distributions. The advantage of this simple model over more complex ones, e.g. LEACHM, is that it requires less input data and computing time, and can still provide useful information for management decision purposes. The model is also flexible in that it allows the soil profile to be divided into soil layers of any thickness instead of fixed equal increments (cf. Nofziger and Hornsby, Appl.Agric. Res. 1, 50, 1986; Foussereau et al., Geoderma 60, 257, 1993), and it allows all the soil and pesticide parameters, rather than some of the parameters, to vary spatially (cf. Jury et al., J. Envir. Qual. 16, 422, 1987; Petach et al., Geoderma, 48, 245, 1991) This flexibility is important as many of the soil data from soil surveys are for soil layers with contrasting pedological features, with both the thickness and properties varying widely. For management purposes, the model is suitable for coupling with a geographic information system to present the results in a map form (Loague et al., J. Contam. Hyd. 5, 171. 1990). Subsequently, PESTSCRN 3 was made available as a user-friendly software

package, which also enables the temporal variability of recharge to be taken into account and illustrates the influence of seasonal patterns of leaching on predicted mobilities and persistence compared with those associated with averaging the recharge rate (100).

A recent detailed survey of literature breakthrough curves and measured solute distributions undertaken in my laboratories (M. Bromly, Honours Thesis, University of Western Australia, 1999), demonstrated that for many purposes, the influence of both pesticide/soil interactions and hydrodynamic processes on the shape of the pesticide distribution with depth in the soil profile, can be effectively described by means of graphical representations based on readily available surrogate parameters such as soil texture, bulk density and degree of aggregation. We employed the Beta distribution for curve fitting as it is able to take the asymmetry of solute spreading into account, allowing for either positive or negative skew. Using Visual Basic software, it has been shown that the Beta distribution incorporated into a simple stochastic model of pesticide mobility with recharge (e.g. the PESTSCRN model, Aylmore and Di, 2000) could be used to provide an approximate description of the spreading which occurs. While it was found that the parameters defining the shape of the Beta distribution were largely consistent within a soil textural class, inadequate details on texture and degree of aggregation in published literature precluded a systematic evaluation across the spectrum of textural classes. A major outcome has been the refinement of the user-friendly software package (PESTSCRN 4) for use by management and regulatory agencies, enabling rapid assessment of pesticide distribution in the soil profile with time for different pesticide/soil combinations under varying environmental conditions (100, 102). These studies have provided a timely and influential contribution not only to soil science but also to environmental science, particularly in relation to water quality (82).

3. STUDIES OF SOIL-PLANT-WATER RELATIONS

An appreciation of the physical, chemical and biological factors determining the supply, availability status and movement of water and solutes in soil-plant ecosystems, together with suitable techniques for the measurement of the forces involved, is essential to the development of an understanding of the mechanisms and dynamics of water movement in soils and their biological implications. The importance of this field of study cannot be over-emphasized in semi-arid and saline environments where the availability of scarce water resources for agriculture makes it imperative that its most efficient utilization by plants is achieved, and where limits to growth and production are most commonly set by limitations on our knowledge of such factors. The following investigations sought to define the part played by the various physico-chemical mechanisms involved in the overall transpiration stream of water and solute from the soil to the plant and into the atmosphere.

To survive in very dry conditions plant cell walls need to be able to retain water against high gradients in total water potential. The suggestion made by Gaff and Carr (Aust. J. Biol. Sci. 14: 299-311, 1961) that the considerable amount of water present in cell walls (actually the Apparent Free.Space) could act as a buffering system during periods of water stress, prompted an investigation of the role which differences in physical structure of the cell walls between xerophytes and mesophytes might play in determining their respective drought resistance. Using classical soil physics techniques for the determination of water content-energy

characteristics it was demonstrated (12, 14) that there were significant differences in the sorption-desorption isotherms for cell wall preparations from the different species. It was concluded that xerophytes must possess a greater resistance to the destruction of the integrity of the two-phase nature of the cell wall (solid-liquid system) than do mesophytes. A greater resistance to dessication was considered the important factor in this regard rather than the presence of a supplementary water reservoir acting as a buffer in the volumetric sense.

The importance of the root-soil interface in controlling the availability of soil water for plant growth had been emphasized by Slatyer (Plant-Water Relationships, Academic Press, 1967). Unfortunately progress in this area of study had been severely limited by the lack of suitable experimental techniques for the detailed study of soil water contents in proximity to plant roots. Questions as to the relative magnitude of soil and plant resistances to water movement under different conditions of soil water potential and transpirational demand (Newman, 1969, J. Appl. Ecol. 6: 261-272), the nature of the water driving forces (Noble, 1974, "Introduction to biophysical plant physiology"), the extent to which root-soil contact resistance (Nye, 1966, Plant and Soil, 25, 81-105; Herkelrath et al., 1977, Soil Sci. Soc. Amer J. 41, 1039-1043), accumulation of soil solute concentrations (osmotic potentials) etc. influence water availability, remained largely unresolved and in some cases, the subject of considerable controversy (Passioura, 1980, J. Exp. Botany, 120, 333-345). Although theoretical treatments had generally predicted (Gardner, 1960, Soil Sci. 89, 63-73; Molz, 1981) that water potential gradients in the soil remain small (i.e. low hydraulic resistance) relative to those in the root (high resistance) except under relatively dry conditions with only 10 to 20 % of available water not extracted (i.e. soil water potentials approaching -5.5 bars), other experimental evidence (Carbon, 1973, Aust. J. Soil Res. 11, 33-42) had strongly contradicted these predictions.

These questions were first tackled by the development of a novel collar tensiometer-potometer system to enable the measurement *in situ* and simultaneously, of the xylem water potential, root-soil interface potential and the rate of water uptake by a maize root actually growing in soil (28, 29, 33). The basis of the tensiometer-potometer was the use of fine ceramic particles to act as an extension of the ceramic wall of the tensiometer to provide intimate contact with the plant root surface in one section, thus providing direct water potential measurements, and soil in direct contact in the adjacent potometer section to allow water uptake at that potential to be measured. Studies with this system showed that root resistance increased linearly with increasing potential difference between the xylem and the external medium. The results also suggested that the rhizosphere resistance to water flow could become significant compared to the plant resistance at low soil moisture tensions contrary to the conclusions of previous workers.

4. APPLICATIONS OF COMPUTER ASSISTED TOMOGRAPHY

4.1 Water and Solute Movement near Plant Roots using CAT Scanning and Ion Specific Microelectrodes

The ideal technique for studying soil water content and soil density distributions in single root studies and across whole root networks, clearly needs to be continuous, non-destructive, sufficiently sensitive to follow the relatively rapid

changes which occur, and be able to resolve differences in water content of less than 0.2% over distances of the order of a few millimeters. This is particularly true in studies of the drawdowns associated with single root systems where accurate measurements of water potentials at the root surface are essential. My application of computer assisted tomography based on X- and Gamma ray attenuation measurements (CAT scanning), to studies of the spatial distribution of soil water content in proximity to growing plant roots (46, 49, 52, 55, 56, 59, 65, 69, 73, 74, 103), provided a major advance in this respect and an extremely exciting method for the detailed investigation of the physics of water uptake by plants (see "The Realization of a Dream", Cassel, D.K. and Nielsen. D.R. in "Tomography of Soil-Water-Root Processes", SSSA Special Publication No. 36, 1994). CAT scanning is a technique developed initially for use in diagnostic radiography to obtain non-destructive 3-dimensional representations of the human brain and for which Hounsfield (1972, Brit. pat. No. 1283915) received the Nobel Prize. Commercially available X-ray CAT scanners are capable of detecting differences in attenuation as low as 0.1% (Brooks and Di Chiro, Phys. Med. Biol. 21, 689, 1976).

Preliminary studies using the E.M.I. C.T. 1007 X-ray scanning facility at the Department of Radiology at the Q.E. II Medical Centre, Nedlands, W.A., demonstrated the ability of this method to resolve spatial variations in soil-water content of the order of 0.006 g/cm^3 over distances of two millimeters or less in an essentially continuous and non-destructive fashion (46) **(ASSSI Publication Medal, 1986).** This X-ray equipment was subsequently used to obtain detailed measurements of the drawdowns in soil water content in close proximity to single radish roots in soil at different water contents and with the plants subjected to different levels of transpirational demand (49, 56, 65). These measurements enabled comparisons to be made between experimentally determined drawdowns and those predicted by both analytical (Cowan, 1965, J. App. Ecol. 2, 221-239) and numerical (Hillel et al., 1975, Soil Science, 120, 385-399) models. While the numerical model gave the closest fit to the experimental data, the measurements illustrated clearly that significant improvements in the physical concepts on which these theoretical approaches were based, were necessary to accurately describe the position and shape of the drawdowns (49, 59, 65). The significance of this advance is illustrated by the comment of one reviewer of paper No.49, that "soil and plant scientists have been waiting for decades to see the type of data presented in this paper".

While commercially available medical scanners provide excellent resolution for the above studies these are prohibitively expensive (circa $2 million), are not conveniently designed for soil-plant studies and are rarely accessible to soil and plant scientists. Modification of the conventional transmission gamma system in my laboratory (Cs-137, Am-241 or Yb-169 sources) to utilize the CAT approach, provided an experimentally more suitable system and vastly reduced the cost of the equipment (55).

Measurement of soil solute concentrations have similarly in the past been totally inadequate to allow detailed investigations of the dynamics of solute accumulation at the soil root interface and the mechanisms involved in determining the influence of osmotic potentials on soil water availability and water and solute uptake by plant roots. The novel approach of using liquid membrane ion specific microelectrodes (Na+-LIX) to measure "single point" solute concentrations at the

soil-root interface, particularly in conjunction with CAT scanning measurements of water content distributions (69, 73), opened up a new dimension for such studies. The data obtained using the above techniques provide the most detailed and continuous description of water and solute movement in proximity to plant roots yet achieved.

Water uptake along the roots was shown to be a function of the root diameter, undoubtedly as a consequence of its influence on both xylem diameter and surface area per unit length of the roots (59, 65, 73). Lupin roots with almost constant diameter along their length showed a uniform water uptake pattern, while for tapering radish roots the water uptake decreased as the diameter of the root decreased with depth. Both plants extracted water at a faster rate than it could be replaced causing the volumetric water content in the vicinity of the root surfaces to fall well below that in the bulk soil. The main water drawdowns occurred within regions one to five mm from the root surfaces. The distances to the outer boundaries of the drawdowns were a function of soil water diffusivity and water extraction rate but varied little with time over the period of measurement. Reductions in the water extraction rates with increase in the Na+ concentration in the soil treatments were illustrated, increasing progressively with time of transpiration. Although the accumulation of Na+ at the root surface of both plants increased gradually with time of transpiration these increases were not exponential as would be expected with non-absorption by the roots. Other considerations suggested that this was due to back diffusion at the relatively high water contents used.

At the soil water contents used in these experiments, the osmotic potentials at the root surface ψ_p, exceeded the matric potentials at the root surface ψ_m, by 3.5 to 10 times and consequently ψ_p had a greater influence on transpiration rate Q than ψ_m. Linear relationships between Q and ΔP, the difference in hydrostatic pressure between the root surface and the leaves, and also between Q and $\Delta\psi$, the total water potential difference between the root surface and the leaves, were observed. The numerical values of ΔP were invariably much higher than the numerical value of the osmotic potential at the root surface. A threshold value of the hydrostatic pressure gradient ΔPo was required to initiate water flow and comparisons of these values with corresponding values of ψ_p at the root surfaces during zero transpiration, indicated that the roots of both plants acted as near perfect osmometers.

Plant resistances R_p, increased with increasing Na+ concentration in the treatments, were higher under a lower transpiration demand but decreased with time of transpiration. Soil resistance R_s between the root surface and bulk soil naturally increased as the water content decreased with time of transpiration remaining lower at the higher solute concentrations due to a lower extraction rate. R_p values were 4 to 20 times higher than the corresponding soil resistances R_s, in the case of lupins and 4 to 60 times higher in the case of the radish plants, depending on the solute concentration and transpiration period.

The development of these innovative experimental techniques using computer assisted tomography and ion specific microelectrodes, has provided a major advance for studies of soil-plant-water relations and undoubtedly has the potential to

elucidate the major controversies surrounding the physics of water and solute uptake by plants (see for example "Tomography of Soil-Water-Root Processes" (S.H. Anderson and J.W. Hopmans Eds.) SSSA Special Publ. No. 36, 1994).

Subsequent studies on the spatial distributions of water content in the vicinity of both single and interacting multiple radish roots and the effects of water stress on root shrinkage and recovery for radish and lupin roots, were undertaken by application of computer assisted tomography to X-ray attenuation measurements (103). Application of CAT was used to compare the drawdowns in soil water content associated with Radish (*Raphanus sativus cv. White Icicle and French Breakfast*) roots at starting soil water contents (θ_v) of 0.3 cm^3 cm^{-3} and 0.1 cm^3 cm^{-3} respectively. Decreasing soil water content resulted in an increase in the appearance of "beam hardening", an artifact which can complicate the interpretation of such measurements. A method of overcoming the complexity arising from "beam hardening" enabled CAT scanning to provide valuable information on processes at the root/soil interface.

Decreasing soil water content from 0.1 to 0.3 cm^3cm^{-3} caused the transpiration rate to decrease by 6 to 10 times. This was presumably due to a reduction in the water potential gradient across the root membrane. The transpiration rate decreased less rapidly than did the water content at the soil-root interface suggesting some osmotic adjustment by the leaves. This osmotic adjustment would allow the plant to maintain transpiration rate even at relatively low soil water content. The drawdown distances associated with roots growing at the lower soil water content were eight times smaller than those at the high soil water content and the value of θ_v at the soil-root interface at the end of the transpiration period was 2.5 times lower. The radish roots exhibited a temporary slight decrease in diameter after the transpiration commenced followed by a significant temporary increase. However, root diameter stabilized around its original diameter when the plant attained an almost steady water uptake rate.

4.2 Soil Water Repellency

Soil water-repellency has been recognised in various parts of the world as causing serious land-use problems on turfs, burned watersheds, horticultural and home gardens and increasingly in agriculture. Its effect in reducing water infiltration has a significant influence in reducing soil water availability for plant growth and in enhancing runoff and hence susceptibility to soil erosion. While soil-wetting agents have been developed as a possible means for overcoming this problem, assessment of the extent of water-repellency in a soil and of the effectiveness of wetting agents, has previously depended largely on simple measurements of water penetration at the soil surface. Application of the CAT technique was used to develop an index, termed the "Soil Water Dispersion Index" (SOWADIN), for quantitatively characterising the enhancement both of soil water content and its spatial distribution throughout the soil with depth resulting from their application (60). This provides a much more definitive assessment of the effectiveness and longevity of soil wetting agents. This approach has been extensively used in a large scale evaluation of soil-water repellency in the Western Australian wheatbelt and in horticultural areas in conjunction with officers of the W.A. Department of Agriculture.

4.3. Soil Structure Determination

In addition the CAT technique using a single radiation source, has been shown to provide a useful approach for directly measuring the spatial distribution of soil macroporosity and for monitoring changes which occur during wetting and drying processes, in a non-destructive manner (61). Total porosity calculated from the bulk density of soil and glass bead samples varying in bulk density from 0.76 to 1.6 g cm^{-3} correlated well with total porosity calculated from CAT scan data. The system was able to detect changes in bulk density for a loam soil of the order of 16 mg cm^{-3}, and objects of 2.0 by 2.0 mm dimensions could be pictorially resolved in the scanning plane. Average macroporosity and the spatial and frequency distribution of macroporosity for soil samples were determined by assigning the value of zero macroporosity to pixels having gamma attenuation coefficients corresponding to the bulk density of a soil aggregate, 100% macroporosity to pixels with zero attenuation coefficients and proportional values to pixels with intermediate coefficients.

The feasibility of applying CAT to dual source (^{137}Cs and ^{169}Yb) scanning to enable the changes in attenuation arising both from changes in soil water content and consequent changes in bulk density, to be monitored concomitantly and continuously has also been demonstrated (70) **(ASSSI Publication Medal, 1992).** This was achieved by simultaneously solving the equations describing attenuation in terms of the attenuation coefficients at the two energy levels for each pixel in the scanned slice. However very large counting times (some 112 h) were required and full realization of the exciting potential of this approach will require substantial improvements in scanning geometry and counting electronics for these sources.

Because limited information existed on non-destructive and repetitive measurements of the changes in soil porosity (ε) that may occur during wetting and drying, particularly at very small scale, techniques were developed to enable changes in structural conditions to be evaluated using a combination of computer assisted tomography (CAT) and fractal dimension (D) to characterise both soil porosity and pore continuity on a microscale. Initial work (93) investigated whether (i) changes in ε at scales as small as 2 x 2 mm, that may occur during wetting and drying, could be discriminated by computer assisted tomography (CAT) and (ii) a published theoretical equation (Feuntes et al., Transport in Porous Media 23, 31, 1966) could be used to estimate surface fractal dimension (D) from ε and to determine whether D is sensitive to wetting and drying. CAT was applied to gamma-ray attenuation to measure dry bulk density (ρ), before and after wetting, at 2 x 2 mm resolution of water stable soil aggregates (WSA) 2 to 4, 0.71 to 1.40, and 0.25 to 0.71 mm in size packed separately in acrylic cylinders. Columns with similar particle size were also prepared for unstable soil aggregates (USA). Before wetting the ε computed from ρ, in WSA ranged from 0.621 to 0.740; after wetting the range was 0.604 to 0. In the USA, ε ranged from 0.489 to 0.562 before wetting, and from 0.457 to 0.516 after wetting. The lack of a 1:1 relationship between the before and after wetting data for ε indicated that there were significant differences between the two. Initial values of D, obtained using a theoretical relation between D and ε, ranged from 2.154 to 2.236 for WSA and from 2.055 to 2.12 for USA. Pore continuity (PC), estimated using the theoretical relation involving PC, ε and D, decreased from 0.45 to 0.30 after wetting in USA and from 0.60 to 0.55 in WSA. The results showed that the CAT technique was useful to discriminate the changes in ε that occurred, at

scales as small as 2 x 2 mm, during wetting and drying. These results showed that D can be computed from ε and used as an index to characterize wetting and drying induced changes in ε and wetting and drying induced changes in pore continuity can be computed from D and ε. Water content and ε data from CAT along with D computed using ε, were used in the Fuentes equation for hydraulic conductivity K distribution estimation (94). Stepwise regression analysis indicated that K estimates were sensitive to structural parameters, D and PC, which changed during wetting of unstable soils. This indicates the importance and the need for the incorporation of data on structural parameters in equations used for K estimations of unstable soils.

These applications of CAT scanning to soil science have attracted considerable international interest and citation **(Invited Keynote Presentation SSS Amer. Nat. Conf., Minneapolis, Nov. 1992)**. A number of senior scientists from overseas have arranged extended visits to our laboratory to study this approach.

5. SOIL PHYSICAL CONDITIONS AND PLANT GROWTH

The physical fertility of a soil as determined by its structure, water retention and transport characteristics, friability etc. can be equally as limiting in determining optimum plant growth as the presence or absence of the necessary chemical nutrients. Unfortunately, while research into the chemical requirements for optimum plant growth has developed rapidly in recent decades and led to major practical advancements, relatively little has yet been achieved in relation to the improvement of soil physical conditions. Soil structure problems, and in particular hard-setting and poor permeability, are in fact major limiting factors in crop production and pasture regeneration as well as constituting a major threat to soil conservation in many of the wheat growing areas of Australia.

5.1 Modulus of Rupture-Exchangeable Sodium Percentage Relations

Traditional procedures for characterising soil structure and classifying soils such as measurements of water stable aggregation, are essentially ineffectual when dealing with the massive a-pedal structures frequently exhibited by many of the deeply weathered soils of the Western Australian wheatbelt and elsewhere. These soils nevertheless vary tremendously in their physical suitability for plant growth (90). In the course of detailed investigations into the susceptibility to waterlogging and hard-setting on drying, characteristic of many of the sandy loam to clay loam soils of the Western Australian wheatbelt, the usefulness of the engineering parameter, the Modulus of Rupture (MOR), as a method for classifying these soils in terms of their strength and structural stability was demonstrated (41). Previous studies of the porous structure of soil systems and clay-water interactions (1-4, 9, 24, 27, 32) provided the basis for further development of this approach.

Modifying the exchangeable sodium percentage (ESP) on the soils by leaching to produce known values before drying, provided an ideal means of subjecting the soil matrix to a range of internal disruptive forces on rewetting as the diffuse double layer development and hence swelling pressure varied. MOR tests on a soil modified in this manner assess the soils structural stability independantly of its original exchangeable cation composition. This greatly broadened the ability of the testing procedure to quantitatively distinguish between soils and to evaluate the

potential behaviour of a given soil under different treatments (41, 81). Because the development of dry strength in soils subjected to the MOR-ESP procedure is dependant on the same forces and mechanisms as are responsible for the strength characteristics of hard-setting soils in the field, the method has proven to be the most reliable indicator of the hard-setting behaviour of these soils and for evaluating the responsiveness of the hard-setting soils to gypsum treatment (50, 53, 68).

A further development of the MOR-ESP assessment procedure, involving variations in the rate of wetting and in electrolyte concentration in the wetting solution prior to the measurement of MOR, provided a method for separate quantitative assessment of the role of both dispersive and non-dispersive mechanisms in contributing to structural instability in hard setting soils (68, 81). This technique was used to assess the impact of various tillage intensity, rotational, stubble management and gypsum amendment practices on structural stability of soils from the W.A. wheatbelt. Dispersive failure was found to be the dominant mechanism contributing to overall structural instability, except where gypsum had been applied on reduced tillage treatments. On average, slaking accounted for only 20% of total instability as opposed to the 66% attributed to dispersive mechanisms. Minimising slaking however, greatly reduced the expression of dispersive behaviour in all treatments examined. This result demonstrated that adoption of management systems which confer on the soil a resistance to slaking, can be as effective a remedial measure as practices such as gypsum application which reduce dispersion directly. While gypsum application can provide a transient remedy for hard-setting behaviour further attention to reduce the effects of non-dispersive failure is essential for long term success (68).

Application of these and other techniques has provided an improved basis for the evaluation of management procedures aimed at the amelioration of poor soil structural conditions. In particular the efficacy of plant residues and root activity (85) in improving aggregate formation and water movement in hard-setting soils and of deep ripping in enhancing productivity of soils susceptible to compacted traffic and plough pan formation (57) have been demonstrated. Deep cultivation has received increasing attention as a means of alleviating subsoil structural constraints on fine textured soils. While significant benefits occur, these effects have been shown to be generally transitory and on the least stable soils, subsoil cultivation can in fact cause long-term structural deterioration unless a stabilizing agent is applied at the same time (57).

5. MISCELLANEOUS STUDIES

In addition to the previous studies I have been involved in several studies on other aspects closely related to plant nutrition and soil and water systems. These include the factors influencing the availability of phosphorus for plant growth (48), the use of soil amendments to improve water and nutrient use efficiency in turf culture (104), urate aggregation in the formation of kidney stones (54), the dynamics of organic matter transport in soil and streams (99) as well as earlier post-doctoral studies on transport through monomolecular surface layers and their application to the retardation of evaporation from water reservoirs (5, 6, 7) at Columbia University in New York (1960-1961) and on gaseous adsorption and diffusion in porous media (8) at Imperial College of Science and Technology, London, U.K. (1961-1963).

6. STATEMENT ON COLLABORATION AND RELATIVE CONTRIBUTIONS

Much of the research described above has been carried out in collaboration with a number of colleagues, post-graduate students, research fellows and research officers. I believe it is fair to say that I have been primarily responsible for the conception and initiation of the research described and in particular its overall synthesis, coherence and direction. Furthermore, I am accustomed to taking as active a role as possible in the bench or experimental aspects of my research. In all of my published work I have played a substantial role in the conduct, interpretation and writing up process. However it has consistently been my policy that first authorship should generally go to post-graduate students and research fellows.

Co-researchers and their appointments are listed below:

Academic Colleagues

Professor S.H. Anderson , University of Missouri-Columbia, U.S.A.
Professor R.M. Barrer F.R.S., Imperial College, University of London, U.K.
Professor J.P. Quirk, University of Adelaide and The University of Western Australia.
Professor W.A. Steele, Pennsylvania State University, U.S.A.
Professor V.K. La Mer, Columbia University, N.Y., U.S.A.
Professor R.S. Mansell, University of Florida, U.S.A.
Professor W.D. Kemper, Colorado State University.
Dr. R.G. Gerritse, C.S.I.R.O. Division of Water Resources.

Research Officers and Research Fellows Under My Supervision

V. Murali; J.H. Adair; C.J. Barnes; I.D. Sills; J.M. Hainsworth; H. R. Cochrane, R.D. Schuller; H. Daniel; R.S. Kookana, H.J.Di; H. Li., Ras.V. Rasiah.

Research Students

I have supervised some 29 Ph.D. degree candidates and 13 Masters degree candidates. Those whose studies are included in the previous outline are listed below.

Ph.D. Degree

M. Karim	P.F. Rolfe
T.S. Teoh	J.M. Hainsworth
S. Olejnik	H. Daniel
F. Giacobbe	N.S. Bolan
H.B. So	R. S. Singh
M. Hamza	V.K. Phogat

Masters Degree

K.R. Brata
Y. Sawada
I.D. Sills

8. SELECTED PUBLICATIONS L.A.G. AYLMORE

* Nos. 1-4 derived from research for the PhD degree, University of Adelaide, 1960.
Estimated percentage contribution indicated in brackets.

*1. Aylmore, L.A.G. and Quirk, J.P. (1959) Swelling of clay-water systems. *Nature* **198**: 1752-1753.

*2. Aylmore, L.A.G. and Quirk, J.P. (1960) Domain or turbostratic structure of clays. *Nature* **187**: 1045-1048.

*3. Quirk, J.P. and Aylmore, L.A.G. (1960) Swelling and shrinkage of clay-water systems. *Proc. 7th Congress Inter. Soc. Soil Sci.* **2**: 378-387.

*4. Aylmore, L.A.G. and Quirk, J.P. (1962) The structural status of clay systems. Proc. 9th National Clay Conf., Indiana, 104-131. *Clays and Clay Minerals* **9**: 104-130.

5. La Mer, V.K. and Aylmore, L.A.G. (1962) Evaporation resistance as a sensitive measure of the purity and molecular structure of monolayers. *Proc. Natl. Acad. Sci.* **48**: 316-324. (70)

6. La Mer, V.K., Aylmore, L.A.G. and Healy, T.W. (1963) The ideal surface behaviour of mixed monolayers of long-chain n-pariffinic alcohols. *J. Phys. Chem.* **67**: 2793-2795. (50)

7. La Mer, V.K., Aylmore, L.A.G. and Healy, T.W. (1964) The transport of water through monolayers of long-chain n-pariffinic alcohols. *J. Colloid Sci.* **19**: 673-684. (50

8. Aylmore, L.A.G. and Barrer, R.M. (1966) Surface and volume flow of single gases and of binary gas mixtures in a microporous membrane. *Proc. Roy. Soc.* **A. 290**: 477-489. (70)

9. Aylmore, L.A.G. and Quirk, J.P. (1966) Absorption of water and electrolyte solutions by kaolin clay systems. *Soil Sci.* **102**: 339-345. (75)

10. Aylmore, L.A.G. and Quirk, J.P. (1967) The micropore size distribution of clay mineral systems. *J. Soil Sci.* **18**: 1-17. (75)

11. Aylmore, L.A.G. and Karim, Mesbahul. (1967) Adsorption and desorption of sulphate ions by soil constituents. *Soil Sci.* **103**: 10-15. (65)

12. Teoh, T.S., Aylmore, L.A.G. and Quirk, J.P. (1967) Retention of water by plant cell walls and implications for drought resistance. *Aust. J. Biol. Sci.* **20**: 41-50. (40)

13. Aylmore, L.A.G. and Karim, Mesbahul. (1968) Leaching of fertilizer ions in soil columns. *Proc. 9th Inter. Congr. of Soil Sci.*, Adelaide, **1**: 143-153. (70)

14. Teoh, T.S., Aylmore, L.A.G. and Quirk, J.P. (1968) Cell wall water and drought tolerance of Ehrharta Calycina. *Aust. J. Biol. Sci.* **31**: 158-159. (40)

15. Olejnik, S., Aylmore, L.A.G., Posner, A.M. and Quirk, J.P. (1968) Infra-red spectra of kaolin mineral-dimethyl sulphoxide complexes. *J. Phys. Chem.* **72**: 241-249. (25)

16. Aylmore, L.A.G., Quirk, J.P. and Sills, I.D. (1969) The effects of heating on the swelling of clay minerals. *Proc. N.R.C. Inter. Symp. H.R.B/*, Washington, D.C., **103**: 31-38. (60)

17. Aylmore, L.A.G., Sills, I.D. and Quirk, J.P. (1970) Surface area of homoionic illite and montmorillonite clay minerals as measured by the sorption of nitrogen and carbon dioxode. *Clays and Clay Minerals* **18**: 91-96. (60)

18. Aylmore, L.A.G., Sills, I.D. and Quirk, J.P. (1970) Location of gas adsorption sites in montmorillonite clay. Reply to Thomas, Bohr and Frost on 17, *Clays and Clay Minerals* **18:** 407-409. (60)

19. Kemper, W.D., Sills, I.D. and Aylmore, L.A.G. (1970) Separation of adsorbed cation species as water flows through clays. *Soil Sci. Soc. Amer. J.* **34**: 946-948. (25)

20. Aylmore, L.A.G. and Quirk, J.P. (1971) Domain and quasicrystalline regions in clay mineral systems. *Soil Sci. Soc. Amer. J.* **35**: 652-654. (60)

21. Aylmore, L.A.G., Karim, Mesbahul and Quirk, J.P. (1971) Dissolution of gypsum, monocalcium phosphate and superphosphate fertilizers in relation to particle size and porous structure. *Aust. J. Soil Res.* **9:** 21-32. (60)

22. Giacobbe, F., Aylmore, L.A.G. and Steele, W.A. (1972) Thermodynamic properties of argon adsorbed on porous glass plus preadsorbed water. *J. Colloid and Inter. Sci.* **38**: 277-284. (40)

23. Sills, I.D., Aylmore, L.A.G. and Quirk, J.P. (1973) A comparision between mercury injection and nitrogen sorption as methods of determining pore size distribution. *Soil Sci. Soc. Amer. J.* **37**: 535-537. (40)

24. Sills, I.D., Aylmore, L.A.G. and Quirk, J.P. (1973) Analysis of pore size in illite-kaolinite mixtures. *J. Soil Sci.* **24**: 480-490. (40)

25. Aylmore, L.A.G. (1974) Hysteresis in gas sorption isotherms. *J. Colloid and Inter. Sci.* **46**: 410-419. (100)

26. Aylmore, L.A.G. (1974) Gas sorption in clay mineral systems. *Clays and Clay Minerals* **22**: 175-183. (100)

27. Sills, I.D., Aylmore, L.A.G. and Quirk, J.P. (1974) Relationships between pore size distributions and physical properties of clay soils. *Aust. J. Soil Res.* **12:** 107-117. (40)

28. So, H.B., Aylmore, L.A.G. and Quirk, J.P. (1976) The measurement of water fluxes and potentials in a single root-soil system. I. The tensiometer-potometer system, *Plant and Soil* **45**: 577-594. (40)

29. So, H.B., Aylmore, L.A.G. and Quirk, J.P. (1976) The resistance of maize roots to water flow. *Soil Sci. Soc. Amer. J.* **40**: 222-225. (40)

30. Aylmore, L.A.G. (1977) Microporosity in montmorillonite from nitrogen and carbon dioxide sorption. *Clays and Clay Minerals* **25**: 148-154. (100)

31. Rolfe, P.F. and Aylmore, L.A.G. (1977) Water and salt flow through compacted clays. I. Permeability of compacted illite and montmorillonite clays. *Soil Sci. Soc. Amer. J.* **41**: 489-495. (50)

32. Aylmore, L.A.G. and Sills, I.D. (1978) Pore structure and mechanical strength of soils in relation to their constitution. Chapter. 8, *Proc. ISSS Comm. and Symp.*, Adelaide: 69-78. (60)

33. So, H.B., Aylmore, L.A.G. and Quirk, J.P. (1978) Measurement of water fluxes and potentials in a single root-soil system. II. Applications of tensiometer-potometer system. *Plant and Soil* **49**: 461-475. (40)

34. Murali, V. and Aylmore, L.A.G. (1979) Predicting the movement of solutes in soil profiles. *Proc. Hydrology and Water Resources Symposium*, Perth: 210-215. (50)

35. Murali, V. and Aylmore, L.A.G. (1980) No-flow equilibration and adsorption dynamics during ionic transport in soils. *Nature*, **283**: 467-469. (50)

36. Rolfe, P.F. and Aylmore, L.A.G. (1980) Water and salt flow through compacted clays. II. Electrokinetics and salt sieving. *J. Colloid and Inter. Sci.* **79**: 301-307. (50)

37. Murali, V. and Aylmore, L.A.G. (1981) Competitive adsorption: its importance in ionic transport in soils. *Search* **12**: 133-135. (50)

38. Murali, V. and Aylmore, L.A.G. (1981) Modelling adsorption in solute flow simulations. Diffuse double layer vs. gas solid interaction approaches. *Soil Sci.* **131**: 76-81. (50)

39. Murali, V. and Aylmore, L.A.G. (1981) A convective-dispersive-adsorptive flow model for solute transport in soils. I. Model description and some simulations. *Aust. J. Soil Res.* **19**: 23-39. (50)

40. Aylmore, L.A.G. and Murali, V. (1981) A convective-dispersive-adsorptive flow model for solute transport in soils II. Evaluation of single and two component adsorption models for phosphate movement in soils. *Aust. J. Soil Res.* **19**: 287-298. (50)

41. Aylmore, L.A.G. and Sills I.D. (1982) Characterisation of soil structure and stability using modulus of rupture- exchangeable sodium percentage relationships. *Aust. J. Soil Res.* **20**: 213-224. (60)

42. Aylmore, L.A.G. and Murali, V (1982) Transport of non-reactive and reactive solutes through soils. *Proc. Inter. Symposium on Salinity*, Murdoch University. **24**, 1-3. (50)

43. Murali, V. and Aylmore, L.A.G. (1983) Competitive adsorption during solute transport in soils. I. Mathematical models. *Soil Sci.* **135**: 145-150. (50)

44. Murali, V. and Aylmore, L.A.G. (1983) Competitive adsorption during solute transport in soils. II. Simulation of competitive adsorption. *Soil Sci.* **135**: 203-213. (50)

45. Murali, V. and Aylmore, L.A.G. (1983) Competitive adsorption during solute transport in soils. III. A review of experimental evidence of competitive adsorption and an evaluation of simple competition models. *Soil Sci.* **136**: 279-290. (50)

46. Hainsworth, J.M. and Aylmore, L.A.G. (1984) The use of computer-assisted tomography to determine spatial distribution of soil water content. *Aust. J. Soil Res.* **21**: 435-443. (50)

47. Barnes, C.J. and Aylmore, L.A.G. (1984) A theoretical treatment of the effects of ionic and non-ionic competitive adsorption during solute transport in soils. *Aust. J. Soil Res.* **22**, 31-41. (25)

48. Bolan, N.S., Robson, A.D., Barrow and Aylmore, L.A.G. (1984) Specific activity of phosphorus in mycorrhizal and non-mycorrhizal plants in relation to the availability of phosphorus to plants. *Soil Biology and Biochemistry* **16**: 299-304. (20)

49. Hainsworth, J.M. and Aylmore, L.A.G. (1986) Water extraction by single plant roots. *Soil Sci. Soc. Amer. J.* **50**: 841-848. (50)

50. Aylmore, L.A.G. and Cochrane, H.R. (1986) Predicting structural amelioration and crop response on hard setting soils *Proc. N.Z./Aust. Soil Sci. Soc. Conf.*, Rotorua, N.Z., November, pp. 49-54. (50)

51. Singh, R., Adeney, J.A., Gerritse, R.G. and Aylmore, L.A.G., (1987) The effects of flow rate on the adsorption of pesticides in soils. *Proc. Inter. Conf. on the Vulnerability of Soil and Groundwater to Pollutants*, Noordwijh, Wageningen, The Netherlands, Ed. W. van Duyvenbooden, 835-844. (25)

52. Law, K.T., Hainsworth, J.M., Aylmore, L.A.G. and Attikiouzel, Y. (1987) Applications of computer assisted tomography, *IASTED Inter. Symp. on Signal Processing and its Applications*, August, 507-512. (25)

53. Aylmore, L.A.G. and Cochrane, H.R. (1988) The quantitative characterisation of soil physical status and potential behaviour - a fundamental approach, **Invited paper,** *Natl. Symposium on the Effects of Management Practices on Soil Physical Properties*, Toowoomba, Qlds., Sept., 1987: 200-203. (75)

54. Adair, J.H., Aylmore, L.A.G., Brockis, J.G. and Bower, R.C. (1988) An electrophoretic mobility study of uric acid with special reference to kidney stone formation. *J. Coll. and Inter. Sci.* **124**: 1-13. (20)

55. Hainsworth, J.M. and Aylmore, L.A.G. (1988) Application of computer assisted tomography (CAT) to gamma attenuation measurement of soil water content. *Aust. J. Soil Res.*, **26**: 105-110. (50)

56. Aylmore, L.A.G. and Hainsworth, J.M. (1988) Studies of soil plant water systems using CAT scanning, *Search*, **19**: 189-190. (50)

57. Daniel, H., Jarvis, R and Aylmore, L.A.G. (1988) Hardpan development in loamy sand and its effect on crop growth. *Proc. 11th Inter. Soil and Till. Res. Organ. Conf.*, Edinburgh, Scotland, July, V.1, 233-238. (30)

58. Singh, Rai, Gerritse, R.G. and Aylmore, L.A.G. (1988) Physico-chemical interaction and mobility of pesticides in soils. *National Workshop on Persistence of Herbicide Residues in Wheat Cropping Systems in Australia* , Melbourne, Oct., 32-47. (35)

59. Hainsworth, J.M. and Aylmore, L.A.G. (1989) Non-uniform water extraction by a single plant root. *Plant and Soil*, **113**, 121-124. (50)

60. Sawada, Y., Aylmore, L.A.G. and Hainsworth, J.M. (1989) Development of a soil water dispersion index (SOWADIN) for testing the effectiveness of soil wetting agents. *Aust. J. Soil Res.*, **27**, 17-26. (40)

61. Phogat, V.K. and Aylmore, L.A.G. (1989) Evaluation of soil structural conditions by application of computer assisted tomography to gamma ray attenuation. *Aust. J. Soil Res.*, **27**, 313-323. (50)

62. Singh, R., Gerritse, R.G. and Aylmore, L.A.G. (1989) Adsorption-desorption behaviour of selected pesticides in some Western Australian soils, *Aust. J. Soil Res.* **28**, 227-243. (35)

63. Singh, Rai, Aylmore, L.A.G. and Gerritse, R.G. (1990) Evaluation of potential for groundwater pollution by some pesticides in a deep sand of Western Australia. *Proc. Natl. Workshop on Herbicide Persistence*, Melbourne, Nov., 1989. (35)

64. R.S.Mansell, Bloom, S.A. and Aylmore, L.A.G. (1990) Simulating cation transport during unsteady flow in water-unsaturated sandy soil. *Soil Science* **150**, 730-744. (20)

65. Aylmore, L.A.G. and Hamza, M. (1990) Water and solute movement to plant roots. *Proc.Inter. Soil Sci. Soc. Congr.*, Kyoto, Japan, August, 1990, **V 2**, 124-129. (75)

66. Aylmore, L.A.G. Singh, Rai and Gerritse, R.G. (1989) Adsorption-desorption behaviour of pesticides and implications for groundwater pollution, *Water 89 Inter. Conf.*, Bangkok, Thailand. EQM, 4-9. (50)

67. Singh, R., Gerritse, R.G. and Aylmore, L.A.G. (1990) Effect of organic co-solvent on adsorption and desorption of Linuron and Simazine in soil, *Aust. J. Soil Res.* **28**, 717-725. (35)

68. Cochrane, H.R. and Aylmore, L.A.G. (1991), Assessing management induced changes in the structural stability of hard setting soils. *Soil and Tillage Res.* **20**, 123-132. (50)

69. Hamza, M and Aylmore, L.A.G. (1991) Liquid ion exchanger microelectrodes used to study soil solute concentrations near plant roots. *Soil Sci. Soc. Amer. J.* **55**, 954-958. (60)

70. Phogat, V.K., Aylmore, L.A.G. and Schuller, R. (1991) Simultaneous measurement of the spatial distribution of soil water content and bulk density, *Soil Sci. Soc. Amer. J.* **55**, 908-915. (30)

71.Aylmore, L.A.G. (1991) The physics of water repellant soils, **Invited Ch.** in "Water Repellency in Soils", (J.M. Oades and P.S. Blackwell eds.) Proc. Natl. Workshop, Adelaide, 13-25. (100)

72. Kookana, R.S., Schuller, R.D. and Aylmore, L.A.G. (1991) Numerical simulation of pesticide transport measured in a sandy soil. Proc. Workshop on 'Modelling the fate of chemicals in the environment', I.D. Moore ed., Centre for Resource and Environmental Studies, Canberra, 75-82. (30)

73. Hamza, M and Aylmore, L.A.G. (1992) Soil solute concentration and water uptake by single lupin and radish plant roots I. Water extraction and solute accumulation. *Plant and Soil.* 145, 187-196. (50)

74. Hamza, M and Aylmore, L.A.G. (1992) Soil solute concentration and water uptake by single lupin and radish plant roots II. Driving forces and resistances. *Plant and Soil.* **145**, 197-205. (50)

75. Kookana, R.S., Gerritse, R.G and Aylmore, L.A.G. (1992) A method for studying nonequilibrium sorption during transport of pesticides in soil. *Soil Sci.* **154**, 344-349. (35)

76. Kookana, R.S., Aylmore, L.A.G. and Gerritse, R.G. (1992) Time dependent sorption of pesticides during transport in soils. Soil Sci. **154**, 214-225. (35)

77. Kookana, R.S., Schuller, R.D. and Aylmore, L.A.G. (1993) Simulation of simazine transport through soil columns using time-dependent sorption data measured under flow conditions. *J. Contam. Hydrol.* **14**, 93-115. (30)

78. Aylmore, L.A.G. (1993) Use of Computer Assisted Tomography in studying water movement around plant roots. **Invited review**, *Advances in Agronomy.* **49**, 1-54. (100)

79. Kookana, R.S. and Aylmore, L.A.G. (1993) Retention and release of Diquat and Paraquat herbicides in soils, *Aust. J. Soil Res.* **31**, 97-109. (50)

80. Aylmore, L.A.G. and Kookana, R.S. (1993) Description and prediction of pesticide leaching, **Invited review**, *J. Aust Geol. and Geophys.* **14**, 287-296. (60)

81. So, H.B. and Aylmore, L.A.G. (1993) How do sodic soils behave? The effects of sodicity on soil physical behaviour. *Aust. J. Soil Res.* , **31**, 761-777. (30)

82. Kookana, R.S. and Aylmore, L.A.G. (1993) Mechanisms and modelling of herbicide mobility and potential for groundwater pollution: An overview, **Invited keynote paper**, *Inter. Symp. on Integrated Weed Management for Sustainable Agriculture*, Haryana, India, Nov. 1993, 129-143. (30)

83. Aylmore, L.A.G. (1994) Application of computer assisted tomography to soil-plant-water studies; An Overview. **Invited Ch. 1** in "Tomography for Measurement of Soil Physical Properties and Processes", (ed. S.H. Anderson and J.W. Hopmans) *Soil Sci. Soc. Amer.Spec. Publ.* No. **36**, 7-15. (100)

84. Kookana, Rai S. and Aylmore, L.A.G. (1994) Estimating the pollution potential of pesticides to groundwater, *Aust. J. Soil Res.* **32**, 1141-1155. (50)

85. Cochrane, H.R. and Aylmore, L.A.G. (1994) The effects of plant roots on soil structure, "Soils "94" Proc. 3rd Trienn. Conf. Aust. Soc. Soil Sci. (W.A.) Sept. 1994, 207-212. (50)

86. G.J. Churchman, Davy, T.J., Aylmore, L.A.G., Gilkes, R.G. and Self, P.G.(1995) Characteristics of fine pores in some halloysites. Clay Miner., 30, 89-98. (20)

87. Kookana, R.S., Di, H. and Aylmore, L.A.G. (1995) A field study of leaching and degradation of nine pesticides in a sandy soil, Aust. J. Soil Res. 33, 1019-1030. (30)

88. Di, H.J., Kookana, R.S. and Aylmore, L.A.G. (1995) Application of a simple model to assess the groundwater pollution potential of pesticides. Aust. J. Soil Res. 33, 1031-1040. (30)

89. Phogat, V.K. and Aylmore, L.A.G. (1996) Computation of hydraulic conductivity of porous materials using computer assisted tomography. Aust. J. Soil Res. 34, 671-678. (50)

90. Aylmore, L.A.G. and Cochrane, H.R. (1995) The importance of soil structure in the management of semi-arid lands of Western Australia, J. Arid Land Studies, 159-162. **, Invited keynote paper**, Proc Inter. Conf. on Desertifiication, Japan, Oct, 1995. (50)

91. Kookana, R.S., Phang, C. and Aylmore, L.A.G. (1997) Transformation and degradation of fenamiphos nematicide and its metabolites in soils, Aust. J. Soil Res. 35, 753-761.. (30)

92. Di, H.J. and Aylmore, L.A.G. (1997) Modeling the probabilities of pesticide groundwater contamination, Soil Sci. Soc. Amer. J. 61, 17-23. (50)

93. Rasiah, V. and Aylmore, L.A.G. (1998) Characterising the changes in soil porosity by computed tomography and fractal dimension, Soil Science 163, 203-211. (40)

94. Rasiah, V. and Aylmore, L.A.G. (1998) Estimating microscale spatial distribution of hydraulic conductivity and pore continuity using computed tomography, Soil Sci. Soc. Amer. J. 62, 1197-1202. (30)

95. Rasiah, V. and Aylmore, L.A.G. (1998) Sensitivity of selected water retention functions to compaction and inherent soil properties. Aust. J. Soil Res. 36, 317-326. (30)

96. Di, H.J., Aylmore, L.A.G. and Kookana, R.S. (1998) Degradation rates of eight pesticides in a sandy soil from laboratory incubation, field study and simulation. Soil Science 163, 404-411. (30)

97. Rasiah, V. and Aylmore, L.A.G. (1998) Computed tomography data on soil structural and hydraulic parameters assessed for spatial continuity by semivariance geostatistics, Aust. J. Soil Res. 36, 485-493. (40)

98. Aylmore, L.A.G. (1998) Soil factors in the transport of pesticides from cotton farms. **Invited Chap. 10** in "Minimising the Impact of Pesticides on the Riverine Environment" LWRRDC Occasional Papers 23/98 (Eds. N. J. Schofield and V.E. Edge) National Capital Publs., Canberra. 58-61. (100)

99. Samson, N., Gerritse, R. and Aylmore, L. (1999) Dynamics of organic carbon in the Ellen Brook Catchment, Perth, Western Australia. Proc. 9th Conf. Inter. Humic Substances Society, Adelaide, Sept. 1998. (30)

100. Aylmore, L.A.G. and Di, H.J. (2000) Predicting the probabilities of groundwater contamination by pesticides under variable recharge, Aust. J. Soil Res. 38, 591-602. (50)

101. Asseng, S., Aylmore, L.A.G., McFall, J.S., Hopmans, J.W. and Gregory, P.J. (2000) Computer Assisted Tomography and Magnetic Resonance Imaging, Ch.11 in "Root Methods – A Handbook", Eds. A.L. Smit, A.G. Bengough, C. Engels, M.van Noordwijk, S. Pellerin and S. van de Geijn, Springer-Verlag. Publ., Berlin, 343-364. (20)

102. Bromley, Melissa J., Aylmore, L.A.Graham and Webb, Kelvin M. (2000) PESTSCRN 4 – An innovative approach to the prediction of groundwater pollution by pesticides, Proc. Aust. Soc. Soil Sci Conference, Northam, 45- 50.

103. Hamza, M.A., S.H. Anderson, and L.A.G. Aylmore. (2001) Studies of soil water drawdowns by single radish roots at decreasing soil water content using computer assisted tomography, Aust. J. Soil Res. 39, 1387-1396. (30)

104. Pathan, S.M., Aylmore, L.A.G. and Colmer, T.D. (2001) Fly ash amendment of sandy soil to improve water and nutrient use efficiency in turf culture. Inter. Turfgrass Soc. Res. J. 9. 33-39. (30)

105. Webb, K.M. and Aylmore, L.A.G. (2002) The role of soil organic matter and water potential in determining pesticide degradation. In Developments in Soil Science Vol. 28A, "Soil Mineral-Organic Matter – Microorganism Interactions and Ecosystem Health, Dynamics, Mobility and Transformations of Pollutants and Nutrients" (Violante, A, Huang, P.M., Bollag, J.M. and Gianfreda, L., eds) Elsevier Publ. Pp. 117-125. (50)

Swelling of clay-water systems

Nature, 198: 1752-1753, (1960)

L.A.G. Aylmore and J.P. Quirk

(*Reprinted from Nature, Vol.* 183, *pp.* 1752–1753, *June* 20, 1959)

Swelling of Clay–Water Systems

CLAY–WATER systems are such that care must be taken to distinguish between systems which describe the final reproducible hysteresis loop and those systems which can be regarded more appropriately as having a gel-like structure.

In a series of papers, Bolt *et al.*[1–3] have reported film thicknesses for clays saturated with sodium or calcium ions. Their results have been obtained in the main by the drying of clay materials from the gel state. Croney and Coleman[4] and also Holmes[5] have clearly demonstrated that in order to obtain the final reproducible hysteresis loop for a clay material it must be dried to its shrinkage limit. Even after drying to a terminal pressure approaching 40 atm., the water content obtained by Warkentin, Bolt and Miller[3] for a Ca^{2+} montmorillonite, on rewetting to a hydrostatic suction of 0·1 atm., is still extremely high. Water contents obtained in this laboratory using Ca^{2+} montmorillonite (Redhill, Surrey) compressed into cores at 1,200 atm., then taken through wetting and drying cycles from 0·01 atm. suction to complete desiccation over phosphorus pentoxide to obtain the final reproducible hysteresis loop are very much less than those obtained by the workers at Cornell University. Furthermore, in calculating the film thicknesses from their data, these authors have assumed that the water retained by the clays was uniformly spread over the entire surface of the montmorillonite. Thus these workers regarded the internal and external surfaces of the montmorillonite crystals as being equivalent. However, Norrish and Quirk[6] have shown that for Ca^{2+} montmorillonite the $d(001)$ spacing does not increase beyond 19 A., which indicates a film thickness considerably less than the overall film thickness calculated by Warkentin, Bolt and Miller.

Before proceeding to an analysis of the water-film thickness on a clay surface, a satisfactory model for the clay mass as a whole is necessary.

The simplest type of model is one in which the clay mass is envisaged as a porous medium; in between the pores we have a clay matrix in which the clay particles are oriented on a micro-scale. From microscopic evidence, these regions of oriented clay are of the order of one micron diameter and are randomly placed with respect to one another throughout the matrix. Each of these regions is thought of as a domain.

When such a clay mass swells without external constraint, the increase in volume arises from addi-

tional water held by the clay surfaces together with an increased pore volume caused by the expansion of the clay matrix. This increase in pore volume is regarded as being proportional to the overall volume change.

For a Ca^{2+} montmorillonite, with a total surface area of 760 m.²/gm. of which 112 m.²/gm. is the external surface of the clay crystals as measured by nitrogen adsorption, the uptake of distilled water at a hydrostatic suction of 0·01 atm. was 0·91 c.c./gm. (about 1·6 c.c./gm. was obtained by Warkentin *et al.*[3]). The volume of the oven-dry clay and the oven-dry porosity of the clay mass were measured as 0·39 c.c./gm. and 0·13 c.c./gm. respectively. Assuming that the pore volume increases proportionally to the total volume of the clay mass, the swollen porosity becomes 0·33 c.c./gm. Hence, the water content associated with the clay surfaces is 0·58 c.c./gm. A $d(001)$ of 19 A. indicates a film thickness of 4·5 A. and for an internal surface of 648 m.²/gm. this film thickness corresponds to 0·29 c.c./gm. of intracrystalline water. Thus 0·29 c.c./gm. of water are associated with the external surfaces and correspond to a film thickness of 26 A. Similar calculation using a Ca^{2+} illite clay (County Grundy, Illinois) where no intracrystalline swelling is involved gives a value of 36 A. for the water film thickness on the illite surface. These film thicknesses could probably be 5–10 A. greater, since an appreciable proportion of the porosity measured in the dry state arises from incomplete contact of crystal cleavage faces, thus giving rise to an over-correction for swollen porosity.

The magnitude of these film thicknesses clearly indicates that the diffuse double layer concepts[7,8] are not applicable to the swelling of clay systems saturated with calcium ions. Furthermore, the reduction in swelling with increasing electrolyte concentration is considerably less than would be expected from diffuse double layer concepts. This is particularly noticeable for the Ca^{2+} illite, where swelling is not reduced until concentrations in excess of M calcium chloride are used. Calculations reveal that the London–van der Waals forces are not sufficient to explain the attraction between clay crystals at separations of this order and it appears likely that further development of the ideas of electrostatic attraction proposed by MacEwan[9,10] are necessary to explain the attractive forces in Ca^{2+} clay systems.

The ideas of pore swelling and the organization of a clay on a domain basis have important implications with respect to the soil mechanics concept of soil strength and soil–water hysteresis other than the final reproducible hysteresis loop. As a clay–water

system dries from a situation approaching the gel state, the formation of domains of oriented crystals and the subsequent re-orientation of these domains to positions of minimum potential energy cause the actual pore volume of the mass to decrease continually. On rewetting from positions on the normal consolidation curve with different basic pore volumes the domains retain their entity and swell as such, causing the pore volume to swell proportionately to the overall volume of the clay mass and giving rise to a series of hysteresis loops. This also enables the same water content (voids ratio) to be obtained with quite different structural arrangements within the clay mass and must of necessity result in appreciable differences in the strength of the soil structure depending on the ratio of the water held in pores to that held within the domains. It is suggested that the concepts of domains and pore swelling obviate the necessity of latent interparticle forces as postulated by Parry[11].

The form of the hysteresis loops can be explained on the basis of Everett and Whitton's[12] domain theory of hysteresis.

The idea of domains as proposed here leads to a much better appreciation of the role of organic matter in bringing about stable aggregation in agricultural soils[13,14]. The polymeric molecules in soil organic matter are thought to exist as binding between adjacent domains.

The detailed presentation of the work discussed here will be published shortly.

L. A. G. Aylmore
J. P. Quirk

Department of Agricultural Chemistry,
Waite Agricultural Research Institute,
University of Adelaide.
March 24.

[1] Bolt, G. H., and Miller, R. D., *Proc. Soil Sci. Soc. Amer.*, **19**, 285 (1955).
[2] Bolt, G. H., *Géotechnique*, **6**, 86 (1956).
[3] Warkentin, B. P., Bolt, G. H., and Miller, R. D., *Proc. Soil Sci. Soc. Amer.*, **21**, 495 (1957).
[4] Croney, D., and Coleman, J. D., *J. Soil Sci.*, **5**, 75 (1954).
[5] Holmes, J. W., *J. Soil Sci.*, **6**, 200 (1955).
[6] Norrish, K., and Quirk, J. P., *Nature*, **173**, 225 (1954).
[7] Schofield, R. K., *Trans. Farad. Soc.*, **42***B*, 219 (1946).
[8] Bolt, G. H., *J. Coll. Sci.*, **10**, 206 (1955).
[9] MacEwan, D. M. C., *Nature*, **162**, 935 (1948).
[10] MacEwan, D. M. C., *Clay Minerals Bull.*, **2**, 73 (1953).
[11] Parry, R. H. G., *Nature*, **183**, 538 (1959).
[12] Everett, D. H., and Whitton, W. I., *Trans. Farad. Soc.*, **48**, 749 (1952).
[13] Panabokke, C. R., Ph.D. thesis, University of Adelaide (1956).
[14] Williams, B. G., honours thesis, University of Adelaide (1958).

Printed in Great Britain by Fisher, Knight & Co., Ltd., St. Albans

2

DOMAIN OR TURBOSTRATIC STRUCTURE OF CLAYS

By L. A. G. AYLMORE and Dr. J. P. QUIRK

(*Reprinted from Nature, Vol.* 187, *No.* 4742, *pp.* 1046–1048, *September* 17, 1960)

(*Reprinted from Nature, Vol.* 187, *No.* 4742, *pp.* 1046-1048, *September* 17, 1960)

Domain or Turbostratic Structure of Clays

It has been realized for some time that plate-shaped clay particles on drying tend to take up a parallel orientation with respect to one another. Further, Terzaghi[1] has indicated that groups of parallel particles behave as a single particle in suspension and has referred to these groups as 'clay clusters'. Aylmore and Quirk[2], in endeavouring to interpret the swelling of clay-water systems, have defined a 'domain' as a parallel arrangement of crystals. Coal research workers[3] have referred to a similar type of organization as 'turbostratic groups' since the elementary particles are arranged in a parallel fashion in groups and these groups are arranged in turbulent array. The present communication presents evidence for the nature of a domain and discusses the consequence of domain formation in swelling phenomena of clays.

An illite clay from the hundred of Willalooka in South Australia was saturated with sodium and calcium by repeated washing with a molar solution of the appropriate cation. The clay was dialysed against distilled water, dried and ground to powder which was then allowed to come to equilibrium with a relative vapour pressure of 0·96 before being compressed into cores[2]. These cores were wet up to pF 2 and dried in stages to complete desiccation over phosphorus pentoxide. Water and nitrogen isotherms were obtained using these cores. This illite, although low in potassium (potassium oxide, 4 per cent), gives no evidence of interstratification.

A complete adsorption–desorption isotherm of nitrogen was obtained at 78° K. The surface area of the clay calculated by the B.E.T. method was 150 m.²/gm. In Fig. 1 a plot of $dV/d(p/p_0)$ against p/p_0 is shown together with a scale to relate values of p/p_0 to the Kelvin cylindrical pore radius. The clay cores have a porosity of 18·8 c.c./100 gm. and at $p/p_0 = 0{\cdot}80$, 18·6 c.c./100 gm. of pores are filled, indicating that almost the entire porosity is contained in pores less than 42 Å. Kelvin radius. Since the plates of this mineral are 700 Å. across and this is large compared with the plate separation, the calculated Kelvin cylindrical radius can more properly be regarded as a measure of the plate separation. The pore peak in Fig. 1 shows that the clay mass can be regarded as a series of parallel crystals, the

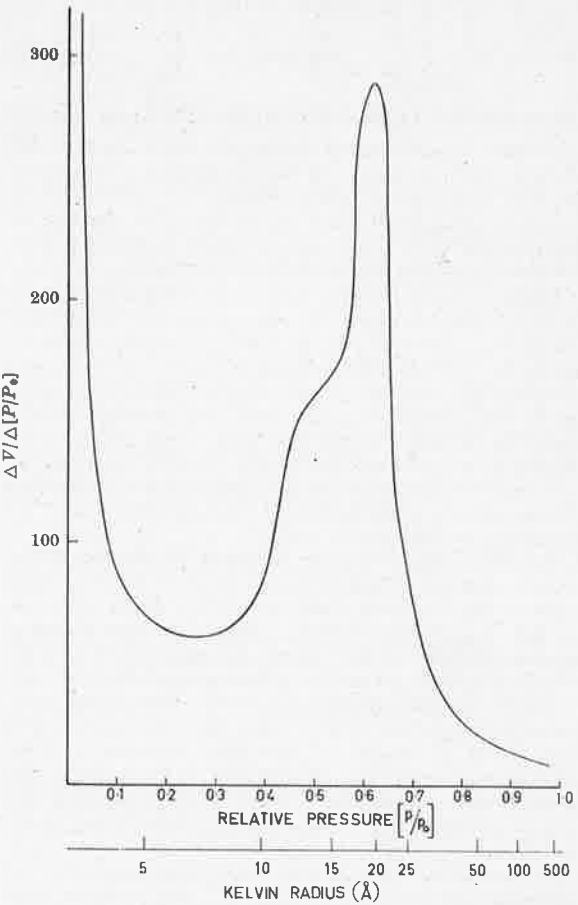

Fig. 1. Pore size distribution of calcium Willaleoka illite. Because the clay crystals are plate-shaped the Kelvin cylindrical radii can be interpreted as crystal separations

separation of which varies between 10 and 30 Å. although closer approach may occur at a few points. This indicates that the pore space of this material is almost exclusively within domains, that is, there is very little interdomain porosity. An electron micrograph of a shadowed replica of the fracture surface of a dry clay core reveals the parallel arrangement of the clay particles and also indicates that there is considerable distortion of the crystals and domain structures undoubtedly caused by stresses set up in drying (Fig. 2).

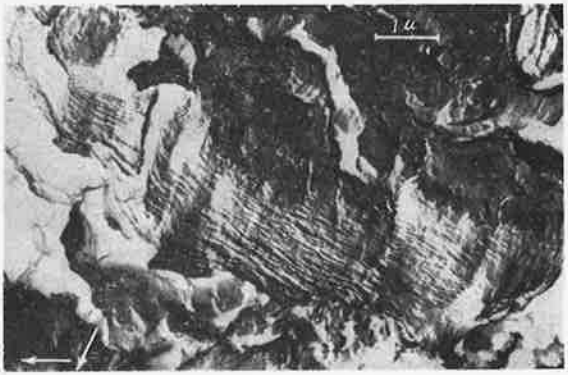

Fig. 2. Electron micrograph of the fracture surface of Willalooka illite core obtained using a replica technique. Arrows indicate the direction of uranium shadowing

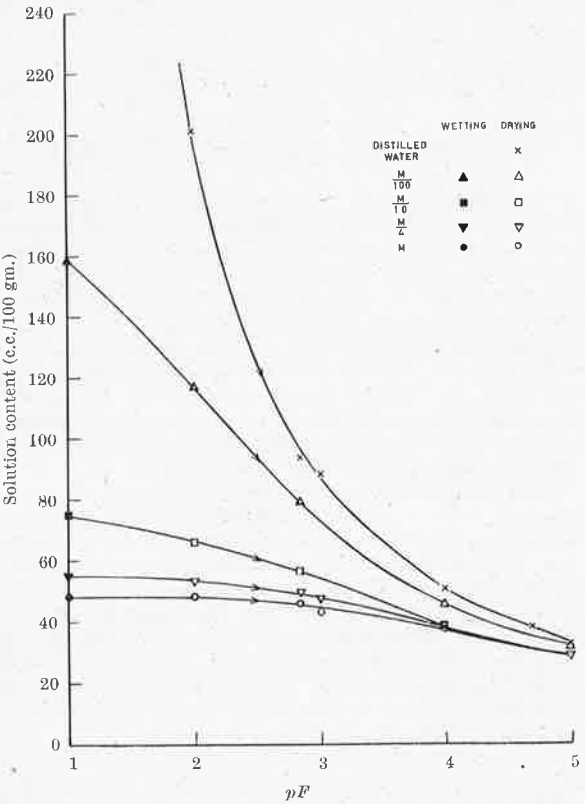

Fig. 3. Solution content–energy curves for sodium Willalooka illite at various electrolyte concentrations (sodium chloride). Note that pF indicates only the logarithm of the hydrostatic suction in cm. of water

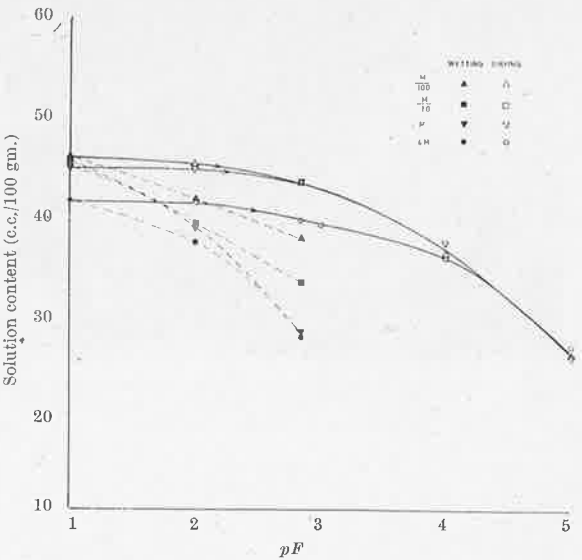

Fig. 4. Solution content–energy curve for calcium Wallalooka illite at various electrolyte concentrations (calcium chloride)

In Figs. 3 and 4 the solution content–energy curves for sodium and calcium Willalooka illite at varying sodium chloride and calcium chloride concentrations are shown. Since the clay is largely organized on a domain basis it appears permissible to divide the solution content by the specific surface area to obtain a first approximation for the film thickness on the clay surface. When this is done, good agreement between Schofield's theory based on the Gouy–Chapman diffuse double layer and the experimental values for sodium-illite are found for 10^{-1}, 10^{-2} and 10^{-4} M sodium chloride concentration.

The remarkable insensitivity of the swelling of the calcium illite to calcium chloride concentration and the appreciable hysteresis in the water content suction curves indicates the non-applicability of diffuse double layer theory to the swelling of this material.

The explanation of the film thickness at pF 1 of 30 Å. even for distilled water and the presence of hysteresis lies in the existence of a potential barrier at a plate separation of < 60 Å. and the formation of a gel structure as the result of the relaxation of strains when sufficient liquid is present in the clay matrix. The limited swelling cannot be ascribed to cementing materials ; when the sodium illite, swollen in distilled water, is converted to a calcium illite and dried, identical swelling behaviour to the calcium

illite prepared directly from the natural material is observed. MacEwan[4] has suggested that coulombic attractive forces exist up to plate separations of 30 Å., at which separation he envisaged the formation of separate double layers by each particle. It seems reasonable to conclude that calcium illite does not overcome this barrier, and that for sodium illite the barrier is overcome, giving rise to high solution contents which are dependent on the sodium chloride concentration. The similarity of this behaviour to that of sodium and calcium montmorillonite[5] is striking and supports the suggestion that a domain structure in some respects resembles a montmorillonite crystal. It is also important to note that on heating to 400° C. the sodium illite swells very little but still retains its exchange capacity of 0·41 m.equiv./gm.

One difficulty in interpreting the water content of a clay in terms of the film thickness developed by the clay particle is that, on wetting, relaxation of strains[6] leads to the formation of a gel structure so that it is difficult to separate that water which is directly associated with the clay surfaces from water which is simply enmeshed within the gel structure. Enmeshed water can be regarded in the following way. When a rigid porous material initially filled with liquid dries out under a falling vapour pressure, pores (capillaries) of particular dimensions will empty at a particular vapour pressure. The remaining liquid is held under a hydrostatic suction which is transmitted to the walls but, as each pore empties, stresses on the walls due to this cause will fall to zero. If, however, the material is easily deformed, the suction in the liquid will cause a reduction in the size of the pore, and evaporation will be delayed until a lower vapour pressure is reached, by which time the suction has further increased. The mechanism has been postulated by Barkas[7] for wood-gels, but is clearly applicable to the interpretation of gel structures and hystereses in clay–water systems.

In conclusion, it is necessary to comment on two recent papers which have overlooked, wholly or in part, suggestions put forward at an earlier date by us. Greacen[8], in discussing the swelling of calcium montmorillonite in terms of the critical voids ratio line, has used a surface area of 800 m.²/gm. and has not adequately taken into account the presence of a gel structure. Blackmore and Warkentin[9] have also claimed that their results support the existence of diffuse double layers on the external surface of montmorillonite crystals. However, they too have not considered the possibility that much of the water retained by their clay was enmeshed in a gel structure.

Further, Norrish[10] and also Blackmore and Warkentin[9] have noted a collapse of swollen crystals or a condensation of elementary silicate sheets of sodium montmorillonite to give a 19 Å. spacing in the presence of dilute calcium chloride solutions. This situation indicates that attractive forces in calcium clay systems must be such that diffuse double layers do not readily form.

The results discussed here, and those obtained for kaolinites and montmorillonites which will be presented elsewhere[11,13], indicate that diffuse double-layer formation is not of any great significance for the swelling of calcium clays. Diffuse double layers may exist for crystals of calcium clays in a suspension, but this is doubtful in view of the negative adsorption results obtained for an illite[13].

We are indebted to Mr. D. M. Hall, of the Department of Scientific and Industrial Research Dominion Physical Laboratory, for obtaining the electron micrograph.

L. A. G. Aylmore
J. P. Quirk

Department of Agricultural Chemistry,
Waite Agricultural Research Institute,
University of Adelaide.

[1] Terzaghi, K., *Geotechnique*, **6**, 191 (1956).
[2] Aylmore, L. A. G., and Quirk, J. P., *Nature*, **183**, 1752 (1959).
[3] Biscoe, J., and Warren, B. E., *J. App. Phys.*, **13**, 364 (1942).
[4] MacEwan, D. M. C., *Nature*, **162**, 935 (1948).
[5] Norrish, K., and Quirk, J. P., *Nature*, **173**, 225 (1954).
[6] Terzaghi, K., Trans. First Int. Congr. Soil Sci., **4**, 127 (1927).
[7] Barkas, W. W., "The Swelling of Wood under Stress" (H.M.S.O., 1948).
[8] Greacen, E. L., *Nature*, **184**, 1695 (1959).
[9] Blackmore, A. V., and Warkentin, B. P., *Nature*, **186**, 823 (1960).
[10] Norrish, K., *Disc. Farad. Soc.*, **18**, 120 (1954).
[11] Quirk, J. P., and Aylmore L. A. G., Seventh Congr. Int. Soil Science Society (1960).
[12] Aylmore, L. A. G., and Quirk, J. P., Ninth National Clay Conf., U.S.A. (1960).
[13] Quirk, J. P., Second Aust. Conf. Soil Sci., Melbourne, Paper No. 26 (1957).

Printed in Great Britain by Fisher, Knight & Co., Ltd., St. Albans.

Reprinted from

TRANSACTIONS OF 7TH INTERNATIONAL CONGRESS OF SOIL SCIENCE

MADISON, WISC., U.S.A., 1960

VOLUME II

J. P. QUIRK
L. A. G. AYLMORE
Department of Agricultural Chemistry,
Waite Institute, University of Adelaide

SWELLING AND SHRINKAGE OF CLAY-WATER SYSTEMS

INTERNATIONAL SOCIETY OF SOIL SCIENCE

Reprint Transactions Vol. II

SWELLING AND SHRINKAGE OF CLAY-WATER SYSTEMS

by

J. P. QUIRK AND L. A. G. AYLMORE
Department of Agricultural Chemistry, Waite Institute, University of Adelaide

The stability of soil aggregates, to processes of wetting and drying and also to mechanical stresses applied during cultivation depends to an appreciable extent upon the forces between individual clay particles and groups of clay particles. An understanding of the relationship between clay and water is therefore essential for a proper appreciation of water retention and movement in soils and the basic mechanisms involved in soil structure.

In 1947, Schofield (13) developed an equation which described the water film thickness on a charged surface in terms of the hydrostatic suction and electrolyte concentration of the solution external to the double layer of the charged surface. In discussing the necessity for this approach he stated 'In these systems it is important to distinguish broadly between irreversible shrinkage due to rearrangement of the particles, and reversible shrinkage associated with the dependence of film thickness on pressure'. Much of the subsequent work seeking to verify Schofield's theory has failed to recognise this situation.

Bolt (4), Bolt and Miller (5) and Warkentin, Bolt and Miller (16) have obtained water content-pressure curves of Na^+ and Ca^{++} montmorillonite on drying from the suspension state. Some of these results were obtained after precompression to pressures between 10 and 100 atmospheres.

Since in nature soils are predominantly Ca^{++} saturated particular importance is attached to the interpretation of the data for Ca^{++} montmorillonite. To obtain film thicknesses which could be compared with theoretical values Bolt and co-workers divided the water content of the clay at a particular pressure by the specific surface area of 800 m^2/g. Since results were obtained in the presence of 10^{-3} or 10^{-4} molar solutions the theory was only tested with respect to one variable (pressure).

Aylmore and Quirk (2) have pointed out this method of reducing the experimental data is not valid and have stressed that for any clay material a series of water content-energy curves can be obtained and these curves depend upon the previous history of the sample. This has been convincingly demonstrated by Croney and Colman (6) and the Ca^{++} montmorillonite results of Warkentin, Bolt and Miller also illustrate the point. Aylmore and Quirk indicated that the problem to be solved before comparisons could be made with theory was to distinguish between the water retained within a double layer at the particle solution interface and that water which is simply enmeshed within a gel structure.

The second point at issue concerned the use of the total surface area for montmorillonite. Because in a Ca^{++} montmorillonite-water system a basal spacing of 19 Å is always found, Aylmore and Quirk suggested that a correction should be made for water contained within the crystal. Instead of calculating the surface film thickness as suggested by Bolt and co-workers Aylmore and Quirk suggested that this should be done by correcting the water content for both crystalline water and gel water and then dividing this corrected water content by the external surface area. They applied these ideas to the swelling of a Ca^{++} montmorillonite sample which had been compressed into a core under a pressure of 1200 atmospheres and was then taken through several complete wetting and drying cycles. This procedure was

adopted so that gel structures would be reduced to a minimum. By usnig the nitrogen surface area and attempting to correct the total water content for enmeshed water and water within the crystal they obtained a film thickness of about 30 Å. They also observed that this film thickness did not change markedly with increase in electrolyte concentration up to molar. In 1954 Quirk (11) reported a similar result for an illitic clay subsoil and he noted that the water content was not susceptible to electrolyte concentration.

More recently Blackmore and Warkentin (3) have corrected Ca^{++} montmorillonite water contents for intracrystalline water on the basis of an external surface area as inferred from line broadening in X-ray diffraction diagrams. However these workers have not made any attempt to separate water simply enmeshed within the gel structure and water associated directly with clay surfaces. They are therefore not justified in the conclusion that 'any swelling which occurs in a Ca^{++} clay water system . . . can be approximated by calculations based on the Gouy-Chapman model'. As the structural status of the medium was not known a more appropriate conclusion would be that the water contents obtained were such that the possibility of diffuse double layer formation still exists for Ca^{++}-clay systems.

It is evident from the foregoing that some model is necessary before interpretation of the behaviour of clay-water systems can be undertaken. Aylmore and Quirk (2) have suggested that clay materials are organized on a domain basis. A domain was defined as the parallel alignment of individual crystals to give a small volume of oriented particles. The adjacent volume would also exist as a domain of oriented crystals but the two domains would be differently orientated with respect to one another. In criticising Bolt's paper (3) Terzaghi (14) has pointed out that the particles in the clay fraction of a soil are considerably larger than the individual crystals and must therefore consist of a group of crystals which he referred to as 'clay clusters'.

Aylmore and Quirk have proposed that the larger amounts of water retained by clays on working is due to the creation of a more open structure by changing the relationship of one domain to another and by the breakdown of domains. On the application of pressure or on drying the separated clay crystals reorganise themselves into domains and the domains take up a closer packing. Condensation of elementary silicate sheets into crystals as takes place in montmorillonite is envisaged as a particular type of domain formation.

Condensation into domains is particularly relevant to the soil mechanics concept of critical voids ratio line (CVR). Greacen (7) has suggested that this line corresponds to that predicted by Schofield's theory. However, as Greacen has used 800 m^2/g as the area for Ca^{++} montmorillonite his novel suggestion is invalidated. Parry (10) has proposed latent interparticle forces to explain the situation which exists between the CVR line, virgin and rebound consolidation curves but the present authors believe that the problem is one of water enmeshed in an open network of clay particles and domains and perhaps the term latent interparticle volume would be more correct. Open structures tend to be condensed when work is done on them and consolidated structures move to a more open structure under similar circumstances.

The present paper is concerned with the amplification of the ideas set out in this introductory review and given elsewhere (Aylmore and Quirk (2), Aylmore (1)).

Experimental Materials and Preparation

Results are reported for the fine fraction of the following materials: an illite from County Grundy, Illinois; an illite from the B horizon of a solonised solonetz soil in the hundred of Willallooka, S.A.; a kaolinite from the pallid zone of a laterite at Rocky Gully, W.A.; Mercks I a kaolinite supplied by Mercks (Germany); a montmorillonite from Upton, Wyoming and a montmorillonite from Redhill, Surrey, England.

Samples of the clays were saturated with the desired cations by repeated washing using molar solutions of the appropriate chlorides. The clays were then washed with distilled water and finally dialysed using 'Visking' cellulose casing. The clays were dried in air and then over P_2O_5. They were gently ground and allowed to come to vapour equilibrium with a saturated solution of potassium sulphate ($p/p_0 = 0.96$ at 20° C). 200 mg. of each of the homoionic clays were placed in a stainless steel mould and compressed under a pressure of 1200 atmospheres by means of a hydraulic jack. After manufacture the cores were wet in stages of pF 4.7→2.8→2.0 and then dried successively at relative vapour pressures of 0.75 and 0.19 to complete desiccation over P_2O_5 before commencing the adsorption isotherm using the same wetting stages at the low suction end. Three weeks were allowed for the attainment of equilibrium at any suction.

Wetting was carried out using constant humidity vacuum desiccators pressure plate and pressure membrane equipment. For salt solutions the film

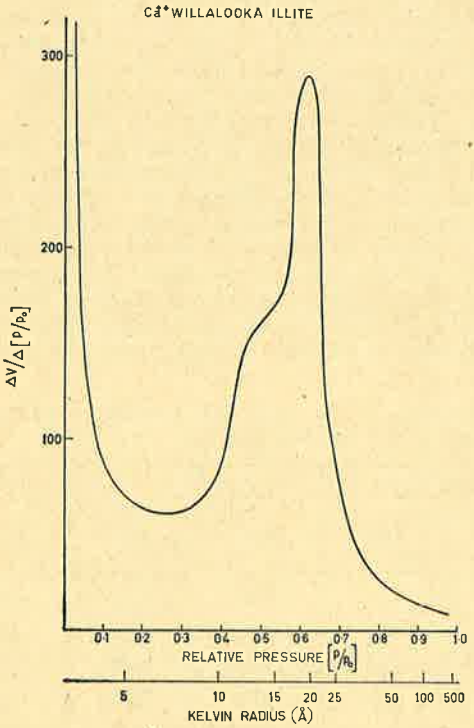

Fig. 1. Pore size distribution of Ca++ Willalooka illite as measured by liquid nitrogen desorption isotherms.

thickness was calculated from the solution content (cc/g) of the clay since the density of some solutions deviated appreciably from unity.

The nitrogen surface areas and the pore size distribution were derived from liquid nitrogen adsorption and desorption isotherms obtained at the temperature of liquid nitrogen using the conventional type of apparatus. The saturation vapour pressure was measured with a liquid nitrogen vapour pressure thermometer. Surface areas were obtained by the B.E.T. method. The clay cores were outgassed at 300° C for 25 hours or until the pressure remained below 10^{-3} mm. after isolation from the pumps for half an hour. To illustrate the distribution of pores within the Willalooka illite cores a differential plot of volume adsorbed per gram with respect to relative vapour pressure against relative vapour pressure i.e. $dV/d(p/p_0)$ against p/p_0 were made. This was considered a more convenient plot than dV/dr against r. The results obtained are shown in Figure 1.

Results and Conclusion

It is interesting to note that almost the entire porosity of the Willalooka cores is accommodated in pores with equivalent cylindrical radii less than 33 Å. From the differential plot it can be seen that the peak of the pore size distribution for this clay occurs at a relative pressure of approximately 0.625 corresponding to an equivalent cylindrical pore radius of 20 Å. Since the crystals of this clay have a cleavage face dimension of about 700 Å, this equivalent cylindrical radius may be interpreted, after allowing for twice the monolayer thickness of nitrogen, as a separation between crystal sheets of the order of 28 Å. If the oven dry porosity (0.188 cc/g) of the clay is divided by the specific surface area the average half distance between crystals so calculated is 13 Å. It may therefore be inferred that the matrix of the Willalooka cores consists of the clay plates highly organized on a microscale into packets or domains with very few large pores between domains. In fact 18.7 cc./g. of liquid nitrogen is condensed in plate separations less than 90 Å. It is difficult to visualize such a relatively narrow band of pore sizes arising in any other fashion than this for plate shaped particles, although the reason for crystals remaining at separations as large as 28 Å in the dry state, is not clear. The presence of surface irregularities on the clay crystals may be envisaged as holding the majority of the surfaces at appreciable separations since other evidence suggests only a very small area of contact. Alternatively the separations may be

Table 1. *A comparison of the effect of hydrostatic suction and electrolyte concentration on gel solution content.*

pF	Electrolyte Concentration Molar	Illite (Co. Grundy)		Illite (Willalooka)		
		Na^+	Ca^{++}	Na^+	Ca^{++}	$Na^+ \rightarrow Ca^{++}$
1	10^{-4}		123		188	264
	10^{-2}	252	117	216	165	329
	10^{-1}	246	118	282	173	313
	1	189	117	377	179	267
2	10^{-4}	—	84.9	—	92.6	
4	10^{-4}	—	27.7	—	38.1	

considered to arise from mutual repulsion of the surface charge distributions. In this regard the approach of one plate to another in the dry state could possibly provide a net repulsive force such as may result from the approach of a positive charge (surface cation) to the dipole which arises from the separation of the exchangeable cation on the adjacent sheet and the site of isomorphous replacement by the layer of oxygen atoms.

The results given in Table 1 for the gels of two illites demonstrate a lack of sensitivity to electrolyte concentration as opposed to the marked response to hydrostatic pressure. It will be subsequently pointed out that the Na^+ Willalooka results conform very well with diffuse double layer theory. It may therefore be argued that lack of sensitivity of the Ca^{++} system to increased electrolyte concentration cannot be taken as evidence against the existence of diffuse double layers in Ca^{++} systems since these double layers could be accommodated within the gel structure in the same way as they must be accommodated for the Na^+ Willalooka illite. However, the important feature to note is that a gel structure clearly exists and the amount of water directly associated with the clay surfaces is not readily obtained. The water content of 123 per cent for the Ca^{++} grundite at pF 1 when divided by the surface area gives a film thickness of approximately 200 Å which corresponds closely to the theoretical prediction even though there is obviously a gel structure present. This calculation reveals how fortuitous agreement with theory can be obtained. The much higher water contents of the $Na^+ \rightarrow Ca^{++}$ gel is further evidence of the domain structure for Willalooka illite. The sodium saturation and washing in distilled water breaks down domains which are not completely reformed until the clay is dried.

BLE 2. *Clay cores — A comparison of the theoretical and calculated film thickness on kaolinites, illites and montmorillonites at a suction of* 10 *cm. of water.*

	Rocky Gully Kaolinite	Mercks I Kaolinite	Illite (Grundite)	Willalooka Illite	Redhill Montmorillonite	Wyoming Montmorillonite	Theoretical Thickness
External Surface Area m^2/g	36	11.5	60	152	102	48*	
Porosity cc./g.	18.5	18.8	12.1	18.8	15.2	13.5	
Particle density g./cc.	2.59	2.61	2.71	2.65	2.58	2.59	
Exchange capacity me./100 g.	4.0	7.0	24	41	100	101	
Na^+ Clay							
Distilled water	98	887	250	550	300**	250**	400
Molar NaCl	97	430	105	32	104	131	20
Ca^{++} Clay							
Distilled water	93	418	71	30	62	117	200
Molar $CaCl_2$	100	414	62	30	42	65	10

* This value is for Na^+ montmorillonite the value used to calculate film thicknesses for ++ montmorillonite was 38 m^2/g. The Na^+ and Ca^{++} Redhill montmorillonite had almost ntical surface areas.

** Area of 760 m^2/g used to calculate these film thicknesses. For other montmorillonite culations external surface area is used to calculate film thickness after the internal water ntent assuming a d(001) of 19Å has been subtracted from the total water content.

The results in Table 2 have in general been calculated by dividing the total solution content by the specific surface area. For Ca^{++} montmorillonite in water and M $CaCl_2$ and Na^+ montmorillonite in M NaCl the water additional to the crystalline water has been divided by the external surface area. These procedures will clearly overestimate the film thickness but will enable several features to be discussed. Mercks I kaolinite gives such large film thicknesses that these can only be attributed to the fact that this clay has a small surface area and a strong tendency to form an open gel network. Rocky Gully kaolinite shows almost identical behaviour in both the Na^+ and Ca^{++} saturated conditions. This behaviour cannot be attributed to the positive edge charges as the Na^+ clay treated with polymetaphosphate gave identical results. Quirk (12) has demonstrated that this clay when K^+ saturated can develop diffuse double layers since it repels chloride in the expected fashion when allowance is made for positive edge charges. The pore swelling theory (2) is probably applicable to swelling of this kaolinite and when applied gives a film thickness of 29 Å.

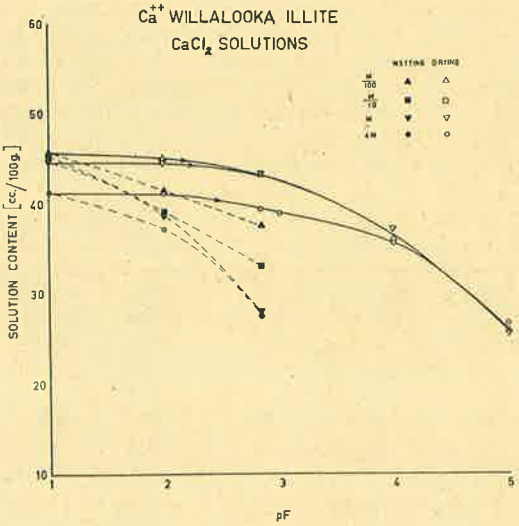

Fig. 2. The solution content — suction relationship for Ca^{++} Willalooka illite at various $CaCl_2$ concentrations.

The results for Willalooka illite are especially interesting since the pore size distribution data indicate that this clay is highly organized and it might be expected that because of this feature corrections for enmeshed water should be at a minimum and hence the film thicknesses obtained by dividing the water contents by surface area may have some reality. The film thicknesses for the Na^+ clay in M NaCl and for the calcium clay in M $CaCl_2$ and distilled water are all about 30 Å (Table 2) suggesting a potential barrier which is overcome in dilute sodium chloride solutions for the Na^+ saturated clay. There is a marked contrast in the behaviour of Na^+ and Ca^{++} Willalooka results presented in Figs 2 and 3. The distilled water 10^{-4} and 10^{-2} and 10^{-1} M NaCl gives results in good agreement with that predicted by diffuse double layer theory, although due to the difficulties

discussed above the agreement here can only be taken as qualitative confirmation of the theory. Schofield's theory only takes account of osmotic repulsive forces and does not consider the role played by attractive forces. Even for the case of Na^+ Willalooka some allowance should be made for enmeshed water and it is possible that the true film thickness bears a closer relationship to those calculated for montmorillonite from X-ray results, (Norrish 9).

The film thickness obtained will to a certain extent depend on the degree of domain development as gel formation on swelling might be expected to be associated with the external surface of the domains because the coherence between domains would be weaker than the coherence between crystals within a domain. The film thickness of 30 Å for Willalooka illite can be regarded as a reasonable approximation of the situation within a domain and the film thicknesses of 42 and 65 Å in M $CaCl_2$ for the two montmorillonites arises from additional water held between adjacent domains. The film thicknesses in 4 molar $CaCl_2$ are 33 and 27 Å for Wyoming and Redhill montmorillonite respectively. For Wyoming montmorillonite the increase from 33 to 65 Å in molar and to 117 in distilled water indicates that electrolyte concentration plays a role in gel formation but the results do not support the suggestion that diffuse double layers have formed between domains. Film thicknesses in excess of 100 Å for both montmorillonites in the presence of M sodium chloride appear unreal and some type of gel formation seems a more appropriate explanation of these values.

It is conceivable that the formation of a gel structure is more dependent on the removal or decrease in attractive forces rather than an increase in repulsive force between the plates. In the presence of liquid, strains due to crystal bending will tend to relax. However, when the solution between the charged surfaces is 4 M $CaCl_2$ the ion distribution would be such that one ion would be only about 5 Å from its neighbour and the water in this region would be largely in the state of dielectric saturation. As the concentration of ions is decreased the attractive force would be lessened since the proportion of water showing dielectric saturation in the vicinity of clay particles would decrease. This suggestion could explain the larger relaxation in M NaCl than in M $CaCl_2$.

The results for Ca^{++} Willalooka can be taken as an indication of the non-applicability of diffuse double layer concepts to the swelling of Ca^{++} clays. At a suction of 10 cm. of water there is virtually no difference between the swelling obtained in M $CaCl_2$ and distilled water. The value of this film thickness 30 Å is considerably larger than the expected 10 Å or thereabouts for a molar solution and considerably less than 200 Å expected for diffuse double layer development in distilled water. It seems reasonable to conclude that diffuse double layer concepts do not apply to the swelling of Ca^{++} clay systems even though the silicate sheets would be separated by an average distance approaching 60 Å. As a potential barrier obviously exists in this system it would still be possible that diffuse double layer concepts can be applied to Ca^{++} clay particles which have moved across this barrier as the result of dispersion or mechanical work.

The nature of the potential barrier is not clear, it could arise from unspecified attractive forces. MacEwan (8) has suggested that coulombic attractive forces exist up to plate separations of 30 Å at which separation he envisaged the formation of separate double layers by each particle. The potential barrier discussed here may be at a somewhat greater distance or alternatively only small areas of opposing crystal faces may not be removed beyond the barrier but may provide sufficient attractive force to resist swelling.

It may be that the surface density of charge plays an important role in controlling the swelling of illite systems since if the clay surfaces approach one another closely mica type bonds may be formed and hence restrict swelling. Since mica shows no crystalline swelling, vermiculite limited crystalline swelling and montmorillonite shows extensive crystalline swelling especially when saturated with Na^+ it may be suggested that there is a fundamental difference between the swelling of illites and montmorillonite.

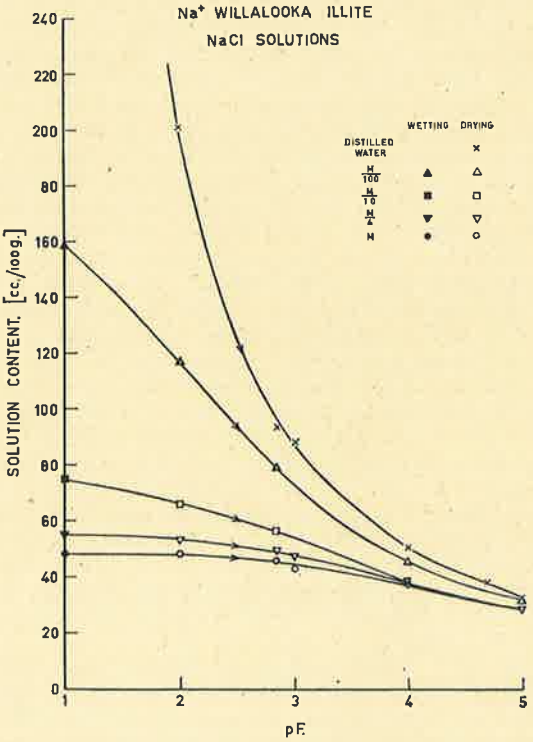

Fig. 3. The solution content — suction relationship for Na^+ Willalooka illite at various NaCl concentrations.

Electron micrographs of the fracture surface of clay cores indicate that clay crystals in the dry clay matrix are subject to considerable distortion. Hence Terzaghi's (15) idea of crystal bending on drying and subsequent relaxation on rewetting could be operative in increasing the solution uptake above that equivalent to surface film development and may account for the large hysteresis observed at pF 2.84 in Fig. 2. With the reduction in the electrostatic attractive forces as envisaged by MacEwan (8) at separations. of about 30—40 Å the elastic properties of the clay crystals may be sufficient to overcome the effective potential barrier and initiate the formation of gel structures. Once the structure has undergone this relaxation of mechanical strain the increase in suction necessary to cause a subsequent recompression of the structure, appears to be comparatively independent of the concentration of electrolyte present.

References

1. Aylmore, L. A. G., (1960). Ph. D. Thesis, University of Adelaide.
2. Aylmore, L. A. G. and J. P. Quirk, (1959). Nature **183:** 1752.
3. Blackmore, A. V. and B. P. Warkentin, (1960) Nature, **186:** 823.
4. Bolt, C. H., (1956). Geotechnique, **6:** 86.
5. Bolt, C. H. and R. D. Miller, (1955). Proc. Soil Sci. Soc. Amer. **19:** 285.
6. Croney, D. and J. A. Colman, (1954). J. Soil Sci. **5:** 75.
7. Greacen, E. L., (1959). Nature, **184:** 1695.
8. MacEwan, D. M. C., (1954). Nature, **174:** 39.
9. Norrish, K., (1954). Disc. Faraday Soc. **18:** 120.
10. Parry, R. H. C., (1959). Nature, **183:** 538.
11. Quirk, J. P., (1954). The Physical & Chemical Properties of Clays. Symposium, Waite Institute.
12. Quirk, J. P., (1957). Second Aust. Conf. in Soil Sci., Melbourne, Paper No. 26.
13. Schofield, R. K., (1946). Trans. Farad. Soc., **42B:** 219.
14. Terzaghi, K., (1927). Trans. First Int. Congr. Soil Sci. **4:** 127.
15. Terzaghi, K., (1956). Geotechnique, **6:** 191.
16. Warkentin, B. P., G. H. Bolt and R. D. Miller, (1957). Proc. Soil Sci. Soc. Amer. **21:** 495.

Summary

From a complete liquid nitrogen desorption isotherm the pore size distribution of an illite core has been obtained. These measurements reveal that a large proportion of the pore space of this clay is held in pores which are 10—30 Å Kelvin radius. Because of the plate shaped particles the Kelvin radius can be interpreted as a plate separation. The pores are therefore between clay crystals which are in parallel array on a microscale. This particle arrangement has been termed a domain and in many circumstances the domain may act as an individual particle. With respect to one another domains are in a turbulent array.

The swelling of Ca^{++} systems are very much smaller than diffuse double layer theory would predict since potential barriers exist within domains. These potential barriers are considered to arise from electrostatic forces of the type proposed by MacEwan. Diffuse double layers could exist between domains in Ca^{++} clay systems.

The large film thickness for all clays in 4 M and M $CaCl_2$ solution is attributed to the relaxation of strains imposed on the clay crystals and domains during the drying process.

Résumé

La répartition, par diamètre, des pores dans un nodule d'Illite a été déduite d'une isotherme de désorption complète, obtenue au moyen d'azote liquide. Ces mesures ont montré qu'une grande partie des vides consistait en pores d'un diamètre compris entre 10 et 30 Å Kelvin. Les particules ayant la forme de plaquettes, le diamètre Kelvin peut être considéré comme une séparation entre plans parallèles. Les pores se trouvent donc entre des cristaux d'argile qui, à l'échelle microscopique, sont disposés en arrangement parallèle. Cet arrangement parallèle des particules a été appelé 'domaine', et souvent le domaine se comporte comme une seule particule. Entr'eux, les domaines sont mélangés de manière désordonnée.

Le gonflement des systèmes Ca^{++} est beaucoup plus petit que la théorie de la double couche diffuse ne le laisse prévoir, car il existe des séparations potentielles à l'intérieur des domaines. L'auteur pense que ces séparations potentielles pourraient avoir leur origine dans des forces électrostatiques, analogues à celles proposées par Mc Ewan. Il est possible qu'il existe des

doubles couches diffuses entre les domaines dans les systèmes d'argile Ca^{++}. La grande épaisseur des films, observée chez toutes les argiles suspendues dans des solutions de $CaCl_2$ 4 M et M, est attribuée à une diminution des tensions qui, pendant le processus du séchage, s'impose aux cristaux d'argile et aux domaines.

Zusammenfassung

Aus einer vollständigen Desorptionsisotherme für flüssigen Stickstoff konnte die Porengrößeverteilung eines Illitkernes erhalten werden. Aus diesen Messungen ging hervor, daß ein großer Teil des Porenraumes dieses Tones von Poren eines Radius zu 10—30 Å Kelvin eingenommen wird. Wegen der Plattenform der Teilchen kann der Kelvin-Radius als eine Plattenscheidung interpretiert werden. Die Poren befinden sich deshalb zwischen Tonkristallen in paralleler Anordnung auf Mikromaßstab. Diese Teilchenanordnung hat man eine 'Domaine' genannt und in vielerlei Umständen wirkt die Domaine wie ein individuelles Teilchen. In Beziehung zu einander liegen die Domainen in völlig verworfener Ordnung.

Die Schwellung von Ca^{++} Systemen ist weit geringer als die diffuse Doppelschicht Theorie verlangen möchte, da die potentiellen Schranken innerhalb der Domainen existieren. Man ist der Meinung, daß die potentiellen Schranken aus elektrostatischen Kraften, der Art wie von MacEwan vorgeschlagen, hervorgehen. Diffuse Doppelschichten könnten zwischen Domainen in Ca^{++} Tonsystemen bestehen.

Die große Filmdicke für alle Tone in 4 M und M $CaCl_2$-Lösung wird der Spannungsverminderung, während des Trockenprozesses den Tonkristallen und Domainen auferlegt, zugeschrieben.

Reprinted from
"Clays and Clay Minerals, Vol. 9"
PERGAMON PRESS
OXFORD – LONDON – NEW YORK – PARIS
1962

THE STRUCTURAL STATUS OF CLAY SYSTEMS

by

L. A. G. AYLMORE AND J. P. QUIRK

Department of Agricultural Chemistry
Waite Agricultural Research Institute, University of Adelaide

ABSTRACT

Illite and montmorillonite have been compressed into cores under a pressure of 1200 atm. The structural status of these clays has been examined by means of detailed nitrogen adsorption–desorption isotherms and by means of electron micrographs of fracture surfaces of the clay cores. The subsequent swelling behavior of sodium and calcium clay cores has been analyzed in terms of the model derived from these measurements and the specific surface area of the clay. A generalized theory for the condensation of plate-shaped particles into domains has been proposed.

Measurements of the effect of electrolyte concentration and hydrostatic suction on the swelling of sodium- and calcium-saturated clay cores indicate that diffuse double layer theory may play a significant part in determining the swelling of monovalent clay systems but not divalent clay systems.

The magnitude of the film thicknesses apparently developed in solutions as concentrated as molar and 4 M, where the condition of ideal solutions required by diffuse double layer theory is certainly not fulfilled, seems to indicate that solution uptake is increased by a relaxation of structural strains within the clay matrix on lubrication by solutions. These strains may arise from the distortion of crystals in packing during the drying process. Such relaxations which appear to occur between pF 4 and 3 could initiate the development of a gel structure.

INTRODUCTION

The reaction of clay with water is of fundamental importance in the fields of agriculture, engineering and clay technology. From an agricultural point of view the stability of soil aggregates to processes of wetting and drying and also to mechanical stresses applied during cultivation depends to an appreciable extent upon the forces between individual clay particles and groups of clay particles. An understanding of the relationship between clay and water is therefore essential for a proper appreciation of water retention and movement in soils and the basic mechanisms involved in soil structure.

Similarly soil engineering studies are concerned with the consolidation and shear strength of the soil–water mass. These properties are determined

by the nature of the clay–water interaction as well as mechanical particle-to-particle interaction. Even for soils of loam texture which exhibit no physical swelling the interaction of clay with water results in swelling, which, although accommodated within the rigid framework of coarser particles, markedly influences soil properties.

A clay mass exists in a series of structural states depending not only on its water content but also on its history. In the dry state the structural status of a clay material can be defined by pore size distribution studies; as swelling takes place the uptake of water can be described in terms of the formation of a gel structure and the film thickness developed by clay particles in repelling one another.

Croney and Coleman (1954) and also Holmes (1955) have shown that at any given hydrostatic suction it was possible for a clay mass to have a range of different water contents depending on its previous history and also that a disturbed clay mass described a series of hysteresis loops on repeated wetting and drying. This effect of terminal pressure on the decompression curve for clays in the gel state is also well illustrated by the results of Warkentin, Bolt and Miller (1957). For many years soil engineering workers (Lambe, 1953; Parry, 1959) also have been aware of the presence of irreversible hysteresis in the water content–suction relationship of a clay material. They use such terms as "virgin consolidation curve," "rebound curves" and "overconsolidated clay."

The results of Croney and Coleman, and Holmes indicate that for a clay mass to describe what may be termed the final or minimum water content hysteresis loop it was necessary to dry the clay material to its shrinkage limit. In this state the clay matrix has settled down to a situation where the clay particles are in a state of minimum potential energy with respect to one another.

Aylmore and Quirk (1959) have suggested that as a clay–water system dries from a situation approaching the gel state (virgin consolidation curve) the formation of domains of oriented crystals and the subsequent reorientation of these domains to positions of minimum potential energy cause the actual volume of water enmeshed within the gel structure to decrease continually. A domain was envisaged as a microscopic or submicroscopic region within which the clay particles (crystals) are in parallel array. These groups of oriented crystals, or domains, are randomly placed with respect to one another throughout the clay matrix; that is, the domains are in turbulent array.

Schofield (1946) regarded the swelling of a clay matrix as arising from the development of diffuse double layers by the clay particles. He has presented a theoretical treatment based on the Gouy–Chapman diffuse double layer, to describe the film thickness in terms of the hydrostatic suction within the water surrounding the clay mass and the electrolyte

concentration of the solution external to the double layers of the clay crystals.

The role of double layers in the retention of water by montmorillonite has been investigated in a series of papers by Bolt (1956), Bolt and Miller (1955) and Warkentin, Bolt and Miller (1957). In questioning the validity of some of the conclusions of these workers, Aylmore and Quirk (1959), and Quirk and Aylmore (1960) have pointed out that the central problem, in trying to interpret the behavior of clay–water systems in terms of double layer formation at the clay liquid interface, was to separate that water which was simply enmeshed within a gel structure from the water retained by physico-chemical forces on the clay particles.

There are few satisfactory experimental data with which a comparison between the internal swelling of expanding lattice minerals and the film thickness developed on the external surfaces of clay crystals can be made. Attempts to correlate physical swelling data for clay minerals with theoretical treatments have proved less conclusive than the more direct X-ray approach.

Early Hofmann and Bilke (1936) reported that, near saturation, Na^+-montmorillonite gave a spacing considerably greater than 30 Å. However, Méring (1946) observed that when flakes of Na^+-montmorillonite were placed in water they increased to 20 times their volume; he concluded that the swelling took place between crystals rather than by crystalline swelling. He attributed the disappearance of the 20 Å basal reflection to disorder in the primary particles rather than their swelling. From permeability and X-ray studies Quirk (1952) concluded that Na^+-montmorillonite expanded beyond the basal reflection of 20 Å and noted that this swelling could be controlled by high sodium chloride concentration (see also Norrish and Quirk, 1954). Norrish (1954) has shown that for concentrations (C) less than 0.25 N the basal spacing increased linearly with respect to $C^{-1/2}$ as predicted by Schofield's theory; however, the film thickness calculated from the X-ray spacing is less than that predicted from theory.

The present paper is concerned with an analysis of the water content-energy curves of clay cores in terms of their structure in the dry state as revealed by complete low temperature nitrogen adsorption–desorption isotherms and the surface area of the crystals. Compressed cores were used so that contributions by water enmeshed within the gel structure to the total water content would be at a minimum.

MATERIALS

Although a number of different clays were examined the results for four clays are discussed to indicate the main features of the investigation. These clays are as follows: an illite from the B horizon of a solodized solonetz in the hundred of Willalooka, South Australia; the B horizon of Urrbrae loam,

a Red-brown earth at the Waite Institute, South Australia, containing 60 percent of particles less than 2 μ; a montmorillonite from Redhill, Surrey, England and Wyoming bentonite from Upton, Wyoming, U.S.A. Willalooka illite is degraded to some extent since it has a low potassium content (4 percent K_2O) but there is no evidence of interstratification. The clay fraction of the Urrbrae loam contained 60 percent illite and 40 percent kaolinite. The illite in the Urrbrae loam appears to have similar characteristics to the Willalooka illite.

EXPERIMENTAL PROCEDURES

(*a*) *Preparation of Clay Materials*

Samples of clay were saturated with the desired cation by repeated washing and centrifuging using a molar solution of the appropriate chloride. Excess salt was removed by washing the materials with distilled water until they commenced to disperse or until the chloride concentration was less than 10^{-3} M. Salt-free samples of clay were obtained by dialyzing for two weeks against distilled water using "Visking" cellulose casing.

Decantation of clay suspension was carried out to remove coarse particles and the suspension was filtered in a Buchner funnel; the clay was then allowed to air-dry. Violent dispersion techniques were specifically avoided to prevent the possible disruption of any natural clay structures which might exist, particularly for the divalent clays.

The air-dry clays then were gently ground to a powder and placed in a desiccator and allowed to come to vapor equilibrium with a saturated solution of potassium sulfate ($p/p_0 = 0.96$ at 20 °C). Samples (200 mg) of homoionic clays were placed in a stainless steel mold and compressed to 1200 atm pressure by means of a hydraulic jack. The water contents of the illite and montmorillonite powder in equilibrium with 0.96 relative vapor pressure were sufficient to give saturation under compression. After compression the cores were wet in stages of pF 4.7 → 2.8 → 2.0 and then dried successively to 0.75 and 0.19 relative vapor pressure before drying over P_2O_5. The water adsorption isotherms, surface areas, and pore size distributions were determined on these cores.

For Urrbrae B the natural aggregates were obtained and the cores were made after Ca^{2+} saturating by the same procedure as was used for the other clays except that coarse particles were not removed. The natural aggregates were largely Ca^{2+} saturated.

(*b*) *Low Temperature Nitrogen Sorption Isotherms*

Complete nitrogen adsorption–desorption isotherms for the clay materials at 78 °K were obtained using a volumetric apparatus based on the original apparatus of Emmett and Brunauer (1934) and incorporating many

of the refinements suggested by Harkins and Jura (1944) and Joyner (1949).

Sufficient weight of clay to give a surface area of approximately 100 m^2 was placed in the sample bulb, connected to the apparatus and outgassed at a temperature of 300 °C for 25 hr or until the pressure remained below 10^{-3} mm after isolation from the pumps for 30 min. The 300 °C outgassing temperature was adopted for most satisfactory reproducibility in the light of results obtained by Brooks (1955). Méring (1946) concluded that montmorillonite retained its hydration capacity up to a temperature of 300 °C. In the present work it was found that montmorillonite still retained its capacity for large physical swelling after outgassing at a temperature of 400 °C.

(c) *Water Content–Energy Relationships*

Water content–energy relationships for the clay materials were obtained by means of pressure plate and pressure membrane apparatus and constant humidity desiccators. The work was carried out in a room maintained at 20 $\pm$ 1/4 °C.

To facilitate comparison between solutions of different electrolyte concentration and also the calculation of surface film thickness, the solution contents are given in volume of solution absorbed per gram of oven dry (110 °C) clay.

(d) *Determination of Exchange Capacity*

Samples of the clays as previously prepared were saturated with strontium by washing with a neutral solution of molar strontium bromide. Excess salt was removed by washing with distilled water and the clays allowed to air-dry. The exchange capacities were obtained as the difference between the strontium and bromide contents determined using an X-ray spectrographic method. In all samples the bromide contents were very low.

The exchange capacities in meq per 100 g of oven dry 110 °C clay are given in Table 1.

TABLE 1.—PROPERTIES OF CLAY MATERIALS

Material	Surface Area (m^2/g)	Exchange Capacity (meq/g)	Porosity (cm^3/g)	Particle Density (g/cm^3)
Willalooka illite	152	0.41	0.185	2.65
Redhill montmorillonite	102	1.00	0.152	2.58
Wyoming bentonite	38	1.01	0.135	2.59
Urrbrae—cores	94	0.28	0.141	2.72
Urrbrae—aggregates	91	0.28	0.191	2.72

(e) *Specific Gravity and Porosity Determinations*

Specific gravity of the clays was determined on the oven-dry (110 °C) material by the volume displacement method using a nonpolar liquid and 25-ml pycnometers. The apparent density of the oven-dried clay cores was determined from the oven dry mass and the overall volume of the clay cores. The volume of the clay cores was calculated from direct measurements of the dimensions obtained with a traveling microscope. For volumes of 0.1–0.2 ml this method gave better than 1 percent accuracy. The porosity was calculated from the particle density and apparent density in the usual way.

RESULTS AND DISCUSSION

Nitrogen Isotherms and Pore Size Distributions

Surface areas of the clay minerals, obtained by the application of the B.E.T. theory to the nitrogen adsorption isotherm are set out in Table 1 together with the exchange capacity, porosity of clay cores and particle density.

To illustrate the distribution of pores differential plots of the volume adsorbed per gram with respect to relative vapor pressure against relative pressure, i.e. $dV/d(p/p_0)$ against p/p_0, were made. The equivalent pore radii calculated on the basis of the Kelvin equation are indicated on the abscissa. The linear (p/p_0) scale was considered more convenient for the purpose of illustration than a true pore size distribution plot of dV/dr against r, since the latter involves the inverse logarithmic relationship between p/p_0 and r and provides little further information.

The isotherm for the Ca^{2+} cores of Willalooka illite together with the pore size distribution are shown in Figs. 1 and 2. Similar results for Redhill montmorillonite are shown in Figs. 3 and 4.

The nitrogen adsorption isotherm of Willalooka illite and Redhill montmorillonite both show appreciable hysteresis above 0.4 relative vapor pressure followed by a small but persistent hysteresis down to a very low vapor pressure. Similar hysteresis effects in nitrogen isotherms on finely divided material have been noted by several other workers. Brooks (1955) explained the presence of hysteresis at low relative pressures (< 0.4) in the nitrogen sorption isotherms for Ca^{2+}-montmorillonite as being due to the propping apart of interlamellar spacings by residual water molecules giving rise to a structural instability of the material. This could account for the augmented nitrogen adsorption capacity on the desorption branch of the isotherm down to very low relative pressures. The disappearance of this micropore hysteresis after the removal of most of the water of adsorption and hydration by a prolonged outgassing for 152 hr at 25 °C and 4 hr at 60 °C

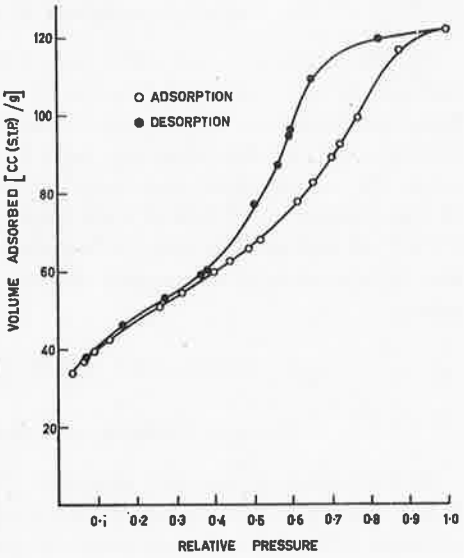

FIGURE 1.—Liquid nitrogen adsorption–desorption isotherm for Ca^{2+} Willalooka illite cores.

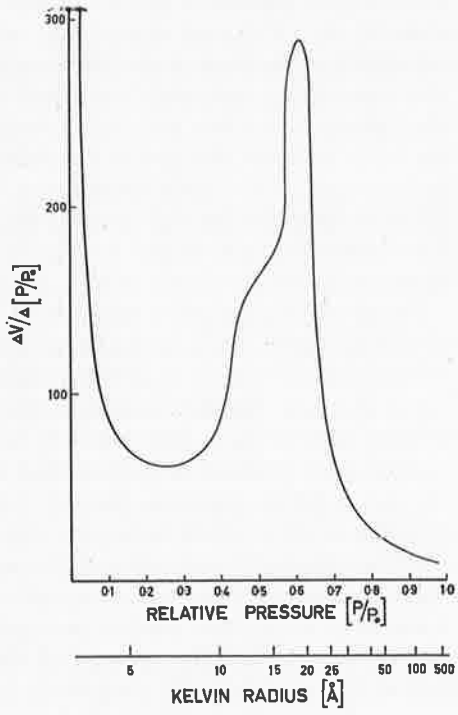

FIGURE 2.—Pore size distribution of Ca^{2+} Willalooka illite cores obtained by differentiating the nitrogen desorption isotherm.

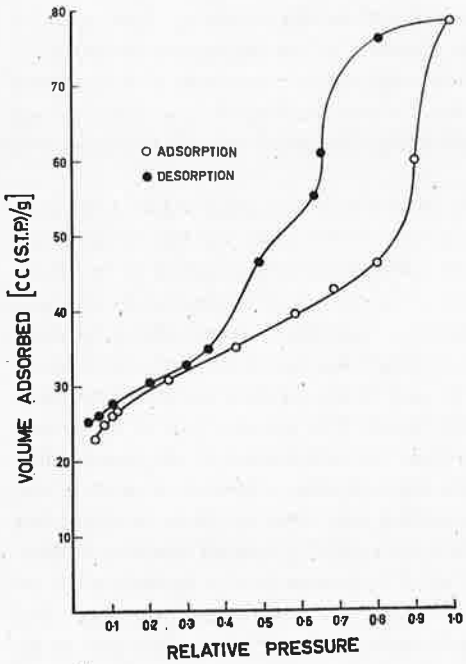

FIGURE 3.—Liquid nitrogen adsorption–desorption isotherm for Ca^{2+} Redhill montmorillonite cores.

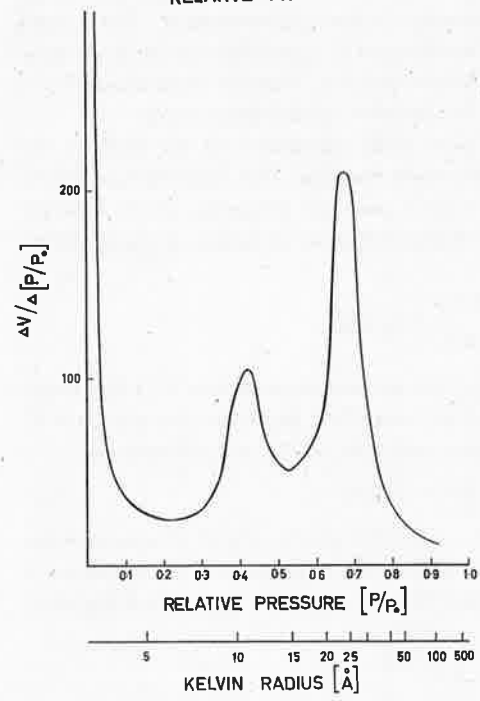

FIGURE 4.—Pore size distribution of Ca^{2+} Redhill montmorillonite cores obtained by differentiating the nitrogen desorption isotherm.

at 10^{-5} mm mercury pressure, gave support to this concept. Low relative pressure hysteresis was not, however, evident in the isotherms obtained by Brooks for native (Na^+) Wyoming bentonite and in this case he considered that the intracrystalline spacing (2.80 Å corresponding to one water layer) was too small to allow nitrogen penetration (diameter of nitrogen molecule = 4.2 Å).

McDermot and Arnell (1955, 1956) in studying the properties of brominated graphites where the situation is not unlike that for the montmorillonites with both intercrystalline and intracrystalline sorption of bromine, have also demonstrated the existence of two types of hysteresis in nitrogen isotherms for these structures with an expanding c-axis. These workers believed the broad hysteresis loop extending from saturation down to relative pressures of approximately 0.45 to be due to the porous nature of the graphite and designated it as "pore" hysteresis. The second type of hysteresis which they termed "swelling" hysteresis was attributed to the availability of volume within the swollen graphite crystals after removal of most of the bromine. The term intercrystalline swelling was used by these workers but the phenomenon as described is probably more aptly termed intracrystalline.

The persistence of this latter type of hysteresis in the present work on Ca^{2+} Redhill montmorillonite after the stronger outgassing procedure and its presence for the illite cores seems to indicate its origin in this case as an intercrystalline rather than an intracrystalline phenomenon. This could arise if there were any appreciable stacking of the platelike crystals of these minerals in the drying or consolidation process. Similar conditions for a structural instability as envisaged by Brooks would then occur.

The interpretation of equivalent pore radii calculated on the basis of the Kelvin equation must be made with some caution. The conventional form of the Kelvin equation relates the vapor pressure lowering above a hemispherical meniscus to the curvature of the meniscus or radius of the cylindrical pore containing the meniscus

$$r_c = -\frac{2V\gamma}{RT}\log_e p/p_0,$$

where p is the desorption pressure, p_0 the saturated pressure, V is the molar volume and γ the surface tension of the adsorbed liquid at temperature T, r_c is the radius of the cylindrical pore and the radius of curvature is

$$(1/r_c + 1/r_c) = 2/r_c.$$

For a meniscus which occurs between parallel plates whose dimensions are large compared with the distance of separation, the radius of curvature is given by $(1/r_p + 1/\infty)$ where r is half the distance of separation between plates. Thus

$$r_p = -\frac{V\gamma}{RT}\log_e\frac{p}{p_0}.$$

so that

$$r_c = 2r_p.$$

Hence the conventional Kelvin radius (hemispherical meniscus) which is given in Figs. 1 and 2 can be better regarded as estimates of the average crystal separations at least for those pores that are small in comparison with plate dimensions (say < 100 Å). If Foster's suggestion (1932) is correct this estimate should be increased by twice the thickness of an adsorbed monolayer (approx. 8 Å).

The volume of liquid nitrogen retained at any particular value of relative pressure is related to the particle size and specific surface area as is to be expected. However, almost the entire porosity of the Willalooka cores is accommodated in pores having equivalent cylindrical radii less than 33 Å. From the differential plot it can be seen that the peak of the pore size distribution for this clay occurs at a relative pressure of approximately 0.625 corresponding to an equivalent cylindrical pore radius of 20 Å. Since the crystal plates of this clay are probably of the order of 700 Å across the cleavage face, this equivalent cylindrical radius may be interpreted, on the addition of twice the monolayer thickness, as a separation between crystal sheets of the order of 28 Å. If the oven-dry porosity of the clay is divided by the specific surface area the average half distance between crystals so calculated is 13 Å. It may be inferred, therefore, that the matrix of the Willalooka cores consists of the clay plates highly organized on a microscale into packets or domains with very few large pores between domains. It is difficult to visualize such a relatively narrow band of pore sizes arising in any other fashion than this for plate-shaped particles, although the reason for crystals remaining at such high separations in the dry state is not clear. The presence of surface irregularities on the clay crystals may be envisaged as holding the majority of the surface at appreciable separations. Alternatively the separations may be considered to arise from mutual repulsion of the surface charge distributions. In this regard the approach of one plate to another in the dry state could possibly provide a net repulsive force such as may result from the approach of a positive charge (surface cation) to a dipole considered as arising from the separation of the exchangeable cation on the adjacent sheet from the site of isomorphous replacement by the layer of oxygen atoms.

It may be argued, of course, that the crystal sheets may be very much closer within domains with a large volume of interdomainal pores of the order of 28 Å, but unless a large proportion of the surface area is not available to nitrogen adsorption this would necessitate the presence of a considerable volume of much larger pores between domains to provide the same total porosity. Isotherms for the adsorption of polar water molecules indicate that essentially the total surface of the illites is available to nitrogen adsorption.

The peak in the pore size distribution for Willalooka illite (Fig. 2) shows a shoulder corresponding to plate separations of approximately 20 Å. On the other hand the pore size distribution for Redhill montmorillonite exhibits two separate peaks corresponding to plate separations of approximately 20 Å and 32 Å, respectively. For Wyoming bentonite these same peaks were in evidence and corresponded to plate separations of approximately 20 Å and 85 Å, respectively. The second peaks may be inter-

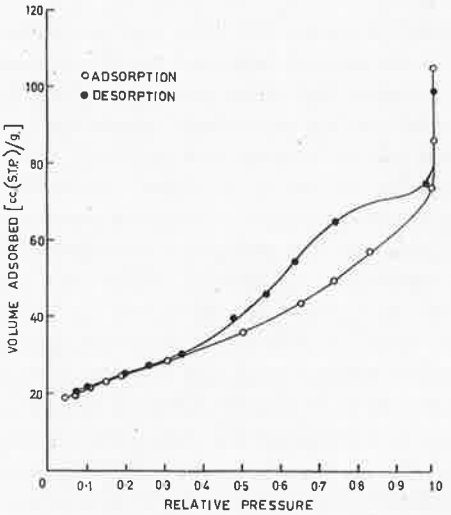

FIGURE 5. – Liquid nitrogen adsorption–desorption isotherm for Ca^{2+} Urrbrae B cores.

preted as arising from larger intradomainal spacings for the montmorillonites than for the illites resulting from the contraction of the montmorillonite crystals after the formation of the clay matrix structure during the drying process. The increased separation for Wyoming bentonite probably arises from the larger number of lamellae per crystal. The first peak on each curve (indicating plate separations of approximately 20 Å in each case) may then correspond either to the areas of closest possible approach of the clay crystals in a fixed structure, as suggested for Willalooka illite, in which case some mechanical hindrance or repulsive force is implied, or else to a reshuffling of the clay crystals by surface tension forces as envisaged by Barrer and MacLeod (1954).

The comparison of the nitrogen sorption isotherms of the manufactured cores and natural aggregates of the Urrbrae loam, B horizon, shown in Figs. 5 and 6 is particularly interesting. Both isotherms are similar to that obtained for the Willalooka illite indicating a high degree of domain structure formation. Below an equivalent cylindrical pore size of 20 Å (0.625 relative vapor pressure) there are no significant differences between the cores and

natural aggregates. This may be interpreted as indicating that the intra-domain pore space is not affected to any appreciable extent by the compression process. The volume of pores between 100 Å and 200 Å is significantly reduced for the cores indicating that domains have been brought into closer packing. Quirk and Panabokke (in press) have studied the pore size distribution for pores greater than 100 Å in some detail and all these pores are eliminated by compression.

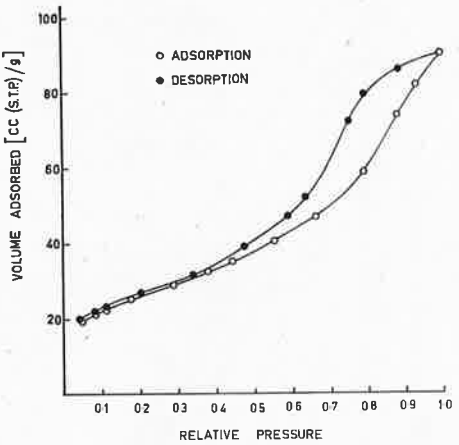

FIGURE 6.—Liquid nitrogen adsorption–desorption isotherm for Urrbrae B, natural aggregates.

An electron micrograph of the fracture surface of a Willalooka illite core obtained using a polyethylene replica technique is shown in Plate 1. The parallel alignment of the plate-shaped particles into an oriented group can be distinguished as the striated area of alternate light and dark strips. The size of the domain area for Willalooka illite (approximately 10 μ long) in comparison to the crystal size for this clay seems to indicate that a domain structure may consist not only of crystal sheets oriented and stacked but also interleaved across a considerable distance. The change in orientation of some of the particles can be clearly seen near the edge of this area.

Physical Swelling of Montmorillonite

(*a*) Ca^{2+} *montmorillonite.*—The effect of previous history on the water content of Ca^{2+} Redhill montmorillonite cores and suspensions is shown in Fig. 7. One feature is the marked hysteresis between the wetting and drying curves for the cores. This hysteresis is clearly dependent on the final wetting point since on drying to pF 3 from a suction of 1 cm the clay retains more water than on drying from 10 cm suction. The hyster-

esis is even more marked where the clay has been dried from a suspension or where it has been saturated with Na^+ and then again saturated with Ca^{2+}. The apparently more open gel network and hence the larger volume of enmeshed water (*i.e.* water held by capillary

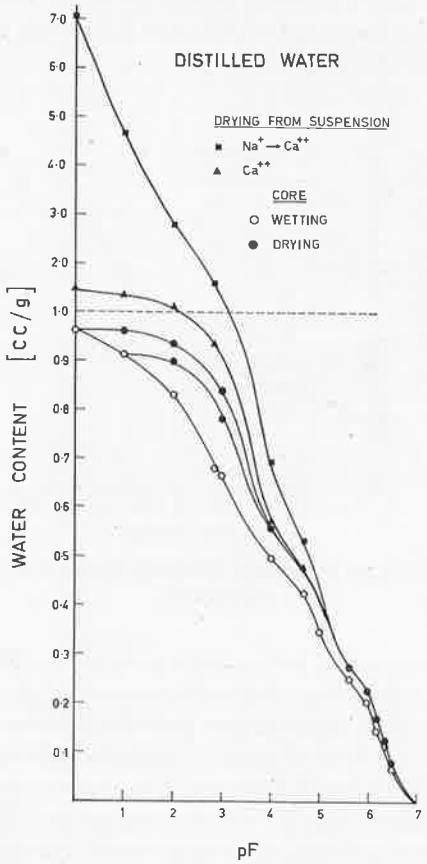

FIGURE 7.—Effect of previous history and hydrostatic suction on the water content of Ca^{2+} Redhill montmorillonite.

forces; see section on enmeshed water in the discussion) in the latter case may be considered to arise from the presence of a larger number of particles due either to the disruption of domains with the crystals retaining their entity or alternatively to the breakup of the crystals themselves whether by dispersion to the elementary silicate sheet level when Na^+ saturated or by a less complete crystal degradation. The identical surface areas obtained for the Ca^{2+} and $Na^+ \rightarrow Ca^{2+}$ montmorillonites (38 m^2/g for Wyoming bentonite and 100 m^2/g for Redhill mont-

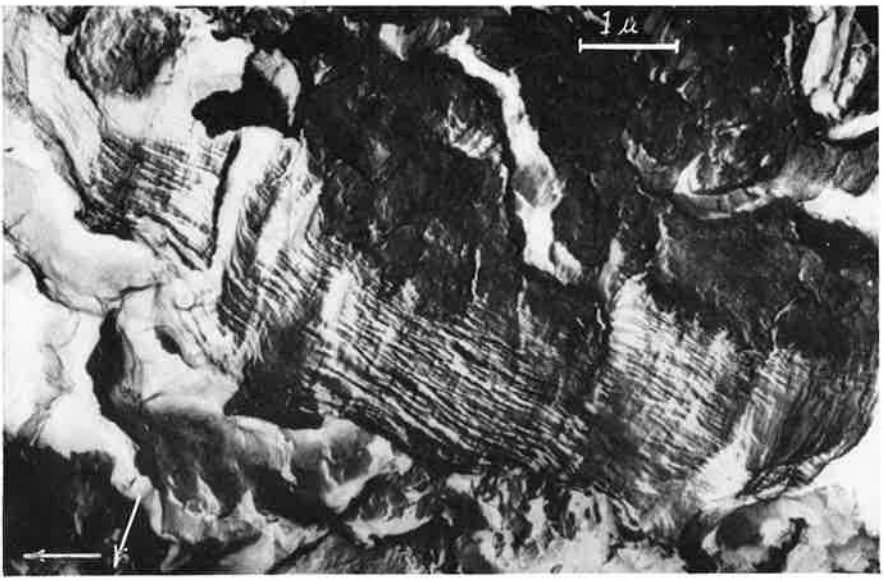

PLATE 1.—A electron micrograph of a replica of the fracture surface of a clay core of Willalooka illite. The arrows show the direction of shadowing. The interleaved and parallel arrangement of the clay crystals can be seen to extend over a considerable distance indicating that a domain is considerably more complex than the simple model.

morillonite) seem to indicate that the crystals either retain their entity throughout the treatment or else result from a statistical re-formation process which for a given type of elementary sheet tends to give the same external surface area when condensation takes place.

Despite the great differences in water content at low suctions, all the drying curves are essentially coincident at pF 5.6 (0.75 relative vapor pressure at 20 °C), the point at which normal shrinkage, as obtained from volume measurements on the cores, ceases. Air entry at this point corresponds to a Kelvin cylindrical radius of <50 Å and since the dry cores have an appreciable volume of pores with equivalent cylindrical radii of several hundred Ångströms it may be concluded that considerable internal accommodation of swelling producing an effective reduction in pore dimensions has occurred. Note that the total volume of liquid nitrogen retained by the Ca^{2+} montmorillonite cores (0.068 cm^3/g and 0.120 cm^3/g for Wyoming bentonite and Redhill montmorillonite respectively) at 0.9 relative vapor pressure (90 Å equivalent Kelvin radius) is appreciably less than the oven-dry porosities of the cores (0.135 cm^3/g and 0.150 cm^3/g, respectively).

At 0.75 relative vapor pressure the intracrystalline spacing is 15.4 Å (Mooney, Keenan and Wood, 1952) and the volume of water (0.258 cm^3/g, assumed density equal to unity) corresponding to two layers of intracrystalline water plus two layers on the external surface of the crystals is only slightly less than the total volume of voids (0.265 cm^3/g) obtained from volume measurements on the Redhill cores.

The results in Table 2 calculated by dividing the water contents given in Fig. 7 by the external surface area after correcting for intracrystalline water [$d(001) = 19$ Å] indicate a film thickness of 19 Å at a suction of 10 atm, and this is considerably more than the predicted value on the basis of the Gouy–Chapman model which would hardly be expected to apply at this point. However, at pF 1 the film thickness of 59 Å is a good deal lower than the theoretical expectation of 200 Å. This film thickness of 59 Å would be an overestimate since the large hysteresis indicates that a considerable

TABLE 2.—EFFECT OF INCREASED SUCTION ON THE FILM THICKNESS FOR Ca^{2+} MONTMORILLONITE CORES WET WITH DISTILLED WATER

pF	Water Content (cm^3/g)	Corrected for Intracrystalline Water — $d(001) = 19$ Å (cm^3/g)	Film thickness (Å) Calculated	Theoretical [1]
1	0.92	61	60	200
2	0.83	52	51	72
3	0.57	26	25	24
4	0.50	19	19	8

[1] 10^{-4}M $CaCl_2$.

amount of the water, held in the clay structure, may not be associated directly with the clay surfaces.

The Gouy–Chapman theory as developed by Schofield relates film thickness on a charged surface to the electrolyte concentration of the solution external to the double layer of the charged surface and the hydrostatic

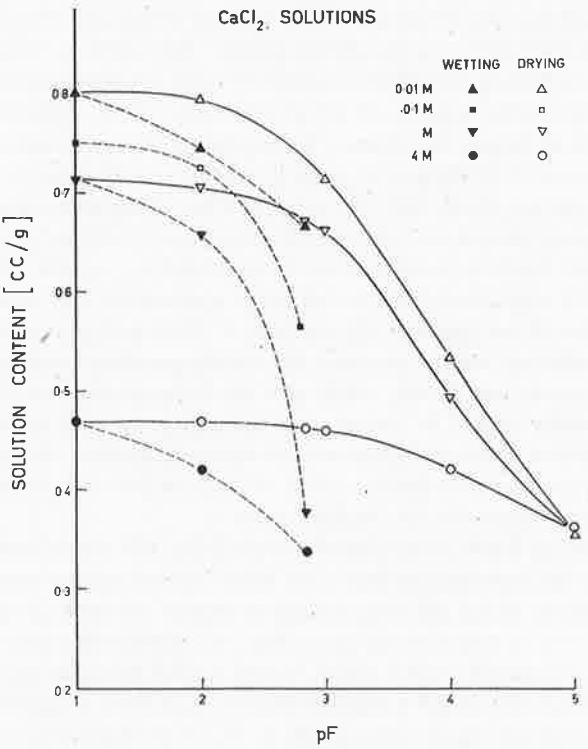

FIGURE 8.—Effect of hydrostatic suction and calcium chloride concentration on the solution content of Ca^{2+} Redhill montmorillonite cores.

suction imposed on the liquid. The results in Fig. 8 show adsorption and desorption isotherm for the montmorillonite cores over the electrolyte concentration range 4 M $CaCl_2$ to 0.01 M $CaCl_2$. All curves show a marked hysteresis and this hysteresis is particularly noticeable at pF 2.8 when the clay contains M $CaCl_2$.

The change in the solution content from 0.72 cm^3/g in molar to 0.80 cm^3/g in 0.01 M does not seem large enough to indicate the presence of diffuse double layers in the system; however, it may be suggested that the particles within a domain do not show appreciable swelling owing to the presence of a potential barrier and that diffuse double layers exist between adjacent

domains. The relatively small amount of swelling (solution content increase from 0.72 to 0.92 cm^3/g) which takes place between molar and distilled water (10^{-4} M) may possibly be attributed to diffuse double layers forming on the external surface of the domains since their surface area would be very much less than the external surface area of the crystals which is 102 m^2/g. At pF 1 the swelling in molar is very much greater than in 4 M although the external surface film thickness calculated for 4 M (basal spacing of 15.4) is 23 Å. This large change in solution content between 4 M and molar would be associated with the swelling of the whole surface including that within domains.

The film thickness calculated on wetting to pF 2.8 with 4 M $CaCl_2$ is 13 Å and this increases to about 23 Å at pF 1. These considerable values for this concentration cannot be regarded as the true film thickness development but probably arise from the relaxation of strains imposed on clay crystals and domains as the result of drying. On wetting, when sufficient liquid is present in the system relaxation may take place creating a gel structure. It should be remembered that as saturation exists for these cores and that the initial pore space has been invaded by intracrystalline swelling.

(*b*) Na^+ *montmorillonite.*—The results of the effect of electrolyte concentration on the swelling of Na^+ montmorillonite (Fig. 9) contrast with those

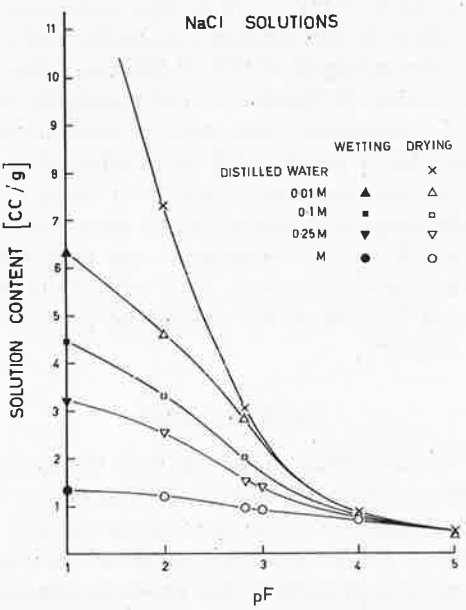

FIGURE 9.—Effect of hydrostatic suction and sodium chloride concentration on the solution content of Na^+ Redhill montmorillonite cores.

for Ca^{2+} montmorillonite. Here solution contents of several hundred percent are obtained at pF 1 for dilute solutions and it seems apparent that diffuse double layers are forming.

The film thickness values in Table 3 were calculated by dividing the solution content by the total surface area of 760 m^2/g except for molar

TABLE 3.—FILM THICKNESS FOR Na^+ REDHILL MONTMORILLONITE

M	Solution Content (cm^3/g)	Film Thickness		
		Calculated from Water Content	X-ray[2]	Theoretical
1.0	1.33	102[1]	4.5	19
0.25	3.20	42	16	33
0.10	4.45	59	25	48
0.01	6.80	83	63	114
0.0001	22.50	295	570[3]	400

[1] External surface area used and a correction applied for intracrystalline water.
[2] Norrish (1954).
[3] Obtained by extrapolation of the X-ray results.

NaCl where the external surface area of the clay was used after correcting for intracrystalline water $d(001) = 19$ Å. The high value obtained by this procedure for the external film thickness in molar NaCl as compared with that obtained at a concentration of 0.25 M NaCl and also as compared with the X-ray measurements of Norrish (1954) highlights the fact that even for the swelling of compressed cores there is considerable reorganization of the structure so that a considerable proportion of the water simply is enmeshed within the gel structure rather than being associated with the clay particles in the form of a diffuse double layer. Owing to the presence of this gel structure it is only possible to say that diffuse double layer theory is obeyed in a qualitative way. It is not possible to decide whether the measurements of Norrish or the theoretical predictions by Schofield's method are more apposite.

Swelling of Illite

(*a*) Ca^{2+} *illite.*—It has been suggested that Willalooka illite possesses a highly organized structure with crystals oriented on a microscale into domains and that almost the entire porosity in the dry state arises from average separations of about 28 Å between these oriented crystals. If this is so, the domain system in an illite has much in common with the montmorillonite crystal and provides an ideal situation for the operation of electrostatic attractions as suggested by MacEwan (1948) with the ex-

changeable cations lying between the negatively charged clay plates. In these circumstances the volume of solution not directly associated with crystal surfaces would be less significant and a more reliable estimate of the film thickness developed on the clay surfaces should be obtained by dividing the solution content by the specific surface area. The effect of

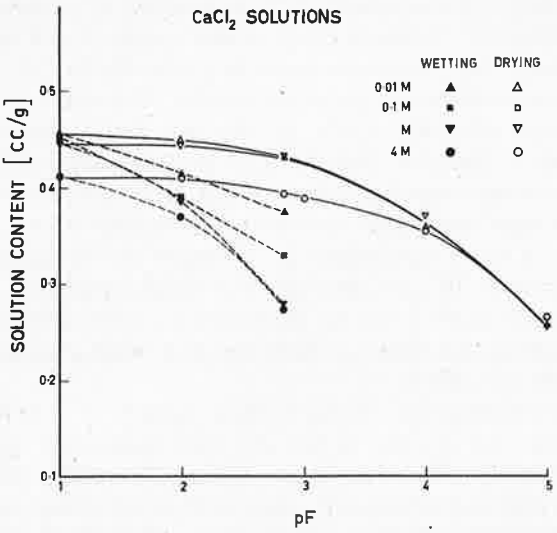

FIGURE 10.—Effect of hydrostatic suction and calcium chloride concentration on the solution content of Ca^{2+} Willalooka illite cores.

TABLE 4.—CALCULATED FILM THICKNESS (Å) FOR Ca^{2+} WILLALOOKA ILLITE FOR DIFFERENT SUCTIONS AND ELECTROLYTE CONCENTRATIONS

Suction	Molar Concentration of $CaCl_2$				
pF	4.0	1.0	0.1	0.01	0.0001
1	27	30	30	30	30
2.8	18	18	22	25	25
4.0	—	—	—	—	20
4.7	—	—	—	—	18

electrolyte concentration on the swelling of the Ca^{2+} Willalooka illite cores is shown in Fig. 10. It is immediately obvious that variations in calcium chloride concentration between distilled water (10^{-4} M) and molar have little if any effect on the solution uptake by this clay at pF1.

From Table 4 it can be seen that the film thickness calculated as above at pF1 is essentially constant at 30 Å for all electrolyte concentrations between 4 M and distilled water. This is reminiscent of Ca^{2+} montmorillonite which has a basal spacing of 19 Å for all calcium chloride concen-

trations less than molar. Thirty Ångströms, whilst considerably larger than the 10 Å or thereabouts expected for a molar solution, is considerably less than 200 Å predicted by diffuse double layer development in distilled water (say 10^{-4}M). It seems reasonable to conclude that diffuse double layer concepts cannot be used to describe the swelling of this Ca^{2+} clay system even though the silicate sheets appear to be separated by a distance of 60 Å. As a potential barrier obviously exists in this system it still may be argued that diffuse double layer concepts could be applicable to Ca^{2+} clay particles which had moved across this potential barrier as a result of dispersion or mechanical work or could apply to the interaction between adjacent domains. There is, however, little indication of any such effects.

The nature of the potential barrier is not clear. MacEwan (1948, 1954) has suggested that coulombic attractive forces exist up to plate separations of 30 Å, at which separations he envisaged the formation of separate diffuse double layers by each particle. The results discussed here indicate a plate separation of 60 Å but no allowance has been made for enmeshed water in obtaining this figure so that the true plate separation could be appreciably less than 60 Å.

The electron micrograph of the fracture surface of a Willalooka illite core shows that clay crystals in the dry clay matrix are subject to considerable distortion (Plate 1). Hence Terzaghi's (1927) idea of crystal bending on drying and subsequent relaxation on rewetting could be operative in increasing the solution uptake above that which would occur if only surface film development took place, as within a montmorillonite crystal. This relaxation may account for the large hysteresis at pF 2.8 in Fig. 10. With the reduction in electrostatic attractive forces as envisaged by MacEwan at separation of about 40 Å the elastic properties of the clay crystals may be sufficient to overcome the effective potential barrier and initiate the formation of gel structures. Once the structure has undergone this relaxation of mechanical strain the increase in suction necessary to cause recompression of the structure, appears to be comparatively independent of the concentration of electrolyte present (Quirk and Aylmore, 1960).

To exclude the possibility that the restricted swelling of the Ca^{2+} Willalooka illite was due to cementing materials, samples of the Na^{+}-saturated clay, which is subsequently shown to exhibit large swelling and considerable response to change in electrolyte concentration, were resaturated with Ca^{2+}. The behavior of this Ca^{2+} clay was identical with that of the material which had been directly Ca^{2+} saturated. One interesting feature was that the $Na^{+} \rightarrow Ca^{2+}$ illite suspension when dried at pF 1 in the presence of molar $CaCl_2$ retained 2.67 cm^3/g of solution whereas the Ca^{2+} illite suspension retained 1.79 cm^3/g. This difference is attributed to domain breakdown in the preparation of the Na^{+} clay. The domains evidently re-formed on drying.

(*b*) Na^+ *illite.*—The effects of concentration of sodium chloride solution on the drying curves of Willalooka illite after wetting to p*F* 1 are shown in Fig. 11. There is a continuous rapid reduction in swelling with increasing sodium chloride concentration as would be expected from diffuse double layer considerations. At p*F* 1 the solution uptake is reduced from 8.41 cm^3/g for distilled water to 0.482 cm^3/g for normal sodium chloride solution. This latter water content is only slightly greater than that for Ca^{2+} Willalooka illite in distilled water, indicating that for molar NaCl the potential barrier

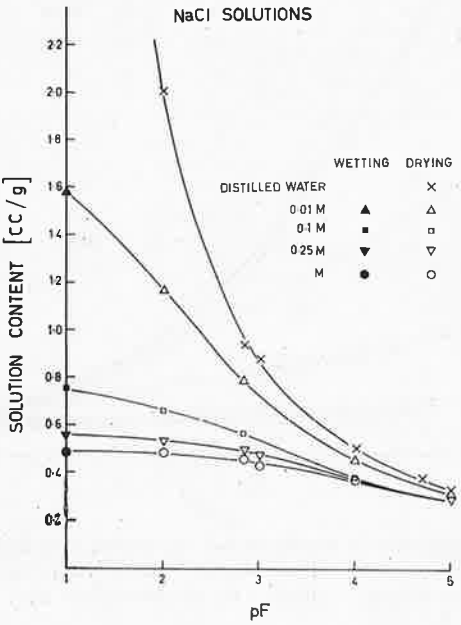

FIGURE 11.—Effect of hydrostatic suction and sodium chloride concentration on the solution content of Na^+ Willalooka illite cores.

has not been exceeded. The same is true for the 0.25 M solution where the film thickness calculated as before is 37 Å. In 0.1 M NaCl there is a considerable increase to 50 Å and in 0.01 M the calculated film thickness is 106 Å. These large film thicknesses for Na^+ Willalooka in dilute salt solutions suggest the possibility of the formation of a diffuse double layer once the potential barrier has been exceeded. When the film thicknesses obtained by dividing the solution content in Fig. 11 by the specific surface area are compared with the theoretical diffuse double layer value (Fig. 12) it can be seen that the agreement for low suctions is good over the range 10^{-1} to 10^{-4} M NaCl. However, no allowance has been made for water that is simply enmeshed in the structure. Even though this would be at a mini-

mum for Willalooka illite because of its highly organized structure, this correction probably would bring the calculated film thickness in 10^{-2} and 10^{-1} M NaCl closer to those calculated for Na^+-montmorillonite from the X-ray results of Norrish (1954). At these respective concentrations film

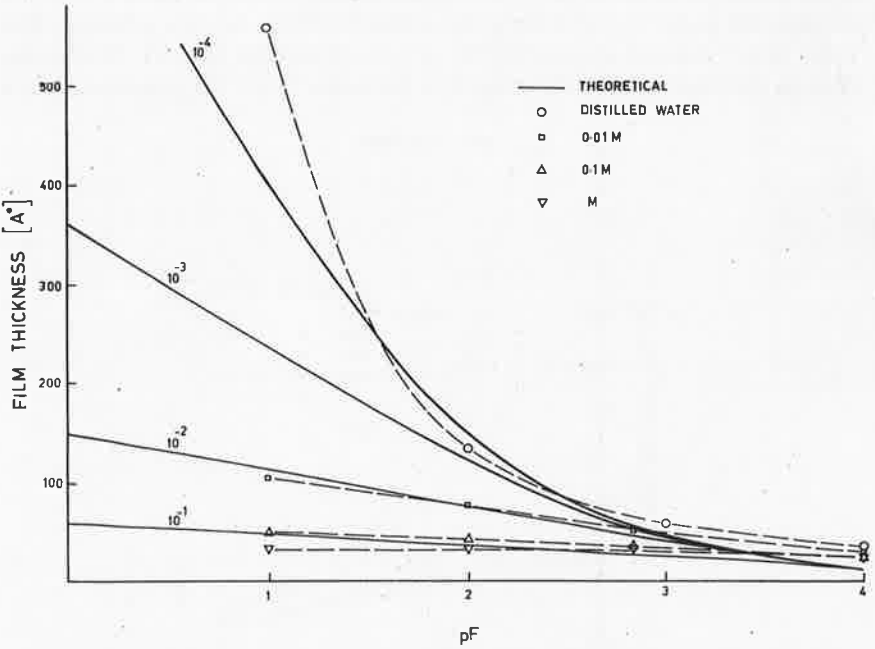

FIGURE 12.—A comparison of calculated and theoretical film thicknesses for Na^+ Willalooka illite cores. The calculated film thicknesses were obtained by dividing the solution content by the specific surface area.

thicknesses of 62 and 23 Å are found for oriented flakes of Na^+-montmorillonite in free solution.

Cores, of the Urrbrae, B horizon, clay show very restricted swelling for divalent ion and high electrolyte concentration monovalent ion systems and large swelling in dilute monovalent ion systems similar to that observed for the Willalooka illite, indicating that domain structure effects are also very apparent for this clay. This contrast in behavior between the Na^+ and Ca^{2+} illite is very similar to the contrast in behavior between Na^+ and Ca^{2+} montmorillonite and reinforces the suggestion that a domain of illite crystals is similar to a montmorillonite crystal since both, when Ca^{2+} saturated, show limited swelling because of the existence of a potential barrier. In this regard a montmorillonite crystal may possibly be regarded as a particular type of domain with the single lamellae constituting the basic units instead of entire crystals as in an illite domain.

The potential barrier limiting the swelling between Ca^{2+} illite crystals would appear to be clearly different from that which limits the crystalline swelling of Ca^{2+} montmorillonite since much greater distances of separation are involved. Furthermore if illite crystals approached within 5 Å of one another as montmorillonite or vermiculite lamellae do on drying, limited swelling would be expected since the surface density of charge of the illite crystals (2.7×10^{-7} meq/cm^2) is considerably greater than vermiculite (approx. 2×10^{-7} meq/cm^2) which gives a maximum lamellae separation of about 5 Å when saturated with sodium or calcium. This potential barrier is overcome by Li^+-vermiculite. However, an alternative explanation of the restricted swelling of the Willalooka illite when Ca^{2+} saturated and in high electrolyte concentration monovalent solutions could be the existence of vermiculite-like bonding at very small areas of closest approach of crystals within domains. Hence the swelling that occurs in these cases may result largely from interdomainal interactions.

GENERAL DISCUSSION

(*a*) *Enmeshed Water*

If the swelling and shrinkage of clay systems were entirely due to the development and contraction of diffuse double layers, the systems would be expected to exhibit little hysteresis. The existence of potential barriers as observed by Norrish (1954) could contribute to hysteresis effects. However, the nature of the irreversible hysteresis observed in the saturated state seems to indicate that structural alterations due to particle readjustment are of major importance in determining this hysteresis (Schofield, 1935). It therefore seems reasonable to suggest that while some of the water is directly associated with the surfaces of the clay particles, some is retained by surface tension forces within a gel structure arising from mechanical interactions of the clay particles. The chief experimental difficulty in trying to test the applicability of diffuse double layer theory, as adapted by Schofield (1946), to the swelling of clay systems is to separate the relative contributions of the two mechanisms to the total water content.

The retention of water within the gel structure can be regarded in the following way. When a rigid porous material, initially filled with liquid, dries out under falling vapor pressures, pores (capillaries) of particular dimensions will empty at particular vapor pressures. The remaining liquid is held under a hydrostatic suction which is transmitted to the walls, but, as each pore empties, the stresses on the walls due to this cause will fall to zero. If, however, the material is easily deformed, the increase in the suction in the liquid will cause a reduction in the size of the pore, and evaporation will be delayed until a lower vapor pressure is reached, by which time the suction has further increased. This mechanism is clearly distinct from

the loss of water from double layers as the result of reducing the vapor pressure or increasing the applied hydrostatic suction. Barkas (1948) has discussed the shrinkage of wood gels in these terms.

Before considering the consequences of this model it is necessary to consider how the gel structure can arise for a compressed clay core or natural clay structure. The electron micrograph (Plate 1) of Willalooka illite shows a region of oriented particles and it is immediately obvious that this region is of considerable extent and conforms in a general way to the idea of the parallel alignment of particles. It can be noticed, however, that this arrangement is far from simple since there is considerable interleaving and bending of the individual crystals. Aylmore and Quirk (1959) have described such a region as a domain. Because the term "domain" could also be taken to mean micro-aggregate the terminology used by coal research workers may be more meaningful. Biscoe and Warren (1942) use the term turbostratic groups to convey the idea that the groups contain particles in a parallel or stratified arrangement and also that the groups with respect to one another are in turbulent array. The above interpretation of the electron micrograph for Willalooka is supported by the peak which occurs in the pore size distribution indicating plate separations between 10 and 30 Å (Fig. 2).

The gel structure appears to form at high suctions (approx. 10–50 atm) and in the presence of strong salt solutions. This would suggest that it is initiated by a mechanical rather than a physico-chemical mechanism although the degree of gel structure development is related to the electrolyte concentration. Terzaghi's (1927) idea of crystal bending on drying and subsequent relaxation on rewetting is probably operative in the formation of this structure. The gel structure development probably is dependent to a certain extent on the removal or decrease in attractive forces rather than an increase in repulsive forces between adjacent clay crystals. It has been suggested that in the presence of sufficient liquid, strains due to crystal bending will tend to relax. However, when the solution between the charged surfaces is 4 M $CaCl_2$ the ion distribution would be such that one ion would be only 5 Å from its neighbor and the water in this region would be largely in the state of dielectric saturation. As the concentration of ions is decreased the attractive force would be lessened since this proportion of water showing dielectric saturation in the vicinity of the clay particles would decrease. This suggestion could explain the larger relaxation in molar NaCl than in molar $CaCl_2$, but of course it would not explain the increase in solution content at pF1 from 0.80 to 0.92 cm^3/g for Redhill montmorillonite when 0.01 $CaCl_2$ and distilled water are used as the wetting liquid. It is interesting to note that Redhill montmorillonite has a much greater tendency to form a gel structure than Willalooka illite, indicating a more extensive or stronger domain structure for the latter material.

(b) *Turbostatic Groups or Domains*

The existence of turbostatic groups or domains and the formation of gel structures are extremely important with respect to the interpretation of the film thickness developed by clay particles and the cause of hysteresis in a two-phase system such as clay and water.

Condensation into domains (Aylmore and Quirk, 1959) is not readily reversible so that each point on the virgin consolidation curve has a different basic pore (capillary) volume; this leads to the series of reversible hysteresis loops since the pores which have not collapsed at a given terminal pressure will continue to function as pores. These remaining pores, however, will show some contraction and expansion and this would not be expected to be completely reversible and hence provides a probable explanation of hysteresis in two-phase systems at relatively low suctions (<5 atm). The series of hysteresis loops enables the same water content (voids ratio) to be obtained with quite different structural arrangements within the clay mass and must of necessity result in appreciable differences in the strength of the soil structure depending on the ratio of the water held in pores to that held within the domains.

The swelling of these domain units for divalent ion systems and also for monovalent ion systems at high electrolyte concentration is controlled by a potential barrier and, since the plates at full swelling are separated by less than 60 Å of water, it seems reasonable to attribute the potential barrier to coulombic attractive forces as discussed by MacEwan (1948, 1954), or to the presence of positive charges on the clay crystals.

The strength of clay materials is clearly dependent on the degree of development and the strength of domain particles since in many circumstances these particles rather than the individual clay crystals are functional.

(c) *Applicability of Diffuse Double Layer Concepts*

Much consideration has been given by many workers to the applicability of diffuse double layer formation to the swelling of clay–water systems. However, it should be remembered that such theories deal exclusively with repulsions and the film thicknesses predicted take no account of possible attractive forces arising from the presence of an opposing surface. MacEwan (1948, 1954) has suggested that electrostatic attractive forces will extend to at least 30 Å. From Norrish's results for the intercrystalline swelling of montmorillonite it appears that these electrostatic attractions extend to separations in excess of 100 Å. Consequently, although diffuse double layer repulsions may exist, the magnitude of the spacings developed may be appreciably lower than those predicted by this theory.

For the monovalent systems it seems likely that once the potential barrier within a domain has been overcome, the development of diffuse

layers as envisaged by the Gouy–Chapman theory plays a significant part in determining the solution uptake. Its applicability in a qualitative way is indicated by the marked effect of electrolyte concentration on the solution content of the sodium cores on wetting from the dry state (Figs. 9 and 11). This sensitivity to electrolyte concentration is far less evident on drying from the suspension state, as shown by the large solution contents retained in molar chloride solution (Quirk and Aylmore, 1960). This seems to indicate that although diffuse double layers are present, their collapse with increasing electrolyte concentration takes place within the gel structure formed and hence does not give rise to an equivalent shrinkage. As diffuse double layer theory in a general way implies an equivalence between mechanical and osmotic components of the free energy, the existence of these gel structures is strongly supported by the sensitivity of the gels to increased mechanical pressure which induces particle rearrangement.

For divalent systems, however, the magnitude of the film thickness developed on wetting from the dry state, and its insensitivity to variations in electrolyte concentrations less than molar, lead to the conclusion that swelling resulting from the formation of diffuse double layers does not become significantly operative in these circumstances. This is presumably because the strong electrostatic attractions prevent the expansion of the domain over the potential barrier. Where surfaces are not directly opposed it is possible that diffuse double layers do form, but such formation appears to be of little significance in regard to divalent clay swelling. It might be argued that the lack of sensitivity to electrolyte concentration at the much higher solution contents obtained on drying from the suspension state could be attributed to the accommodation of diffuse double layers within the gel structure as for the sodium clays. However, there is at present no evidence to substantiate this suggestion and the low values reported for chloride exclusion by calcium systems (Quirk, 1957) indicate that diffuse double layer formation seems unlikely. Further experiments are necessary to establish this point but it is clear that the diffuse double layer theory cannot be used to describe the swelling of calcium clay systems.

ACKNOWLEDGMENT

We are indebted to Mr. D. M. Hall of the D.S.I.R. Dominion Physical Laboratory for obtaining the electron micrograph presented in Plate 1 and other electron micrographs. We also wish to thank Dr. K. Norrish of the C.S.I.R.O. Division of Soils for the X-ray spectrographic determination of strontium and bromide.

REFERENCES

Aylmore, L. A. G. and Quirk, J. P. (1959) Swelling of clay–water systems: *Nature*, v. 183, pp. 1752–1753.

Barkas, W. W. (1948) *The Swelling of Wood under Stress*: H.M. Stationery Office, London.

Barrer, R. M. and MacLeod, D. M. (1954) Intercalation and sorption by montmorillonite: *Trans. Faraday Soc.*, v. 50, pp. 980–989.

Biscoe, J. and Warren, B. E. (1942) An X-ray study of carbon black: *J. Appl. Phys.*, v. 13, pp. 364–371.

Bolt, G. H. (1956) Physico-chemical analysis of the compressibility of pure clays: *Geotechnique*, v. 6, pp. 86–93.

Bolt, G. H. and Miller, R. D. (1955) Compression studies of illite suspensions: *Soil. Sci. Soc. Amer. Proc.*, v. 19, pp. 285–288.

Brooks, C. S. (1955) Nitrogen adsorption experiments on several clay minerals: *Soil Sci.*, v. 79, pp. 331–347.

Croney, D. and Coleman, J. D. (1954) Soil structure in relation to soil suction (p*F*): *J. Soil Sci.*, v. 5, pp. 75–84.

Emmett, P. H. and Brunauer, S. (1934) The adsorption of nitrogen by iron synthetic ammonia catalysts: *J. Amer. Chem. Soc.*, v. 56, pp. 35–41.

Foster, A. C. (1932) The sorption of condensible vapours by porous solids. Part 1, The applicability of the capillary theory: *Trans. Faraday Soc.*, v. 28, pp. 645–657.

Harkins, W. D. and Jura, G. (1944) Surface of solids. Extension of the attractive energy of a solid into an adjacent liquid or film, the decrease of energy with distance and the thickness of the films: *J. Amer. Chem. Soc.*, v. 66, pp. 919–927.

Hofmann, U. and Bilke, W. (1936) Über die innerkristalline Quellung und das Basenaustauschvermögen des Montmorillonits: *Kolloid-Z.*, v. 77, II, pp. 238–251.

Holmes, J. W. (1955) Water sorption and swelling of clay blocks: *J. Soil Sci.*, v. 6, pp. 200 to 208.

Joyner, L. G. (1949) *Scientific and Industrial Glass Blowing and Laboratory Techniques* (chap. 12, by Barr, W. E. and Anhorn, V. J.): Instruments Publishing Co., Pittsburgh.

Lambe, T. W. (1953) Structure of inorganic soil: *Proc. Amer. Soc. Civil Eng.* 79, paper no. 315.

MacEwan, D. M. C. (1948) Adsorption by montmorillonite and its relation to surface adsorption: *Nature*, v. 162, pp. 935–936.

MacEwan, D. M. C. (1954) Short range electrical forces between charged colloid particles: *Nature*, v. 174, pp. 39–40.

McDermot, H. L. and Arnell, J. C. (1955) The adsorption of nitrogen, oxygen and argon by graphite: *Canad. J. Chem.* v. 33, pp. 913–922.

McDermot, H. L. and Arnell, J. C. (1956) The adsorption of nitrogen by brominated graphite and carbon black: *Canad. J. Chem.*, v. 34, pp. 1114–1126.

Méring, J. (1946) On the hydration of montmorillonite: *Trans. Faraday Soc.*, v. 42B, pp. 205–219.

Mooney, R. W., Keenan, A. C., and Wood, L. A. (1952) Adsorption of water vapor by montmorillonite, II. Effect of exchangeable ions and lattice swelling as measured by X-ray diffraction: *J. Amer. Chem. Soc.*, v. 74, pp. 1371–1374.

Norrish, K. (1954) The swelling of montmorillonite: *Disc. Faraday Soc.*, v. 18, pp. 120–134.

Norrish, K. and Quirk, J. P. (1954) Crystalline swelling of montmorillonite: *Nature*, v. 173, pp. 225–256.

Parry, R. H. G. (1959) Latent interparticle forces in clays: *Nature*, v. 183, pp. 538–539.

Quirk, J. P. (1952) Deflocculation of soil colloids: Ph. D. Thesis, University of London.

Quirk, J. P. (1957) The negative adsorption of chloride ions by clay surfaces: *2nd Aust. Conf. in Soil Sci., Melbourne*, v. I, paper no. 26.

Quirk, J. P. and Aylmore, L. A. G. (1960) Swelling and shrinkage of clay–water systems: *7th Int. Cong. Soil Sci.* In press.

Quirk, J. P. and Panabokke, C. P. (in press) Pore volume-size distribution and swelling of natural soil aggregates: *J. Soil Sci.*

Schofield, R. K. (1935) The p*F* of the water in soil: *Trans. 3rd Int. Cong. Soil Sci.*, v. 2, pp. 37–48.

Schofield, R. K. (1946) Ionic forces in thick films of liquid between charged surfaces: *Trans. Faraday Soc.* v. 42 B, pp. 219–228.

Terzaghi, Karl (1927) Soil classification for foundation purposes: *Trans. 1st Int. Cong. Soil Sci.*, v. 4, pp. 127–157.

Warkentin, B. P., Bolt, G. H. and Miller, R. D. (1957) Swelling pressure of montmorillonite: *Soil Sci. Soc. Amer. Proc.*, v. 21, pp. 495–497.

Reprinted from the Proceedings of the NATIONAL ACADEMY OF SCIENCES
Vol. 48, No. 3, pp. 316–324. March, 1962.

*EVAPORATION RESISTANCE AS A SENSITIVE MEASURE OF THE PURITY AND MOLECULAR STRUCTURE OF MONOLAYERS**

BY VICTOR K. LA MER AND L. A. G. AYLMORE

COLUMBIA UNIVERSITY

Read before the Academy, April 26, 1961

This report is a continuation of studies on monolayers reported in 1959.[1] The primary objective was to extend the temperature coefficient studies of Archer and La Mer on the saturated straight chain fatty acids to the corresponding alcohols to ascertain the effects of replacement of COOH by OH on the energy barrier to evaporation.

Before undertaking temperature coefficient studies, the reproducibility of the evaporation resistance measurements required further examination. Further samples purified for laboratory studies and also commercial materials or mixtures for practical application on reservoirs have been examined. A number of the evaporation resistance-surface pressure curves reported in the previous work have been confirmed, in particular those for pure octadecanol, hexadecanol, and stearic acid. The extreme sensitivity of evaporation resistance measurements to the presence of minute amounts of impurities is illustrated by these results. Such measurements on samples purified by different methods indicate appreciable differences in purity which are not apparent from melting point determinations. The effects of impurities predominate at low surface pressures, yielding abnormally low values of evaporation resistance accompanied by poor reproducibility. At higher pressures, these effects are less significant due to the impurities being squeezed out of the monolayer. Also a higher degree of reproducibility can be obtained for a given specimen. The squeezing out of impurities is time-dependent, which is evidenced by an increase in evaporation resistance when the monolayer is maintained under pressure. The variability observed at lower surface pressures (<15 dynes/cm) in the previous work and confirmed in present measurements is now attributed to uncontrollable differences in the rate at which minute amounts of contaminants or of solvent are squeezed out.

The behavior of the monolayers under pressure as a function of time provides a criterion of the purity and rearrangement of molecular structure. In general, higher purity results in greater stability under compression.

The resistance to evaporation through monolayers of a particular chain length is determined primarily by the nature of the polar head group and its influence on compressibility of the monolayer through packing of the hydrocarbon chains. The region of relative independence of evaporation resistance upon surface pressure observed for compounds with a divided head group in the liquid condensed phase is attributed to a rearrangement of the polar head groups before the transition to the solid condensed phase.

Previous investigations carried out by La Mer and co-workers have noted the importance of the purity of a monolayer in fundamental studies in the laboratory. Using the method proposed by Langmuir and Schaefer[2] in 1943, Archer and La Mer[3] showed in 1955 that by taking precautions against contamination of the monolayer by impurities from the air, from the aqueous subphase and by the retention of the spreading solvent, reproducible and meaningful measurements of the rate of evaporation of water molecules through surface monolayers could be obtained. These precautions included spreading the monolayer from solutions of high concentration at high initial surface pressure to prevent the entry of impurities. More recently (1959), La Mer and Barnes[1, 4] have shown that provided sufficient precautions are taken to prevent contamination of the monolayer from external sources, the conventional technique of spreading from dilute solutions at zero initial surface pressure yields satisfactory results. This finding permits measurements to be made of evaporation resistance for mixed monolayers. In addition, these workers showed that the purity of sample used for the monolayer was of critical importance in determining the evaporation resistance. Before undertaking temperature coefficient studies of the alcohols and their mixtures, it became

necessary to investigate further the reproducibility of evaporation resistance measurements in these systems.

The initial work has been concerned mainly with (1) the development of a reliable technique for the measurement of evaporation resistance of the long chain *primary alcohols*, (2) the testing of various samples of long chain saturated fatty acids and alcohols available in this laboratory, (3) the checking of data obtained by previous workers, (4) preparing samples of high purity, and (5) an examination of some commercial products for practical application to the control of evaporation from reservoirs.

The film balance-evaporation resistance apparatus is the same as that used by La Mer and Barnes[1] in 1959.† The evaporation resistance of the samples of octadecanol, hexadecanol, and stearic acid available in this laboratory were tested for comparison with the curves obtained by Archer (1955), Barnes (1959), etc. This was done using a variety of different spreading techniques as reported by the previous workers. These included spreading from solutions of both high and low initial concentrations and spreading at both high and zero initial surface pressures.

Strict precautions against contamination of the monolayer by external sources were observed. The apparatus was maintained in a dust-free cabinet the walls of which were greased to retain air-borne particles. Water from the trough was obtained by the double distillation of ordinary distilled water from potassium permanganate solution. The spreading solvent, petroleum ether (40–50°C fraction) was twice distilled. Several monolayers were spread on the water and swept off as a means of cleansing the surface before commencing evaporation resistance measurements.

The compounds employed and their sources were as follows:

	M.P., °C
Octadecanol $CH_3(CH_2)_{16}CHOH$ ($C_{18}OH$)	
(1) Applied Science Laboratories	56.5–56.8
(2) Fisher Chemical Co.	56.2–56.5
(3) Archer, Daniels, Midland Co.	58.4–58.9
(4) Sample of unknown origin	58.5–59.0
Hexadecanol $CH_3(CH_2)_{14}CHOH$ ($C_{16}OH$)	
(1) Department of Agriculture	49.2
(2) Dytol F-11 (Rohm and Haas)	46.8–47.8
(3) Adol 52 (Archer, Daniels, Midland Co.)	46.8–47.6
Stearic acid $CH_3(CH_2)_{16}COOH$ ($C_{17}COOH$)	
(1) Sample of unknown origin	69.8
(2) Hormel Foundation	69.5
(3) Fisher Chemical Co.	69.1

Of the samples of *octadecanol* tested, only samples (3) and (4) gave anything like satisfactory results, the remaining samples providing poor resistance to evaporation except at high surface pressures (see Fig. 1). The sensitivity of evaporation resistance measurements to the presence of minute quantities of impurities is well illustrated by these results. Melting point determinations show no significant difference in purity between samples (1) and (2), while evaporation resistance measurements indicate a considerable difference in purity between these two materials. It is important to recognize that the stability of the monolayer under compression provides in itself a good criterion of the purity of the monolayer. Sample (1) was particularly unstable to compression, the surface pressure falling off rapidly with time. This rapid collapse of the monolayer appears to result from the ejection of impurities, as the evaporation resistance was found to increase

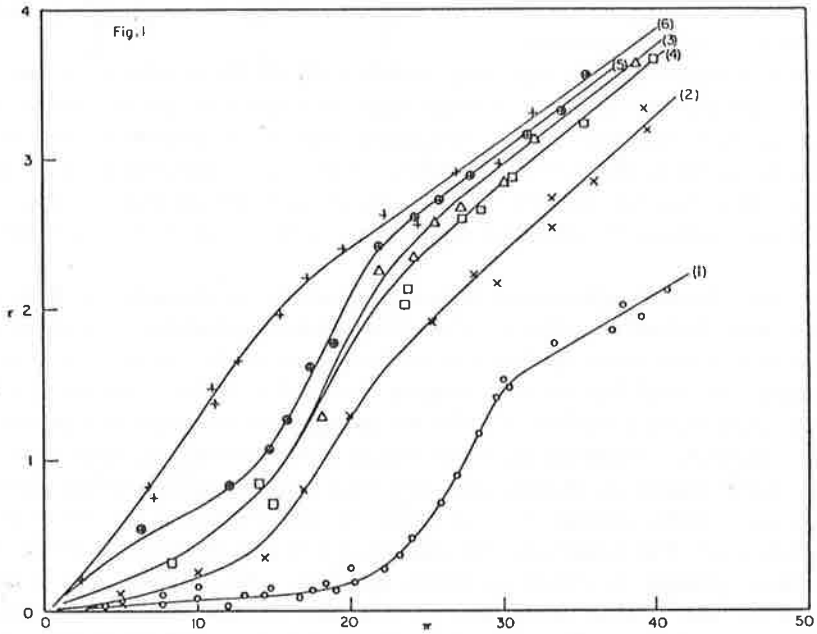

FIG. 1.—Specific resistance to evaporation, r, versus surface pressure, π, of monolayers prepared from a variety of samples of octadecanol ($C_{18}OH$) nos. 1 to 4, as well as the effect of purification of sample 4 (nos. 4 to 6).

1. Applied Science Laboratory sample (1) M.P. 56.6 (○)
2. Fisher Chemical Co. sample (2) M.P. 56.2 (×)
3. Archer, Daniels, Midland M.P. 58.5 (△)
4. Unknown source M.P. 58.4 (□)
5. Unknown source (recrystallized) M.P. 58.6 (⊕)
6. Unknown source (molecularly distilled) M.P. 58.5 (+)

when the monolayer was maintained at a particular surface pressure. The purer sample (2) exhibited a similar, but less striking instability to compression and increase in evaporation resistance on maintaining the monolayer at surface pressure.

Differences in purity between samples (3) and (4), again not apparent from melting point determination, could also be detected from measurements of evaporation resistance; the monolayers of both samples were reasonably stable to compression.

Similarly, appreciable difference in purity between the Dytol F 11 and Adol 52 (commercial hexadecanol) samples, which are not apparent from their melting points, became apparent from evaporation resistance measurements (Fig. 2). The π-r isotherm for monolayers of the Adol 52 samples (3) hexadecanol, like that for the Applied Science Laboratory sample (1) of octadecanol, is indicative of the squeezing out of impurities from the monolayer with increasing surface pressure, since the resistance to evaporation increases on maintaining the film at a particular surface pressure.

Results for samples (1) and (2) of stearic acid were comparable with those obtained by La Mer and Barnes (1959). Sample (3) on the other hand yielded poor resistance to evaporation even at high surface pressures.

From the previous results (ref. 1), it is apparent that the determination of

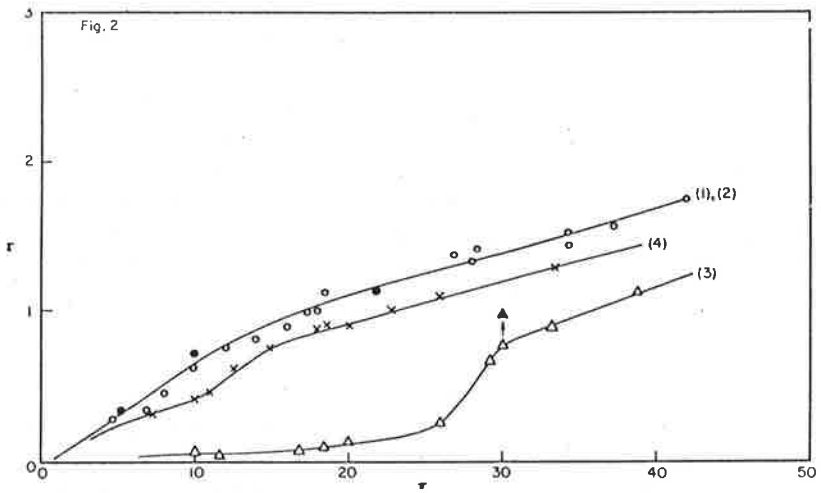

FIG. 2.—Specific resistance to evaporation, r, versus surface pressure, π, of monolayers of hexadecanol ($C_{16}OH$). Source of samples.

		M.P.	
1.	Department of Agriculture		(●)
2.	Department of Agriculture (molecularly distilled)	49.4	(○)
3.	Dytol F-11	46.8–47.8	(×)
4.	Adol 52	46.8–47.6	(△)

The resistance of *Adol* 52 is poor and requires compression to 30 dynes/cm before appreciable resistance is exhibited.

standard or absolute values of evaporation resistance for pure compounds is difficult. There is a considerable variation in evaporation resistance between samples of supposedly high purity from different sources. Since impurities are more likely to consist of lower rather than higher homologues, it seems reasonable to assume higher evaporation resistance to indicate higher purity.

Purification of Materials.—1. *Recrystallization:* A portion of sample (1) of octadecanol was recrystallized from petroleum ether after filtering the warm solution through a 100 mμ millipore filter. An appreciable increase in the evaporation resistance was obtained (curve 4 to 5, Fig. 1).

2. *Molecular distillation:* Portions of sample (4) of octadecanol and sample (1) of hexadecanol were distilled under vacuum in a molecular still at 100°C on a steam bath. The evaporation resistance of the octadecanol sublimate is considerably better than that of the original material (curve 4 to curve 5, Fig. 1), particularly at surface pressures below about 20 dynes/cm. The evaporation resistance of hexadecanol sample (1) was not however changed significantly, nor was there any further improvement apparent for the octadecanol on subsequent redistillation.

The most significant difference between the curve obtained by Barnes for pure octadecanol and the present results for octadecanol distilled under vacuum lies in the absence of the "kink" observed by Barnes and the more rapid rise in evaporation resistance at low surface pressures for the material after molecular distillation. Although further work will be necessary to elucidate this difference, it seems possible that the rapid drop in evaporation resistance (r) observed by Barnes for the range approximately $\pi = 8$ to $\pi = 16$ results mainly from the difficulty in measur-

ing r accurately at low surface pressures, due to the presence of impurities. This may account for the apparently anomalously high values of evaporation resistance observed by Barnes at low surface pressures for mixtures of the alcohols.

In these measurements, no significant difference could be detected between results obtained using the conventional spreading technique (i.e. low concentration at zero initial surface pressure) and alternative methods of spreading at higher concentrations or high initial surface pressure. This result supports the conclusion of Barnes that the conventional spreading technique can be made to yield satisfactory results, provided sufficient precautions are taken to prevent contamination of the monolayer.

Cetyl-Stearyl Alcohol Mixtures.—For practical application to the control of evaporation from water storage the greatest efficacy, i.e. maximum retardation of evaporation consistent with efficient spreading, is achieved using mixtures of cetyl and stearyl alcohols. Studies have been initiated on a number of commercial products in use at the present time in the hope of establishing some criterion by which the relative efficiency of these materials can be evaluated. In Figure 3, π-r isotherms for several of these commercial products are shown in comparison with the curve obtained for a 1:1 mixture of octadecanol and hexadecanol purified by molecular distillation. The solution of the 1:1 mixture of pure cetyl-stearyl alcohol was prepared by weighing the powders into a volumetric flask and dissolving in petroleum ether.

The evaporation resistances of the commercial materials are obviously con-

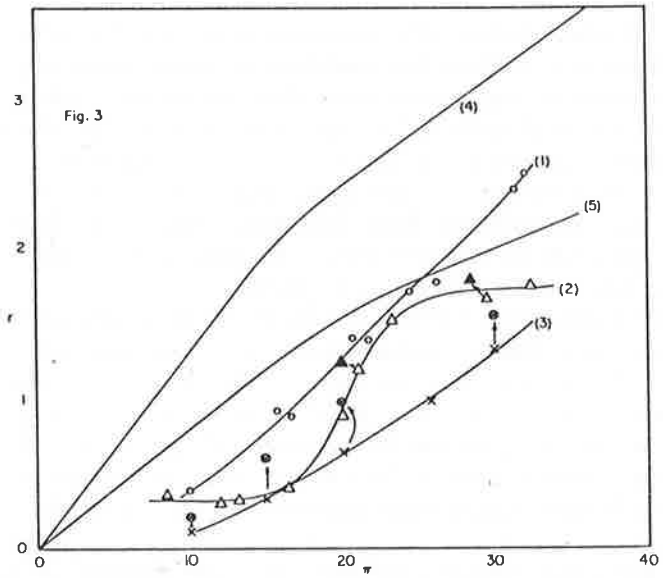

FIG. 3.—Behavior of monolayers of commercial samples of cetyl ($C_{16}OH$) and stearyl ($C_{18}OH$ alcohols and their mixtures).

1. Cetyl to stearyl 1 to 5 Proctor-Gamble ○
2. Cetyl to stearyl 1 to 2 Proctor-Gamble △
   Cetyl to stearyl 1 to 2 Proctor-Gamble after compression ▲
3. Cetyl-stearyl alcohol Prices (Bromborough) before compression ×
   after compression ⊗
4. Pure octadecanol for comparison
5. 1 to 1 pure cetyl-stearyl mixture

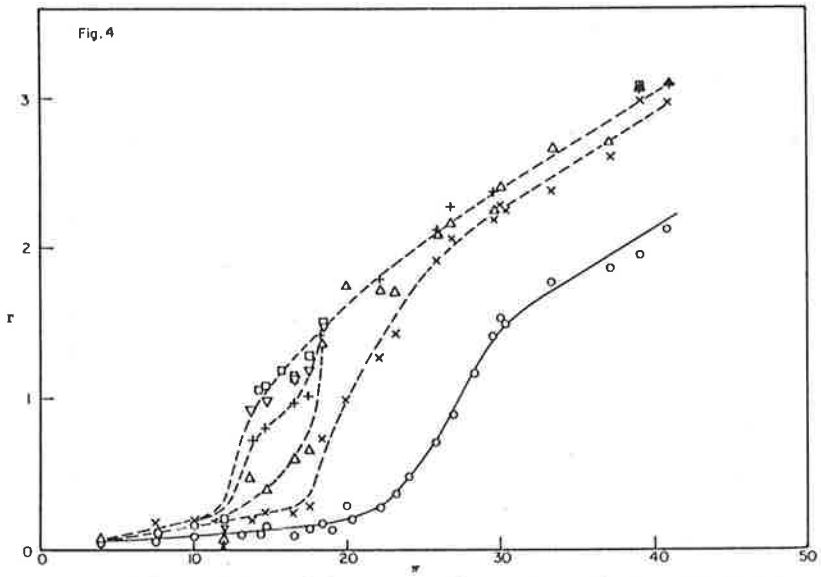

FIG. 4.—Effect of maintaining a monolayer of octadecanol ($C_{18}OH$) for a period of time at surface pressure π indicated before measurement of evaporation resistance is made. Period of time (seconds) at surface pressure π during which r was measured:

0–200	○	measurement of r made
200–400		box was weighed for 200-sec period between measurements
400–600	×	measurement of r made
800–1000	△	measurement of r made
1,200–1400	+	measurement of r made
1,600–1800	▽	measurement of r made
2,000–2200	□	measurement of r made

siderably inferior to those for the pure materials. In addition, monolayers of the commercial products show varying degrees of instability to compression while those for the pure mixture remain reasonably stable to compression. The evaporation resistances of all three commercial materials are improved appreciably by maintaining the films under pressure (shown by arrows in Fig. 3). The length of time taken to reach a stable value varied between compounds and is presumably determined by the amount and nature of the impurities present. These data offer a ready explanation for certain of the disappointing results obtained in the field. They indicate that commercial products should always be tested and then be further purified before field application. It is a waste of time and money to apply materials in the field unless they have been adequately checked by laboratory tests to ascertain their effectiveness (see ref. 4, preface, pp. 35–37).

This variation of evaporation resistance with time for impure materials due to the squeezing out of the impurities under pressure is particularly interesting. In specifying materials for practical use, it obviously becomes necessary to distinguish between those impurities which are retained in the monolayer to high surface pressures and thus exert a deleterious effect on the evaporation resistance and those which are rapidly squeezed out of the monolayer under lower pressure and therefore have relatively little effect on the efficiency of the monolayer. It is intended to continue these studies to the time dependency of evaporation resistance measure-

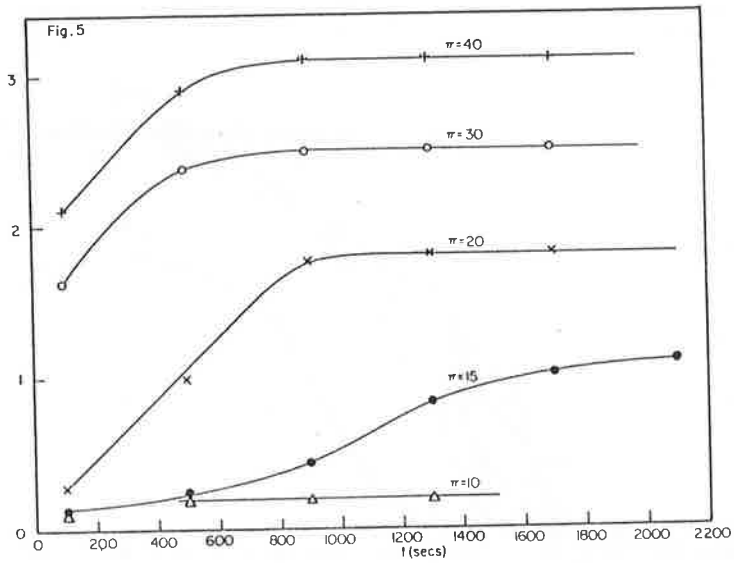

FIG. 5.—Plot of data of Fig. 4 with time (t) for period of measurement as abscissa at various constant surface pressures π as the parameter.

ments to determine the effect of different compounds (e.g. lower homologues, branched chain compounds, etc.) introduced as impurities.

Time Dependence of Evaporation Resistance.—To examine further the variation with time of the evaporation resistance of an impure monolayer, monolayers of the impure sample (1) of octadecanol were spread by the conventional technique, compressed to a particular surface pressure and maintained at that pressure by adjusting the movable teflon barrier. The rate of evaporation was measured over successive intervals of 200 seconds followed by 200-second intervals between measurements. The intervening periods were used to weigh the desiccant box and to adjust its temperature.

The manner in which the π-r isotherm varies with the length of time the monolayer is held under compression is shown in Figure 4. In Figure 5, the variation of evaporation resistance with time at constant surface pressure is shown for several different pressures. At high surface pressures (say $>$ 25 dynes/cm), the evaporation resistance increases rapidly to a maximum value for the particular surface pressure, indicating that those impurities which can be "squeezed out" are rapidly ejected from the monolayer. At surface pressures below the transition from the liquid condensed to the solid condensed state ($<$ about 12 dynes/cm), the impurities appear to be retained in the monolayer, resulting in very low values of evaporation resistance. At intermediate surface pressures, the impurities are only gradually squeezed out of the monolayer, and a considerable time is necessary for the evaporation resistance to reach a maximum value.

Even after being subjected to high surface pressure for some time, the evaporation resistance is still considerably less than that of the pure material. This seems to indicate that some additional impurities are strongly retained in the

monolayer. It is also possible that contamination of the monolayer by external sources begins to exert an influence after such a time.

In view of this considerable change in the π-r isotherm with time, it seems likely that the variability in evaporation resistance measurements observed by previous workers, particularly at low surface pressures, may be attributed at least in part to differences in the extent to which minute amounts of contaminants or of solvent are squeezed out.

* This investigation was supported by Grant NSF G-7348 from the National Science Foundation for the period July 1960 to June 1961.

† Constant factors such as the calibration for the surface balance and the effect of the air gap on the rate of absorption were checked and found to be essentially the same as reported by Barnes.

[1] La Mer, V. K., and G. T. Barnes, these PROCEEDINGS, **45**, 1274–1280 (1959).

[2] Langmuir, I., and V. Schaefer, *J. Franklin Inst.*, **235**, 119 (1943).

[3] Archer, R. J., and V. K. La Mer, *J. Phys. Chem.*, **59**, 200 (1955).

[4] *Retardation of Evaporation by Monolayers: Transport Processes*, ed. V. K. La Mer (New York: Academic Press, February 1962), preface and chapters 1 and 2.

[Reprinted from the Journal of Physical Chemistry, 67, 2793 (1963).]

The Ideal Surface Behavior of Mixed Monolayers of Long-Chain *n*-Paraffinic Alcohols

By Victor K. La Mer, L. A. G. Aylmore, and Thomas W. Healy

[Reprinted from the Journal of Physical Chemistry, **67**, 2793 (1963).]

THE IDEAL SURFACE BEHAVIOR OF MIXED MONOLAYERS OF LONG-CHAIN *n*-PARAFFINIC ALCOHOLS

By Victor K. La Mer, L. A. G. Aylmore, and Thomas W. Healy

Chemistry Department, Columbia University, New York, New York

Received July 19, 1963

The rate of evaporation of water through mixed monolayers of high purity 1-alcohols of alkyl chain length from 16 to 20 carbons has been used to verify the ideal surface behavior of these mixed monolayers. The ideal behavior exists at all surface pressures of the monolayers. It has been established that deviations from ideality observed at low surface pressures by previous workers are due to impurities in the alcohols or in the water subphase.

Introduction

Certain monomolecular films will markedly retard the evaporation of water through the water–air interface. The theoretical and practical aspects of this phenomenon have been discussed in detail recently in a monograph by La Mer[1] and need not be repeated. To investigate quantitatively the rate of evaporation as a function of parameters of the monolayer such as chain length, surface compression, etc., the reciprocal of the rate of uptake of water by a desiccant suspended a few millimeters above the water surface may be expressed as a specific evaporation resistance (r) by the equation

$$r = a(w_w - w_d)(t/m_f - t/m_w) \qquad (1)$$

where a is the area of water surface under the desiccant; w_w and w_d are the concentrations of water vapor in equilibrium with water and desiccant, respectively; t/m is the reciprocal evaporation rate with the subscripts f and w referring to the surface with and without monolayer, respectively. The resistance, r, is a property of the monolayer alone, and is expressed in absolute units (sec./cm.).

Previous work by Barnes and La Mer[2] showed that at *high surface pressures* (>15 dynes cm.$^{-1}$), mixtures of long-chain alcohols, *i.e.*, 1-hexadecanol and 1-octadecanol, behaved as ideal surface layers, obeying a mixture law that can be derived from the additivity of the free energies of activation for the kinetic process of transporting a molecule of water through the monolayer, *viz.*

$$\ln r_{12} = x_1 \ln r_1 + x_2 \ln r_2 \qquad (2)$$

Here r_1 and r_2 are specific resistance values of pure components at a given pressure, r_{12} is the specific resistance of a binary mixture of the pure component at the same pressure, and x_1 and x_2 are the mole fractions of the pure components in the mixture. In the low pressure region (<15 dynes cm.$^{-1}$) considerable divergence from

(1) V. K. La Mer, Ed., "Retardation of Evaporation by Monolayers," Academic Press, Inc., New York, N. Y., 1962.

(2) G. T. Barnes and V. K. La Mer in ref. 1, pp. 9–39.

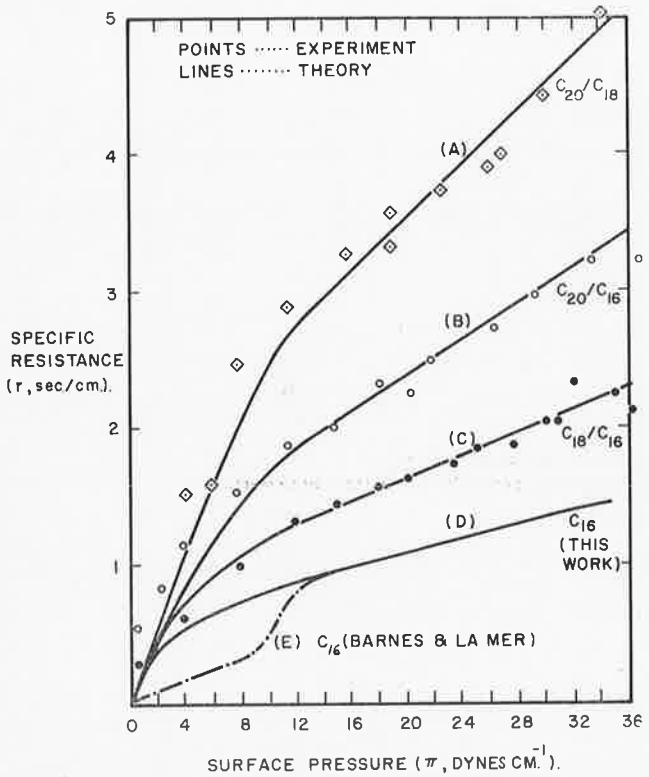

Fig. 1.—Specific resistance–surface pressure isotherms for mixtures (curves A–C) of C_{20}, C_{18}, and C_{16} *n*-alcohols as 1:1 mixtures. Curve D is for 1-hexadecanol (present work) and curve E is from data of Barnes and La Mer.[2]

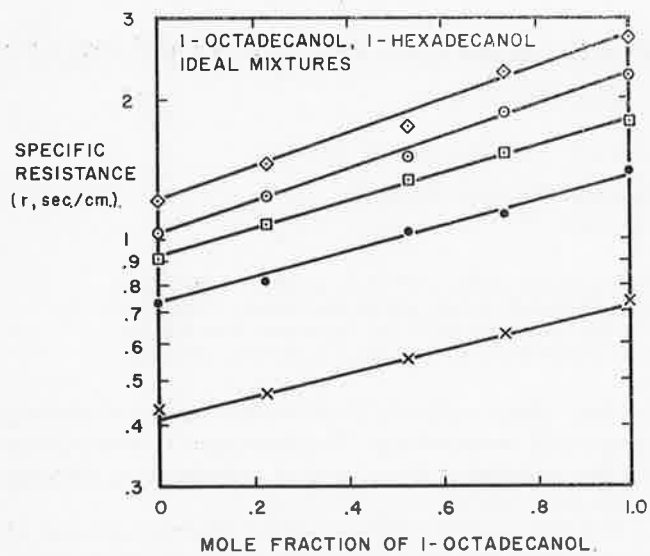

Fig. 2.—Logarithm of the specific evaporation resistance as a function of composition for mixed monolayers of 1-octadecanol and 1-hexadecanol at various surface pressures and at 25°: ◇, 30 dynes cm.$^{-1}$; ⊙, 20 dynes cm.$^{-1}$; ⊡, 15 dynes cm.$^{-1}$; ●, 10 dynes cm.$^{-1}$; and ×, 5 dynes cm.$^{-1}$.

ideality was observed, the mixtures giving higher resistances than pure components.

Recent work by La Mer and Aylmore[3] has shown that it was likely that the 1-hexadecanol and 1-octadecanol used by Barnes and previous workers[4–6] contained trace impurities, since the "kink" in the resistance–pressure curve at low pressures, observed by Barnes and La Mer, can be removed by successive purification of the long-chain alcohols. The impurity levels discussed here are exceedingly small and cannot always be detected by techniques such as gas chromatography.

In this paper we shall show that with *sufficiently purified materials*, alcohol–alcohol monolayers exhibit ideal surface mixing behavior at all pressures.

Experimental

The apparatus, described elsewhere,[1–6] was used without further modification. Briefly, it consists of a shallow Pyrex glass trough with lightly paraffined edges, a desiccant box assembly, a Wilhelmy plate, and fixed and movable Teflon barriers. The water in the trough was kept at 25.0 ± 0.2° by pumping water from a thermostat bath through a long glass serpentine lying in the trough.

Water in the trough was prepared by double distillation of the laboratory-distilled water. Several monolayers were spread on the water surface and swept off prior to each set of experiments. The middle fraction of predistilled *n*-hexane was used as the spreading solvent. The volume of solution spread was measured with an Agla micrometer syringe.

The C_{20},C_{18},C_{16} alcohols (Fig. 1) were supplied by C. Michel of Molecular Technology, Inc., New York, N. Y., and were not purified further. The C_{18}, C_{16} alcohols (Fig. 2) were the middle fractions of the molecular distillation of 1-hexadecanol and 1-octadecanol of unknown source. All alcohols used showed only one peak in gas chromatographic analysis.

Results

The solid lines for curves A, B, and C of Fig. 1 are calculated from the ideal mixture law (eq. 2) and the values of the specific resistance of the pure components. The mixtures shown are 1:1 mixtures of $C_{20}OH/C_{18}OH$ (curve A), $C_{20}OH/C_{16}OH$ (curve B), and $C_{18}OH/C_{16}OH$ (curve C).

Curve D is the resistance–pressure behavior of the 1-hexadecanol used in the present investigation. The dotted curve E illustrates the "kink" observed by previous works[3] for impure 1-hexadecanol at low pressures. Notice that the impurity is effectively "squeezed out" at higher pressures so that the two curves superimpose.

In Fig. 2 we have plotted the logarithm of specific resistance at various pressures as a function of the mole fraction of 1-octadecanol in 1-octadecanol–1-hexadecanol mixtures at 25°. This type of plot, suggested by Barnes and La Mer[2] is suitable for checking ideal surface solution behavior, *i.e.*, eq. 2.

Discussion

The results of Fig. 1 and 2 demonstrate that mixed alcohol monolayers exhibit ideal surface behavior at all surface pressures below the collapse pressure. Three types of mixed monolayer behavior can now be differentiated.

1. Ideal Surface Mixtures.—This behavior is exhibited by mixtures of close members of a homologous series. The present system is of this type. La Mer and Robbins[7] have shown that benzene trapped in 1-hexadecanol or 1-octadecanol monolayers forms an ideal solution in that the areas are additive, at least for low mole fractions of benzene. Essentially ideal surface solution behavior has been shown[8] for two similar long-chain fatty acids.

(3) V. K. La Mer and L. A. G. Aylmore, *Proc. Natl. Acad. Sci. U. S.*, **48**, 316, 1962.

(4) R. J. Archer and V. K. La Mer, *J. Phys. Chem.*, **59**, 200 (1955).

(5) H. L. Rosano and V. K. La Mer, *ibid.*, **60**, 348 (1956).

(6) V. K. La Mer and G. T. Barnes *Proc. Natl. Acad. Sci. U. S.*, **45**, 1274 (1959).

(7) M. L. Robbins and V. K. La Mer, *J. Colloid Sci.*, **15**, 123 (1960).

(8) T. Isemura and K. H. Hamaguchi, *Mem. Inst. Sci. Ind. Res. Osaka Univ.*, **8**, 131 (1951); see *Chem. Abstr.*, **46**, 2373 (1952).

2. Nonideal Surface Solutions.—Mixtures of 1-octadecanol and stearic acid for example, show positive deviations from ideal behavior.[2]

3. Ideal or Nonideal Behavior with Complex Formation or Rearrangement at Specific Compositions.—Mixed monolayers of 1-hexadecanol and 1-hexadecyl sulfate are of this type.[9] We point out that the behavior shown in Fig. 2, ref. 9, is by no means unique. Robbins and La Mer [Fig. 11, ref. 7] found that pressure-area isotherms for octadecanol as the excess of spreading solvent, benzene, diffuses into the subphase, showed the same type of progressive discontinuities—which some have arbitrarily called phase transitions.

The evaporation resistance technique is most useful in distinguishing between these types of surface behavior of mixed monolayers, provided precautions are taken to ensure purity of reagents and of the water–air interface.

At low surface pressures, both Rosano and La Mer[5] and Barnes and La Mer[2,6] observed a sharp rise in the evaporation resistance of the pure alcohols between $\pi = 8$ dynes cm.$^{-1}$ and $\pi = 15$ dynes cm.$^{-1}$. Barnes and La Mer suggested that this sharp angle could be associated with the transition from the liquid condensed to the solid state which occurs at the same pressure. However, in measuring the evaporation resistance of mixtures of these and other alcohols in the low surface pressure region, these authors obtained values much higher than those of either pure compound. The higher resistance values obtained for these materials in the low surface pressure range indicates clearly that the sharp change in slope (curve E, Fig. 1) observed by the previous workers resulted either from contamination of the monolayer from external sources or the presence of impurities in the spreading material. We interpret the "kink" in specific resistance–surface pressure isotherms (curve E, Fig. 1) to the process where the decrease in area results in squeezing out of impurities rather than to increase in pressure [ref. 5, Fig. 7, and ref. 1, p. XV].

The extreme sensitivity of the evaporation resistance of surface monolayers to the presence of minute quantities of impurities or contamination, particularly at low surface pressures, is further emphasized by these results. In practice it was found that only by using freshly prepared solutions and by rigorous acid and steam cleaning of the still for preparation of the subphase water, that these higher resistance values could be reproduced at low surface pressures. Frequently, solutions left overnight, while yielding similar values at higher surface pressures, were found to produce much lower values in the low surface pressure region and to exhibit the sharp change in evaporation resistance observed by previous workers. A similar deterioration in evaporation resistance at lower surface pressures resulted from even the slightest deterioration in the quality of the water used in the subphase.

The isotherm of specific resistance–surface pressure for the C_{20} alcohol did have a slight sigmoidal discontinuity at very low pressures (<10 dynes cm.$^{-1}$). This undoubtedly is due to trace impurities in this longer chain material and accounts for the fact that in the low pressure region for curves A and B of Fig. 1 some disagreement between theory and experiment is observed. It may be noted that the C_{20} alcohol, and indeed all alcohols used in this investigation showed only one peak in gas chromatography analysis. This finding highlights the importance of the evaporation resistance technique in studying architecture of monolayers; the "probe" in such measurements is a water molecule.

Acknowledgment.—This work was supported by a grant from the U. S. Bureau of Reclamation No. 14-06-D-4018.

(9) F. M. Fowkes, *J. Phys. Chem.*, **67**, 1982 (1963); p. 1983, Fig. 2.

THE TRANSPORT OF WATER THROUGH MONOLAYERS OF LONG-CHAIN *n*-PARAFFINIC ALCOHOLS

Victor K. La Mer, Thomas W. Healy, and L. A. G. Aylmore

Department of Mineral Engineering, Columbia University, New York, New York

Reprinted from JOURNAL OF COLLOID SCIENCE, Volume 19, No. 8, October 1964

Reprinted from JOURNAL OF COLLOID SCIENCE, Volume 19, No. 8, October 1964

JOURNAL OF COLLOID SCIENCE **19**, 673–684 (1964)

THE TRANSPORT OF WATER THROUGH MONOLAYERS OF LONG-CHAIN *n*-PARAFFINIC ALCOHOLS

Victor K. La Mer,[1] Thomas W. Healy,[2] and L. A. G. Aylmore[3]

Department of Mineral Engineering, Columbia University, New York, New York

Received February 17, 1964

INTRODUCTION

Studies of the rate of transport of water molecules through compressed monolayers of saturated long-chain fatty acids and alcohols are presently of considerable academic interest in correlating this property with molecular architecture. They are technically important for the control of evaporation from water storages.

The studies on retardation of evaporation that preceded the present investigation have been summarized in detail in reference 1. When the present work was initiated, the situation that existed in 1962 may be summarized as follows:

1. Archer and La Mer (2, 3) had presented a theory that describes the process in terms of well-established concepts of chemical kinetics. This theory has been verified in various details (1).

2. Long straight-chain (i.e., greater than 14 carbons) fatty alcohols and acids have been shown to produce the most resistant monolayers (4). Branched-chain molecules or esterified compounds exhibit much less resistance to evaporation.

3. In the case of mixtures of long-chain compounds the resistance to evaporation is controlled either by the ideal mixture law involving the additivity of free energies of activation for alcohol-alcohol mixtures or by a nonideal (nonlinear) mixture law for alcohol-acid mixtures (5, 6).

The specific resistance-surface pressure diagram of reagents containing impurities in small amounts invariably exhibits an inflection best described as a "kink" in the curve at low pressures. La Mer and Aylmore (7) have demonstrated that this "kink" is removed by successive reduction in the

[1] Professor Emeritus Chemistry, Senior Researcher in Mineral Engineering, Columbia University, New York.

[2] Now Lecturer in the Department of Mineral Technology, University of California, Berkeley, California.

[3] Department of Soil Science, University of Western Australia, Nedlands, Western Australia, Australia.

content of impurities of the sample. High-purity reagents give a smooth evaporation resistance-surface pressure curve. The "kink" results when the compression "squeezes out" an impurity at constant lateral pressure rather than increasing this pressure. At high pressures monolayers formed from an impure reagent almost invariably approach the behavior of a monolayer made from a high-purity reagent (4, 6).

Archer and La Mer (2, 3) showed that the erratic results of Langmuir and Schaefer (8) could be transformed into reproducible results by spreading the monolayer from solutions at initial high concentration and by using other precautions to prevent contamination of the monolayer. These precautions included the use of an all-Pyrex glass trough instead of a paraffined metal trough, the use of *n*-hexane in preference to benzene as a spreading solvent, and the exclusion of impurities from the subphase and atmosphere. Using these techniques Archer was able to establish a satisfactory relation for the calculation of specific evaporation resistance (r) reciprocal of the rate constant. He showed that for a homologous series of saturated fatty acids in the liquid condensed phase, the monolayer resistance (r) was virtually independent of the surface pressure and subphase pH; $\log r$ was a linear function of chain length. For a particular fatty acid monolayer, in the liquid condensed phase, the logarithm of the resistance was found to be a linear function of the reciprocal of the absolute temperature which led to the description of the evaporation resistance in terms of an exponential energy barrier, i.e., free energy of activation dependent on chain length.

Rosano and La Mer (4) confirmed the results of Archer and La Mer, using a similar technique but decompressing the film to the required surface pressure after initially spreading under high pressure instead of compressing to the required pressure as Archer and La Mer had done. They showed that the evaporation resistance of the long-chain compounds was correlated with the compressibility of the monolayer.

To extend these investigations to *mixed monolayers* Barnes and La Mer re-examined the conventional (dilute solution) spreading technique since the spreading of monolayers from solutions of high concentration results in the formation of small islands of crystalline or associated material within the films. This crystal formation is of little consequence in the case of pure monolayers but prevents an accurate estimation of the composition of mixed monolayer systems. Barnes and La Mer showed that by applying sufficiently stringent precautions to prevent contamination of the monolayer, identical results for evaporation resistance could be obtained regardless of the spreading technique used. Their results for pure monolayers in comparison with the results of previous workers illustrated the high sensitivity of the evaporation resistance to the presence of impurities in the sample used for the monolayer.

Although all mass transfers are basically diffusion processes, on the

molecular scale, the evaporation process follows the single-step energy barrier relation established by Archer and La Mer, i.e., Fick's law of diffusion is not obeyed. Barnes and La Mer (5) analyzed their results on mixed monolayers in terms of the free energy of activation and showed that the basic requirements of their equation derived for mixtures were compatible with their experimental results. For mixed monolayers of octadecanol and hexadecanol the resultant resistance obeyed a logarithmic addition rule which follows as a corollary of the energy barrier theory and not the reciprocal addition rule originally suggested by Langmuir and Schaefer (8) and accepted by Rosano and La Mer (4). Recent work (6) at Columbia has established that alcohol-alcohol mixed monolayers obey the logarithmic additivity rule at *all* pressures below collapse.

In the previous studies the monolayer had been spread from petroleum ether. This choice of solvent, used in the Columbia University Laboratories, was further substantiated by La Mer and Robbins (9), who established from pressure-area isotherms that benzene, for example, was retained in the film as Archer had predicted. However, except for some preliminary experiments by Archer, no resistance-pressure curves had been obtained for monolayers spread from various solvents or from the solid, whether the solid was in the form of a dry powder or in the molten state.

The activation theory developed by Blank and La Mer (10) has been verified with the results of Barnes (5) and Robbins (9). However, the extremely high purity reagents prepared later by Aylmore (7) were not available to these workers. It therefore became important to redetermine the E_{CH_2} "radius" plots with the purified alcohols now available; E_{CH_2} is the experimental activation energy per CH_2 group associated with the separation of chains as a water molecule escapes. The "radius" is the measure of the distance between polar groups in the monolayer.

Apparatus and Experimental Procedures

The apparatus was similar to that used by the previous workers (1–5, 7). The edges of a glass Langmuir surface balance trough were lightly waxed and Teflon barriers were used to confine and compress the surface films. Surface pressures were measured by means of a Wilhelmy dipping plate of roughened mica suspended from a calibrated torsion balance. The temperature of the subphase was controlled to ±0.2°C. by pumping water from a constant-temperature bath through a glass serpentine tube in the trough. Room temperature was maintained in the range of 25°–27°C. Redistilled *n*-hexane (boiling range 40°–50°C. fraction) was the spreading solvent, and an "Agla" micrometer syringe was used to dispense accurately known volumes of solution. The water subphase was obtained by the double distillation of New York City tap water from alkaline potassium permanganate solution in an all-Pyrex distillation assembly.

The rate of evaporation from the water surface was determined from the increase in weight of a container filled with a desiccant (Lithium Chloride) and held at a precisely fixed distance (usually 2 mm.) above the water surface for a specific time (2, 3).

The monolayers were spread using the conventional or dilute solution spreading technique following Barnes and La Mer (5). The standard procedure was as follows:

Before commencing evaporation resistance measurements several monolayers were spread and swept off to remove contaminants which come to the surface. The monolayer was spread and compressed immediately to the required surface pressure. The bridge and desiccant box were then placed in position and the timer was started. Any drift in the surface pressure during the time of measurement was noted.

At the end of the measuring period (usually 200 to 400 seconds, depending on the rate of evaporation) the desiccant box was reweighed and the resistance to evaporation of the monolayer calculated. The evaporation rate is determined by measuring the rate of uptake of water by a desiccant suspended a few millimeters above the water surface. From measurements with and without a monolayer, the specific evaporation resistance (r) of the monolayer can be calculated from the equation

$$r = a(w_w - w_d)(t/m_f - t/m_w), \qquad [1]$$

where a is the area of water surface under the desiccant; w_w and w_d are the concentrations of water vapor in equilibrium with water and desiccant, respectively; t/m is the reciprocal evaporation rate with the subscripts f and w referring to the surface with film and without film, respectively.

The factor $a(w_w - w_d)$ was obtained experimentally by varying the height of the desiccant box above the surface of the water.

A small correction for the extraneous water vapor absorbed from the atmosphere during the measuring period was applied to the measured mass of water absorbed.

The samples of C_{14}, C_{16}, C_{18}, C_{20}, and C_{22} alcohols used in these measurements were provided by Curtis Michel of M. Michel & Co. Gas chromatographs of these materials revealed single peaks only. The final check for purity of the sample was to measure the evaporation resistance-surface pressure isotherm; if no "kink" or point of inflexion exists in the low-pressure region, the sample may be taken as pure. La Mer and Aylmore (7) have discussed this point in detail.

A second sample of octadecanol (C_{18}) was one of the unknown source available in the laboratory; it had been purified by us by recrystallization from petroleum ether and subsequent molecular distillation.

Results and Discussion

a. Effect of Solvents on the Resistance to Evaporation of Monolayers

The effect of the spreading solvent on the resistance to evaporation of hexadecanol and octadecanol monolayers is shown in Fig. 1. Petroleum ether (*n*-hexane) as spreading solvent has no deleterious effect on the resistance of the hexadecanol monolayer at any given pressure. This is evident from the close correlation with monolayers spread from the solid. The shape of the resistance-pressure curve for hexadecanol spread from benzene is of the same general form as the petroleum ether curve, *but at any given pressure the resistance of monolayers spread from benzene* is *considerably less than the resistance of monolayers spread from n-hexane*. This is in agreement with Archer's work of 1954. At pressures greater than 35 dyne cm.$^{-1}$ the two curves approach each other and would meet if such high pressures (45–50 dyne cm.$^{-1}$) could be attained.

These findings confirm the suggestion made by Archer and La Mer (2, 3) and later examined in detail by La Mer and Robbins (9), that since benzene

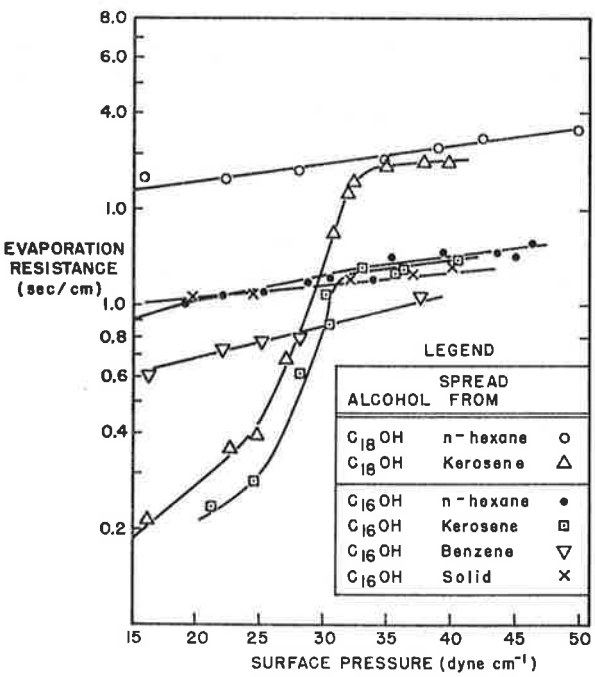

Fig. 1. Effect of spreading solvent on the resistance to evaporation of monolayers of pure hexadecanol. The behavior of monolayers spread from the solid hexadecanol is included for comparison.

is retained in the monolayer, the use of benzene as a spreading solvent will have detrimental effects on the resistance behavior.

Note that the resistance-pressure curve for hexadecanol spread from benzene has no "kink" due to "squeezing out" or rejection of the benzene into the water. Benzene is apparently retained rather than squeezed out!

On the other hand, when using *kerosene* as the spreading solvent we find a most pronounced "kink" due to "squeezing out" of nonvolatile constituents of the kerosene. The effectiveness of this rejection process is evidenced by the fact that the resistance-pressure curves for hexadecanol and octadecanol spread from *n*-hexane and from kerosene superimpose at pressures greater than 30 dyne cm.$^{-1}$.

A further example of the "squeezing out" process was given by La Mer and Aylmore (7) in which they compared resistance-pressure isotherms for pure hexadecanol and a typical commercial hexadecanol. Successive purification eliminates this kink. The presence of relatively large quantities of impurities in these materials often causes a serious deterioration in the evaporation resistance with time. When, however, such impurities are of the type which are rapidly squeezed out of the monolayer, particularly at high surface pressures, the effectiveness of the film in retarding evaporation may not be severely affected. Such impurities can be considered as permissible in contrast to those which are retained and continue to exert a deleterious effect to high surface pressures.

b. Effect of Chain Length on Resistance to Evaporation

The evaporation resistance-surface pressure isotherms obtained for the pure samples of C_{14}, C_{16}, C_{18}, C_{20}, and C_{22} alcohols at 25°C. are shown in Fig. 2. Monolayers of all these materials were fairly stable at surface pressures below their respective collapse pressures, indicating acceptable purity. The surface pressure of the C_{20} and C_{22} alcohol films showed a tendency to increase for some time after the initial spreading and compression. This is probably a result of the slower spreading rates of these longer chain materials.

At higher surface pressures (above about 15 dynes/cm.) the evaporation resistance of these alcohols shows a very marked dependence on the chain length, increasing with increasing surface pressure. The isotherms obtained for the C_{16} and C_{18} alcohols at pressures about 15 dynes/cm. are essentially the same as those reported by Barnes and La Mer (5); however, the shape of the curves at lower surface pressures is significantly different.

At lower surface pressures both Rosano and La Mer (4) and Barnes and La Mer (5) observed a sharp rise in the evaporation resistance of the pure alcohols (between $\Pi = 8$ and $\Pi = 15$ dynes/cm.). Barnes and La Mer (5) suggested that this sharp change could possibly be associated with the transition from the liquid condensed state to the solid state which occurs

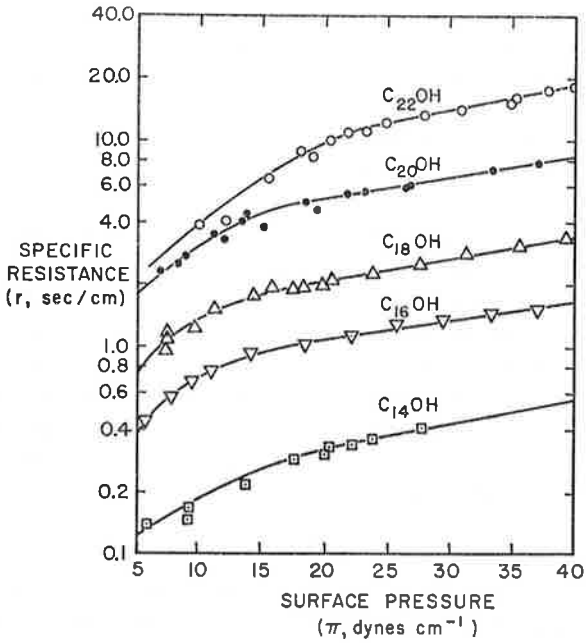

FIG. 2. Effect of alkyl chain length of n-paraffinic alcohols on the resistance to evaporation at 25°C.

at the same pressure. However, in measuring the evaporation resistance of mixtures of these and other alcohols in the low surface pressure region, these authors obtained values higher than those of either pure compounds. Recent work from these laboratories (6) has shown that alcohol-alcohol mixed monolayers exhibit ideal mixing at *all* pressures.

The continuous rise in evaporation resistance from zero observed in the present results and the higher resistance values obtained for these materials in the low surface pressure range indicate clearly that the sharp change in slope observed by the previous workers results either from contamination of the monolayer by external sources or from the presence of impurities in the spreading materials.

The extreme sensitivity of the evaporation resistance of surface monolayers to the presence of minute quantities of impurities or contamination, particularly at low surface pressures, is further verified by these results. It was found that only by using freshly prepared solutions, by sweeping the surface clean by the successive application of monolayers, and by rigorously cleaning the still for preparation of the subphase water, could these higher resistance values at low surface pressure be reproduced. Frequently solutions left overnight were found to produce much lower values in the low surface pressure region and to exhibit the sharp change in evapo-

ration resistance observed by previous workers. A similar deterioration in evaporation resistance at lower surface pressures resulted from even the slightest deterioration in the quality of the water used in the subphase.

The somewhat sigmoidal shape of the isotherm for the C_{22} alcohol can therefore be taken as an indication of the presence of a certain amount of impurity in the longer chain material. It is significant that gas chromatography did not always detect this impurity.

According to the exponential energy barrier theory the plot of the logarithm of the resistance against the surface pressure for a homologous series of long-chain compounds should give a series of parallel straight lines the separation of which is determined by the increment in chain length. The results of Fig. 2 for the long-chain alcohols are in excellent agreement with this theoretical prediction. The experimental points for the C_{22} alcohol tend to lie slightly below the equivalent points indicated by the C_{16}, C_{18}, and C_{22} alcohol isotherms, but as previously mentioned C_{22} appears to contain a light amount of impurity.

c. Energy Barrier Theory

The resistance r, defined by Eq. [1], is a property of the monolayer alone and does not depend on any apparatus constant; it is expressed in absolute units (sec./cm.).

The resistance of the monolayer is given by Archer and La Mer (2, 3) as

$$r = C \exp\left(\frac{E(n)}{RT}\right), \qquad [2]$$

where C is a frequency constant, in which case $E(n)$, a function of the number (n) of CH_2 groups in the molecule, must be regarded as a *free energy* of activation. Blank and La Mer (10) have shown how from resistance data for say C_{16} and C_{18} alcohols it is possible to express $E(CH_2)$ as a function of surface pressure. Here $E(CH_2)$ is the energy associated with the process of addition of one CH_2 group to the long-chain alcohol or acid. Furthermore, with the aid of surface pressure-area equilibrium data, $E(CH_2)$ can be expressed as a function of the average distance between centers of molecules that make up the monolayer (called "radius x" by Blank and La Mer).

We have redetermined the dependence of $E(CH_2)$ on surface pressure using the very high purity materials now available, and the results are shown in Fig. 3 (see La Mer and Aylmore (7) for the effect of successive purifications of the resistance of long-chain alcohol monolayers). The value of 246 cal./mole for $E(CH_2)$ at the saturation pressure of about 45 dynes/cm. is somewhat lower than the value of 308 cal./mole of Blank and La Mer.

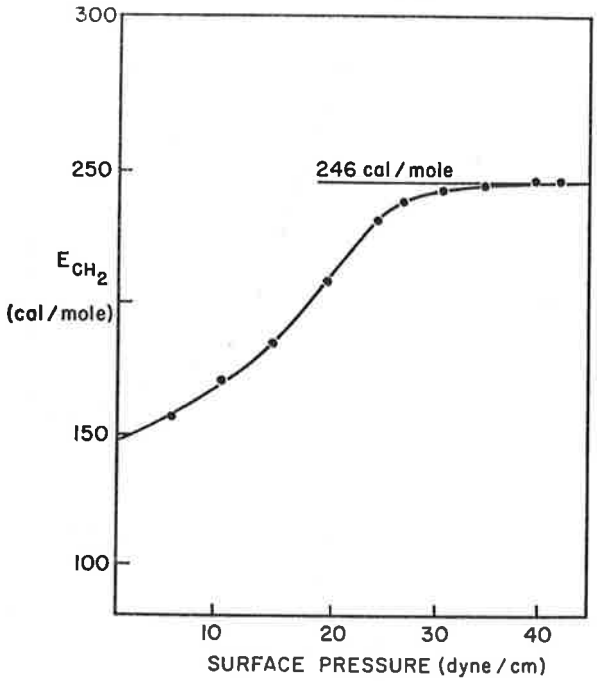

FIG. 3. E_{CH_2} as a function of surface pressure; E_{CH_2} was calculated from the evaporation resistance-surface pressure isotherms for pure C_{16} and C_{18} alcohols.

Similar calculations from two sets of results obtained by Aylmore yield values of $E(CH_2)$ of 264 and 234 cal./mole, respectively. Several experimenters have now shown that for all alcohols from the C_{14} to the C_{22} alcohol (inclusive) $E(CH_2)$ increases by approximately 300 cal. for each CH_2 group added.

In Fig. 4, the results of Fig. 3 together with the pressure-area results of Robbins and La Mer (9) have been used to obtain log $E(CH_2)$ as a function of log "radius." The limiting slope at high pressure for these results is found to be -9.6. This new value for n, in

$$E(CH_2) = Kx^{-n}, \qquad [4]$$

strengthens the previous suggestion (10) that the forces involved in the formation of a hole in a close-packed monolayer are primarily those of *repulsion* between the chains.

The discussion above emphasizes the importance of chain length on the resistance to evaporation of water through a monolayer of a fatty alcohol. Chain length is a variable that allows one to characterize the most important requirements of a monolayer that is to be used in the field. The

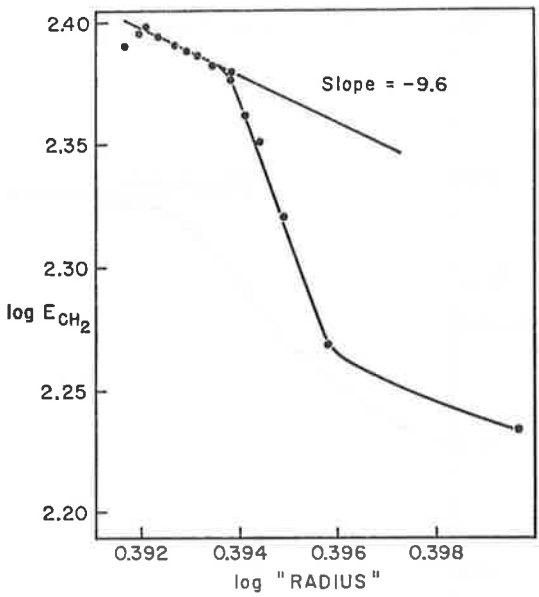

FIG. 4. E_{CH_2}—"radius" relationship. The E_{CH_2} data are taken from Fig. 3, and the surface pressure-area per molecule data of Robbins and La Mer (9) were used to calculate the "radius" parameter.

chain length of individual members of a homologous series of long-chain alcohols determines the following:

a. resistance to evaporation;
b. spreading rate;
c. "squeezing out" of one component of a monolayer by another;
d. "squeezing out" of nonvolatile solvent impurities for monolayers spread with the aid of a solvent;
e. resistance to wave and/or wind action;
f. regeneration or sublimation of the long-chain alcohol itself;
h. solubility of the alcohol in water.

The effect of chain length on evaporation and solution of the alcohol itself ((*g*) and (*h*)) has been examined by other workers (11). The resistance of monolayers to wave action has been investigated recently by Healy and La Mer (12).

To conform to the exponential energy barrier theory the logarithm of the evaporation resistance should be a linear function of the reciprocal of the absolute temperature. The results of Archer and La Mer for the C_{19} long-chain fatty acid and of Barnes and La Mer for C_{16} and C_{18} alcohols showed excellent agreement with this requirement.

The effect of temperature on the evaporation resistance of the C_{20} alcohol

has been redetermined. If ln r for any particular pressure is plotted against the reciprocal of the absolute temperature, the experimental points lie fairly close to linear ln $r - \pi$ plots for all but the 15°C. temperature, where the experimental errors are probably quite high. The values of the residual activation energy ($E^{\ddagger}$) and the activation energy per CH_2 group, $E(CH_2)$, 6955 cal./mole and 264 cal./mole, respectively, were calculated from these data and agree very well with the values of 6,460 cal./mole and 276 cal./mole obtained by Barnes and La Mer for the C_{16} and C_{18} alcohols.

Summary

The importance of the chain length of the monolayer-forming molecule on evaporation resistance and spreading rate has been emphasized.

Evaporation resistance-surface pressure isotherms show that n-hexane as the spreading solvent does not have a deleterious effect on the resistance; whereas benzene, since it is retained to some extent in the monolayer, reduces the resistance of a monolayer at all pressures. Kerosene, although retained at low pressures, is effectively squeezed out of the monolayer at high pressures.

We have used resistance-pressure isotherms of high-purity materials to show more conclusively that the forces involved in the formation of a hole in a close-packed monolayer are primarily those of repulsion between the chains.

Finally we have shown how the Columbia University quiescent evaporation resistance-surface pressure apparatus (Evaporimeter) is a valuable tool for specifying materials suitable for field tests in respect to many properties.

Acknowledgments

We thank Mr. M. Jefferis and Mr. J. Glickson for assistance with some of the experimental work.

We are indebted to the Bureau of Reclamation for financial assistance through Research Contract #14-06-D-4018 which was conducted in the laboratories of Mineral Engineering, Columbia University, and which supported the investigation which yielded the new data of 1963 obtained by one of us (T. W. H.) and which appears in the figures of this paper. It should be noted that the statements in this paper are solely the responsibility of the authors and are not be to construed as conveying the impression that the Bureau of Reclamation is in any way advocating one method of application or a particular apparatus or product over another.

References

1. La Mer, V. K., ed., "Retardation of Evaporation by Monolayers." Academic Press, New York, 1962.
2. Archer, R. J., and La Mer, V. K., *J. Phys. Chem.* **59**, 200 (1955).
3. Archer, R. J., and La Mer, V. K., *Ann. N. Y. Acad. Sci.* **58**, 807 (1954).
4. Rosano, H. L., and La Mer, V. K., *J. Phys. Chem.* **60**, 348 (1956).

5. BARNES, G. T., AND LA MER, V. K., *In* "Retardation of Evaporation by Monolayers," V. K. La Mer, ed., p. 9, 35, Academic Press, New York, 1962.
6. LA MER, V. K., AYLMORE, L. A. G., AND HEALY, T. W., *J. Phys. Chem.* **67,** 2793 (1963).
7. LA MER, V. K., AND AYLMORE, L. A. G., *Proc. Natl. Acad. Sci. U. S.* **48,** 316 (1962).
8. LANGMUIR, I., AND SCHAEFER, V. J., *J. Franklin Inst.* **235,** 119 (1943).
9. ROBBINS, M. L., AND LA MER, V. K., *J. Colloid Sci.* **15,** 123 (1960); LA MER, V. K., AND ROBBINS, M. L., *J. Phys. Chem.* **62,** 1291 (1958).
10. BLANK, M., AND LA MER, V. K., *In* V. K. LA MER, ed., "Retardation of Evaporation," p. 59. Academic Press, New York, 1962.
11. BROOKS, J. H., AND ALEXANDER, A. E., *In* V. K. LAMER, ed., "Retardation of Evaporation," p. 245. Academic Press, New York, 1962.
12. HEALY, T. W., AND LA MER, V. K., *J. Phys. Chem.* 1964 (In Press).

Reprinted without change of pagination from the
Proceedings of the Royal Society, A, *volume* 290, *pp.* 477–489, 1966

Surface and volume flow of single gases and of binary gas mixtures in a microporous carbon membrane

By L. A. G. Aylmore† and R. M. Barrer, F.R.S.

Physical Chemistry Laboratories, Chemistry Department, Imperial College, London, S.W. 7

(*Received* 27 *May* 1965)

Surface and volume flow have been studied in a microporous carbon membrane of high surface area for He, Ar, N_2, Kr and CO_2 and for the mixtures $Kr + N_2$ and $CO_2 + Kr$. Although the adsorption extended beyond the range in which Henry's law was valid, the permeability coefficient, K, remained independent of amount sorbed and isotherm curvature. For a given gas the permeability coefficient was also identical for the pure gas and for the gas in binary mixtures in which competitive adsorption was occurring. These results indicate that, in the range investigated, surface flow occurred by a random walk diffusion mechanism (surface hopping), rather than by a viscous flow mechanism. The products $K\sqrt{M}$ (M denoting molecular weight) show smooth correlations with parameters determining the adsorbability of the flowing gases.

1. Introduction

When an adsorbed gas flows through a microporous medium the presence of a mobile adsorbed film may greatly augment the flow (Flood 1952; Carman & Raal 1951; Kammermeyer & Rutz 1959; Haul and Peerbohms 1958; Gilliland, Baddour & Russell 1958; Ash, Barrer & Pope 1963). The mechanism of the additional flow is of considerable interest. Two extreme views are that surface flow occurs by a viscous, hydrodynamic mechanism only; or that this transport takes place by a diffusive, random walk mechanism only. In earlier studies in these laboratories the diffusion mechanism has been considered to be dominant for dilute adsorbed films, with the viscous flow mechanism dominating above monolayer coverage (Barrer 1963). However, in a recent review (Field, Watts & Weller 1963) it was considered that the viscous flow mechanism was dominant even for dilute adsorbed films approaching, or in, the range of Henry's law. By studying the surface flow of mixtures it should be possible to decide between these opposing views. If transport on the surface were entirely viscous in character the film should flow with no unmixing, as in Poiseuille flow. On the other hand, if transport in dilute films took place purely by a diffusion mechanism then each component should migrate independently of the others, as in Knudsen flow.

In this paper we report measurements of surface flow of single gases and of binary mixtures of these gases for adsorptions in or near the range of Henry's law. It was of interest, through these experiments, to attempt to elucidate the mechanism of surface migration, and to study the possibility of net interconversion of surface to gas-phase flux with increasing distance through the porous medium. Some evidence of flux interconversion has been obtained (Ash *et al.* 1963; Barrer 1963), but in each case partial blockage of gas-phase flow by the sorbed film appears to be

† Now in Department of Soil Science and Plant Nutrition, Institute of Agriculture, University of Western Australia, Nedlands, Western Australia.

at least partly responsible. It has not as yet been established whether other causes of flux interconversion exist, at what concentration of adsorbed molecules interconversion begins, and how general the phenomenon is.

2. Experimental

The gases used were spectrally pure helium, argon, nitrogen, krypton and carbon dioxide supplied by the British Oxygen Company. As porous medium a Carbolac carbon plug was prepared by compressing approximately 0·5 g increments of dry powder within a steel cylindrical container under a hydrostatic pressure of 50 000 Lb./in.^{2} for 60 s. It was hoped by this means to obtain greater uniformity of packing over the full length of the plug than is obtained by compaction in a single step. Before use the plug was outgassed for several days at 200 °C. Between flow runs outgassing overnight at 200 °C was found to be adequate.

Pure gas adsorption measurements using the standard volumetric procedure were carried out on the plug constrained between grooved plungers to prevent possible swelling and fracture, particularly at 90·2 °K. The comparisons between the 273 °K isotherms for pure nitrogen, krypton and carbon dioxide and the component gases in the mixture $Kr+N_2$ and CO_2+Kr were carried out on pieces of a similar plug constructed in an identical fashion to that used for the flow measurements. During the determination of the mixture isotherms the gas mixture was gently circulated within a closed system to prevent variations in mixture composition within stagnant regions due to preferential adsorption of one gas. Circulation was stopped only briefly during pressure measurement. Analysis of the gas mixtures was carried out by a thermal conductance method (Ash *et al.* 1963). The plug characteristics are:

length	$3{\cdot}10_2$ cm	estimated outgassed weight	0·599 g
diameter	$0{\cdot}47_6$ cm	porosity	0·497 cm^3/cm^3
cross-sectional area	0·180 cm^2	volume of plug	0·560 cm^3
weight of carbon	0·6574 g		

The specific surface area determined on the plug was 725 m^2/g (from the argon isotherm at 90·2 °K) to 735 m^2/g (from the nitrogen isotherm at 90·2 °K).

The diffusion cell was similar to that previously described (Ash *et al.* 1963) incorporating circulation of the ingoing gas within a closed system, and was operated under the following boundary conditions. The flow occurs in the x direction. Normal to this direction the porous medium is bounded by the planes $x = 0$ and $x = l$. The pressure at $x = 0$ was maintained constant during the experiment. The porous medium was free of gas before the experiment, and by the use of buffer volumes the pressure at the outgoing face during the experiment remained negligible compared with that maintained at the face of entry. There was no measurable change in plug characteristics over the period of experimentation.

3. Results

(*a*) *Helium flow*

This gas is often used as a non-sorbed calibrating gas for deriving the gas phase as distinct from the surface flow. The time lags, L, and the permeability coefficients, K_{He}, are seen from the results in table 1 to be independent of pressure. This means, in the case of the permeability, that the streamline flow component is negligible in the porous medium. The permeability is the integrated diffusion coefficient, i.e.

$$K_{\mathrm{He}} = \frac{1}{C'_0}\int_0^{C'_0} \epsilon D_{gs}^{\mathrm{He}}\, \mathrm{d}C'_g,$$

but since K_{He} is not dependent on C'_g neither is D_{gs}^{He}, so that $K_{\mathrm{He}}/\epsilon = D_{gs}^{\mathrm{He}}$. Here D_{gs}^{He} denotes the steady-state diffusion coefficient of helium, that is, the diffusion coefficient of helium in the channels involved in steady-state flow. C'_g is the gas-phase concentration in molecules per cm^3 and C'_0 is the value of C'_g at $x = 0$. ϵ is the porosity in cm^3 per cm^3.

From the time lags, assuming negligible adsorption, we can derive a time-lag diffusion coefficient D_g^{He} from the relation

$$D_g^{\mathrm{He}} = l^2/6L. \tag{1}$$

Values of D_g^{He} are given in table 1, and are a little larger than $D_{gs}^{\mathrm{He}} = 2{\cdot}9 \times 10^{-3}$ cm^2/s.

Table 1. Flow measurements with helium at 273 °K

ingoing pressure (cmHg)	time lag, L (min)	$10^3 D_g^{\mathrm{He}}$ (cm^2/s)	flux, J (erg/s)	permeability, $10^3 K_{\mathrm{He}}$ (cm^2/s)
5·29	7·8	3·4	5·81	1·43
5·82	7·8	3·4	6·48	1·44
10·04	8·0	3·3	10·94	1·42
15·85	7·9	3·4	17·69	1·44
16·12	7·9	3·4	17·80	1·43
20·27	7·9	3·4	22·25	1·43

From the helium data we may derive the values of K which would be found for other gases at temperature T °K, if there were no surface flow, i.e.

$$K = K_{\mathrm{He}}\left(\frac{T}{273}\,\frac{M_{\mathrm{He}}}{M}\right)^{\frac{1}{2}}, \tag{2}$$

where the M's are the molecular weights. Similarly for the time lags if there were no adsorption or surface flow

$$L = L_{\mathrm{He}}\left(\frac{273}{T}\,\frac{M}{M_{\mathrm{He}}}\right)^{\frac{1}{2}}. \tag{3}$$

Deviations from these values for K and L therefore indicate surface flow, or (for L) adsorption and surface flow.

(b) Adsorption constants

From the adsorption isotherms the Henry's law adsorption constants could be derived at 273, 298 and 323 °K for Ar, N_2 and Kr. These constants defined as

$$k_s = \frac{\text{molecules per cm}^2 \text{ of surface } (C_s')}{\text{molecules per cm}^3 \text{ of gas phase } (C_g')},$$

TABLE 2. HENRY'S LAW ADSORPTION CONSTANTS

gas	$10^7 k_s$ at 273 °K	$10^7 k_s$ at 298 °K	$10^7 k_s$ at 323 °K	$-\Delta E$ (kcal/mole)	$-\Delta H$ (kcal/mole)
Ar	$8{\cdot}3_2$	$5{\cdot}9_1$	$4{\cdot}5_6$	$2{\cdot}1_3$	$2{\cdot}7_3$
N_2	$9{\cdot}4_3$	$6{\cdot}3_8$	$4{\cdot}5_6$	$2{\cdot}5_7$	$3{\cdot}1_7$
Kr	47·1	35·6	$15{\cdot}1_5$	$4{\cdot}0_1$	$4{\cdot}6_1$
CO_2	—	—	—	$5{\cdot}3_5$	$5{\cdot}9_5$

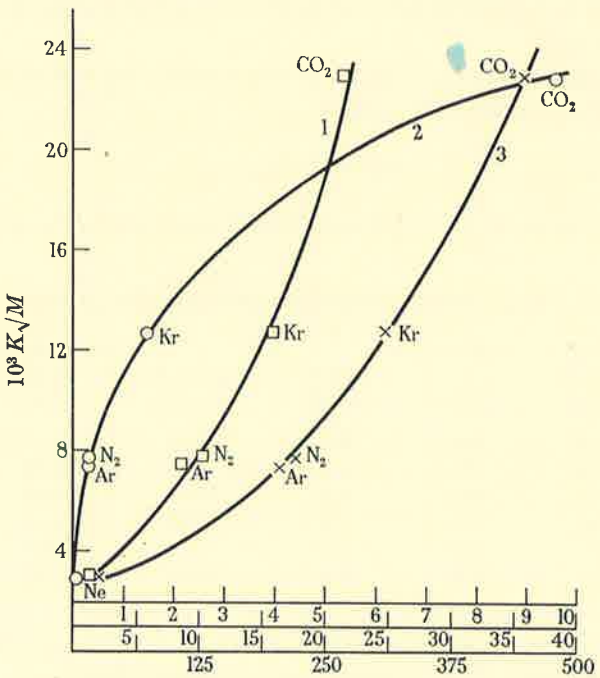

top scale and curve 1, $-\Delta E$ (kcal/mole)
middle scale and curve 3, $10^{25}\alpha$ (cm³ per molecule)
bottom scale and curve 2, Ak_s/ϵ

FIGURE 1. Correlations between $K\sqrt{M}$ at 0 °C and quantities related to sorbability.

where C_s' denotes the surface concentration in molecules per cm², are given in table 2, together with the corresponding energy (ΔE) and enthalpy (ΔH) values given respectively by

$$-\Delta E = 4{\cdot}60 \frac{\partial \ln k_s}{\partial (1/T)}$$

and

$$\Delta H = \Delta E + P\Delta V \sim \Delta E - RT.$$

The values of k_s are very similar to corresponding values obtained previously for adsorption on Carbolac carbon plugs of comparable porosity (Barrer & Strachan 1955). This is also true of the energies and entropies of sorption.

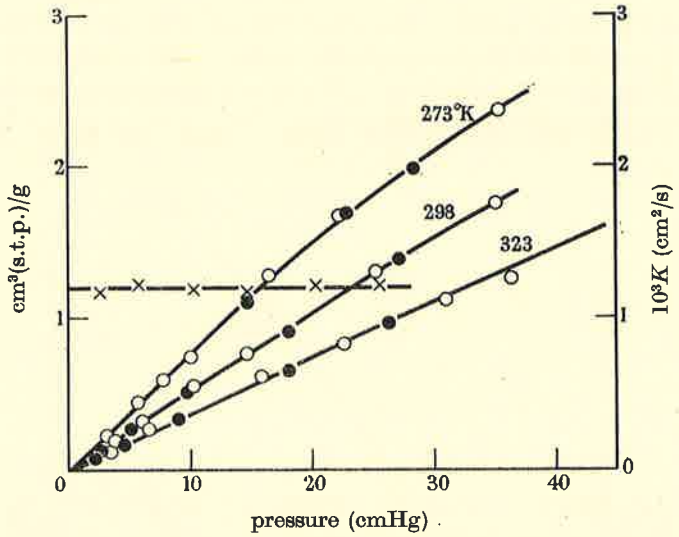

FIGURE 2. Isotherms of argon on the carbon plug at 273, 298 and 323 °K (○, sorption; ●, desorption); and permeability coefficient at 273 °K as a function of pressure (points ×).

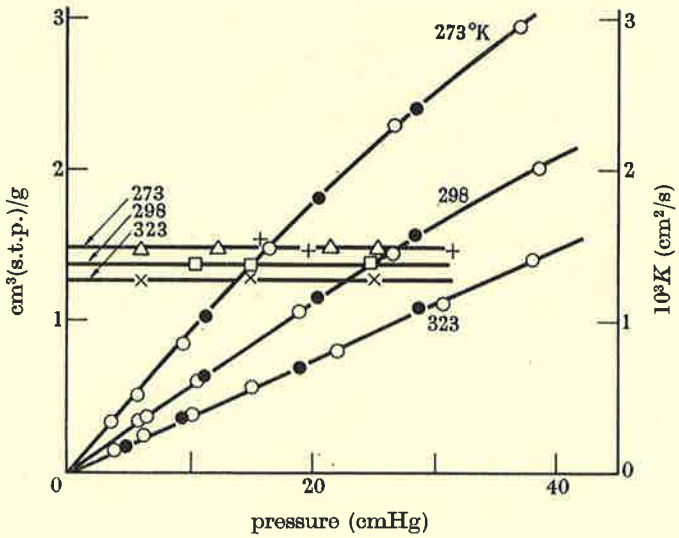

FIGURE 3. Isotherms of nitrogen on the plug at 273, 298 and 323 °K; and permeability coefficients at these temperatures as functions of pressure, for pure nitrogen and (at 273 °K) for nitrogen in krypton. Isotherms: ○, sorption; ●, desorption. K values: Δ, pure N_2 at 273 °K; +, N_2 in Kr at 273 °K; □, pure N_2 at 298 °K; ×, pure N_2 at 323 °K.

(c) *Flow of adsorbed gases*

There is significant adsorption of Ar, N_2 and Kr, and of carbon dioxide, as shown from the Henry's law constants of table 2 and from the isotherms of figures 2 to 4.

That this adsorption results in a considerable surface flux is clearly shown from plots of $K\sqrt{M}$ against Ak_s/ϵ (a parameter characterizing the total sorption); against $-\Delta E$; and against the polarizabilities, α (important in governing the dispersion interaction between sorbate and sorbent). If there were no surface flow $K\sqrt{M}$ would be constant for all gases at the same temperature; as it is, $K\sqrt{M}$ increases with increasing sorbability (figure 1) whether Ak_s/ϵ, $-\Delta E$ or α is used to assess this. In the extreme case of carbon dioxide $K\sqrt{M}$ is about eight times its value for helium; while for krypton the ratio is more than four.

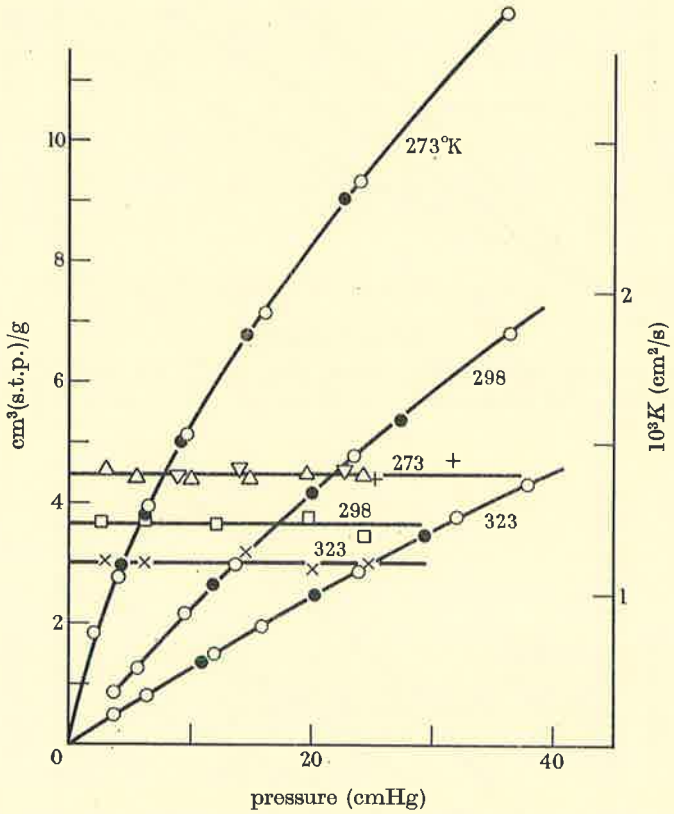

FIGURE 4. Isotherms of krypton on the plug at 273, 298 and 323 °K; and permeability coefficients at these temperatures as functions of pressure, for pure krypton, and (at 273 °K) for krypton in carbon dioxide and in nitrogen. Isotherms: ○, sorption; ●, desorption. K values: Δ, pure Kr at 273 °K; +, Kr in CO_2 at 273 °K; ▽, Kr in N_2 at 273 °K; □, pure Kr at 298 °K; ×, pure Kr at 323 °K.

(*d*) *Permeability coefficient and isotherms*

The isotherms for pure Ar, N_2, Kr and CO_2 are shown in figures 2 to 5 together with the permeability coefficients obtained for the gases both as single gases and as components of binary mixtures. In figures 6 and 7 respectively the 273 °K isotherms of the component gases in the mixtures $Kr + N_2$ and $CO_2 + Kr$ are compared with each other and with the isotherms of each pure component. For the mixture isotherms successive points on the isotherm of one component correspond to the

presence of the second component as indicated by successive points on the other isotherm, from the lowest partial pressures upwards. From the results presented in these figures several conclusions may be drawn:

(i) The permeability coefficients for combined surface and gas-phase transport in the ranges investigated are independent of pressure and amount sorbed.

(ii) These coefficients are not changed when the isotherms become curved.

(iii) The permeability coefficients for N_2, Kr and CO_2 in the mixtures N_2+Kr and CO_2+Kr remain the same as when the respective pure gases are flowing through the medium, despite the decrease in sorption of each component in the mixture.

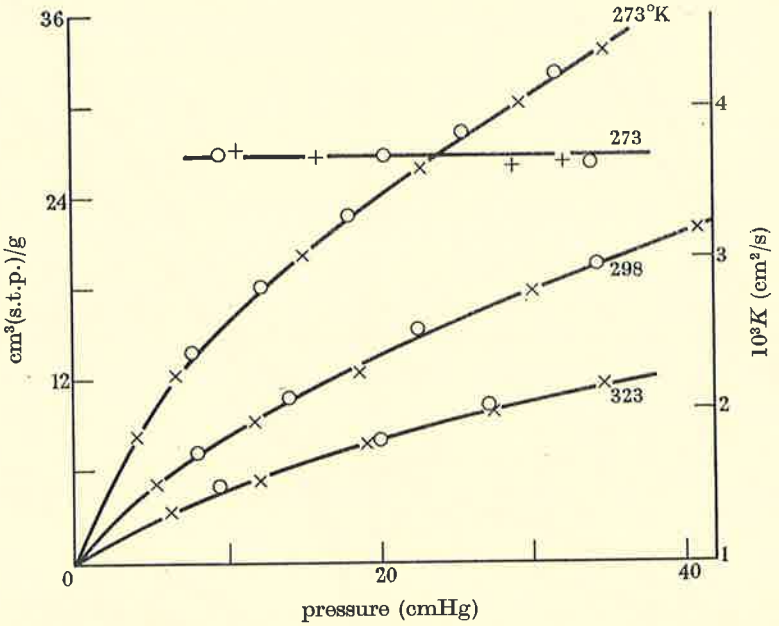

FIGURE 5. Isotherms of carbon dioxide on the plug at 273, 298 and 323 °K, and permeability coefficients of pure carbon dioxide (○) and of carbon dioxide in krypton (+) at 273 °K. Isotherms: ×, sorption; ●, desorption.

A possible exception to (i) and (ii) above is a slight decrease in permeability coefficient with pressure shown for pure CO_2 particularly at higher pressures. This is not apparent for the CO_2 component of the mixture, but these measurements are subject to greater variation than is the case for the runs for the pure gas.

The permeability coefficients of argon, nitrogen and krypton, determined at 273, 298 and 323 °K, show negative temperature coefficients, which can be understood in terms of a decreasing population of adsorbed molecules as the temperature rises.

4. Discussion

The significance of these results and conclusions may be considered further.

(*a*) *The permeability coefficients*

The total flux, J, can be divided in two ways. Through any cross-section there is the flux J'_s which is *only* on the surface and the flux J'_g which is *only* in the gas phase.

However, the total 'surface' flux, J_s, created by the existence of a mobile adsorbed film is partly in the gas phase and partly on the surface through any cross-section (Barrer & Gabor 1960), and the remaining gas-phase flow, J_g, is that estimated by the helium calibration method i.e. at equal pressures

$$J_g = J_g^{\mathrm{He}}(M_{\mathrm{He}}/M)^{\frac{1}{2}}$$

Then

$$J = J'_g + J'_s = J_g + J_s, \tag{4}$$

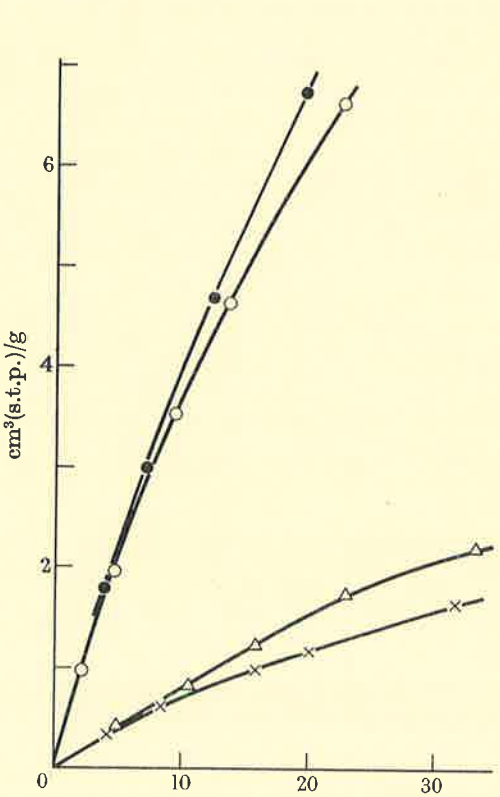

FIGURE 6

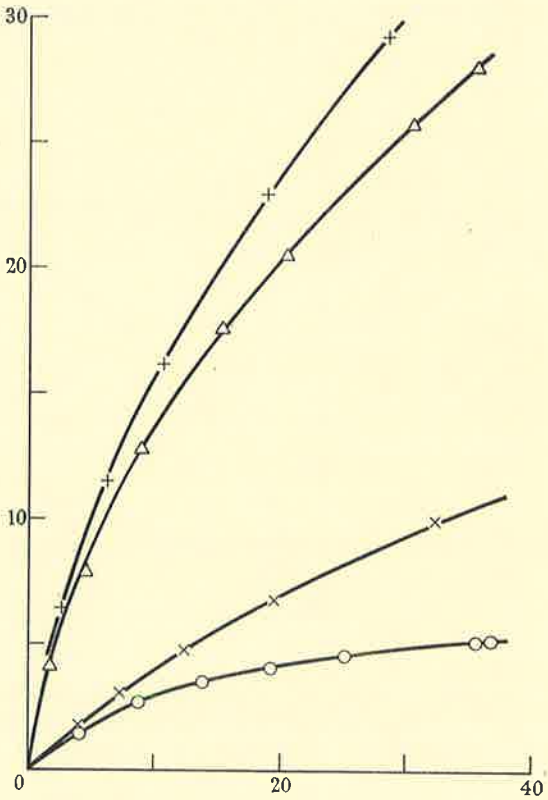

pressure or partial pressure (cmHg)

FIGURE 7

FIGURE 6. Comparison of isotherms of krypton and nitrogen as pure gases and in their mixtures, on the plug at 273 °K. ●, Pure krypton; ○, krypton in presence of nitrogen; △, pure nitrogen; ×, nitrogen in presence of krypton.

FIGURE 7. Comparison of isotherms of carbon dioxide and krypton as pure gases and in their mixtures, on the plug at 273 °K. +, Pure carbon dioxide; ∠, carbon dioxide in presence of krypton; ×, pure krypton; ○, krypton in presence of carbon dioxide.

where $J'_g > J_g$ and $J_s > J'_s$. In terms of Fick's law, if C_g and C_s are the numbers of molecules per cm³ of porous medium in the gas phase and on the surface respectively, (4) can formally be written in the steady state and per unit cross-section as

$$J = -\left(D'_{gs}\frac{\mathrm{d}C_g}{\mathrm{d}x} + D'_{ss}\frac{\mathrm{d}C_s}{\mathrm{d}x}\right) = -\left(D_{gs}\frac{\mathrm{d}C_g}{\mathrm{d}x} + D_{ss}\frac{\mathrm{d}C_s}{\mathrm{d}x}\right). \tag{5}$$

D'_{gs} and D'_{ss} are the steady-state diffusion coefficients relevant to J'_g and J'_s, and D_{gs} and D_{ss} are those appropriate for J_g and J_s. By integrating (5) from $x = 0$ to $x = l$ we obtain

$$Jl = \int_0^C \left(\epsilon D'_{gs} + D'_{ss}\frac{dC_s}{dC'_g}\right) dC'_g = \int_0^{C'_0} \left(\epsilon D_{gs} + D_{ss}\frac{dC_s}{dC'_g}\right) dC'_g. \tag{6}$$

The permeability coefficient, K, is however defined as before by $C'_0 K = Jl$, and so if (6) is written with $C'_0 K$ replacing Jl and is differentiated with respect to C'_0,

$$K = \left(\epsilon D'_{gs} + D'_{ss}\frac{dC_s}{dC'_g}\right)_{x=0} = \left(\epsilon D_{gs} + D_{ss}\frac{dC_s}{dC'_g}\right)_{x=0} \tag{7}$$

since K is constant (figures 2 to 5). Thus the bracketed terms in (7) are each constant. Since, moreover, the helium permeability coefficient is independent of concentration, D_{gs} or D'_{gs} will also be expected to be independent of concentration for gases other than helium. It follows that

$$D'_{ss}\frac{dC_s}{dC'_g} = K - \epsilon D'_{gs} = \text{constant (absolute surface permeability coefficient } K'_s),$$

and

$$D_{ss}\frac{dC_s}{dC'_g} = K - \epsilon D_{gs} = \text{constant (helium method surface permeability coefficient } K_s).$$

Therefore D'_{ss} and D_{ss} each have the same concentration dependence which is compensated by the isotherm slope, dC_s/dC'_g. This property has been shown to follow if there is no net interconversion of J'_s and J'_g as x increases (Barrer 1963) (J_g and J_s are each necessarily independent of x). Our results accordingly imply that J'_s and J'_g do not vary with x.

There is a further consequence of the constancy of K'_s or K_s. At any given pressure it can be seen from figures 6 and 7 that the slope of the isotherm for the pure gas exceeds that of the isotherm of the same gas when admixed with another which is competitively adsorbed. Since, however,

$$D^0_{ss} A k_s = \left[D_{ss}\frac{dC_s}{dC'_g}\right]^{\text{pure Ar}}_{C'_g = C'_0} = \left[D_{ss}\frac{dC_s}{dC'_g}\right]^{\text{Ar in mixture}}_{C'_g = C'_0}, \tag{8}$$

it follows that in the mixture D_{ss} has increased as compared with D_{ss} for the pure gas. A similar conclusion holds for D'_{ss}. In the range of Henry's law D_{ss} has the same value, D^0_{ss}, for pure Ar, and Ar in the mixture, because the Henry's law constant, k_s, is the same in both cases.

(*b*) *Mechanism of surface flow*

The surface permeability coefficient K (or K'_s) for any one gas has been shown over the range investigated here to be characteristic for each gas; independent of the amount sorbed and therefore of whether the isotherm obeys Henry's law or is curved; and unaltered when there is a second flowing, adsorbed species competing for the same surface (§ 3 (*d*)). This behaviour is fully compatible with a diffusion mechanism of surface migration in which each species upon activation moves along

the surface by a series of hops, the permeability coefficients having values independent of those of another species migrating simultaneously. It is not in agreement with a viscous flow mechanism of transport, analogous to Poiseuille flow, for this should give a surface flow rate J_s, and permeability coefficient K_s, characteristic of the mixed film as a whole. As sorption approaches and passes the monolayer value, one would expect viscous flow to become of significance, although it is of interest that even when liquid mixtures flow through Vycor porous glass, some unmixing of the components occurs (Kammermeyer & Hagerbaumer 1955). Evidently not even then is there the same permeability coefficient for all the components in the mixture.

TABLE 3. $\lambda^s_{12}/\lambda^s_{11}$ FOR CO_2 AND Kr AT 273 °K IN THE CO_2 + Kr MIXTURES

p_{CO_2} (cmHg)	p_{Kr} (cmHg)	$(\lambda^s_{12}/\lambda^s_{11})_{CO_2}$	$(\lambda^s_{12}/\lambda^s_{22})_{Kr}$
1·7	4·0	0·122	0·180
3·6	8·8	0·134	$0{\cdot}33_3$
9·0	14·0	0·142	$0{\cdot}48_5$
15·4	19·3	0·152	$0{\cdot}63_4$
20·6	25·2	0·170	0·78
30·7	35·6	0·191	1·06

It is possible to discuss surface migration in mixtures usefully in terms of the phenomenological coefficients of the irreversible thermodynamic formulation. For simultaneous surface and gas-phase flow of one component in a binary mixture (Barrer 1963)

$$K = RT\{(\lambda^s_{11}+\lambda^s_{12})(C_s/C'_g)_m + (\epsilon - Ad)(\lambda^g_{11}+\lambda^g_{12})\}, \tag{9}$$

while for this component flowing in the pure state

$$K = RT\{\lambda^s_{11}(C_s/C'_g) + (\epsilon - Ad)\lambda^g_{11}\}_{x=0}. \tag{10}$$

The subscript m in (9) refers to the mixture: d is the thickness of a monolayer, and thus Ad is effectively the sorption volume per cm³ of medium below monolayer coverage (Barrer 1963). Then $(\epsilon - Ad)$ is the volume available for gas-phase flow per cm³ of medium. λ^s_{11} and λ^g_{11} are the phenomenological coefficients for surface and gas-phase flow of component 1 and λ^s_{12} and λ^g_{12} are the corresponding cross-coefficients. Experimentally we have established that K in (9) and (10) is the same, so that at $x = 0$

$$\lambda^s_{11} = \left\{\lambda^s_{12}\left(\frac{C_s}{C'_g}\right)_m + (\epsilon - Ad)\lambda^g_{12}\right\} \Big/ \left\{\frac{C_s}{C'_g} - \left(\frac{C_s}{C'_g}\right)_m\right\}.$$

However, λ^g_{12} must depend on molecular collisions between components 1 and 2 in the gas phase. When the mean free path is much larger than $2\epsilon/A$ the number of such collisions must be negligible compared with the number of molecule-wall collisions, which in turn will then determine λ^g_{11}. Thus, in (9) we expect $\lambda^g_{12} \ll \lambda_{11}$, and so at $x = 0$ and for the same value of C'_g,

$$\frac{\lambda^s_{12}}{\lambda^s_{11}} = \left\{\frac{C_s}{(C_s)_m} - 1\right\}.$$

In the particular Kr + CO_2 mixtures we have studied the ratios of λ^s_{12} to λ^s_{11} and of λ^s_{12} to λ^s_{22} can therefore be calculated for each component. Values of these ratios are given in table 3. As expected, they become small as the Henry's law range is approached. These ratios are larger for Kr than for CO_2, reflecting the greater interference of CO_2 with the sorption of Kr than conversely. One would expect λ^s_{12} to be determined mainly by collisions of adsorbed molecules of component 1 with component 2, while λ^s_{11} should be determined mainly by collisions between pairs of adsorbed molecules of component 1 and vibrational collisions of these molecules with surface atoms of the carbon.

(c) *Numerical analysis of flow measurements*

Terms in (10) are to be identified with those in (7) as follows:

$$\left.\begin{aligned} RT(\epsilon - Ad)\lambda^g_{11} &= \epsilon D'_{gs}, \\ RT\lambda^s_{11}\frac{C_s}{C'_g} &= D'_{ss}\frac{\mathrm{d}C_s}{\mathrm{d}C'_g}. \end{aligned}\right\} \tag{11}$$

However, no general method exists for evaluating D'_{gs} or D'_{ss} (Barrer 1963). On the other hand, the helium calibration method readily gives D_{gs} and D_{ss}. An analysis of the results is therefore given using the method of Barrer & Gabor (1959). In this procedure the permeability coefficient was defined as

$$K_1 = \frac{K}{\epsilon} = \frac{Jl}{\epsilon C'_0} \tag{12}$$

and in the Henry's law range K_1 was expressed as

$$K_1 = D_{gs} + D_{ss}\frac{A_s k_s}{\epsilon_s} = D_{gs} + \frac{D_{ss}}{\beta}\frac{Ak_s}{\epsilon}. \tag{13}$$

Here A_s and ϵ_s are the surface area and pore volume involved in steady-state flow (and so do not include blind pores), and $\beta = A_s\epsilon/\epsilon_s A$. It should then be noted, in comparing (13) and (5) that in (5), β is included in D_{ss} which also has its limiting value appropriate to adsorption obeying Henry's law.

The results of the analysis are presented in table 4. D_s and D_g are surface and gas phase diffusion coefficients based on the time-lag measurements, still using helium as calibrating gas (Barrer & Gabor 1959). The time lags for krypton at 273 °K decreased appreciably with increasing pressure, but all other values given were effectively constant for each gas at a particular temperature. $D^{\mathrm{cyl.}}_g$ is the Knudsen diffusion coefficient in a cylindrical capillary having ϵ/A equal to that of the actual porous medium. It is given by

$$D^{\mathrm{cyl.}}_g = \frac{8}{3}\frac{\epsilon}{A}\left(\frac{2RT}{\pi M}\right)^{\frac{1}{2}}, \tag{14}$$

and serves as a reference value with which to compare D_g and D_{gs} in the actual porous medium. The structure factors κ are then defined by

$$\left.\begin{aligned} D_g &= \kappa_g D^{\mathrm{cyl.}}_g, & D_s &= \kappa_s D^{\mathrm{cyl.}}_s; \\ D_{gs} &= \kappa_{gs}\beta\,.\,D^{\mathrm{cyl.}}_g, & D_{ss} &= \kappa_{ss}\beta\,.\,D^{\mathrm{cyl.}}_s. \end{aligned}\right\} \tag{15}$$

Because no certain value can be given to $D_s^{cyl.}$, the surface diffusion coefficient on the perfectly smooth wall of the reference capillary, only the ratio κ_s/κ_{ss} can be found.

TABLE 4. ANALYSIS OF FLOW AND TIME-LAG DATA FOR Kr, N_2 AND A BY METHOD OF BARRER & GABOR (1959). POROSITY OF PLUG = 0·49$_7$, ϵ/A = 6·4 Å

gas	Kr			N_2			Ar		
T (°K) ...	273	298	323	273	298	323	273	298	323
average L (min)	720*	430	285	125	92	64	140	98	77
$10^3 D_g^{cyl.}$ (cm²/s)	2·24	2·36	2·44	3·86	4·04	4·21	3·24	3·38	3·53
$10^3 D_g$ (cm²/s)	0·740	0·771	0·804	1·27	1·33	1·38	1·07	1·110	1·156
$10^3 D_s$ (cm²/s)	0·0277	0·0445	0·0643	0·142	0·187	0·281	0·127	0·182	0·234
$10^3 D_{gs}$ (cm²/s)	0·634	0·664	0·691	1·096	1·148	1·195	0·917	0·961	1·00
$10^3 D_{ss}/\beta$ (cm²/s)	0·0292	0·0452	0·0639	0·125	0·159	0·191	0·109	0·137	0·156
κ_g	0·330	0·330	0·330	0·330	0·330	0·330	0·330	0·329	0·328
$\kappa_{gs}\beta$	0·283	0·281	0·284	0·283	0·284	0·284	0·283	0·284	0·283
κ_{ss}/κ_s	1·054	1·015	0·995	0·884	0·855	0·680	0·862	0·752	0·667
D_g/D_{gs}	1·16	1·16	1·16	1·16	1·16	1·16	1·16	1·16	1·16
$D_s k_s A/D_g \epsilon$	2·77	2·32	1·90	1·64	1·41	1·46	1·56	1·52	1·45
$D_{ss} k_s A/D_{gs} \epsilon\beta$	3·40	2·74	2·20	1·69	1·38	1·14	1·64	1·32	1·12
$k_s A/\epsilon$	73·9	40·2	23·75	14·8	10·0	7·15	13·1	9·27	7·15

* Obtained by extrapolation of L against p to zero pressure.

The present plug gives considerably smaller structure factors than those previously found (Barrer & Gabor 1959) for two plugs made from the same carbon (Barrer & Strachan 1955), having respectively $\epsilon = 0{\cdot}37$, and $\epsilon/A = 3{\cdot}0$ Å; $\epsilon = 0{\cdot}64$ and $\epsilon/A = 9{\cdot}3$ Å. The permeability of porous media made by compaction is not readily reproducible even for plugs compressed to the same porosity. From their mode of compaction the above two plugs were expected to be less uniform in texture throughout their lengths than that used in the present study. The small structure factors κ_g and $\kappa_{gs}\beta$ (table 3, lines 7 and 8) suggest tortuous conduction channels or channels with bottlenecks.

In addition to these geometrical considerations, however, the mechanism of flow in the porous medium is somewhat altered as compared with that in a long, straight capillary. Weber (1954) has emphasized three components which determine D_g or D_{gs}. There is a Knudsen flow component (self-diffusion down a pressure gradient); a slip component (conduction flow); and a stream-line flow component. As already noted, the latter is negligible in this work. In tortuous channels the Knudsen value of $D_g^{cyl.}$ is reduced, as shown by Hiby & Pahl (1956), because the maximum lengths of axial molecular flights are reduced by the tortuosity. Also the slip component, when expressed by an equation analogous to (14), has a smaller numerical coefficient than 8/3. These considerations, therefore, like the geometrical ones of the previous paragraph, will result in values of κ_g and $\kappa_{gs}\beta$ less than one. Nevertheless it is also possible for these structure factors to approach or exceed unity if some flow channels are unusually wide and so contribute a large part of the total transport (Barrer & Gabor 1959).

The ratio D_g/D_{gs} (table 4, line 10) is close to unity, implying similarity of the pore geometry of the conducting channel system involved during the transient time-lag period (D_g) and the somewhat different (Barrer & Gabor 1959) system involved in steady-state flow (D_{gs}). This similarity is further emphasized by the similar magnitudes of J_s/J_g for the two states (lines 11 and 12). In each state of flow the 'surface' flow assessed by the helium method exceeds the gas-phase flow. Finally, in line 13, $k_s A/\epsilon$ is a measure of the ratio of the total numbers of molecules within the porous medium which are on the surface and in the gas phase, in the range in which Henry's law is valid. Since C'_s in the expression $k_s = C'_s/C'_g$ should be the absolute number of molecules on the surface per unit area, whereas the adsorption measurements give only the surface excess, unity must be added to $k_s A/\epsilon$ as given in the table to make this measure quantitatively the ratio of the previous sentence.

5. Conclusion

This investigation shows that the combined study of transport of pure gases and of mixtures of these gases through a microporous medium, can give valuable information regarding the nature of surface flow. The independence of the permeability coefficients of isotherm curvatures and gas pressures means that the ratio of gas phase to surface flow remains constant throughout the medium, i.e. there is no interconversion of fluxes. The measurements made, however, still refer to relatively dilute adsorbed films. As one approaches monolayer coverage flux interconversion can be expected through blockage of gas-phase flow by the adsorbed film, particularly near the ingoing surface. Moreover, as monolayer coverage is replaced by denser, multilayer film or capillary condensate, one must expect the diffusive mechanism to become in part a viscous flow mechanism. Intermediate regions of coverage therefore remain for further investigation of the relative importance of the two surface-flow mechanisms.

We are indebted to Mr R. Ash of this department for helpful criticism and comment.

References

Ash, R., Barrer, R. M. & Pope, C. G. 1963 *Proc. Roy. Soc.* A, **271**, 1, 19.
Barrer, R. M. 1963 *Canad. J. Chem.* **41**, 1768.
Barrer, R. M. & Gabor, T. 1959 *Proc. Roy. Soc.* A, **251**, 353.
Barrer, R. M. & Gabor, T. 1960 *Proc. Roy. Soc.* A, **256**, 267.
Barrer, R. M. & Strachan, E. 1955 *Proc. Roy. Soc.* A, **231**, 353.
Carman, P. C. & Raal, F. A. 1951 *Proc. Roy. Soc.* A, **209**, 38.
Field, G. J., Watts, H. & Weller, K. R. 1963 *Rev. Pure Appl. Chem.* **13**, 2.
Flood, E. A., Romlinson, R. H. & Leger, A. E. 1952 *Canad. J. Chem.* **30**, 389.
Gilliland, E. R., Baddour, R. F. & Russell, J. L. 1958 *A.I.Ch.E.Jl.* **4**, 90.
Haul, R. & Peerbohms, R. 1958 *Naturwissenschaften*, **45**, 109.
Hiby, J. W. & Pahl, M. 1956 *Z. Naturforsch.*, **11***a*, 80.
Kammermeyer, K. & Hagerbaumer, D. H. 1955 *A.I.Ch.E.Jl*, **1**, 215.
Kammermeyer, K. & Rutz, L. O. 1959 *Chem. Eng. Progr. Symp. Ser.*, no. 24, **55**, 163.
Weber, S. 1954 *K. Mat. fys. Medd.* **28**, no. 2.

SOIL SCIENCE
Vol. 102, No. 5

Printed in U.S.A.

ADSORPTION OF WATER AND ELECTROLYTE SOLUTIONS BY KAOLIN CLAY SYSTEMS

L. A. G. AYLMORE AND J. P. QUIRK

University of Western Australia[1]

Received for publication December 13, 1965

The mineral kaolin has many industrial applications (18) in addition to its agricultural importance as a major constituent of many soils. In both fields its interaction with water and electrolytes plays a dominant role in determining its behavior characteristics.

Several investigators (11–13, 16) have studied the water vapor sorption characteristics of homoionic kaolins with particular reference to the variation of the sorption isotherms with exchangeable cation. Considerable information has also been obtained concerning the electrical charge distribution in proximity to the kaolin crystals and their consequent dispersion characteristics in aqueous suspension (10, 19, 21). The present paper is concerned with the swelling behavior of kaolin clay systems in the intermediate region between these extremes of hydration, that is under conditions encountered by natural soil materials in nature. In this region the clay crystals are in close juxtaposition. Initially, water adsorption by the porous matrix is controlled mainly by surface-adsorption and surface-tension forces. As saturation is approached, a gradual transition occurs to equilibrium governed by the balance between repulsive forces attributed to the formation of diffuse distributions of the exchangeable cations associated with the clay crystals, and electrical attractions and other bonding mechanisms within the matrix.

Although the swelling behavior of soils containing predominantly mica-like minerals has been examined in some detail (6, 9), this region of hydration, which determines to a large extent the structural characteristics of soils largely containing kaolin has as yet received little attention.

EXPERIMENTAL AND MATERIALS

Homoionic samples of the $<2\ \mu$ fraction of a number of kaolinite clays and one halloysite clay were obtained by repeated washing and centrifuging, using a molar solution of the appropriate chloride. At least two of these washes contained 10^{-3} N hydrochloric acid to facilitate the removal of aluminum ions from exchange sites. After washing and dialyzing with distilled water, the clays were allowed to air-dry before being gently ground to a powder. These powders were placed in a vacuum desiccator over a saturated solution of potassium sulfate, giving a relative vapor pressure of 0.96 at 20°C., and allowed to equilibrate. Samples (400 mg. each) of the clays were then placed in a stainless steel mold and compressed to 1200 atmospheres pressure by means of an hydraulic jack (2). The small clay cores produced in this manner were used for all subsequent experimental determinations.

Solution-content–suction data for these materials were obtained by means of perspex-ceramic pressure plates, brass pressure membrane chambers using cellulose casing and vacuum desiccators containing saturated salt solutions, to provide a range of constant water vapor pressures[2]. This equipment was set up in a laboratory maintained at a temperature of 20°C. ± ¼°C. Core volumes were obtained by direct measurement of core dimensions, using a traveling microscope in the region where the cores were not completely saturated with solution and a displacement technique for the saturated cores (15). Equilibrium of the cores with a given suction was usually attained within 2 to 3 days but, in general, 5 days were allowed.

Cation-exchange capacities were determined by strontium-saturating the clays, using strontium bromide and determining the strontium content by x-ray spectrography. Surface areas of the clay cores were obtained by application of the BET (3) theory to measurement of nitrogen adsorption at low temperature by the standard volumetric procedure.

[1] Institute of Agriculture, Nedlands, Australia.

[2] L. A. G. Aylmore, Ph.D. thesis, University of Adelaide, 1960.

The kaolin clays were obtained from the following sources:

Rocky Gully kaolinite. From pallid zone of laterite, Rocky Gully, Western Australia.

Merck I kaolinite. From Merck Chemical Company, Germany: labeled DAB-6.

Merck II kaolinite. Colloidal kaolinite from Merck Chemical Company, U.S.A.

New Zealand kaolinite. Hydrothermal kaolinite, supplied by Ceramic Research Section, D.S.I.R., New Zealand.

Malone kaolinite. From Malone, Victoria, Australia: supplied by the Ceramic Section, Chemical Research Laboratories, C.S.I.R.O. Victoria, Australia.

Eureka halloysite. From Eureka, Utah: supplied by Wards Natural Science Museum, U.S.A.: preheated to 110°C. to remove intracrystalline water.

Eureka halloysite contained an appreciable amount of gibbsite, but only a very small amount was detected in the Rocky Gully kaolinite by x-ray examination, and none was detected in the remaining clays.

RESULTS AND DISCUSSION

The BET nitrogen specific surface areas, exchange capacities, surface densities of charge, and porosities of the compressed cores are given in table 1. The exchange capacity of the Merck I kaolin is very high in relation to its specific surface area, and subsequent x-ray examination revealed the presence of a small amount of montmorillonite impurity (<5%) in this sample.

The effect of electrolyte concentration and exchangeable cation on the solution contents of the kaolin on wetting to 10 millibars suction is shown in table 2. Although kaolin clay systems are frequently referred to as non-swelling, it is apparent from this table that appreciable swelling can occur and that wide variations in behavior are possible. Volume increases ranging from 6.7 per cent for the Eureka halloysite cores to 145 per cent for the Merck I kaolinite occur, with increases of approximately 30 per cent or less for the remaining clays. With the exception of Merck I kaolin, the outstanding feature of this table, however, is the complete lack of correlation between the solution contents obtained at this low suction and both specific surface areas and electrolyte concentration such as would be expected from surface adsorption and osmotic considerations arising from diffuse distributions of the exchangeable cations at the solid-liquid interface (20).

TABLE 1

Data for kaolin clay cores

Clay	Specific Surface Area ($m.^2/g.$)	Exchange Capacity (*me./100g.*)	Surface Density of Charge ($esu \times 10^4/cm.^2$)	Porosity (*cc./g.*)
Rocky Gully kaolinite	36.3	4.0	3.19	0.185
Merck I kaolinite	11.5	7.0	17.6	0.188
Merck II kaolinite	11.2	2.1	5.42	0.196
Malone kaolinite	17.4	4.3	7.15	0.189
New Zealand kaolinite	40.2	3.3	2.37	0.259
Eureka halloysite	109.8	7.7	2.03	0.189

Eureka halloysite shows almost negligible swelling, and in view of its large specific surface area and consequent small particle size, the rigidity of this material, even when saturated with monovalent ions, indicates the existence of very strong binding forces between individual clay particles.

The remainder of the kaolins, excluding Merck I, exhibit a limited amount of swelling with varying small dependence on the exchangeable cation present. The Rocky Gully cores (fig. 1) describe approximately the same water-content–energy curves on wetting and drying regardless of the exchangeable cation present, and behave rather like rigid structured materials whose pores fill and empty in the vicinity of 10^5 millibars suction corresponding to equivalent cylindrical pore radii in excess of 100 A. At lower-suction values there is a relatively small swelling accompanied by a narrow hysteresis between wetting and drying curves.

Since there is no apparent correlation between swelling and specific surface areas, it would seem that the total uptake of solutions by these materials is determined more by the structural strength of the system than by the physico-chemical development of diffuse double layers associated with the clay surfaces. This is in marked contrast to the 2:1 layer lattice alumino-silicate clay minerals which, in general, exhibit extensive swelling for sodium systems, at least qualitatively consistent with the formation of diffuse distributions of the exchangeable cations, but only limited swelling for divalent systems (2). For example, from Schofield's equation (20) the calculated theoretical value of

TABLE 2

Effect of electrolyte concentration and exchangeable cation on solution content of kaolins on wetting to 10 millibars suction

Clay	4M	M	$\frac{M}{4}$	$\frac{M}{10}$	$\frac{M}{100}$	Distilled Water	Calculated Average Film Thickness in Distilled Water* (A.)
	cc./ 100 g.						
Rocky Gully							
Na^+	—	37.3	35.3	35.1	35.1	35.5	98
K^+	—	—	—	—	—	34.0	95
Ca^{++}	38.6	36.2	—	34.9	33.8	33.8	93
Mg^{++}	—	—	—	—	—	35.5	98
Merck I							
Na^+	—	49.4	59.5	69.5	77.7	102	887
K^+	—	—	—	—	—	66.8	581
Ca^{++}	41.7	47.5	—	47.4	46.4	48.0	418
Mg^{++}	—	—	—	—	—	54.0	470
Merck II							
Na^+	—	28.4	27.8	27.2	28.0	27.8	248
Ca^{++}	25.2	24.8	—	23.3	23.9	24.3	217
Malone							
Na^+	—	34.3	35.1	35.5	36.5	37.3	214
Ca^{++}	33.3	31.7	—	29.4	29.1	28.3	163
New Zealand							
Na^+	—	46.0	47.4	47.7	48.4	46.9	117
Ca^{++}	45.6	42.7	—	41.3	40.7	39.6	99
Eureka Halloysite							
Na^+	—	24.0	24.2	22.9	22.7	22.7	21
Ca^{++}	23.0	22.5	—	21.5	21.3	20.5	19

* Calculated by dividing the water content at 10 millibars suction by the specific surface area.

surface film thickness for a concentration of monovalent ions of 10^{-4} molar at 10 millibars suction is some 400 A. The average values for distilled water film thickness (table 2), calculated by dividing the water content at 10 millibars suction by the specific surface area, clearly shows that for all but the Merck I clay any possible formation of diffuse double layers is severely restricted. This calculation should, if anything, overestimate the actual average surface film thickness (1).

The Merck I sample, despite its relatively small specific area, exhibits considerable swelling and a large variation in water content with change in valency of the exchangeable cation at low values of suction (fig. 2). There is a large hysteresis effect evident between 10 and 10^5 millibars suction, suggesting the possibility of a considerable rearrangement of particle configuration between the wetting and drying curves. The water contents attained, for the calcium clay in particular, exceed those to be expected simply from the addition of some 5 per cent montmorillonite clay to the matrix [*cf.* approximately 96 per cent water content for calcium montmorillonite at 10 millibars suction (2)].

It would appear from these variations in swelling behavior that both particle to particle interactions giving rise to gel structures and the physico-chemical development of surface adsorbed films are involved to some extent. The relative contribution of these factors has been the subject of much discussion and the considerations involved have been well reviewed by Williamson (23).

Schofield and Samson (21) demonstrated the existence of strong positive edge to negative face attractions in kaolinite clays causing flocculation in salt-free suspensions, and these same forces could be expected to influence the swelling behavior of the compacted clay matrix. Deflocculation of their clays was found to be brought about in several ways: (*a*) by proton transfer on addition of NaOH and consequent

removal of positive edge charge; (*b*) by anion adsorption, causing neutralization of positive charges, and (*c*) by the presence of small negatively charged platelets of another clay, such as montmorillonite or illite, overlying the positive charges on the edge faces of the larger kaolinite crystals.

In view of the distinctive swelling behavior of Merck I, the possibility of a blanketing effect as noted above (*c*) allowing the unimpeded development of surface layers for this clay seemed significant. However, neither the pre-adsorption of sufficient sodium tripolyphosphate to cause deflocculation of the sodium Rocky Gully, sodium New Zealand, or sodium Malone clays in suspension (14), or the addition in suspension of 5 or 10 per cent by weight of the $<0.1\ \mu$ fraction of illite or montmorillonite clays, produced any significant change in the swelling of these materials at 10 millibars suction other than that equivalent to the water content of the clays added in the latter cases. This does not, of course, eliminate the possibility that a particular set of conditions may be necessary to reproduce a sufficiently intimate association of the

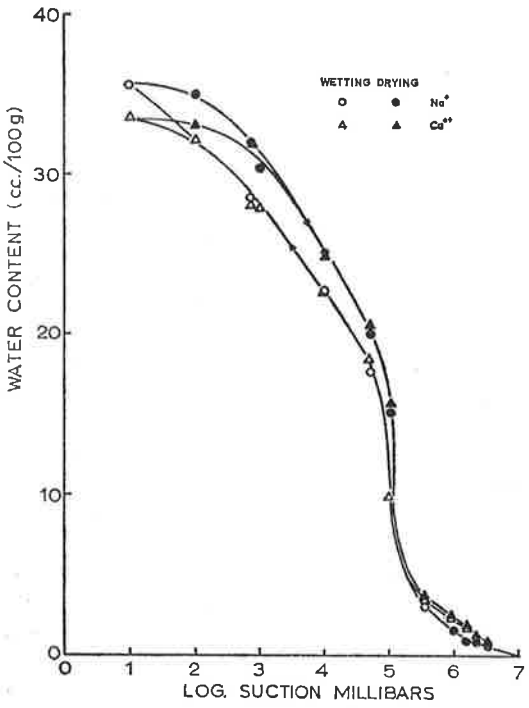

FIG. 1. Water-content–suction relationship for Rocky Gully kaolinite cores on distilled water.

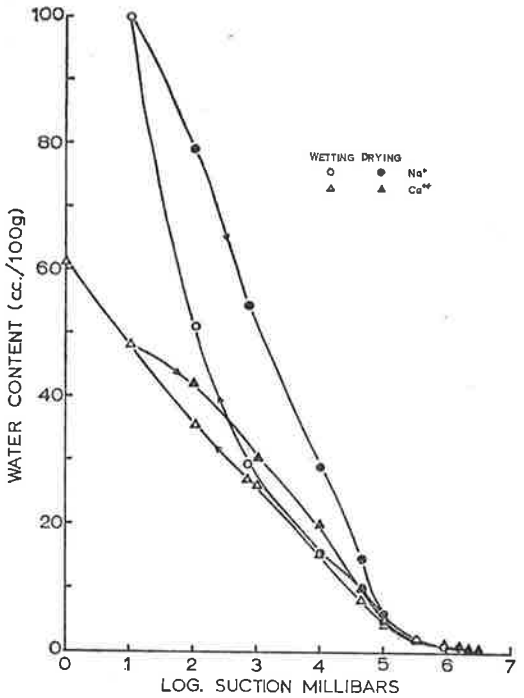

FIG. 2. Water-content–suction relationship for Merck I kaolinite cores on distilled water.

montmorillonite lamellae with the kaolin crystals to nullify the effect of positive-edge to negative-face attraction on the initial swelling.

Perhaps the most significant feature of the data in table 2 is the behavior of the clay systems with changes in electrolyte concentration. With the exception of Merck I kaolinite, and perhaps also Malone kaolinite, there is no significant difference in solution content for the monovalent clays over the concentration range from *M* to distilled water. Desorption curves to 10^5 millibars suction for Rocky Gully kaolinite for all the concentrations used were effectively the same as that obtained for distilled water. In contrast, the marked effect of increasing concentration of sodium chloride on the behavior of the Merck I kaolinite is illustrated by the drying curves obtained after wetting to 10 millibars suction (fig. 3). Here the presence of even a very small proportion of sodium montmorillonite would, of course, greatly affect the change in solution content with decreasing electrolyte concentration.

The calcium clays, on the other hand, again with the exception of the Merck I kaolin, ex-

hibit a somewhat anomalous behavior by retaining a slightly larger solution volume at the higher concentrations. This increase persists with increasing suction, as illustrated by the drying curves for calcium Rocky Gully in figure 4(*A*) and is accompanied by a slightly more plastic and sticky texture for the clay cores. The Merck I kaolinite (*B*, fig. 4), while showing little significant variation in volume taken up between distilled water and *M* calcium chloride, shows an appreciable restriction in swelling in 4 *M* calcium choride solution.

Evidence has been obtained by several workers (10, 19) that diffuse double layers are formed on the surface of kaolinite clays in suspension. In these circumstances the lack of response to changes in electrolyte concentration of the clay cores in the present work clearly requires some other explanation. It is possible that the inertial and frictional resistance to movement of the large kaolinite crystals may also provide a significant hindrance to swelling forces. Although such impediments would be of greater significance than for, say, montmorillonite lamellae, it is difficult to explain on this basis the lack of correlation between the swelling values obtained and specific surface area and electrolyte concentration. It is conceivable, however, that with such relatively large crystals, the major development of diffuse double layers may be accommodated within the large pores of the clay matrix or, alternatively, in stepping of the crystal surfaces, without producing any appreciable swelling pressure. Total solution uptake may be less affected, since the porous structure would retain the majority of the solution by capillary action.

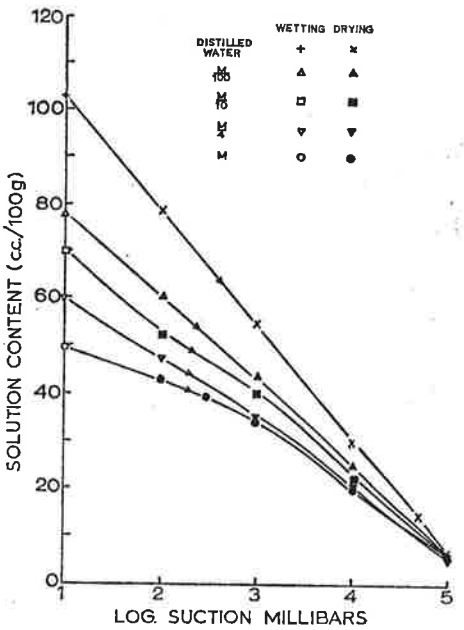

FIG. 3. Effect of sodium chloride concentration on solution-content–suction relationship for sodium Merck I kaolinite cores.

One possible source of a strong short-range bonding mechanism between kaolin clays is that of hydrogen bonding with water molecules be-

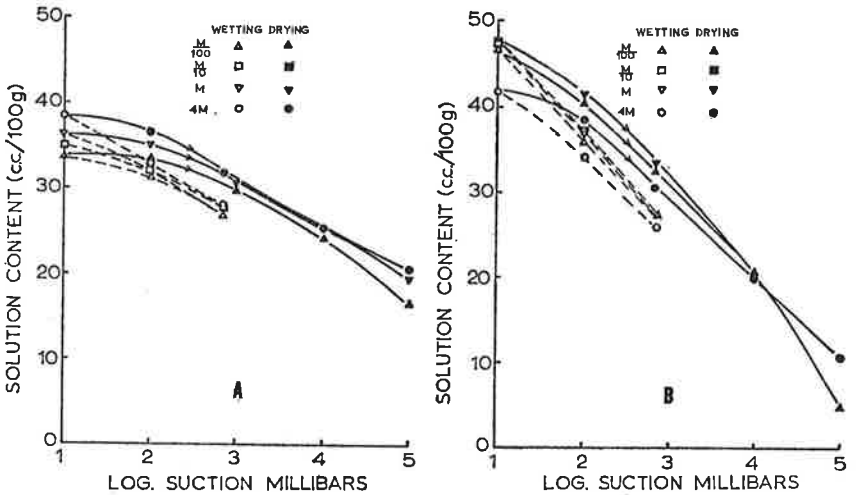

FIG. 4. Effect of calcium chloride concentration on solution content-suction relationship for (*A*) sodium Rocky Gully kaolinite cores and (*B*) sodium Merck I kaolinite cores.

tween the close-packed hydroxyl sheet of the octahedral layer of one crystal and the open-packed oxygen network of the tetrahedral layer of an adjacent crystal. Such forces have been suggested as responsible for the restriction of the interlamellar spacings of an hydrated halloysite to one layer of water molecules. If, as seems probable, the small halloysite crystals are oriented into groups of parallel crystals on drying or compaction (2), a similar restriction to one layer of water molecules where crystal surfaces overlap is conceivable and could account for the negligible swelling of this material. Although the surface area of the halloysite crystals is readily accessible to nitrogen adsorption, it is possible that there are small areas where close, near contact is achieved, and the restricted swelling of the kaolin clays in general may result, in part, from a number of hydrogen bonds in these areas of closest approach. The number of such hydrogen bonds could determine the force necessary to cause appreciable swelling in much the same fashion as the swelling of exchange resins is determined by the number of cross linkages present (7).

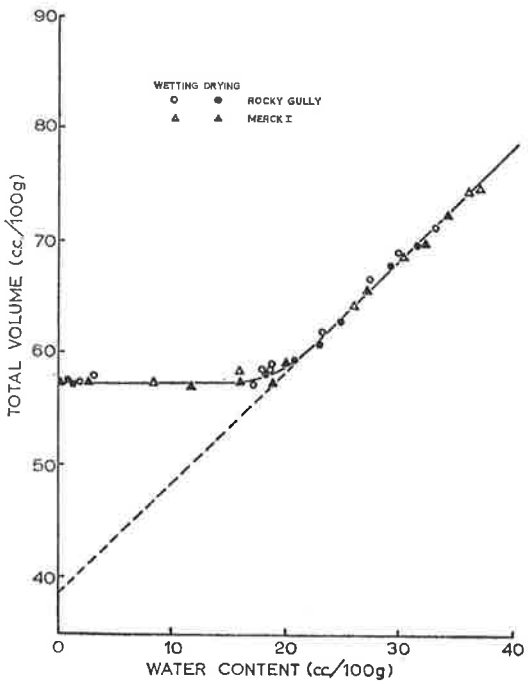

FIG. 5. Experimentally determined relationship between total volume and water content for kaolinite cores.

A further possible explanation for the restriction of swelling arises from the suggestion by Cashen (4) that, as the kaolinite clays are washed free of electrolyte, the crystals become unstable, due to a rise in potential differences between negative planar and positive edge faces allowing the migration of edge-face aluminum ions to exchange sites on the planar faces. Thus, by the present method of preparation the swelling of the kaolinite clays could possibly be dominated by the presence of aluminum ions. If this, however, is the case the treatment with sodium tripolyphosphate should nullify the effect of aluminum on planar faces and prevent further migration from the edge faces, as shown by Cashen (4) with pyrophosphate. In addition, Muljadi, Posner, and Quirk (17) concluded from phosphate-adsorption measurements that during a similar preparation transference of aluminum ions from the edge to cleavage faces occurs, if at all, to only a very minor extent.

Clearly, at close distances of approach electrostatic forces would also be involved, and here the region of dielectric saturation associated with the exchangeable cations would exert an influence. This could possibly explain the differences in swelling exhibited by the monovalent and divalent ion kaolinites. There is, however, no apparent correlation between swelling and surface density of charge. It has been suggested (22) that the electrostatic charge on kaolin clay crystals may be located entirely on one cleavage face. Under such conditions of high surface density of charge approaching that of the mica-like clays, significant ion binding may occur, resulting in little tendency to form diffuse double layers, with consequent reduction in repulsive forces as discussed by Edwards, Posner, and Quirk (8). The present data, where the swelling of the kaolins shows little sensitivity to electrolyte concentration and exchangeable cation, may thus support Weiss' conclusion (22).

The experimentally determined relationships between total volume and water content for Rocky Gully and Merck I kaolins are shown in figure 5. The points plotted are those for the calcium-saturated clays, but within experimental error the curve is equally representative of the relationships obtained for the other cations. For both clays, normal shrinkage ceases sharply at a pore volume approximately equal to the oven-dry value (5). Any further reduction in

water content is accomplished by pore drainage within the rigid network formed by the large kaolinite crystals.

Osmotic and hydrostatic components of free energy do not appear to exert equivalent effects, the latter being far more effective in reducing the swelling of even the sodium Merck I clay (fig. 3). This seems to be due to the presence of the gel structure, since an increase in hydrostatic force on the gel structure could collapse it more effectively than a change in electrolyte concentration, which does not apply as an actual force on the pore water.

SUMMARY AND CONCLUSION

The swelling of homoionic kaolin clay cores has been examined in relation to hydrostatic suction, electrolyte concentration, specific surface area, and exchangeable cation. The outstanding feature of the data is the lack of correlation between solution contents and the physico-chemical characteristics of the clay systems. Swelling appears to be governed by variations in the structural strength of the clay matrix. The origin of these restraints is not clear and requires further investigation.

REFERENCES

(1) Aylmore, L. A. G., and Quirk, J. P. 1959 Swelling of clay-water systems. Nature 183: 1752–1753.

(2) Aylmore, L. A. G., and Quirk, J. P. 1962 The structural status of clay systems. Proc. 9th Natl. Conf. Clays and Clay Minerals, pp. 104–139. Pergamon Press, New York.

(3) Brunauer, S., Emmett, P. H., and Teller, E. 1938 Adsorption of gases in multimolecular layers. J. Am. Chem. Soc. 60: 309–319.

(4) Cashen, G. H. 1959 Electric charges of kaolin. Trans. Faraday Soc. 55: 477–486.

(5) Childs, E. C., and Collis-George, N. C. 1948 Soil geometry and soil-water equilibria. Discussions Faraday Soc. 3: 78–85.

(6) Croney, D., and Coleman, J. D. 1954 Soil structure in relation to soil suction (pF). J. Soil Sci. 5: 75–84.

(7) "Dowex" 1958 "Ion Exchange." Dow Chemical Co., Midland, Michigan.

(8) Edwards, D. G., Posner, A. M., and Quirk, J. P. 1966 The repulsion of chloride ions by negatively charged clay surfaces. Parts I, II, and III. Trans Faraday Soc. 61: 2808–2823.

(9) Holmes, J. W. 1955 Water sorption and swelling of clay blocks. J. Soil Sci. 6: 200–208.

(10) Holtzman, W. 1962 The application of the Verwey and Overbeek theory to the stability of kaolinite-water systems. J. Colloid Sci. 17: 363–382.

(11) Jurinak, J. J. 1961 The effect of pretreatment on the adsorption and desorption of water vapor by lithium and calcium kaolinite. J. Phys. Chem. 65: 62–64.

(12) Jurinak, J. J. 1963 Multilayer adsorption of water by kaolinite. Soil Sci. Soc. Am. Proc. 27: 269–272.

(13) Keenan, A. G., Mooney, R. W., and Wood, L. A. 1951 The relation between exchangeable ions and water adsorption on kaolinite. J. Phys. and Colloid Chem. 55: 1462–1474.

(14) Lyons, J. W. 1964 Sodium tri-(poly)phosphate in the kaolinite-water system. J. Colloid Sci. 19: 399–412.

(15) McIntyre, D. S., and Stirk, G. B. 1954 A method for determination of apparent density of soil aggregates. Australian J. Agr. Research 5: 291–296.

(16) Martin, R. T. 1959 Water-vapour sorption on kaolinite: hysteresis. Proc. 6th Natl. Conf. Clays and Clay Minerals, pp. 259–278. Pergamon Press, New York.

(17) Muljadi, D., Posner, A. M., and Quirk, J. P. 1966 The mechanism of phosphate adsorption by kaolinite, gibbsite, and pseudoboehmite. J. Soil Sci. (in press).

(18) Murray, H. H. 1961 Industrial applications of kaolin. Proc. 10th Natl. Conf. Clays and Clay Minerals, pp. 291–298. Pergamon Press, New York.

(19) Quirk, J. P. 1960 Negative and positive adsorption of chloride by kaolinite. Nature 188: 253–254.

(20) Schofield, R. K. 1947 Calculation of surface areas from measurements of negative adsorption. Nature 160: 408–410.

(21) Schofield, R. K., and Samson, H. R. 1954 Flocculation of kaolinite due to the attraction of oppositely charged crystal faces. Discussions Faraday Soc. No. 18, pp. 135–145.

(22) Weiss, A., and Russow, J. 1963 Über die Lage der austauschbaren Kation bei Kaolinit. Proc. International Clay Conf., Stockholm 14: 203–213.

(23) Williamson, W. O. 1951 The physical relationships between clay and water. Trans. Brit. Ceram. Soc. 50: 10–34.

Offprint from

THE JOURNAL OF SOIL SCIENCE

Volume 18 · Number 1 · March 1967

OXFORD
AT THE CLARENDON PRESS

Subscription (for 2 numbers) 40s. post free

THE MICROPORE SIZE DISTRIBUTIONS OF CLAY MINERAL SYSTEMS

L. A. G. AYLMORE AND J. P. QUIRK

(*Institute of Agriculture, University of Western Australia*)

Summary

The micropore (<100 Å) size distributions of compacted clay mineral systems have been examined by means of low-temperature N_2 sorption isotherms to saturation. The calculation of pore sizes was based on the application of the Kelvin equation, corrected for the adsorbed film thickness, to the parallel plate model.

Clay-mineral systems have been shown to exist with a high degree of parallel alignment of the plate-shaped crystals. This results in a high proportion of microporosity and in relatively discrete pore sizes.

In montmorillonite clays much intercrystalline overlap area in the dry matrix is inaccessible to N_2 sorption. The structure of these systems may be governed partly by the effect, in suspension, of electrostatic interaction between the charged particles on crystal size, but largely by mechanical interaction on sedimentation and the size of the exchangeable cations present.

Introduction

MOST chemical reactions in soils take place at surfaces within the pores and the clay-water interaction determines, to a large extent, the mechanical consistence and properties of the soil system. In addition, the nature of the pore space controls the transport of soil water and nutrient ions needed for plant growth.

Although the term 'pore size distribution' (P.S.D.) is used freely in soil science literature, there is little quantitative information on pore sizes. Some emphasis has been given to the macropores, those drained of water at suctions of less than 100 cm, $> 10^5$ Å radius (Quirk and Panabokke, 1962), but there is little information on smaller pore sizes, especially those < 100 Å (Brunauer, 1943).

The sorption of N_2 and other inert gases at temperatures near their boiling points has been used by many workers (Barrett *et al.*, 1951; Innes, 1957; Lippens *et al.*, 1964) to study the nature and extent of void spaces within microporous systems. The Brunauer, Emmett, and Teller, 1938 (B.E.T.), method of estimating the specific surface-area of finely divided materials from such adsorption isotherms has, despite its apparent theoretical shortcomings, received general acceptance and has been used extensively in the characterization of these systems (Keenan *et al.*, 1951; Brooks, 1955; Barrer and McLeod, 1955).

Estimations of pore sizes and their volume distribution are usually based on the phenomena of capillary condensation and the application of the Kelvin equation to either the complete adsorption or desorption isotherm after correcting for the thickness of the physically adsorbed layer. There are limitations to the accuracy of the Kelvin equation in estimating the radius of curvature of the liquid meniscus (Derjaguin, 1957) but for most purposes of comparison it is acceptable.

The major difficulty in investigating the role of physico-chemical forces in determining the behaviour of clay-water systems arises from the necessity to distinguish between the water which is actually held at the clay surface by physico-chemical forces and that which is simply enmeshed within the gel structure and retained by capillary forces (Aylmore and Quirk, 1959). The present work was undertaken to give basic information on soil- and clay-particle arrangement which would assist in interpreting the swelling of soil and clay materials and in studies on the movement of ionic solutions through reactive materials such as soil- and clay-gel systems. The location of organic and inorganic binding materials which enhance soil stability similarly depends on satisfactory determinations of micropore size distributions.

Experimental and Materials

In general, homoionic samples of the $< 2\mu$ fraction of the clays were obtained by repeated washing and centrifuging with a molar solution of the appropriate chloride. The samples were washed and finally dialysed against distilled water, using Visking cellulose casing. After air-drying, the clays were gently ground to a powder and allowed to equilibrate with water vapour over a saturated solution of K_2SO_4 ($p/p_0 = 0{\cdot}96$ at 20° C) in a vacuum desiccator. The resultant water content was usually sufficient to ensure the development of pore-space saturation on subsequent compression of small samples (200 mg) of the clays in a stainless steel mould. The small cores so produced were taken through repeated wetting-and-drying cycles to ensure the maximum natural rearrangement of particle configuration (Aylmore and Quirk, 1959).

Clay samples were obtained from the following natural deposits:

Wyoming bentonite—montmorillonite from Upton, Wyoming, U.S.A.

Redhill montmorillonite—from Redhill, Surrey, England: supplied by Fullers Earth Company.

Rocky Gully kaolinite—from pallid zone of laterite, Rocky Gully, Western Australia.

Merck kaolinite—obtained from Merck Chemical Company, Germany: labelled DAB-6.

Willalooka illite—B horizon from a solonized solonetz: Hundred of Laffer, South Australia.

Urrbrae B clay—B_1 horizon of Urrbrae loam, a red-brown earth, Adelaide, South Australia. Clay fraction 60 per cent illite and 40 per cent kaolinite.

Sorption isotherms. Conventional volumetric adsorption equipment (Aylmore, 1960) based on the original apparatus of Emmett and Brunauer (1934) and incorporating many of the refinements suggested by Harkins and Jura (1944) and Joyner (1949), was used to obtain complete N_2 adsorption-desorption isotherms for each material. Approximately 1 g of cores was placed in the sample bulb and outgassed at a temperature of 300° C for 25 h or until the pressure remained below 10^{-3} mm after isolation from the pumps for 30 min. The sample bulb was then immersed in a liquid-N_2 bath (78° K) and the N_2-sorption isotherm determined in the usual fashion.

Hysteresis and the Calculation of Pore Size Distribution

In the dry state the compacted clay system forms a rigid matrix which does not swell or appear to undergo any significant structural rearrangement in the presence of non-polar liquids. The hysteresis present in the complete N_2 adsorption-desorption isotherms therefore arises entirely from the nature of the porous structure formed by these materials on drying.

Reversible hysteresis over the range in which capillary condensation is taking place arises entirely from the occurrence of different mechanisms on the adsorption and desorption branches of the isotherm, depending on the shape of the capillaries involved. Where irregular tubular and so-called 'ink-bottle' pores (McBain, 1935) predominate, spontaneous emptying of condensate retained in larger chambers behind narrower pore openings produces irreversibility in the desorption branch of an isotherm. The adsorption branch, on the other hand, will correspond to a reversible filling of the pores, governed by the curvature of the condensate meniscus. This has been verified experimentally by Kington and Smith (1964) for Ar sorption in porous glass and, in these circumstances, the correct pore radii can be determined by applying the Kelvin equation to the adsorption branch of the hysteresis loop.

In systems where the porous structure is such that meniscus formation is delayed until the adsorbed multilayers merge in the narrowest part of the void space, pore-filling may occur by spontaneous nucleation at these points, thus giving rise to irreversibility on the adsorption branch. This 'open-pore' concept (Foster, 1932) seems most applicable to the open-sided, slit-shaped pores which occur in many systems (de Boer, 1958). On the desorption branch, the meniscus is present and, provided there are no bottle-shaped pores, the relative pressure in the pore, and hence evaporation, is governed solely by the curvature of the meniscus and the correct pore radii can be obtained by applying the Kelvin equation to the desorption branch of the isotherm.

If the total cumulative surface-area of pores is calculated from the increments in surface area of the adsorbed film obtained, on the basis of pore-geometry over small intervals of relative pressure, the presence of an irreversible or spontaneous process in the adsorption or desorption branch will produce a displacement of the calculated pore-size distribution to higher or lower values of relative pressure respectively. This will result in the under- or over-estimation respectively of the true surface area. Hence, a comparison between B.E.T. area and cumulative pore surface-areas should serve as a guide to the validity of the basic assumptions of pore-shape and the mechanisms controlling capillary condensation. De Boer *et al.* (1964) have examined the isotherms obtained for systems of each pore-shape and record striking agreement between B.E.T. surface-areas and surface-areas obtained from the adsorption branch for bottle-shaped pores, and from the desorption branch for open slit-shaped pores. Use of the alternative branch for either system resulted in considerable disagreement.

It is not always possible to state categorically *a priori* which mechanism is producing reversible hysteresis in a particular system. As pointed out by Adamson (1963), thermodynamic pronouncements on the basis of an assumed model are only as valid as the model itself. However, models proposed for the arrangement of soil particles (e.g. Terzaghi, 1956; Lamb, 1953; Aylmore and Quirk, 1960) invariably consist of a parallel arrangement of the plate-shaped clay crystals or something intermediate between this and the card-house structure which is often invoked to explain the behaviour of thixotropic gels (van Olphen, 1962). The detailed knowledge of the physical dimensions of the plate-shaped crystals, electron micrographs of the clay matrix (Bates, 1958; Aylmore and Quirk, 1960), and the values obtained for dry porosity leave little doubt that the void-spaces between these crystals are, in fact, of the open-sided slit-shaped type, in which case the mechanisms of pore-filling and emptying suggested by Foster (1932) are the most logical to assume. Application of the Kelvin equation to the desorption branch in this model is therefore reasonably justified, certainly as a first approximation for comparison of the pore-size distributions in different clay systems.

Since the dimensions of the plate-shaped crystals are large compared with the distances separating them, it seems reasonable to assume a cylindrical rather than a hemispherical meniscus for the desorption branch of the isotherm. Following Innes (1957) the modified Kelvin equation, allowing for the surface-film thickness, is then expressed

$$d-2t = \frac{2\gamma M}{RT\ln p/p_0} \qquad (1)$$

where d is the maximum distance of plate-separation at which capillary evaporation can occur for a given relative pressure p/p_0; t is the thickness of the adsorbed layer; M is the molar volume and γ the surface tension of the condensate and R is the gas constant and T the absolute temperature.

The physical meanings of the quantities involved in the Kelvin equation and hence the validity of the calculated dimensions, are uncertain at relative pressures corresponding to plate-separations < 20 Å. Nevertheless the results of such calculations can be accepted as illustrating, at least for the purposes of comparison, the relative availability of pore-space for sorbate retention (Everett, 1958).

The main difficulty in carrying out these calculations arises from the concurrence at any point on the isotherm of both capillary condensation and multilayer surface-adsorption. A correction to the total volume sorbed for the volume of the surface adsorbate is therefore necessary before the application of the Kelvin equation. This volume of surface adsorbate can be obtained from measurements of sorption isotherms on non-porous or very coarse crystalline solids where capillary condensation is negligible. Schull *et al.* (1948) and Lippens *et al.* (1964) have shown that, for many such adsorbates, the ratio of the volume adsorbed at a particular relative pressure to the volume required to form a

monolayer is essentially constant, thereby providing a satisfactory estimate of the surface-film thickness at that relative pressure. The values for film thickness used here are those obtained by Lippens *et al.* (1964) for N_2 adsorption on coarse aluminas.

As surface desorption takes place only within the pores already emptied of capillary condensate, some method of estimating the surface area of these pores is required and this is usually accomplished by a cumulative addition of the average area increments calculated from pore-geometry over successive small decrements of relative pressure.

A similar series of calculations to those suggested by Innes (1957) and by Lippens *et al.* (1964) to obtain the pore-size distribution for a parallel plate model was programmed for an *IBM*/1620 data-processing unit and is available on request from the authors.

Results and Discussions

Specific surface-areas obtained by both the B.E.T. method and from the pore-size distribution (P.S.D.) calculation, together with the porosities after outgassing of the compressed cores and natural aggregates are given in Table 1. The N_2 isotherms obtained for samples of the kaolinite, illite, and montmorillonite clays are shown in Figs. 1(*a*) and (*b*) and 3(*a*) to 9(*a*) and the corresponding cumulative and differential pore-size distribution and surface-area versus plate-separation curves obtained from the desorption branches in Figs. 3(*b*) to 9(*b*). The cumulative pore-volume is given as a percentage of the total desorbed pore-volume.

TABLE 1

Surface Areas and Porosities of Clay Materials

Material	*Cation*	*Surface area* (m^2/g)		*Porosity* (*cc/g*)
		B.E.T.	*P.S.D.*	
Rocky Gully kaolin	Ca^{++}	36·3	36·6	0·185
Merck kaolin	Ca^{++}	11·5	10·5	0·188
Willalooka illite (<2 μ)	Ca^{++}	163	163	0·188
(<0·1 μ)	Ca^{++}	227	210	0·297
Urrbrae loam				
B-horizon cores	Ca^{++}	90·7	87·1	0·131
Natural Urrbrae loam				
B-horizon aggregates		93·8	90·2	0·191
Wyoming bentonite	Ca^{++}	38·1	37·5	0·135
	Na^{+}	48·1	51·7	0·104
	K^{+}	47·7	..	0·104
	Cs^{+}	113	104	0·123
Redhill montmorillonite	Ca^{++}	99·4	94·0	0·152
	Na^{+}	104	99·4	0·152
	Cs^{+}	141	131	0·155

The isotherms for the two kaolins, Figs. 1(*a*) and 1(*b*), are characteristic for materials of relatively coarse particle-size and approach Type II of Brunauer's 1938 classification. Both isotherms show little hysteresis

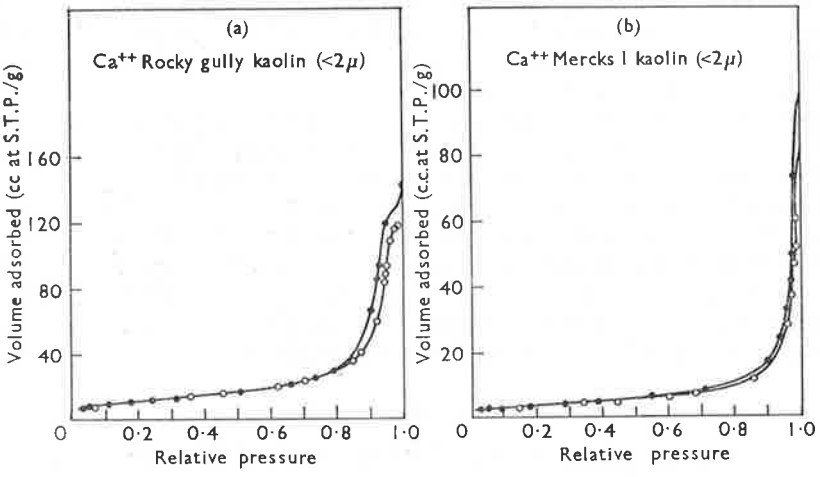

FIG. 1. Nitrogen sorption isotherms at 78° K for (*a*) Calcium Rocky Gully and (*b*) Calcium Merck kaolin. ○ Adsorption, ● Desorption.

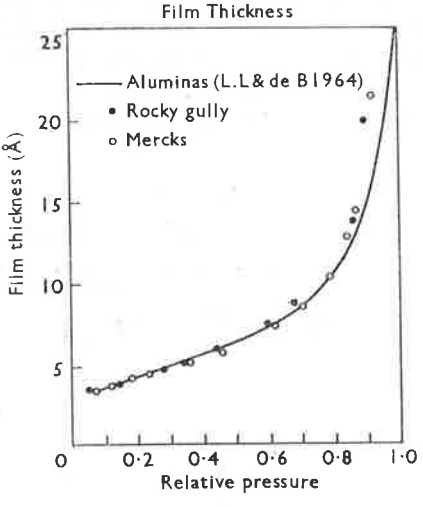

FIG. 2. Surface film thickness for nitrogen on kaolin at 78° K compared with coarse aluminas (5).

and the majority of the porosity is contained in relatively large plate-separations > 100 Å ($p/p_0 = 0{\cdot}88$) for Rocky Gully kaolinite and 200 Å ($p/p_0 = 0{\cdot}94$) for the Merck kaolinite. With the relatively large crystals in kaolinites, such surface-separations of the order of 100 Å at least, could arise from steps in the crystal surface as well as from separations between neighbouring crystals. As the majority of the pore-sizes for these kaolins are outside the range to be examined by the present method, no pore-size distributions are shown for these materials.

However, the ratio of the volume adsorbed at a particular relative pressure to the volume required to form a B.E.T. monolayer for these coarse materials, agrees well with the ratio obtained by Lippens *et al.* (1964) for N_2 adsorption on coarse aluminas until the capillary condensation began at approximately $p/p_0 = 0{\cdot}86$ (Fig. 2).

In contrast, however, the remaining isotherms for the illite and montmorillonite cores are all characterized by appreciable hysteresis above 0·4 relative pressure, followed by a small but persistent hysteresis down to very low relative pressures. The broad hysteresis loop extending from saturation down to relative pressures of approximately 0·4 is generally attributed to the porous nature of the adsorbent material and has been described as 'pore' hysteresis (McDermot and Arnell, 1956). The presence of hysteresis at lower relative pressures in N_2 sorption isotherms has been observed by previous workers for the expanding-lattice montmorillonite clays (Brooks, 1955; Barrer and McLeod, 1955) and for partially brominated graphites (McDermot and Arnell, 1956). In each case this hysteresis, termed 'swelling hysteresis' by McDermot and Arnell (1956) has been attributed to the availability of space between the individual lamellae due to their being propped apart by residual water, Br or other molecules and has been removed by further outgassing. However, the persistence of this latter type of hysteresis in the present measurements on montmorillonite after prolonged outgassing, and particularly its presence for the non-expanding lattice illite cores, seems to indicate that its origin in this case is intercrystalline rather than intracrystalline.

Parallel interleaving of clay crystals. De Boer (1958) has classified adsorption-desorption isotherms on the basis of their shape. The isotherms in Figs. 3(*a*) to 9(*a*) could arise from a combination of his Type B and Type D hysteresis loops and thus could represent a capillary system of open slit-shaped pores (Group IX) together with wedge-shaped pores (Group XII) with a closed-edge at the narrower side preventing a hysteresis loop being formed. The former pore-shape could arise from the parallel interleaving of clay crystals and the latter by the propping apart of crystals to form wedge-shaped voids. Such a capillary system seems highly probable for a dry, aggregated matrix of thin, flat plates.

Since almost the entire porosity of the Ca-Willalooka illite (Fig. 3) arises from pores of less than 60 Å, for this clay at least, with plates of the order of 700 Å across the planar surfaces, the porosity must result largely from the void spaces between nearly parallel aligned plates. Electron microscopic studies of fracture surfaces of similar clay cores (Aylmore, 1960) verify this general picture of the dry-clay matrix. Similarly, varying degrees of alignment are apparent from the pore-size distributions obtained for the other clays. In these circumstances, it seems quite probable that interleaving would produce peaks in the differential pore-size distribution curves corresponding to the predominance of a particular thickness of clay-unit whether individual alumino-silicate sheets, larger crystals, or groups of crystals forming domains (Aylmore and Quirk, 1960). This interleaving could result in

a maximum in the differential pore-size distribution curve at something less than the predominant crystal-thickness, depending on the proportion of wedge- to slit-shaped voids. Peaks of this type are very much in evidence for both the illite and montmorillonite samples.

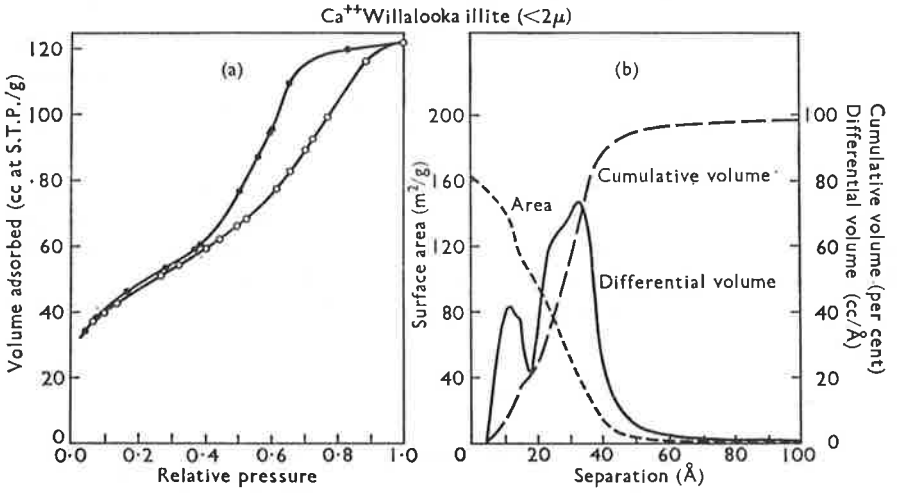

FIG. 3. (*a*) Nitrogen sorption isotherm at 78° K, ○ Adsorption, ● Desorption and (*b*) Surface-area, cumulative and differential pore-size distributions for calcium Willalooka illite.

The residual hysteresis in the isotherms observed below $p/p_0 = 0{\cdot}4$ may, therefore, result at least partially from the interleaving of thin crystals consisting of one or two alumino-silicate sheets producing open, slit-shaped, and wedge-shaped pores with points of maximum separation $\simeq$ 10 Å and 20 Å respectively. However, the characteristic pore-size distribution peak at or near 10 Å, present for the majority of these materials, could arise equally well between areas of overlap of crystal units or within book-like stacks of crystals if there were sufficient surface irregularities, plate buckling, or molecular props to allow some penetration of N_2 molecules similar to that which occurs for a partially hydrated montmorillonite clay (Brooks, 1955). It is difficult to see why this penetration of N_2 should occur between the external surfaces of the illite crystals in contact, when it does not occur between the interlamellar surfaces of a dry montmorillonite. On the other hand, the good agreement obtained between N_2 surface-areas for illites and those obtained from methods involving the adsorption of polar molecules (Greenland and Quirk, 1962) indicates that any loss of surface area to N_2 adsorption through planar crystal-contact is relatively small.

By far the largest proportion of void space occurs in the Willalooka illite, in plate separations of the order of 30 Å, with an upper limit to the pore size of about 60 Å. Since the surface area of this material is 163 m^2/g, of which some 10 per cent would be edge-area, there would be some five elementary silicate sheets per crystal. Interleaving would

therefore be expected to produce a predominant pore-size of about 50 Å and the smaller value observed may mean that wedge-shaped pores predominate. In the case of wedge-shaped pores, the breadth and pliability of the clay-crystals could be expected to exert some influence on the average pore-dimensions measured by N_2 desorption. This may explain the variations in dimensions observed for the pore-size distribution peaks corresponding to crystals of the same thickness but for different materials. Possible deficiencies in the accuracy of the Kelvin equation should also be borne in mind in considering separations of this magnitude.

The separation of the $< 0{\cdot}1\ \mu$ fraction of this illite clay increases the specific surface-area to 227 m^2/g, sharpens the 30–35 Å peak and virtually eliminates the volume in pores larger than 40 Å. Incomplete dehydration does not result in an increase in the volume of the hysteresis below $p/p_0 = 0{\cdot}4$ as is the case for the swelling hysteresis of a montmorillonite clay (Brooks, 1955), but instead, in the removal of this hysteresis by the filling with water and consequent unavailability of these spaces to N_2 sorption.

The Urrbrae B horizon clays (Figs. 4 and 5) are coarser materials and exhibit a broader spectrum of pore-sizes than the Willalooka illite, but again discrete predominant pores of similar dimensions are present for both materials. The presence of some 40 per cent of kaolinite could produce this greater range of pore dimensions. Compression of the natural aggregates of Urrbrae B loam into cores reduces the total porosity from 0·19 cc/g to 0·13 cc/g and a comparison of the pore-size distributions for these two materials (Figs. 4 and 5) shows that the narrower distribution for the cores arises principally from a redistribution of the pore-sizes of less than 100 Å, probably as the result of better packing. The results are sufficiently similar to indicate that the cores have the same structure as the natural aggregates, except that the coarse pores have been removed. Hence, the use of compressed cores facilitates the interpretation of water content-energy data for these materials (Aylmore and Quirk, 1960).

The high proportion of the volume retained in pores of less than 100 Å for these natural soil aggregates is also significant in relation to the penetration of microbes into intra-aggregate voids (Greacen and Rovira, 1957). Even the smallest bacteria of some 2000 Å dimensions would be excluded from some 75 per cent of aggregate porosity. Organic matter adsorbed within such plate separations would, therefore, be very effectively protected against bacterial attack.

The specific surface area and pore-size distribution obtained for the dry matrix of both kaolinite and illite materials are apparently determined solely by the size of the clay-crystals and the degree and type of packing appears unaffected by variations in charge or size of the exchangeable cations. Essentially the same specific surface-areas and pore-size distributions are obtained by N sorption for these materials regardless of the exchangeable cation present.

Expanding lattice clays. In the case of the montmorillonite clays where polar water molecules are able to penetrate between and separate the

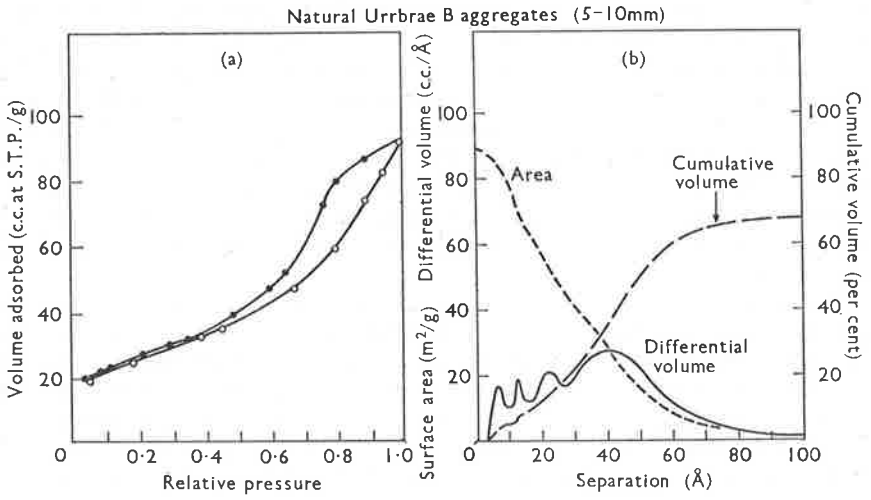

FIG. 4. (*a*) Nitrogen sorption isotherm at 78° K, ○ Adsorption, ● Desorption and (*b*) Surface-area, cumulative and differential pore-size distributions for natural Urrbrae B aggregates.

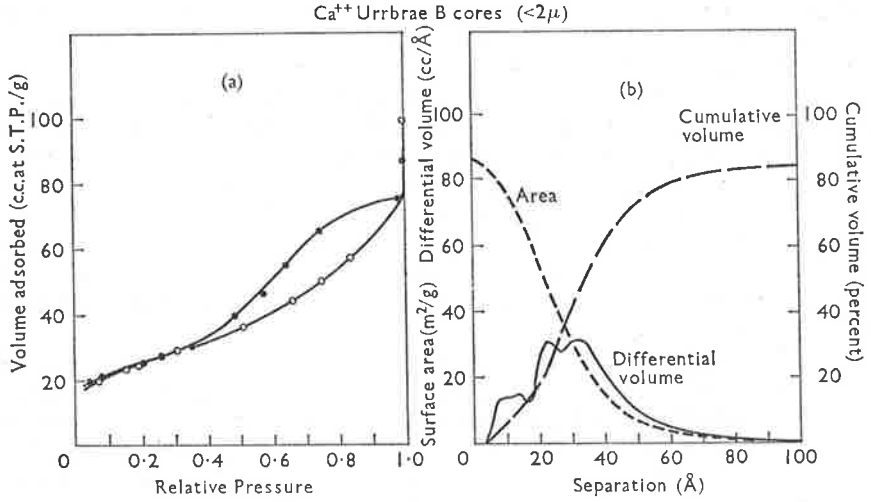

FIG. 5. (*a*) Nitrogen sorption isotherm at 78° K, ○ Adsorption, ● Desorption and (*b*) Surface-area, cumulative and differential pore-size distributions for calcium Urrbrae B cores.

individual alumino-silicate sheets, the matrix obtained on drying a suspension will naturally depend to a large extent on the degree to which these individual lamellae are dissociated in aqueous suspension. The extent to which montmorillonite clays disperse to the unit lamellae in dilute aqueous suspension is still open to question. Norrish (1954) has shown that, when saturated with small monovalent ions (Li^+, Na^+, and K^+), the crystal lattice of montmorillonite does expand to give large

separations ($>$ 100 Å) in distilled water. On the other hand, there is evidence (Edwards *et al.*, 1965) that varying degrees of association of the lamellae into crystal units do, in fact, persist in aqueous suspension to an extent determined largely by the size and charge of the exchangeable cation.

The relatively small reproducible specific surface-areas obtained here for the montmorillonite samples after drying from suspension (cf. total theoretical area of some 700 m^2/g) could mean either that larger crystals, of several sheets in thickness, retain their entity to an appreciable extent even in distilled water or that they result from some statistical reformation process which, for a given size of elementary sheet and physico-chemical environment, tends to give the same external surface-area when condensation of the unit lamellae to crystals takes place on drying (Aylmore and Quirk, 1959).

The fact that the alumino-silicate sheets of montmorillonite are able to approach sufficiently closely to prevent the penetration and adsorption of N results in the well-known discrepancy between B.E.T. N surface-areas and the total surface area available for cation exchange in aqueous suspension. Hence, in discussing such a complexly interwoven mass of platelets as must result from the dehydration of a montmorillonite suspension, the distinction between internal and external surfaces of crystals becomes largely a matter of definition in terms of their accessibility to N molecules when in the dry state. In certain circumstances a single alumino-silicate sheet may be interleaved in two or more regions of inaccessibility to N molecules, each region being considered as a separate crystal unit. Similarly, where crystal units, each of several lamellae thick, overlap, the surface area involved may or may not be accessible, depending on various geometrical factors including the dimensions of the exchangeable cations. In these circumstances, the definition of crystal size must be somewhat arbitrary.

The samples of montmorillonite clay show marked differences in apparent crystal-size and consequent specific surface-area and pore-size distribution, not only between different clay species, but also between samples of the same species saturated with different exchangeable cations. As for the Willalooka illite, almost all the porosity of the Redhill Ca-montmorillonite (Fig. 6) is contained in pore dimensions of $<$ 60 Å and pores of 20 Å and 40 Å separation respectively predominate. Also, an appreciable area involved either in overlap of the crystal units or possibly in staggering of the lamellae at crystal edges (i.e. in separations of $<$ 10 Å) is available for N adsorption. By contrast, only some 60 per cent of the porosity of the Wyoming Ca-bentonite (Fig. 7) is held in pores of less than 100 Å and a very much smaller volume of sorbate is retained in areas where crystal surfaces overlap. In fact, although some hysteresis is apparent at low relative pressures in the isotherm for this material the volume available in separations of $<$ 10 Å, as indicated by the pore-size distribution, is extremely small.

Electron micrographs of Redhill montmorillonite show an elementary sheet of considerably smaller lateral dimensions (approx. 200 Å) than that of the Wyoming bentonite (approx. 1000 Å). This alone cannot account for the difference in specific surface-area of the two materials

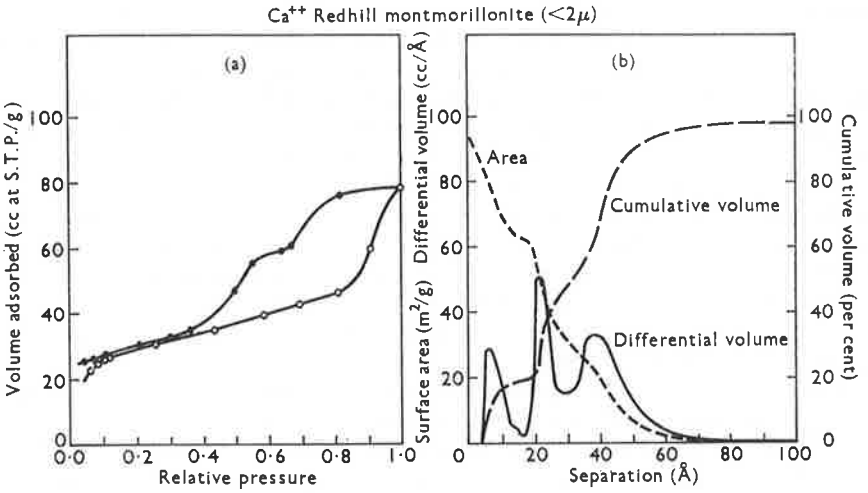

FIG. 6. (*a*) Nitrogen sorption isotherm at 78° K, ○ Adsorption, ● Desorption and (*b*) Surface-area, cumulative and differential pore-size distributions for calcium Redhill montmorillonite.

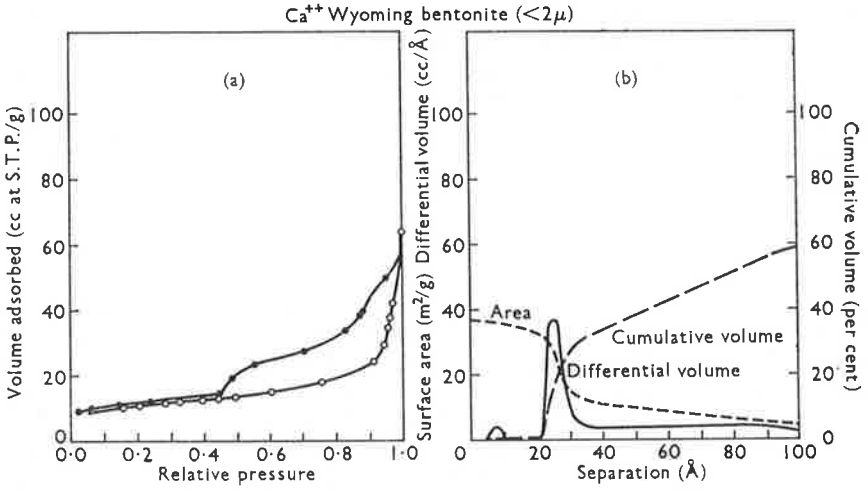

FIG. 7. (*a*) Nitrogen sorption isotherm at 78° K, ○ Adsorption, ● Desorption and (*b*) Surface-area, cumulative and differential pore-size distributions for calcium Wyoming bentonite.

and, from the pore-size distributions, larger areas of inaccessibility to N_2 and hence thicker effective crystals, occur for the Wyoming bentonite matrix than for the Redhill montmorillonite.

Conversion of the Ca-saturated Wyoming bentonite to the Na form produces an increase in the B.E.T. N_2 surface-area from 38·1 to 48·1 m^2/g and increases the relative volume in micropores of approximately 26 Å separation whilst still providing an appreciable proportion of

larger (> 100 Å) pores (Fig. 8). Once again the areas of crystal-overlap accessible to N_2 adsorption are almost negligible. This structural alteration with the valency of the exchangeable cation is to a large extent reversible, as the reconversion of the Na- to Ca-saturated clay produced an almost identical specific surface-area (38·3 m^2/g) and pore-size distribution to that of the original Ca-saturated clay.

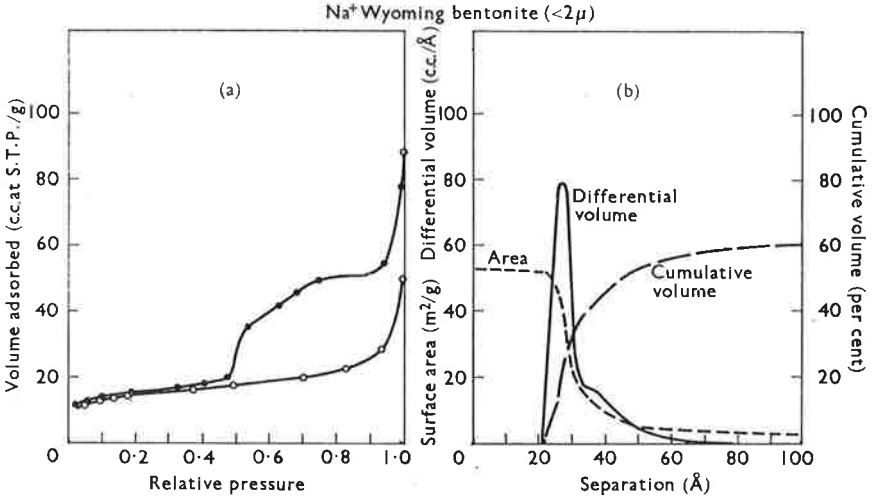

FIG. 8. (*a*) Nitrogen sorption isotherm at 78° K, ○ Adsorption, ● Desorption and (*b*) Surface-area, cumulative and differential pore-size distributions for sodium Wyoming bentonite.

The repulsive potential between neighbouring particles in aqueous suspension depends on the charge, size, and resultant hydration-energy of the exchangeable cation present. This would be expected to govern, to some extent, the size of the crystal-units formed by a dynamic association of given elementary sheets in suspension, and hence the subsequent accessibility of the surfaces to N_2 adsorption on drying. Attempts to measure the total internal plus external surface-area of Wyoming bentonite in dispersed aqueous suspension by the negative adsorption of chloride method (Edwards *et al.*, 1965) yield values considerably less than the total theoretical value of approximately 700 m^2/g, decreasing with the charge and ionic radius of the exchangeable cation present but far larger than those obtained by N_2 adsorption. The apparent variation in average crystal-size between the Na and Ca Wyoming bentonite could, therefore, be explained in terms of the difference in repulsive potential between the lamellae in suspension when saturated with the divalent and monovalent ions respectively. The higher valency apparently produces a larger effective crystal unit in suspension and hence, on drying, the formation of larger aggregates could be expected. However, saturation with larger and hence less strongly hydrated monovalent cations than Na would also be expected to produce, if anything, slightly larger crystal units than would the Na ion, due to the decrease

in the repulsive potential. Instead, K-Wyoming bentonite with a B.E.T. surface area of 47·7 m²/g has a pore-size distribution almost identical with that of the Na clay, and saturation with the large Cs ion (d(001) ≈ 12 Å) results in a dramatic increase to 113 m²/g in the surface-area accessible to the N molecule and effectively eliminates the macro-porosity (Fig. 9). This increase in surface-area of the Cs-Wyoming bentonite over the Ca, Na, and K forms occurs almost entirely in the < 10 Å separations.

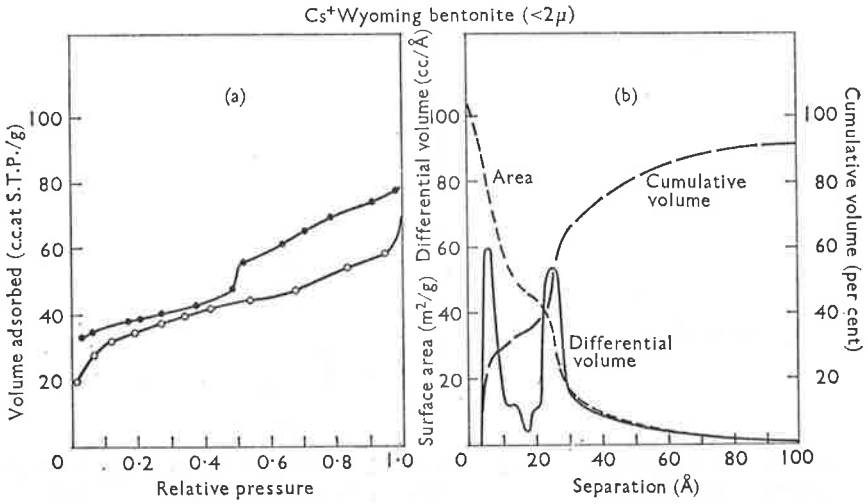

FIG. 9. (*a*) Nitrogen sorption isotherm at 78° K, ○ Adsorption, ● Desorption and (*b*) Surface-area, cumulative and differential pore-size distributions for caesium Wyoming bentonite.

Cs-montmorillonite gives a fixed lattice-spacing of 13·8 Å even in distilled water (Norrish, 1954). Hence, the value for the specific surface-area of Cs-Wyoming bentonite (150 m²/g) obtained by Edwards *et al.* (1965) by negative-adsorption measurements should represent only the external surface-area of the crystals in aqueous suspension. The accessibility of crystal surfaces on drying the Cs-clay (113 m²/g) is therefore much greater than with the other ions.

Brooks (1955) noted that the specific surface-area of Ca-Wyoming bentonite increased to a value above 120 m²/g with decreasing hydration, due to the accessibility to N_2 of surfaces propped apart by water molecules, before decreasing to a value of 41·3 m²/g on effectively complete desorption. Similarly, the maximum N_2-area obtained by Barrer and McLeod (1955) after the intercalation of large alkylammonium ions ($N(CH_3)_4^+$) in Wyoming bentonite (d(001) = 13·5 Å) is again some 169 m²/g. This seems to indicate that a similar matrix is formed on drying, regardless of the exchangeable cation present, but that for all but the larger or partially hydrated ions, an appreciable amount of the areas of crystal overlap becomes inaccessible to N_2 adsorption. On the

basis of previous definition, this is effectively the same as saying that two or more crystals merge except that the regions of crystal overlap must be less stable mechanically than the remaining internal surfaces.

From the comparison of the surface-areas obtained for Wyoming bentonite there does not appear to be any considerable penetration of N_2 into intracrystalline spacings even in the presence of these large intercalated ions, but rather an increase in the accessibility of the external surfaces of the bentonite crystals within the matrix.

It appears significant that the area of pores of greater than 20 Å separation is always of the order of 40 to 50 m^2/g for the Wyoming bentonite and this may represent the natural area of the bentonite matrix, allowing for the inaccessibility of crystal-overlap areas, when prepared by the present method.

The reproducibility of the structure of the systems in the present work is illustrated by the fact that even freeze-drying does not prevent an almost identical structural reformation at this level. However, previous experiments (Greene-Kelly, 1964) have shown that careful sedimentation and drying of suspension films to oriented flakes can reduce the specific surface-area of Na Wyoming bentonite to a value as low as 5 m^2/g. Hence, the mechanical and geometrical considerations can play a greater role in determining the structural configuration of the dry montmorillonite matrix than do electrostatic forces.

The greater accessibility, to N_2 adsorption, of the overlap-areas between the fixed-lattice illite crystals than between the expanding-lattice Wyoming bentonite crystals is probably due to the greater flexibility of these bentonite crystals in the later stages of dehydration after the formation of the matrix structure. The presence of one layer or more of water molecules, acting as a lubricant between each lamella, would greatly facilitate the moulding of each surface to its neighbour and hence the exclusion of N_2 molecules when dry.

Possibly as a result of the smaller lateral dimensions of the Redhill montmorillonite lamellae, the area of overlap of the Ca-Redhill montmorillonite crystals accessible to nitrogen adsorption is greater than for Ca-Wyoming bentonite. Although there is only a small increase in the B.E.T. specific surface-area between the Ca and Na Redhill samples, Cs saturation again produces a marked increase in surface-area (Table 1) and in the volume of smaller micropores similar to that shown for the Wyoming bentonite.

Surface-area determination. It is difficult to assess the accuracy of surface-areas obtained where the possibility of N_2 sorption between two surfaces in close proximity exists. However, the comparison between specific surface-areas calculated by the B.E.T. and P.S.D. methods (Table 1) shows an agreement which, in view of the approximations involved, particularly in the second method, is quite remarkable. Whilst possibly fortuitous for some samples, this agreement increases confidence in the general picture proposed for the structural configuration of the dry clay-matrix which, in turn, has proved very useful in interpreting wide variations in swelling behaviour observed for the various materials (Aylmore, 1960).

Conclusion

Clay-mineral systems exist with a high degree of parallel alignment of the clay-crystals, resulting in a high proportion of microporosity. The following regions of microporosity, accessible to N molecules are indicated by the present investigation:

(*a*) Crevices of up to some 10 Å in width mainly between nearly contacting areas of overlap of crystal units. Staggering of the lamellae at crystal-edges and interleaving of unit-lamellae may contribute to the pore volume of these dimensions.

(*b*) Slit- and wedge-shaped pores resulting from the interleaving of crystal-units of several elementary sheets in thickness, giving rise to discrete differential pore-size distribution peaks at or near plate-thickness values. With clay-plates of the order of 1000 Å across the planar surfaces, it is possible that nearly parallel sided separations of up to 30 Å could also be produced by the presence of surface-irregularities and plate-buckling.

The N surface-area and pore-size distribution obtained for montmorillonite clays varies considerably with the exchangeable cation present: this is due to the inaccessibility of much inter-crystalline overlap area to N adsorption and may be governed, to some extent, by the effect in suspension of electrostatic interaction between the charged particles on crystal-size, but largely by mechanical interactions on sedimentation and the size of the exchangeable cations present.

Detailed experimental observations of particular aspects of these systems are being undertaken to facilitate the complete definition of their structural configurations.

Acknowledgement

We wish to thank Mr. I. D. Sills for carrying out a number of the experimental determinations.

REFERENCES

ADAMSON, A. W. 1963. In discussion. J. phys. Chem. **67**, 1959.

AYLMORE, L. A. G. 1960. Ph.D. Thesis, University of Adelaide.

—— and QUIRK, J. P. 1959. Swelling of clay-water systems. Nature, Lond. **183**, 1752–3.

—— —— 1960. Domain or turbostratic structure of clays. Ibid. **187**, 1046–8.

BARRER, R. M., and MCLEOD, D. M. 1955. Activation of montmorillonite by ion exchange and sorption complexes of tetra-alkyl ammonium montmorillonite. Trans. Faraday Soc. **51**, 1290–1300.

BARRETT, E. R., JOYNER, L. G., and HALENDA, P. P. 1951. The determination of pore volume and area distributions in porous substances. J. amer. Ceram. Soc. **73**, 373–80.

BATES, T. F. 1958. Circular No. 51, College of Mineral Industries, Penn. State University.

BROOKS, C. S. 1955. Nitrogen adsorption experiments on several clay minerals. Soil Sci. **79**, 331–47.

BRUNAUER, S. 1943. The Adsorption of Gases and Vapours. Oxford Univ. Press, London.

BRUNAUER, S., EMMETT, P. H., and TELLER, E. 1938. Adsorption of gases in multimolecular layers. J. amer. chem. Soc. **60**, 309–19.

DE BOER, J. H. 1958. The shapes of capillaries. p. 68 in 'The Structure and Properties of Porous Materials'. Butterworths, London.

—— VAN DEN HEUVAL, A., and LINSEN, B. G. 1964. Studies of pore systems in catalysis. IV. The two causes of reversible hysteresis. J. Catalysis **3**, 268–73.

DERJAGUIN, B. V. 1957. Correct form of the equation of a capillary condensation in porous bodies. Proc. 2nd Int. Congr. Surface Activity, **2**, 153–9.

EDWARDS, D. G., POSNER, A. M., and QUIRK, J. P. 1965. The repulsion of chloride ions by negatively charged clay surfaces. Parts II and III. Trans. Faraday Soc. **61**, 2816–23.

EMMETT, P. H., and BRUNAUER, S. 1934. The adsorption of nitrogen by iron synthetic catalysts. J. amer. chem. Soc. **56**, 35–41.

EVERETT, D. H. 1958. Some problems in the investigation of porosity by adsorption methods. p. 95 in 'The Structure and Properties of Porous Materials'. Butterworths, London.

FOSTER, A. G. 1932. The sorption of condensible vapours by porous solids. Part I. The applicability of capillary theory. Trans. Faraday Soc. **28**, 645–57.

GREACEN, E. L., and ROVIRA, A. D. 1957. The effect of aggregate disruption on the activity of microorganisms in the soil. Aust. J. agric. Res. **8**, 659–73.

GREENE-KELLY, R. 1964. The specific surface areas of montmorillonite. Clay Miner. Bull. **5**, 392–400.

GREENLAND, D. J., and QUIRK, J. P. 1962. Surface areas of soil colloids. Trans. Int. Soc. Soil Sci. Conf. Comm. IV and V. New Zealand, 79–87.

HARKINS, W. D., and JURA, G. 1944. Surface of solids, X, XII and XIII. J. amer. chem. Soc. **66**, 919–27, 1362–6, 1366–72.

INNES, W. B. 1957. Use of a parallel plate model in calculation of pore size distribution. Anal. Chem. **29**, 1069–73.

JOYNER, L. G. 1949. Chap. 12: 'Scientific and Industrial Glass Blowing and Laboratory Techniques' by Barr, W. E., and Anhon, V. J. Instruments Publishing Co., Pittsburg.

KEENAN, A. G., MOONEY, R. W., and WOOD, L. A. 1951. The relation between exchangeable ions and water adsorption on kaolinite. J. Phys. Coll. Chem. **55**, 1462–74.

KINGTON, C. L., and SMITH, P. S. 1964. Thermodynamics of adsorption in capillary systems. Parts I and II. Trans. Faraday Soc. **60**, 705–28.

LAMB, T. W. 1953. The structure of inorganic soils. Amer. Soc. Civil Eng. Proc. **79**, Paper No. 315.

LIPPENS, B. C., LINSEN, B. G., and DE BOER, J. H. 1964. Studies of pore systems in catalysis, I, II, and III. J. Catalysis, **3**, 32–49.

MCBAIN, J. W. 1935. An explanation of hysteresis in the hydration and dehydration of gels. J. amer. chem. Soc. **57**, 699–700.

MCDERMOT, H. L., and ARNELL, J. C. 1956. The adsorption of nitrogen by brominated graphite and carbon black. Canad. J. Chem. **34**, 1114–26.

MOONEY, R. W., KEENAN, A. G., and WOOD, L. A. 1952. Adsorption of water vapour by montmorillonite. I. Heat of desorption and application of B.E.T. theory. II. Effect of exchangeable ions and lattice swelling as measured by X-ray diffraction. J. amer. chem. Soc. **74**, 1367–71, 1371–4.

NORRISH, K. 1954. The swelling of montmorillonite. Disc. Faraday Soc. No. **18**, 120–34.

QUIRK, J. P., and PANABOKKE, C. R. 1962. Incipient failure of soil aggregates. J. Soil Sci. **13**, 60–70.

SCHULL, C. G., ELKIN, P. B., and ROESS, L. C. 1948. Pore size distribution from gas adsorption data. J. amer. chem. Soc. **70**, 1405–14.

TERZAGHI, K. 1956. In Correspondence, Geotechnique, **6**, 191–2.

VAN OLPHEN, H. 1962. Unit layer interaction in hydrous montmorillonite systems. J. Coll. Sci. **17**, 660–7.

(Received 13 September 1965)

SOIL SCIENCE
Vol. 103, No. 1

Printed in U.S.A.

ADSORPTION AND DESORPTION OF SULFATE IONS BY SOIL CONSTITUENTS

L. A. G. AYLMORE, MESBAHUL KARIM, AND J. P. QUIRK

The University of Western Australia[1]

Received for publication December 28, 1965

Recent studies of the retention of sulfate fertilizers by soils have indicated that movement of this ion through the soil profile occurs by a stepwise adsorption–desorption process similar to that which occurs in chromatographic columns. The main soil constituents thought to be responsible for sulfate adsorption are those clays possessing positive edge charges and the oxides of iron and aluminum.

Studies in our laboratories have been aimed at correlating the movement through leaching of fertilizers with factors such as water movement, soil structure, and interaction of the fertilizer with soil constituents. Of interest in this latter regard is the shape and, in particular, the reversibility of the isotherms governing the sorption processes for different ions. Chao, Harward, and Fang (2) have reported adsorption isotherms for sulfate (for a number of sulfate-retentive soils) which obey Freundlich-type equations with no indication of an adsorption maxmum up to equilibrium concentrations of 500 ppm. S. This concentration is 31 me. per l. of sulfate, which may be compared with a concentration of 28.0 me. per l. for saturated gypsum at 20°C. Most of this sulfate was easily desorbed, with as much as 45 per cent of the sulfate initially adsorbed being recovered by a single water extraction. Below a limiting equilibrium concentration of 15 ppm. S, the adsorption data conformed to a Langmuir-type equation, but at higher concentrations good agreement with the Freundlich equation was indicated. Kamprath, Nelson, and Fitts (7), on the other hand, have reported a linear Langmuir relationship for sulfate adsorption on Cecil soil up to and above an equilibrium concentration of 300 ppm. S.

[1] Department of Soil Science and Plant Nutrition, Institute of Agriculture. Mesbahul Karim wishes to acknowledge support from the Colombo Plan which enabled him to participate in this work. The authors are grateful to A. M. Posner for much helpful discussion.

In view of the many components present in natural soils and the possibility of the superposition of several different adsorption mechanisms, the importance of the various soil constituents in relation to sulfate retention can best be examined by direct measurement of sulfate adsorption on and desorption from the individual constituents rather than the soil mass in toto.

EXPERIMENTAL

Preparation of materials

Hydrated aluminum oxide was prepared by a modification of the methods of Weiser (10) and Gastuche and Herbillon (5). To a 1-liter solution of molar aluminum chloride at 20°C. 4 *N* sodium hydroxide was added slowly with continuous stirring until the pH reached 8.4. The gelatinous precipitate was centrifuged and washed repeatedly with distilled water to remove excess salt and then dialyzed against double-distilled water for 40 days. Controlled aging induces the gradual transformation from γ-$Al_2O_3 \cdot H_2O$ (pseudoboehmite) through metastable α-$Al_2O_3 \cdot 3H_2O$ (bayerite) to stable γ-$Al_2O_3 \cdot 3H_2O$ (gibbsite). The suspension was dried in an oven at 70°C. for 24 hours and the material ground to pass through an 80-mesh sieve. X-ray analysis indicated that the material obtained was largely pseudoboehmite with some gibbsite.

The ferric oxide precipitate was prepared by the hydrolysis of ferric nitrate solution by boiling for 18 days under reflux conditions to prevent the escape of nitric acid (9). The precipitate was dialyzed against double-distilled water until free from nitrate, dried at 70°C. for 24 hours, and then gently ground to a powder. X-ray analysis showed the end product to be α-Fe_2O_3 (haematite).

Samples of kaolinite clays from Clackline, Western Australia, and the American Petroleum Institute Clay No. 9 (API-9) were potassium-

saturated by repeated washing and centrifuging, using a molar solution of potassium chloride. The clays were washed free of chloride with distilled water, air-dried, and gently ground to powders. The Clackline clay contained a very small quantity of iron oxide, but x-ray and infrared analysis indicated that the API-9 clay did not contain iron or aluminum oxides.

All chemicals used were of analytical reagent standard.

Sulfate adsorption–desorption under equilibrium conditions

Samples of the iron and aluminum oxides and kaolinite clays were shaken with 25 ml. of various concentrations of potassium sulfate ranging from 1 me. per l. to 100 me. per l. The pH of the solution was adjusted to the required value by successive additions of dilute sulfuric acid between six hourly end-over-end shaking periods. At equilibrium a small known quantity of potassium sulfate containing S35 tracer was added and allowed to equilibrate; the amount of sulfate adsorbed was then calculated from the measured distribution of S35 in both the solid and liquid phases.

The concentration of sulfate in solution was determined chemically by the reduction method of Johnson and Nishita (6), and the total amount of sulfate in the liquid phase calculated from the known weight of solution present.

When the change in S35 concentration in solution due to adsorption was small in comparison to the total isotope present, the following technique was used. The tubes were centrifuged, the supernatant poured off, and the tube and contents re-weighed. The contents were extracted with sodium fluoride, and the total sulfate in the extract corrected for that due to the entrained solution to give the amount adsorbed on the known weight of material.

Desorption points were obtained by successive small dilutions of the supernatant concentrations at the highest adsorption levels, using distilled water pre-adjusted to the appropriate pH. This was done in such a way as to keep the ratio of solid to solution constant.

RESULTS AND DISCUSSION

Figure 1 shows the adsorption–desorption isotherms at pH 4.6 and 20°C. obtained for sulfate on the samples of pseudoboehmite and haema-

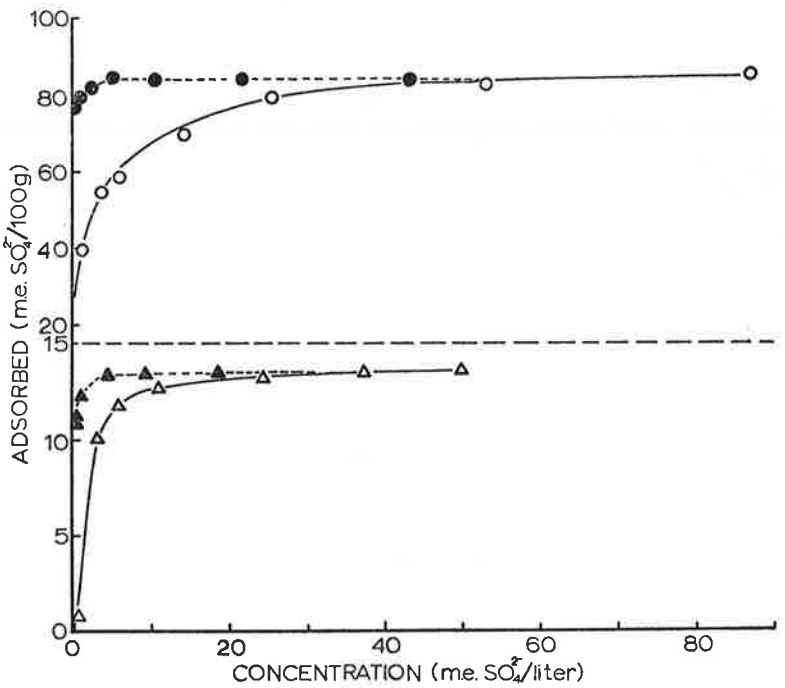

FIG. 1. Adsorption–desorption isotherms at 20°C. for sulfate on iron oxide (△ adsorption, ▲ desorption) and aluminum oxide (○ adsorption, ● desorption).

TABLE 1

Sulfate adsorption maxima and specific surface areas for kaolin clays and iron and aluminum oxides

Adsorbent	Adsorption maximum	Nitrogen surface area	Adsorption per unit area
	me./100 g.	*m.²/g.*	*me./m.²*
API-9 kaolinite.....	1.86	17.7	—
Clackline kaolinite....	1.0	16.9	—
Haematite.....	13.4	26.7	0.50
Pseudoboehmite.....	84.2	165.5	0.50

tite prepared in our laboratories. The adsorption isotherms for both oxides obey a Langmuir-type equation over this concentration range (fig. 2) and give adsorption maxima at 13.4 me. per 100 g. and 84.2 me. per 100 g. for iron and aluminum oxides, respectively. This is in exact proportion to the B.E.T. surface areas of the oxides as determined by low-temperature nitrogen adsorption (table 1), and indicates that the mechanisms of adsorption for both materials are related to the amount of available surface. This result is interesting, since similar adsorption mechanisms would be expected in the adsorption of sulfate by iron and aluminum oxides.

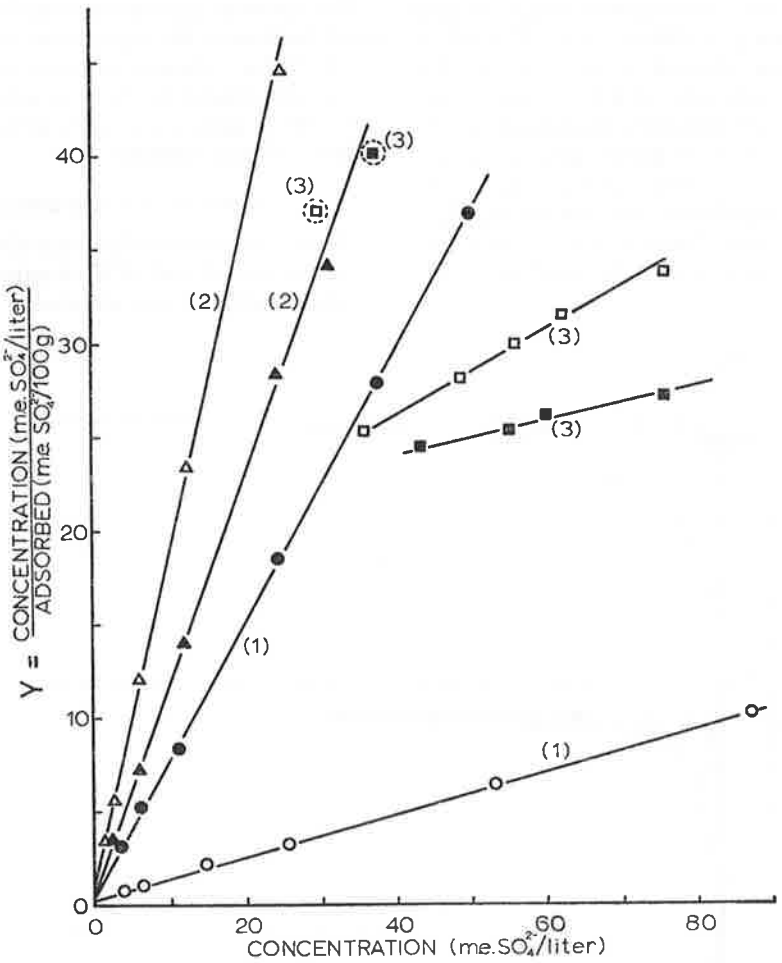

FIG. 2. Langmuir plots for sulfate adsorption on (*1*) aluminum oxide (○) and iron oxide (●), Y × 10; (*2*) API-9 kaolin (▲) and Clackline kaolin (△), first region Y; and (*3*) API-9 kaolin (■) and Clackline kaolin (□), second region, Y × 10^{-1}.

The most important result from the point of fertilizer leaching, however, is the almost complete irreversibility of the sorption process with respect to concentration as indicated by the desorption isotherms for the oxides. The term "irreversibility" is here used in the thermodynamic sense to indicate the presence of hysteresis between adsorption and desorption paths. Although the recovery of sulfate at infinite dilution has not been examined, parallel studies with leaching columns containing artificial admixtures of sand and oxide show that no significant displacement of this adsorbed sulfate occurs with up to 20 inches equivalent rainfall. Adsorption of sulfate was pH-dependent for both materials, decreasing with increasing pH but exhibiting similar isotherm characteristics at any given value. The adsorption data at pH 4.6 has been given here because of the increased adsorption, to better illustrate the irreversibility with respect to equilibrium concentration.

The sorption isotherms for sulfate on the kaolinite clay (fig. 3), on the other hand, clearly show two distinct regions of adsorption for each clay, and in contrast to the two oxides the adsorption is largely reversible with respect to concentration. The first adsorption plateau conforms to a Langmuir equation (fig. 2), but interpretation of the initial steep slope of the second region appears to require the assumption of a co-operative adsorption mechanism.

Muljadi, Posner, and Quirk (8) reported two Langmuir equations for the adsorption of phosphate on kaolinite API-9 and obtained 1.62 me. per 100 g. for the total amount adsorbed in the two regions. Although the nature of the second part of the isotherm for sulfate adsorbed onto API-9 is not clear, the points approaching the plateau conform with a Langmuir plot and the sum of the initial Langmuir and second part of the isotherm is 1.86 me. per 100 g. It thus appears that the two regions involved in sulfate

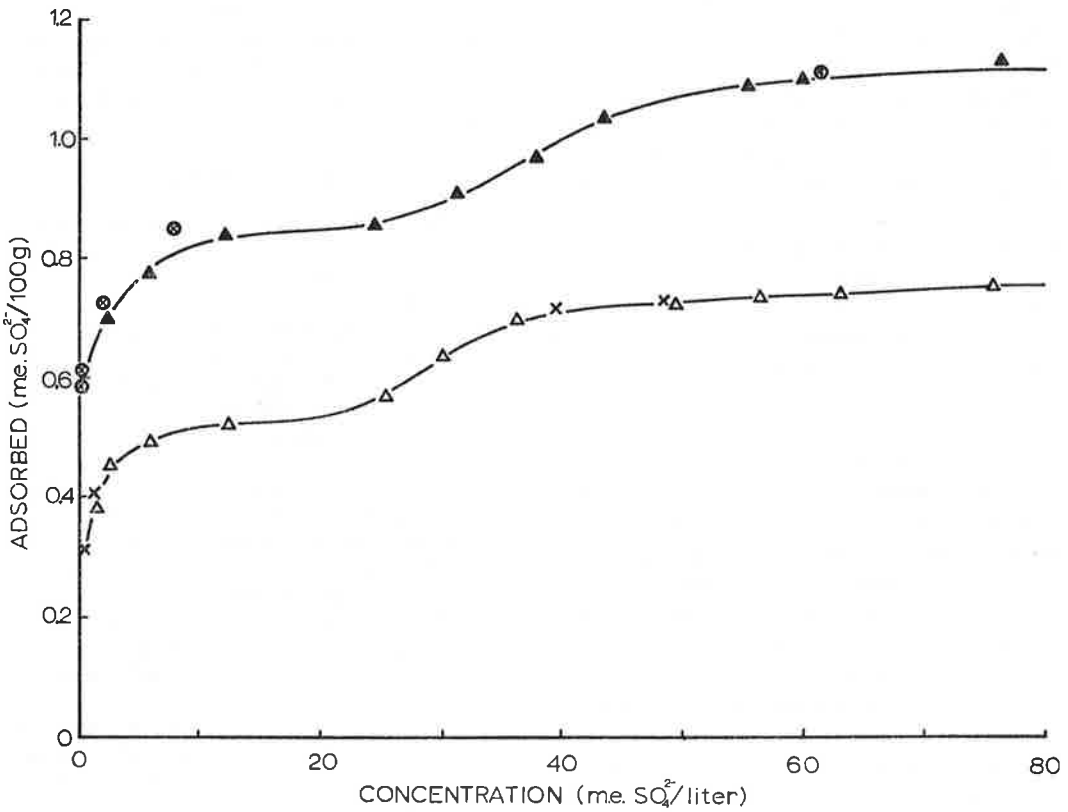

FIG. 3. Adsorption-desorption isotherms at 20°C. for sulfate on API-9 kaolin (▲ adsorption, ⊗ desorption) and Clackline kaolin (△ adsorption, X desorption).

adsorption are probably those described by Muljadi, Posner, and Quirk (8) for phosphate.

The most likely mechanism of significance for the sorption of sulfate and other anions by these materials within this range of equilibrium concentrations is by exchange with hydroxyl ions associated with the soil constituents. This is supported by the variations in adsorption capacities with pH observed by numerous workers (1, 3, 7, 8). Muljadi, Posner, and Quirk (8) have designated three regions in the adsorption isotherms of phosphate ions by kaolinite, gibbsite, and pseudoboehmite. They suggest that the first two regions are related to the affinity of the phosphate ion for energetically different reaction sites associated with the first and second hydroxyl of an $Al(OH)_2$ as part of the edge faces of the kaolinite and hydrated aluminum oxide crystals, and possibly on the kaolinite exchange sites occupied by aluminum. Similar sites would also exist for the hydrated iron oxide. Further adsorption was apparently produced by occlusion of phosphate within amorphous or semi-crystalline regions of the crystals.

The plateaus shown for sulfate adsorption on the kaolinite clays in figure 3 confirm the presence of at least two energetically different sets of sites for these materials, the small affinity of the sulfate ion accentuating the distinction between the two regions above that observed by the previous workers for the more strongly adsorbed phosphate. It appears, however, from the initial high affinity for region 2 after the completion of region 1, that something other than a simple adsorption on less reactive sites is occurring.

Close inspection of the curves obtained for iron and aluminum oxides suggests that each of these may also represent a composite of two adsorption processes, the first being largely completed at low equilibrium concentrations below some 3 me. per l. similar to the adsorption of phosphate in regions 1 and 2 for gibbsite and pseudoboehmite (8).

The cause of the irreversibility in the sorption of sulfate by iron and aluminum oxides may be related to a change in phase or re-orientation of the adsorbed phase in accord with the domain concept of hysteresis suggested by Everett and Whitton (4).

SUMMARY

The shape and reversibility with respect to concentration of the adsorption isotherms for sulfate ions on haematite, pseudoboehmite and kaolinite clay have been examined at equilibrium concentrations up to 100 me. per l. The isotherms for the two oxides conform to a Langmuir-type equation and are almost completely irreversible with respect to equilibrium concentration. On the other hand the isotherm for the kaolinite clays exhibit two distinct regions of adsorption and are largely reversible with respect to equilibrium concentration.

It is apparent that the adsorption of sulfate by soil constituents occurs at a number of energetically different reaction sites and cannot be adequately described by a single equation at all concentrations.

The proportions of clay minerals in soil are likely to be much higher than those of iron and aluminum oxides. While the sulfate adsorbed on the kaolinite clay is weakly held and easily released, that sorbed on iron or aluminum oxides as soil constituents will be highly resistant to leaching but may also be less available for plant growth.

REFERENCES

(1) Chang, M. L., and Thomas, G. W. 1963 A suggested mechanism for sulfate adsorption by soils. Soil Sci. Soc. Am. Proc. 27: 281–283.

(2) Chao, T. T., Harward, M. E., and Fang, S. C. 1962 Adsorption and desorption phenomena of sulfate ions in soils. Soil Sci. Soc. Am. Proc. 26: 234–237.

(3) Chao, T. T., Harward, M. E., and Fang, S. C. 1964 Iron and aluminum coatings in relation to sulfate adsorption characteristics of soils. Soil Sci. Soc. Am. Proc. 28: 632–635.

(4) Everett, D. H., and Whitton, W. I. 1952 A general approach to hysteresis. Trans. Faraday Soc. 48: 749–757.

(5) Gastuche, M. C., and Herbillon, A. 1962 "No. 243 Etude des gels d'alumine: cristallisation en milieu désionisé." Bull. Soc. Chim. Fr. 1404.

(6) Johnson, C. M., and Nishita, H. 1952 Microestimation of sulfur-plant materials, soils and irrigation waters. Anal. Chem. 24: 736.

(7) Kamprath, E. J., Nelson, W. L., and Fitts, J. W. 1956 The effect of pH, sulfate and

phosphate concentrations on the adsorption of sulfate in soils. Soil Sci. Soc. Am. Proc. 20: 463–466.

(8) Muljadi, D., Posner, A. M., and Quirk, J. P. 1966 The mechanism of phosphate adsorption by kaolinite, gibbsite and pseudoboehmite. J. Soil Sci. 17: 212–247.

(9) Smith, F. G., and Kidd, D. J. 1949 Haematite-goethite relations in neutral and alkaline solutions under pressure. Am. Mineralogist 34: 403.

(10) Weiser, H. D. 1935 "Inorganic Colloid Chemistry," vol. II, p. 90. John Wiley and Sons, New York.

Reprinted from the
AUSTRALIAN JOURNAL OF BIOLOGICAL SCIENCES

RETENTION OF WATER BY PLANT CELL WALLS AND IMPLICATIONS FOR DROUGHT RESISTANCE

By T. S. Teoh,* L. A. G. Aylmore,* and J. P. Quirk*

[*Manuscript received July* 20, 1966]

Summary

The water-retaining properties of cell wall materials from the roots of two monocotyledons (*Ehrharta calycina* Sm. and *Triticum vulgare* Vill. cv. Gabo) and two dicotyledons (*Salicornia australis* Banks & Soland and *Vicia faba* L.) have been studied.

Differences in the sorption–desorption isotherms found for the various wall materials suggest that an important factor enabling a drought-resistant species to endure prolonged water stress is the relatively greater tenacity with which its cell wall water is held in comparison with that of mesophytes.

I. Introduction

A considerable proportion of "apparent free space" (AFS) or "outer space" is present in plant tissue (Kramer 1957). For example the AFS of wheat roots has been estimated to be as high as 33·5% of the root volume (Butler 1953). Estimates of the amount of AFS vary with the method of determination, but values for the free space of roots obtained by various investigators range from about 12 to 35%.

Many workers, including Butler (1953), Levitt (1957), Dainty and Hope (1959), Laties (1959), Kramer and Kozlowski (1960), hold the view that the AFS resides entirely or largely in the cell wall. More recently electron-microscopic and other studies of the AFS of root cells of pine seedlings by Salyaev (1963, 1964) in Russia have provided convincing evidence that the AFS is in fact confined to the cell wall, and that a mass flow of water along the wall does actually occur. These findings are reasonable in view of the numerous interfibrillar spaces present in plant cell walls. The cell wall is considered as a micro- and macropore system (Dainty and Hope 1959) with the micropores ($\leqslant$100 Å in diam.) leading into the macropores ($\geqslant$100 Å in diam.). As a result of the numerous electron-microscopic studies on plant cell walls the presence in cellulose of individual microfibrils can now be considered as well established (Odintsov 1957).

Recent electron-microscopic work by Gaff, Chambers, and Markus (1964) have also demonstrated the presence of a "facile transport system" in the cell wall in which channels intercommunicate freely. The cell wall is generally considered a direct flow extension of the xylem system (Scholander *et al.* 1965). According to Raney and Vaadia (1965) the macropores of the root system are probably in the cell walls, and under hydrodynamic conditions of transpiration most of the water flow occurs in these larger pores.

* Department of Soil Science and Plant Nutrition, Institute of Agriculture, University of Western Australia.

In studies of the water relations of plants, the water in the cell wall has received increasing attention in recent years. It has been suggested that the considerable amount of water present in cell walls (actually the AFS) could act as a buffering system during periods of water stress since the resistance to movement is relatively lower along the wall than through the wall (Carr and Gaff 1961; Gaff and Carr 1961; see also May and Milthorpe 1962). However, no explanation has so far been put forward as to why this so-called buffering capacity is not as effective in drought-sensitive species as in drought-tolerant ones during drought periods.

In this paper the sorption–desorption isotherms for root cell wall materials of different species are compared. The implications of the relative amount of water sorbed, as well as the accompanying hysteresis, are discussed in relation to drought resistance. As pointed out by Slatyer (1965), an understanding of the relative mobility and physiological activity of various cell water fractions is a desirable prerequisite to further progress in studies of cell water relations.

II. Materials and Methods

Cell walls from which the amorphous constituents have been extracted are sometimes referred to as pure cell walls. These "purified" wall materials are in fact simply cellulose skeletons and unrepresentative of the natural condition as found in the plant. For this reason, cell wall materials used in this study were prepared by removing only the cytoplasm from the cells, leaving the amorphous matrix of the wall intact. It was hoped that the use of wall materials prepared in this manner would provide a more meaningful comparison between the several species studied.

Two dicotyledons (*Salicornia australis* Banks & Soland and *Vicia faba* L.) and two monocotyledons (*Ehrharta calycina* Sm. and *Triticum vulgare* Vill. cv. Gabo) were chosen for their contrasting botanical differences. Wall materials from the young roots of these plants were prepared using a standard method, so that data obtained could be directly compared.

The freshly harvested roots were washed thoroughly until free of soil particles; they were comminuted in 0·5M sucrose in a MSE Ato-Mix for 15 sec, and the mixture strained through muslin. This process was repeated a further two times. The residue was then washed with 10% NaCl four times (again using the Ato-Mix), each time the excess solution being squeezed out by hand as it would not drain of its own accord. To saturate the material with calcium, it was then washed four times with 20% $CaCl_2$. Finally, it was washed with distilled water until free of chloride; the absence of chloride was tested by adding $AgNO_3$ to the washings. The above operations were carried out in a cold-room at 4°C. After air-drying at 20°C the wall material was passed through a 1-mm sieve of an EBC mill (Casella, London).

For ease of handling, particularly in sampling, the wall materials (air dry) were compressed into small cores at a pressure of 500 lb/in^2. This was achieved by means of a stainless steel mould and a hydraulic press: 30 mg was found to be the minimum amount of material necessary to make suitable cores, both from the point of view of coherence and the time taken to reach equilibrium.

The cores were allowed to sorb water until equilibrium was reached at particular values of water stress. A range of equivalent water suctions was obtained by using

improved versions of pressure plates (Richards and Fireman 1943), pressure membranes (Richards 1941, 1947), and vacuum desiccators containing saturated salt solutions (O'Brien 1948) for the low, middle, and high suction ranges, respectively. The first two techniques involve the application of a constant air pressure to one side of a ceramic plate or cellulose membrane, the other side being in contact with a reservoir of the appropriate solution. This air pressure induces a curvature in the meniscus of each membrane pore equivalent to that produced by a hydrostatic suction applied to the solution in the membrane. Higher equivalent suctions (i.e. lower vapour pressures) are more conveniently obtained by equilibration with the constant vapour pressures obtained over various saturated salt solutions. Sorption of electrolyte solutions was examined by replacing the water in the pressure plates and pressure membranes with solutions of different concentrations. These determinations were confined to the liquid transport range, since the vapour pressure measurements involve a continuous variation in osmotic pressure component of the total water potential as the water content changes, for all but salt-free materials.

This equipment was housed in a constant-temperature room maintained at 20 ± 1°C. Due to the enclosed nature of the equipment thermal fluctuations in the immediate environment of the cores would be much smaller than those in the room itself. In the use of the pressure plates a system of precision air-pressure regulators (Negretti and Zambra, London) in conjunction with mercury manometers and water columns was used to adjust the water potential to any desired value.

Sampling was carried out by removing cores in duplicate from the apparatus and immediately transferring them into stoppered weighing bottles. Water contents were calculated on the basis of the oven-dry weight of the cores at 105°C. After drying, the cores were discarded since heating to 105°C did in fact lower the sorptive capacity of the wall materials when re-wetted. Many fibres including wool and cotton also show an appreciable decrease in sorption after they have been dried at 105°C for 24 hr (Chabert and Diemunsch 1962). However, weight losses between drying under vacuum over P_2O_5 and drying in the oven at 105°C were found to be insignificant. The former method was not used as several days were required for the wall material to attain constant weight.

The growth of *Mucor* spp. and other Phycomycetes on the cores at low suction was prevented by painting a solution of thymol in alcohol on the roof of each Perspex dome of the pressure plates.

Preliminary experiments indicated that the approach to equilibrium (using 30-mg cores) was asymptotic, but in general some 18, 8, and 12 days were found to be satisfactory times for pressure plates, pressure membranes, and desiccators, respectively. The penetration of the water molecules into the internal network of fine capillaries in the cell wall could be expected to be a relatively slow process, proceeding initially with interfibrillar and finally with intrafibrillar swelling.

III. Results and Discussion

Figure 1 shows the sorption–desorption isotherms obtained for the four species. Water content has been plotted versus water potential expressed as the logarithm of

the applied suction in millibars (Slatyer and Taylor 1960, 1961; Taylor and Slatyer 1961*a*, 1961*b*). In general, the water uptake increases exponentially as the water stress decreases. This may be attributed to the nature of the internal adsorption.

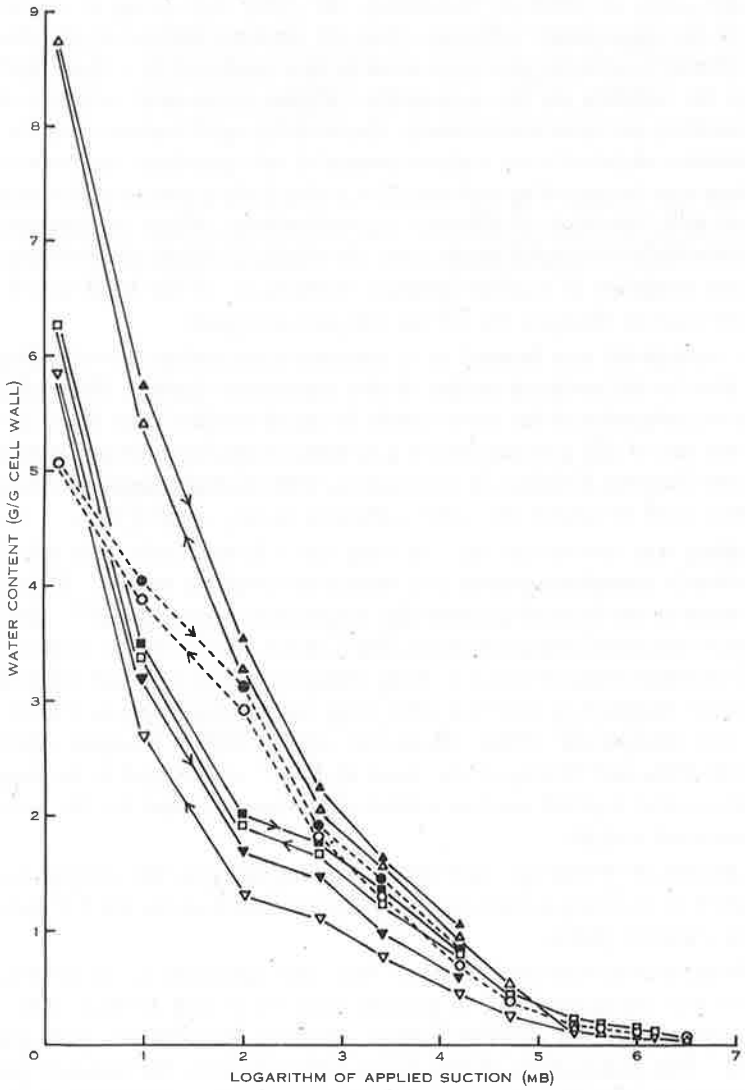

Fig. 1.—Sorption–desorption isotherms at 20°C for the cell wall–water system for the four species. Cell wall preparation saturated with calcium as described in the text. Solid symbols denote desorption, open symbols sorption. ▲, △, *T. vulgare*; ●, ○, *S. australis*; ■, □, *V. faba*; ▼, ▽, *E. calycina*.

As swelling of the cell walls proceeds, the opening up of the matrix exposes fresh sites for the further adsorption of water molecules, the amount sorbed depending on the number and position of the polar groups present on the macromolecular chains. However, the large water uptake at low water stress is probably due to capillary

absorption between the wall fragments constituting the core. In the absence of this absorption, the isotherms may well be sigmoid-shaped as has been observed for many cellulosic materials. It is difficult to make an exact distinction between such capillary absorption and purely surface-adsorbed water. However, preliminary studies with fractions of wall materials of various particle sizes indicated that the contribution from such macrocapillary water is insignificant at values of water suction greater than some $10^{1\cdot3}$ mb.

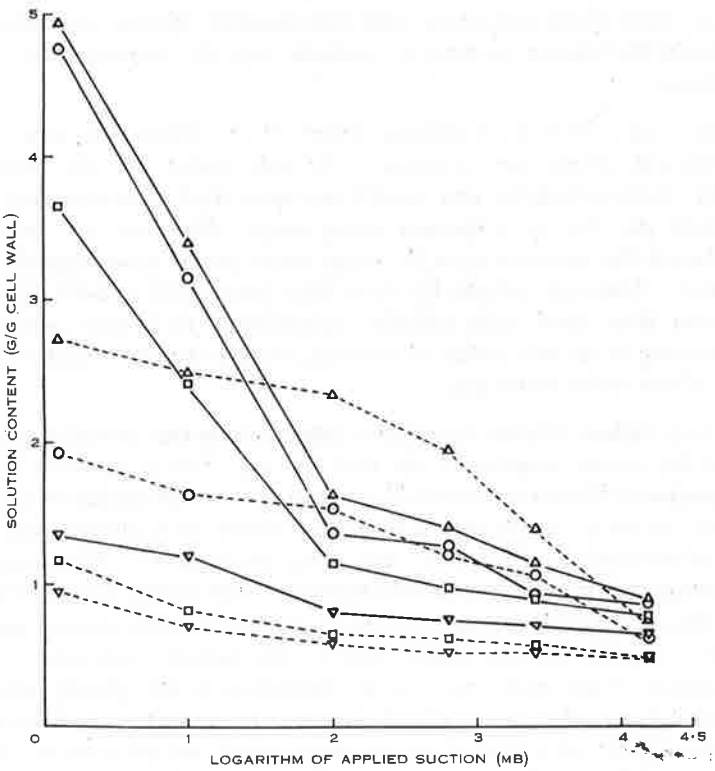

Fig. 2.—Sorption isotherms at 20°C for the cell wall–calcium chloride system for two species at four concentrations of calcium chloride: △ 0·01M; ○ 0·1M; □ 1M; ▽ 4M. Cell wall preparation saturated with calcium as described in the text. ——— *T. vulgare*; – – – – *S. australis*.

Except at very low values of applied suction, it is seen that the drought-resistant *E. calycina* (perennial veldt grass) exhibits the smallest sorptive capacity amongst the four species. Classical experiments have shown that under comparable environmental conditions, there are marked differences in the water requirements of various crop plants and even between varieties of a particular crop, with the amount of water needed for normal growth decreasing from drought-sensitive to drought-tolerant species. It is possible that a common factor enabling perennial veldt grass and other xerophytes to withstand water stress is their smaller water use as compared with more mesophytic species, coupled with the fact that the cell wall water in

xerophytes is held by relatively stronger forces so that it is not easily lost under dehydrating conditions. The latter effect is discussed in relation to the hysteresis phenomenon.

The perennial veldt grass used in this study (an introduced species in Western Australia) is thriving particularly well in its competition with more well-adapted indigenous species (Teoh 1964). From time to time during the last couple of decades, various measures have been tried to eradicate this "weed" from large areas of bushland reserve near Perth, but as yet with little success. Its wiry drought-resistant roots have helped the species to survive recurrent long dry summers with frequent high temperatures.

Salicornia was collected at Pelican Point, W.A., where the roots of these highly salt-tolerant plants are submerged in salt water all the year round. Physiologically, both halophytes and xerophytes have often been regarded as being similar, i.e. both are able to withstand water stress. However, one fundamental difference between the environments in which these plants exist appears to have been overlooked. Although halophytes have been considered to have difficulty in extracting water from their salty habitat, nevertheless their roots generally are bathed continuously in the salt water; in contrast, xerophytes are subject to recurrent long spells of actual water deficiency.

At the very highest relative humidities (approaching free water) it is seen that Salicornia has the lowest sorption of the four species. This is probably due to an inherent adaptation of the plant whereby it is able to control the intake of excess water into its system; unless it can do this, it would not thrive in its natural wet habitat. The sorption of electrolyte solutions of various concentrations by Salicornia and by wheat over a range of suctions is shown in Figure 2. The values for water potential indicate only that component arising from the applied hydrostatic suction and do not include the lowering of the free energy due to the osmotic component. For all electrolyte concentrations used, sorption by Salicornia is not greatly affected by changes in water stress below some 10^3 mb suction. In contrast, wheat increases its solution uptake rapidly at values of water stress below 10^2 mb suction. (Sorption isotherms obtained for the bean and the veldt grass in electrolyte solutions are similar to those of the wheat). It is seen that with increasing salt concentration to 1M, solution uptake by Salicornia decreases rapidly but thereafter shows only slight changes. On the other hand, concentrations approaching 1M are necessary to significantly restrict the solution uptake by the wheat, and at 4M a marked reduction is observed, particularly at low water suctions. The characteristic behaviour of Salicornia is probably related to its ability to limit the uptake of electrolyte solutions.

Recently the mangroves of Cape York (northern Australia) were studied by Scholander *et al.* (1965) who reported that the xylem sap in these salt-tolerant plants consisted essentially of fresh water. In most of the species they studied, the salt concentration averaged only 1% of that of the sea water. The negative hydrostatic pressure of the sap of *Salicornia* was found to average -50 atm; since the osmotic potential of sea water is about -25 atm, *Salicornia* has an ample margin for extracting fresh water from the ocean.

The ease with which fresh water is available to *S. australis* may be associated with the narrower hysteresis loop as compared with that found for perennial veldt grass (Fig. 1). There are many causes for hysteresis, depending on the nature of the system under study. Hysteresis in a swelling polymer has been interpreted by Cassie (1945) as a reflection of the mechanical constraints present in the resultant swelling gel. Since perennial veldt sorbs the smallest amount of water over most of the range, its cell walls probably have a more tightly bound structure in comparison with wheat, broad bean, and Salicornia. It follows that the sorbed water molecules in the wall structure of perennial veldt would probably be held by stronger forces than the majority of those in the other three species. Regardless of how hysteresis is interpreted it is clear that the ability of the cell wall material to retain water when desorbed to a particular water potential varies amongst the four species. The work done in completing an adsorption–desorption cycle, as given by the areas within the respective hysteresis loops, is smallest for the bean and largest for perennial veldt. The cell wall water of drought-sensitive species is likely to be easily depleted under drought conditions. As soil moisture approaches a critical low level, the root probably shrinks slightly due to the withdrawal of water from its AFS to supply the tops. It is possible that permanent damage to the ultrastructure of the cell walls may occur as a result of such volume changes.

The work needed to remove the same quantity of water from various types of cell wall (different matrices with different physicochemical properties) will vary. It seems reasonable that the tenacity with which the cell wall holds onto water would increase as the drought-resisting capacity of the species increases. It is well known that under conditions of water stress the consequent physiological responses in the plant differ from species to species. If a xerophyte and a mesophyte were simultaneously subjected to an identical drying regime, wilting symptoms will appear in the latter long before they do in the former.

Discussing the evidence from various investigations of the relative exchangeability of water in different cell components, Petinov (1962) states that, in general, the ease of exchangeability decreases in the following order: water in cell walls and vascular system, vacuolar water, cytoplasmic water, and water in chloroplasts; this implies that the water in the cell wall and vascular system is relatively free. Under conditions of dehydration the water stored in the microcapillary systems in the fibrillar wall structure can be readily transported and distributed to other cell components where more vital processes are going on.

Adsorption theories applicable to polymeric systems have been reviewed in detail by Chabert and Diemunsch (1962). The applicability of these theories to the present and additional data at low water potentials will be discussed in a separate paper.

IV. Concluding Remarks

Drought resistance in plant species undoubtedly involves a multiplicity of factors; factors such as sunken stomata, thick cuticle, water-storage mechanisms, etc. obviously contribute to the water economy of plants. However, these specialized adaptations are often characteristic of a particular species or family only. They

assist the plant, in a limited degree, to overcome the initial stages of dehydration. In the final analysis, the drought resistance of a species would depend on its ability to endure increasing intensity of dehydration until internal water deficits become critical. Plants which are adapted to drought conditions and yet possess no obvious morphological features suggesting such adaptability may be called "physiological xerophytes" (Lemée 1946).

The development of an extensive root system is without doubt another means of overcoming inadequate rainfall (e.g. Satoo 1956; see also Palmer, Trickett, and Linacre 1964), but again, not all drought-resistant species possess this characteristic. The roots of perennial veldt grass are generally very fine. In the sandy soils of the Perth area, the adventitious root system of this grass does not penetrate the soil deeper than a depth of about 1 ft. Plants of dry habitats which tap water by means of extensive root systems cannot be regarded as true xerophytes, since they are not subject to actual water stress. More than 50 years ago, Kamerling (1914) had shown that certain so-called xerophytes in fact transpire freely, and he termed them "pseudoxerophytes" in contrast to true xerophytes which have a smaller transpiration rate.

It is suggested that the cell wall plays an important role in the water regime of all arid and semi-arid vegetation with regard to drought resistance, irrespective of whether other adaptive features are developed or not. During periods of drought, xerophytes must possess a greater resistance to the destruction of the integrity of the two-phase nature of the cell wall (solid–liquid system) than do mesophytes. It should be emphasized that it is this greater resistance to desiccation which is considered to be important in this regard rather than the presence of a supplementary water reservoir acting as a buffer in the volumetric sense. It is known that a plant subjected to water stress frequently develops thicker cell walls. "In many plants, the volume of cell wall can reach significant proportions and in xerophytic and sclerophytic tissue the volume of the vacuole can be less than one-half of the total cell volume" (Slatyer and Taylor 1960).

Provided that a rigorously standardized procedure is used in the preparation of cell wall materials, the simple quantitative approach of assessing the comparative drought hardiness of various species as described in this paper may be of practical value in selection trials. However, more studies on plants with varying degrees of known drought resistance would be needed. It is hoped to include the drought-sensitive species *E. brevifolia* and *E. longiflora* (annual veldt grasses) in subsequent studies using this method. Annual veldt grass has a relatively broader leaf lamina and is more mesophytic than perennial veldt grass. A comparison of closely related species having different capacities in withstanding water stress may throw further light on the present findings.

V. Acknowledgment

One of us (T.S.T.) expresses his gratitude to the University of Western Australia for financial assistance.

VI. References

Butler, G. W. (1953).—Ion uptake by young wheat plants. II. The "apparent free space" of wheat roots. *Physiol. Plant.* **6**, 617–35.

Carr, D. J., and Gaff, D. F. (1961).—In "Plant–Water Relationships in Arid and Semi-arid Conditions". Proc. Madrid Symp. pp. 117–25. (UNESCO: Paris.)

Cassie, A. B. D. (1945).—Absorption of water by wool. *Trans. Faraday Soc.* **41**, 458–64.

Chabert, J., and Diemunsch, J. (1962).—Contribution to the study of sorption in textile fibres. *Bull. Inst. Text. Fr.* **99**, 205–63.

Dainty, J., and Hope, A. B. (1959).—Ionic relations of cells of *Chara australis*. I. Ion exchange in the cell wall. *Aust. J. Biol. Sci.* **12**, 395–411.

Gaff, D. F., and Carr, D. J. (1961).—The quantity of water in the cell wall and its significance. *Aust. J. Biol. Sci.* **14**, 299–311.

Gaff, D. F., Chambers, T. C., and Markus, K. (1964).—Studies of extrafascicular movement of water in the leaf. *Aust. J. Biol. Sci.* **17**, 581–6.

Kamerling, Z. (1914).—Which plants should we call "xerophytes"? *Flora, Jena* **106**, 433–54.

Kramer, P. J. (1957).—Outer space in plants: some possible implications of the concept. *Science* **125**, 633–5.

Kramer, P. J., and Kozlowski, T. (1960).—"Physiology of Trees". (McGraw-Hill Book Co., Inc.: New York.)

Laties, G. G. (1959).—Active transport of salt into plant tissue. *Ann. Rev. Pl. Physiol.* **10**, 87–112.

Lemée, G. (1946).—Investigations on the water use by small xeromorphic shrubs of sandy tracts. *Ann. Sci. Nat. Bot.* (11) **7**, 53–85.

Levitt, J. (1957).—The significance of "apparent free space" (AFS) in ion absorption. *Physiol. Plant.* **10**, 882–8.

May, L. H., and Milthorpe, F. L. (1962).—Drought resistance of crop plants. *Field Crop Abstr.* **15**, 171–9.

O'Brien, F. E. M. (1948).—The control of humidity by saturated salt solutions. *J. Sci. Instrum.* **25**, 73–6.

Odintsov, P. N. (1957).—Present-day views on the structure of cellulose and cell walls of plants. *Trudy Akad. Nauk Latviiskoi SSR* **12**, 5–24.

Palmer, J. H., Trickett, E. S., and Linacre, E. T. (1964).—Transpiration response of *Atriplex nummularia* Lindl. and upland cotton vegetation to soil–moisture stress. *Agric. Meteorol.* **1**, 282–93.

Petinov, N. S. (1962).—"The Physiology of Irrigated Agricultural Plants." [In Russian.] (U.S.S.R. Acad. Sci.: Moscow.)

Raney, F., and Vaadia, Y. (1965).—Movement of tritiated water in the root system of *Helianthus annuus* in the presence and absence of transpiration. *Plant Physiol.* **40**, 378–82.

Richards, L. A. (1941).—A pressure-membrane extraction apparatus for soil solution. *Soil Sci.* **51**, 377–85.

Richards, L. A. (1947).—Pressure-membrane apparatus—construction and use. *Agric. Engng.* **28**, 451–4.

Richards, L. A., and Fireman, M. (1953).—Pressure-plate apparatus for measuring moisture sorption and transmission by soils. *Soil Sci.* **56**, 395–404.

Salyaev, R. K. (1963).—The problem of the mechanism of water absorption by plant roots. *Dokl. Akad. Nauk SSSR* **152**, 1253–5.

Salyaev, R. K. (1964).—Electron-microscopic examination of the "apparent free space" of root cells, and the role it plays in water absorption. *Dokl. Akad. Nauk SSSR* **158**, 737–8.

Satoo, T. (1956).—Drought resistance of some conifers at the first summer after their emergence. *Bull. Tokyo Univ. Forests* **51**, 1–108.

Scholander, P. F., Hammel, H. T., Bradstreet, Edda D., and Hemmingsen, E. A. (1965).—Sap pressure in vascular plants. *Science* **148**, 339–46.

Slatyer, R. O. (1965).—Abstr. of paper by N. S. Petinov (1962), with commentary.

Slatyer, R. O., and Taylor, S. A. (1960).—Terminology in plant– and soil–water relations. *Nature, Lond.* **187**, 922–4.

SLATYER, R. O., and TAYLOR, S. A. (1961).—Terminology in plant– and soil–water relations. (Discussion.) *Nature, Lond.* **189**, 207–9.

TAYLOR, S. A., and SLATYER, R. O. (1961*a*).—Proposals for a unified terminology in studies of plant–soil–water relationships. Proceedings of a conference on plant–water relationships in arid and semi-arid conditions. *Arid Zone Res.* **16**, 339–49.

TAYLOR, S. A., and SLATYER, R. O. (1961*b*).—Water soil–plant relations terminology. Trans. 7th Int. Congr. Soil Sci. Vol. 1. pp. 394–403.

TEOH, T. S. (1964).—"Some Ecological Studies of the Vegetation at King's Park with special reference to *Casuarina fraseriana*." Hons. Thesis, University of Western Australia.

9th INTERNATIONAL CONGRESS OF SOIL SCIENCE
TRANSACTIONS

VOLUME I PAPER 16

LEACHING OF FERTILIZER IONS IN SOIL COLUMNS

L. A. G. AYLMORE
AND MESBAHUL KARIM

LEACHING OF FERTILIZER IONS IN SOIL COLUMNS

L. A. G. Aylmore and Mesbahul Karim
Department of Soil Science and Plant Nutrition, University of Western Australia

Introduction

The movement of salt solutions through the soil is subject to the complexities of soil structure and, in addition, to the extent to which solute ions interact with the various soil constituents. Dispersion and dilution of solute concentration have been attributed to such factors as ion exchange, adsorption and molecular diffusion, as well as to hydrodynamic effects due to the distortion of flow lines and velocity differences within the porous medium.

Recently attention has been focussed on the ability of a number of theories of ion exchange, adsorption and dispersion in flow systems to successfully predict the movement and distribution of salt and fertilizer ions in soil columns. In these approaches the differential equation describing the material balance at a point within the column is set up on the assumption of a specific dispersion process, and solved for the particular boundary conditions applicable.

Two types of experiment are of most general interest. The distribution of a slug or band of solution moving through the column can be determined either by sectioning the column at the appropriate time, or by measuring the concentration of the effluent. The boundary conditions are usually simpler however, when the displacement of one solution from the column by another is examined by means of the effluent concentration. Plots of concentration versus effluent volume for this case are generally referred to as breakthrough curves.

The velocity of movement of a solution through a porous medium varies in magnitude and direction from point to point because of the viscous characteristics of the liquid and the complex geometry of the medium. This distribution of velocities induces a movement of the solute at diverse rates, thus causing a spreading of the boundary between solution and pure solvent, quite independently of diffusive and sorptive effects. Day (1956) adapted the statistical theory of disordered movement developed by Scheidegger (1954) to describe the dispersion of a salt water front moving through a soil column as a result of these effects.

Some controversy exists as to the relative importance of simple longitudinal molecular diffusion and of hydrodynamic dispersion in determining the amount of spreading which occurs at a boundary during displacement. Spreading through molecular diffusion should occur for any given solution and porous structure at a relatively constant rate. Thus, the faster the inter-

face is displaced from one end of a soil column to another, the less significant will this mechanism be. On the other hand, the process of hydrodynamic dispersion is controlled largely by the range of pore sizes and distribution of pores in the medium and, for a given length of displacement, the amount of spreading of the boundary is essentially independent of the velocity with which the displacement occurs. For any given system the relative importance of these two factors will thus be determined by the flow velocity, and it seems logical to expect that there would be a gradual transition in importance from one effect to the other over a certain velocity range. However, it is not clear at just what flow velocity the diffusion mechanism becomes significant.

In reactive media the analysis is further complicated by the nature of the sorption process. Glueckauf (1949) extended the "theoretical plate" model of Martin and Synge (1941) and obtained solutions to a continuous mass balance equation on the assumptions of a diffusive mechanism for dispersion, subject to local equilibrium and a linear adsorption isotherm. Similarly, Lapidus and Amundson (1952) obtained solutions to a differential equation in which the effects of both molecular diffusion and average flow velocity through the medium on solute movement are taken into account. A linear adsorption isotherm is again assumed, and the solution for the case of local equilibrium is of most practical use.

In contrast to the theories assuming instantaneous equilibrium between solution and solid, Hiester and Vermeulen (1952) have developed Thomas' (1944) approach in which an attempt is made to account quantitatively for dispersion in terms of a finite rate of adsorption in the column. The equation describing the material balance is solved in conjunction with a Langmuir isotherm equation, and an equation describing the surface reaction. No account is taken of molecular diffusion or the effects of flow velocity.

A complete formulation incorporating all possible dispersion mechanisms presents considerable mathematical difficulty, and may not be warranted in many circumstances. Hence, it is of interest to examine the relevance of the many mechanisms which can be imagined, to any particular system. So far, very little information has been obtained on the dynamics of anion adsorption and desorption during flow in soil columns, and this has been largely in the nature of qualitative or semi-qualitative comparisons (Berg and Thomas 1959, Chao, Harward and Fang 1962).

Experimental

The columns used for leaching experiments were constructed from acrylic tubing of 4·4 cm internal diameter. Simple breakthrough measurements were carried out using a suitable length of the tubing closed at the bottom end, except for an 0·1 cm internal bore stopcock to control the flow rate. Sectionable columns for the measurement of solute distribution were constructed from 2-cm segments of acrylic tubing taped together. The columns were coated with a thin layer of paraffin wax by immersing the inverted columns and slowly withdrawing them from a tube containing hot paraffin. This was done to prevent leakage from the sectionable columns

and to provide a good seal between the contents and the walls of the columns.

Before filling the columns, a piece of fine metal gauze was placed on the bottom of the column to facilitate drainage. The columns were filled by a standard procedure to maintain as near uniformity of packing as possible. The material was spread on a plastic sheet and slightly moistened by a fine water spray. It was thoroughly mixed and then packed into the column by tamping small constant increments with a steel plunger. Preliminary experiments on sorptive capacity and water content showed that there was no significant movement of the clay within the sand columns at much higher flow velocities than those reported here.

The columns were saturated from below by gradually raising the level of water in a tube attached to the outlet. In general water and solutions were added to the top of the columns by means of a constant head device adjusted to maintain a thin layer. Constant flow rates were maintained by preadjustment of the outlet stopcock. In the experiments involving the movement of a slug of solution, the slug was applied uniformly to the top of the column and just allowed to disappear before subsequent leaching. Sectioning of the columns was carried out as soon as the level of the applied water reached that of the soil surface. The contents of the segments were placed in tins, weighed before and after oven drying, and analysed for solute content.

Chloride contents were obtained by extracting with 50 ml of $0{\cdot}05N$ sulphate solution followed by electrometric titration. Sulphate was extracted using $0{\cdot}1N$ sodium fluoride. S^{35} radioisotope labelled sulphate was used to facilitate measurements of the concentration of this ion by scintillation counting.

For studies on sulphate movement, the *pH* of the column was preadjusted to the required value by continuous leaching with the appropriate chloride solution of this *pH*. Both the tracer and non-tracer solutions were also preadjusted to the required *pH*, using sulphuric or hydrochloric acid respectively.

The Clackline kaolinite was obtained as soft blocks of material from the pallid zone of a laterite, Clackline, Western Australia. The material was hand ground and passed through an 80 mesh sieve before use. X-ray analysis indicated that this clay does not contain any significant amounts of iron or aluminium oxides. The clay was saturated with the required cation by repeated washing and centrifuging, using a molar solution of the appropriate chloride and then washed free of chloride with distilled water. It was air dried and gently hand ground to a powder.

The clay as prepared had a specific surface area of $16{\cdot}9 m^2/g$ and a cation exchange capacity of $1{\cdot}5$ me/$100g$.

Aggregates of Clackline kaolinite were obtained by mixing the powdered clay with water, forcing the resultant thick paste through appropriate sized sieves and allowing the globules produced to dry out at 100°C. To restrict any possible swelling and disintegration on wetting of the aggregates, these were heated to 300°C in a furnace (Aylmore 1960).

The sand used in these experiments was a yellow sand from the Swan Coastal Plain, Western Australia. Before use, the sand was washed repeatedly with dilute *NaOH* solution to remove some 0·5% of colloidal coatings. The particle size distribution of this sand is 99 per cent within the 0·1 mm to 0·5 mm range.

Results and Discussion

The chloride breakthrough curves obtained for flow velocities of 1·0 cm/hr, 0·75 cm/hr, 0·45 cm/hr and 0·1 cm/hr in a 30 cm column containing a mixture of sand and 5 per cent powdered Clackline kaolinite are shown in Figure 1. To prevent any slight adsorption of chloride by the clay (Berg and Thomas 1959), the columns were pre-equilibrated with a 0·01*N* solution of potassium sulphate and the chloride eluting solution also contained this concentration of sulphate. At higher flow velocities, the breakthrough curves obtained were essentially the same as that obtained using 1·0 cm/hr.

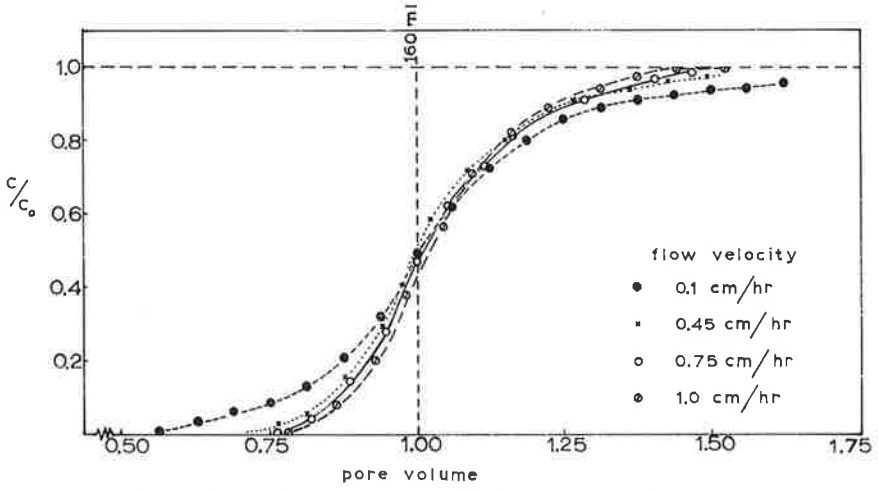

Fig. 1.—Chloride breakthrough curves for flow velocities of 1·0 cm/hr, 0·75 cm/hr, 0·45 cm/hr and 0·1 cm/hr in saturated columns containing sand plus 5 per cent powdered Clackline clay.

With decreasing flow velocity below 1·0 cm/hr, the point of breakthrough is progressively shifted to lower effluent volumes, and the approach to $C/C_0 = 1·0$ is substantialy delayed with respect to that of a symmetrical breakthrough curve. This skewed nature of the curves and their slight displacement to the right of $C/C_0 = 0·5$ at one pore volume (160 mls), presumably indicates the increasing effect of longitudinal molecular diffusion in addition to the simple hydrodynamic dispersion effect.

The variation in the breakthrough curves with flow velocity below 1 cm/hr observed here is much less than that observed by Nielsen and Biggar (1963) for mixing in glass beads. This and the conflicting con-

clusions reached by authors on the relevance of molecular diffusion and hydrodynamic dispersion (cf. Gardner and Brooks 1956, Day and Forsythe 1957, Nielsen and Biggar 1963) suggest that the manner in which these two phenomena are coupled differs with the pore size distribution of the system. In any event, longitudinal molecular diffusion seems unlikely to be of appreciable significance at the flow rates which normally occur during the leaching of soils. The usefulness of Day's relatively simple approach in predicting both the extent of movement and distribution for a non-adsorbed species has been well illustrated by comparisons between experimental and predicted distributions (Karim 1967).

The effects of molecular diffusion are likely to be of most importance in aggregated soils when there is an appreciable delay between dissolution of a salt and its subsequent leaching. In Figures 2 a, b and c, the relevance of molecular diffusion of chloride ions into intra-aggregate pores has been examined by comparing the differences in the distributions obtained when a chloride slug is leached immediately after application, and when some 24 hours is allowed to elapse between the addition of the chloride slug to the top of the column and its subsequent leaching. In Figure 2a, the slugs

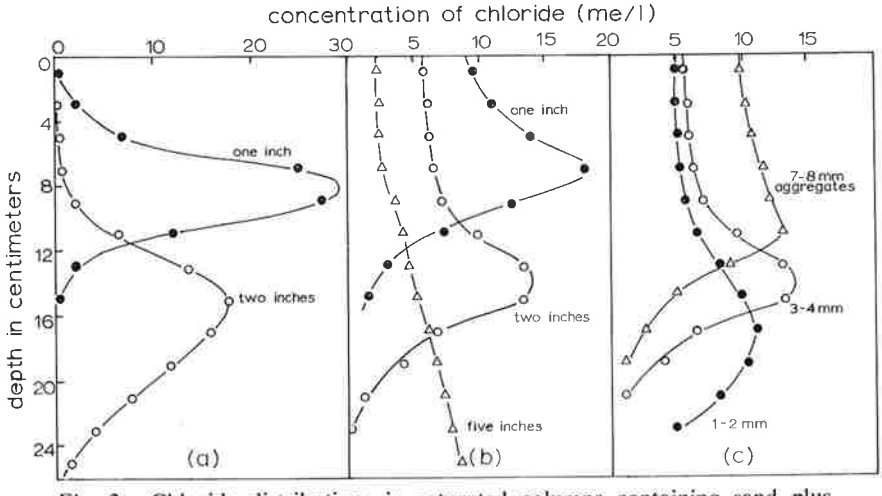

Fig. 2.—Chloride distributions in saturated columns containing sand plus 25 per cent aggregated Clackline clay plus 15 per cent powdered Clackline clay (a) leached immediately after application of slug (3-4 mm aggreg.), (b) leached 24 hours after application of slug (3-4 mm aggreg.) and (c) effect of aggregate size when leached with 2 in. water 24 hours after application of slug.

leached immediately after application move coherently through the column with virtual complete displacement of the slug from the top sections by the following non-tracer solution. However, leaving the tracer band overnight before leaching (Figure 2b) allows the chloride to diffuse into the relatively stagnant intra-aggregate pores. Subsequent leaching moves the

main peaks downward almost as far as for the columns leached immediately after placement, but leaves a significant residual concentration in the upper sections. Increased aggregate size increases the magnitude of this retention (Figure 2c). The practical implications of this result are illustrated by the field measurements of Cooke, Bates and Tinker (1957) and of Cunningham and Cooke (1958).

When the solute reacts with the porous medium through which the solution is moving, e.g. by exchange or adsorption, the change in distri-

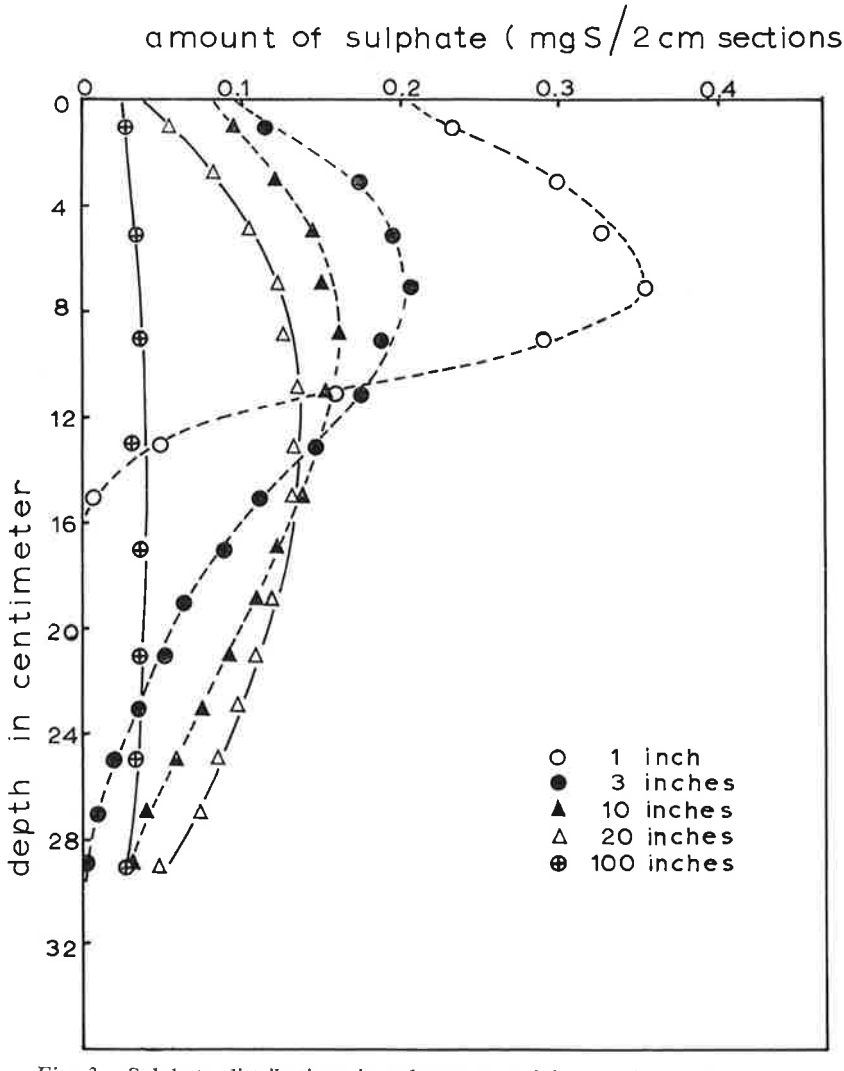

Fig. 3.—Sulphate distributions in columns containing sand plus 5 per cent powdered Clackline clay with increasing water application at *pH* 4·6. Concentration of initial 3 ml slug 37·5 me/l.

bution with displacement is further modified from that produced by diffusion or dispersion effects alone to an extent depending on the strength of the interaction. In a previous paper (Aylmore, Karim and Quirk 1967), iron and aluminium oxides were shown to have high adsorption capacities for sulphate ions which were largely irreversible with respect to concentration. Thus, in similar experiments to the previous using columns containing sand plus 2% iron oxide, an identical sulphate distribution profile was obtained regardless of the amount of water subsequently applied, the sulphate being irreversibly adsorbed from the band of solution as it moved through the column. As the concentration in solution was depleted, so the amount adsorbed in successive sections decreased in accord with a Langmuir adsorption isotherm.

Figure 3 shows the effect of leaching with increasing amounts of water up to 100 inches on the movement of bands of potassium sulphate solution at *pH* 4·6 through columns containing sand plus 5 per cent potassium saturated Clackline kaolinite. In contrast to the absolute retention

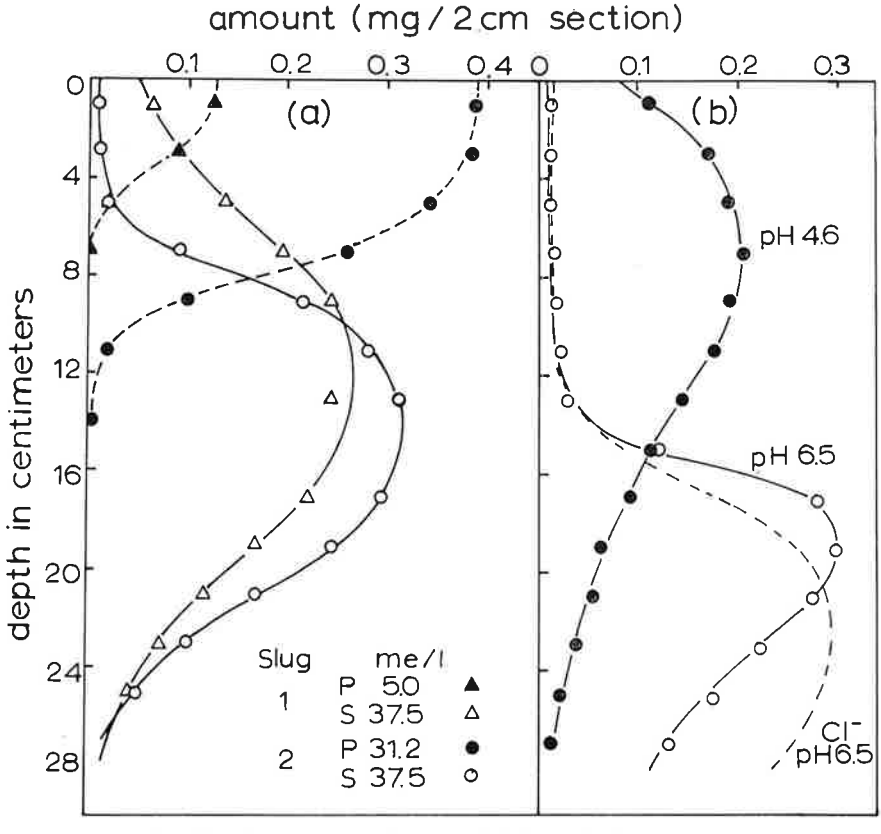

Fig. 4.—(a) Simultaneous leaching of sulphate and phosphate in saturated columns containing sand plus 5 per cent powdered Clackline clay at *pH* 4·6. (b) Effect of *pH* on sulphate distribution.

of sulphate exhibited by the iron oxide columns, the distribution of sulphate in the kaolinite columns changes progressively with increasing water application, spreading gradually along the length of the column and decreasing in peak height. Since the adsorption capacity of the column is some 0·7 mg S/2cm section, the movement of the sulphate distribution occurs by an alternative adsorption-desorption process similar to that which occurs in chromatographic columns.

The presence of competitive ions in solution and of an increase in pH markedly reduce the amount of sulphate ions adsorbed at any given sulphate concentration (Karim 1967). In Figure 4a, the displacement of the less strongly adsorbed sulphate from adsorption sites by phosphate ions results in a displacement of the sulphate distribution to greater depths. As the concentration of phosphate in the 3 ml slug is increased from 5·0 me/1 to 31·2 me/1, so the sulphate distribution is further displaced. Similarly in Figure 4b, an increase in pH of the system from 4·6 to 6·5 reduces the sulphate adsorption capacity to negligible proportions, and the distribution obtained is almost identical to that obtained for chloride movement in the same system.

In Figure 5 the breakthrough curves obtained at pH 4·6 for potassium sulphate through columns containing 5 per cent Clackline kaolinite saturated with potassium, calcium and aluminium ions respectively, are compared. The concomitant exchange of potassium for calcium cations on the kaolin clay appears to exert little influence on the sulphate breakthrough curve, even though the potassium breakthrough curve lags considerably behind that for sulphate. The potassium breakthrough curve is flatter and is displaced to higher effluent volumes than the corresponding sulphate break-

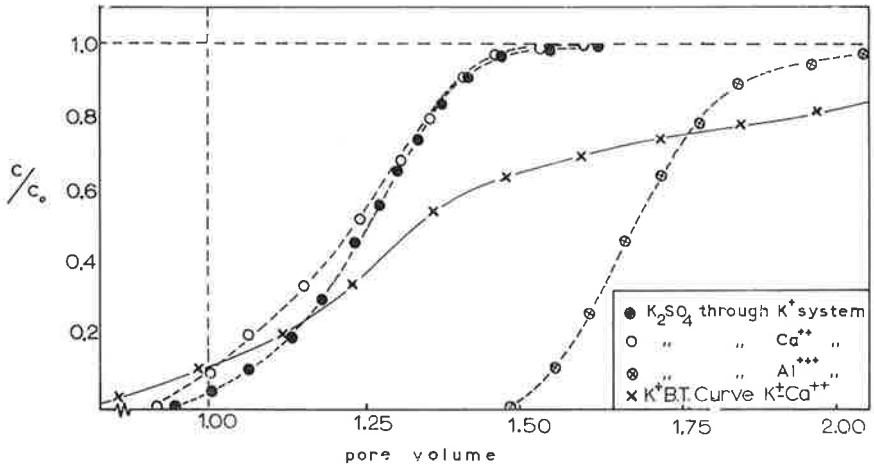

Fig. 5.—Sulphate breakthrough curves at pH 4·6 for potassium sulphate solutions for columns containing sand plus 5 per cent powdered Clackline clay saturated with potassium, calcium and aluminium. Also potassium breakthrough curve for potassium sulphate through calcium saturated column.

through curve, but it is interesting to note that the potassium ion appears in the effluent before the sulphate. This can be attributed to differences in the rates and isotherms governing the exchange processes for $SO_4^{--} - OH^-$ and $K^+ - Ca^{++}$ exchange respectively and consequent mixing. The sulphate breakthrough curve for potassium sulphate in an aluminium saturated column is displaced to higher effluent volumes by the increased adsorption capacity due to sulphate exchange with hydroxyls associated with the exchangeable aluminium ions (Aylmore, Karim & Quirk 1967).

A comparison of the experimental sulphate breakthrough curve for the potassium saturated column, with the curves predicted by the theories of Glueckauf (1949), Lapidus and Amundson (1952) and of Hiester and Vermeulen (1952) when the necessary parameters are obtained from a point on the experimental curve is given in Figure 6. Qualitatively the models all give a reasonable prediction of the position and shape of the experimental observation. The Glueckauf theoretical plate approach gives the best fit to the experimental data by this means. This method is, however, somewhat more empirical than are the other two theories, since the parameters are uniquely determined by the shape and position of the experimental curve. In this regard the method is similar to Day's (1956) method for non-reactive ions and could be of most use in predicting subsequent distributions from one determined experimentally.

Although somewhat more fundamental in their derivation, both the Lapidus and Amundson and the Hiester and Vermeulen models contain parameters which are difficult to evaluate independently, and also require interpretation from the experimental breakthrough curves. Both predict the approximate displacement of the breakthrough curve with respect to

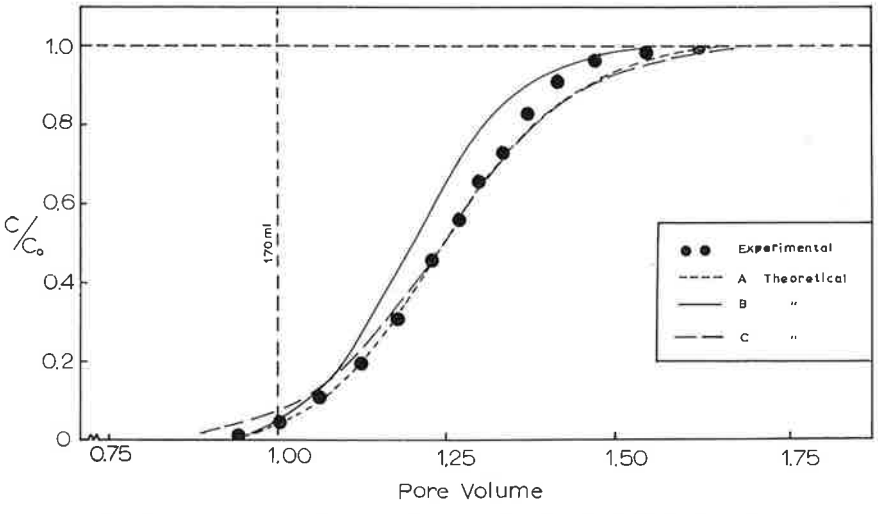

Fig. 6.—Comparison of theoretical (A) Glueckauf (1949), (B) Lapidus and Amundson (1952), (C) Hiester and Vermeulen (1952), and experimental sulphate breakthrough curves for columns containing sand plus 5 per cent powdered Clackline clay saturated with potassium.

effluent volume. The Hiester and Vermeulen theory attempts to account for dispersion in terms of rate dependent processes involved in the diffusion of ions to adsorption sites and in subsequent adsorption. Such rate dependent processes are probably of negligible importance in this system, and the values of the column capacity and solution capacity parameters incorporating an exchange rate constant, estimated from the experimental curve, would have a doubtful physical significance. Although physically more reasonable, the Lapidus and Amundson model suffers from the incorrect assumption of a linear adsorption isotherm and the uncertainty in coupling of hydrodynamic and any diffusive effects. Use of a Langmuir isotherm in the equation of continuity presents considerable mathematical difficulty and will await a satisfactory solution.

The physical models on which these theories have been developed thus seem inadequate to provide other than approximate descriptions of the movement of reactive ions through the more complex soil systems. However, much useful information may be obtained for practical purposes within the limits of their applicability.

References

Aylmore, L. A. G. (1960)—Ph.D. Thesis, University of Adelaide.
Aylmore, L. A. G., Karim, M. and Quirk, J. P. (1967)—*Soil Sci.* **103**, 10-15.
Berg, W. A. and Thomas, G. W. (1959)—*Proc.Soil Sci.Soc.Am.* **23**, 348-350.
Chao, T. T., Harward, M. E. and Fang, F. C. (1962)—*Proc.Soil Sci.Soc.Am.* **26**, 27-32.
Cooke, G. W., Bates, J. A. R., and Tinker, P. B. (1957)—*J.Sci.Fd Agric.* **8**, 248-252.
Cunningham, R. K., and Cooke, G. W. (1958)—*J.Sci.Fd Agric.* **9**, 317-330.
Day, P. R. (1956)—*Trans.Am.geophys.Union.* **37**, 595-601.
Day, P. R. and Forsythe, W. H. (1957)—*Proc.Soil Sci.Soc.Am.* **21**, 477-480.
Gardner, W. R. and Brooks, R. H. (1956)—*Soil Sci.* **83**, 295-304.
Glueckauf, E. (1949)—*J.chem.Soc.* (4 , 3280-3285.
Hiester, N. K. and Vermeulen, T. (1952)—*Chem.Engng Prog.* **48**, 505-516.
Karim, M. (1967)—Ph.D. Thesis, University of Western Australia.
Lapidus, L., and Amundson, N. R. (1952)—*J.phys.Chem.* **56**, 984-988.
Martin, A. J. P. and Synge, R. L. M. (1941)—*Biochem.J.* **35**, 1358-1368.
Nielsen, D. R. and Biggar, J. W. (1963)—*Proc.Soil Sci.Soc.Am.* **27**, 10-13.
Scheidegger, A. (1954)—*J.appl.Physics.* **25**, 994-1001.
Thomas, H. C. (1944)—*J.Am.chem.Soc.* **66**, 1664-1666.

Summary

The movement of non-reactive and of reactive ions through columns containing artificial soils has been studied and the results compared with the distributions predicted by the chromatographic theories of Day (1956), Lapidus and Amundson (1952), Glueckauf (1949) and Hiester and Vermeulen (1952) for the particular conditions of the experiments. Evidence has been obtained that the spreading of a solution-solvent boundary through longitudinal molecular diffusion is only of significance at flow rates of the order of 1 cm/hr or less. The holdback of non-adsorbed ions by diffusion into intra-aggregate pores at slow flow velocities has been illustrated.

Comparatively good agreement between experimental and theoretical distributions was obtained under these controlled conditions for both non-

reactive and reactive species. The results, however, illustrate the dependence of the progressive adsorption-desorption process by which the movement of a particular ionic species occurs on the presence of other ions, *pH* value and the complicities of soil constitution. These factors make a generalized theoretical approach to the movement of ions in solution through soils extremely difficult.

Résumé

Le mouvement des ions non-réactifs et réactifs à travers des colonnes qui contenaient des sols artificiels fut étudié et les résultats furent comparés avec les distributions prédites par les théories chromatographiques de Day (1956), Lapidus et Amundson (1952), Gluekauf (1949) et Hiester et Vermeulen (1952) sur les conditions spéciales des expériences. Des indices furent recueillis indiquant que la répartition d'une limite de solution-solvant comme résultat d'une diffusion moléculaire longitudinale a une signification seulement à une vitesse d'écoulement de l'ordre de 1 cm heure ou moins. La rétention d'ions non-adsorbés par diffusion dans les pores intra-agrégats à des vélocités de courant lents a été illustrée.

Un accord comparativement bon entre les distributions expérimentales et théoriques fut obtenu sous ces conditions contrôlées pour les espèces non-réactives et réactives. Cependant les résultats démontrent la dépendance du processus progressif d'adsorption-désorption par lequel le mouvement d'une espèce ionique particulière a lieu sur la présence d'autres ions, la valeur *pH*, et les complicités de la constitution du sol. Ces facteurs ont rendu très difficile la considération théorique générale du mouvement des ions dans une solution à travers les sols.

Zusammenfassung

Es wurde die Bewegung von nicht-reagierenden und reagierenden Ionen durch Röhren, die kuenstlichen Böden enthalten, geprueft und die Ergebnisse, die durch die chromatographischen Theorien von Day (1956), Lapidus und Amundson (1952), Glueckauf (1949) und Hiester und Vermeulen (1952) fuer die besonderen Bedingungen der Experimente vorausgesagt worden waren, wurden mit der Verbreitung verglichen.

Es hat sich herausgestellt, dass das Fortschreiten einer Lösungsmittel—Grenzlinie durch longitudinale Molekulardiffusion nur bei einer Stroemungsgeschwindigkeit von 1 cm/Stunde, oder weniger, von Bedeutung ist.

Das Zurückhalten von nicht adsorbierten Ionen durch Diffusion in die Intra-Aggregat Poren bei niedriger Geschwindigkeit ist illustriert worden. Verhaeltnismaessige gute Uebereinstimmung zwischen experimentellen und theoretischen Verbreitungen wurden unter diesen kontrollierten Bedingungen fuer beide,—nicht-reagierende und reagierende Arten erzielt. Jedoch illustrieren die Ergebnisse die Abhaengigkeit des progressiven Adsorptions-Desorptions-Prozesses, in welchem die Bewegung einer besonderen Ionenart in Gegenwart anderer Ionen vor sich geht, sowie vom *pH*-Wert und von der Beteiligung der Bodenzusammensetzung.

Diese Faktoren machen eine verallgemeinernde theoretische Stellungnahme zur Bewegung von Ionen in Loesung in Boeden besonders schwierig.

Reprinted from *The Australian Journal of Science*, Volume 31, Number 4, October, 1968, page 158

Cell Wall Water and Drought Tolerance of *Ehrharta calycina*

In a recent Letter to the Editor, Tothill (1968) has misunderstood the implications of our paper (Teoh, Aylmore and Quirk, 1967) dealing with the retention of water by plant cell walls and its implications for drought resistance. In our paper (see p. 48) the suggestion clearly stated was that xerophytes must possess a greater resistance to the destruction of the integrity of the two-phase nature of the cell wall (solid-liquid system) than do mesophytes. It was emphasized that it is this greater resistance to desiccation which is considered important in this regard rather than the presence of a supplementary water reservoir acting as a buffer in the volumetric sense. Nowhere is there any suggestion that bound water is made available to the plant during periods of drought as is implied by Tothill whatever his interpretation of water bound by root cell wall. The wall is viewed not only as giving identity to the cell but also affording protection to the cell contents.

Again it is difficult to understand the statement by Tothill that our comparison of a perennial plant with an annual is misleading, since this was one specific aim of the investigation. The same organ (*i.e.*, the root) of several species of contrasting botanical differences was chosen in our work so that data obtained could be directly compared. The perennial veldt grass also produces seeds just as the wheat plant does. In fact, the perennial veldt grass used in our work (an introduced species in Western Australia) is thriving particularly well in its competition with more well-adapted indigenous species, partly because it spreads by producing an abundance of seeds.

Recently McWilliam and Kramer (1968) and McWilliam (1968) have compared the behaviour of a typical perennial (*Phalaris tuberosa*) with a closely related annual (*P. minor*) under field and simulated drought conditions. They reported that an important factor in the survival of this perennial is the ability of its deep root system to supply water during the summer to the dormant culms at the soil surface. In field soils under drought conditions the roots of this perennial were found to reach a depth of 7 ft. in subsoil containing available moisture. Amongst the other features contributing to summer survival, the capacity of certain organs to resist senescence and retain viability and function is of major importance (McWilliam, 1968). McWilliam states that one of the most important factors controlling the plant survival of these two species is the difference in the rate and pattern of senescence after flowering under the influence of moisture stress. In the annual, senescence is rapid and complete, but in the perennial it is retarded, and function is retained in certain organs, including the lower stem and root system, throughout the summer stress.

The perennial veldt grass was obtained from Mount Eliza near Perth. The depths to the water table (summer levels) recorded by Rossiter (1938) at 11 sites near the base of Mount Eliza indicate a minimum depth of 13 ft. and a maximum depth of 14½ ft. The depth to the water table at the elevated locality (sandy soils) where the plants were collected would be much greater than that recorded by Rossiter. Under high summer temperatures the sandy soils of the perennial veldt grass root zone would lose their water rapidly until below the wilting percentage. Thus, although the development of a deep rooting system may be of significance for drought survival in some circumstances, it seems very unlikely that this alone could account for the survival of this xerophyte in this situation where its roots are clearly not in contact with the water table. The observation by Tothill and Love (1964, 1966) of *E. calycina* commencing growth in autumn prior to the onset of rainfall is therefore not significant to our consideration.

Tothill's argument concerning the quiescence of *E. calycina* in relation to the continuous availability of soil moisture appears inconsistent. He states that the plant can be reactivated at any time by watering. However, if the plant has been in contact with ' available soil moisture ' throughout the summer the commencement of growth prior to the onset of rainfall must reflect some physiological response quite apart from contact with available water. It is obviously a question of the degree of availability of water, *i.e.*, whether just sufficient to maintain viability or to initiate growth. The fact remains that xerophytic species are able to withstand greater water stress for longer periods than are mesophytic species, and it seemed likely that this ability is *inter alia* related to differences in the physico-chemical properties of the cell wall. Our investigations were prompted partially by the observation that a plant subjected to water stress frequently develops thicker cell walls.

We would also like to point out that Tothill's statement that a considerable proportion of the root system sloughs off each dry season does not appear particularly relevant since we are concerned only with that part of the root system in which the integrity of the cell wall and viability of the protoplasm are in fact maintained.

We consider that our tentative suggestion that the simple quantitative approach described in our paper (Teoh *et al.*, 1967) may be of practical value in assessing the comparative drought hardiness of various species is worthy of further investigation.

T. S. Teoh
L. A. G. Aylmore
J. P. Quirk.

Department of Soil Science and
Plant Nutrition,
Institute of Agriculture,
University of Western Australia,
Nedlands,
Western Australia, 6009.

19 June 1968.

References

McWilliam, J. R. (1968): *Aust. J. agric. Res.*, **19**, 397.
McWilliam, J. R., and Kramer, P. J. (1968): *Aust. J. agric. Res.*, **19**, 381.
Rossiter, R. C. (1938): Hons. thesis, University of Western Australia.
Teoh, T. S., Aylmore, L. A. G., and Quirk, J. P. (1967): *Aust. J. Biol. Sci.*, **20**, 41.
Tothill, J. C. (1968): *Aust. J. Sci.*, **30**, 273.
Tothill, J. C., and Love, R. M. (1964): *Adv. Front. Pl. Sci.*, **8**, 83.
Tothill, J. C., and Love, R. M. (1966): *J. Aust. Inst. Agr. Sci.*, **32**, 300.

AUSTRALASIAN MEDICAL PUBLISHING CO. LTD.
71-79 ARUNDEL ST., GLEBE, SYDNEY, N.S.W., 2037

[Reprinted from the Journal of Physical Chemistry, 72, 241 (1968).]

Infrared Spectra of Kaolin Mineral–Dimethyl Sulfoxide Complexes

By S. Olejnik, L. A. G. Aylmore, A. M. Posner, and J. P. Quirk

Infrared Spectra of Kaolin Mineral–Dimethyl Sulfoxide Complexes

by S. Olejnik, L. A. G. Aylmore, A. M. Posner, and J. P. Quirk

Department of Soil Science and Plant Nutrition, University of Western Australia, Nedlands, Western Australia
(Received July 17, 1967)

Dimethyl sulfoxide (DMSO) intercalates into the kaolin minerals and increases the basal spacing $d(001)$ from 7.14 A to approximately 11.16 A. The rate of intercalation has been measured and found to increase in the order: halloysite > kaolinite > dickite. An explanation of the observed intercalation rates based on the structure of the kaolin minerals and the numbers of interlayer hydrogen bonds is given. The infrared spectra of the kaolin minerals–DMSO complexes were examined. DMSO hydrogen bonds *via* its oxygen atom to the clay hydroxyl surface. The hydrogen bonding involves predominantly the 3690-cm^{-1} hydroxyls of the clay and results in the appearance of sharp peaks at approximately 3658, 3535, and 3499 cm^{-1}. Deuteration of the complex confirms that these peaks are due to perturbed hydroxyls. A model consistent with the infrared and X-ray data is suggested to account for the bonding of the DMSO to the internal surfaces of the clay.

Introduction

Intercalation of potassium acetate and certain other compounds into kaolinite has been examined by a number of workers,[1–4] using measurements of the change in basal spacing. Infrared techniques were also used by Ledoux and White[3,4] to determine the nature of the bonding of these molecules to kaolinite.

The compounds examined by Ledoux and White,[3,4] potassium acetate, hydrazine, formamide and urea, can be classed as protic type compounds; that is, they can either accept or donate protons with suitable molecules to form hydrogen bonds. They can therefore hydrogen bond to both the hydroxyl and oxygen surfaces of kaolinite.

Dimethyl sulfoxide (DMSO) is classed as a dipolar aprotic solvent. It has a large dipole moment (4.3 D.)[5] and is a proton acceptor, not having any labile hydrogens that it can donate; hence it can only hydrogen bond with suitable donors.

Preliminary X-ray studies indicated that DMSO intercalates into kaolinite with an increase of the basal spacing $d(001)$ to 11.16 A. The infrared spectrum of intercalated DMSO was deemed of interest: first, because of the unusual properties of DMSO, and secondly, because of the possibility of its hydrogen bonding to the hydroxyl surfaces of kaolinite.

Experimental Section

Kaolinite and dickite were obtained from Ward's Natural Science Establishment Inc. and are the standard clay minerals No. 9 and 15 of API Project No. 49, respectively. X-Ray diffraction showed the kaolinite to be well crystallized with no oxide impurities and a $d(001)$ of 7.14 A. The dickite contains a small amount of unidentified impurity, and its $d(001)$ spacing is 7.15 A. A sample of hydrated halloysite was kindly supplied by the Government Chemical Laboratories and originated from near Boorabbin, Western Australia. Electron microscopy revealed it to have the characteristic tubular morphology of halloysites and its $d(001)$ spacing is 10.01 A.

Other kaolinites used originated from Clackline and Rocky Gully, Western Australia. The Rocky Gully kaolinite, which is a *b*-axis disordered form, contains some iron oxides and gibbsite as impurity[6] and was used in the K^+ saturated form. A dickite from Pottsville, Pa., was also examined. The Pottsville dickite is a coarse crystalline material and some of it was used as received. A sample was gently ground before use, but even so its particle size was considerably greater than 2 μ. The specific surface areas of the clay minerals were determined by application of the BET method to low-temperature nitrogen sorption isotherms and are given in Table I.

Homoionic samples of the clays (Na^+ saturated form) were prepared by the method of Posner and Quirk,[7] and the <2 μ esd fraction was obtained by sedimentation in distilled water at pH 8.6. Metahalloysite was prepared by freeze-drying a portion of the

(1) K. Wada, *Am. Mineralogist*, **46**, 78 (1961).

(2) A. Weiss, W. Thielepape, G. Goring, W. Ritter, and H. Schafer *Intern. Clay Conf.*, **1**, 287 (1963).

(3) R. L. Ledoux and J. L. White, *J. Colloid Interface Sci.*, **21**, 127 (1966).

(4) R. L. Ledoux and J. L. White, *Proc. Intern. Clay Conf.* **1**, 361 (1966).

(5) A. J. Parker, *Quart. Rev.* (London), **16**, 163 (1962).

(6) D. Muljadi, Ph.D. Thesis, University of Adelaide, 1964.

(7) A. M. Posner and J. P. Quirk, *Proc. Roy. Soc.* (London), **A278**, 35 (1964).

hydrated halloysite paste and then heating at 140° for 13 hr. It gave a $d(001)$ spacing of 7.34 A.

Table I: Specific Surface Areas of Kaolin Minerals

	Specific surface area, m^2/g
API No. 9 kaolinite (Na^+)	17.7
Clackline kaolinite (Na^+)	27.04
Rocky Gully kaolinite (K^+)	40.0
Boorabbin halloysite (Na^+)	76.27
API No. 15 dickite (Na^+)	8.23
Pottsville dickite (natural)	1.01
Pottsville dickite (ground)	13.39

BDH laboratory reagent grade DMSO was dried over molecular sieve Type 5A with intermittent shaking for several days, then distilled through a short fractionating column at reduced pressure. The first few milliliters of distillate was discarded. No water was present in the DMSO as shown by the infrared spectrum of a thin liquid film between AgCl plates forming the cell. Heavy water, of high isotopic purity 99.75% by weight of D_2O, was supplied by the Australian Institute of Nuclear Science and Engineering.

DMSO (2 ml) was added to 20 mg of kaolinite (predried over P_2O_5) and the suspension shaken in an end-over-end shaker at 20 ± 2° for various lengths of time. To obtain uniform oriented clay films for the infrared studies, a portion of the suspension was evaporated onto AgCl disks in a vacuum desiccator at approximately 0.05 mm pressure till all the liquid disappeared. Continuous evacuation, up to 15 hr at 0.005 mm, did not remove intercalated DMSO and had negligible effect on the infrared spectra.

Infrared spectra were recorded with a Perkin-Elmer Model 337 double-beam infrared spectrometer. For the orientation studies, a mask was placed around the disk to eliminate nonuniformity of the clay film near the disk edges. The orientation spectra were all recorded for the same clay film and so are comparable. The clay films on the AgCl disks were unprotected from atmospheric moisture, since the spectra obtained were unaffected by standing in air for a considerable length of time.

X-Ray measurements were obtained using a Philips PW-1010 X-ray generator and Model PW-1050 diffractometer, using iron filtered Co Kα radiation at 40 kv and 15 ma and a scanning rate of 0.5° 2θ/min.

For the kinetic studies, a sample of the clay suspension in DMSO was spread on an unglazed porcelain tile to form a uniform thin layer, covered with thin polythene film to prevent drying and moisture adsorption, and X-rayed. Integrated peak intensities were obtained by the method of Norrish and Taylor[8] for minimizing background errors, after correcting the recorder peak heights to the same scale factor of the recorder, and assuming the peak half-width does not change significantly with peak height for different scale factors of the diffractometer. X-Ray spacings were also determined on the specimens used for the infrared measurements.

Results

I. Kaolinite A. Rate of Intercalation. Intercalation of DMSO into kaolinite results in a considerable portion of the clay expanding from a basal spacing $d(001)$ of 7.14–11.16 A. The $d(001)$ value obtained, 11.16 A, is close to the reported value of 11.18 A.[9] The proportion expanded increases with the time of contact with DMSO, suggesting that the rate of intercalation is governed by time-dependent factors. However, even after several months, there is still some clay with a $d(001)$ of 7.14 A left.

Figure 1 shows a plot of the ratio $I_{(001)\text{complex}}$: $(I_{(001)\text{complex}} + I_{(001)\text{kaolinite}})$ *vs.* time for DMSO and several water–DMSO mixtures. The use of this relationship assumes approximately the same degree of particle orientation for both the expanded and unexpanded forms and for different specimens. The figure shows an initial rapid expansion of portion of the kaolinite to $d(001)$ of 11.16 A, followed by a slower rate of expansion of the remainder. The process is obviously enhanced by the presence of water, which must act as a catalyst in promoting the expansion since its spectrum is never observed together with that of the intercalated DMSO. There appears to be an optimum water content favorable to expansion of approximately 9% (v/v), beyond which the presence of water decreases the rate of expansion of kaolinite.

B. Infrared Spectra. The infrared spectrum of the API-9 kaolinite–DMSO complex, after 38 days shaking, is shown in Figure 2 together with the spectra of kaolinite and liquid DMSO. Hydroxyl stretching bands at 3690, 3664, 3646, and 3617 cm^{-1} are observed for the kaolinite and correspond to those at 3695, 3670, 3650, and 3620 cm^{-1}, reported previously.[3,10,11] Vibrational assignments of kaolinite in the low-frequency region are based on those of Farmer and Russell,[12] *viz.*, 1117, 1035, and 1016 cm^{-1} to in-plane SiO vibrations; 941 and 917 cm^{-1} to AlOH vibration; 797, 789, 751, and 693 cm^{-1} to vibrations of the gibbsite-like layers of kaolinite; and 542, 476, 434, and 421 cm^{-1} to SiOAl skeletal vibrations.

(8) K. Norrish and R. M. Taylor, *Clay Minerals Bull.*, **5**, 98 (1962).

(9) S. Gonzalez Garcia and M. Sanchez Camazano, *Anales Edafol. Agrobiol.* (Madrid), **24**, 495 (1965).

(10) R. L. Ledoux and J. L. White, "Proceedings of the 13th National Conference on Clays and Clay Minerals," Pergamon Press, London, 1966, p 289.

(11) J. M. Serratosa, A. Hidalgo, and J. M. Vinas, *Intern. Clay Conf.* 1, 17 (1963).

(12) V. C. Farmer and J. D. Russell, *Spectrochim. Acta*, **20**, 1149 (1964).

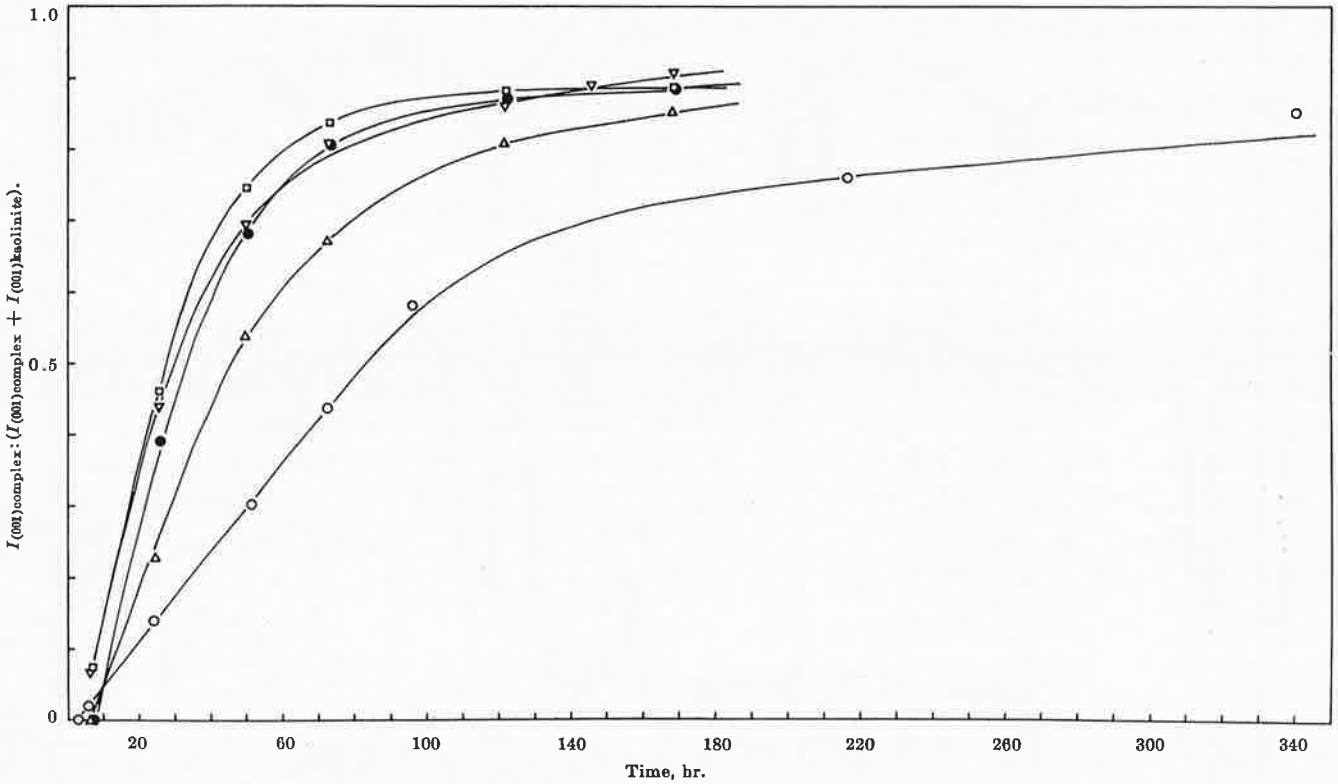

Figure 1. Rate of intercalation of DMSO into API-9 kaolinite in DMSO and water–DMSO solutions: △, 0.99% H_2O; ▽, 4.77% H_2O; □, 9.09% H_2O; ●, 20% H_2O; and ○, pure DMSO.

Table II: Vibrational Frequency Assignments of DMSO, Cm^{-1}

Liquid				
[a]	[b]	Solution[c]	Vapor[d]	Assignment
2994	2965	3000	2973	Asym CH stretching
2913	2880	2918	2908	Sym CH stretching
1445		1436	1440	
	1412–1436	1416	1419	Asym CH_3 deformation
1414		1404	1405	
1320	1312	1325	1319	
1303		1306	1304	Sym CH_3 deformation
1288		1291	1287	
1057	1007–1075	1055	1102	SO stretching
		1012	1016	
			1006	
953	950	946	929	CH_3 rocking
929	930	921	915	
896	897	887	898	
699	696	690	689	Asym CS stretching
669	665	661	672	Sym CS stretching

[a] This work. [b] Salonen.[13] [c] In chloroform and carbon disulfide solvents. [d] F. A. Cotton and W. D. Horrocks.[15]

The infrared spectrum of the liquid DMSO used here is similar to that published by Salonen,[13] with the exception that he obtained broad bands at approximately 3430 and 1650 cm^{-1} due to incomplete removal of water from his sample. Vibrational assignments have been made for the liquid,[13] in dilute solution in chloroform and carbon disulfide,[14] and in the vapor phase.[15] Although the vibration frequencies differ slightly, the assignments are similar and are given in Table II, together with the present results.

Sharp absorption bands appear at 3658, 3535, and

(13) A. K. Salonen, *Ann. Acad. Sci. Fennicae*, **67A**, 5 (1961).

(14) F. A. Cotton, R. Francis, and W. D. Horrocks, *J. Phys. Chem.*, **64**, 1534 (1960).

(15) F. A. Cotton and W. D. Horrocks, *Spectrochim. Acta*, **17**, 134 (1961).

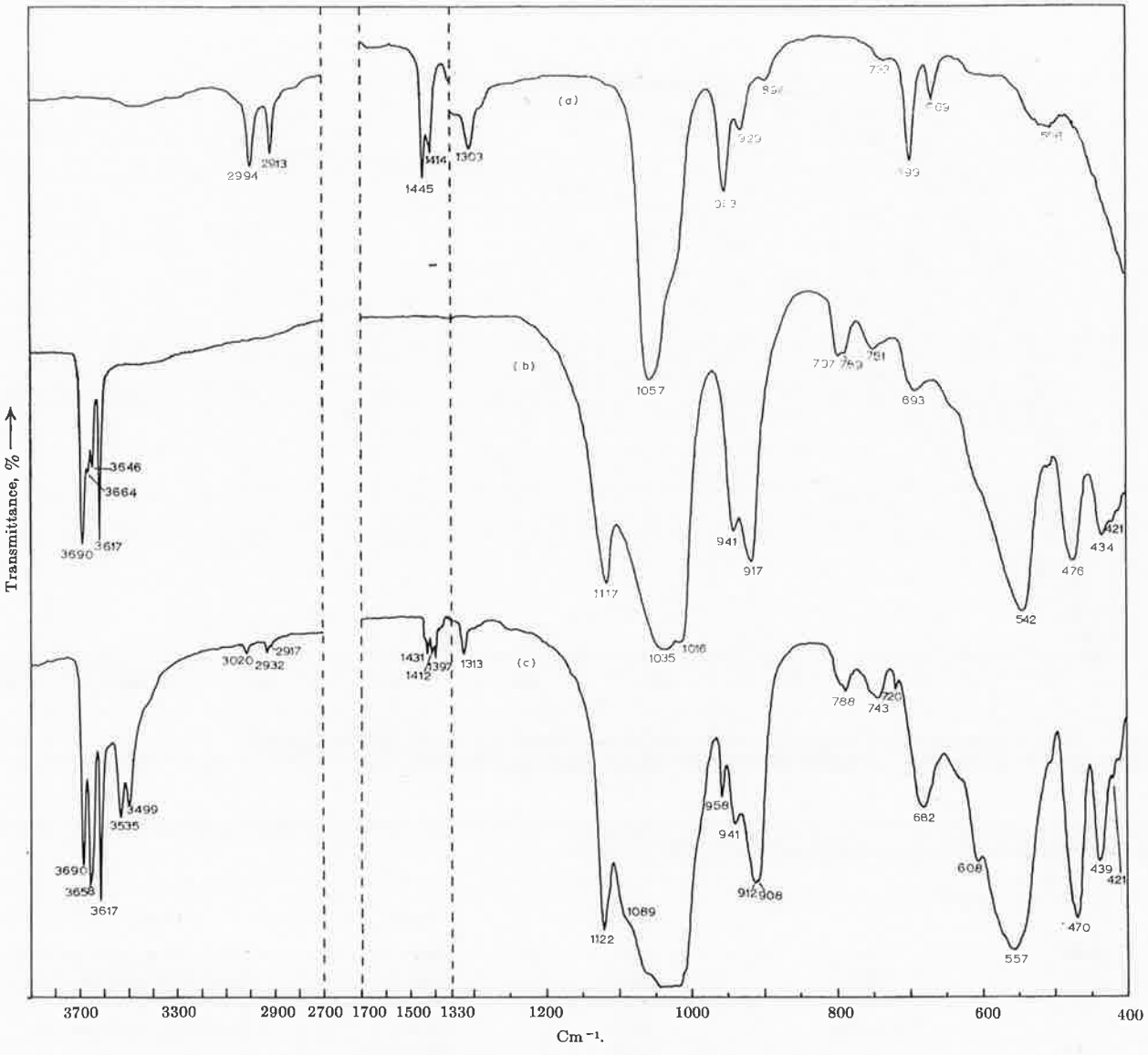

Figure 2. Infrared spectra of (a) liquid DMSO, (b) API-9 kaolinite, and (c) API-9 kaolinite–DMSO complex.

3499 cm^{-1} in the infrared spectrum of the complex. These peaks increase in intensity with time as the 3690-cm^{-1} peak intensity decreases. An increasing sharpness and delineation of the shoulder at approximately 1089 cm^{-1} and the peak at 608 cm^{-1}, and also a marked intensity decrease of the AlOH vibration of 941 and 917 cm^{-1} occur with the amount of DMSO intercalated, the 941-cm^{-1} peak decreasing more than the 917-cm^{-1} peak. These results indicate that bonding of DMSO is to the hydroxyl surface of the kaolinite sheets. Intercalation of DMSO shifts the perpendicular modes of kaolinite at 751 and 693 to 743 and 682 cm^{-1}, respectively, with an intensity increase. The other kaolinites showed similar behavior to the API-9 kaolinite in the appearance of sharp peaks at around 3655, 3530, and 3497 cm^{-1}.

C. Effect of Heating and Evacuation on the Complex. Continuous evacuation of the API-9 complex on a AgCl disk for 2 hr over silica gel slowly removes the DMSO, increasing slightly the 3690-cm^{-1} peak intensity while decreasing the 3658-, 3535-, and 3499-cm^{-1} peak intensities. Longer evacuation, up to 15 hr, restores the original hydroxyl peaks of kaolinite, except for an additional small peak at 3540 cm^{-1} (Figure 3). Although the X-ray patterns show that evacuation over silica gel for several hours collapses most of the kaolinite to a $d(001)$ of 7.14 A, the infrared spectra still show the presence of some DMSO on the kaolinite. Peaks in other regions of the infrared associated with the complex gradually disappear on evacuation. Removal of DMSO from the complex apparently causes some irreversible changes in the kaolinite structure, as the infrared spectrum after evacuation is not the same as for the original kaolinite (compare Figures 2b and 3). Heating the DMSO complex has the same effects as evacuation over silica gel, the rate of removal of the

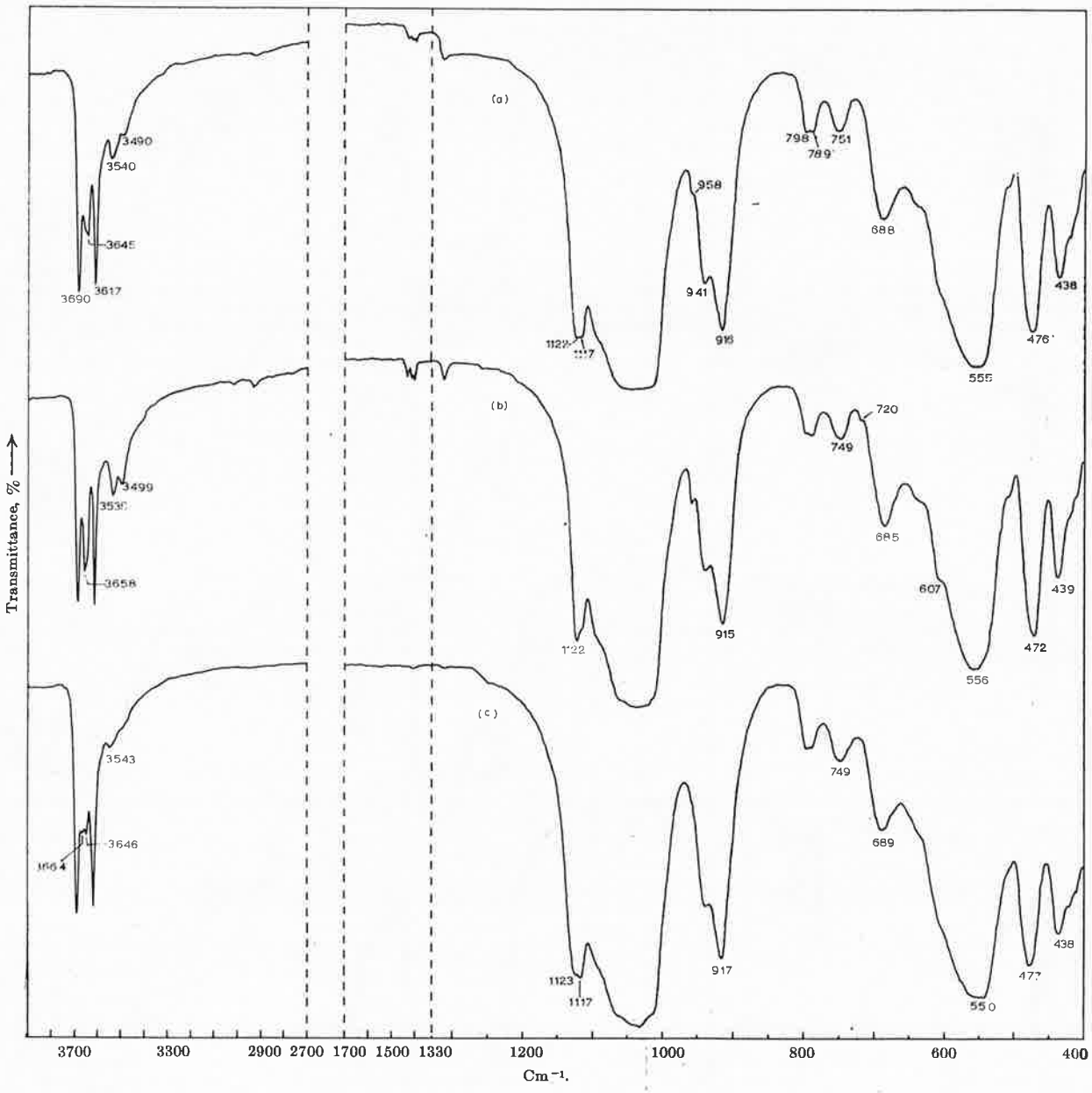

Figure 3. Infrared spectra of kaolinite–DMSO complex (a) evacuated over silica gel approx 5 hr, (b) heated 65° for 30 min, and (c) heated 100° for 15 min.

DMSO depending on the temperature of heating. A slight peak appears at 3543 cm^{-1} and remains even after heating for 9 hr at 105°.

D. Deuteration of the Kaolinite–DMSO Complex. Only a small amount of OH–OD exchange occurred after 7 days when the clay was expanded by DMSO containing 10% D_2O. However, considerably more exchange took place after 2 months (Figure 4d). If the clay–DMSO complex is washed with pure D_2O for 3 1-hr periods, partial deuteration of the kaolinite takes place and effects complete removal of intercalated DMSO with a collapse of $d(001)$ to 7.14 A. Figure 4a, b, c shows the successive stages in this deuteration. The X-ray patterns demonstrate that complete removal of DMSO and collapse of the $d(001)$ spacing occurs only during the third wash. Apart from a shift of some peak positions due to deuteration, washing with D_2O or H_2O appears to restore the kaolinite to its original form, unlike evacuation or heating.

Peaks at 2623 and 2597 cm^{-1} appear in the deuterated DMSO complex. The isotopic ratio of frequencies νOH:νOD to the 3535- and 3499-cm^{-1} peaks is 1.3477 and 1.3473, respectively. Hence, the 3535- and 3499-cm^{-1} peaks are due to perturbed hydroxyls on the kaolinite surface hydrogen bonded to DMSO. It appears that only the 3690-cm^{-1} hydroxyls of kaolinite are largely involved in hydrogen bonding. A peak at 2672 cm^{-1} is attributed to deuteration of the inner hydroxyls, Figure 4d.[10]

E. Pleochroism of the Kaolinite–DMSO Complex.

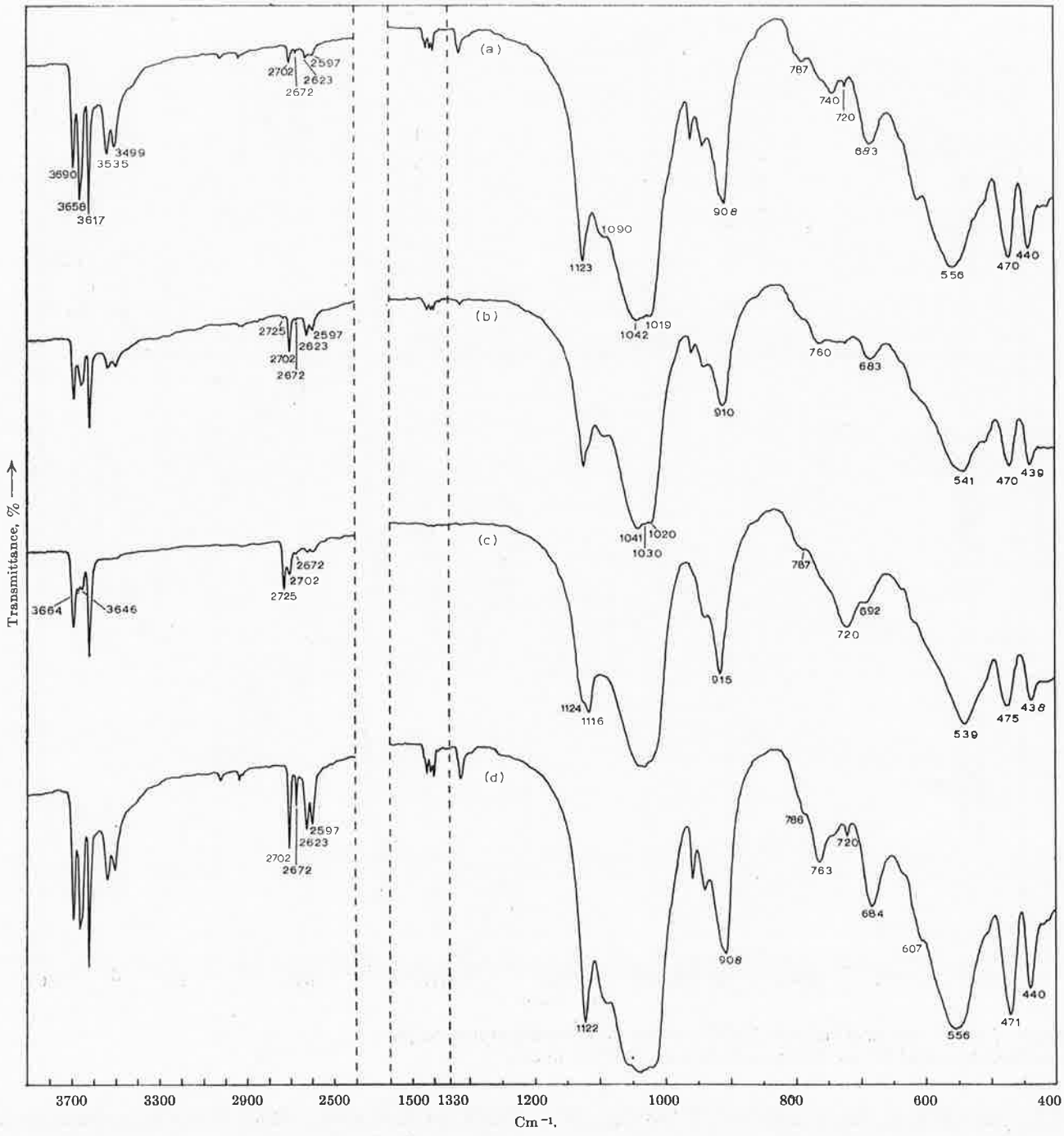

Figure 4. Infrared spectra of deuterated kaolinite–DMSO complex: (a) kaolinite–DMSO complex washed with D_2O for 1.25 hr; (b) D_2O in (a) replaced by fresh D_2O and washed for a further hour; (c) as (b) and washed for another hour; and (d) kaolinite treated for 2 months with DMSO containing 10% D_2O.

The pleochroism of an oriented film of the kaolinite–DMSO complex on an AgCl disk was examined at several angles of incidence. The pleochroism of the peaks is essentially the same in the hydroxyl region of the complex as in pure kaolinite, indicating that the dipole moment change of the perturbed hydroxyls, which are hydrogen bonded, is much the same as in the original unexpanded kaolinite. A shoulder at approximately 3646 cm^{-1} appears to be slightly more pleochroic than the 3658-cm^{-1} peak.

II. Halloysite. A. Infrared Spectra. Intercalation of DMSO into hydrated halloysite displaces the interlamellar water and expands halloysite to $d(001)$ of 11.13 A, as in kaolinite. Metahalloysite similarly expands to 11.16 A, though more slowly than hydrated halloysite. The infrared spectra of the halloysite–DMSO complex and hydrated halloysite are shown in Figure 5. The interlayer water of the hydrated halloysite is shown by the bands at approximately 3440 and at 1630 cm^{-1}. The infrared spectrum of fully

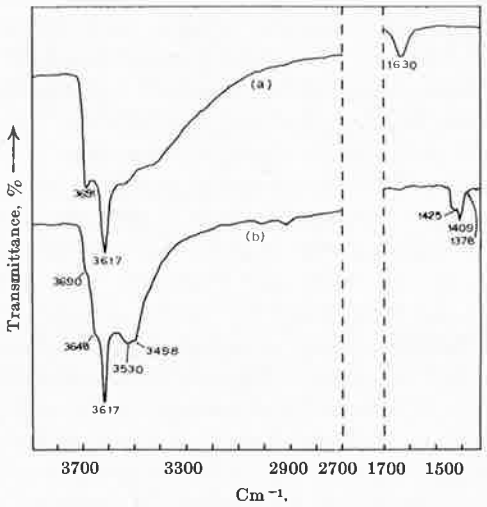

Figure 5. Infrared spectra of (a) hydrated halloysite, and (b) hydrated halloysite–DMSO complex.

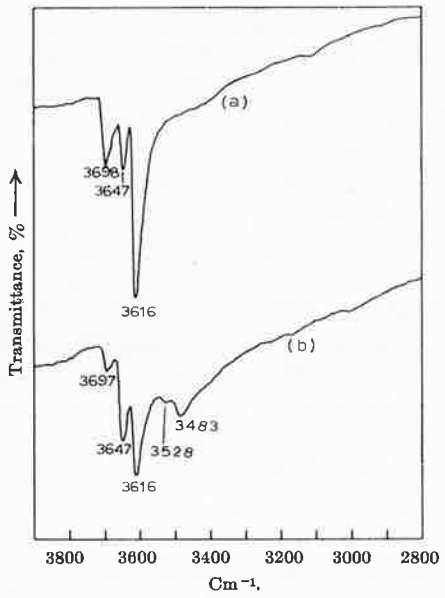

Figure 6. Infrared spectra of (a) Pottsville dickite, and (b) Pottsville dickite–DMSO complex.

hydrated halloysite was difficult to obtain by the methods used.

Two hydroxyl bands were observed in halloysite at 3691 and 3618 cm^{-1}; they correspond to bands at 3695 and 3620 cm^{-1}, respectively, previously reported[10,11] for halloysite. A broad band from approximately 3498 to 3530 cm^{-1} and two shoulders at 3690 and 3648 cm^{-1} are seen in the infrared spectrum of the halloysite–DMSO complex. The broad-band contour suggests that it consists of two slightly broadened overlapping peaks, just unresolved by the instrument and thereby appearing as one (compared with Figure 2c for the kaolinite–DMSO complex). Intercalation of DMSO into the kaolin clays therefore involves hydrogen bonding between the 3690-cm^{-1} hydroxyls and DMSO, as shown by the similar infrared spectra and reduction of the 3690-cm^{-1} peaks in the kaolinite–DMSO and halloysite–DMSO complexes.

B. Deuteration and Heating of the Halloysite–DMSO Complex. Analogous behavior to the kaolinite–DMSO complex is observed for the halloysite–DMSO complex on D_2O washing for hourly periods or heating. Heating collapses the halloysite to $d(001)$ of 7.34 A. A weak band at approximately 3665 and a shoulder at 3641 cm^{-1} appear in the heated sample. These bands could be the halloysite analogs of the kaolinite peaks at 3664 and 3646 cm^{-1}, respectively. Washing the metahalloysite–DMSO complex with water rehydrates the halloysite and the $d(001)$ spacing collapses from 11.16 to 9.97 A; Wada[1] similarly rehydrated metahalloysite using potassium acetate.

III. Dickite. The unground Pottsville dickite gave no intercalation of DMSO even after 3 months. Intercalation of DMSO took place with the ground Pottsville and API-15 dickites with the $d(001)$ spacing increasing to 11.14 A. However, the intercalation rate is much slower than with kaolinite. Virtually no expansion occurs after 8 days and even after 40 days the ratio $I_{(001)\,complex} : (I_{(001)\,complex} + I_{(001)\,dickite})$ is only 0.339 (compare with 0.72 for kaolinite after 7 days, Figure 1).

The infrared spectrum of the dickite–DMSO complex is essentially similar to the kaolinite–DMSO complexe spectra (Figure 6) with a few slight differences. The two new peaks at 3528 and 3483 cm^{-1} appear broader and more intense for the same amount of expansion, compared to their kaolinite counterparts, and the 3483 cm^{-1} peak is the stronger. There is also an intensity increase of the peak at 3647 cm^{-1} and a decrease in the 3698-cm^{-1} peak intensity. The infrared spectrum of the API-15 dickite–DMSO complex is less distinct but essentially similar to the others.

No evidence could be obtained of any intercalation of DMSO into gibbsite or geothite, presumably because of the stronger interlayer hydrogen bonding in gibbsite.

Discussion

A. Nature of the Hydroxyl Interactions. The interesting feature of the infrared spectrum of intercalated DMSO is the appearance of sharp peaks in the regions of 3658, 3535, and 3499 cm^{-1} and decreased intensity of the peak at about 3690 cm^{-1}. In contrast, the intercalation of potassium acetate, hydrazine, formamide, and urea markedly decreases the 3695-, 3670-, and 3650-cm^{-1} peak intensities[3,4,10] and new broader bands at lower frequencies are seen instead. To explain these observations, Ledoux and White[3,4,10] propose hydrogen bonding between these hydroxyls and the intercalated molecules.

The intensity increase of the 3658-, 3535-, and 3499-cm^{-1} peaks occurs simultaneously with an intensity decrease of the 3690-cm^{-1} peak as more DMSO is intercalated. Removal of DMSO and collapse to

$d(001)$ of 7.14 A, by heating, restores the original hydroxyl peaks of kaolinite. Hence, bonding of DMSO to kaolinite involves only the 3690-cm^{-1} hydroxyls and is responsible for the appearance of peaks at 3658, 3535, and 3499 cm^{-1}.

It is suggested that intercalation of DMSO results from the DMSO breaking the interlayer hydrogen bonds and reforming them with itself. In addition, new hydrogen bonds are formed. The sharpness of the new peaks at 3535 and 3499 cm^{-1} and marked increase in intensity at 3658 cm^{-1} is uncommon for hydrogen bonding. The DMSO hydrogen bonds to some of the 3690-cm^{-1} hydroxyls *via* its oxygen atom (see below) and gives rise to the hydroxyl peaks at 3535 and 3499 cm^{-1}. Crystal-field effects, caused perhaps by distortion in the kaolinite lattice, symmetry factors, or degeneracy of the vibrations, cause two relatively sharp peaks instead of one broad band to be observed. The geometry of the system may also permit different arrangements of the DMSO oxygens with respect to the hydroxyl layer leading to a splitting of the bands.

Dimethyl sulfoxide hydrogen bonds *via* its oxygen atom and so may be relatively mobile between the layers compared to substances such as formamide that bond to both the hydroxyl and oxygen surfaces of kaolinite and are restricted in their mobility. The DMSO will arrange itself to give the least expansion consistent with minimum interaction between adjacent molecules. This may lead to some of the oxygen atoms of DMSO being positioned in a similar situation with respect to the hydroxyl layer as the oxygen atoms of the adjacent tetrahedral layer in unexpanded kaolinite. The increase in number of such weak hydrogen bonds would result in the increased intensity of the 3658-cm^{-1} band. Its broadened band width compared to the 3690-cm^{-1} peak is consistent with a slight shift to lower frequencies of the 3690-cm^{-1} peak.

The reduced crystallinity and randomness in structure of halloysite probably does not allow such marked splitting to occur, resulting in two closely overlapping bands at 3530 and 3498 cm^{-1} and a shoulder at approximately 3648 cm^{-1}, instead of the sharper peaks observed for the kaolinite–DMSO complex. Two bands at 3528 and 3483 cm^{-1}, corresponding to those obtained for the kaolinite couple at 3535 and 3499 cm^{-1}, respectively, are also observed for the ground Pottsville dickite complex. Their large intensity and overlap may be related to the frequency shift resulting from an increase in bond strength, once entry of DMSO has been gained. The appearance of the 2725-cm^{-1} peak and simultaneous disappearance of the 2623- and 2597-cm^{-1} peaks upon deuteration, when all the DMSO has been washed out, (Figure 4c) is further evidence that bonding of DMSO to kaolinite predominantly involves the 3690-cm^{-1} hydroxyls of kaolinite.

B. Bonding Interactions of DMSO. Bonding of DMSO can occur either through the sulfur or oxygen atoms.[16] Bonding *via* the oxygen may involve the resonance form $R_2S^+–O^-$, which lowers the S–O vibration frequency and is the most likely.[14] An examination of the broad band at approximately 1030 cm^{-1} in a thin sample of the kaolinite complex shows that it may be composed of three overlapping peaks at 1042, 1030, and 1019 cm^{-1}, with the 1042-cm^{-1} peak the strongest. If two of these are the in-plane SiO vibrations corresponding to the 1035 and 1016 cm^{-1} vibrations of kaolinite, the other could be the SO stretching vibration of DMSO. From a comparison of relative intensities and assuming a slight upward frequency shift of the SiO vibration, the SO stretch in the complex is assigned to the 1030-cm^{-1} peak. The results for dickite in this region support the above assignment of peaks. A peak at 720 cm^{-1} in the kaolinite–DMSO complex is assigned to the asymmetric CS stretching occurring at 699 cm^{-1} (Table II) in liquid DMSO. The downward frequency shift of the SO stretching vibration and the absence of the symmetric CS vibration[12] shows that hydrogen bonding of DMSO to the hydroxyl surfaces of the clay takes place *via* the oxygen atom, rather than the sulfur atom.

A shoulder at 2917 cm^{-1} appears on the symmetric CH stretching vibration of 2932 cm^{-1}, and the asymmetric CH bending mode is split into three components of approximately equal intensity in the kaolinite complex (Figure 2c). The halloysite complex is similar except for the asymmetric bending vibration peak intensities, which are in the reverse order to that in liquid DMSO (compare Figures 2a and 5b). Clearly the CH bonds of DMSO in the complexes are perturbed by the clay lamellae in different ways, depending upon the clay. The upward frequency shift of the CH stretching vibration in all the complexes is difficult to reconcile with the possibility of CH$\cdots$O hydrogen bonding to the tetrahedral oxygen layer.

The interlayer space of 3.96 A (11.16–7.2 A) (MacEwan's "Δ value")[17] is less than the dimensions of the DMSO molecule, since the diameter of the methyl group alone is 4.0 A.[18] Some "keying" of the DMSO molecules into the kaolinite surface must therefore occur, especially when the DMSO molecular structure is considered to consist of a trigonal pyramid with sulfur at the apex.[19] An orientation consistent with the X-ray and infrared data is one where the sulfur atom points toward the tetrahedral oxygen layer and the pyramid base is nearly parallel to the hydroxyl surface. Hence, weak C–H$\cdots$O hydrogen bonds may exist, but these are masked and cannot be seen. Vig-

(16) M. J. Bennett, F. A. Cotton, and D. L. Weaver, *Nature*, **212**, 286 (1966).

(17) D. M. C. MacEwan, *Trans. Faraday Soc.*, **44**, 349 (1948).

(18) L. Pauling, "Nature of the Chemical Bond," Cornell University Press, Ithaca, N. Y., 1960, p 260.

(19) R. Thomas, C. B. Shoemaker, and K. Eriks, *Acta Cryst.*, **21**, 12 (1966).

orous removal of DMSO, as by heating, may cause permanent distortions in the tetrahedral oxygen layer, hence the broadened appearance of some SiO vibrations, compared to the original kaolinite.

C. Intercalation Rates and Interlayer Bonding. Intercalation rates of DMSO into the kaolin minerals may reflect variations in the strength of interlayer bonding related to the degree of order in the structures. Intercalation is slowest with dickite, the most crystalline kaolin polymorph with probably the strongest interlayer hydrogen bonding, intermediate with kaolinite, and fastest with halloysite, the least crystalline polymorph with very weak hydrogen bonding (if any) between the lamellae. The infrared spectra of the uncomplexed kaolin minerals in the hydroxyl stretching region indicate that the strength and number of interlayer hydrogen bonds increases from halloysite through kaolinite to dickite. For example, the peak in the region of 3650 cm^{-1} increases markedly in this order. This is in the same order as the rates of intercalation.

Some variation in the intercalation rate is also observed between the kaolinites themselves. Intercalation in Clackline kaolinite appears to be faster than in API-9 kaolinite, whereas that in Rocky Gully kaolinite is somewhat slower, in spite of its significantly higher surface area. Removing the iron oxides from the Rocky Gully kaolinite by treatment with dithionite[20] does not increase the intercalation rate. Grinding of the Pottsville dickite increases the rate of intercalation more than would be expected from the decrease in particle size. Also the finer API-15 dickite intercalates at much the same rate as the ground Pottsville dickite, despite the larger specific surface area of the latter. In general, it would appear that factors other than particle size have a significant effect on the intercalation rate of DMSO into the kaolin minerals. From the above, it appears that grinding produces other changes in particle morphology which allow a faster penetration of the DMSO.

The presence of water also affects the intercalation rates into kaolinite. The rate increases up to a certain water content and then falls. Apparently, water may break up the cyclic hydrogen bonded structure of liquid DMSO[5] allowing the individual molecules, with perhaps some attached water molecules, to act in opening up the lamellae. Without water, the rate appears to be governed by the availability of single DMSO molecules and hence intercalation is slower. With more than the optimum amount of water present, the DMSO molecules may again be further intermolecularly bonded with the water molecules and the intercalation rate decreases.

A tentative explanation of the reason for the hydration of halloysite and not kaolinite may be attempted. The crystalline lattice distortions of the lamellae in halloysite may result in conditions favorable to the weak bonding of water to the interlamellar surfaces. Once water is removed and interlayer bonds formed, halloysite behaves similarly to kaolinite with regard to intercalation of DMSO. If, however, water can reenter the interlamellar spaces with the help of an external agent, *e.g.*, DMSO, the water-surface bonds are reformed and halloysite hydrates. The lesser degree of lamellae distortion and absence of water in the infrared spectra of kaolinite complexes, confirmed by the D_2O washings, favor the explanation given. Further evidence comes from the work of Wada,[21] who found that kaolinite forms a partial water complex and dickite none at all.

Acknowledgment. The authors wish to express their thanks to Dr. L. H. Little of the Chemistry Department, University of Western Australia, for helpful discussions.

(20) T. L. Deshpande, Ph.D. Thesis, University of Adelaide, 1964.
(21) K. Wada. *Am. Mineralogist.* **50**, 924 (1965).

Reprinted from Special Report 103 (1969)
Highway Research Board, Washington, D.C.

Effects of Heating on the Swelling of Clay Minerals

L. A. G. AYLMORE, J. P. QUIRK, and I. D. SILLS
Department of Soil Science and Plant Nutrition, University of Western Australia

The effects of dehydration by evacuation and heating to progressively higher temperatures up to 400 C on the subsequent hydration and swelling behavior of homoionic predominately illite clay minerals has been studied. Water vapor sorption isotherms for 200-mg tablets at 25 C were determined using a volumetric doser technique, and swelling of the clays at low water suctions was measured on ceramic suction plates.

The swelling of certain illitic clays is subject to a marked reduction (e.g., from 200 percent to 35 percent water content at 10 millibars suction) after preheating, indicating the formation of very strong binding forces between individual clay particles. Although water vapor sorption at low relative vapor pressures shows that part of the water loss on heating is irreversible, it seems unlikely that any deterioration of the crystal lattice has occurred at the temperatures used. The cation exchange capacities of the clays are unaltered, and the specific surface areas are essentially the same after heating.

The nature of the bonding mechanism is not yet clear, but there is evidence that small amounts of kaolinite impurities present may be involved. It seems likely that the formation of hydrogen bonds between silicate and aluminate surfaces can occur on complete removal of the adsorbed water molecules.

IT HAS been known for some time that heating can markedly alter the physicochemical behavior of clay mineral systems. Such techniques have been used to some extent in road research (9, 10) and also in agriculture to increase the stability of surface soils. Heating to temperatures in excess of 600 C generally results in at least some irreversible destruction of the crystal lattice with consequent deterioration in sorptive properties. However, there is a substantial amount of data to indicate that the hydrophilic properties of certain clay minerals are modified quite appreciably by desorption long before there is any significant lattice deterioration.

The data of Mooney, Keenan, and Wood (14) and others for montmorillonite show that subsequent rehydration at low relative humidities can depend markedly on the severity of the predrying technique used to obtain an "oven-dry" weight. This is largely a result of the influence of the hydration energy of the exchangeable cations on the intercalation of water. Similarly, Martin (13) and Jurinak (11) found that the sorption of water at low relative vapor pressures by kaolinite clays was influenced by preheating to temperatures up to 300 C and attributed these effects to interparticle adhesion.

During detailed studies of water sorption and swelling by clay mineral systems it was observed that the swelling of certain clays was considerably reduced by the outgassing procedure used in the determination of specific surface area and pore size distribution by low-temperature nitrogen adsorption (3). The ability of montmorillonite clays to exhibit extensive crystalline swelling [$d(001) > 40$ Å] at low water suctions when sodium-saturated was found to be essentially unaltered by preheating even as high as 600 C. Similarly, the relatively small swelling exhibited by kaolinite clays even when sturated with water (2) was unaffected. In contrast, several samples of clays containing predominantly illite minerals showed large reductions in swelling after desorption. This effect has been examined in some detail in the present paper.

MATERIALS AND METHODS

The clay samples used were obtained from the following natural deposits:

•Willalooka illite—B horizon from a solonized solonetz, Hundred of Laffer, South Australia.

•Urrbrae B clay—B horizon of Urrbrae loam, a red-brown earth, Adelaide, South Australia. Clay fraction 60 percent illite and 40 percent kaolinite.

•Fithian illite—from Ward's Natural Science Establishment Inc., Illite No. 35 of the American Petroleum Institute's Research Project No. 49 (1951).

•Rocky Gully kaolinite—from pallid zone of laterite, Rocky Gully, Western Australia.

In general, samples of the clays were sodium-saturated by repeated washing with molar sodium chloride, during which the pH of the suspension was adjusted to 3.0 using hydrochloric acid. The samples were washed and finally dialyzed against distilled water using Visking cellulose casing. Initially a simple decantation process was used to remove the coarse fractions. These samples are labeled R. F. to indicate the rough fractionation used. Subsequently the $< 2\mu$ fractions were obtained by accurate sedimentation. Samples saturated with other cations were prepared from these materials using the appropriate molar chloride solution.

The air-dried clays were gently ground to a powder, equilibrated with 0.75 relative water vapor pressure, and compressed into 200-mg cores at 1200 atmospheres pressure by means of a hydraulic jack (1). This was done to facilitate subsequent experimental handling and to ensure that the clays were in an overconsolidated condition.

Heating of the clays was carried out by allowing a number of cores in weighing bottles to equilibrate for 3 days at a given temperature in a muffle furnace and cooling the ground glass stoppered bottles over phosphorus pentoxide powder before weighing.

Water content-energy data at low suctions were obtained using ceramic-perspex pressure plate systems. The cores were wet up in small stages using vacuum desiccators containing saturated salt solutions to prevent disruption of the cores by rapid differential swelling.

Surface areas were determined by application of the B. E. T. theory (7) to low-temperature nitrogen adsorption isotherms determined volumetrically in the usual way. Water vapor sorption isotherms were determined volumetrically in equipment similar to that used by Jurinak (11) incorporating a modified Pearson gage (16).

Cation exchange capacities were obtained by first saturating the clays using a neutral solution of molar strontium bromide and removing excess salt by washing with distilled water. The exchange capacities were then determined as the difference between the strontium and bromide contents of the dried clays determined using an X-ray fluorescence spectrographic method.

RESULTS AND DISCUSSION

The specific surface areas and cation-exchange capacities of the clay cores are given in Table 1. In Table 2 the decrease in weight of the Willalooka illite and Urrbrae

TABLE 1

SPECIFIC SURFACE AREAS AND CATION EXCHANGE CAPACITIES OF CLAY MATERIALS

Clay	Specific Surface Area (m^2/g)	Cation Exchange Capacity (me/100 g)
Willalooka illite (R. F.)	150	39.1
Willalooka illite ($< 2\mu$)	188	—
Urrbrae B clay (R. F.)	91	27.6
Fithian illite ($< 2\mu$)	99	—
Rocky Gully kaolinite ($< 2\mu$)	39.3	4.0

TABLE 2

WEIGHT LOSS BETWEEN SUCCESSIVE TEMPERATURES AND 400 C FOR ILLITIC CLAYS

Clay	Weight Loss (g/100 g clay at 400 C)			
	20 C	110 C	200 C	300 C
Ca^{++} Willalooka illite	16.39	4.92	2.47	1.22
Mg^{++} Willalooka illite	21.07	4.82	2.36	1.20
Na^{+} Willalooka illite	18.47	4.58	2.28	1.21
K^{+} Willalooka illite	17.36	3.89	1.87	1.10
Ca^{++} Urrbrae B clay	12.83	3.71	1.67	0.75
Mg^{++} Urrbrae B clay	13.07	3.92	1.80	0.85
Na^{+} Urrbrae B clay	13.47	3.27	1.58	0.80
K^{+} Urrbrae B clay	11.27	3.24	1.53	0.73

B clay cores between successive temperatures and 400 C has been expressed as a percentage on the basis of the weight of clay after drying to 400 C. The possible sources of weight loss on heating are surface-adsorbed water, water of hydration of the exchangeable cations, hydroxonium ions in interlayer positions normally occupied by potassium ions in unweathered micas (6), and hydroxyl groups from the clay lattice. Some weight loss may also occur from the charring of any organic matter present but this is relatively small in these materials. In general, the water contents from 110 C to higher temperatures show some relationship to the hydration energies of the exchangeable cations and the specific surface areas of the clays but the variation between different ions is not as large as might be expected if the weight losses were entirely associated with dehydration of the exchangeable cation [see Table 1 in Keenan, Mooney, and Wood (12)].

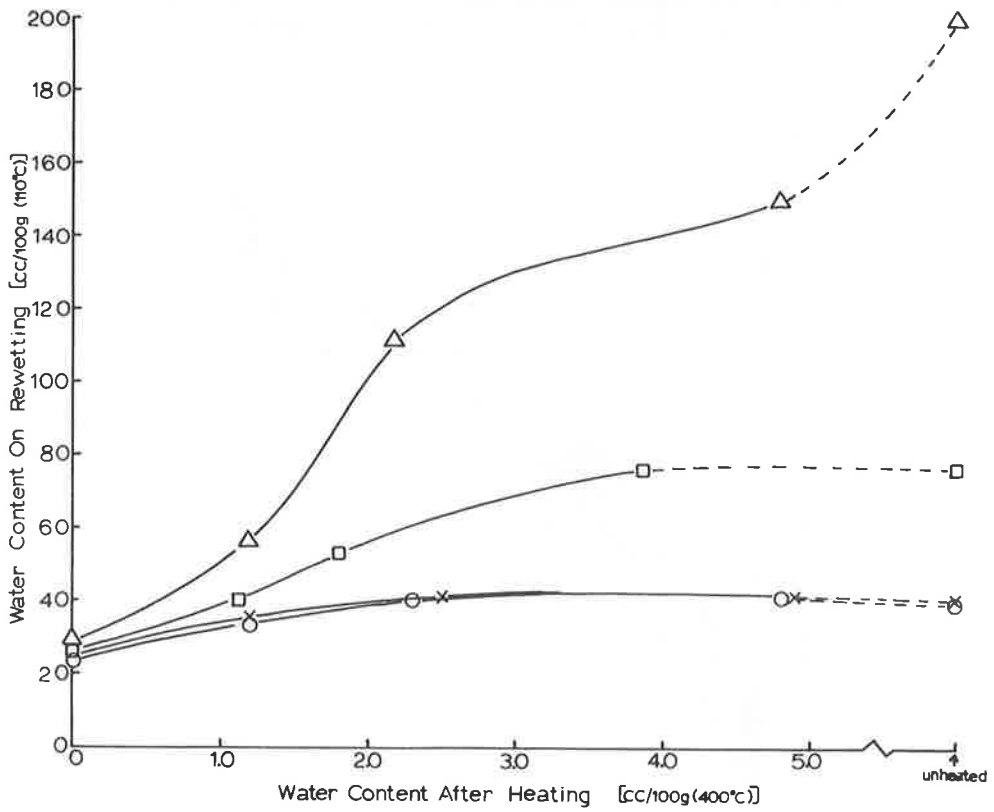

Figure 1. Water contents (cc/100 g at 110 C) for Willalooka illite cores saturated with sodium (Δ), potassium (□), calcium (X), and magnesium (O) cations on rewetting at 100 mB suction vs initial water content (cc/100 g at 400 C) after preheating to various temperatures.

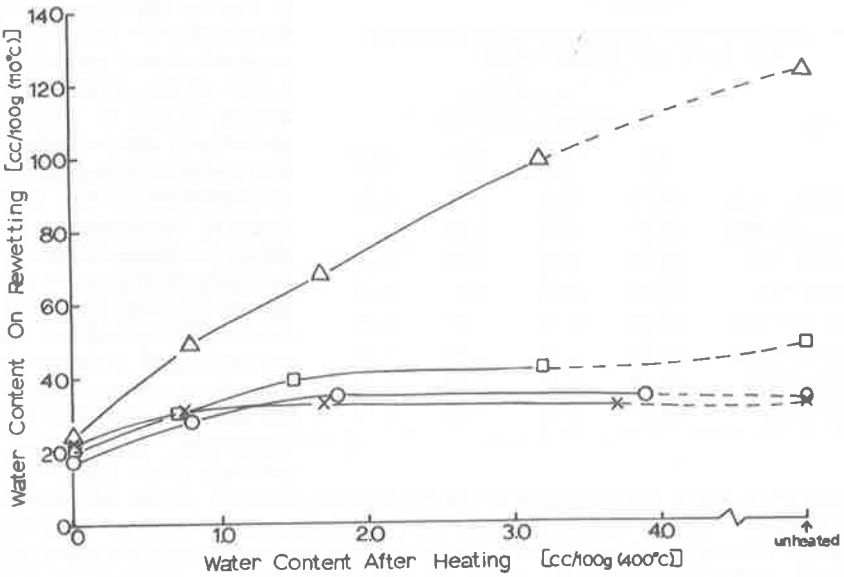

Figure 2. Water contents (cc/100 g at 110 C) for Urrbrae B cores saturated with sodium (Δ), potassium (□), calcium (X), and magnesium (O) cations on rewetting at 100 mB suction vs initial water content (cc/100 g at 400 C) after preheating to various temperatures.

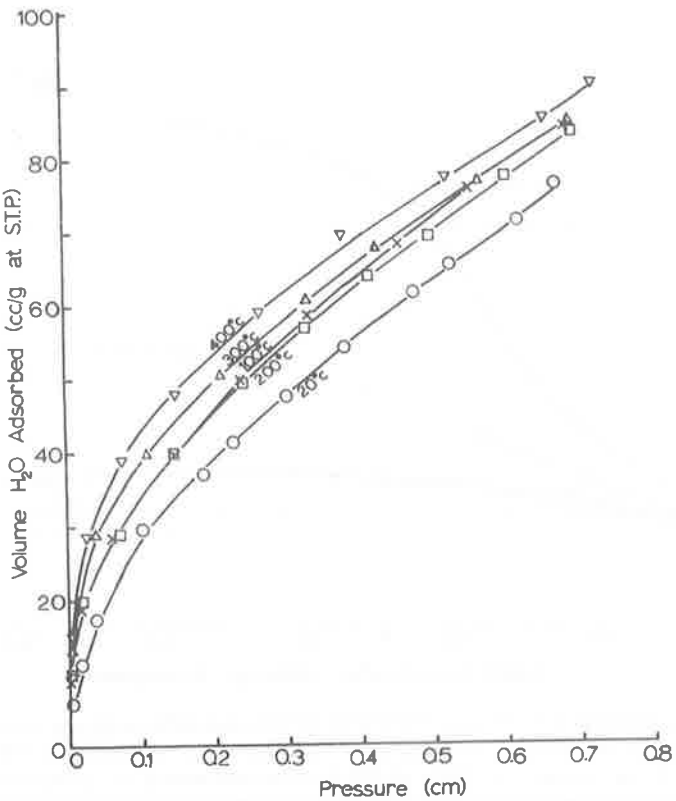

Figure 3. Water vapor adsorption isotherms at 25 C for sodium Willalooka illite degassed at various temperatures.

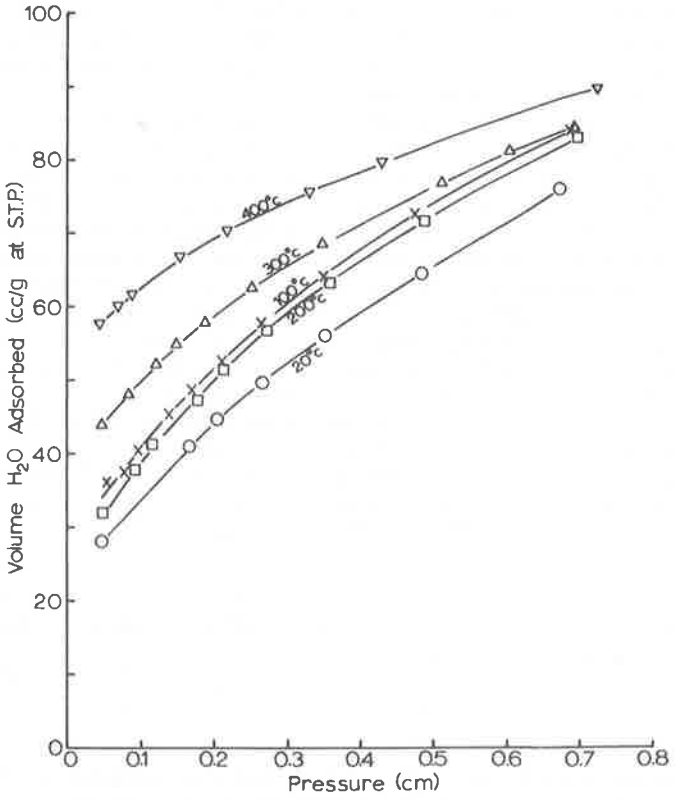

Figure 4. Water vapor desorption isotherms at 25 C for sodium Willalooka illite degassed at various temperatures.

The water contents on wetting the cores against 100 millibars (mB) suction after heating to successively higher temperatures up to 400 C, calculated on the subsequent oven-dry (110 C) basis, are shown in Figures 1 and 2 for Willalooka illite and Urrbrae B clay cores respectively when saturated with sodium, potassium, calcium, and magnesium cations. At this low suction the differences in swelling due to the exchangeable cation and increasing heat treatments become most apparent. For both clays the cores saturated with divalent magnesium and calcium cations, although unaffected by preheating to 200 C, show appreciable reductions in swelling after preheating to higher temperatures. The cores saturated with monovalent cations, and in particular those sodium-saturated, show a marked continuous reduction in swelling with increasing temperature. The large swelling of the unheated sodium clays can be attributed to the unrestrictricted development of diffuse ionic double layers. However, previous work (1) has indicated that there is an electrostatic potential barrier restricting the swelling of these clays when saturated with polyvalent ions. It is apparent that the restrictions due to the heating process either enhance or exceed these restrictions.

The cause of these restrictions is not immediately apparent. Grim (8), in reviewing the dehydration properties of illites used by numerous workers, indicates that there is no loss of structure even with the loss of hydroxyl groups until temperatures exceed 850 C. In addition, Brooks (5) found that the surface area of an illite clay was essentially constant after the loss of surface-adsorbed water and cation hydration water, until temperatures in excess of 600 C were reached. In Figures 3 and 4 are shown water sorption and desorption isotherms obtained on sodium-saturated Willalooka illite cores outgassed at various temperatures until the pressure in the volumetric system remained below 10^{-3} mm mercury after 30 minutes isolation from the pumps. Since

these isotherms were obtained on the $< 2\mu$ fraction of the clay and the clays were heated under vacuum there is of course no direct correspondence in weight loss at a particular temperature between these and the previous samples. Evacuation should result in greater dehydration at any given temperature.

The adsorption isotherms (Fig. 3) are of similar shape with the main vertical displacement occurring between outgassing at room temperature (20 C) and at 100 C. The additional water uptake obtained on the 100 C sample above the uptake after outgassing at 20 C is essentially equivalent to the additional loss of 2.7 cc at STP that occurs on heating from 20 C to 100 C. The weight loss to this stage is thus probably due largely to a reversible dehydration of the surface and cations. On further outgassing at 200 C the subsequent water uptake is slightly less and this may be attributed to a small drop in specific surface area resulting from a more intimate contact of the clay crystals on removal of the last water molecules most strongly held between regions of closest approach. Both Martin (13) and Jurinak (11) have reported such a loss of surface area. Also a decrease in B. E. T. nitrogen area of some 5 to 10 percent on desorption between 100 C and 200 C for Willalooka illite has been repeatedly observed by the authors in studies on the surface area of clays with presorbed water (4).

The weight losses on outgassing at temperatures above 100 C are far greater than those regained on subsequent water sorption. These values are given in the following table for convenience in comparing with Figures 3 and 4:

Temperature	100 C	200 C	300 C	400 C
Water loss (equivalent cc at STP/g)	2.7	16.3	25.1	47.3

The increases in subsequent water uptake observed after outgassing at 300 C and 400 C required considerably longer times for equilibration; this and the increased hysteresis effect on desorption (Fig. 4) suggest that these weight losses could be due to the loss of hydroxonium or hydroxyl ions from within the clay lattice. However, it is apparent that at least part of this loss is regained under these conditions.

Thus it seems unlikely that the reduction in swelling on heating can be attributed to deterioration of crystal structure or marked changes in the sorptive properties of the clay surfaces.

Since there is a decrease in surface area evident on vigorous outgassing it is reasonable to assume that the subsequent restrictions to swelling arise from the formation of bonds at the regions of contact of the individual clay crystals. A conceivable origin for strong electrostatic attractive forces at these points would be through the dehydrated cations sandwiched between the negatively charged clay crystals. However, this would require that the cation exchange capacity of the heated material be significantly reduced, and accurate measurements indicate that there is no such loss of exchangeable cations.

Martin (13) observed a decrease in the specific surface area and water uptake of kaolinite clays stored under a vacuum of 10^{-5} mm pressure for long periods and attributed this effect to twinning of the crystals in close juxtaposition. The mechanism of twin formation was considered to be hydrogen bonding between the oxygen surface of one crystal and the hydroxyl surface of its neighbor. Similarly, Jurinak (11) observed a degree of "coalescence" of kaolinite crystals after desorption that was related to the size of the exchangeable cation on the clay surface. The Urrbrae B clay used in the present work contains some 40 percent and the Willalooka illite about 2 percent kaolinite. Hence, it seems quite possible that the formation of interparticle hydrogen bonds on the removal of adsorbed water molecules may prevent the re-expansion of the domains of oriented clay particles despite the formation of diffuse ionic distributions on the surfaces. Such forces have been suggested by Aylmore and Quirk (2) as being responsible for the small swelling exhibited by kaolin clays.

TABLE 3

WATER CONTENTS ON WETTING TO 10 mB SUCTION FOR SODIUM FITHIAN ILLITE (< 2μ) SAMPLES

Treatment	Water Content (g/100 g)
Unheated	92.5
Preheated 300 C	133.9
Unheated plus 1 percent Rocky Gully kaolinite	92.8
1 percent Rocky Gully kaolinite added and heated to 300 C	90.8

This suggestion is strongly supported by the data in Table 3 for sodium-saturated Fithian illite that X-ray examination shows to be free of kaolinite impurity. Far from restricting the swelling of this clay, heating to 400 C results in an appreciable increase in water uptake at 10 mB suction, probably through the removal of organic binding materials. The addition of 1 percent Rocky Gully kaolinite as an impurity before heating seems to cancel this increase due to the removal of organic matter. However, it is difficult to control the intimacy of mixing of the two constituents and this would obviously influence the extent of bonding that occurs.

Dimethyl sulfoxide (DMSO) has been shown to be an effective hydrogen bond breaker (15) and hence it should be possible to at least partially restore the swelling of these clays by treatment with DMSO if hydrogen bonding is in fact responsible. This possibility was investigated by shaking samples of preheated sodium Willalooka illite with a 90 percent solution of DMSO in water for periods of two weeks and two months at 60 C. The samples were washed with distilled water, air-dried and compressed into cores as before. The water contents of these DMSO-treated cores at 10 mB suction are compared in Table 4 with control cores of the unheated clay and heated samples shaken for two weeks with distilled water.

It is apparent that the DMSO treatment is not only capable of restoring the swelling capacity of the Willalooka clay but actually increases the water uptake of the heated material beyond that of the unheated clay if carred out long enough. This may indicate the presence of some restrictions in the original clay but obviously a more detailed investigation of the DMSO treatment is warranted to establish the nature of this interaction.

From the previous results it is reasonable to conclude that the presence of the kaolinite clay is responsible for the restriction to swelling observed on heating the Willalooka and Urrbrae B clay samples. It seems very likely that the formation of hydrogen bonds between oxygen and hydroxyl surfaces on the complete removal of adsorbed water is in fact the mechanism of crosslinking that occurs. Further work is at present being undertaken in an attempt to confirm these conclusions and to determine the extent of hydrogen bonding that occurs in the different systems.

TABLE 4

EFFECT OF DMSO TREATMENT ON WATER CONTENT OF SODIUM WILLALOOKA ILLITE (< 2μ) ON WETTING TO 10 mB SUCTION

Treatment	Water Content (g/100 g)
Untreated	246
Heated 300 C, shaken with water for 2 weeks	80
Heated 300 C, shaken with 90 percent DMSO for 2 weeks	154
Heated 300 C, shaken with 90 percent DMSO for 2 months	355

REFERENCES

1. Aylmore, L. A. G., and Quirk, J. P. The Structural Status of Clay Systems. Proc. Ninth Natl. Conf. Clays and Clay Minerals, Pergamon Press, New York, 1962, p. 104.
2. Aylmore, L. A. G., and Quirk, J. P. Adsorption of Water and Electrolyte Solutions by Kaolin Clay Systems. Soil Sci., Vol. 102, p. 339, 1966.
3. Aylmore, L. A. G., and Quirk, J. P. The Micropore Size Distributions of Clay Mineral Systems. Jour. Soil Sci., Vol. 18, p. 1, 1967.
4. Aylmore, L. A. G., Quirk, J. P., and Sills, I. D. The Surface Area of Clays With Preadsorbed Water. (In preparation.)
5. Brooks, C. S. Nitrogen Adsorption Experiments on Several Clay Minerals. Soil Sci., Vol. 79, p. 331, 1955.
6. Brown, G., and Norrish, K. Hydrous Micas. Miner. Mag., Vol. 29, p. 929, 1952.
7. Brunauer, S., Emmett, P. H., and Teller, E. Adsorption of Gasses in Multimolecular Layers. Jour. Amer. Chem. Soc., Vol. 60, p. 309, 1938.
8. Grim, R. E. Clay Mineralogy. McGraw-Hill Ltd., London, 1953, 237 p.
9. Gupta, G. C., and Dutta, A. K. Water Stability of Aggregates in a Heated Black Cotton Soil. Soil Sci., Vol. 104, p. 210-216, 1967.
10. Irvine, R. H. Road Making by Heat Treatment of Soils. Jour. Inst. Eng. Australia, Vol. 11, Paper No. 332, 1930.
11. Jurinak, J. J. The Effect of Pretreatment on the Adsorption and Desorption of Water Vapour by Lithium and Calcium Kaolinite. Jour. Phys. Chem., Vol. 65, p. 62, 1961.
12. Keenan, A. G., Mooney, R. W., and Wood, L. A. The Relation Between Exchangeable Ions and Water Adsorption on Kaolinite. Jour. Phys. and Coll. Chem., Vol. 55, p. 1462, 1951.
13. Martin, R. T. Water Vapor Sorption on Lithium Kaolinite. Proc Fifth Natl. Conf. Clays and Clay Minerals, Natl. Acad. Sci.-Natl. Res. Council Pub. 566, 1958, 23 p.
14. Mooney, R. W., Keenan, A. G., and Wood, L. A. Adsorption of Water Vapour by Montmorillonite: I. Heat of Desorption and Application of B. E. T. Theory. Jour. Amer. Chem. Soc., Vol. 74, p. 1367, 1952.
15. Olejnik, S., Aylmore, L. A. G., Posner, A. M., and Quirk, J. P. Infra-Red Spectra of Kaolin Mineral-Dimethyl Sulfoxide Complexes. Jour. Phys. Chem., Vol. 72, p. 241, 1968.
16. Pearson, T. G. Uber ein Manometer zur Messung niederer Drucke leichtkondensierbarer Gase. Zeitschrift Physik. Chem., Vol. A 156, p 86, 1931.

Clays and Clay Mi[illegible] 1970, Vol. 18, pp. 91–96. Pergamon Press. Printed in Great Britain

SURFACE AREA OF HOMOIONIC ILLITE AND MONTMORILLONITE CLAY MINERALS AS MEASURED BY THE SORPTION OF NITROGEN AND CARBON DIOXIDE

L. A. G. AYLMORE, I. D. SILLS and J. P. QUIRK

Department of Soil Science and Plant Nutrition, Institute of Agriculture, University of Western Australia, Nedlands, W.A. 6009

(*Received* 15 *September* 1969)

Abstract—The surface areas obtained by application of the B.E.T. theory to adsorption isotherms of nitrogen and carbon dioxide gases at 77°K and 195°K respectively on homoionic samples of illite and montmorillonite clays have been examined. The isotherms were obtained using a standard volumetric adsorption system and the results are compared with those obtained by Thomas and Bohor (1968) using a dynamic sorption system.

Small amounts of residual water have been shown to have a marked influence on the accessibility of the internal surfaces of the montmorillonite clays to nitrogen and carbon dioxide adsorption. In this respect the standard outgassing procedure under high vacuum seems more efficient than that used in dynamic systems. The present data indicate that provided the sample has been satisfactorily outgassed there is little penetration of nitrogen or carbon dioxide gases into the quasi-crystalline regions of montmorillonite clays. With the exception of the caesium saturated montmorillonites the surfaces of the clays are more accessible to the smaller nitrogen molecules than to carbon dioxide assuming the values used for molecular area are correct.

IN A RECENT paper Thomas and Bohor (1968) have examined the accessibility of the surfaces of homoionic montmorillonite clays to nitrogen and carbon dioxide adsorbates at 77°K and 195°K respectively using a dynamic measuring system (Nelson and Eggertsen, 1958). From variations in the surface area obtained by application of the B.E.T. (1938) theory to these measurements these authors considered that there was a certain degree of penetration of both nitrogen and carbon dioxide between the unit platelets or lamellae forming the crystals of montmorillonite. Their experimental data indicated that the extent of penetration was time dependent and also a function of the interlayer forces as governed by the size and charge of the replaceable cations.

Aylmore and Quirk (1967) have recently pointed out that in the dry state montmorillonite clay forms a complexly interwoven matrix in which one lamella may conceivably pass through several apparently crystalline regions. It is considered that the term "quasi-crystalline" (Aylmore and Quirk, 1969) may be the most appropriate description here since in these regions the lamellae are stacked in parallel array but not necessarily in perfect crystalline order. In these circumstances the definition of apparent crystal size must be somewhat arbitrary. It was considered that the area determined by nitrogen adsorption at low temperatures was essentially a measure of the surface area external to these quasi-crystalline regions. The differences in specific surface area observed between montmorillonite saturated with different exchangeable cations was attributed partly to differences in the degree of association of the lamellae in aqueous suspensions (Edwards, Posner and Quirk, 1965) and the subsequent statistical arrangement of the units on drying, and partly to variations in accessibility of areas of overlap of quasi-crystalline regions with size of the exchangeable cations.

Since the data reported by Thomas and Bohor (1968) was obtained using a dynamic sorption system (Nelson and Eggertsen, 1958) the results of similar sorption measurements obtained using a standard volumetric adsorption system are reported here.

MATERIALS

The clay samples used were obtained from the following natural deposits.

Fithian illite—from Ward's Natural Science

Establishment Inc., Illite No. 35 of the American Petroleum Institute Research Project No. 49 (1951).

Willalooka illite—B horizon from a solonized solonetz: Hundred of Laffer, South Australia.

Wyoming bentonite—montmorillonite from the John C. Lane Tract, Upton, Wyoming. Standard clay mineral No. 25b of the American Petroleum Institute Research Project No. 49.

Redhill montmorillonite—from Redhill, Surrey, England: supplied by Fullers Earth Company.

In general, samples of the clays were sodium saturated by repeated washing and centrifuging with molar sodium chloride during which the pH of the suspension was adjusted to 3·0 using hydrochloric acid. The samples were washed and dialysed against distilled water using Visking cellulose casing, and the $< 2\mu$ fractions obtained by accurate sedimentation. In addition, several size fractions of the sodium saturated Wyoming bentonite clay were obtained by centrifugation as described by Laffer, Posner and Quirk (1969). Samples saturated with other cations were prepared from these materials by washing with the appropriate molar chloride solution and finally dialysing against distilled water as before.

The air-dried clays were gently ground to a powder, equilibrated with 0·75 relative water vapour pressure and compressed into 200 mg cores at 1200 atmosphere pressure by means of an hydraulic jack (Aylmore and Quirk, 1962).

PROCEDURE

The volumetric apparatus used (Aylmore 1960) was based on the original apparatus of Emmett and Brunauer (1934) and incorporated many of the refinements suggested by Harkins and Jura (1944) and Joyner (1949), including a mercury cut-off between the sample tube and mercury manometer to minimize free space volume. Saturation vapour pressures were measured by means of a vapour pressure thermometer.

In general, the clays were outgassed overnight at 300°C and 10^{-6} mm mercury pressure. Provided the pressure in the system remained below 10^{-3} mm mercury pressure after 30 min isolation from the pumps the sample was regarded as thoroughly outgassed. Previous determinations have shown that further outgassing for an extended period produces no significant change in the specific surface area obtained.

Nitrogen adsorption isotherms were determined by the usual doser technique after immersing the sample bulb in a liquid nitrogen bath. The sample was then allowed to return to room temperature and re-evacuated for 30 min to remove adsorbed nitrogen. Carbon dioxide adsorption isotherms at 195°K were obtained by immersing the sample bulb in a gently stirred solid carbon dioxide–ethanol slush. The saturated vapour pressure of carbon dioxide was taken as 760 mm. In some cases the entire procedure was repeated to check that the sorptive properties of the clay were unaltered by the previous sorption determination.

RESULTS AND DISCUSSION

The surface areas obtained by application of the B.E.T. theory to the nitrogen and carbon dioxide absorption isotherms on homoionic illite and montmorillonite clays are given in Table 1. The B.E.T. plots so obtained all had positive intercepts with C-values ranging from 20 to several hundred. In general the C-values for the nitrogen plots were higher than those for carbon dioxide. Surface areas were calculated using molecular areas of 16·2 Å² for nitrogen adsorption at 78°K and 22·1 Å² for carbon dioxide adsorption at 195°K. These values are the most consistently accepted in the literature and make the results directly comparable with those of Thomas and Bohor (1968).

Because of the time dependence of adsorption observed by Thomas and Bohor, the approach of equilibrium for a number of points on each isotherm were followed carefully for periods up to 48 hr. For the illite clays where there is little likelihood of penetration of adsorbate within the crystal structure, equilibrium pressures were always obtained within a period of some 20 min or less. Subsequent variations in relative vapour pressure within the volumetric system were considerably less than the limits of experimental error.

In the case of the montmorillonite clays the time

Table 1. B.E.T. surface areas from nitrogen and carbon dioxide adsorption on $< 2\mu$ fractions of homoionic illite and montmorillonite clays

Clay	Surface area, m²/g	
	Nitrogen adsorption	Carbon dioxide adsorption
Sodium Fithian illite	105	72·4
Sodium Willalooka illite	195	162
Caesium Willalooka illite	184	159
Sodium Wyoming bentonite	39·8	40·6
Caesium Wyoming bentonite	99·1	189
Sodium Redhill montmorillonite	147	132
Caesium Redhill montmorillonite	158	215

required for equilibration varied with the exchangeable cation present on the clay surface. For the sodium saturated samples a definite equilibrium, within the limits of experimental error, was established in less than 20 min for both nitrogen and carbon dioxide adsorption. On the other hand longer equilibration times up to some 4 hr were required for the initial dose for the caesium saturated samples for both nitrogen and carbon dioxide adsorption, indicating that some regions were less readily accessible than others. This was evidenced by a very small but measurable uptake after the initial rapid sorption. Equilibrium on subsequent points was again well established within 20 min.

The differences in B.E.T. specific surface area estimated on the basis of amounts adsorbed after periods of 30 min and 16 hr respectively were in all cases very small. The maximum difference observed was for example for carbon dioxide adsorption on 0·14μ–0·27μ e.s.d. caesium saturated Wyoming bentonite*, the sample equilibrated for 30 min giving a surface area of 198 m²/g and that equilibrated for 16 hr giving 206 m²/g. Other differences were generally less than 0·5 per cent of the 30 min value.

Previous investigations by others (Barrer and McLeod, 1955; Brooks, 1955) and in these laboratories, have shown that the sorption of non-polar gases and hence the B.E.T. area obtained for a montmorillonite clay is particularly dependent on the efficiency of the outgassing procedure used. Brooks (1955) noted that the specific surface area of Ca-Wyoming bentonite increased to a value of about 120 m²/g with decreasing hydration due to the accessibility to nitrogen of surfaces propped apart by water molecules, before decreasing to a value of 41·3 m²/g on effectively complete desorption. Similar effects have been noted in these laboratories in detailed studies of the surface areas of both illite and montmorillonite clays with small amounts of presorbed water. Invariably the specific surface area increased to a maximum with the gradual removal of adsorbed water from the clay surfaces, followed by a decrease due to the collapse of regions between surfaces propped apart by the last remaining water molecules.

In view of the results obtained by Thomas and Bohor (1968) and the different outgassing procedure used in the dynamic system the effect of incomplete outgassing on the relative sorption of nitrogen and carbon dioxide was investigated. The changes in nitrogen and carbon dioxide B.E.T. specific surface areas with percentage residual water based on the weight of sample outgassed at 300°C and 10^{-6} mm mercury pressure are shown in Fig. 1. After outgassing at room temperature for 30 min the area obtained using carbon dioxide is considerably greater than that using nitrogen. During the initial stages of further dehydration at 50°C and then at 110°C the nitrogen area increased rapidly, presumably due to the increased accessibility of surfaces previously blocked by water molecules. The carbon dioxide area increases slightly at first for the same water loss between room temperature and 50°C suggesting that the presence of the water molecules causes sufficient separation of some surfaces to enable the penetration of the more strongly adsorbed carbon dioxide. However, further dehydration above 110°C causes a decrease in specific surface area as these regions collapse and become inaccessible to the larger carbon dioxide molecules. The magnitude of the area involved suggests that in this case it may be only the surfaces between quasi-crystalline regions (i.e. within discontinuities in ordering) which are involved and that much of the internal area of the clay matrix is in fact not accessible to nitrogen or carbon dioxide adsorption.

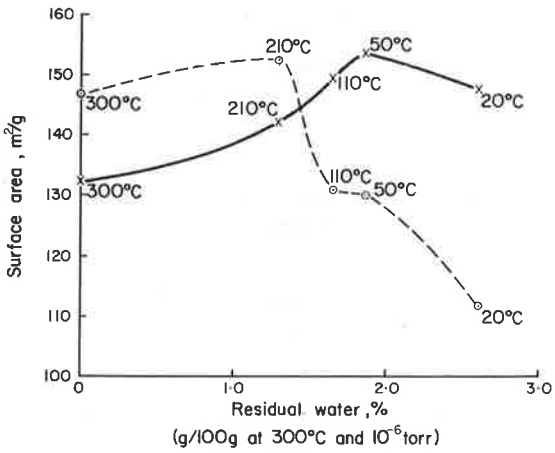

Fig. 1. Changes in nitrogen and carbon dioxide specific surface areas of sodium Redhill montmorillonite with percentage residual water based on the weight of sample outgassed at 300°C and 10^{-6} torr. ○ Nitrogen; × Carbon dioxide.

The outgassing procedure used in dynamic sorption systems involves the passing of a stream of helium gas over the heated sample usually at pressure of 5–10 p.s.i. Under these conditions the mean free path for water vapour movement and hence the rate of desorption of water from the clay surfaces, would be considerably less than in systems evacuated at 10^{-6} mm mercury pressure

*The CO_2 surface area for < 2μ Cs Wyoming bentonite is 189 m²/g.

at any given temperature. Thus it seems likely that the samples of montmorillonite examined by Thomas and Bohor contained considerably more residual water than those in the present study. This is also indicated by the observation that the data of Thomas and Bohor for temperature effects follow the same general trends as shown in Fig. 1 except that the temperatures at which the final stages of dehydration and collapse of regions propped apart by residual water molecules occur, are higher for the dynamic outgassing procedure. That is, the nitrogen surface areas for most clays show a slight increase as the temperature of outgassing increases from 110°C to 175°C followed by a decrease at the highest temperatures (300°C–500°C). The carbon dioxide areas decrease considerably and continuously as the outgassing temperature is raised.

Comparison of the specific surface areas given in Table 1 shows that with the exception of the caesium saturated montmorillonites the internal areas of the completely outgassed clay cores are less accessible to the larger carbon dioxide molecule than to nitrogen, i.e. assuming the given values for molecular area. Even for the non-expanding illite clays there are obviously regions of overlap of the clay crystals which are accessible to nitrogen but not to carbon dioxide. Only for the caesium montmorillonites which apparently have a much less well ordered packing arrangement, is the greater affinity of the carbon dioxide molecule for the surface more effective in penetrating between the quasi-crystalline regions.

Thomas and Bohor (1968) in comparing the marked tailing of the adsorption peak which they obtained with Cs-montmorillonite suggest that there is no reason to believe that this is due to a significant difference in the mean particle size or in pore characteristics (greater proportion of micropores) that evolves during sample preparation. However, specific surface areas obtained by measurements of chloride exclusion from homoionic Wyoming Bentonite in aqueous suspension (Edwards, Posner & Quirk, 1965) indicate that there is a marked variation in the degree of association of the lamellae with the size and charge of the exchangeable cation. The size of these units in aqueous solution could be expected to have some influence on the porous structure formed on drying. Since these chloride exclusion areas are invariably much larger than the nitrogen areas obtained on the dried clay we may infer that overlap of these units results in larger quasi-crystalline regions.

In addition, the pore size distributions obtained by Aylmore and Quirk (1967) on Cs and Na saturated montmorillonites indicate that there is a far greater proportion of micropores of less than 10 Å plate separation, presumably between quasi-crystalline regions, which is available to rapid nitrogen adsorption, in the Cs clays than in the Na clays. As pointed out by these authors the distinction between internal and external surfaces is essentially one of alignment of the lamellae and its effect on the accessibility of these surfaces to the adsorbate. The larger Cs cation results in greater accessibility of the areas of overlap between quasi-crystalline regions but it is apparent from Table 1, that even here much less than the total interlamellar surface area of more than 700 m^2/g is available to nitrogen adsorption, even doubling the values of 99 m^2/g and 158 m^2/g on the assumption that a single layer is adsorbed between two adjacent surfaces. Even for the more strongly absorbed carbon dioxide, it is evident that the surface area remains inaccessible.

In Table 2, the specific areas obtained from nitrogen and carbon dioxide adsorption on homoionic samples of the different size fractions of the Wyoming bentonite clay are given. One particularly interesting feature is the small area and slight variation in area obtained by nitrogen adsorption for the different sodium fractions despite electron microscopic confirmation that the lateral dimensions of the lamellae forming the smaller size fractions were of the order of one tenth those of the larger fraction. The authors have repeatedly observed this reproducibility in surface area for a given homoionic montmorillonite despite wide variations in the preparative technique. Thus, it is apparent that the exchangeable cation on the clay surface can be more important in determining the accessibility of the dry clay matrix to gas sorption than the lateral dimensions of the lamellae.

Table 2. B.E.T. surface areas from nitrogen and carbon dioxide adsorption on different size fractions of Wyoming bentonite obtained by centrifugation

Size fraction	Exchangeable cation	Surface area m^2/g Nitrogen adsorption	Carbon dioxide adsorption
0·14 μ-	Na^+	39·8	41·1
0·27 μ e.s.d.	Cs^+	120	207
0·041 μ-	Na^+	44·6	54·9
0·065 μ e.s.d.	Cs^+	147	228

CONCLUSIONS

Provided the sample has been satisfactorily outgassed there is little penetration of nitrogen or carbon dioxide gases into the quasi-crystalline

regions of these montmorillonite clays. The gas sorption which does occur appears, with the possible exception of the Cs montmorillonites, to be essentially between rather than into quasi-crystalline regions. Although it is reasonable to expect that there will be some delayed diffusion of even non-polar adsorbates into less accessible surfaces of the clay matrix the present data indicate that this is very small for all but the caesium clays. Under these conditions the sorption of such gases can be used to estimate the external surface area of these regions.

The increase in area which occurs with initial outgassing is probably due to the removal of water from and hence the greater accessibility of the surfaces between quasi-crystalline regions in the same way as it is for nonexpanding crystals such as illites. Subsequently the presence of a few residual water molecules will allow some penetration between lamellae forming quasi-crystals (see Brooks, 1955).

When the removal of adsorbed water is essentially complete the surface area obtained will depend, for a given clay, and on the size and charge of the exchangeable cations and their effects on the porous matrix formed during preparation, and the size of the adsorbate molecules. Differences in area obtained with different sorbate molecules will occur as a result of variations in molecular exclusion from the smallest micropores between crystals and quasi-crystalline regions and in micropore filling (see Dubinin, 1967). For this reason the surface area of the clays is generally more accessible to nitrogen than to carbon dioxide.

In the case of larger exchangeable cations such as caesium the imperfections in packing of the lamellae are sufficiently large to permit a more extensive penetration of the gases into the clay matrix. However, even for carbon dioxide sorption the increase in volume sorbed after 16 hr is very small compared with that after 30 min and much of the clay matrix remains essentially inaccessible.

The penetration of gas molecules between the lamellae is enhanced by the presence of residual water molecules and it seems likely that the outgassing used in dynamic systems is less efficient than standard procedures under high vacuum.

REFERENCES

Aylmore, L. A. G. (1960) The hydration and swelling of clay mineral system. Ph.D. Thesis. University of Adelaide.

Aylmore, L. A. G. and Quirk, J. P. (1962) The structural status of clay systems. *Clays and Clay Minerals* **9**, 104–139. Pergamon Press, New York.

Aylmore, L. A. G. and Quirk, J. P. (1967) The micropore size distributions of clay mineral systems. *J. Soil Sc.* **18**, 1–17.

Barrer, R. M. and McLeod, D. M. (1955). Activation of montmorillonite by ion exchange and sorption complexes of tetra-alkyl ammonium montmorillonite. *Trans. Faraday Soc.* **51**, 1290–1300.

Brooks, C. S. (1955). Nitrogen adsorption experiments on several clay minerals. *Soil Sci.* **79**, 331–347.

Brunauer, S., Emmett, P. H. and Teller, E. (1938). Adsorption of gases in multimolecular layers. *J. am. Chem. Soc.* **60**, 309–310.

Dubinin, M. M. (1967). Adsorption in micropores. *J. Colloid Interface Sci.* **23**, 487–499.

Edwards, D. G., Posner, A. M. and Quirk, J. P. (1966). The repulsion of chloride ions by negatively charged clay surfaces. Parts I, II and III. *Trans. Faraday Soc.* **61**, 2808–2823.

Emmett, P. H. and Brunauer, S. (1934) The adsorption of nitrogen by iron synthetic catalysts. *J. Am. Chem. Soc.* **56**, 35–41.

Harkins, W. D. and Jura, G. (1944) Surface of solids, X, XII, XIII. *J. Am. Chem. Soc.* **66**, 919–927, 1362–1366, 1366–1372.

Joyner, L. G. (1949) Chap. 12 *Scientific and Industrial Glass Blowing and Laboratory Techniques* by Barr, U. E. and Aukon, V. J. Instrument Publishing Co. Pittsburgh.

Laffer, B. G., Posner, A. M. and Quirk, J. P. (1969) Optical Density of Montmorillonite Suspensions During Sodium–Calcium Exchange. *J. Colloid Interface Sci.* **30**, 355–358.

Nelsen, F. M. and Eggertsen, F. T. (1958). Determination of surface area: adsorption measurements by a continuous flow method. *Ann. Chem.* **30**, 1387–1390.

Thomas, J. Jr. and Bohor, B. F. (1968). Surface area of montmorillonite from the dynamic sorption of nitrogen and carbon dioxide. *Clays and Clay Minerals* **16**, 83–91.

Résumé—Les ares de surface obtenues par l'application de la théorie B.E.T. aux isothermes d'adsorption du nitrogène et du gaz carbonique, à 77°K et 195°K respectivement, sur des échantillons homoioniques d'argiles illite et montmorillonite, ont été étudiées. Les isothermes ont été obtenus en utilisant un système standard d'adsorption volumétrique et les résultats sont comparés à ceux obtenus par Thomas et Bohor (1968) qui emploient un système d'adsorption dynamique.

De petites quantités d'eau résiduelle ont fait apparaître une influence marquée sur l'accessibilité des surfaces internes des argiles montmorillonites à l'adsorption du nitrogène et du gaz carbonique. A cet égard, la méthode de dégazéification standard, sous un vide élevé, semble plus efficace que celle utilisée dans les systèmes dynamiques. Les données actuelles indiquent que, pourvu que l'échantillon ait été dégazéifié d'une manière satisfaisante, il se produit une faible pénétration de gas carbonique et de nitrogène dans les régions quasi-cristallines des argiles montmorillonites. A l'exception des mont-

morillonites saturés de Cs, les surfaces des argiles sont plus accessibles aux plus petites molécules de nitrogène qu'au gaz carbonique en supposant que les valeurs utilisées pour le are moléculaire soient correctes.

Kurzreferat—Die durch Anwendung der B.E.T. Theorie auf Adsorptionsisothermen von Stickstoff und Kohlendioxyd Gasen bei 77°K bzw. 195°K an homoionische Proben von Illit und Montmorillonit Tonen erhaltenen Oberflächen wurden untersucht. Die Isothermen wurden unter Anwendung eines Standard volumetrischen Adsorptionssystems erhalten, und die Resultate werden mit jenen durch Thomas und Bohor (1968), unter Verwendung eines dynamischen Sorptionssystems erhaltenen, verglichen.

Es konnte festgestellt werden, dass kleine Mengen von Restwasser einen deutlichen Einfluss auf die Zugänglichkeit innerer Oberflächen der Montmorillonit Tone für die Adsorption von Stickstoff und Kohlendioxyd ausüben. In dieser Hinsicht scheint das Standard Ausgasungsverfahren im Hochvakuum wirksamer zu sein als das in dynamischen Systemen verwendete. Die gegenwärtig verfügbaren Werte deuten darauf hin, dass, vorausgesetzt die Probe ist genügend ausgegast worden, nur geringfügige Eindringung von Stickstoff oder Kohlendioxyd Gasen in die quasikristallinen Bereiche der Montmorillonit Tone stattfindet. Mit der Ausnahme der an Caesium abgesättigten Montmorillonite sind die Oberflächen der Tone für die kleineren Stickstoffmoleküle besser zugänglich als für Kohlendioxyd, angenommen, dass die für die Molekülfläche verwendeten Werte korrekt sind.

Резюме—Изучены поверхностные области, выявленные при применении теории B.E.T. к анализу изотерм адсорбции газов NO_2 и CO_2 при 77°K и 195°K, соответственно, для гомоионных образцов иллитовых и монтмориллонитовых глин. Изотермы сняты с использованием стандартной волюметрической адсорбционной системы и полученные результаты сравнимы с результатами, полученными Томасом и Боором (1968) при использовании динамической сорбционной системы.

Показано, что небольшие количества остаточной воды оказывают заметное влияние на чувствительность внутренних поверхностей монтмориллонитовых глин к поглощению NO_2 и CO_2. В связи с этим стандартная методика дегазации в условиях высокого вакуума очевидно является более эффективной, чем методика, используемая в динамических системах. Полученные данные показывают, что при условии удовлетворительной дегазации образца имеет место лишь незначительное проникновение газов NO_2 и CO_2 в квази-кристаллические области монтмориллонитовых глин. За исключением монтмориллонита, насыщенного катионами цезия, поверхности глин более чувствительны к небольшим молекулам NO_2, чем к молекулам CO_2, при предположении, что значения, используемые для молекулярных поверхностей, являются правильными.

over techniques employing standard apparatus in determining the total amount of gas adsorbed via the elution (desorption) of the adsorbate. The dynamic method is based on gas chromatography principles, and is very sensitive to volume changes and quite accurate with proper calibration. We are not surprised that Aylmore *et al.*, with standard pressure–volume apparatus, were unable to detect the very slight additional adsorption, with time, on Na-montmorillonite as they were able to do more easily with Cs-montmorillonite.

To reiterate our position, from our data and that of others, we believe that penetration occurs between layers and we feel that, had Aylmore *et al.* used the proper combination of parameters for carbon dioxide, they would have found greater penetration by carbon dioxide than by nitrogen, as we did.

Illinois State Geological Survey
Urbana, Illinois
U.S.A.

JOSEPHUS THOMAS, Jr.
BRUCE F. BOHOR
ROBERT F. FROST*

REFERENCES

Anderson, R. B., Hofer, L. J. E. and Bayer, J. (1962) Surface area of coal: *Fuel* (London) **41**, 559–560.
Anderson, R. B., Bayer, J. and Hofer, L. J. E. (1965) Determining surface areas from CO_2 isotherms: *Fuel* (London) **44**, 443.
Aylmore, J. G., Sills, I. D., and Quirk, J. P. (1970) Surface area of homoionic illite and montmorillonite clay minerals as measured by the sorption of nitrogen and carbon dioxide: *Clays and Clay Minerals* **18**, 91.
Bridgeman, O. C. (1927) A fixed point for the calibration of pressure gauges; the vapor pressure of liquid carbon dioxide at 0°: *J. Am. Chem. Soc.* **49**, 1174–1183.
de Boer, J. H. (1968) *The Dynamical Character of Adsorption*, 2nd Edn., Chap. 10. Oxford University Press, London.
Emmett, P. H. and Brunauer, S. (1937) The use of low temperature van der Waals adsorption isotherms in determining the surface area of iron-synthetic ammonia catalysts: *J. Am. Chem. Soc.* **59**, 1553–1564.
Lamond, T. G. (1962) Ph. D. Thesis, University of Durham, Durham, England.
Lamond, T. G. and Marsh, H. (1964) The surface properties of carbon II, III: *Carbon* **1**, 281–307.
Maggs, F. A. P. (1952) Anomalous adsorption of nitrogen at 90°K: *Nature* **169**, 793–794.
Nandi, S. P. and Walker, P. L. Jr. (1964) The diffusion of nitrogen and carbon dioxide from coals of various rank: *Fuel* (London) **43**, 385–393.
Pickering, H. L. and Eckstrom, H. C. (1952) Physical adsorption of gases on anatase: *J. Am. Chem. Soc.* **74**, 4775–4777.
Thomas, Josephus, Jr. and Bohor, B. F. (1968) Surface area of montmorillonite from the dynamic sorption of nitrogen and carbon dioxide: *Clays and Clay Minerals* **16**, 83–91.
Walker, P. L. Jr. and Kini, K. A. (1965) Measurement of the ultra fine surface area of coals: *Fuel* (London) **44**, 453–459.

*The comments presented in this paper are those of Thomas and Bohor in defense of their published work. Frost contributed the valuable supplementary data and calculations in the plot of Fig. 1.

Clays and Clay Minerals, 1970, Vol. 18, pp. 407–409. Pergamon Press. Printed in Great Britain

Reply to comments of Thomas, Bohor and Frost on Aylmore, L. A. G., Sills, I. D. and Quirk, J. P. (1970) The surface area of homoionic illite and montmorillonite clay minerals as measured by the sorption of nitrogen and carbon dioxide, *Clays and Clay Minerals* **18**, 91.

IN THEIR comments on our paper (Aylmore, Sills and Quirk, 1970), Thomas, Bohor and Frost (1970) have discussed the way in which the relative magnitude of the B.E.T. specific surface area obtained for clay mineral systems using carbon dioxide at 195°K and nitrogen at 78°K depends upon the values of saturation vapour pressure and molecular area accepted for carbon dioxide when nitrogen is taken as the standard. This variation is not disputed. However, the question of the correct values to use for the saturation vapour pressure and molecular area of carbon dioxide at 195°K will await further elucidation and should not be allowed to obscure the real point of contention debated in our paper which is whether or not these gases penetrate into the quasi-crystalline (Aylmore and Quirk, 1960; Quirk, 1967) regions of the montmorillonite matrix and their use for measurement of the external surface area of these regions. As indicated in the following notes, acceptance of the values assigned by Thomas and Bohor (1968) would not reverse our conclusions with respect to these points.

As pointed out in both their papers and by various other authors, the "absolute" values for surface area obtained by gas sorption depend entirely on the values assigned to the molecular area and saturation vapour pressure for a particular gas. These considerations recently led Pierce and Ewing (1964) to reiterate the conclusions of Brunauer (1943) that it is perhaps unrealistic to expect even nitrogen adsorption to give the absolute surface areas within better than 20 per cent. We have in fact, attempted to "calibrate" the molecular area for carbon dioxide on various clay

minerals and other materials having only "external" surfaces, against nitrogen at 78°K as standard. The values obtained ranged from 22Å² to 42Å² when using the measured saturation vapour pressure of approximately 76 cm. Thus although we concluded that for the values of molecular area assumed, the nitrogen appeared to have access to a greater area of the clay matrix than carbon dioxide, our paper was concerned less with this point than with the location of adsorption, the interpretation of the organisation of the clay lamellae into quasi-crystalline regions and the effects of residual water molecules on the sorption of these two gases.

The major difference in our views apparently stems from a difference in concept of the organisation of the montmorillonite lamellae in the clay matrix and its susceptibility to adsorption. Thomas *et al.* (1968, 1970) appear to regard the organisation of the montmorillonite matrix as essentially the same for all exchangeable cations with penetration of nitrogen or carbon dioxide depending solely on the adsorbate and exchangeable cation and not being subject to previous history or preparative technique. Although undoubtedly much more complex the dry montmorillonite matrix can, in the simplest picture, be regarded as a pile of books, each book containing a number of parallel aligned lamellae in close juxtaposition and sufficiently regular array to provide a $d(001)$ X-ray spacing characteristic for the particular exchangeable cation. The average size of these books or "quasi-crystals" will be determined by a number of factors including, in particular, the degree of association of the lamellae in suspension prior to sedimentation (Edwards, Posner and Quirk, 1965) and the drying technique used. It is worth noting in this regard that by careful preparation of oriented flakes it is possible to reduce the nitrogen specific surface area of sodium Wyoming Bentonite to some 5m²/g compared with the 40m²/g to 50m²/g frequently obtained (e.g. Greene-Kelly, 1964).

Pore size distributions (Aylmore and Quirk, 1967) show that for most of these materials the majority of the surface area external to the quasi-crystalline regions lies in pores of some 25Å–30Å plate separation. The $d(001)$ spacings for dry sodium and calcium montmorillonites are, for example, some 9.8Å and 10.4Å respectively. Since the width of the montmorillonite lamellae is approximately 9.5Å, separation between lamellae in these regions will be something less than 1.0Å. Under these conditions penetration of most simple adsorbates into a given montmorillonite matrix will be determined almost entirely by the ability of the adsorbate to intercalate into the quasi-crystals, i.e. to do mechanical work in actually expanding the $d(001)$ spacings of the quasi-crystals. In these circumstances much of the discussion by Thomas, Bohor and Frost (1970) on diffusion in micropores and analogies with coal and molecular sieves of 4Å–5Å pore size would appear irrelevant. For the caesium cation the $d(001)$ spacing in the dry clay is approximately 11.8Å leaving roughly 2.3Å between the lamellae. In this case much of the work of expansion has already been accomplished and as suggested in our paper the question of possible intercalation in this adsorbent is much more open.

When intercalation does occur as with strongly polar molecules such as water, this is usually evidenced by discontinuities in the adsorption isotherm indicative of a threshold pressure for entry, and appreciable hysterisis in the desorption branch persistent to very low pressures (Barrer and MacLeod, 1954). We have never observed such discontinuities in the adsorption branch of complete adsorption–desorption isotherms for nitrogen on montmorillonite and only for the particular case of the large caesium cation does any appreciable hysterisis persist to low relative pressures. The narrow hysteresis loops evident in our isotherms for carbon dioxide adsorption on montmorillonite are much the same as those obtained for carbon dioxide adsorption on a number of materials which have only "external" surfaces in the previous sense, i.e. non-expanding, such as kaolinite, illite and vycor porous glass. This would again suggest very little if any intercalation of carbon dioxide in the montmorillonite quasi-crystals.

It is conceivable that if one waits a sufficiently long time some carbon dioxide or nitrogen will eventually penetrate into parts of the quasi-crystalline regions by a gradual levering apart at points of weakness perhaps enhanced at higher relative pressures. It would be unreasonable not to expect some penetration of gases into the edges of the quasi-crystals as these are unlikely to be well defined. However, the increases in calculated specific surface area which we observed after 16 hr equilibration compared with 30 min equilibration, were of the order of 0.5 per cent of the 30 min value for all but the clays saturated with the large caesium ion (where it was still only some 4 per cent). We are not aware of any reason why our volumetric system should not be sufficiently sensitive to detect *significant* time dependencies of sorption. We are aware of features of the chromatographic technique which could lead to enhancement of these effects particularly with measurements extended over a considerable time (Cahen and Marechal, 1963). In view of the limitations of the B.E.T. method of surface area determination from gas adsorption the effects of any such delayed diffusion into less accessible surfaces of the clay matrix can certainly be neglected from this point of view.

On the other hand as clearly shown in our paper and previous publications the presence of even a few residual water molecules greatly facilitates the entry of nitrogen and carbon dioxide into the quasi-crystalline regions. The earlier work by Brooks (1955) with nitrogen adsorption shows that in these circumstances large hysteresis, persistent to low relative pressures, is obtained with even sodium and calcium saturated montmorillonites and that this hysteresis decreases rapidly with the progressive removal of residual water as the nitrogen gas is excluded from these regions. The recent data of Thomas and Bohor (1969) for nitrogen and carbon dioxide sorption on vermiculite clays which have essentially the same structure as the montmorillonites but a somewhat higher surface density of charge, are particularly interesting in this regard. Thomas and Bohor conclude that these gases are essentially excluded from the interlamellar regions of vermiculite but that some slight edge penetration of adsorbate gas does occur, since in each case the carbon dioxide areas are appreciably greater than the corresponding nitrogen areas. Significantly they also conclude that the amount of water retained, co-ordinated with the interlayer cations, appears to have a considerable influence on the degree of adsorbate penetration. For example the carbon dioxide area of a magnesium vermiculite decreases from 70m²/g after outgassing at 110°C to 44m²/g when outgassed at 300°C. This behaviour is almost identical to that which we reported for the effects of outgassing on the carbon dioxide areas obtained for montmorillonite. The

significant difference between the structure of the montmorillonite and vermiculite systems is however that the montmorillonite lamellae are subject to various degrees of dissociation in suspension during preparation which results in variations in susceptibility to gas adsorption with quasi-crystal size on drying. This dissociation is largely prevented by the larger surface density of charge of the vermiculites. However, it is clear that in both cases increased outgassing progressively restricts penetration of these adsorbates into the crystalline or quasi-crystalline regions.

Use of the extrapolated vapour pressure for super-cooled liquid carbon dioxide at 195°K (i.e. 145 cm approx.) instead of the measured 76 cm (approx.) increases the specific surface areas obtained for our clays by carbon dioxide sorption to values greater than or approximately equal to those obtained by nitrogen adsorption at 78°K. This is true for the non-expanding illite clays as well as for the montmorillonites. Thus, it is clear that if 145 cm and 22Å² are accepted as the correct saturation vapour pressure and molecular area respectively for CO_2 at 195°K, the conclusion to be reached is that the area of a clay matrix accessible to carbon dioxide at 195°K is frequently greater than that for nitrogen at 78°K. (Whether this conclusion is reversed or not if the measured value of 76 cm is accepted as P_0 for CO_2 at 195°K will of course depend on which particular calibration molecular area is accepted for carbon dioxide). However it does not follow that larger carbon dioxide areas c.f. nitrogen occur through significant penetration of carbon dioxide into the quasi-crystalline regions of the montmorillonite clay for the reasons outlined below.

The slightly larger CO_2 area ($207 m^2/g$) c.f. N_2 ($195 m^2/g$) obtained for sodium Willalooka illite (under the previous assumptions) agrees remarkably well with the increased value ($210 m^2/g$) observed in these laboratories for N_2 adsorption with very small amounts of preadsorbed water on this clay. The latter result was interpreted as resulting from the accessibility of areas of crystal overlap through a "propping apart" of these regions by a few residual water molecules. This would indicate that the carbon dioxide was sufficiently polar to penetrate between the areas of overlap of the illite crystals perhaps yielding a better measure of the total surface area than is obtained with non-polar nitrogen. In the case of the montmorillonite clays it is likely that the surfaces between quasi-crystalline units brought about by discontinuities in ordering of the lamellae, would vary in their accessibility to gas sorption with such factors as the exchangeable cation, size of the quasi-crystalline units, size of the lamellae, nature of the adsorbate and preparative technique. Greater penetration of CO_2 than N_2 as suggested by use of the extrapolated saturation vapour pressure for the super-cooled liquid could be expected to occur initially in these regions of quasi-crystal overlap in a similar fashion to the previous suggestion for the illite crystals. We have suggested in previous publications that this effect and edge effects brought about by incomplete alignment of lamellae, both contribute to variations in adsorption between different gases.

To summarize our position we agree that the question of the relative areas of a montmorillonite clay accessible to nitrogen and carbon dioxide is open to further clarification of the appropriate molecular areas and saturation vapour pressures. We believe however that our data and that of others clearly indicate that with the possible exception of large cations such as caesium or except when residual water molecules are present, carbon dioxide at 195°K and certainly nitrogen at 78°K, are essentially excluded from the quasi-crystalline regions of the montmorillonite matrix. Bearing in mind the inherent limitations of surface area definition there seems little justification for the conclusion by Thomas and Bohor (1968) that time dependency of the sorption of nitrogen "negates the generally accepted concept that nitrogen provides a satisfactory measure of the external surface area" of the quasi-crystalline regions.

REFERENCES

Aylmore, L. A. G. and Quirk, J. P. (1960). Domain or turbostratic structure of clays: *Nature* **187**, 1046–1048.

Aylmore, L. A. G. and Quirk, J. P. (1967) The micropore size distribution of clay mineral systems: *J. Soil Sci.* **18**, 1–17.

Barrer, R. M. and McLeod, D. M. (1954) Intercalation and sorption by montmorillonite: *Trans. Faraday Soc.* **51**, 1290–1300.

Brooks, C. S. (1955) Nitrogen adsorption experiments on several clay minerals: *Soil Sci.* **79**, 331–347.

Brunauer, S. (1943): *The adsorption of gases and vapours*. Princeton University Press, Princeton, N.J. p. 297.

Cahen, Raymond M. and Marechal, Joseph (1963): *Anal. Chem.* **35**, 259–260.

Edwards, D. G., Posner, A. M. and Quirk, J. P. (1965) The repulsion of chloride ions by negatively charged clay surfaces. Parts II and III: *Trans. Faraday Soc.* **61**, 2816–2823.

Greene-Kelly, R. (1964) The specific surface areas of montmorillonite: *Clay Minerals Bull.* **5**, 392–400.

Quirk, J. P. (1968) Particle interaction and soil swelling: *Israel J. Chem.* **6**, 213–234.

Thomas, Josephus Jr. and Bohor, B. F. (1968) Surface area of montmorillonite from the dynamic sorption of nitrogen and carbon dioxide: *Clays and Clay Minerals* **16**, 83–91.

Thomas, Josephus Jr. and Bohor, Bruce F. (1969) Surface area of vermiculite with nitrogen and carbon dioxide as adsorbates: *Clays and Clay Minerals* **17**, 205–209.

Thomas, Josephus Jr., Bohor, Bruce F. and Frost, Robert R. (1970) Comments on The Surface Area of Homoionic Illite and Montmorillonite Clay Minerals as Measured by the Sorption of Nitrogen and Carbon Dioxide: *Clays and Clay Minerals* **18**, 91.

Department of Soil Science and Plant Nutrition
University of Western Australia
Nedlands, W.A. 6009
Australia

L. A. G. AYLMORE
I. D. SILLS
J. P. QUIRK

Reprinted from the *Soil Science Society of America Proceedings*
Volume 34, no. 6, November-December 1970
677 South Segoe Rd., Madison, Wis. 53711 USA

SEPARATION OF ADSORBED CATION SPECIES AS WATER FLOWS THROUGH CLAYS[1]

W. D. KEMPER, I. D. SILLS, AND L. A. G. AYLMORE[2]

Abstract

Theory predicts that adsorbed divalent cations move upstream and monovalent cations move downstream in a mixed ion system, when solutions of low concentration are forced through this clay. Data from small size mica support this prediction.

Additional Key Words for Indexing: **demixing, streaming potential, ionic refluxing.**

THE MOBILE cationic charge in a clay-water system exceeds the mobile anionic charge. Consequently, solution forced through a clay tends to carry a net positive charge with it, building up a positive electrical potential at the low pressure side of the clay. This "streaming potential" gradient continues to grow until it forces the cations upstream and pulls the anions downstream at rates such that the flux of anionic charge equals the flux of cationic charge through the clay. The streaming potential, water, and ion velocities shown in the following presentation were calculated by the general procedures outlined by Kemper (1960).

When mobile anionic charge in the system is less than 5% of the mobile cationic charge, most of the downstream cationic movement in the middle of the pore must be balanced by upstream movement of cations near the edges of the pore film as indicated in Fig. 1. When mono- and divalent cations coexist in the system, the divalent ions in the "adsorbed" diffuse layer tend to be closer to the walls of the pore as indicated in Fig. 2. Consequently, the average divalent ion is not carried downstream as fast as the average monovalent ion. Moreover, since it is doubly charged, the streaming potential forces the divalent cation upstream faster than the monovalent cation. (This difference is generally less than a factor of 2 because hydrated divalent cations are generally bigger and less mobile than hydrated monovalent cations.)

Considering a film of thickness 2b between two clay platelets as indicated in Fig. 1 and 2, the convected velocity, V_{ci}, of the ions of species i is the same as that of the solution (i.e., V) with both measured with respect to the clay. The migration velocity of the ions with respect to the water, V_{mi} (usually negative), caused by the streaming potential gradient $d\psi/dx$ is,

$$V_{mi} = Z_i \epsilon U_i \, d\psi/dx \qquad [1]$$

where Z_i and U_i are the valence and mobility of the ion species, and ϵ is the charge on an electron (esu). In the following calculations ion velocities are calculated from measured and published electrical mobilities, U_i, rather than from the estimated hydrated radii of the ions and Stokes law as was done by Kemper (1960).

In the following treatment Na^+ and Ca^{2+} are used as examples of mono- and divalent ion species, but the general principals discussed should apply to all such monodivalent mixed ion systems. Net velocities ($V_{ci} + V_{mi}$) are indicated for Na^+ and Ca^{2+} as a function of distance from the mineral surface in Fig. 1. The flow of ions (millimoles/sec) through a unit width of a film of thickness 2b, be-

[1] Contribution from the Dept. of Soil Science and Plant Nutrition, Univ. of Western Australia at Nedlands, and the US Soils Laboratory, Soil & Water Conservation Research Division, ARS, USDA, Beltsville, Md. Received Apr. 24, 1970. Approved Aug. 3, 1970.

[2] Director, US Soils Laboratory; Research Associate, Univ. of Western Australia; and Senior Lecturer in Soil Science, Univ. of Western Australia, respectively.

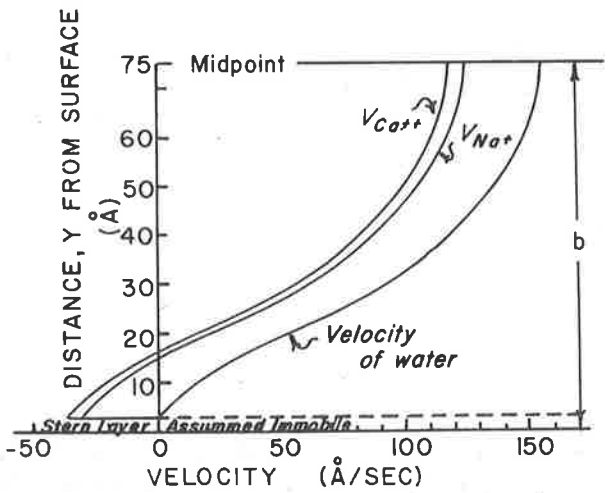

Fig. 1—Velocities of water, Na^+, and Ca^{2+} in films between clay platelets. (Pressure gradient forcing water through was assumed to be 0.1 bar/cm. Calculated streaming potential, involving the cation distribution shown in Fig. 2, was 2×10^{-6} esu/cm.)

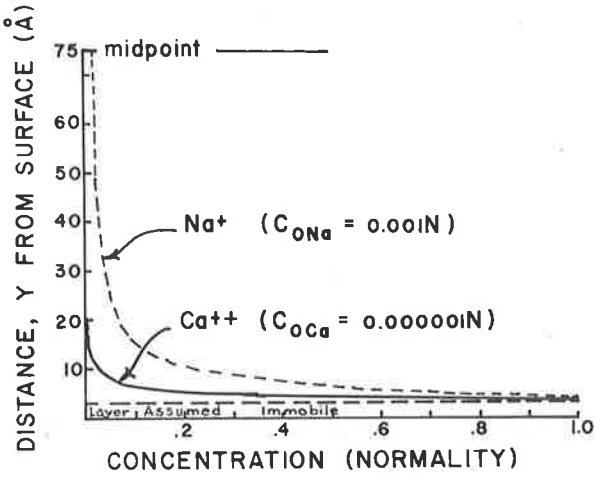

Fig. 2—Distribution of diffuse layer (adsorbed) cations in a mixed Na-Ca system. (Estimated from diffuse layer theory assuming a charge density associated with diffuse layer ions of 24,000 esu/cm^2.)

tween mineral surfaces assuming that Stern layer ions (0 to 3A) are immobile will be,

$$j_i = 2 \int_{y=3A}^{b} V C_i \, dy + 2 Z_i \epsilon U_i \, d\psi/dx \int_{y=3A}^{b} C_i \, dy \qquad [2]$$

where C_i is the concentration (molarity) of cations at the plane y distant from the mineral surface. In the case of no appreciable anionic flow, the net downstream flow of the sodium must be balanced by the net upstream flow of the calcium. Consequently, there should be a tendency for a net movement of divalent cations upstream when solutions of low anionic concentration are forced through porous materials that have mono- and divalent cations adsorbed on their surfaces.

The equilibrium solution concentrations $0.001N$ Na^+ and $0.000001N$ Ca^{2+} assumed in Fig. 2 were the approximate Na^+ content measured in the solution coming out of the clay and a Ca^{2+} concentration which would allow about 20% of the adsorbed ions in the diffuse layer to be Ca^{2+}. Electrical potentials in the diffuse layer were estimated assuming an effective surface charge density at the outside of the Stern layer equal to the Na^+ ions in the diffuse layer. Neglecting the effects of the diffuse layer Ca^{2+} ions and the exchange spots associated with them causes a slight underestimation of the electrical potential from which Na^+ and Ca^{2+} concentrations of Fig. 2 were calculated. Double layer theory to handle mixed ion systems has been developed and will soon be in the literature (private communication from N. Collis-George) from which more precise estimates of this electrical potential may be obtained. Further refinement of the electrical potential values was not attempted in this paper because the conclusions would be the same for practically any appreciable potential associated with the clay mineral surface.

Materials

The mica used was isolated from a pegmatic outcrop near Corrigin, W. Australia, and was identified by X-ray diffraction techniques as biotite. It was ground to pass a 325 mesh sieve and half was saturated with Na^+ and half with Ca^{2+} by repeated washing with a molar solution of the appropriate chloride. After washing free of salt, the material was dried and approximately equal proportions by weight of the Na^+ and Ca^{2+} mica were thoroughly mixed.

Experimental Procedure

The $Na^+ + Ca^{2+}$ mica mixture was packed into glass tubes 0.6 cm in diameter and 2 cm long. After carefully wetting the plug from below to eliminate air bubbles, distilled water was forced through the compacted mineral plugs at the pressure differentials and for the time intervals indicated in Table 1. The distilled water picked up some ions while passing through the plug and this solution coming out of the plug was analyzed for Na^+ and Ca^{2+}. After the indicated time intervals, the flow was stopped, the glass tube broken open, and the plug was divided into an upstream and a downstream section.

The cations were washed out of each section using $1N$ NH_4Ac and the amounts of Na^+ and Ca^{2+} were determined by atomic absorption spectroscopy, employing the appropriate standards prepared in the same batch of $1N$ NH_4Ac to cancel out any interference. Concentrations of Na^+ and Ca^{2+} were calculated on the basis of the oven-dried weight of mica in each section.

Table 1—Conditions leading to, and extent of, cationic separation by streaming potentials

Pressure difference	Flow time	Flow volume	Ca^{2+}	Na^+	Half of tube
bars	days	cc	μeq/gm	μeq/gm	
0.12	3	6.0	36.5	38.8	Upstream
			35.4	47.7	Downstream
0.12	6	6.5	36.7	34.2	Upstream
			34.7	41.0	Downstream
0.68	2	17.0	29.2	22.8	Upstream
			26.0	30.7	Downstream
0.68	3	31.0	36.2	24.8	Upstream
			27.9	37.2	Downstream
0.68	4	29.0	40.2	13.8	Upstream
			33.2	33.3	Downstream

Results and Discussion

The flow through the plugs is shown in Column 3. As shown in Columns 4 and 6, Ca^{2+} tended to move to the upstream half of the plug. This upstream movement was greater if the pressure forcing solution through the plug was greater and generally increased when more solution had been forced through the plug.

It was expected that the sum of the Na^+ and Ca^{2+} concentrations in the upstream and downstream sections should be equal to the exchange capacity and as such should not vary appreciably. However, this apparent exchange capacity tends to decrease with time of flow and also with flow rate.

The decrease in milliequivalents of combined $Na^+ + Ca^{2+}$ in the upstream sections as compared to the downstream sections probably indicates some decomposition of the mica in the distilled water and a replacement of some of the Na^+ and Ca^{2+} by potassium (e.g., see Mortland, 1958), or possibly aluminum. Amounts of Na^+ in the outflow water were of the order of magnitude of this decrease in combined $Na^+ + Ca^{2+}$ in the upstream section (as compared to the downstream), but were generally larger, indicating some replacement of these ions in even the downstream sections. However, the amount of Ca^{2+} in the outflow was negligible. Despite the decomposition reactions that were probably occurring, we can visualize no mechanism other than the streaming potential induced migration, which would move the Ca^{2+} upstream as was observed.

Unfortunately, this decomposition of the clay and slow replacement of the adsorbed ions precludes the attainment of a steady state system in which the assumptions made in the general theory could be checked quantitatively. However, the data indicate that streaming potential separation of mono- and divalent ions does occur, qualitatively in accord with the theory presented. The role of this phenomena in leaching processes, using solutions of higher concentrations, should be determined.

The separation of ion species predicted and observed in this paper is similar in some respects to the "sorting effects" predicted by Helfferich (1962, p. 408) which may occur across charged membranes. Helfferich pointed out that different mobilities of ions would tend to cause different rates of electric migration of ions and result in some degree of species separation. We add that when valences are different, there will be large differences in the convective transport of species of mobile adsorbed cations due to their different average distances from the mineral surface. In compacted clays, this difference in convective velocities is more important than the differences in mobility in causing the separation of mono- and divalent cations.

Literature Cited

1. Helfferich, F. 1962. Ion exchange. McGraw-Hill Book Company, New York.
2. Kemper, W. D. 1960. Water and ion movement in thin films as influenced by the electrostatic charge and diffuse layer of cations associated with clay mineral surfaces. Soil Sci. Soc. Amer. Proc. 24:10–16.
3. Mortland, M. M. 1959. Kinetics of potassium release from biotite. Soil Sci. Soc. Amer. Proc. 26:503–508.

Reprinted from the *Soil Science Society of America Proceedings*
Volume 35, no. 4, July-August 1971
677 South Segoe Rd., Madison, Wis. 53711 USA

Domains and Quasi-Crystalline Regions in Clay Systems[1]

L.A.G. AYLMORE AND J.P. QUIRK[2]

ABSTRACT

A number of terms have been used by different authors to describe regions of near-parallel alignment of the plate-shaped crystals in clay materials. This has resulted in some confusion through inadequate definition and misconceptions in the usage of these terms. Use of the term *quasi-crystal* to describe the regions of parallel alignment of individual alumino-silicate lamellae in montmorillonite and of the term *domain* to describe the regions of parallel alignment of crystals for illite and other fixed lattice clays is recommended in preference to terms such as *tactoid* or *crystal of montmorillonite*.

The similarity in behavior of a domain of illite crystals and a montmorillonite quasi-crystal is illustrated. These regions show a marked difference in swelling behaviour between sodium and calcium systems.

Additional Key Words for Indexing: **quasi-crystal, swelling of clays, tactoid.**

IN PAPERS reporting research on clay-water relations and particle arrangement some confusion exists in the use of the terms—*crystal, domain,* and *tactoid*. The following comments are provided in an attempt to produce some uniformity and consistency in the use of these terms.

Clay mineral systems have been shown to exist with varying degrees of near-parallel alignment of the plate-shaped crystals in randomly oriented regions which electron microscopic evidence indicates are of the order of several microns across for some clay materials (2). Examination of thin sections of clay materials under a microscope with crossed nicols during rotation also indicates that these regions of alignment are of the order of 1 μ or somewhat greater in extent. The extinction in different parts of the field under examination reveals that these regions are in turbulent array with respect to one another, and thus for natural soil aggregates and compressed clay cores the swelling is approximately isotropic (14) although the swelling within each micro-region would be predominantly unidirectional.

In the case of the montmorillonite clays which possess a variable *c*-axis spacing, the regions of parallel alignment of the alumino-silicate lamellae have generally been referred to as *crystals,* although the term *tactoid* has also frequently been used. The term *domain* was used by Aylmore and Quirk (1) to describe an analogous stacking of clay crystals, but this term has also been applied to the grouping of montmorillonite lamellae.

The significance of this near-parallel alignment of clay crystals is most evident in its effect on the development of ionic distributions in the vicinity of clay surfaces. The large swelling of clay systems with lithium and sodium ions balancing the net negative charge arising from isomorphous replacement within the alumino-silicate lattice, is particularly sensitive to both electrolyte concentration and applied hydrostatic suction (3) or mechanical load (18). This is true for those clays such as noninterstratified illites, which exhibit only *inter*-crystalline swelling, as well as for clays with a variable *c*-axis spacing (*intra*-crystalline swelling) such as the montmorillonites. Both swell-

[1] Contribution from Inst. of Agr., Univ. of Western Australia, Nedlands. Received Nov. 9, 1970. Approved Mar. 22, 1971.
[2] Senior Lecturer in Soil Science and Professor of Soil Science, respectively.

ing studies (3) and chloride exclusion measurements (9, 11) with sodium clays have shown that this behavior is more or less consistent with the development of diffuse ionic distributions over most of the clay surfaces and can be qualitatively, if not completely quantatively, described by theoretical treatments of the diffuse double layer as developed by Schofield (22), Verwey and Overbeek (23), and Bolt (8).

In contrast, clay systems saturated with divalent cations show only limited swelling, and it is apparent from the results reported (1, 3, 7, 16) that the development of diffuse ionic distributions between the parallel-aligned clay crystals within a domain, or between the elementary silicate sheets for montmorillonite, is largely prevented.

The most striking example of the difference in behavior between sodium and calcium clays is provided by X-ray measurements of montmorillonite saturated with these ions in free solution in the presence of varying electrolyte concentrations. At concentrations less than 0.3*N* NaCl, sodium montmorillonite gives X-ray spacings which are > 43Å and are proportional to $C^{-1/2}$ (15, 16). Thus, it can be stated that diffuse double layers develop on the surface of each elementary silicate sheet or on the total surface area of some 750 m^2/g. On the other hand, calcium montmorillonite exhibits a fixed 19Å $d(001)$-spacing over the concentration range from 1.7*M* to distilled water (16, 20). Even in suspension, negative adsorption measurements (11) indicate that for calcium montmorillonite there is an external and internal surface. The magnitude of the external surface ($\approx 100 m^2/g$) measured in this way would indicate that for this clay each "crystal" contains on the average about five to seven elementary silicate sheets separated by 10Å of water giving rise to the fixed $d(001)$-spacing of 19Å.

The net effects of these differences in *c*-axis spacing on the physical swelling of montmorillonite were clearly demonstrated by the results reported by Aylmore and Quirk (2, 3) for the effects of electrolyte concentration and hydrostatic suction on the swelling of Na- and Ca-saturated clays. Similarly, in contrast to the large swelling and sensitivity to electrolyte concentration exhibited by a sodium illite, the swelling of calcium illite was less than one-tenth of the value predicted by diffuse double layer theory at low water potentials and was insensitive to large changes in electrolyte concentration, thus illustrating the limited inter-crystalline swelling of a calcium illite domain.

Blackmore and Miller (7), using different methods, arrived at essentially the same conclusion with respect to calcium montmorillonite; however, their use of the term *tactoid* to describe the constant relationship between the elementary alumino-silicate sheets in calcium montmorillonite (fixed d(001) —19Å) is at variance with the definition of tactoid accepted in colloid science. The term *tactoid*, originally used by Freundlich and later by Langmuir, has been discussed by Overbeek (19) in terms of the spacing between units within a tactoid being sensitive to electrolyte, and as such, the term is much more appropriate in describing the behavior of sodium montmorillonite at concentrations of NaCl less than 0.3*M*.

The evidence cited above illustrates the similarity between the behavior of a domain of illite crystals and a "crystal" of montmorillonite. Aylmore and Quirk (1, 3) considered that in many circumstances a domain would have appreciable stability and would behave as a single entity in determining the water content-energy characteristics and mechanical properties of a clay-water system. They presented electron microscopic evidence and surface area, porosity, and pore size distribution measurements (4) illustrating the relationship between particles within a domain. A significant feature of these results was the average separation of some 30Å between illite surfaces within a domain, even on complete drying, which was unaffected by the exchangeable cation present on the clay surface. Studies with small amounts of preadsorbed water indicate that less than 10% of the surfaces in this clay matrix are in sufficiently close proximity to one another to prevent the adsorption of nonpolar nitrogen gas at 78K (L. A. G. Aylmore, I. D. Sills, and J. .P Quirk. 1971 (in preparation). Surface area of clay systems with preadsorbed water.). This characteristic pore structure must arise through the interleaving and bending of the irregular clay crystals within each domain and will undoubtedly be influenced by both the thickness and lateral dimensions of the particular illite crystals.

In the case of the montmorillonite clays, however, since polar water molecules are able to penetrate between and separate the individual alumino-silicate sheets, these lamellae become the basic particles involved in the swelling process. It is clear that in this context, the montmorillonite "crystal" represents a particular type of "domain" formed by the alignment of individual alumino-silicate sheets. Unlike the surfaces of the larger crystal units forming an illite domain, the surfaces between the parallel montmorillonite lamellae are in close juxtaposition in the dry state. During the late stages of the drying process, the presence of water layers between individual lamellae may help to lubricate the movement of lamellae with respect to one another, thus enhancing the moulding of one unit to the next. Usually much less than some 20% of the total surface area of the lamellae forming the dry clay matrix is accessible to nitrogen adsorption and the BET (10) nitrogen area probably provides a measure of the external area of these regions of parallel alignment (5).

The nitrogen surface area obtained on drying a montmorillonite clay from suspension is essentially reproducible for a given exchangeable cation and preparation despite the near complete dispersion of the lamellae apparent in suspension for the Na-saturated clay (11). However, wide variations in the area measured are obtained for the same montmorillonite saturated with different cations (4). Similarly it is important to note that by careful preparation of oriented flakes it is possible to reduce the nitrogen surface area of sodium Wyoming Bentonite to some 5 m^2/g (13) compared with the 40 to 50 m^2/g usually obtained. Since the individual lamellae vary considerably in their lateral dimensions it is evident that the matrix formed on drying a suspension will be somewhat more complex than the simple booklet or packet structure suggested by the term

crystal. For example, it is possible that one particular lamella may be interleaved in more than one region of parallel array and there will be areas of discontinuity of perfect overlap of adjacent lamellae even within these regions. Discrete *c*-axis spacings are obtained by X-ray diffraction from the regions in which the montmorillonite lamellae are stacked in parallel array, but these are not necessarily in perfect crystalline order as shown by the absence of (hhl) reflections. Consequently, it is considered by the authors that the term *quasi-crystal* may be a more appropriate description for these characteristic regions unique to this type of layer-lattice alumino-silicate clay mineral. This proposal has been supported by O'Connor and Kemper (17) in discussing cation exchange in sodium-calcium montmorillonite systems. The reproducibility of the nitrogen surface areas obtained on drying from the dispersed suspension for a given montmorillonite clay and preparation suggests that quasi-crystal formation takes place by a statistical process dependent on factors such as the average lateral dimensions of the lamellae, surface density of charge, exchangeable cation, and degree of association in suspension.

To summarize, we consider that use of the term *quasi-crystals* to describe the regions of parallel alignment of individual alumino-silicate lamellae in montmorillonite and of the term *domain* to describe the regions of parallel alignment of crystals for illite and other fixed lattice clays will eliminate much of the confusion which has arisen through inadequate definition and also avoid the misconceptions inherent in the terms *tactoid* or *crystal of montmorillonite*. A characteristic of the quasi-crystalline regions of montmorillonite and fixed lattice clays with a well-formed domain structure is the marked difference in swelling behavior between Na- and Ca-saturated systems, reflecting the effects of changes in ionic distribution between charged surfaces in parallel array. These swelling processes have recently been reviewed by Quirk (21) and the nature of a quasi-crystal has been investigated by electron microscopic, light scattering, and sorption techniques (5, 6, 12).

LITERATURE CITED

1. Aylmore, L. A. G., and J. P. Quirk. 1959. Swelling of clay-water systems. Nature 183:1752–1753.
2. Aylmore, L. A. G., and J. P. Quirk. 1960. Swelling and shrinkage of clay-water systems. Int. Congr. Soil Sci. Trans. 7th (Madison, Wis.) 2:378–387.
3. Aylmore, L. A. G., and J. P. Quirk. 1962. The structural status of clay systems. Clays Clay Min. 9:104–130.
4. Aylmore, L. A. G., and J. P. Quirk. 1967. The micropore size distributions of clay mineral systems. J. Soil Sci. 18: 1–17.
5. Aylmore, L. A. G., I. D. Sills, and J. P. Quirk. 1970. Surface area of homoionic illite and montmorillonite clay minerals as measured by the sorption of nitrogen and carbon dioxide. Clays Clay Min. 18:91–96.
6. Aylmore, L. A. G., I. D. Sills, and J. P. Quirk. 1970. Clays Clay Min. 18 (in press). Reply to comments of Thomas Bohor and Frost. Clays Clay Miner. 18:407–409.
7. Blackmore, A. V., and R. D. Miller. 1961. Tactoid size and osmotic swelling in calcium montmorillonite. Soil Sci. Soc. Amer. Proc. 25:169–173.
8. Bolt, G. H. 1956. Physico-chemical analysis of the compressibility of pure clays. Geotechnique 6:86–93.
9. Bolt, G. H., and B. P. Warkentin. 1958. The negative adsorption of anions by clay suspensions. Kolloid Z. 156: 41–46.
10. Brunauer, S., P. H. Emmett, and E. Teller, 1938. Adsorption of gases in multimolecular layers. J. Amer. Chem. Soc. 60: 309–319.
11. Edwards, D. G., and J. P. Quirk. 1962. Repulsion of chloride by montmorillonite. J. Colloid Sci. 17:872–882.
12. Fitzsimmons, R. F., A. M. Posner, and J. P. Quirk. 1970. Electron microscopic and kinetic study of the flocculation of calcium montmorillonite. Israel J. Chem. 8:301–314.
13. Greene-Kelly, R. 1954. The specific surface areas of montmorillonite. Clay Miner. Bull. 5:392–400.
14. Holmes, J. W. 1955. Water sorption and swelling of clay blocks. J. Soil Sci. 6:200–208.
15. Norrish, K. 1954. The swelling of montmorillonite. Disc. Faraday Soc. 18:120–134.
16. Norrish, K., and J. P. Quirk. 1954. Crystalline swelling of montmorillonite. Nature 173:225–226.
17. O'Connor, G. A., and W. D. Kemper. 1969. Quasi-crystals in Na-Ca systems. Soil Sci. Soc. Amer. Proc. 33:464–469.
18. Olson, R. E., and F. Mitronovas. 1962. Shear strength and consolidation characteristics of calcium and magnesium illites. Clays Clay Min. 9:185–209.
19. Overbeek, J. T. G. 1952. p. 326–327. *In* H. R. Kruyt (ed.) Colloid science. Elsevier, Amsterdam.
20. Posner, A. M., and J. P. Quirk. 1964. The adsorption of water from concentrated electrolyte solutions by montmorillonite and illite. Proc. Roy. Soc. 278:35–56.
21. Quirk, J. P. 1968. Particle interaction and swelling. Israel J. Chem. 6:213–234.
22. Schofield, R. K. 1946. Ionic forces in thick films of liquid between charged surfaces. Trans. Faraday Soc. 42B: 219–228.
23. Verwey, E. J. W., and J. T. G. Overbeek. 1948. Theory of the stability of lyophobic colloids. Elsevier Pub. Co. London.

Reprinted from the
AUSTRALIAN JOURNAL OF SOIL RESEARCH

DISSOLUTION OF GYPSUM, MONOCALCIUM PHOSPHATE, AND SUPERPHOSPHATE FERTILIZERS IN RELATION TO PARTICLE SIZE AND POROUS STRUCTURE

By L. A. G. AYLMORE,* M. KARIM,* and J. P. QUIRK*

[*Manuscript received January* 25, 1971]

Abstract

The effect of variations in physical form such as particle size and mixing with other materials, on the rate of dissolution of sulphate and phosphate from solid fertilizers, has been investigated. It is apparent from these results that the degree of subdivision of a solid fertilizer is particularly important in determining its susceptibility to leaching. It has been demonstrated that leaching of sulphate is appreciably restricted when the granule size is 2 mm or greater in diameter. Except when leached immediately after application, the retention of phosphate is determined largely by "reversion" to the relatively insoluble dicalcium phosphate form.

Combination of sulphate with phosphate in superphosphate or the addition of various additives to gypsum markedly reduces the rate of sulphate leaching in comparison to pure gypsum. A comparison of pore size distribution suggests that pores within the intermediate range from approximately 500 Å to 10^5 Å play a significant part in the dissolution process.

I. INTRODUCTION

Since most fertilizers are applied to the soil in the form of powdered or granulated material spread over the surface or in a band in the soil, variations in the physical form of the fertilizer (largely degree of subdivision and compaction) will undoubtedly play a significant part in determining the rate of dissolution of the material applied. The rate of dissolution, and hence both availability to plants and liability to leaching, will depend in the first instance on the solubility in water of the solid material. In some cases (e.g. superphosphate, Cal-Nitro, calurea) more than one essential nutrient is contained in the same physical matrix, and the less soluble material may thus protect the more soluble component from rapid dissolution. In the particular case of monocalcium phosphate dissolution results in the precipitation of the considerably less soluble dicalcium phosphate or aluminium or iron phosphates, as also can reaction of the triple point solution with the soil. This process is frequently referred to as "reversion" of the phosphate.

In many instances, particularly in heavier-textured soils, the efficiency of a fertilizer as a source of plant nutrients and its susceptibility to leaching will be comparatively independent of its rate of dissolution because of its reaction with the colloids near the original site of placement. In light-textured soils, the rate of dissolution may serve as the only effective control over fertilizer movement and preventative to rapid leaching.

* Department of Soil Science and Plant Nutrition, Institute of Agriculture, University of Western Australia, Nedlands, W.A. 6009.

Despite the difficulties involved in separating the many variables applicable, much useful progress has been made in a number of recent investigations concerned with the dissolution of fertilizer materials: e.g. Huffman 1957; Huffman *et al.* 1960; Elphick 1955; Caro and Hill 1956; Caro and Freeman 1961; Lehr, Brown, and Brown 1959; Lawton and Vomicil 1954; Lindsay and Stephenson 1959. Until recently, however, there has been surprisingly little information available on the effects of granule size and the presence of associated salts on the rate of dissolution and leaching of sulphate and phosphate from fertilizers. Papers by Williams (1969, 1970) and Williams and Lipsett (1970) and Millington and Powrie (1968) have indicated that such information can be extremely useful in determining the optimum techniques for fertilizer usage.

The present work was undertaken as part of a general study of the factors affecting the leaching of fertilizer sulphate (Karim 1967; Aylmore, Karim, and Quirk 1967; Aylmore and Karim 1968), and specifically to obtain information on the practical implications of different preparations and granule sizes of superphosphate in comparison with pure gypsum and monocalcium phosphate.

II. Materials

A number of samples of different superphosphate preparations were supplied by CS-BP and Farmers Ltd of Western Australia. These samples were considered by the manufacturers to represent the full range of variability of their product both in the origin of the rock phosphates used and in the mechanics of production. For convenience the samples have been designated A to E and their descriptions are outlined below:

Sample A.—Prepared in Bassendean Works from 50% Pacific Islands Rock, 25% Christmas Rock, and 25% African Rock.

Sample B.—Prepared in Fremantle works from 70% Pacific Islands Rock and 30% African Rock. This sample has undergone a special process to reduce the amount of fine material in the end product. Prior to the second setting, water was added and the material rolled in granulating drums to produce circular particles of high density (79–90 lb/cu ft) and relatively dust-free character.

Sample C.—Prepared in Geraldton Works from 50% Christmas Island Rock and 50% Pacific Islands Rock.

Sample D.—Prepared in Bunbury Works from 50% Pacific Islands Rock, 23% Christmas Island Rock, and 27% African Rock.

Sample E.—Prepared in Albany works from 7% African Rock, 40% Christmas Island Rock, and 53% Pacific Islands Rock.

The contents of P and S in these superphosphates were approxiamtely 11 g/100 g and varied only slightly between the samples.

The powdered gypsum (calcium sulphate dihydrate) and monocalcium phosphate were both of A. R. standard.

The plaster of paris preparations were obtained from Gypsum House Pty Ltd, W.A. Sample 1, labelled Casting Plaster, is relatively pure calcium sulphate hemi-hydrate. Sample 2, labelled Super-fine Plaster, is identical in composition to sample 1 but of much finer particle size to produce a smooth finish in use. The remaining samples contain relatively small amounts of additives to promote desirable characteristics as building materials. Sample 3, labelled Hardwall Plaster, contains some 5% of a mixture of hydrated lime and gum arabic, the effect of which is to harden and strengthen the plaster during the setting process. Sample 4, labelled Retarded Plaster, contains some 9% gelatinous glue to retard the setting process.

Particular particle size fractions of plaster were obtained by mixing the powdered samples with 45% water, forcing the resultant pastes through various sized sieves, and allowing the globules produced to set and dry.

The sand used in these experiments was a yellow sand from the Swan Coastal Plain, W.A. Before use, the sand required repeated washing with dilute NaOH solution to remove some 0·5% colloidal coatings, as it was found that these caused appreciable adsorption of both sulphate and phosphate. The particle size distribution of this sand is 99% within the 0·1–0·5 mm range.

III. Experimental Methods

In general, the leaching experiments were carried out with the fertilizer materials spread uniformly over an area of 2 sq cm on the surface of a pad of sand (100 g) in a small Buchner funnel (7 cm diameter) and covered with a thin layer of sand. The sand had previously been pre-wet to some 8% water content, which corresponds approximately to field capacity for the sand. The rates of application of fertilizers were 200 mg of superphosphate and 100 mg of gypsum and monocalcium phosphate respectively. No attempt was made to reproduce the equivalent of field application rates since the dissolution process was considered to depend primarily on conditions in the immediate environment of the applied granules.

Water was applied by means of a constant head device at a rate just sufficient to maintain a thin film over the surface during the run. The equivalents of amounts up to 30 in. of water were applied, either immediately after placement of the fertilizer or progressively in small amounts at successive periods of time as indicated on the diagrams.

The determination of inorganic sulphate was based on the method of Johnson and Nishita (1952) incorporating improvements suggested by Johnson and Ulrich (1959), Steinbergs *et al.* (1962), and Gustafsson (1960). The phosphate contents of the solutions were determined using the heteropoly blue method of Boltz and Mellon (1947).

The determination of pore size distributions was carried out by application of either the Kelvin or Jurin equations to desorption isotherms obtained using a non-polar liquid to prevent volume changes due to swelling forces. The appropriate equation is determined by convenience of measurement, that is, whether by the low temperature sorption of liquid nitrogen (Aylmore and Quirk 1967) or by liquid transport at constant suction head using tetrachlorethane and benzene (Quirk and Panabokke 1962); the suitability of each method depends largely on the pore sizes to be examined.

Total specific surface areas were determined by application of the Brunauer, Emmett, and Teller (1938) theory to nitrogen adsorption isotherms obtained at 78°K.

IV. Results and Discussion

The data obtained for the dissolution of the various samples of superphosphate supplied by CS–BP and of pure gypsum and monocalcium phosphate are shown in Figures 1–3. The susceptibility to leaching of the whole samples of superphosphate was first examined under conditions of leaching immediately after placement, and of progressive leaching with the same amount of water over a period of some 19 days. When leached immediately after placement, there are significant differences (up to 35%) between the five perparations in terms of both percentage sulphate and percentage phosphate retained (Figs. 1(*a*) and 1(*b*)). The order of susceptibility to dissolution from the various preparations is essentially the same for both sulphate and phosphate. Sample B which was specifically prepared in a compact high density form with a minimum amount of fine material (i.e. granulated) is noticeably better retained than the other materials. An interesting point which is immediately apparent, however, is that although the phosphate is more rapidly leached than the sulphate, the difference is considerably less than could be expected from differences in solubility measured at 20°C between pure gypsum (2·4 g/l) and monocalcium phosphate (18 g/l).

When leached progressively over a period of 19 days with increasing amounts of water the differences in sulphate retention between the superphosphate preparations

is still apparent (Fig. 1(*c*)), although, as can be expected, the amount of sulphate retained is reduced in each case, presumably as a result of the greater time allowed for dissolution and diffusion. In contrast, however, the amount of phosphate retained is virtually the same for all samples under these conditions of progressive leaching (Fig. 1(*d*)).

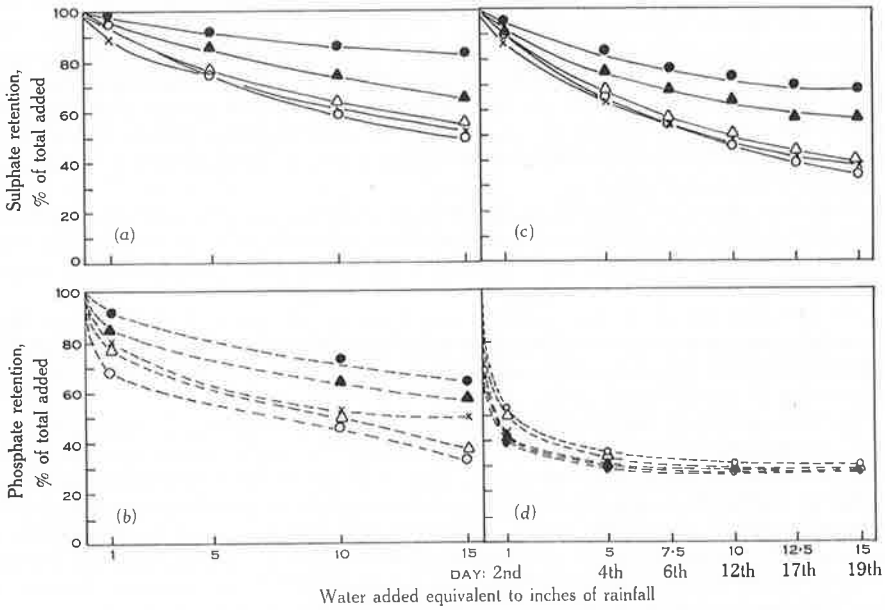

Fig. 1.—Sulphate and phosphate retained against leaching from whole samples of different preparations of superphosphate. ○, A; ●, B; △, C; ▲, D; ×, E. (*a*) Sulphate and (*b*) phosphate retained on leaching immediately after placement; (*c*) sulphate and (*d*) phosphate retained after progressive leaching for up to 19 days.

The less rapid dissolution of phosphate than would be expected compared with the sulphate on immediate leaching may result partly from the protection afforded the phosphate component within the granules by the somewhat less soluble sulphate under these conditions. However, progressive leaching over a longer period (Fig. 1(*d*)) probably allows as much of the phosphate as possible to dissolve and diffuse from within the granules. Under these conditions the phosphate retained (some 28–30%) is largely that which reverts to the relatively insoluble dicalcium phosphate form. Preliminary experiments in which pure monocalcium phosphate was allowed to equilibrate overnight with 40 mesh glass beads containing 8% water before dissolution had shown that some 28% reversion to the less soluble dicalcium phosphate form occurred under these conditions. This is comparable with the figure of 22·4% for phosphate reversion obtained by Lindsay and Stephenson (1959) by shaking monocalcium phosphate in water. Experiments with monocalcium phosphate in soils at different relative humidities showed that this reaction went to completion provided the water vapour pressure was greater than that (96%) corresponding roughly to a saturated solution of monocalcium phosphate. Below this value no reversion occurred.

The variations on immediate leaching and for sulphate on progressive leaching could result either from differences in the state of subdivision of the materials as applied and possibly also from variations in other physical characteristics of the fertilizer matrix: e.g. internal pore space distribution, and intimacy of mixing of sulphate and phosphate. As indicated earlier, there is little significant difference in the proportions of sulphate and phosphate in the different preparations.

TABLE 1

PERCENTAGE OF DIFFERENT SIZE FRACTIONS OF FIVE SUPERPHOSPHATE SAMPLES

Superphosphate Samples	$< 0{\cdot}5$ mm Diameter	0·5–1·0 mm Diameter	1·0–2·0 mm Diameter	$> 2{\cdot}0$ mm Diameter
A	46·8	18·6	14·4	20·2
B	17·8	17·8	30·0	34·4
C	37·1	19·8	17·0	26·1
D	24·3	15·2	29·0	31·5
E	29·6	29·2	18·7	22·5

A comparison between nitrogen specific surface areas and percentage sulphate retained after the equivalent of 15 in. of water did not suggest any correlation between total specific surface area of the materials and susceptibility to leaching, so the samples were next sieved into > 2 mm, 2–1 mm, 1–0·5 mm, and $< 0{\cdot}5$ mm equivalent diameter fractions and the proportions of each size fraction for the various samples are shown in Table 1.

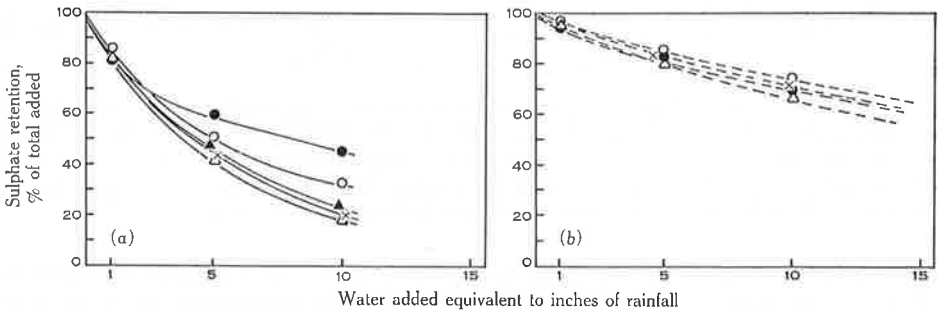

Fig. 2.—Sulphate retained against leaching immediately after placement from different size fractions of superphosphate. ○, A; ●, B; △, C; ▲, D; ×, E. (*a*) $< 0{\cdot}5$ mm diameter fraction, (*b*) 1–2 mm diameter fraction.

A definite correlation between the degree of subdivision of the fertilizers as a whole and their susceptibility to leaching is immediately apparent. The most rapidly leached, Sample A, has by far the highest proportion of fine material of $< 0{\cdot}5$ mm equivalent diameter, and the order of susceptibility to leaching of the remainder of the samples correlates well with the aggregate size distributions as indicated by Table 1.

The effect of the drum rolling of Sample B in its preparation is obvious in the reduced percentage of fine material as indicated in Table 1 and by the higher percentage retention of both sulphate and phosphate. A comparison of the susceptibility of the sulphate in the $< 0{\cdot}5$ mm fractions and the 1–2 mm fractions on leaching immediately after placement given in Figures 2(*a*) and 2(*b*) shows that there is little

variation between the preparations when sufficiently aggregated to form granules above about 1 mm. Larger particle size fractions were more uniform in size and showed even less variation between the samples. However, the $< 0 \cdot 5$ mm fractions still exhibit a marked differentiation, and this probably reflects further variations in the degree of subdivision below this particle size limit. Sample B is still the most retained but the order of susceptibility of the remaining samples has changed.

From Figures 3(*a*) to 3(*b*) showing the effect of particle size on the dissolution of Sample A, it is obvious that losses of sulphate and phosphate are both significantly restricted by increasing the particle size from fine powder to large granules. Minimum retention of sulphate and phosphate occurs for the powdered gypsum and mono-

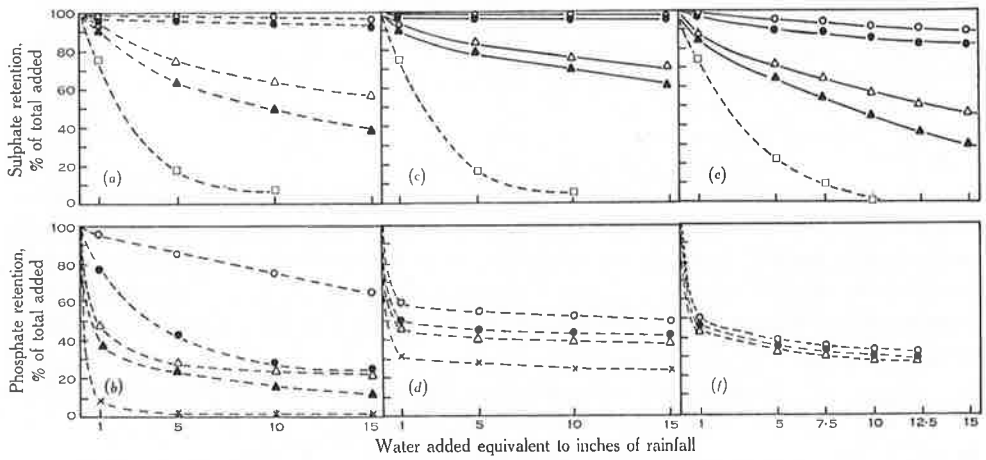

Fig. 3.—Sulphate and phosphate retained against leaching from □, powdered gypsum; ×, powdered monocalcium phosphate; and different size fractions of superphosphate A: ▲, powdered; △, 1 mm; ●, 2 mm; ○, 4 mm. (*a*) Sulphate and (*b*) phosphate retained on leaching immediately after placement; (*c*) sulphate and (*d*) phosphate retained on leaching 24 hr after placement; (*e*) sulphate and (*f*) phosphate retained after progressive leaching for up to 19 days.

calcium phosphate respectively in comparison with the superphosphate fractions, and increasing superphosphate granule size results in decreasing losses of both nutrients. This enhanced retention by the superphosphate granules compared with the pure materials must result from the lower external surface area exposed to leachate by the aggregated material.

In the case of the sulphate ions, only negligible amounts are lost from granules greater than 2 mm median diameter after 15 in. equivalent rainfall, whilst more than 60% is lost from the powdered superphosphate preparations and virtually 100% of of the powdered gypsum (Fig. 3(*a*)). It is particularly interesting to note that loss of sulphate from the superphosphate samples, particularly for the powdered material, is appreciably less when 24 hr have elapsed between placement and leaching. Losses from the pure gypsum on the other hand were unchanged. This decrease is suggestive of the gypsum retention observed by Lehr, Brown, and Brown (1959) in tablets containing both monocalcium phosphate and gypsum, and may be related either to the development of high acidity (pH 1·01) in the presence of monocalcium

phosphate dissolution (Lindsay and Stephenson 1959), or more probably to the presence of high calcium concentrations. The possible protection provided by the formation of an insoluble dicalcium phosphate shell may also be involved. With leaching immediately after placement rapid displacement of the highly soluble monocalcium phosphate may prevent such developments.

The effect of reversion of the monocalcium phosphate to dicalcium phosphate on the retention of phosphate ions is apparent from a comparison of Figures 3(*b*) and 3(*d*). Immediate leaching results in almost complete removal of the powdered monocalcium phosphate. Within 24 hr however, some 22·5% has been converted to the less soluble form and is retained against 15 in. water. Aggregation into the granular forms affords appreciable protection to the highly soluble monocalcium phosphate against immediate leaching (Fig. 3(*b*)), but with sufficient time to permit dissolution in the soil solution the amount retained will be controlled largely by the amount left as dicalcium phosphate at the site of placement. This in turn will depend on phase equilibrium considerations as influenced by water content, temperature, etc. (Lehr, Brown, and Brown 1959).

The data in Figures 1 and 3, where leaching was carried out progressively over a period of 19 days, again suggests that under these conditions phosphate retention is governed largely by the extent of reversion. Sulphate retention is, on the other hand, still influenced by particle size.

This dependence of rate of dissolution on particle size suggests that it is the external surface area exposed by the granules per unit mass which governs the rate of dissolution. This suggestion can perhaps best be tested by application of the equal reduction hypothesis (Elphick 1955), which postulates that the rate of particle diameter reduction is unaffected by particle size, on the assumption that the granules are spherical in shape and of uniform size, density, and composition. If the rate of dissolution is directly proportional to the total instantaneous surface area of the spheres, i.e. if

$$\mathrm{d}m/\mathrm{d}t = kS,$$

where m is the mass that has disappeared in time t, k is the proportionality or rate constant, and S is the total area of the spherical surfaces, then plotting $(1-u)^{\frac{1}{3}}$ versus time t or volume of water applied at constant rate should give a straight line of slope $-c = 2k/\rho D_0$, where ρ is the bulk density and D_0 the initial diameter of the granules, and an ordinate intercept of 1 if the theory is obeyed (Swartzendruber and Barber 1965). $u = m/m_0$ is the fractional mass dissolution, and the rate constant k will depend on, amongst other things, the solubility of the solid material.

If the internal surface area of the porous particles is involved in dissolution, this relationship will no longer hold, since the external surface area of a sphere decreases proportionately to the two-thirds power of the volume (and hence mass), whilst the internal surface area is directly proportional to the mass of the particle. Since the rate of dissolution is proportional to the surface from which it is occurring, this means that the negative slope of the plot of $(1-u)^{\frac{1}{3}}$ versus time will decrease with time if the internal area is involved, thus giving a curved relationship.

These plots for total phosphate plus sulphate dissolution from superphosphate granules of different sizes on leaching immediately after placement are given in Figure

4(*a*). Instead of straight lines, the points specify a curved relationship in which the slope is steep initially and flattens progressively with time. This indicates an increasing retardation of the rate of dissolution compared with the initial rate. Similar plots for sulphate dissolution alone from superphosphate granules are given in Figure 4(*b*). Provided the more soluble monocalcium phosphate does not interfere with the progressive dissolution of the sulphate the latter could be expected to conform to the equation derived by Swartzendruber and Barber (1965) if the rate of dissolution is in fact directly proportional to the external surface area of the granules. Again however, a curved relationship is obtained, and it must be concluded that either there is some interdependence of the rates of dissolution of the sulphate and phosphate constituents or alternatively that the internal pore structure of the superphosphate granules does exert some influence on their rates of dissolution.

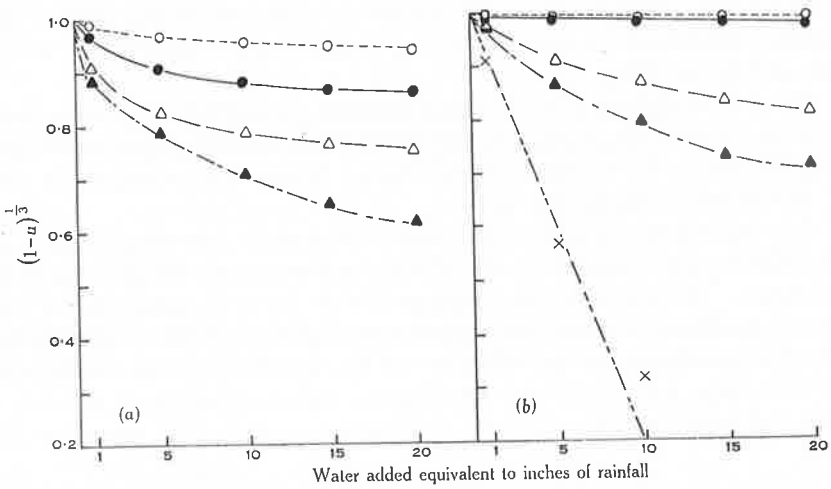

Fig. 4.—Plots of $(1-u)^{\frac{1}{3}}$ versus inches of water applied for dissolution of (*a*) sulphate plus phosphate and (*b*) sulphate alone from different size fractions of superphosphate and gypsum. Test of applicability of equal reduction hypothesis (Swartzendruber and Barber 1965): ×, approx. 0·1 mm diameter gypsum; ▲, approx. 0·1 mm diameter superphosphate A; △, 1 mm diameter superphosphate A; ●, 2 mm diameter superphosphate A; ○, 4 mm diameter superphosphate A.

Dissolution of the monocalcium phosphate constituent may result in a high concentration of phosphate in the solution, in and surrounding the granules with a resultant decrease in pH. Measurements of the effect of pH and of phosphate concentration separately on the solubility of gypsum at 20°C demonstrated that whilst the pH value is unimportant the concomitant dissolution of the phosphate constituent could markedly restrict the susceptibility of the sulphate component to dissolution.

For comparison, the effect of granule size on the rate of dissolution of gypsum alone was examined using granules prepared from the pure plaster of paris preparation No. 1. Plots of $(1-u)^{\frac{1}{3}}$ versus volume applied for this data give excellent straight lines (Fig. 5) and the negative slopes of these lines, c, fall on the same straight line passing through the origin when plotted against $1/D_0$ (Fig. 6) in accord with the

equation $c = 2k/\rho D_0$. Initially the only exception was the powdered gypsum, but this was found to be due to the tendency of this material to aggregate when placed in the wet soil. Prior mixing with dry sand before application prevented this aggregation, and the resultant dissolution data conformed to the equal reduction formula.

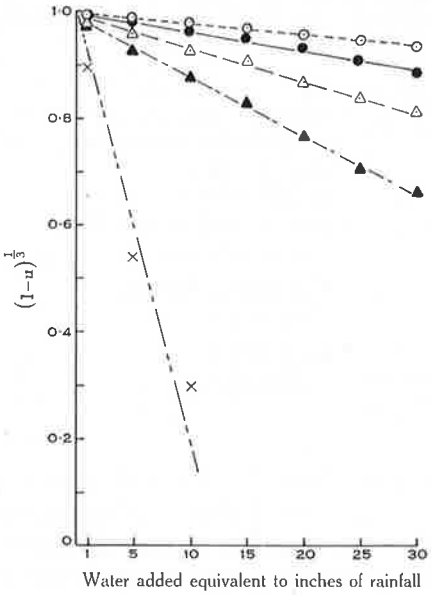

Fig. 5.—Plots of $(1-u)^{\frac{1}{3}}$ versus inches of water applied for five different size fractions of gypsum.
×, approx. 0·1 mm diameter;
▲, 0·5 mm diameter;
△, 1·0 mm diameter;
●, 2 mm diameter;
○, 4 mm diameter.

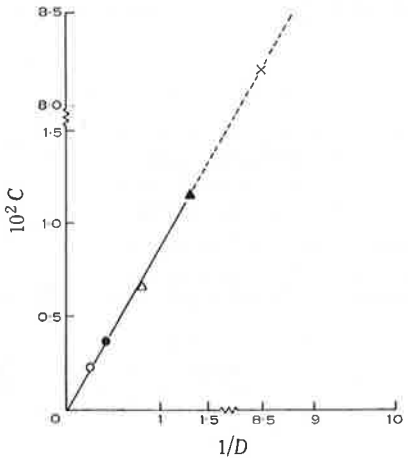

Fig. 6.—Plot of C versus $1/D$, (D, diameter in mm of gypsum particles), where C is taken as the negative slope of straight lines in Fig. 5.

Caro and Freeman (1961) suggested that differences in reactivity between three types of triple superphosphate examined by them could be attributed to difference in internal porous structure between some 600 Å and 5 μm equivalent cylindrical diameter. In Figure 7, the cumulative pore size distributions obtained for superphosphate Samples A and B are given and compared with those obtained by Caro and Freeman for their three triple superphosphate preparations. The superphosphate samples have a broader pore spectrum than the triple superphosphates which contain

the majority of their pore volume within the range 10^5 Å down to 10^3 Å. Triple superphosphate is prepared from rock phosphate using phosphoric acid and hence contains no sulphate. In contrast, the pore size distribution for the gypsum samples prepared from plaster of paris, given in Figure 8, show a high proportion of pores of greater than 10^5 Å and virtually no pores between 10^5 Å and 500 Å. The broad pore

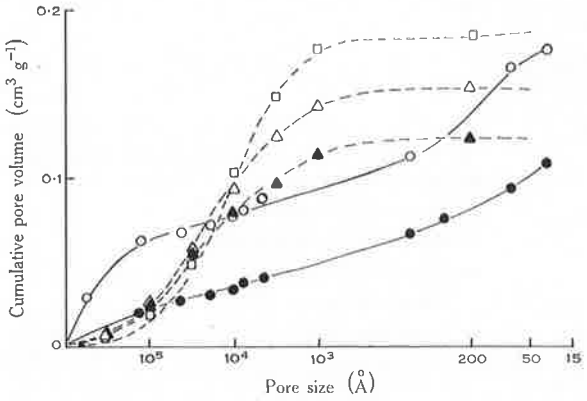

Fig. 7.—Comparison of cumulative pore size distributions for superphosphate samples A and B and three triple superphosphate products (Caro and Freeman 1961).
○, superphosphate A;
●, superphosphate B;
△, product 1;
▲, product 2;
□, product 3.

spectra for the superphosphate thus obviously arises from the combination of those for the sulphate and phosphate constituents. The total porosities of the gypsum preparations (Table 2) vary with the amount of water added in their preparation (e.g. Sample 1 prepared with 100% water content, cf. 45% water content) and are considerably higher than those for the superphosphate samples.

Fig. 8.—Cumulative pore size distribution for gypsum prepared from plaster of paris samples:
⊗, plaster 1 (100% water content);
▲, plaster 1 (45% water content);
△, plaster 2;
○, plaster 3;
●, plaster 4.

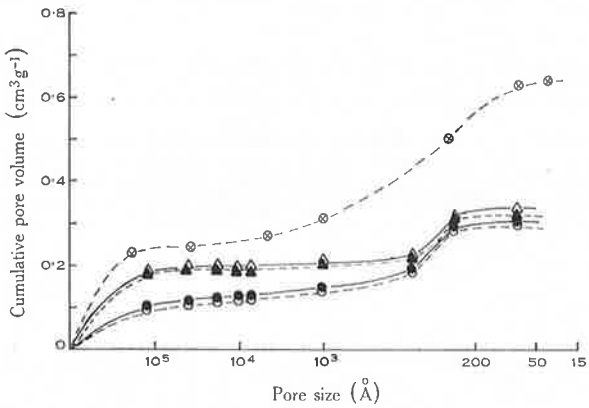

Superphosphate Sample A has an appreciably larger volume of pores of greater than 10^5 Å than has Sample B (0·063 cm^3 g^{-1}, cf. 0·033 cm^3 g^{-1}), but the distributions of pores between about 10^5 Å down to some 500 Å are remarkably similar for both materials. Since for a given particle size there is little difference in the susceptibility to leaching of these two samples, the conclusion which can be drawn is that pores of greater than 10^5 Å exert little influence on the dissolution process. The relative area in such pores would of course be very small.

The good agreement with the equal reduction hypothesis obtained for the gypsum Sample 1 compared with superphosphate thus probably results from its lack of pores within the intermediate range 500 Å to 10^5 Å. Smaller pores do not appear to contribute much to dissolution.

The presence of the additives in gypsum Samples 3 and 4 reduces the macroporosity ($> 10^5$ Å) of these samples compared with the pure gypsum samples (Fig. 8).

TABLE 2

TOTAL POROSITY OF SUPERPHOSPHATE AND GYPSUM PREPARATIONS

Sample	Porosity (c.c./g)	Sample	Porosity (c.c./g)
Superphosphate A	0·197	Gypsum Sample 2	0·362
Superphosphate B	0·136	Gypsum Sample 3	0·343
Gypsum Sample 1 (45% water content)	0·366	Gypsum Sample 4	0·344
Gypsum Sample 1 (100% water content)	0·704		

Comparison of the rates of dissolution of the 1 mm particle size fractions of the gypsum samples given in Figure 9 indicates that the presence of these additives also significantly retards the leaching of the sulphate. This cannot be attributed to the larger volume of the pores of greater than 10^5 Å in the pure samples 1 and 2 since the gypsum prepared from sample 1 using 100% water content has a much greater volume in pores of greater than 10^5 Å but gives identical dissolution results with those obtained for the sample prepared with 45% water content.

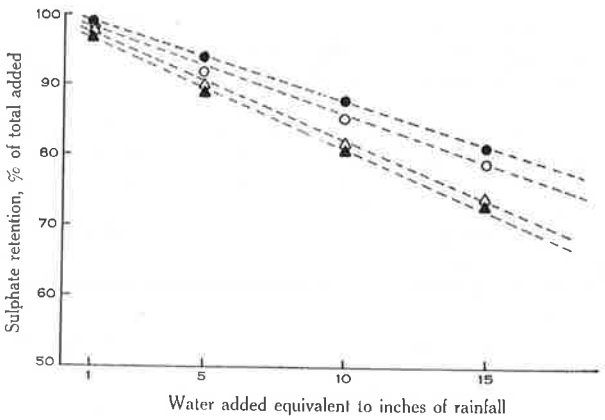

Fig. 9.—Sulphate retained against leaching from 1 mm particle size fraction of gypsum prepared from plaster of paris samples:
▲, plaster 1;
△, plaster 2;
○, plaster 3;
●, plaster 4.

V. CONCLUSIONS

It is apparent from the results of these experiments that the degree of subdivision of a solid fertilizer is particularly important in determining its susceptibility to leaching. In this respect it has been demonstrated that leaching of sulphate is appreciably restricted when the granule size is 2 mm or greater in diameter. This conclusion agrees with the view of Williams and Lipsett (1969), who examined the effect of particle size on the availability of phosphate and sulphate to plants.

Similarly, combination of sulphate with phosphate in superphosphate or the addition of various additives to gypsum markedly reduces the rate of sulphate leaching in comparison to pure gypsum. A comparison of pore size distributions suggests that pores within the intermediate range from approximately 500 Å to 10^5 Å play a significant part in the dissolution process.

VI. References

Aylmore, L. A. G., and Karim, M. (1968).—Leaching of fertilizer ions in soil columns. Trans. 9th int. Congr. Soil Sci. Vol. 1, p. 143.

Aylmore, L. A. G., Karim, Mesbahul, and Quirk, J. P. (1967).—Adsorption and desorption of sulphate ions by soil constituents. *Soil Sci.* **103**, 10.

Aylmore, L. A. G., and Quirk, J. P. (1967).—The micropore size distribution of clay mineral systems. *J. Soil Sci.* **18**, 1.

Boltz, D. F., and Mellon, M. G. (1947).—Determination of phosphorus, germanium, silicon and arsenic by the heteropoly blue method. *Analyt. Chem.* **19**, 873.

Brunauer, D., Emmett, P. H., and Teller, E. (1938).—Adsorption of gases in molecular layers. *J. Am. chem. Soc.* **60**, 309.

Caro, J. H., and Freeman, H. P. (1961).—Pore structure of phosphate rock and triple superphosphate. *J. agric. Fd. Chem.* **9**, 182.

Caro, J. H., and Hill, W. L. (1956).—Characteristics and fertilizer value of phosphate rock from different fields. *J. agric. Fd. Chem.* **4**, 684.

Elphick, B. L. (1955).—Studies in uses of agricultural limestone. *N.Z. J. Sci. Tech.* **37**(A), 156.

Gustafsson, L. (1960).—*Talanta* **4**, 227.

Huffman, E. O. (1957).—Rates of solutions of calcium phosphate in phosphoric acid solution. *J. agric. Fd. Chem.* **5**, 266.

Huffman, E. O., Cate, W. E., Dening, M. E., and Elmore, K. L. (1960).—Rates and mechanisms of dissolution of some iron and aluminium phosphates. Trans. 7th int. Congr. Soil Sci. Vol. 2, p. 404.

Johnson, C. M., and Nishita, H. (1952).—Microestimation of sulphur. *Analyt. Chem.* **24**, 736.

Johnson, C. M., and Ulrich, A. (1959).—Bull. Div. Agric. Univ. Calif. No. 766.

Karim, M. (1967).—Physico-chemical factors affecting the leaching of fertilizer sulphate. Ph.D. Thesis, University of Western Australia.

Lawton, K., and Vomocil, J. A. (1954).—The dissolution and migration of phosphorus and granular superphosphate in some Michigan soils. *Proc. Soil Sci. Soc. Am.* **18**, 26.

Lehr, J. R., Brown, W. E., and Brown, E. H. (1959).—Chemical behaviour of mono-calcium phosphate monohydrate in soils. *Proc. Soil. Sci Soc. Am.* **23**, 3.

Lindsay, W. L., and Stephenson H. F. (1959).—Nature of the reaction of mono-calcium phosphate mono-hydrate in soils. *Proc. Soil Sci. Soc. Am.* **23**, 12.

Millington, R. J., and Powrie, J. K. (1968).—Dissolution and leaching of fertilizer granules. Trans. 9th int. Congr. Soil Sci. Vol. 3, p. 385.

Quirk, J. P., and Panabokke, C. R. (1962).—Pore volume-size distribution and swelling of natural soil. *J. Soil Sci.* **13**, 72.

Steinbergs, A., Iismaa, O., Freney, J. R., and Barrow, N. J. (1962).—Determination of total sulphur in soil and plant material. *J. Soil Sci.* **13**, 72.

Swartzendruber, D., and Barber, S. A. (1965).—Dissolution of limestone particles in soil. *Soil Sci.* **100**, 287.

Williams, C. H. (1969).—Moisture uptake by surface applied superphosphate and movement of the phosphate and sulphate into the soil. *Aust. J. Soil Res.* **7**, 307.

Williams, C. H. (1970).—Effect of particle size on the availability of the phosphorus and sulphur in superphosphate. Proc. 11th int. Grassland Congr., p. 384.

Williams, C. H., and Lipsett, J. (1969).—The effect of particle size of superphosphate on the availability of its phosphorus and sulphur to pasture plants. *Aust. J. agric. Res.* **20**, 265.

Reprinted from JOURNAL OF COLLOID AND INTERFACE SCIENCE, Volume 38, No. 1, January 1972

Printed in U.S.A.

Thermodynamic Properties of Argon Adsorbed on Porous Glass plus Preadsorbed Water[1]

FREDERICK GIACOBBE, L. A. G. AYLMORE,[2] AND WILLIAM A. STEELE

Department of Chemistry, The Pennsylvania State University, University Park, Pennsylvania

Received January 31, 1971; accepted May 3, 1971

Precise isotherms and calorimetric heats of adsorption have been determined for argon adsorbed on a sample of porous Vycor glass containing one monolayer of preadsorbed frozen water and on the sample containing sufficient water to form a triple layer. Pore size distributions were calculated from the isotherms for these two systems as well as for the bare porous glass adsorbent. Hysteresis effects were observed in the calorimetric heats of adsorption and desorption; these are compared with hysteresis in the isotherms, and in the Clausius–Clapeyron heats. The data indicate that most of the first increment of preadsorbed water is located in micropores and pore necks, but that pore filling occurs when three statistical layers of water are adsorbed.

INTRODUCTION

The problem of elucidating the details of the pore structure of high area solids remains one of the most difficult in surface science. In spite of considerable elegant theory (1, 2) and many careful experiments (1–5) much remains to be learned about these systems. The present paper contains a report of some thermodynamic measurements of adsorption on a particularly simple and extensively studied solid, namely, porous Vycor glass. After determining an adsorption–desorption isotherm for argon on the outgassed sample, precise measurements were made of calorimetric heats and of isotherms at two neighboring temperatures for two systems which had been prepared by preadsorbing water in the pores of the original solid. The first system studied in detail contained approximately one monolayer of water; this was followed by an investigation of the porous glass containing sufficient preadsorbed material to cover the surface with three layers of water. The thermodynamic measurements were of the same type and had roughly the same accuracy as those reported by Kington and Smith (4) in their study of argon adsorbed on the bare surface of a somewhat different sample of porous glass.

The only other study known to the authors of the effect of preadsorption upon the properties of porous Vycor glass is that of Ferguson and Wade (6), who have determined the change in N_2 BET area of the glass as a function of the quantity of water in the system. Although our results are much less extensive than those reported by Ferguson and Wade, we also observed the expected decrease in area with increasing amounts of preadsorbed water. However, our intensive studies on a limited number of systems made it possible to determine several quantities of interest in addition to BET area; in particular, pore-size distributions, saturation volumes, and measurements of the total apparent heat and work generated in the hysteresis loop were obtained. Although the detailed theoretical interpretation of these and other data is far from complete, it seemed of interest to report on

[1] This work supported by a grant from the Army Research Office-Durham.

[2] Permanent address: Department of Soil Science, University of Western Australia, Nedlands, Australia.

the conclusions drawn from this work to date.

EXPERIMENTAL

Thermodynamic measurements were made in a conventional Nernst–Giauque type adiabatic calorimeter that has been often described in the literature (7, 8). Indeed, the cryostat was identical to that used by Chon, Fisher, and Aston (9), with the substitution of a copper calorimeter filled with 25 gm of powdered porous Vycor glass for the platinum container of Chon, *et al.* Pressures were measured with a Texas Instruments fused quartz spiral gauge that had been calibrated against mercury manometers in our laboratory; the gauge had a sensitivity of 0.01 mm Hg, and an estimated accuracy of ±0.02 mm Hg (or 2 parts in 10^4 at pressures greater than 200 mm Hg). Temperatures were measured with a platinum resistance thermometer; potential drop across the thermometer and across a standard resistor in series with the thermometer were determined on a Leeds and Northrup White double potentiometer; the sensitivity of the galvanometer used as a detector was sufficient to allow one to observe temperature differences of 0.001°K, although the estimated accuracy of the absolute temperature measurements was ±0.01°K. If one takes account of the errors from all sources in the measurements including those due to small deviations from adiabatic conditions, the estimated precision of the calorimetric data is ±0.3%; this is confirmed by our determinations of the heat capacity of the system as a function of the amount of argon adsorbed. When these data are corrected to a common temperature, they could be fitted to straight lines, as shown in Fig. 1, with a root mean square deviation of 0.4%. Note that the calculation of heat capacity from the raw data requires that one make the well-known corrections for the heat of desorption and PV work in the calorimeter (8), so that a variety of effects contribute to the observed scatter of the points.

One complete adsorption–desorption isotherm was determined for argon on the bare porous glass surface at 83.0°K; similar isotherms were obtained at 80.5 and 84.6°K on the glass containing roughly one monolayer

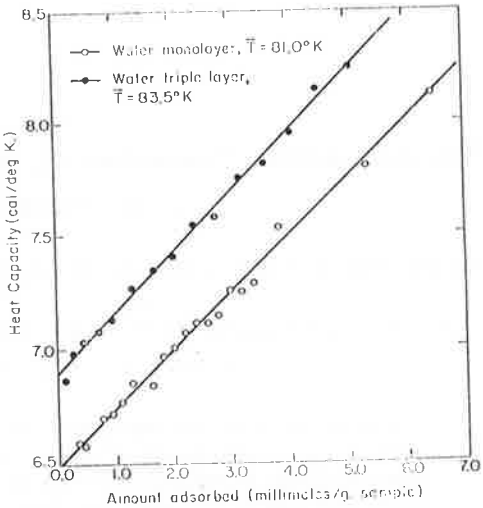

FIG. 1. Heat capacities of the calorimeter plus adsorbed argon are shown here as a function of the amount adsorbed. The heat capacity data have been corrected to a single average temperature using a value of (dC/dT) obtained from data on the calorimeter plus adsorbent.

of preadsorbed water, as calculated from the BET N_2 area (the exact amounts of water preadsorbed are listed in Table I), and at 83.0 and 86.0°K in the system with three times the monolayer quantity of water. One isotherm for each of the three adsorbents is shown in Fig. 2, with the amounts adsorbed in units of millimoles per gram of sample. These data have been replotted in Fig. 3 in units of micromoles per square meter of sample calculated from the Ar BET areas shown in Table 1. Although the Ar isotherms gave good BET plots, it should be noted that the area of 81 m²/gm obtained in this way for the bare porous glass differs considerably from our measured N_2 BET area of 111 m²/gm; consequently, the results shown in Table I are of value primarily as relative quantities. In particular, the fact that the BET area drops to 93% of its original value when 27.5 mg/gm of water is preadsorbed, and to 55% when 70.5 mg/gm is preadsorbed, can be compared to Ferguson and Wade's results. They find that the original BET N_2 area of 125 m²/gm has decreased to 85% of its original value at 30 mg/gm of water and to 55% at 70 mg/gm. The disagreements between the two investigations

TABLE I

SUMMARY OF RESULTS

Statistical layers of preadsorbed water	Zero	One	Three
Amount of preadsorbed H_2O (mg/gm sample)	0	27.5	70.5
Ar BET monolayer capacity (mmoles/gm)	1.05	0.98	0.57
Ar BET Area (m^2/gm)	82	76	44
BET c	30	26	14
Total pore volume (cm^3/gm)	0.214	0.200	0.156
Irreversible work (cal/gm)	0.100	0.106	0.094
"Irreversible heat" (cal/gm)	—	0.106	0.098
Beginning of hysteresis (P/P_0)	~0.42	~0.40	~0.40
Beginning of hysteresis (mmoles adsorbed/gm)	1.69	1.53	0.83
Beginning of hysteresis (Kelvin radius in Å)	13.2	13.0	12.5
Beginning of hysteresis (negative pressure on adsorbate—atm)	200	207	211
Heat capacity of adsorbed Ar (cal/mole deg K)	—	9.9	10.5

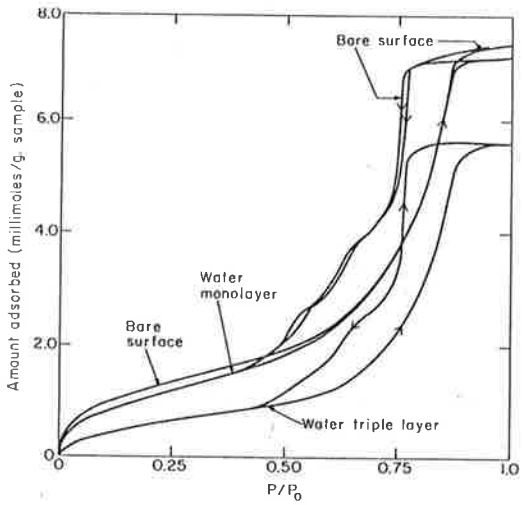

FIG. 2. Typical argon isotherms are shown here. The isotherm for the bare surface was measured at 83.0°K, that for the system containing a monolayer of preadsorbed water, at 80.5°K, and the curve for the system with a triple layer of water, at 83.0°K. However, the temperature dependence of the points is quite small when they are plotted as a function of P/P_0, so that all three isotherms are comparable.

are slight and are probably due to the more stringent outgassing procedure of Ferguson and Wade—the construction of our calorimeter made it impractical to outgas *in situ* at temperatures greater than 80°C, whereas Ferguson and Wade heated to 200°C.

The points shown in Fig. 3 give some indication of the quantity and quality of the isotherm data; they have been omitted from Fig. 2 and from the isotherm for the bare surface in Fig. 3 for the sake of clarity. It is evident that the quantities shown in Table I such as total pore volume, P/P_0 and amount adsorbed at the beginning of the hysteresis loop, and the total irreversible work required to take the systems around their hysteresis loops are readily obtainable from these data. (Of course, the irreversible work was evaluated from the area in the loops in plots of amount adsorbed vs. ln (P/P_0) which are not shown here).

Isosteric heats of adsorption were calculated in two ways: from the temperature dependence of the isotherm data, and from direct calorimetric measurements (8). These heats are shown in Fig. 4 for argon adsorption in the porous glass plus one monolayer of water, and in Fig. 5 for the system containing three monolayers of water. The calorimetric heats of Fig. 4 were measured at an average temperature of 81.0°K. The Clausius–Clapeyron heats were obtained from isotherms at 80.5 and 84.6°K. For the water triple layer experiments shown in Fig. 5, temperatures were slightly higher, with the average temperature of the calorimetric heats set at 83.5°K, and the isotherm data taken at 83.0 and 86.0°K. Thus, these experiments were run at temperatures rather close to 83.82°K, the melting point of bulk argon; however, the bulk of the data indicate that the appropriate reference state for this work is the liquid, supercooled when neces-

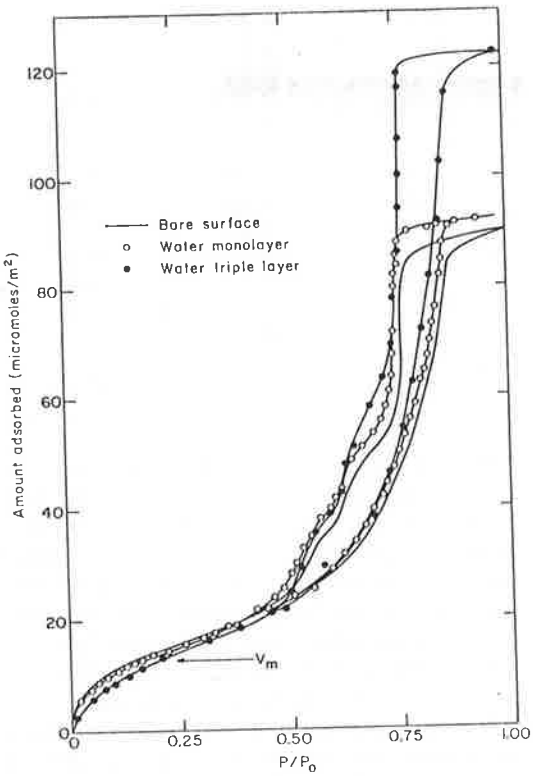

FIG. 3. The data of Fig. 2 are replotted here as amount adsorbed per unit area of surface. Experimental points are shown for two of the isotherms to help distinguish them and to give an indication of the number and precision of the data points taken in this work. The argon BET monolayer volume of 12.6 μmoles/m² is shown by the horizontal arrow.

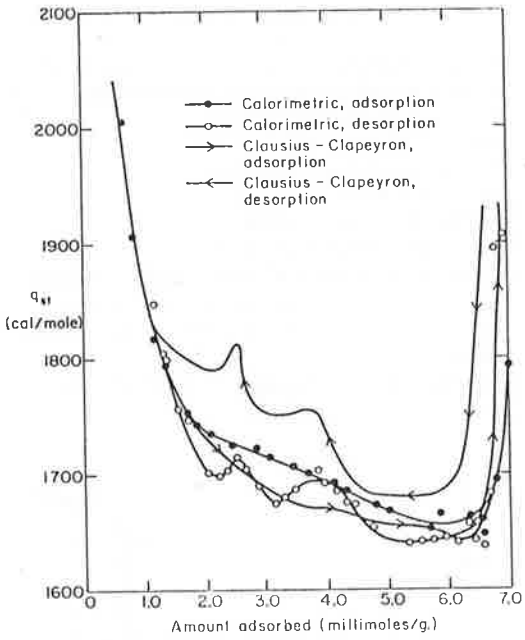

FIG. 4. Isosteric heats of adsorption are shown for the adsorption of argon at 81°K on porous glass plus one monolayer of frozen preadsorbed water. Individual calorimeteric data points are plotted, but continuous curves are drawn for the Clausius–Clapeyron heats. A few points at low coverage (and high q_{st}) have been omitted in this figure and in Fig. 5 in order to enlarge the vertical scale in the hysteresis region.

sary. If one omits the highest coverage data for the moment, it is clear that the heats of adsorption approach the heat of vaporization of bulk liquid argon (1575 cal/mole at 84°K) rather than the heat of sublimation (1856 cal/mole at 84°K). Also, the heat capacity measurements give a value of 9.9 ± 0.5 cal/mole deg for argon adsorbed on a monolayer of water at 81.0°K, and 10.5 ± 0.5 cal/mole deg for adsorption on the triple layer at 83.5°K. These results are much closer to the bulk liquid value of 10.1 cal/mole deg than to the bulk solid value of 7.5 cal/mole deg (at 84°K). Consequently, the bulk vapor pressures (P_0) were calculated for the liquid, and pore volumes were computed from moles adsorbed using a liquid molar volume of 28.2 cc/mole.

In a calorimetric adsorption experiment, the calorimeter was equilibrated at a convenient initial temperature; electrical heat was added to give a temperature rise of ~1°K, and the final temperature determined after equilibration under adiabatic conditions; the calorimeter and thermal shields were then cooled back to the initial temperature and equilibrated. Sufficient argon gas was added to give a temperature rise of ~1°K, and the temperature change was determined. In this way, a value of the heat capacity and the heat of adsorption could be calculated. Subsequently, the calorimeter was again cooled to the initial temperature and the sequence of measurement of heat capacity, heat of adsorption was repeated until the entire coverage range had been investigated.

Calorimetric heats of desorption were measured somewhat differently: as gas was

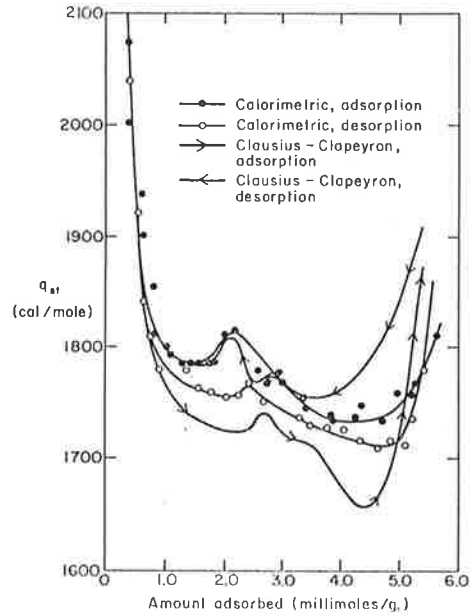

FIG. 5. Isosteric heats of adsorption are given here for argon adsorbed at 83.5°K on porous glass plus a triple layer of preadsorbed water.

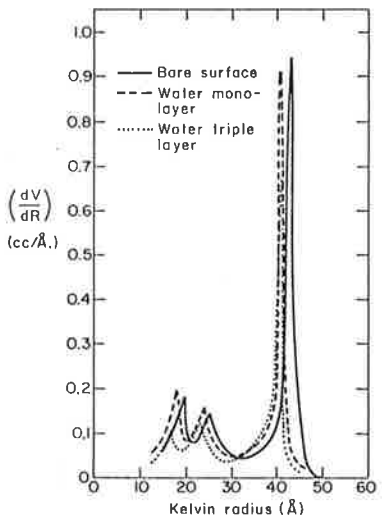

FIG. 6. Differential pore size distributions are shown for the three adsorbents used in this work. These curves were obtained by calculating the cumulative pore size distributions from the application of the Kelvin equation to the isotherms shown in Fig. 2, and subsequent differentiation of these curves.

drawn out of the calorimeter, electrical heat was added to hold the temperature of the system constant. With care, it was possible to complete a desorption point without changing the temperature of the system by more than 0.01°K; the heat of desorption is then equal to the amount of electrical heat added, plus a term for the PV work of desorption in the calorimeter, plus a small correction term for the heat involved in whatever temperature change actually resulted in the course of the experiment (8).

ISOTHERMS

One of the most interesting features of this work emerged when the pore size distributions were calculated from the isotherms in the usual way (5). The curves of differential pore volume vs. Kelvin radius are plotted in Fig. 6. In these calculations, no allowance was made for radius corrections due to the thickness of an adsorbed multilayer in the capillary; however, terms of this type will not appreciably affect the relative pore size distributions for the three systems. It is obvious from Fig. 6 that the distribution of the preadsorbed water is considerably different in the triple layer case than in the monolayer system. The first water adsorbed causes the pore size distribution to shift almost uniformly; by 2.5 Å for the 40 Å pores, and by lesser amount for the smaller size pores. Inasmuch as this corresponds reasonably well to the diameter of a water molecule, it is tempting to conclude that the first addition of preadsorbed water is spread evenly as a monolayer, at least in the largest pores. In contrast, the pore radii that characterize the triple layer system are essentially identical to those for the monolayer case, and one sees that the additional water has completely filled some of the capillaries, thus removing them from the distribution curve. Although this pore filling is most noticeable for the smaller radii of 18 and 23 Å, appreciable filling occurs in the 40 Å pores as well.

However, it is necessary to ensure that these conclusions are consistent with other data such as the total pore volumes shown in Table I. If the frozen water has a density not too different from 1 gm/cc, one anticipates that the total pore volume in the glass will decrease by 0.028 cc/gm when a mono-

layer of water is added, and by an additional 0.043 cc/gm when the extra layers of water are added. Although the second value is in excellent agreement with the experimental change of 0.044 cc/gm, the data in Table I indicates the pore volume change upon addition of one layer of water is only 0.014 cc/gm. Two questions arise immediately: First, what happened to 0.014 cc/gm of water in the preadsorbed monolayer? Secondly, how can one reconcile this result with the behavior of the pore size distribution curves?

Of the various possible explanations of the "loss" of preadsorbed water (anomalously high water density or anomalous density of the argon are two rejected possibilities), it seems most likely that many of the water molecules have adsorbed in microcracks or micropores that are not accessible to argon atoms because of their larger molecular size (~3.7 Å for Ar compared to ~2.5 Å for H_2O). This molecular sieving is well known for other systems (10), and its reverse (blocking effects by use of preadsorbed atoms that are larger than those of the adsorbate) was observed some time ago (11, 12). If some of the water is indeed adsorbed in this way, it would also give a simple rationalization for the relatively small loss in Ar BET area upon the initial addition of water.

Burgess and Everett (13) have suggested that capillary condensation cannot occur in sufficiently small micropores because the negative pressures associated with the sharply curved menisci exceed the limiting tensile strength of the liquid. In this case, the lower point of closure of the hysteresis loop should be characteristic of the adsorbate, rather than the adsorbent. Furthermore, the limiting negative pressure P_n is given by

$$P_n = P_v - 2\gamma/r, \qquad [1]$$

where P_v is the gas pressure, r is the calculated Kelvin radius at the point of closure, and γ is the surface tension of the adsorbate. Their suggestions are nicely validated by our measurements, as shown by the data in Table I. Evidently, the limiting Kelvin radius and the limiting tension for argon are independent of the amount of preadsorbed water and of any changes in surface properties associated with the preadsorption process.

It would follow that the pore size distribution curves obtained from Ar isotherm data are incapable of yielding information about possible pores of Kelvin radius less than 12 Å. It is altogether possible that appreciable numbers of such pores and cracks are present, and that some of these are accessible to water but not to Ar. However, if this behavior is postulated, our previous interpretation of the change in pore size distribution with one monolayer of preadsorbed water must be revised. That is, if much of this water is "lost" in microcracks, the amount remaining will be insufficient to cover the surface with a monomolecular layer. At this point, it is well to recollect that the pore size distributions are obtained using a highly oversimplified theory; in particular, it is assumed that the pore structure is composed of uniform cylindrical capillaries. If we make the most obvious refinement of this model by assuming cylindrical pores with nonuniform cross-sections, the theory becomes at least qualitatively consistent with the results. Evaporation from a nonuniform capillary is controlled by the pore neck radii, and one need only postulate that the preadsorbed water forms monomolecular films in these narrow regions, thereby changing the critical pore radii without necessarily affecting the wider portions of the pores.

A final bit of supportive evidence for this picture is provided by the calculations of the total irreversible work shown in Table I. If this work is taken to be a measure of the total amount of capillary condensed material that evaporates irreversibly, the results indicate that no large changes occur in this quantity as the amount of preadsorbed water is increased. No quantitative conclusions can be drawn in light of the possibility that the irreversible work of capillary emptying may depend upon the capillary radius as well as the amount of material evaporated.

HEATS

The heats of adsorption and desorption shown in Figs. 4 and 5 present a number of puzzling aspects, not all of which are ex-

plicable at present. One of the most interesting results is that these heats are generally quite a bit larger than the heat of vaporization of the liquid (1575 cal/mole), even at coverages several layers thick (BET monolayer capacities are listed in Table I), but not yet in the region of the sharp rise at the end of the pore filling process. In the intermediate region, it seems reasonable to assume that the adsorbed argon has liquid-like properties (as in the Frenkel–Halsey–Hill model), but is in the potential field of the solid. In this case, one would estimate the differential heat of adsorption in a film of thickness t from (14)

$$q_{st} = -u(t) + (E^\sigma/\rho)(dS/dV), \qquad [2]$$

where $u(t)$ is the average gas–solid interaction energy of an atom at a distance t from the solid, E^σ is the surface energy of the adsorbate per unit area, ρ is the molar density of the adsorbate and (dS/dV) is a geometrical factor giving the rate of change of the film area with its volume. For example, in the case of multilayer adsorption in a cylindrical capillary, $(dS/dV) = -1/(r - t)$, where r is the capillary radius.

Rough estimates of the quantities in Eq. [2] would indicate that $u(t)$ is probably of the order of -120 cal/mole in the second layer and one third of that in the third; however, E^σ/ρ is about equal to 1300 cal Å/mole, and we see that the last term in Eq. [2] can make a contribution to the heat of adsorption which is of the same order of magnitude as the gas–solid energy, and which could combine with this energy to give heats such as those shown in Figs. 5 and 6. [In a detailed treatment, one would also need to include terms to take account of the change in enthalpy due to stresses under a curved interface, as was done by Kington and Smith (4).]

The reason for the upsweep in the heat curves at high amounts adsorbed is well known (4, 15): as the menisci flatten out during the completion of the pore filling process, the stresses on the fluid in the pores change considerably, and the enthalpy of the liquid changes concomitantly. The structure observed in the curves in the intermediate region is not well understood, although it seems reasonable to associate this with pore filling; the fact that relatively discrete values for the radii are indicated by the pore size distribution curves encourages the speculation that relatively discrete changes may be induced in the thermodynamic properties.

Kington and Smith (4) have given an excellent discussion of the thermodynamics of irreversible processes as applied to heats of adsorption and desorption in porous systems. Among other things, they point out that the integrated difference between the true (calorimetric) heats of adsorption and desorption must be equal to zero because of the First Law, and thus the irreversible work obtained by integrating around the loop in a plot of the isotherm data vs. $RT \ln P$ is equal to $T\Delta S_{\text{irr}}$, where ΔS_{irr} is the irreversible entropy produced in scanning the entire hysteresis loop. Unlike Kington and Smith, we find that calorimetric heats of adsorption lie above the heats of desorption in the intermediate region. The two curves cross just before they begin rapid rises due to the completion of pore filling. It is an interesting, but so far inexplicable, fact that the integrated differences in calorimetric heats for coverages below that of the crossing point amount to 0.106 cal/gm for one layer of preadsorbed water and 0.098 for three layers, and are equal to the values given in Table I for the total irreversible work in the two systems. Our heat curves differ from those of Kington and Smith in yet another significant fashion; although they found that the Clausius–Clapeyron and the calorimetric adsorption heats were in reasonably good agreement, such is not the case in the present work. Thus, it would appear that neither the adsorption or the desorption processes in our systems can be considered as reversible. We note in passing that Kington and Smith obtained agreement between calorimetric and Clausius–Clapeyron adsorption heats only after applying a correction to the calorimetric data for the heat of expansion under the curved surface; this procedure is incorrect, since the equilibrium Clausius–Clapeyron heats give the enthalpy of the same system as the equilibrium calorimetric heats, and any corrections for enthalpy of

expansion should be applied to both sets of data or to neither. Consequently, it appears that neither adsorption or desorption was reversible in their system as well as in ours. If the magnitude of the difference between a calorimetric and the Clausius–Clapeyron curve is taken to be a measure of the degree of irreversibility, one would conclude that desorption is the more irreversible of the two processes in Kington and Smith's investigation of the bare porous glass and in our investigation of the porous glass plus a monolayer of preadsorbed water; in the triple water layer case, adsorption and desorption appear to be comparably irreversible.

REFERENCES

1. Everett, D. H., *in* "The Solid-Gas Interface, Vol. 2," (E. A. Flood, ed.) Dekker, NY (1967).
2. Everett, D. H. and Stone, F. S., "The Structure and Properties of Porous Materials" Butterworths, London (1958).
3. Linsen, B. G., and van den Heuvel, A., *in* "The Solid-Gas Interface, Vol. 2," (E. A. Flood, ed.) Dekker, NY (1967).
4. Kington, G. L., and Smith, P. S., *Trans. Faraday. Soc.* **60**, 705 (1964).
5. Gregg, S. J., and Sing, K. S. W., "Adsorption, Surface Area and Porosity," Academic Press, NY (1967).
6. Ferguson, C. B., and Wade, W. H., *J. Colloid Interface Sci.* **24**, 366 (1967).
7. McCullough, J. P., and Scott, D. W., Eds. "Experimental Thermodynamics, Vol. I," Chapts. 5 and 13, Plenum Press, NY (1968).
8. Young, D. M. and Crowell, A. D., "Physical Adsorption of Gases," Butterworth, London (1962).
9. Chon, H., Fisher, R. A., and Aston, J. G., *J. Amer. Chem. Soc.* **82**, 1955 (1960); R. A. Fisher, Ph.D. dissertation, The Penn. State University, 1961.
10. Barrer, R. M., *in* "The Structure and Properties of Porous Materials," Butterworths, NY (1958).
11. Holmes, J. M., and Beebe, R. A., *Advan. Chem. Ser.* **33**, 291 (1961); A. I. Sarakhov, M. M. Dubinin, and Yu. F. Berezkina, *Bull. Acad. Sci. USSR, Div. Chem. Sci* 1069 (1963); A. I. Sarakhov, M. M. Dubinin, Yu. F. Berezkina, and E. D. Zaverina, *Bull. Acad. Sci. USSR, Div. Chem. Sci.* 902 (1961).
12. Steele, W. A., and Aston, J. G., *J. Amer. Chem. Soc.* **79**, 2393 (1957); W. A. Steele, *J. Phys. Chem.* **61**, 1551 (1957).
13. Burgess, C. G. V., and Everett, D. H., *J. Colloid Interface Sci.* **33**, 611 (1970).
14. Kington, G. L., and Smith, P. S., *Trans. Faraday Soc.* **60**, 121 (1964).
15. Kiselev, A. V., *in* "Proc. 2nd Int. Congress on Surface Activity, Vol. 2", Butterworths, London (1957).

A Comparison Between Mercury Injection and Nitrogen Sorption as Methods of Determining Pore Size Distributions[1]

I. D. SILLS, L. A. G. AYLMORE, AND J. P. QUIRK[2]

ABSTRACT

A comparison of mercury injection and nitrogen sorption methods of pore size distribution analysis was made on a sample of goethite using the slit-shaped pore model. Using the commonly accepted contact angle of 140° for mercury, the mercury pore-size distribution plot is displaced by approximately 20% in plate separation with respect to the nitrogen plot. The assumption of a contact angle of 153° for mercury is required to make the plots coincide. This value is regarded as not unrealistic. Combination of the two techniques provide a useful method of pore size distribution analysis over a continuous range of pore sizes from 10Å to 50μm. This approach is particularly appropriate to the investigation of the pore structure of soil materials.

Additional Index Words: **slit-shaped pores, contact angle for mercury.**

UNTIL RECENTLY the characterization of soil structure has been carried out largely in terms of particle size distribution, degree of aggregation, and bulk density. While such measurements remain of considerable significance in interpreting the behavior of a soil, increasing emphasis has been placed over the past decade on measurements of the pore size distribution (2, 3, 12, 13). The distribution of pore sizes controls to a large extent the retention and transport of water within the soil, aeration, and microbial activity.

Since soils may contain a wide range of constituents, the pore size distribution will vary with the proportion of different particle sizes present (14). Pore sizes may thus range from less than 100Å for clay materials to several hundred μm for sands. Techniques used to measure pore size distributions on soils should therefore be capable of measuring a very wide range of pore sizes with reasonable accuracy. At present no suitable single method is able to encompass the complete range of pore sizes present in soils. However, combination of the low temperature nitrogen sorption and mercury injection porosimetry techniques should make this possible if the techniques are equivalent.

The nitrogen sorption method involves the analysis of either the adsorption or desorption branch of the nitrogen sorption isotherm usually obtained at 78K by application of the Kelvin equation. This equation relates the pore radius, r, to the relative pressure, p/p_o, by the expression:

$$\frac{RT}{V} \ln \frac{p}{p_o} = -\frac{2\gamma \cos\theta}{r} \qquad [1]$$

where R is the gas constant, T is the absolute temperature, γ is the surface tension, and V is the molar volume of liquid nitrogen.

Mercury injection porosimetry involves the measurement of the volume of mercury injected into the porous medium with increasing applied pressure. The minimum pressure, P, which must be applied to force mercury into a pore with radius, r, is calculated from the Jurin equation:

$$P = -2\gamma \cos\theta / r \qquad [2]$$

where γ is the surface tension of the mercury and θ is the contact angle of the mercury.

The nitrogen sorption technique provides considerable detail over the range of pore sizes from approximately 10Å to 200Å but becomes insensitive for larger pore sizes. While the mercury injection technique is capable of measurements down to approximately 30Å (depending on the pressure capability of the equipment) the accuracy of the measurements decreases at very high pressures. For pores of less than about 50Å more detailed information can be obtained using the nitrogen technique.

There does not appear to be a great deal of experimental verification of the equivalence of the two techniques in the literature. However, Joyner, Barrett, and Skold (11), using a variety of chars, and Zwietering (15), using iron oxide, obtained good agreement between the two techniques using a cylindrical pore model.

Since slit-shaped pores occur in many systems, including soil and clay materials, the present work was undertaken using a material for which electron microscopy indicated the applicability of this model. To examine the compatability of the two methods, it was necessary to use a material in which the predominant pore size lies in the region that can be accurately measured by both, i.e. 50Å–150Å. This was achieved by using a sample of goethite in which the predominant pore size was approximately 100Å.

MATERIALS

The goethite was prepared according to the method described by Atkinson, Posner, and Quirk (1) by adding 200 ml of 2.5*M* NaOH to a solution of 404.2 g of $Fe(NO_3)_3$ in 1,800 ml of water, mixing, and standing for 55 hours at room temperature. This was then added to a mixture of 800 ml of 2.5*M* NaOH and 1,200 ml of water and placed in an oven at 60C for 3 days. Sodium nitrate ($NaNO_3$) was added to flocculate the suspension and the goethite was washed by decantation until the supernatant was clear. The pH was adjusted to 8.0 and washing continued until dispersion commenced. The material was then dried at 60C to form aggregates.

X-ray analysis showed the material to be poorly-crystallized goethite. Figure 1 shows an electron micrograph of the oxide which appears as needle-like crystals joined along their length forming plate-shaped particles. The specific surface area of this material obtained by application of the BET method to nitrogen adsorption at 78K was 130 m^2/g.

[1] Contribution from the Dep. of Soil Science and Plant Nutrition, University of Western Australia, Nedlands, W. Australia 6009. Received Jan. 2, 1973. Approved April 3, 1973.

[2] Research Officer, Senior Lecturer in Soil Science, and Professor of Soil Science, respectively, Department of Soil Sci. and Plant Nutrition, Univ. of Western Australia, Nedlands, W. Australia,6009.

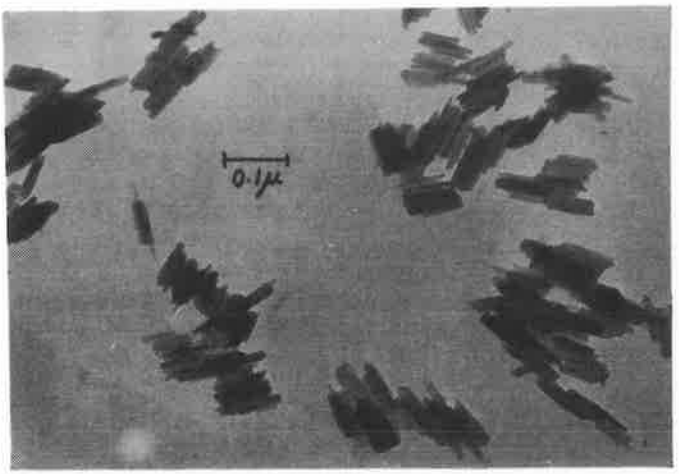

Fig. 1—Electron micrograph of goethite crystals.

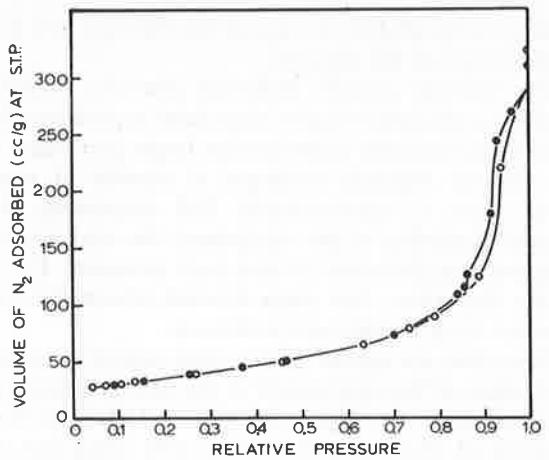

Fig. 2—Nitrogen sorption isotherm at 78K for goethite, O adsorption, ● desorption.

EXPERIMENTAL PROCEDURE

Nitrogen sorption data were obtained by sealing approximately 1 g of goethite into a sample bulb and degassing under a vacuum of better than 10^{-4} torr at 60C until the pressure remained below 10^{-3} torr for 15 min when the vacuum pumps were isolated. Conventional volumetric adsorption apparatus based on the original apparatus of Emmett and Brunauer (6) and incorporating many of the refinements suggested by Harkins and Jura (7) and Joyner (10) was used. The sample bulb was connected to this apparatus, evacuated, and the nitrogen sorption isotherm was determined at 78K using a liquid nitrogen bath.

The pore size distribution was calculated by the method of Innes (9) for slit-shaped pores using the desorption isotherm. This method utilizes a modification of the Kelvin equation, incorporating the thickness of the adsorbed film, to determine the plate separation. The modified Kelvin equation is

$$d - 2t = -\frac{2\gamma V}{RT \ln p/p_o} \qquad [3]$$

where d is the maximum distance of plate separation at which capillary evaporation can occur for a given relative pressure p/p_o and t is the thickness of the adsorbed layer (obtained from sorption onto essentially nonporous solids).

Mercury injection data were obtained using a modified version of the apparatus described by Ingles (8). The volume of mercury injected into approximately 3 g of sample was monitored by measuring the change in resistance of 0.004 inch diameter tungsten wire strung down the capilllary around a glass bridge and returned. A resistance bridge reading to 0.01 ohms was used for this purpose. Pore sizes were obtained by substituting the pressure readings into the Jurin equation [2]. For slit-shaped pores the parameter r in the Jurin equation is replaced by the plate separation d.

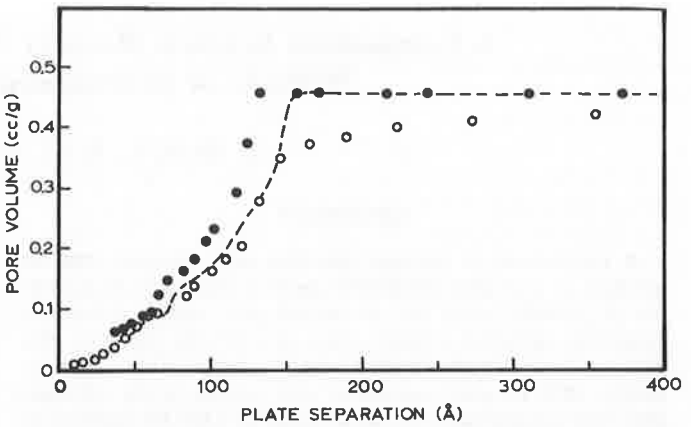

Fig. 3—Pore size distributions of goethite using O, nitrogen sorption and ●, mercury injection ($\theta = 140°$) techniques; --- mercury injection calculated for $\theta = 153°$.

RESULTS AND DISCUSSION

The nitrogen sorption isotherm obtained for the goethite appears in Fig. 2. Its significant features are the sharply rising section at high relative pressures and the hysteresis closure at a relative pressure above 0.70. Analysis of this isotherm using the method of Innes (9) resulted in a cumulative pore volume distribution with increasing pore size. On the other hand the mercury injection results are measured as increasing volume injected with increasing pressure, i.e. with decreasing pore size. A comparison of the two methods thus requires the mercury data to be plotted as the unfilled pore volume vs. pore size; the unfilled pore volume being the volume of pores remaining unfilled by mercury at any given pressure. The total pore volume is that derived from the nitrogen sorption data (0.46 cc/g).

Because of the cosine relationship in the Jurin equation, the pore size calculated from mercury injection data is particularly sensitive to the contact angle used. Contact angles have been reported to vary from 117° for mercury on cement paste (4) to 147° on kaolinite and illite (3). Previously, most workers had assumed contact angles of 140° since a number of commonly tested materials gave values close to this figure. Ellinson et al. (5) found that a variety of materials gave angles ranging from 130° to 139° at 25C. In most of these cases the contact angles were determined on the powdered sample in air and consequently they may vary from the actual values occurring within small pores and under vacuum.

Since no contact angle data for mercury on goethite was available, the commonly accepted value of 140° was used to calculate the pore size distribution from the mercury injection results and these are combined with the nitrogen results in Fig. 3. The mercury plot, is displaced in plate separation by approximately 20% with respect to the nitrogen plot.

In view of the assumptions made with respect to contact angle, surface tension, density, and adsorbed film thickness for the liquids used, the compatability of the results is particularly good. The applicability of values for statistical quantities such as surface tension and density measured on bulk liquids to liquid in pores in which the size approaches molecular dimensions is at best uncertain, as are the values estimated for the thickness of physically adsorbed layers at high relative vapor pressures. In particular, as indicated by the dashed line plot in Fig. 3, only a change in the value of the contact angle assigned for mercury onto goethite to 153° is required to give virtual coincidence of the two plots. Such a value would not appear unreasonable compared with previous experimental determinations. Accurate determinations of contact angles for mercury are obviously necessary to clarify whether there is a unique or general value for soil materials.

Since generally it is the shape of the pore size distribution rather than the estimation of absolute pore size which is important, it may be concluded that for most purposes of pore size distribution application the agreement between the methods is more than adequate to justify their combination as a means of obtaining fairly detailed pore size distributions from about 10Å to 50μm (14).

LITERATURE CITED

1. Atkinson, R. J., A. M. Posner, and J. P. Quirk. 1968. Crystal nucleation in Fe(III) solutions and hydroxide gels. J. Inorg. Nucl. Chem. 30:2371–2381.
2. Aylmore, L. A. G., and J. P. Quirk. 1960. Domain or turbostratic structure of clays. Nature 187:1046–1048.
3. Diamond, Sidney. 1970. Pore size distributions in clays. Clays Clay Miner. 18:7–23.
4. Diamond, Sidney, and W. L. Dolch. 1972. Generalised log-normal distribution of pore sizes in hydrated cement pastes. J. Colloid Interface Sci. 38:234–244.
5. Ellinson, A. H., R. B. Klemm, A. M. Schwartz, L. S. Grubb, and D. A. Petrash. 1967. Contact angles of mercury on various surfaces and the effect of temperature. J. Chem. Eng. Data 12:607–609.
6. Emmett, P. H., and S. Brunauer. 1934. The adsorption of nitrogen by iron synthetic catalysts: J. Amer. Chem. Soc. 56:35–41.
7. Harkins, W. D., and G. Jura. 1944. Surfaces of solids, X, XII, and XIII. J. Amer. Chem. Soc. 66:919–927, 1362–1366, 1366–1372.
8. Ingles, O. G. 1958. Design and operation of a high pressure mercury porosimeter. Aust. J. Appl. Sci. 9:120–126.
9. Innes, W. B. 1957. Use of a parallel plate model in calculation of pore size distribution. Anal. Chem. 29:1069–1073.
10. Joyner, L. G. 1958. *In* W. E. Barr and V. J. Anhorn (ed.) Scientific and industrial glassblowing and laboratory techniques. p. 257–283. Instruments Publishing Co., Pittsburgh, Pennsylvania.
11. Joyner, L. G., E. P. Barrett, and R. Skold. 1951. The determination of pore volume and area distributions in porous substances: II. Comparisons between nitrogen isotherm and mercury porosimeter methods. J. Amer. Chem. Soc. 73:3155–3158.
12. Nagpal, N. K., L. Boersma, and L. W. De Backer. 1972. Pore size distributions of soils from mercury intrusion porosimeter data. Soil Sci. Soc. Amer. Proc. 36:264–267.
13. Panabokke, C. R., and J. P. Quirk. 1962. Pore volume-size distribution and swelling of natural soil aggregates. J. Soil Sci. 13:71–81.
14. Sills, I. D., L. A. G. Aylmore, and J. P. Quirk. 1973. A pore size distribution analysis of illite-kaolinite mixtures. J. Soil Sci. 24:(in press)
15. Zwietering, P. 1958. Discussions in The structure and properties of porous solids. Proc. 10th Symposium of the Colston Res. Soc., Univ. of Bristol. Butterworths, London. p. 287.

Reprinted from the *Soil Science Society of America Proceedings*
Volume 37, no. 4, July-August 1973
677 South Segoe Rd., Madison, Wis. 53711 USA

AN ANALYSIS OF PORE SIZE IN ILLITE-KAOLINITE MIXTURES

I. D. SILLS, L. A. G. AYLMORE, AND J. P. QUIRK

(*Department of Soil Science and Plant Nutrition, Institute of Agriculture, University of Western Australia, Nedlands, Western Australia 6009*)

Summary

When API-9 kaolinite and Willalooka illite clays were mixed in various proportions, the pore-size distributions obtained using nitrogen sorption and mercury injection techniques were found to be characteristic of neither of the components but showed a progressive reduction in the pore size as the concentration of illite was increased. The plate separation of the mixtures showed a marked decrease with initial added illite, approaching that of the illite when the mixture contained approximately 40 per cent illite. This is indicative of a homogeneous mixture in which the fine illite particles fill in the pores bounded by the relatively coarse kaolinite particles.

The relationship between particle dimensions (derived from crystallographic parameters and specific surface area) and pore size of single clays and clay mixtures is consistent with a model in which slit-shaped pores result from the parallel interleaving of clay crystals for the single clays. Some deviations occur for the mixtures.

Introduction

SOILS are usually composed of mixtures of clay minerals, together with oxides and organic matter. One of the most common mixtures of clay found in soils is comprised of kaolinite and illite in various proportions. Changes in the proportion of fine-grained illite to relatively coarse-grained kaolinite could be expected to influence the physical properties and in particular the structure of natural soil aggregates.

Within a clay system where the length and breadth of the crystals are much greater than the thickness, it is reasonable to assume the majority of the porosity results from slit-shaped voids formed by the interleaving of clay plates. This general picture has been proposed by Aylmore and Quirk (1960, 1967) and is supported by electron microscopy observations. In these circumstances it seems likely that the size of the pores would be equal to the thickness of the particular clay units involved, whether they be crystals or groups of crystals forming domains.

The present work was undertaken to examine the way in which the pore-size distribution of kaolinite-illite mixtures varies with composition and the relationship which exists between particle dimensions and the pore structure of aggregated clay systems in general.

Materials

The following clays were used: Kaolinite from Canada del Camino, Mesa Alta, New Mexico. Sample Number 9 of the American Petroleum Institute project No. 49 (API-9), specific surface area of 17 m^2/g (< 2 μm fraction). Willalooka illite from B horizon of a solonized solonetz, Hundred of Laffer, South Australia. The < 2 μm fraction has a specific surface area of 190 m^2/g.

Preparation

Sodium saturated suspensions of the less than 2 micron fraction of clay were obtained by the method used by Posner and Quirk (1964), washed free of salt by repeated centrifugation in the case of the kaolinite and dialysed against distilled water in the case of the illite. Water was removed by filtering with Visking cellulose casing in a pressure-membrane apparatus followed by air-drying. The samples were then lightly ground.

Mixtures of Willalooka illite and API-9 kaolinite were prepared by weighing the sodium-saturated illite and kaolinite in the desired proportions, water was added to the mixture in a beaker, and a magnetic stirrer was used to produce a dilute suspension. This was then filtered under vacuum through a porosity-5 sintered-glass filter while being stirred to prevent differential sedimentation. When the total amount had been filtered it was scraped off the filter and air-dried into lumps which were broken into smaller aggregates between 2 mm and 5 mm across. These were dried in an oven at 110 °C and divided into two portions; one was weighed and placed into a sample tube for the nitrogen sorption determination; the second was used to determine the porosity of the mixture, after which it was placed in a dilatometer and examined by mercury injection porosimetry.

API-9 is normally self-flocculating (Schofield and Samson, 1954). To determine whether the pore structure of the dry material was influenced by deflocculation, a dispersed sample was prepared by mixing 5 g clay with 55 ml water and 10 ml 0·1 per cent solution of sodium tripolyphosphate and dried into aggregates in the same way as described above.

Experimental

Nitrogen sorption

Conventional volumetric adsorption apparatus based on the original equipment of Emmett and Brunauer (1934) and incorporating many of the refinements suggested by Harkins and Jura (1944) and Joyner (1949), was used to obtain complete adsorption-desorption isotherms for the mixtures. Outgassing was achieved by heating under vacuum at 300 °C until the pressure remained below 10^{-3} torr for 15 min after isolation from the pumps while still being heated. This usually required between 8 and 24 h. Nitrogen sorption isotherms were then obtained in the usual way with the sample bulb immersed in liquid nitrogen. Specific surface areas were obtained using the B.E.T. method from sorption data between relative pressures of 0·05 and 0·35.

Evidence presented by Aylmore and Quirk (1967) indicates that the majority of the pore volume of dried clays is contained within slit-shaped pores and consequently the method of Innes (1957) was used to calculate the pore-size distributions of the clay mixtures from the desorption isotherms. This requires a modified Kelvin equation, incorporating the thickness of the adsorbed film, to determine the plate separation. The modified Kelvin equation is expressed:

$$d-2t = \frac{-2\gamma M}{RT\ln p/p_0}, \qquad (1)$$

where d is the maximum distance of plate-separation at which capillary evaporation can occur for a given relative pressure p/p_0; t is the thickness of the adsorbed layer (obtained from sorption on to essentially non-porous solids); M is the molar volume and γ the surface tension of the liquid; R is the gas constant and T the absolute temperature. The concept of slit-shaped pores undoubtedly becomes less valid for pore sizes comparable with the cleavage face dimensions of the clay plates. However, the calculation of an 'equivalent plate separation' provides a useful measure of the pore dimensions particularly for comparative purposes and is used in a similar way to the 'equivalent spherical diameter' term in applying Stokes's law to the sedimentation of particles of various shapes.

The application of the Kelvin equation to estimate pore sizes smaller than 2 nm has been questioned by Schofield (1948) and further discussed by Everett (1967) and Kadlec and Dubinin (1969) who attribute the hysteresis closure point to the limitations imposed by the tensile strength of the liquid adsorbate. Nevertheless, Burgess and Everett (1970) have estimated that the lower limit for nitrogen sorbed at 78 °K is closer to 1·0 nm before such a breakdown occurs.

Mercury injection

The porosimeter used for the mercury injection technique was constructed by the Weapons Research Establishment, Salisbury, South Australia, to a design by Ingles (1958) and has a pressure capability of $4{\cdot}83 \times 10^8$ N/m^2 (70 000 psi). Initially the change in the height of mercury in the dilatometer was measured using a hydraulically operated probe which formed part of the pressure vessel closure. This was lowered into the dilatometer until an electrical contact was made when it touched the mercury surface and the height of mercury in the capillary was measured from a vernier scale on the probe. Later, modifications were made and the resistance of a tungsten wire 0·016 cm diam strung down the capillary was measured using a resistance bridge capable of reading to 0·01 ohms. As the mercury level dropped, the length of wire not immersed increased and the resistance also increased. This method has the advantage that the mercury level can be monitored continuously. No significant differences in volume distributions were evident when the two methods were compared on samples of the same material. The relationship between the plate separation, d, and the applied pressure, P, is given by the Jurin equation:

$$P = \frac{-2\gamma \cos\theta}{d}, \qquad (2)$$

where γ is the surface tension of the liquid (480 dynes/cm for mercury) and θ is the angle of contact of mercury with the clay (140°).

The following method was used to obtain the mercury injection results:

The 2–3 g oven-dried sample was placed in the sample tube of the dilatometer, which was connected to a constant-bore capillary of approximately 3 mm inside diameter. The dilatometer was then placed

in a specially designed vacuum chamber, evacuated and sufficient mercury was run on to the sample almost to fill the dilatometer to the top of the capillary. The dilatometer was then placed inside a pressure vessel filled with silicone oil which enabled the hydraulic pressure to be transmitted to the mercury. The volume of mercury injected was then related to the resistance change. Simultaneous pressure and resistance readings enabled a plot of mercury injected against plate separation to be made.

Porosity

Porosity was measured by immersing the aggregates in kerosene ($\rho = 0{\cdot}80$ g/cc) under vacuum and then touching them lightly on a piece of filter paper to remove surface liquid. The volume of kerosene absorbed was determined by oven drying to constant weight at 110 °C.

Results and discussion

The nitrogen-sorption isotherms for some of the illite-kaolinite mixtures are shown in Fig. 1. For clarity, a number of experimental

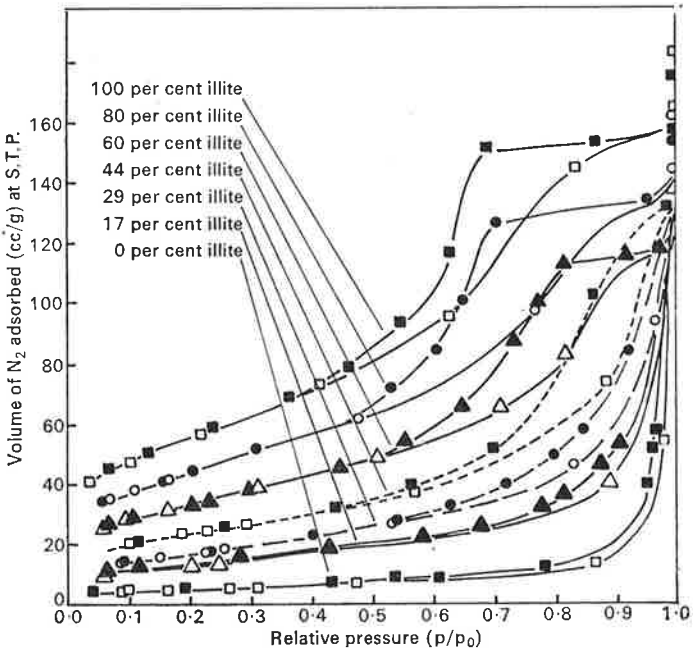

FIG. 1. Nitrogen sorption isotherms at 78 °K for mixtures of Willalooka illite and API-9 kaolinite.

points have been omitted from some of the isotherms. With increasing percentage of illite the isotherms change gradually from that characteristic of the relatively coarse kaolinite to that characteristic of the high surface-area illite. This is indicated by an increase in volume of nitrogen

sorbed at low relative pressures due to the increase in specific surface area and by the expansion of the hysteresis envelope in the higher ranges of relative pressure.

The cumulative pore-size distributions for the mixtures calculated from the nitrogen-sorption isotherms are shown in Fig. 2. For clarity they are plotted relative to the total pore volume. The mercury injection data are presented in Fig. 3 as cumulative volume injected with increasing pressure, i.e. decreasing plate separation.

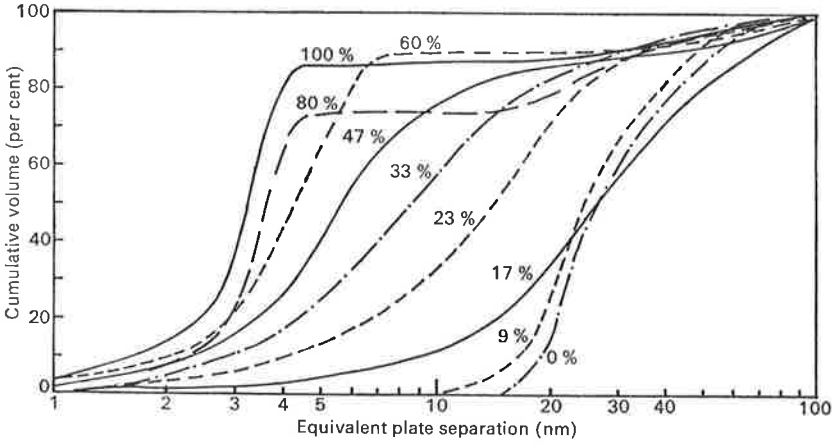

FIG. 2. Cumulative volume—pore-size distributions for mixtures of Willalooka illite and API-9 kaolinite from nitrogen desorption data.

Mixed clay models

Perhaps the most significant point illustrated by these data is that the position of the rapid change in pore volume with pore size moves gradually across the scale from the pore size corresponding to 100 per cent kaolinite to that corresponding to 100 per cent illite. This would indicate a complete mixing of the two materials resulting in a continuous decrease in pore dimensions as the illite crystals fill in the pores bounded by the larger kaolinite particles. A mixture of distinct kaolinite and illite regions would on the other hand be expected to produce pore sizes characteristic of each component in the mixture resulting in steps in the curve related in size to the volume of pores in each region.

Additional evidence for the homogeneous model is derived from the porosity results. A heterogeneous mixture of the two clays would result in a total porosity given by the addition of the porosities of the amount of each clay present, i.e.

$$E_t = E_i\theta + E_k(1-\theta)$$

where E_t is the total specific pore volume in cc/g,

E_k is the specific pore volume of the kaolinite,

E_i is the specific pore volume of the illite, and

θ is the proportion of illite in the mixture.

As Fig. 4 shows, the specific pore volumes of the mixtures in fact drop more rapidly with increase in per cent illite than is indicated by the above relation, and exhibit a minimum porosity for mixtures containing 40 per cent illite.

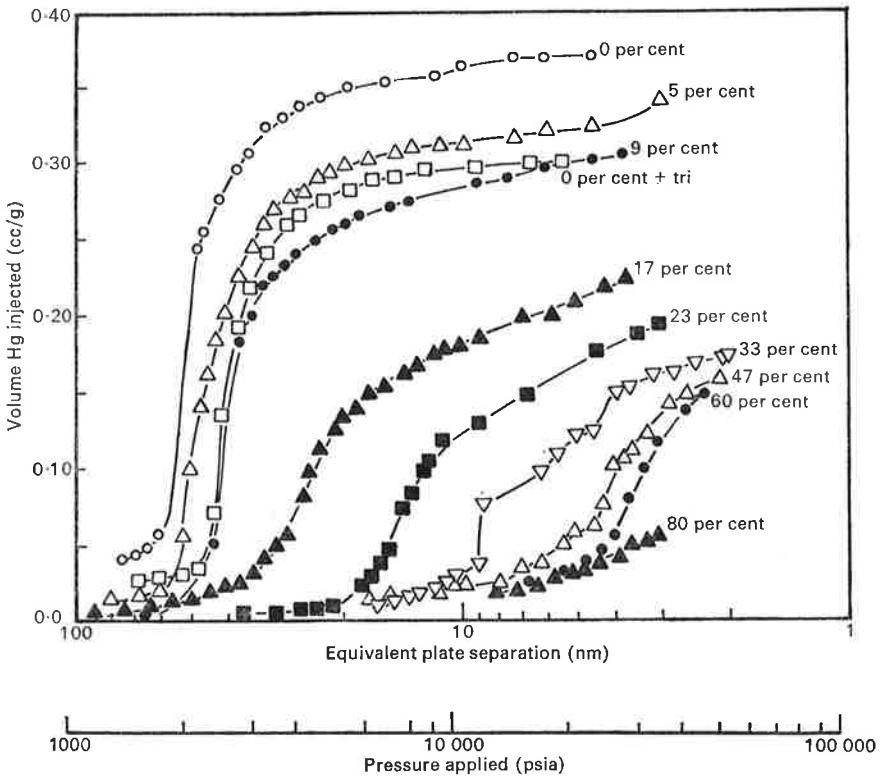

FIG. 3. Mercury injection pore-size distributions for mixtures of Willalooka illite and API-9 kaolinite; also API-9 kaolinite treated with sodium tripolyphosphate.

The relationship between specific surface area and per cent illite is also shown in Fig. 4 and is linear, indicating that the accessibility of the clay surfaces to nitrogen is unaffected when the clays are mixed.

Deflocculated kaolinite

Deflocculation of the kaolinite by the use of sodium tripolyphosphate causes a shift from 50 nm to 40 nm in the predominant plate separation (Fig. 3). In addition, there is a decrease in porosity from 0·408 cc/g for pure kaolinite to 0·363 cc/g for the sodium tripolyphosphate-treated clay and an obvious increase in aggregate strength. These results point to better orientation of the particles in the treated aggregates.

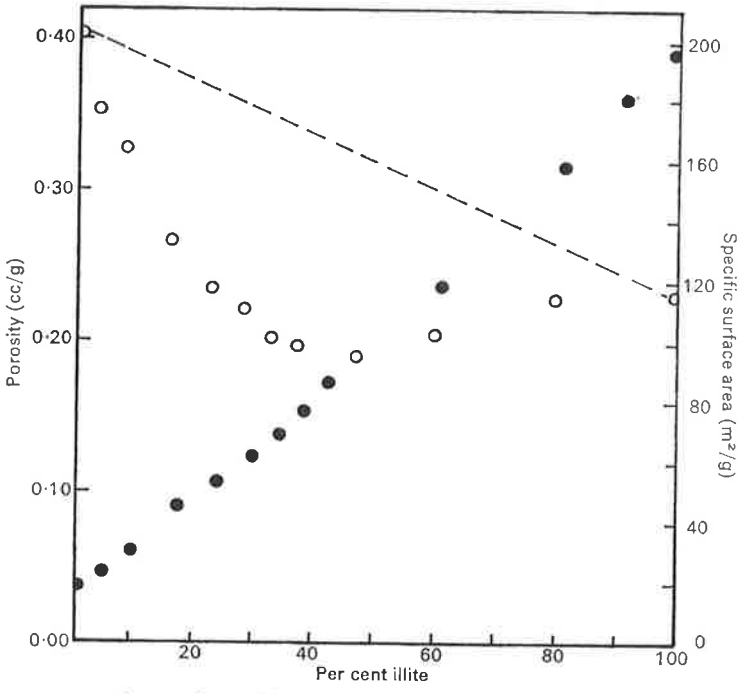

FIG. 4. Porosity, and specific surface area as a function of per cent illite. – – – – Theoretical porosity. ● Specific surface area. ○ Porosity.

Matching of nitrogen and mercury distributions

The pore-size range covered by each method is illustrated in Figs. 2 and 3. The majority of pores for mixtures with 17 per cent or less illite is larger than 20 nm which is outside the useful range of the nitrogen sorption method. These pore sizes are well within the capability of the mercury injection method. On the other hand, a significant fraction of the pores, for those mixtures with a high proportion of illite, is too small to be penetrated by mercury at pressures approaching the limit of the instrument. These pores, however, are in the range of maximum sensitivity of the nitrogen method. The two techniques are thus complementary in that each is most useful in the range of pore size in which difficulties are experienced using the other.

It is easier to compare the mercury and nitrogen curves by plotting the mercury data as cumulative unfilled pore volume against equivalent plate separation. The volume of pores remaining unfilled with mercury at the applied pressure concerned is calculated by subtracting the volume of mercury injected from the total pore volume. When plotted this way the curve for mercury was invariably displaced towards higher volumes with respect to the nitrogen curve. This is thought to be caused by the failure of the mercury method to measure cracks or interaggregate pores larger than 50 μm since these are already filled by the head of mercury (10 cm) present at the beginning of the experimental determination in

the equipment. The kerosene method of porosity determination would, however, include this volume.

The curve for mercury was displaced vertically to match the nitrogen curve at 5 nm. This pore size was selected as it falls within the overlap region of the two methods and the curves could be expected to coincide at this point. This displacement does not alter, in any way, the size distribution of pores over the range being studied, but merely serves to compensate for the uncertainty in the volume of pores at plate separations greater than those measured in this study. Pore size distributions treated in this way are shown in Fig. 5 for the mixtures possessing 33, 47,

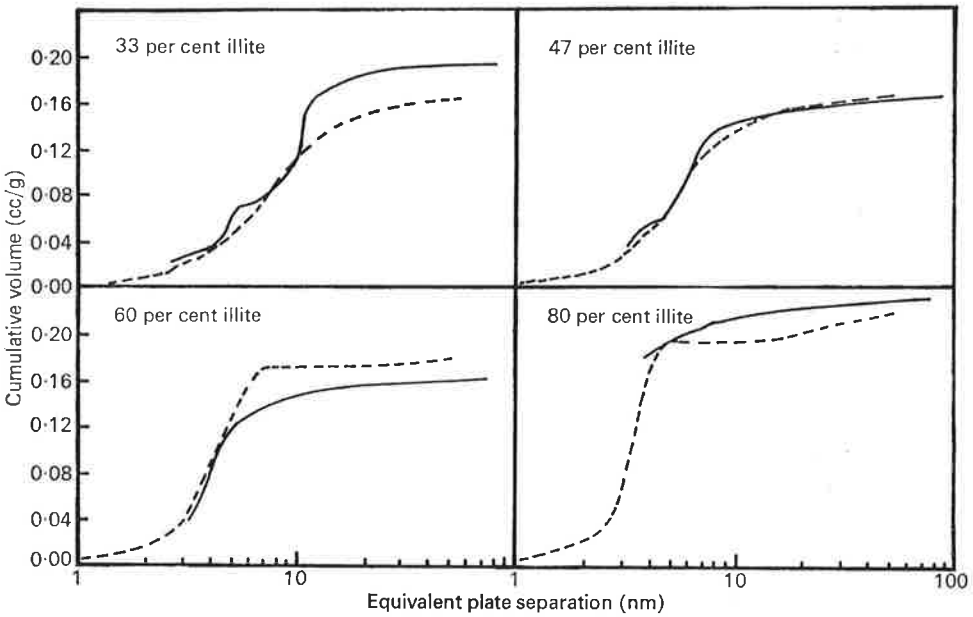

FIG. 5. Comparison of nitrogen sorption and mercury injection pore-size distributions for mixtures of Willalooka illite and API-9 kaolinite. – – – – Nitrogen desorption data; —— Mercury injection data.

60, and 80 per cent illite and show reasonable agreement between the shapes of the curves obtained where the majority of the pores have plate separations which lie within the overlap region of the two techniques. The mixture containing 80 per cent illite has most of its pore volume below 4 nm plate separation which is at the limit of the mercury method and so the curves in this case do not compare well.

Interleaved model

As mentioned previously, the pores formed in a single clay system are thought to be the result of interleaving of the plate-shaped particles. If this is so the plate separations indicated by their pore-size distributions should approximate to the crystal thicknesses calculated from their

crystal parameters and B.E.T. surface areas. The molecular weight of Willalooka illite, based upon the ideal muscovite unit cell formula of

$$(Si_6Al_2)^{IV}(Al)_4^{VI}O_{20}(OH)_4$$
$$\downarrow$$
$$K_2$$

is 796 and its face area based on the a and b dimensions (0·90 and 0·52 respectively) is:

$$2 \times 0{\cdot}90 \text{ nm} \times 0{\cdot}52 \text{ nm} = 9{\cdot}4 \times 10^{-19} \text{ m}^2$$

since two faces are involved. This leads to a theoretical unit cell area of 706 m^2/g and since the actual face area of the illite based on the B.E.T. area, allowing about 10 per cent for edge area, is about 170 m^2/g there would be on average $706/170 = 4{\cdot}1$ sheets per crystal. Since mica materials have a c-axis thickness of 1·0 nm the average crystal thickness of Willalooka illite will be about 4·1 nm which is similar to the predominant nitrogen sorption pore-size distribution plate separation of 3·3 nm. In a similar way the average crystal thickness of API-9 kaolinite which has a face area of about 15 m^2/g may be calculated from the molecular formula:

$$Si_4Al_4O_{10}(OH)_8 = 516$$

and the unit cell dimensions:

$$a = 0{\cdot}516 \text{ nm}, \quad b = 0{\cdot}893 \text{ nm}, \quad c = 0{\cdot}739 \text{ nm}.$$

This indicates that the average crystal thickness is 53 nm for this clay, which is in excellent agreement with the predominant mercury injection plate separation of 50 nm. The agreement observed here supports the pore model of interleaved clay crystals proposed by Aylmore and Quirk (1967).

It is obvious from the previous calculation that there is a relationship between particle size (and hence specific surface area) and pore size. Very satisfactory agreement is obtained between the average crystal thickness (calculated from surface area data and crystallographic parameters) and the average plate separation (obtained from the nitrogen desorption and mercury injection results) for illite and kaolinite. A similar procedure was used to predict values of plate separation (crystal thickness) for various values of specific surface area. Two calculations were carried out, one using the kaolinite parameters and one using the illite parameters, and both gave similar results because of the compensation between molecular weight and c-axis spacing. The average of these two calculations is plotted in Fig. 6 along with a curve for the change in the measured plate separation with specific surface area.

The curves shown in Fig. 6 are also a measure of the decrease in plate separation with increase in illite content of the mixtures. This is because the abscissa can be used as a measure of illite content as there is a nearly linear relationship between per cent illite and specific surface area as shown in Fig. 4, ranging from 17 m^2/g for no illite to 190 m^2/g for 100 per cent illite. A marked decrease in plate separation for the

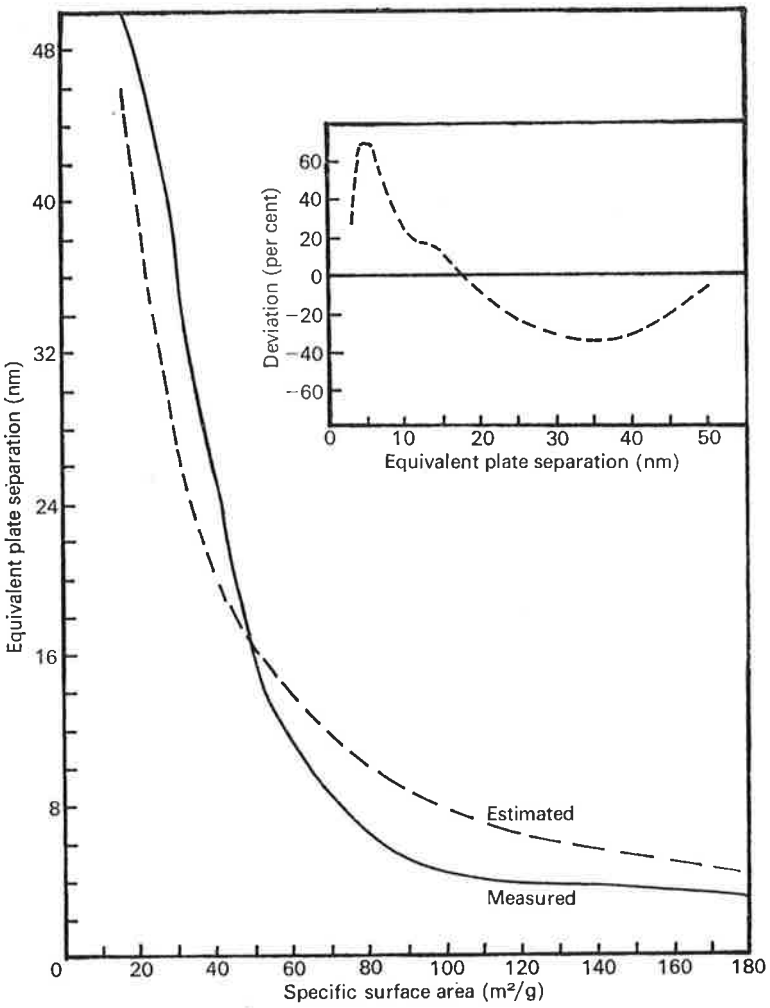

FIG. 6. Change in equivalent plate separation with specific surface area for clay crystals. Inset: per cent deviation of estimated plate separation from measured plate separation.

addition of some 30–40 per cent illite with little change thereafter is illustrated in Fig. 6. Thus small increases in fine clay content in a mixture in which a relatively coarse clay predominates could have significant implications with respect to those properties of the system which are related to pore-size distribution, in particular water retention and transport.

A comparison of the predicted and measured plate separation-specific surface area curves in Fig. 6 shows that, although there are deviations, the trends of the two curves are similar. The inset illustrates the deviation of the calculated pore size as a percentage of the measured

pore size and shows that, while there is close agreement when only a single clay is present, the mixing of coarse and fine clays creates a situation that is more complex than the simple interleaving model envisaged here. Nevertheless, the agreement is sufficiently good to permit approximate estimates of plate separations in clay mixtures below about 25 nm using specific surface area and crystallographic parameters. However, more direct techniques such as mercury injection porosimetry are necessary to measure distributions in the coarse pore range.

REFERENCES

AYLMORE, L. A. G., and QUIRK, J. P. 1960. Domain or turbostratic structure of clays. Nature, Lond. **187,** 1046–8.

—— —— 1967. The micropore size distribution of clay mineral systems. J. Soil Sci. **18,** 1–17.

BURGESS, C. G. V., and EVERETT, D. H. 1970. The lower closure point in adsorption hysteresis of the capillary condensation type. J. Colloid and Interface Sci. **33,** 611–14.

EMMETT, P. H., and BRUNAUER, S. 1934. The adsorption of nitrogen by iron synthetic catalysts. J. Amer. Chem. Soc. **56,** 35–41.

EVERETT, D. H. 1967. Adsorption hysteresis. In The Solid Gas Interface (ed. E. A. Flood), vol. ii, p. 1086. Dekker, N.Y.

HARKINS, W. D., and JURA, G. 1944. Surfaces of solids, X, XI, and XII. J. Amer. Chem. Soc. **66,** 919–27, 1362–6, 1366–72.

INGLES, O. G. 1958. Design and operation of a high pressure mercury porosimeter. Aust. J. Appl. Sci. **9,** 120–6.

INNES, W. B. 1957. Use of a parallel plate model in calculation of pore size distribution. Anal. Chem. **29,** 1069–73.

JOYNER, L. G. 1949. Scientific and Industrial Glass-blowing and Laboratory Techniques (eds. W. E. Barr and V. J. Anhorn), Chapter 12. Instruments Publishing Co., Pittsburgh.

KADLEC, O., and DUBININ, M. M. 1969. Comments on the limits of applicability of the mechanism of capillary condensation. J. Colloid and Interface Sci. **31,** 479–89.

POSNER, A. M., and QUIRK, J. P. 1964. The adsorption of water from concentrated electrolyte solutions by montmorillonite and illite. Proc. roy. Soc. A. **278,** 35–6.

SCHOFIELD, R. K. 1948. In discussions. Disc. Faraday Soc. **3,** 105–6.

—— and SAMSON, H. R. 1954. Flocculation of kaolinite due to the attraction of oppositely charged crystal faces. Ibid. **18,** 135–45.

(*Received 27 November 1972*)

Hysteresis in Gas Sorption Isotherms

L. A. G. AYLMORE

Department of Soil Science and Plant Nutrition, Institute of Agriculture, University of Western Australia

Reprinted from JOURNAL OF COLLOID AND INTERFACE SCIENCE, Volume 46, No. 3, March 1974

Hysteresis in Gas Sorption Isotherms

L. A. G. AYLMORE

Department of Soil Science and Plant Nutrition, Institute of Agriculture, University of Western Australia

Received April 2, 1973; accepted August 31, 1973

Hysteresis in the nitrogen sorption isotherm for a system containing slit-shaped pores has been shown to conform to the "open-pore" theory suggested by Foster [*Trans. Faraday Soc.* **28**, 645 (1932)]. Adsorption takes place largely by the development of multilayers on the surfaces of the plate-shaped crystals and ceases when opposite films merge thus filling the pore. Desorption is then governed by the curvature of the semicylindrical meniscus formed. Hysteresis thus arises essentially from a delay in the formation of a meniscus during the adsorption process.

In a system containing cylindrical capillaries capillary condensation occurs during both the adsorption and desorption processes. Neither process appears thermodynamically reversible with a delay in adsorption resulting from the presence of cylindrical menisci in open-ended pores being followed by a delay in desorption due to the retention of liquid behind narrow restrictions.

INTRODUCTION

The origin of hysteresis in gas sorption isotherms has been the subject of numerous theories ranging from the angle of contact theory of Zsigmondy (1) which has been largely discounted, to various theories based either on the structural properties of the medium or on differences in the fundamental processes involved in sorption and desorption. The "ink-bottle" theory put forward by Kraemer (2) in 1931 and later developed by McBain (3) attributes hysteresis to a delay in desorption due to the retention of liquid sorbate in large pores behind narrow necks. On the other hand Cohan (4) and Coelingh (5) have suggested that the meniscus of a liquid condensed in a capillary has a cylindrical shape on adsorption and a spherical shape on desorption. This leads to the result that the equivalent radius of curvature during the adsorption process is twice as large as during desorption.

Where slit-shaped pores are present the "open-pore" theory of Foster (6) suggests that hysteresis arises from the operation of different mechanisms in the adsorption and desorption processes. Adsorption is seen as occurring solely by the development of physically adsorbed multilayers on the surface of the pore with no meniscus being formed until the physically adsorbed layers merge in the center of the pore. With the filling of the pore a semicylindrical meniscus will be formed and desorption will then be governed by the curvature of this meniscus.

The lowering of the vapor pressure over a curved meniscus is given by the Kelvin equation,

$$\ln \frac{p}{p_0} = \frac{-M\gamma}{RT}\left(\frac{1}{r_1} + \frac{1}{r_2}\right)\cos\theta, \qquad [1]$$

where p is the equilibrium pressure, p_0 is the saturation vapor pressure, γ is the surface tension and M the molar volume of the liquid at temperature T, R is the gas constant and θ is the angle of contact generally assumed equal to zero so that $\cos\theta = 1$.

Journal of Colloid and Interface Science, Vol. 46, No. 3, March 1974

r_1 and r_2 are the principal radii of curvature of the meniscus. For a hemispherical meniscus $r_1 = r_2$ and the equation reduces to:

$$\ln \frac{p}{p_0} = \frac{-2M\gamma}{rRT}. \qquad [2]$$

For a cylindrical or semicylindrical meniscus $r_2 = \infty$ and the equation reduces to:

$$\ln \frac{p}{p_0} = \frac{-M\gamma}{rRT}. \qquad [3]$$

Thus the curvature of the meniscus at which the pore empties and by allowing for the thickness of the physically sorbed layer t, the dimensions of the pore, can be calculated from the corresponding relative vapor pressure, provided the correct pore shape and sorption mechanisms involved are assumed.

The verification of such assumptions is of considerable importance in studies dealing with the application of thermodynamic derivatives such as the Kelvin and Clausius-Clapeyron equations, to sorption isotherms (7–9). For example clay mineral systems are known to exist with a high degree of parallel alignment of the plate-shaped crystals forming slit-shaped pores (10, 11). On the basis of Foster's theory it has been argued (9) that pore size distribution analyses using the Kelvin equation in form [3] should be applied to the desorption rather than the adsorption branch of the complete adsorption–desorption isotherm to saturation. Similarly numerous studies on porous glass (12–14) have debated the virtues of the "ink-bottle" theory or the Cohan theory as an explanation of hysteresis in gas sorption isotherms on this material.

Recently a great deal of evidence has been published (15–18) showing that nitrogen adsorption on a large number of nonporous materials of large crystal size, produces essentially the same isotherm when plotted in the reduced form $n(=V/V_m)$ versus (p/p_0) where V is the volume adsorbed at relative vapor pressure (p/p_0) and V_m is the volume required to form a monolayer. V–n plots for other materials using n from this "universal nitrogen adsorption isotherm" enable deviations from simple monolayer–multilayer adsorption, such as capillary condensation, to be detected as departures from a linear relation. The specific surface area of the sample can be calculated from the slope of the plot which gives V_m.

Using a combination of the previous considerations a number of significant features of the sorption processes in slit-shaped and cylindrical-shaped pores can be illustrated.

SLIT-SHAPED PORES

Curve 1 in Fig. 1 shows a complete adsorption–desorption isotherm at 78 K for nitrogen on a sample of compacted <2 μm size fraction Willalooka Illite, a member of the layer-lattice aluminosilicate clay minerals. Electron microscopy shows the crystals of this material to be plate-shaped particles on the average some 40 Å thick by 1000 Å across the planar surfaces. The sorption isotherm was obtained in the usual way using a volumetric system. Curve 2 shows the differential pore size distribution obtained by application of the Kelvin equation to the desorption branch of this isotherm using a method for slit-shaped pores essentially similar to that of Innes (19). In this method the plate separation d at any relative vapor pressure is given by Eq. [3] with d equal to $2(r + t)$. The cumulative area obtained from this analysis was 183 m^2/g in excellent agreement with the BET area of 185 m^2/g. Curve 2 indicates that most of the porosity of this clay arises from pores of some 20 to 50 Å equivalent plate separation with the maximum in the pore peak occurring at about 33 Å. This is similar to the curve published by Aylmore and Quirk (9).

Curve 3 in Fig. 1 shows a V–n plot for the adsorption branch of the nitrogen isotherm on Willalooka Illite constructed using the data provided by Shull (15) for nitrogen adsorption on crystalline materials of large crystal size, as a standard isotherm. The linearity of this plot up to the point at which the curve flattens, indicates that over this region adsorp-

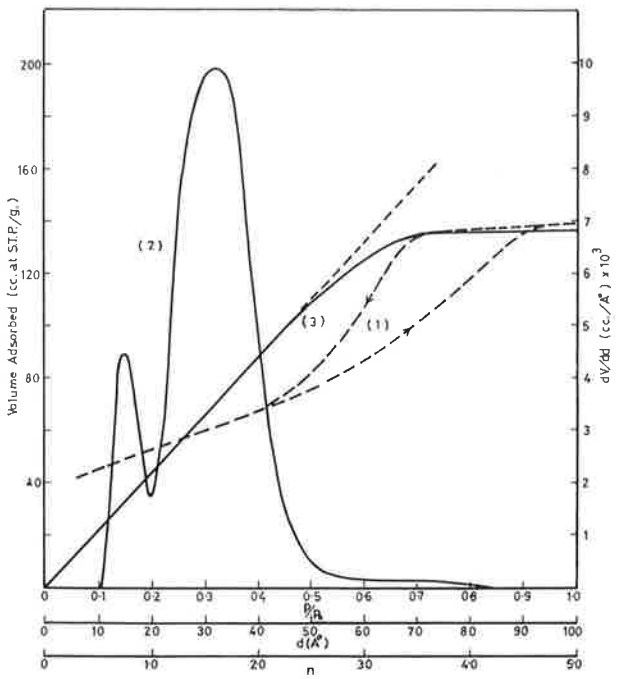

FIG. 1. Nitrogen sorption on Willalooka Illite: (1) Adsorption–desorption isotherm at 78°K; (2) differential pore size distribution from desorption isotherm; (3) V–n plot from adsorption isotherm. Note: legends on abscissa do not correspond.

tion has taken place entirely by multilayer formation on the surface of the clay crystals, i.e., the shape of the isotherm is identical with that obtained on the nonporous standards. Measurements by the author on many other aluminosilicate clay mineral systems indicate that this result is general for these plate-shaped particles except in particular circumstances such as where sorption into intracrystalline regions is occurring. The slope of the linear region corresponds to a specific surface area of 187 m²/g in excellent agreement with both the BET and the pore size distribution analyses.

Note that the legends on the abscissa of Fig. 1 do not correspond. The point at which the V–n plot begins to deviate from linearity ($n \approx 2.4$) does in fact correspond to a relative vapor pressure of about 0.8. Assuming a layer thickness for nitrogen adsorption of some 4 Å, $n = 2.4$ means that a film thickness of some 9.6 Å exists at the point where the physically adsorbed layers merge thus filling the pore, i.e., a plate separation of some 19 Å. This value agrees well with the lower limit of pore size (about 19 Å) indicated by the main peak in the pore size distribution curve 2. According to Eq. [3] these pores are not emptied until a relative pressure of about 0.35 is reached during desorption.

These results seem entirely consistent with the processes suggested by Foster (6) for the filling and emptying of slit-shaped pores with adsorption taking place entirely by multilayer formation on the surfaces of the pores and ceasing abruptly when opposite layers merge at a high relative vapor pressure ($p/p_0 = 0.8$). Subsequently desorption occurs by capillary evaporation governed by the curvature of the semicylindrical meniscus formed, with the result that the pores are not emptied until the lower relative vapor pressure ($p/p_0 = 0.35$) given by the Kelvin equation in form [3] is reached. Hysteresis is thus essentially due to a delay in the formation of a meniscus in the

pores during the adsorption process. In this type of open-pore structure it is unlikely that hysteresis due to ink-bottle retention will occur during desorption.

One difficulty arises with respect to the simple picture indicated by these results. The pore size distribution curve 2, obtained in this case by continuing the analysis until the volume of capillary condensate (estimated by correcting the volume desorbed for the thinning of physically adsorbed layers) was exhausted, indicates the presence of a small volume of pores of some 15 Å equivalent plate separation. These are emptied at a relative vapor pressure below the point of closure of the hysteresis loop at $p/p_0 = 0.4$; that is, in the reversible region of the isotherm. The cumulative specific surface area obtained in the pore size distribution analysis of the desorption isotherm reaches a value of 143 m^2/g at the point where the hysteresis loop closes, leaving some 40 m^2/g in pores still filled. The fact that the isotherm is reversible at lower vapor pressures would suggest that the pores being filled or emptied are probably wedge shaped (20, 21). However, the filling of such pores is difficult to reconcile with the linearity of the V–n plot. A decrease in specific surface area of 40 m^2/g should produce a readily apparent change in slope unless this is largely compensated for by the increase sorption due to capillary condensation. The discrepancy is not removed by any reasonable variation in the values attributed to multilayer film thickness or Kelvin radii in the pore size distribution analysis. However, other factors such as the values assumed for density and surface tension of liquid nitrogen may account for this apparent anomaly.

It has been suggested (22, 23) that the lower closure point of the hysteresis loop may correspond to the limit of the tensile strength of the liquid adsorbate in which case the pore size distribution analysis should terminate at this point. However, this is not necessarily the case. For example, the lower closure point for nitrogen adsorption at 78 K on various clay minerals occurs at relative vapor pressures ranging from 0.3 to 0.8 and within these limits clearly reflects variations in the pore structure of the adsorbents. For other materials (24) the shape of the isotherm sometimes indicates a rapid desorption associated with the lower closure point of the hysteresis loop and this may possibly reflect a spontaneous emptying by the previous mechanism. A number of other factors such as limitations on the accessibility of pores to the adsorbate may produce a similar effect. If spontaneous nucleation does occur the emptying of pores at higher relative vapor pressures than corresponds to their size would result in an underestimate of the true cumulative surface area. However, the present isotherm for Willalooka Illite shows no such rapid desorption at the point of closure but rather a more gradual merging of the desorption isotherm with the adsorption isotherm.

The results of many workers (25) would suggest a minimum pore size, to which pore size distribution analyses based on the Kelvin equation can be extended, of roughly 20 Å diameter for cylindrical pores and somewhat smaller in the case of slit-shaped pores. In the present case it seems likely that the procedure has some validity to relative pressures below the closure of the hysteresis loop.

CYLINDRICAL SHAPED PORES

In Fig. 2 similar plots for nitrogen sorption on a sample of Vycor porous glass are given. The available evidence (13, 14) suggests that the pores in this material are roughly cylindrical in shape with narrow necks leading into larger volumes. The differential pore size distribution analysis was calculated from the desorption branch using a method similar to that described by Gregg and Sing (26) for cylindrical pores and shows the majority of porosity to be in two pore classes of approximately 47 and 28 Å mean radius, respectively.

In the V–n plot, in contrast to that for the Willalooka Illite, the initial linear region is followed by an upturn in the curve at about $n = 1.8$. This clearly indicates enhanced sorption due to the onset of capillary condensation

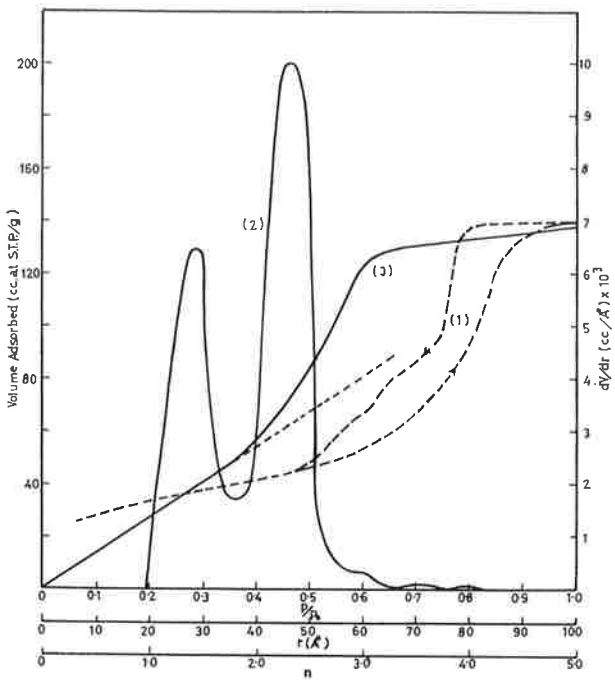

FIG. 2. Nitrogen sorption on Vycor porous glass: (1) Adsorption–desorption isotherm at 78°K; (2) differential pore size distribution from desorption isotherm; (3) V–n plot from adsorption isotherm. Note: legends on abscissa do not correspond.

and the corresponding relative vapor pressure is approximately 0.58. Up to this point sorption probably occurs by monolayer formation followed by condensation on cylindrical menisci as suggested by Cohan (4). Provided the pores are open-ended, then as the radius of the cylindrical meniscus is reduced by continued adsorption with increasing vapor pressure, a point must be reached at which the cylindrical meniscus becomes unstable at the particular relative vapor pressure and the channel through the center of the pore will fill spontaneously, leaving hemispherical menisci at the ends. $n = 1.8$ corresponds to a film thickness of some 7.2 Å. For the cylindrical meniscus which exists just before condensation occurs, a relative vapor pressure of 0.58 indicates a channel radius of approximately 9 Å using the Kelvin equation in form [3]. That is the pore radius would be some 16.2 Å. Since the radius of curvature for a hemispherical meniscus at $p/p_0 = 0.58$ using Eq. [2] is some 18 Å, the hemispherical menisci formed in the pore will be quite stable at this vapor pressure.

Depending on pore continuity the hemispherical menisci in these small pores may be propagated throughout the pore structure with increasing vapor pressure causing large pores to fill by normal capillary condensation according to Eq. [2]. Alternatively, larger pores containing cylindrical menisci, if isolated, will go "critical" progressively with the increase in relative vapor pressure.

Capillaries with one end closed would undoubtedly form hemispherical menisci once the adsorbed film developed properties akin to the bulk liquid. In these circumstances capillary condensation at $p/p_0 = 0.58$ would, according to Eq. [2], indicate that pores some 24 Å radius were being filled. However, it can be noted that the point of closure of the hysteresis loop during desorption occurs at a lower relative vapor pressure ($p/p_0 = 0.48$) than that at which capillary condensation

commences during adsorption. $p/p_0 = 0.48$ corresponds to a Kelvin radius of 12.5 Å for a hemispherical meniscus or a pore radius of some 19 Å (including $t = 6.5$ Å) as indicated by the minimum pore size in the differential pore size distribution. Thus it appears unlikely that this material contains any appreciable volume of pores with one end closed. A value of 12.5 Å for the limiting radius of curvature for nitrogen is close to the 10.8 and 11.9 Å quoted by Burgess and Everett (23) for nitrogen adsorption on porous glass and silica/alumina catalysts, respectively. Thus, although the V–n plot indicates that the smallest pores are of some 16.2 Å radius, these may be emptied of their hemispherical menisci at $p/p_0 = 0.48$ during desorption for the reasons outlined by Burgess and Everett. However, once again the shape of the isotherm does not suggest any significant desorption resulting from such a process.

The excellent agreement between the specific surface area obtained from the initial slope of the V–n plot (114 m²/g) and the BET area (116 m²/g) for porous glass would suggest that only monolayer–multilayer formation has occurred in this region. In a cylindrical capillary one would normally expect the specific surface area available for sorption to be progressively reduced as the radius of the cylindrical meniscus is reduced by adsorption beyond the monolayer, i.e., the V–n plot should begin to curve downward. However, increased sorption due to condensation on the cylindrical meniscus may tend to compensate for the effects of the decrease in specific surface area available.

The cumulative specific surface area obtained from the pore size distribution analysis of the desorption branch of the nitrogen isotherm on porous glass was 136 m²/g. This is somewhat higher than the values obtained from the BET calculation and V–n plot and lends weight to the possibility of narrow necks controlling desorption from larger volumes. Volumes of liquid nitrogen held back in larger pores behind narrow necks would be attributed to smaller pore radii in the pore size distribution analysis thus yielding excessive surface area estimates for each decrement of volume. Although the pores appear to be open-ended the presence of narrow constrictions in tubular pores would result in effectively the same behavior as suggested by the simple "ink-bottle" concept.

On the other hand a similar analysis carried out on the adsorption branch of this isotherm gives a specific surface area of 96 m²/g thus considerably underestimating the BET and V–n values. If the mechanism of filling of the pores is as suggested earlier this would in fact result in the reverse phenomenon of pore volumes being attributed to larger pore radii with a consequent underestimate of the true specific surface area.

The previous considerations lead to the conclusions that irreversible processes occur in both the adsorption and desorption branches of the nitrogen isotherm for porous glass with a delay in adsorption through the presence of cylindrical menisci being followed by a delay in desorption due to retention behind narrow restrictions. From comparisons between Clausius-Clapeyron and calorimetric heats of sorption of argon on a sample of the same batch of porous glass used here, Giacobbe, Aylmore and Steele (27) came to the conclusion that neither the adsorption or the desorption processes could be considered as reversible. Although Kington and Smith (8) had earlier obtained agreement between calorimetric and Clausius-Clapeyron adsorption heats for argon on porous glass, Giacobbe, Aylmore and Steele have pointed out that the correction applied by these authors to the calorimetric data for the heat of expansion under a curved surface should also have been applied to the Clausius-Clapeyron data. Also it is clear from the shapes of the argon isotherms obtained by Kington and Smith (8) and by Giacobbe, Aylmore, and Steele (27) that there are significant differences in the pore structures of the two samples of porous glass used. A similar difference exists between the nitrogen isotherms obtained by Emmett and DeWitt (12) and that in the present work. The materials used by Kington and Smith and by Emmett and DeWitt show

single sharp pore size distribution peaks compared with the bimodal distribution for the present material. However, a V–n plot of the adsorption data obtained by Emmett and DeWitt is very similar to that shown in Fig. 2 although the upturn after the initial linear region rises more sharply to the limit as could be expected from the narrower pore size distribution.

To summarize it is clear that the origin of hysteresis in gas sorption isotherms varies with the configuration of the porous structure. Hysteresis can arise from the structural properties of the medium and from differences in the fundamental processes involved in adsorption and desorption. In slit-shaped pores of the type formed in clay mineral systems adsorption appears to occur largely by multilayer formation on the flat surfaces of the clay particles. With the filling of the pores, desorption is then governed by the curvature of the semicylindrical menisci formed. In contrast capillary condensation occurs during both the adsorption and desorption processes in porous glass. Hysteresis appears to arise partly from a delay in the formation of hemispherical menisci during adsorption and partly from the retention of liquid behind narrow restrictions during desorption.

ACKNOWLEDGMENT

This paper results from a project financed by the Australian Research Grants Committee, whose support is gratefully acknowledged.

REFERENCES

1. Zsigmondy, R., *Z. Anorg. Allg. Chem.* **71**, 356 (1911).
2. Kraemer, E. D., *in* "A Treatise on Physical Chemistry," (H. S. Taylor, ed.), p. 1661. Macmillan & Co., London, 1931.
3. McBain, J. W., *J. Amer. Chem. Soc.* **57**, 699 (1935).
4. Cohan, L. H., *J. Amer. Chem. Soc.* **60**, 433 (1938).
5. Coelingh, M. B., *Kolloid Z.* **87**, 251 (1939).
6. Foster, A. G., *Trans. Faraday Soc.* **28**, 645 (1932).
7. La Mer, V. K., *J. Colloid Interface Sci.* **23**, 297 (1967).
8. Kington, G. L., and Smith, P. S., *Trans. Faraday Soc.* **60**, 705 (1964).
9. Aylmore, L. A. G., and Quirk, J. P., *J. Soil Sci.* **18**, 1 (1967).
10. Bohor, B. F. and Hughes, R. E., *Clay Minerals* **19**, 49 (1971).
11. Aylmore, L. A. G., and Quirk, J. P., *Nature (London)* **187**, 1046 (1960).
12. Emmett, P., and DeWitt, T., *J. Amer. Chem. Soc.* **65**, 1253 (1943).
13. Amberg, C., and McIntosh, R., *Can. J. Chem.* **30**, 1012 (1952).
14. Kington, G. L., and Smith, P. S., *Trans. Faraday Soc.* **60**, 721 (1964).
15. Shull, C. G., *J. Amer. Chem. Soc.* **70**, 1405 (1948).
16. Harris, R. M., and Sing, K. S. W., *Chem. Ind.* 487 (1959).
17. Lippens, B. C., Linsen, B. G., and De Boer, J. H., *J. Catal.* **3**, 32 (1964).
18. Pierce, A. C., *J. Phys. Chem.* **72**, 3673 (1968).
19. Innes, W. B., *Anal. Chem.* **29**, 1069 (1957).
20. de Boer, J. H., *in* "The Structure and Properties of Porous Materials," p. 68. Butterworths, London, 1958.
21. Everett, D. H., *in* "The Solid–Gas Interface" (E. A. Flood, Ed.), Vol. 2, p. 1078. Dekker, New York, 1967.
22. Schofield, R. K., *Discuss. Faraday Soc.* **3**, 105 (1948).
23. Burgess, C. G. V., and Everett, D. H., *J. Colloid Interface Sci.* **33**, 611 (1970).
24. Everett, D. H., *in* "The Solid–Gas Interface" (E. A. Flood, Ed.), Vol. 2, p. 1061. Dekker, New York, 1967.
25. Flood, E. A., *in* "The Solid–Gas Interface" (E. A. Flood, Ed.), Vol. 1, p. 54. Dekker, New York, 1967.
26. Gregg, S. J., and Sing, K. S. W., "Adsorption, Surface Area and Porosity," p. 163. Academic Press, New York, 1967.
27. Giacobee, F. Aylmore, L. A. G., and Steele, W. A., *J. Colloid Interface Sci.* **38**, 277 (1972).

Clays and Clay Minerals, Vol. 22, pp. 175–183. Pergamon Press 1974. Printed in Great Britain

GAS SORPTION IN CLAY MINERAL SYSTEMS

L. A. G. AYLMORE

Department of Soil Science and Plant Nutrition, Institute of Agriculture,
University of Western Australia, Nedlands, W.A. 6009, Australia

(*Received* 14 *June* 1973)

Abstract—Sorption isotherms for four gases (N_2, A, Kr and CO_2), commonly used in specific surface area and pore structure measurements, have been accurately determined on a number of clay mineral and oxide systems.

Specific surface areas obtained by application of the BET theory to these isotherms illustrate the extent to which the apparent cross-sectional areas for these sorbed gases vary with surface structure, exchangeable cation and microporosity.

V–n plots for nitrogen adsorption on these materials using nitrogen adsorption on crystalline materials of large crystal size as a standard isotherm provide appreciable ranges of linearity in each case. The specific surface areas obtained from these straight line plots agree well with the corresponding BET values. The linearity of these plots for illite clays indicates the absence of capillary condensation and that adsorption in slit-shaped pores takes place largely by the formation of physically adsorbed layers on the surfaces.

Much larger BET specific surface areas were obtained from carbon dioxide sorption at 196°K on goethite, hematite and gibbsite than from nitrogen, argon and krypton sorption at 78°K. It is suggested that enhanced sorption of CO_2 into microporous regions of the oxides, inaccessible to the other gases, occurs in a similar fashion to that frequently observed for coal and charcoal materials. V–n plots for CO_2 sorption in these materials using that for an illite clay as a standard isotherm, support this conclusion.

Considerably lower BET specific surface areas were obtained for CO_2 sorption on kaolinite than were obtained for nitrogen, argon and krypton sorption. The shape of the V–n plots for CO_2 sorption on kaolinite compared with illite suggest that an initial specific adsorption of CO_2 on the kaolinite is followed by a change in state with the completion of this layer, allowing normal multilayer formation to proceed.

INTRODUCTION

The specific surface area and pore structure of a compacted clay system are undoubtedly two of its most important characteristics in determining both its chemical and physical interactions with its surroundings. Most chemical reactions in soils take place at the surface of the pores, and experimental studies of such reactions are almost invariably referred back to a unit area basis. Similarly the interpretation of physical properties such as swelling behavior, aggregate structure formation, and permeability requires an accurate measurement of specific surface area and a knowledge of the pore structure.

The most universally accepted method of determining the surface area of finely divided and porous materials is that of Brunauer, Emmett and Teller (1938), the BET method. A number of gases have been utilized in the application of this method to the physical adsorption of gases at low temperature. Since the method is accepted, sometimes without question, by numerous workers concerned with the properties of clays and clay minerals, it is important to establish the limits within which such acceptance can be sustained for the different gases in use.

When vapor adsorption methods were first developed, Emmett and Brunauer (1937) advocated the use of nitrogen as adsorbate, and this gas has been generally accepted as the most satisfactory. However, use of nitrogen as the primary standard has recently been questioned (Aristov and Kiselev, 1963; Pierce and Ewing, 1964), there being suggestions that the quadrupole moment of nitrogen can interact with hydroxyl or other polar groups, leading to a change in the cross-sectional area of the adsorbed molecule.

Argon adsorption at 78°K has been preferred by some workers, since this is a symmetrical non-polar atom which should be less subject to specific interactions affected by changes in the chemical nature of surfaces. However argon is less strongly adsorbed than nitrogen, raising some doubts as to whether the BET procedure provides a satisfactory estimate of the monolayer capacity ($C < 50$). Also there are strong suggestions that the effective saturation vapor pressure (p_0) for argon varies between that for solid argon above non-porous materials to that of the supercooled liquid within micro- (< 20 Å) and transitional (20—200 Å) pores (Harris and Sing, 1967; Carruthers *et al.*, 1971).

Carbon dioxide adsorption at 196°K has been favored and extensively used in studies on carbon blacks, charcoals and similar materials (Anderson, Bayer and Hofer, 1965; Walker and Kini, 1965). The surface areas obtained using carbon dioxide on these materials frequently vastly exceed those obtained by nitrogen adsorption at 78°K, indicating the presence of large volumes of microporous regions inaccessible to the less energetic nitrogen adsorption. Similar effects have been noted with the expanding lattice alumino–silicates such as montmorillonite and vermiculite (Thomas and Bohor, 1968; Aylmore, Sills and Quirk, 1970).

For the measurement of very small surface areas ($<1\ m^2\ g^{-1}$) krypton sorption at 78°K has the advantage of providing a low saturation vapor pressure at the working temp. and hence a marked reduction in the volume of unadsorbed gas which has to be corrected for (Beebe, Beckwith and Honig, 1945; Sing and Swallow, 1960). Krypton adsorption also offers the benefit that its inertness makes it unlikely that it will interact specifically with the solid surface.

Because krypton and carbon dioxide sorption at 78 and 196°K respectively, like that of argon at 78°K, take place below the bulk triple point, the use of these two gases in specific surface area measurements is likewise subject to considerable uncertainty in the correct values for saturation vapour pressure to be used in the BET analysis.

Uncertainties in the validity of the BET approach when micro- and transitional pores are present (Gregg and Sing, 1967) and in the absolute values of molecular areas and how these will vary with substrate, have led to the recent development of alternative methods for comparison of adsorption isotherms. Amongst these the *t*-method of Lippens and De Boer (1965) and similar variations (Sing, 1968; Pierce, 1968) have attracted attention as a means of interpreting vapor adsorption isotherms and characterizing the porosity of solid adsorbents. These methods involve the use of 'reduced isotherms' in which the volume adsorbed V, is plotted against the corresponding statistical thickness (t) of the adsorbed layer on a non-porous reference solid (Lippens and de Boer, 1965), or alternatively against some arbitrarily chosen parameter $V_s = V/V_x$, where V_x is the volume adsorbed at $p/p_0 = 0{\cdot}4$ (Sing, 1968). Where adsorption results entirely from monolayer–multilayer formation straight line plots with slope proportional to the surface area of the sample will be obtained. The presence of complications such as specificity in adsorption, micropore filling and capillary condensation will almost invariably result in characteristic deviations from linearity (Gregg and Sing, 1967). Pierce (1968) has pointed out the advantage of V–n plots where n is the number of statistical layers on a reference standard, since these give directly the value of V_m, while t values are themselves based on n values and involve an assumption about the thickness of an adsorbed layer.

Considerable use has been made of V–n plots to examine nitrogen sorption in a variety of materials. In the present work this approach has been used to illustrate features of both nitrogen and CO_2 sorption in clay mineral and sesquioxide systems.

MATERIALS AND METHODS

The clay samples used were obtained from the following natural deposits:

Fithian illite—From Ward's Natural Science Establishment Inc., Illite No. 35 of the American Petroleum Institute Research Project No. 49 (1951).

Willalooka illite—B horizon from a solonized solonetz: Hundred of Laffer, South Australia.

A.P.I. No. 5 kaolinite—From Ward's Natural Science Establishment Inc., Kaolinite No. 5 of the American Petroleum Institute Research Project No. 49 (1951).

In general, samples of the clays were sodium saturated by repeated washing and centrifuging with molar sodium chloride during which the pH of the suspension was adjusted to 3·0 using HCl. The samples were washed and dialysed against distilled water using Visking cellulose casing, and the $<2\ \mu m$ fractions obtained by accurate sedimentation.

Samples saturated with cesium, calcium and lanthanum were prepared from the Na saturated suspensions by repeated washing with the appropriate molar chloride solution and finally with distilled water using dialysis tubing. During this procedure extreme care was taken to ensure that no material was lost from the samples.

The air-dried clays were gently ground to a powder, equilibrated with 0·75 relative water vapor pressure and compressed into 200 mg cores to facilitate subsequent handling. Previous studies have shown that this compaction into cores has little if any effect on the specific surface area or micropore structure of the clays.

Gibbsite was prepared by adding 4 N sodium hydroxide to 1 M hydrated aluminum chloride until the pH remained constant at 4·6. The precipitate formed was heated for 2 hr at 40°C and then dialysed in cellulose bags against distilled water for 28 days.

Goethite was prepared by dissolving 400 g ferric nitrate in 1800 ml water and adding approx 1500 ml of 2·5 M sodium hydroxide solution at 60°C over a period of some 24 hr to raise the pH to 12.

To prepare hematite 100 g of ferric nitrate was placed in 400 ml of water and refluxed for 3 weeks.

The materials were air dried and lightly compressed into 200 mg cores. In each case the preparations were verified by X-ray diffraction analysis.

Sorption isotherms were determined using standard volumetric equipment based on that described by Emmett and Brunauer (1934) and including many of the refinements suggested by Harkins and Jura (1944) and Joyner (1949). In general the aluminosilicate clay minerals and hematite samples were outgassed overnight at 300°C and 10^{-6} mm mercury pressure. The goethite and gibbsite samples were outgassed at 60°C to avoid decomposition of the samples. Provided the pressure in the system remained below 10^{-3} mm mercury pressure after 20 min isolation from the pumps the sample was regarded as thoroughly outgassed.

Nitrogen, argon and krypton adsorption isotherms were determined by the usual doser technique after immersing the sample bulb in a liquid nitrogen bath. Carbon dioxide adsorption isotherms at 195°K were obtained by immersing the sample bulb in a gently stirred solid carbon dioxide–ethanol slush. In between individual isotherms the samples were outgassed overnight at room temp. Nitrogen, argon and carbon dioxide pressures were measured using a wide bore manometer and cathetometer; krypton pressures by means of a McLeod gauge. Nitrogen, argon and carbon dioxide adsorption isotherms were measured to the appropriate saturation pressures while only sufficient adsorption points to provide accurate specific surface area calculations were obtained for krypton.

RESULTS AND DISCUSSION

Isotherms

The isotherms obtained for nitrogen, argon and carbon dioxide adsorption on the various materials are shown in Figs. 1–4. For nitrogen and argon the saturation vapor pressures, measured on an appropriate vapor pressure thermometer with the bulb immersed in the bath alongside the sample bulb, have been used to calculate the relative pressure (p/p_0). For carbon dioxide and krypton the extrapolated vapor pressures for the super-cooled liquids at the temperature of the bath have been used in calculating p/p_0. The validity of this latter procedure has been discussed by various authors (Beebe *et al.*, 1945; Gregg and Sing, 1967, pp. 84 and 90). It is used here since more linear plots were obtained in applying the BET theory than when the measured saturation vapor pressure was used.

The values for specific surface areas obtained by application of the BET theory to the various adsorption isotherms using the molecular areas and saturation

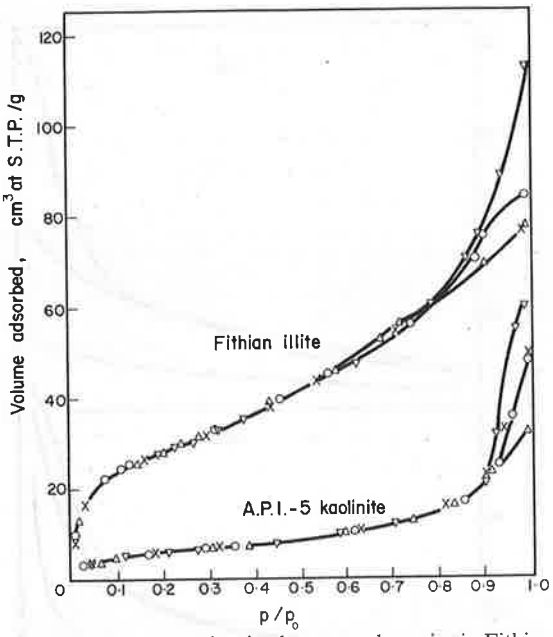

Fig. 1. Argon adsorption isotherms on homoionic Fithian illite and A.P.I.–5 kaolinite; × sodium, ○ caesium, △ calcium, ▽ lanthanum.

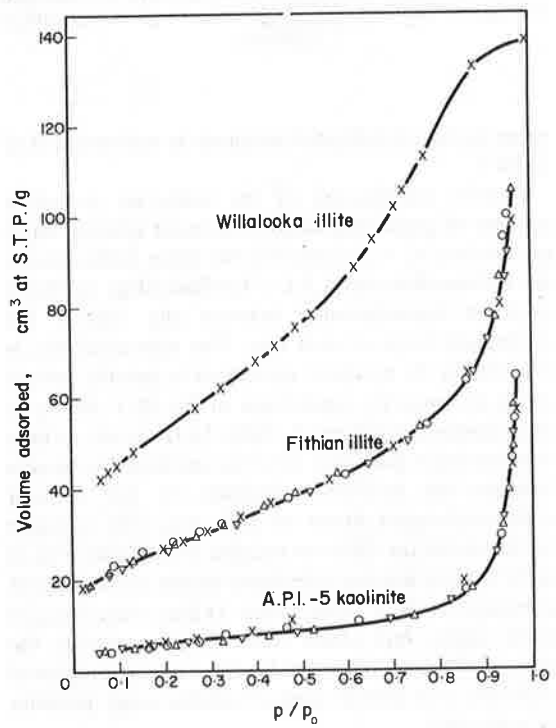

Fig. 2. Nitrogen adsorption isotherms on homoionic Willalooka illite, Fithian illite and A.P.I.–5 kaolinite; × sodium, ○ caesium, △ calcium, ▽ lanthanum.

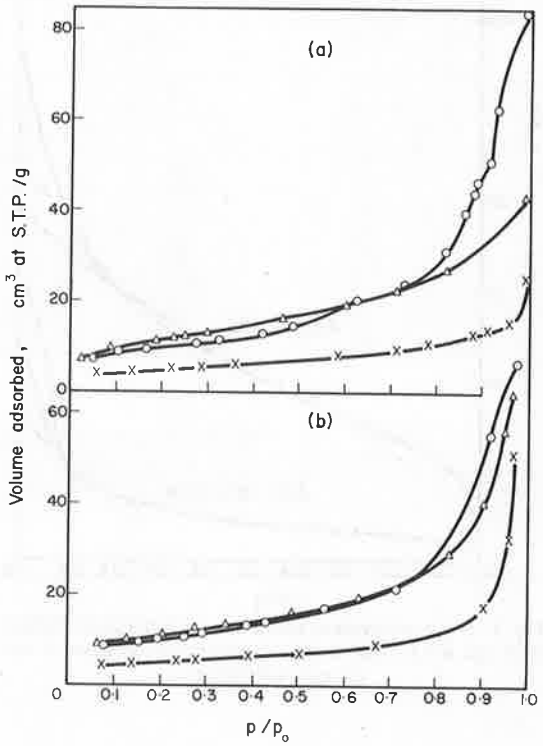

Fig. 3. (a) Argon adsorption isotherms and (b) Nitrogen adsorption isotherms on △ goethite, × hematite and ○ Gibbsite.

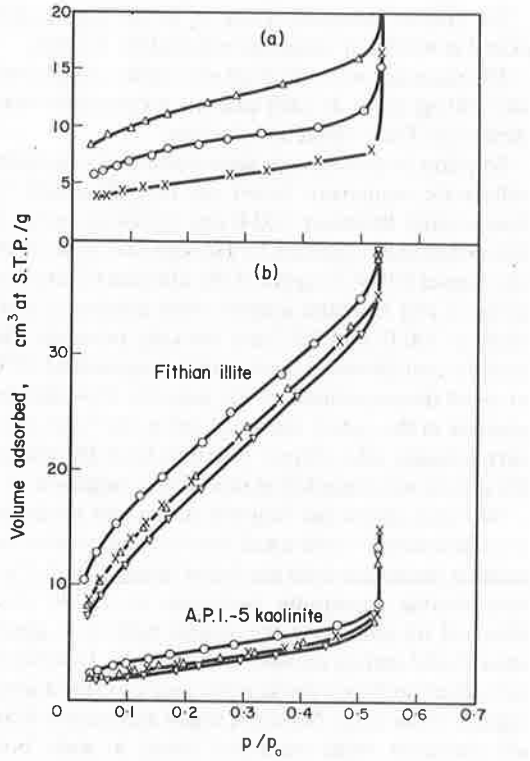

Fig. 4. Carbon dioxide adsorption isotherms on (a) △ goethite, × hematite and ○ gibbsite (b) homoionic fithian illite and A.P.I.–5 kaolinite; × sodium, ○ caesium, △ calcium, ▽ lanthanum.

vapor pressures indicated are given in columns 2–5 of Table 1.

Careful examination of the isotherms reveals a number of interesting features. At lower relative vapor pressures (p/p_0 < approx. 0·6) the argon isotherms for the Fithian illite and A.P.I.–5 kaolinite (Fig. 1) exhibit excellent reproducibility between the various ion exchanged forms of each clay. This reproducibility is reflected in the excellent agreement in specific surface areas obtained by application of the BET theory to these isotherms (column 3, Table 1). However, at high relative vapor pressures there are marked divergences between the isotherms obtained on the different cation-exchanged forms of each clay. The nitrogen isotherms for the different samples of each clay (Fig. 2) show slightly less reproducibility at low relative vapor pressures (cf. BET areas, Table 1) than was obtained using argon, but within these limits essentially the same isotherm is obtained for the various samples of each clay over the full range of relative vapor pressure to saturation.

The divergence of the argon isotherms at relative vapor pressures above the onset of capillary condensation would suggest the presence of different pore structures for the different ion exchanged forms. However, this suggestion is contradicted by the reproducibility of the nitrogen isotherms on the identical samples. A more logical explanation would seem to lie in the susceptibility of the argon sorption to changes in the effective saturation vapor pressure within porous media (Harris and Sing, 1967).

Comparison of the specific surface area results for the clay mineral samples saturated with various exchangeable cations using nitrogen and argon gases (columns 2 and 3, Table 1) suggests that the nature of the exchangeable cations has little if any significant effect on the values obtained. For each gas the variation in the specific surface areas obtained for a given clay mineral is within the limits of reproducibility normally acceptable in such measurements.

Nitrogen values are consistently higher on all materials than the corresponding values obtained for argon. Therefore, if nitrogen is taken as the standard adsorbate, larger molecular areas than 14·1 Å^2 are indicated for argon sorption on these materials. It is also evident that the relative molecular areas for nitrogen and

Table 1. Specific surface areas obtained by application of BET theory and from slope of V–n plots for gas sorption on clay materials

	Surface area ($m^2\ g^{-1}$)					
	BET				(V–n)	
Gas	N_2	A	CO_2	Kr	N_2	CO_2
Molecular area $(Å)^2$	16·2	14·1	22·1	19·5	16·2	22·1
Clay						
Sodium A.P.I.–5 Kaolinite	23·1	17·6	12·1	22·2	25·3	20·8
Caesium A.P.I.–5 Kaolinite	22·7	17·6	21·7		24·8	22·8
Calcium A.P.I.–5 Kaolinite	18·9	16·9	13·5		21·6	18·1
Lanthanum A.P.I.–5 Kaolinite	20·7	18·3	12·9		23·5	18·1
Sodium Fithian Illite	95·6	86·8	95·6	123	103	
Caesium Fithian Illite	97·2	87·4	104·4		107	94·6
Calcium Fithian Illite	96·8	89·2	94·3		103	94·9
Lanthanum Fithian Illite	87·2	87·7	86·4		101	92·5
Sodium Willalooka Illite	185		183	200	187	185
Goethite	39·2	35·9	56·3	42·0	43·8	30·4
Hematite	18·0	14·4	25·2	13·8	19·8	16·1
Gibbsite	35·2	29·5	40·9	39·3	42·0	21·7

argon change significantly with the structure of the adsorbent surface.

The most obvious discrepancies occur between the values obtained using CO_2 and those obtained using the other gases under the present assumptions for molecular areas. This is particularly noticeable in the cases of the sodium, calcium and lanthanum saturated kaolinite clays for which the carbon dioxide values are considerably lower than the corresponding nitrogen and argon values. On the other hand, the carbon dioxide areas obtained for the iron and aluminum oxides are considerably higher than the corresponding nitrogen and argon areas. In view of the larger quadrupole moment and high polarizability of the CO_2, greater variation in the area occupied by 1 molecule with variation in the structure of the adsorbent surface would be expected than for the non-polar nitrogen and argon gases. Since the sorbed carbon dioxide could be removed by outgassing overnight at room temp., it is unlikely that chemisorption contributes significantly to the observed effects. The fact that much better agreement is obtained for the three gases on the Fithian illites than for the kaolinites would suggest that the presence of hydroxyl groups on one surface of the plate shaped kaolinite crystals might somehow result in a reduced adsorption of carbon dioxide. This suggestion appears to be contradicted by the considerably higher values obtained for carbon dioxide on gibbsite and goethite. Both materials possess hydroxyl groups on their surfaces. However, a considerably higher specific surface area is also observed with carbon dioxide than with nitrogen for the hematite sample with its oxygen surfaces. This result suggests strongly that an enhanced sorption of the more energetic CO_2 into microporous regions of the oxides, inaccessible to nitrogen and argon, is occurring in a fashion similar to but less dramatic than that observed with carbon dioxide sorption on coal and charcoal materials (Anderson *et al.*, 1965; Walker and Kini, 1965). Explanations for this phenomenon (seemingly anomalous on the basis of molecular size) have been given in terms of activated diffusion of the two gases at their respective adsorption temperature. If this is the case, it is clear that interpretation of the reactivities of these materials based on nitrogen specific surface areas may be subject to some qualification. Just how the presence of hydroxyl groups would reduce so markedly the extent of physical adsorption on kaolinite is not clear.

It is interesting to note from Fig. 4(b) that for both Fithian illite and A.P.I.–5 kaolinite the sorption of CO_2 is apparently significantly dependent on the nature of the exchangeable cation, following the sequence $Cs^+ > Ca^{2+} \approx Na^+ > La^{3+}$ for both materials. Since the isotherms were not obtained in any regular sequence it is unlikely that this order results from some experimental anomaly. The constancy of the differences between the isotherms with increasing relative vapor pressure indicates that they result from initial interactions with the exchangeable ions which displace the remainder of the isotherms with respect to each other.

V–n *plots*

Nitrogen adsorption on a large number of nonporous materials has been shown to produce essentially the same isotherm when plotted in the reduced

form $n\,(=V/V_m)$ vs p/p_0 (Shull, 1948; Harris and Sing, 1959; Lippens and de Boer, 1965; Pierce, 1968). V–n plots for other materials using this 'universal nitrogen adsorption isotherm' enables deviations from simple monolayer–multilayer adsorption to be detected and the specific surface area of the sample to be calculated from the slop of the plot which yields V_m. In Fig. 5, V–n plots have been constructed for nitrogen adsorption on a number of the materials used in this study using as a standard isotherm the data provided by Shull (1948) for nitrogen adsorption on crystalline materials of large crystal size.

In each case an appreciable range of linearity of the curves is obtained and the specific surface areas obtained from these straight line regions, given in column 6, Table 1, agree well with the corresponding BET values. The linearity of these plots up to the point at which deviations occur indicates that over this region the shape of the isotherms is essentially the same as that obtained on the non-porous reference solids (Shull, 1948). That is, adsorption appears to have taken place entirely by the formation of physically adsorbed layers on the surface with no indication of capillary condensation.

In the case of the illite clays where the pores between the plate-shaped crystals are likely to be slit-shaped,

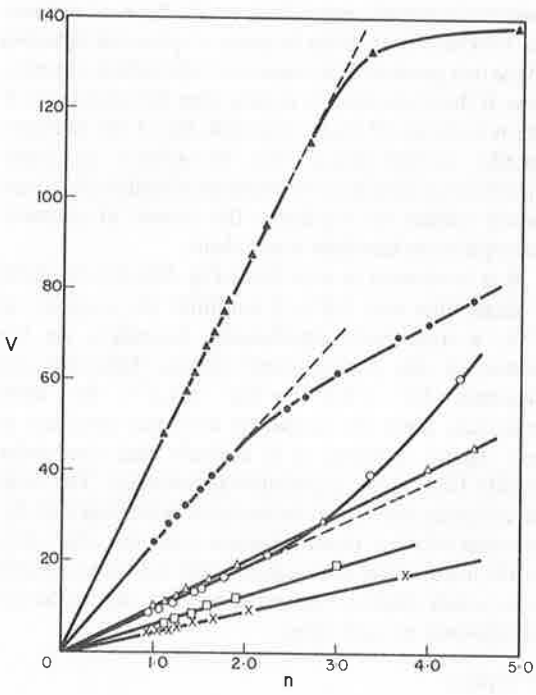

Fig. 5. V–n plots for nitrogen adsorption on ▲ sodium Willalooka illite, ● sodium Fithian illite, □ sodium A.P.I.–5 kaolinite, △ goethite, × hematite, ○ gibbsite.

filling of the pores occurs when the physically adsorbed layers merge in the center of the pore. This filling results in a reduction of the surface area available for subsequent adsorption. For the Fithian illite this point corresponds to the presence of about 2·1 layers on each surface or parallel plate separations of roughly 16 Å (taking the layer thickness as about 4 Å). Similarly for the Willalooka illite, the filling of the smallest pores is completed with approx. 2·4 layers on each surface corresponding to parallel plate separations of some 19 Å. For both materials this filling takes place at relative pressures above about 0·8.

Subsequent desorption would then occur by capillary evaporation governed by the curvature of the semi-cylindrical menisci formed. Both the previous values agree well with the lowest pore sizes indicated by pore size distribution analyses obtained by application of the Kelvin equation, in the form appropriate to semi-cylindrical menisci (Innes, 1957), to nitrogen desorption data on the same materials (Aylmore and Quirk, 1967; Aylmore, unpublished data). These pores are not emptied of capillary condensate until the relative vapor pressure is reduced to about 0·35. Thus, the hysteresis which is almost invariably observed in adsorption–desorption isotherms carried to saturation, results at least partly, for systems such as clay materials containing slit-shaped pores, from a delay in the formation of a meniscus during the adsorption process. These observations are consistent with the 'open-pore' theory of the origin of hysteresis first outlined by Foster (1932). Thus the use of desorption isotherms in pore size distribution analyses on such materials is more valid than the use of adsorption isotherms.

In contrast to the plots for the illite clays, that for gibbsite curves upwards after the initial linear region. This behavior is characteristic of materials in which enhanced sorption, above that corresponding to multilayer formation, occurs as a result of the onset of capillary condensation in transitional pores. The presence of such pores would explain the way in which the argon and nitrogen isotherms in Fig. 3 cross over the corresponding isotherms for goethite at roughly 0·65 relative vapor pressure and thereafter increase more rapidly. The V–n plots for both goethite and hematite remain linear to high n values indicating the absence of transitional pores. Pores in which such condensation occurs are more likely to approximate a cylindrical shape and a relative vapor pressure of 0·65 indicates a pore radius of 30 Å for the onset of condensation.

The apparent susceptibility to change in substrate of the molecular area for CO_2 makes it less feasible to construct a 'universal isotherm' for this gas. However,

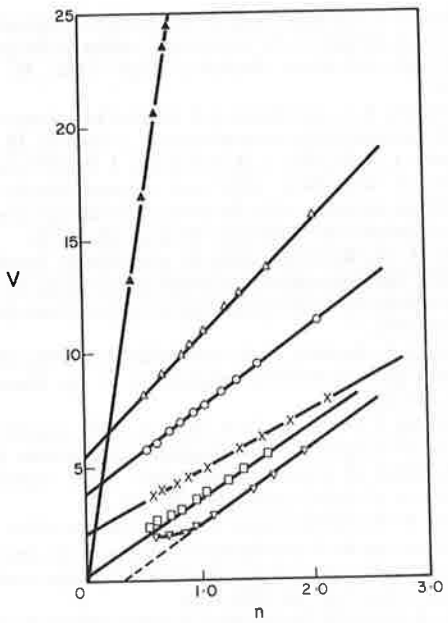

Fig. 6. V–n plots for carbon dioxide adsorption on △ goethite, × hematite, ○ gibbsite, ▽ sodium A.P.I.–5 kaolinite, □ caesium A.P.I.–5 kaolinite, ▲ sodium Willalooka illite.

an interesting comparison can be made between the various materials using the carbon dioxide isotherm on sodium Fithian illite as a standard. This isotherm was chosen because the carbon dioxide area agrees well with the nitrogen area under the present assumptions. In addition, the adsorption of carbon dioxide on Fithian illite is completely reversible up to high relative vapor pressures indicating the absence of capillary condensation. The V–n plot obtained in this way for carbon dioxide sorption on sodium Willalooka illite, shown in Fig. 6, yields a straight line passing through the origin. The specific surface area obtained from the slope agrees well with both the nitrogen and carbon dioxide BET values (Table 1). In contrast, similar V–n plots for carbon dioxide sorption on goethite, hematite and gibbsite provide good straight lines with positive intercepts on the volume axis. This behavior is characteristic of materials in which micropore filling has occurred and strongly supports the previous interpretation of the larger BET specific surface areas obtained with carbon dioxide than with nitrogen. A simple variation in molecular area with respect to that on the illite would alter the slope of the V–n plot for these materials but the plots would still pass through the origin. The specific surface areas obtained from the slopes of these lines (column 7, Table 1) are smaller than the nitrogen BET areas; however, this difference could be accounted for either by variations in molecular area or degree of accessibility to nitrogen and carbon dioxide sorption in the different materials.

The V–n plot for carbon dioxide sorption on sodium A.P.I.–5 kaolinite is equally interesting. The linear region of the plot gives a specific surface area close to that for the BET nitrogen value but intersects the abscissa. Below $n \approx 0{\cdot}9$ there is little change in sorption at least down to an n value of about 0·6. This suggests that the initial sorption of carbon dioxide on this material takes places with a considerably larger effective cross-sectional area per molecule, presumably as a result of some specific interaction, than occurs with the illite–clay. With the completion of this layer a change in state for subsequent adsorption occurs allowing normal multilayer formation to proceed. Although not shown in Fig. 6, similar effects occur with both the calcium and lanthanum saturated kaolinites. However in the case of the cesium saturated kaolinite this effect is less evident and a more normal V–n plot is obtained (Fig. 6), providing a specific surface area in excellent agreement with both the nitrogen and carbon dioxide BET values. The structure breaking properties of the large cesium ion thus appear to hinder the formation of a specifically adsorbed layer.

It is possible that the development of this dilute layer arises from an interaction between the large permanent quadrupole moment of the carbon dioxide molecule and the electric field gradient in the neighborhood of the exchangeable cations. Thus, the strength of the interaction would increase with increasing ionic charge and decrease with increasing ionic dia. Alternatively, it seems more likely that the development of a surface induced structure in the first layer of adsorbed molecules is disrupted to an extent determined by the size and frequency of cations on the surface. Although the initial adsorption of carbon dioxide on both illite and kaolinite is subject to the nature of the exchangeable cation, the sorption on kaolinite is clearly much more inhibited, despite similar surface densities of charge for both materials. This behavior is at present under more detailed study.

CONCLUSIONS

It is clear that specific surface areas obtained by application of the BET theory to gas sorption isotherms on clay mineral systems are subject to significant variations in apparent molecular areas with variations in surface structure, exchangeable cation and microporosity. Argon sorption appears the least subject to such variations at lower relative vapor pressure and is thus likely to provide the most reproducible areas by application of the BET theory. Uncertainties in the effective saturation vapor pressure for argon sorption at

higher relative vapor pressures where capillary condensation occurs, and the reproducibility of the nitrogen isotherms in this region, indicate that nitrogen is a better choice for pore size distribution analyses based on the Kelvin equation.

The range of linearity of the V–n plots for nitrogen sorption on the clay minerals indicates that adsorption in the slit-shaped pores within these systems takes place largely by the formation of physically adsorbed multilayers on the surfaces. With the filling of the pores desorption would then be governed by the curvature of the semi-cylindrical meniscii formed. Hysteresis in such systems thus results at least partly from a delay in the formation of a meniscus during the adsorption process in accord with the 'open-pore' theory.

The larger specific surface areas obtained by application of the BET theory and the positive intercepts on the volume axis in the V–n plots for carbon dioxide sorption at 196°K on goethite, hematite and gibbsite suggest the presence of micropores in these oxides, inaccessible to nitrogen, argon and krypton sorption at 78°K. Interpretations of the reactivities of these materials based on nitrogen, argon or krypton sorption would not take such micropores into account. Thus for many purposes, particularly in comparisons between similar oxides, the greater penetration and absence of capillary condensation indicated by the V–n plots for carbon dioxide sorption at 196°K, may make this gas a more appropriate adsorbate than the conventional use of nitrogen and argon.

The lower BET specific surface areas and the shape of V–n plots for carbon dioxide sorption on sodium, calcium and lanthanum saturated kaolinite suggest that an initial specific adsorption of carbon dioxide on these kaolinites is followed by a change in state for subsequent adsorption allowing normal multilayer formation to proceed.

Acknowledgements—This paper results from a project financed by the Australian Research Grants Committee whose support is gratefully acknowledged.

REFERENCES

Anderson, R. B., Bayer, J. and Hofer, L. J. E. (1965) Determining surface areas from CO_2 isotherms: *Fuel* **44,** 443–452.

Aristov, B. C. and Kiselev, A. V. (1963) Effect of dehydration of silica surface on the adsorption isotherms for gaseous nitrogen and argon: *Russian J. Phys. Chem.* **37,** 1359–1363.

Aylmore, L. A. G. and Quirk, J. P. (1967) The micropore size distributions of clay mineral systems: *J. Soil Sci.* **18,** 1–17.

Aylmore, L. A. G., Sills, I. D. and Quirk, J. P. (1970) Surface area of homoionic illite and montmorillonite clay minerals as measured by the sorption of nitrogen and carbon dioxide: *Clays and Clay Minerals* **18,** 91–96.

Beebe, R. A., Beckwith, John B. and Honig, Jurgen M. (1945) The determination of small surface areas by krypton adsorption at low temperatures: *J. Am. Chem. Soc.* **67,** 1554–1558.

Brunauer, S., Emmett, P. H. and Teller, E. (1938) Adsorption of gases in multimolecular layers: *J. Am. Chem. Soc.* **60,** 309–310.

Carruthers, J. D., Payne, D. A., Sing, K. S. W. and Stryker, L. J. (1971) Specific and non-specific interactions in the adsorption of argon, nitrogen and water vapour on oxides: *J. Colloid Interface Sci.* **36,** 205–216.

Emmett, P. H. and Brunauer, S. (1937) The use of low temperature van der Vaals adsorption isotherms in determining the surface area of iron synthetic ammonia catalysts: *J. Am. Chem. Soc.* **59,** 1553–1564.

Foster, A. G. (1932) The sorption of condensible vapours by porous solids—I. The applicability of the capillary theory: *Trans. Farad. Soc.* **28,** 645–657.

Gregg, S. J. and Sing, K. S. W. (1967) *Adsorption, Surface Area and Porosity*. Academic Press, New York.

Harkins, W. D. and Jura, G. (1944) Surface of solids X, XII and XIII: *J. Am. Chem. Soc.* **66,** 919–927.

Harris, M. R. and Sing, K. S. W. (1967) Use of argon adsorption for the determination of specific surface area: *Chem. Ind.* 757–758.

Innes, W. B. (1957) Use of a parallel plate model in calculation of pore size distribution: *Anal. Chem.* **29,** 1069–1073.

Joyner, L. G. (1958) *Scientific and Industrial Glass Blowing and Laboratory Techniques* (Edited by Barr, W. E. and Anhorn, V. J.). Chap. 12. Instruments Publishing Co., Pittsburgh.

Lippens, B. C. and de Boer, J. H. (1965) Studies on pore systems in catalysis—V. The t method: *J. Catalysis* **4,** 319–323.

Pierce, Conway (1968) The universal nitrogen isotherm: *J. Phys. Chem.* **72,** 3673–3676.

Pierce, Conway and Ewing, Bland (1964) Areas of uniform graphite surfaces: *J. Phys. Chem.* **68,** 2562–2568.

Shull, C. G. (1948) The determination of pore size distribution from gas adsorption data: *J. Am. Chem. Soc.* **70,** 1405–1414.

Sing, K. S. W. (1968) Empirical method for analysis of adsorption isotherms: *Chem. Ind.* 1520–1521.

Résumé—Les isothermes de sorption de quatre gaz (N_2, A, Kr et CO_2) utilisés couramment pour les mesures de surface spécifique et de structure des pores, ont été déterminées avec précision sur un certain nombre de minéraux argileux et d'oxydes.

Les surfaces spécifiques obtenues en appliquant la théorie de BET à ces isothermes montrent bien jusqu'à quel point les surfaces projetées apparentes de ces gaz sorbés varient avec la structure superficielle, le cation échangeable et la microporosité.

Les courbes V–n pour l'adsorption d'azote sur les matériaux étudiés, en considérant l'adsorption d'azote sur des matériaux cristallins de grande taille particulaire comme une isotherme de référence, ont des

domaines de linéarité appréciables dans chaque cas. Les surfaces spécifiques obtenues à partir de ces droites sont en accord avec les valeurs BET correspondantes. La linéarité de ces diagrammes pour les illites indique qu'il n'y a pas de condensation capillaire et que l'adsorption dans les pores en forme de fente se fait, pour une grande part, par suite de la formation de couches adsorbées physiquement sur les surfaces.

Des surfaces spécifiques BET beaucoup plus grandes qu'avec la sorption à 78°K de l'azote, de l'argon et du krypton, ont été obtenues avec la sorption du gaz carbonique à 196°K sur la goethite, l'hématite et la gibbsite. On fait l'hypothèse que la sorption accrue du CO_2 dans la microporosité des oxydes inaccessible aux autres gaz, relève d'un processus similaire à celui que l'on observe fréquemment sur les carbones et charbons de bois. Les courbes *V–n* pour la sorption du CO_2 sur ces matériaux étayent cette conclusion si l'on utilise l'illite comme isotherme de référence.

Sur la kaolinite, la sorption du gaz carbonique conduit à des surfaces spécifiques BET considérablement plus basses que celles que l'on obtient avec la sorption de l'azote, de l'argon et du krypton. La forme des courbes *V–n* pour la sorption du CO_2 sur la kaolinite comparée à l'illite suggère qu'une adsorption spécifique initiale du CO_2 sur la kaolinite est suivie par un changement d'état de cette couche adsorbée lorsqu'elle est complète, ce qui permet par la suite la formation d'un système normal à plusieurs couches adsorbées.

Kurzreferat—Sorptionsisothermen für 4 Gase (N_2, A, Kr, CO_2), die gewöhnlich für Messungen der spezifischen Oberfläche und der Porenstruktur benutzt werden, wurden für eine Anzahl von Tonmineralen und Oxidsystemen genau bestimmt. Die spezifischen Oberflächen, die durch Anwendung der BET-Theorie auf diese Isothermen erhalten wurden, illustrieren das Ausmaß, in dem die scheinbaren Querschnittsflächen für diese Gase mit der Oberflächenstruktur, dem austauschbaren Kation und der Feinporosität schwanken.

V-n-Diagramme für die Stickstoffadsorption an diesen Stoffen unter Verwendung der Stickstoffadsorption an grobkristallinem Material als Standardisotherme liefern in jedem Fall merkliche Linearitätsbereiche. Die spezifischen Oberflächen, die von diesen linearen Bereichen der Diagramme erhalten wurden, stimmen gut mit den zugehörigen BET-Werten überein. Die Linearität dieser Kurven für Illittone zeigt, daß Kapillarkondensation fehlt und daß die Absorption in spaltförmigen Poren weitgehend durch Bildung physikalisch adsorbierter Schichten an den Oberflächen stattfindet. Viel größere spezifische BET-Oberflächen wurden aus der Kohlendioxidsorption bei 196°K an Goethit, Hämatit und Gibbsit erhalten als aus der Sorption von Stickstoff, Argon und Krypton bei 78°K. Es wird angenommen, daß die verstärkte Sorption von CO_2 in die Mikroporenbereiche der Oxide, die für andere Gase unzugänglich sind, in ähnlicher Weise erfolgt, wie es häufig für Kohle und Holzkohle beobachtet wurde. *V-n*-Kurven für die CO_2-Sorption an diesen Stoffen unter Verwendung der für Illitton erhaltenen als einer Standardisotherme stützen diese Schlußfolgerung. Bedeutend geringere spezifische BET-Oberflächen wurden aus der CO_2-Sorption an Kaolinit erhalten als aus der Sorption von Stickstoff, Argon und Krypton. Die Form der *V-n*-Kurven für die CO_2-Sorption an Kaolinit im Vergleich zu Illit legt nahe, daß einer anfangs spezifischen CO_2-Sorption an Kaolinit eine Zustandsänderung mit der Vervollständigung dieser Schicht folgt, die es gestattet, daß die Bildung einer normalen Vielschicht abläuft.

Резюме — Изотермы сорбции четырех газов (N_2, A, Kr и CO_2), обычно используемых для измерения специфических площадей поверхности и структуры пор, точно определяли на ряде глинистых минералов и систем окислов. Специфические площади поверхности, полученные применением теории В.Е.Т. к этим изотермам, иллюстрируют до какой степени очевидные профили этих сорбированных газов меняются в зависимости от структуры поверхности, катионообмена и микропористости.

Для определения адсорбции азота на этих материалах построили *V–n*-диаграмму, используя адсорбцию азота на крупнокристаллических материалах в качестве стандартной изотермы и получили заметные области линейного изменения в каждом случае. Специфические площади поверхности, полученные посредством этих графиков прямых линий почти полностью соответствуют значениям В.Е.Т. Линейность этих графиков для иллитовой глины, указывает на отсутствие капиллярной конденсации и на адсорбцию в щелеобразных порах, происходящей большей частью вследствие образования на поверхности физически адсорбированных слоев.

Более крупные специфические площади поверхности В.Е.Т. были получены сорбцией угольного ангидрида при температуре 196°К на гетите, гематите и гибсите, чем от сорбции азота, аргона и криптона при температуре 78°К. Предполагают, что улучшенная сорбция CO_2 в микропоры окислов, недоступные для других газов, происходит таким же образом, как это нередко наблюдается с углем и древесным углем. *V–n*-диаграмма сорбции CO_2 на этих материалах, подтверждает этой заключение.

При сорбции CO_2 на каолине получили значительно меньшие специфические площади поверхности В.Е.Т., чем при сорбции азота, аргона и криптона. Форма *V–n*-диаграммы сорбции CO_2 на каолине по сравнению с иллитом наводит на мысль, что за начальной удельной сорбцией CO_2 на каолине следует изменение состояния слоя, допуская продолжение нормального образования свиты пластов.

Aust. J. Soil Res., 1974, **12**, 107–17

Relationship between Pore Size Distributions and Physical Properties of Clay Soils

I. D. Sills, L. A. G. Aylmore, and J. P. Quirk

Department of Soil Science and Plant Nutrition, Institute of Agriculture, University of Western Australia, Nedlands, W.A. 6009.

Abstract

Pore size distributions using mercury injection and nitrogen sorption techniques were determined on a number of soils classified as clays on the basis of particle size analysis. Some of these soils exhibit markedly different consistencies during texturing and undergo changes in texture during prolonged manipulation, e.g. subplastic, superplastic and self-mulching soils. The pore size distributions for these soils do not differ significantly from those obtained for the normal labile clay soil in the pore size range 2 nm to 50 μm. The clay soils examined, with the exception of the krasnozem, have the majority of their pore volume within pores smaller than 10 nm with the predominant pore size centred around 3 nm plate separation.

In the case of the krasnozem, the particle size analysis does not correspond to the texture assessment as a clay loam. Surface and subsoil samples of the krasnozem have high porosities and predominant plate separations of 6 nm. They consequently possess significantly different pore size distributions from the other clays. In the case of the surface sample, only a small proportion of its total pore volume is in pores smaller than 10 nm. These differences in pore structure observed between the krasnozem and the other soils examined may result from differences in mineralogy, and in particular from the high sesquioxide content of the krasnozem.

Introduction

This paper investigates the possibility of a relationship between the pore size distributions of natural soil aggregates and their physical properties as assessed by the consistency measurement of texture. The techniques used involve a combination of low temperature nitrogen sorption and mercury injection porosimetry as described by Sills *et al.* (1973).

A number of soils, classified as clay soils on the basis of particle size analysis, but exhibiting different consistencies during texturing, were chosen for investigation; these soils belong to the categories of superplastic, normally plastic, self-mulching and subplastic as described by Butler (1955). Butler observed that some 'clays' had the consistence of gravels, sands or loams and behaved accordingly in their influence on drainage. However, when manipulated during the texturing process their apparent clayiness progressively increased. After a period of some 5 min their textural behaviour conformed to the particle size analysis for heavy clay, and so these soils were designated 'subplastic'. On the other hand 'superplastic clays' progressively lost their apparent clayiness with manipulation, while self-mulching clays quickly increased their plasticity to that of a normal clay. Normal labile clay undergoes no significant change during texturing. Since the particle size distribution for these soils were similar, it was thought that differences between these four classifications of clays could result from different particle arrangements which would be reflected in their pore size distributions.

Differences between the textural assessment and particle size analysis are also observed in the krasnozems sometimes known as the Red Loam Soils which have the consistence of loams and yet are clearly clays when judged from the standpoint of their particle size analyses. This stability has been attributed to the presence of cementing materials, and pore size distributions determined on these soils could be expected to reflect the presence of such materials.

Very little work has been done using these pore size distribution techniques on natural soil aggregates, and essentially no information is available on Australian clay soils. Diamond (1970) used the mercury injection technique to examine several silt loams and silty clay loams from the U.S.A., and Nagpal *et al.* (1972) have compared the technique with water content–suction techniques on several U.S.A. soils ranging in texture from sand through to clay. Unfortunately, these investigations have been restricted to the examination of pores larger than 20 nm. On combining with the nitrogen sorption technique, the range of pore sizes covered can be extended down to 2 nm plate separation and so includes regions dominated by the clay fraction.

Materials Used

The following soils were used:

Subplastic clay III. Tharbogang loam profile 23, 122–137 cm Hanwood S. L., Griffith, N.S.W. B_{Ca} horizons of a red-brown earth (Taylor and Hooper 1938).

Self-mulching clay. Yooroobla, 0–38 cm Coleambally, from surface of a grey soil of heavy texture (Churchward and Flint 1956).

Normal labile clay. Thulabin, Vic., 15–23 cm B horizon, grey soil of heavy texture (Smith 1945).

Superplastic clay. Katandra, from a buried land surface, Axdale Creek, N.S.W. (Butler, unpublished data).

Ruthven clay loam. A virgin krasnozem with laterized clays derived from basalt as parent material from Toowoomba, Qld, and described in CSIRO Division of Soils Report 1/60.

Surface sample (0–10 cm) is a reddish brown light clay of moderate fine blocky structure 3–6 mm.

Subsoil sample (22–40 cm) of heavy clay with moderate blocky structure 6–12 mm; few pieces of very weathered basalt.

Knapdale clay. Virgin black earth from the Darling Downs, Queensland (Stace *et al.* 1968), exhibiting well-developed gilgai up to 3 m across and 4·5 m apart with 10–15 cm vertical interval.

Surface sample (0–10 cm) heavy, black clay.

Subsoil sample (10–30 cm) similar to surface.

Kimberley soil. Weaber Plains, Kimberley area of Western Australia. Western Australian Main Roads Department No. 69 Km 19. A grey soil of heavy texture.

Surface sample has considerable swelling and shrinkage properties making it a poor road base.

Subsoil sample 1·7 m below surface soil.

Preparation

Field samples of each soil were thoroughly mixed and then sieved to obtain the 2·5 mm fraction. In all cases the soils contained appreciable amounts of aggregates of this size and no crushing was required.

Experimental

Nitrogen Sorption

Conventional volumetric adsorption apparatus similar to that described by Aylmore and Quirk (1967) was used. About 1 gram of soil aggregates was heated to 300°C while under a vacuum of better than 10^{-5} torr until the pressure remained below 10^{-3} torr for 15 min while still being heated with the sample isolated from the pumps. This usually required between 8 and 16 hr outgassing. The adsorption of nitrogen with increasing pressure at 78°K was then measured in the usual way. Surface areas were obtained by application of the B.E.T. equation to the section of the adsorption isotherm between 0·05 and 0·35 relative pressure. Measurements by the authors on the present soils indicate that the specific surface area and pore size distributions obtained are not appreciably affected by the temperature of outgassing up to 300°C, provided effective outgassing is achieved.

Since it has been shown (Aylmore and Quirk 1967) that slit-shaped pores predominate in the pore space of dried clays, pore size distributions were calculated using the method of Innes (1957). This determines the plate separation from the desorption isotherm using a modification of the Kelvin equation which incorporates the thickness of the adsorbed film. The modified Kelvin equation is expressed:

$$d - 2t = -2\gamma V/\mathbf{R}T \ln p/p_0, \tag{1}$$

where d is the maximum distance of plate separation at which capillary evaporation can occur for a given relative pressure p/p_0; t is the thickness of the adsorbed layer obtained from sorption onto essentially non-porous solids (Aylmore and Quirk 1967); V is the molar volume and γ the surface tension of liquid nitrogen; $\mathbf{R}$ is the gas constant and T the absolute temperature. The concept of slit-shaped pores undoubtedly becomes less valid for pore sizes comparable with the cleavage face dimensions of the clay plates. However, the parameter 'equivalent plate separation' constitutes a useful measure of the pore dimensions, particularly for comparative purposes and is used in a similar way to the 'equivalent spherical diameter' term in applying Stokes' law to the sedimentation of particles of various shapes.

Mercury Injection

The porosimeter used to obtain the mercury injection results was constructed by the Weapons Research Establishment, Salisbury, S.A., to a design originating from the CSIRO Division of Industrial Chemistry (Ingles 1958), and has a pressure capability of $4{\cdot}83 \times 10^8$ Pa (70,000 p.s.i.). The volume of mercury injected was obtained by measuring the electrical resistance of a 0·016 cm tungsten wire strung down the capillary of the dilatometer. As the mercury level dropped, the length of wire not immersed increased, thus increasing the resistance.

Pore sizes corresponding to any pressure, P, were calculated by applying a form of the Young–Laplace equation sometimes referred to as the Jurin equation:

$$P = -\frac{2\gamma \cos \theta}{d}, \tag{2}$$

where d is the plate separation (applicable to slit-shaped pores), γ is the surface tension of mercury and θ is the angle of contact of mercury on the soil.

The value for the surface tension of mercury varies to a small degree with the purity of the mercury used. Since triple distilled mercury, free of oxide, was used, it was assumed that the surface tension would be that of pure mercury (taken as 0·480 N/m). The value of plate separation calculated from equation (2) is particularly sensitive to the angle of contact of mercury on the material being examined. The usual values employed have been either 130° (Winslow and Shapiro 1959) or 140° (Ritter and Drake 1945), and in many cases a single value has been used for a variety of substances. More recently, contact angles have been estimated on various substances, but little information has been published on soil constituents. Diamond (1970) has found values of 139° for montmorillonite minerals and 147° for illite and kaolinite minerals. However, it is possible that oxides and organic matter present in soils will modify these values and so precise values cannot be stated. In this work a value of 140° has been used for the contact angle of mercury on soil materials, since it is close to the range of values found for the common clay minerals. The soil aggregates were oven dried at 110°C before mercury injection measurements were carried out.

Table 1. Porosity, specific surface area, particle size analysis and mineralogy of soils
K, kaolinite; M, montmorillonite; H, haematite; I, illite

Soils	Porosity (c.c./g)	Surface area (m^2/g)	Particle size analysis CS (%)	FS (%)	SI (%)	C (%)	Mineralogy (< 2 μm fraction)
1 Normal labile	0·166	81	7	25	20	48	K, 40%; I, 40%
2 Self-mulching	0·180	81	3	12	14	71	K, 35%; I, 35%
3 Subplastic	0·165	61	4	37	18	41	K, 45%; I, 45%
4 Superplastic	0·146	66	11	24	13	52	K, 45%; I, 35%
Knapdale clay:							
5 Surface	0·125	49	7	29	18	40	K, 20–30%; M, 50–65%
6 Subsoil	0·110	59	5	25	17	46	K, 30–40%; M, 50–65%
Kimberley soil:							
7 Surface	0·126	72		24	23	53	M, 60%; K, 20%; I, 5%
8 Subsoil	0·126	82		1	24	75	M, 60%; K, 20%; I, 5%
Ruthven krasnozem:							
9 Surface	0·317	47	2	15	18	46[A]	K, 87%; H, 13%
10 Subsoil	0·218	67	1	12	14	69	K, 86%; H, 14%

[A] Low summation due to high organic matter content.

Porosity

Porosity determinations were carried out by immersing the aggregates in kerosene ($\rho = 0{\cdot}80$ g/cm^3) under vacuum and then touching them lightly on a piece of filter paper to remove surface liquid. The volume of kerosene absorbed was determined by oven drying to constant weight, at 110°C.

Particle Size Analysis

The mechanical analyses were determined by the method of Hutton (1955).

Mineralogy

The major clay minerals present in the soils were determined by pipetting a suspension of the clay fraction, obtained from the mechanical analyses onto a ceramic

tile and subjecting it to X-ray analysis using a Philips PW1050 diffractometer with Co Kα radiation.

Results and Discussions

Results of porosity, specific surface area, particle size analysis and mineralogical determinations for the soils are presented in Table 1. It may be noted that the Ruthven soils have clearly higher porosities than the other soils (i.e. lower bulk densities). This does not, however, appear to be related to differences in particle size analyses, since all the soils have relatively high clay contents. The clay fractions of the soils contain montmorillonite, illite or kaolinite, and in addition the Ruthven soils contain haematite.

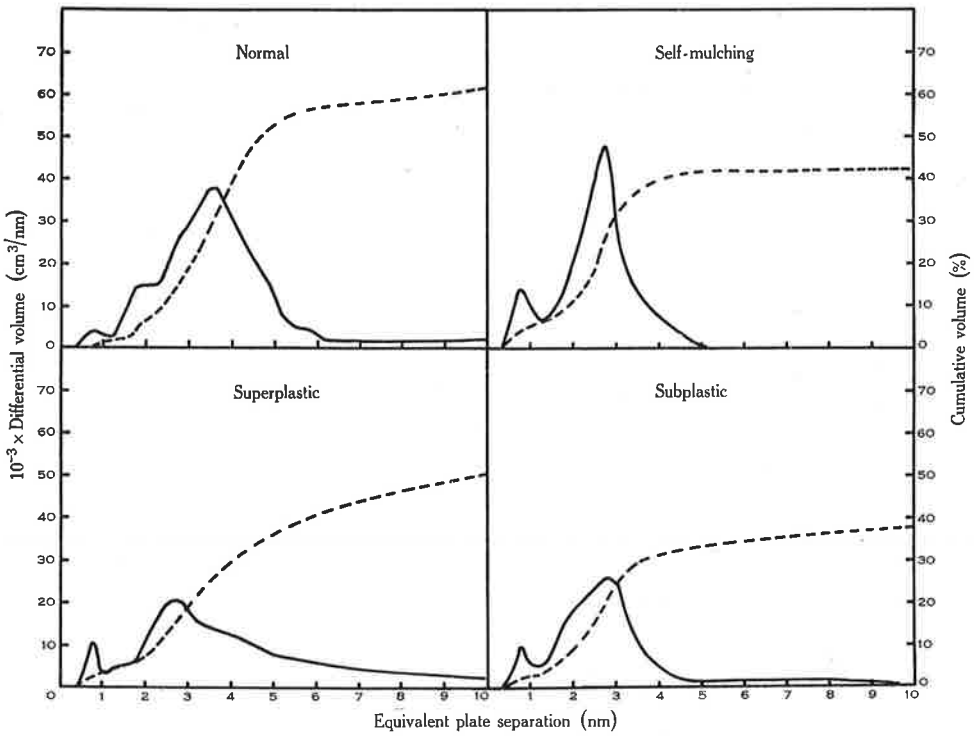

Fig. 1. Cumulative pore volume (- - - - -) and differential pore volume (———) distributions for normal labile, self-mulching, superplastic and subplastic soils.

Pore size distributions derived from the nitrogen sorption results are presented for the normal, self-mulching, superplastic and subplastic soils in Fig. 1. The dashed and solid lines represent the cumulative volumes as a percentage of the total porosity and differential curves respectively. No large differences can be seen between four soils with the exception of the differential peak exhibited by the labile soil which appears at 3·4 nm plate separation compared with the 2·8 nm observed for the other soils. In addition, the superplastic soil has a wider distribution of pore sizes than the other three.

In order to combine the mercury injection results with those from the nitrogen sorption method, it is necessary to plot the mercury injection results as unfilled pore volume versus equivalent plate separation; unfilled pore volume being the volume of

Table 2. Volume displacement needed to match the unfilled pore volume plot from the mercury injection results with the cumulative volume plot from the nitrogen results at 5 nm plate separation

Soil	Downward displacement (c.c./g)	Soil	Downward displacement (c.c./g)
Normal labile	0·021	Knapdale subsoil	0·015
Self-mulching	0·022	Kimberley surface	0·000
Superplastic	0·024	Kimberley subsoil	0·019
Subplastic	0·032	Ruthven surface	0·060
Knapdale surface	0·045	Ruthven subsoil	0·040

pores remaining empty at any given applied pressure. This means that both the mercury and nitrogen results are plotted as increasing pore volume against equivalent plate separation.

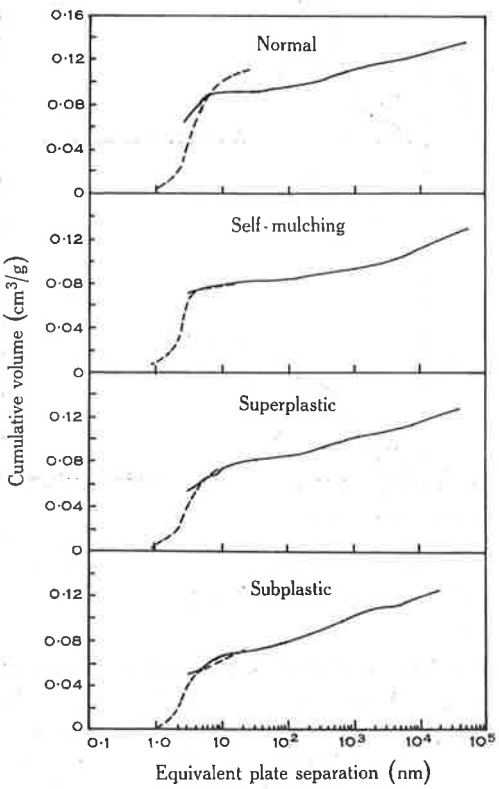

Fig. 2. Combined nitrogen sorption and mercury injection pore size distributions for normal labile, self-mulching, superplastic and subplastic soils. - - - - - - Nitrogen desorption data; ——— mercury injection data.

When this is done, the mercury curves are displaced to larger volumes compared with the nitrogen curves. This is undoubtedly due to the filling of some macroporosity (which would be included in the porosity values) by the head of mercury present at

the start of the mercury injection determinations. Since the curves are displaced with respect to volume, they are matched by a displacement of the mercury injection curve in the y direction to coincide with the nitrogen sorption curve at 5 nm equivalent plate separation. This pore size was chosen since it is well within the overlap region of both techniques. The displacement volumes necessary to achieve coincidence of the two curves are given for each soil in Table 2. It must be emphasized that this displacement is made only with respect to volume in order to compensate for that volume included in pores too large to be measured by the mercury technique used here. It does not affect the distribution of pore sizes.

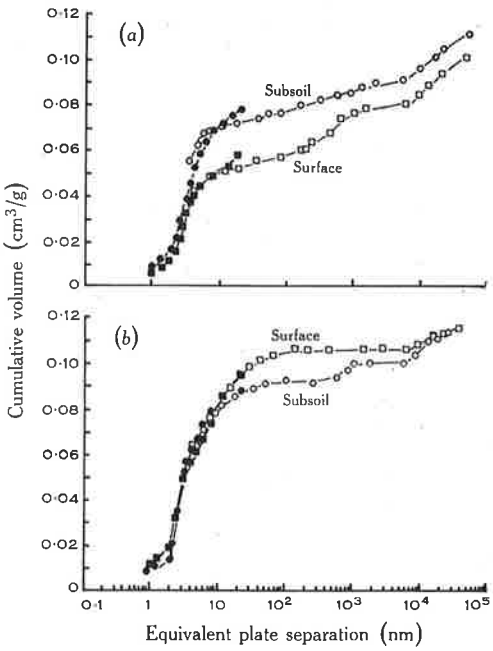

Fig. 3. Combined nitrogen sorption and mercury injection pore size distributions for (*a*) Knapdale clay; (*b*) Kimberley soil. Closed symbols, nitrogen data; open symbols, mercury data.

The combined curves are shown in Figs 2–4, and show good agreement in the overlap region leading to reasonably continuous pore size distributions from below 2 nm to 50 μm. It is interesting to note that, when a similar matching was attempted (Sills 1972) between the mercury injection results and nitrogen sorption pore size distributions calculated from the adsorption branch instead of the desorption branch of the isotherm for the same samples, smooth combined curves were not produced, and appreciable displacements of the mercury injection results were necessary to achieve coincidence at 5 nm. This evidence thus supports the view that the desorption branch of the nitrogen isotherm is the correct one to use for slit-shaped pores. This is not surprising since de Boer *et al.* (1964) obtained excellent agreement between surface areas obtained from the desorption isotherm and the B.E.T. surface areas in the case of slit-shaped pores, whereas considerable disagreement resulted from a comparison using the surface areas from the adsorption isotherm.

The combined nitrogen and mercury pore size distributions for the normal labile, self-mulching, superplastic and subplastic soils are shown in Fig. 2 and show few significant differences. In fact the surprising feature is the similarity of the distributions for soils possessing different physical properties and obtained from diverse

sites. Pore size distributions of the Knapdale and Kimberley soils are illustrated in Fig. 3, and in common with the soils in Fig. 2 these have a large proportion of the pore volume in pores smaller than 10 nm. However, the Knapdale and Kimberley soils differ from the normal, self-mulching, subplastic and superplastic soils in that the Knapdale soil has a higher proportion of its pore volume in pores larger than 10 nm, while the Kimberley soil has a smaller proportion.

It is reasonable to expect that a subsoil containing a higher proportion of clay than a surface soil would exhibit a higher volume in pores attributable to the clay fraction, in this case below 10 nm. Such a difference is in fact observed between the Knapdale surface and subsoils. In the case of the Kimberley soils the surface and subsoil distributions are in the opposite order to that expected. However, the differences are relatively small.

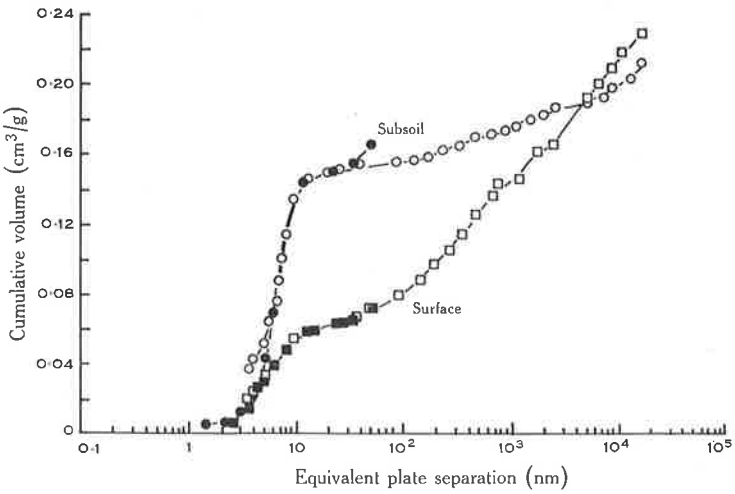

Fig. 4. Combined nitrogen sorption and mercury injection pore size distributions for Ruthven surface and subsoils. Closed symbols, nitrogen data; open symbols, mercury data.

It is still possible that the observed differences in textural classification arise partly from differences in structural organization of the soils in the wet state. However, the present data clearly indicate that any such differences are not reflected in the pore size distributions of the dried materials within the pore size range examined.

The pore size distributions of the Ruthven clay soils (Fig. 4) are significantly different from those of the other soils tested. Total pore volumes of both the surface and subsoil samples are greater than for the other clay soils. The porosity of the surface soil is derived from a wide spectrum of pores ranging from a few nm to greater than 10^4 nm. In contrast, the major proportion of the subsoil porosity is accommodated in pores smaller than 10 nm. These differences between the surface and subsoil pore size distributions could possibly be attributed to the difference in clay content (46% as against 69% for the subsoil). However, similar differences in clay content occur between the surface and subsoil samples of the Kimberley soil (53% and 75%), and yet their pore size distributions are not significantly different.

Sills *et al.* (1973) determined pore size distributions and specific surface areas on mixtures of kaolinite and illite in various proportions, and published a curve to illustrate the relationship. The lower part of this curve appears as the solid line in Fig. 5 and shows that little change in the predominant plate separation occurs in the mixtures having specific surface areas greater than 100 m^2/g. Previous investigations have shown that most high surface area clays, such as those contained in many clay soils, have plate separations of about 3 nm. With this in mind, it is interesting to compare the plate separation for the soils examined in this report with those obtained in the previous study. Since the majority of the surface area of a soil is due to the clay fraction, the surface area per gram of soil needs to be proportionally increased to a figure representing surface area per gram of clay. The method of

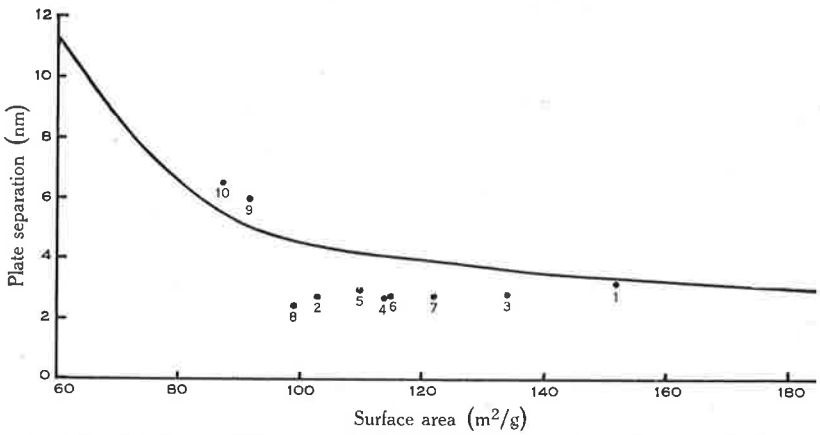

Fig. 5. Relationship between surface area and average plate separation for kaolinite-illite mixtures (solid line) and clay soils (numbered dots) calculated on 100% clay basis. 1, Normal labile; 2, self-mulching; 3, subplastic; 4, superplastic; 5, Knapdale surface; 6, Knapdale subsoil; 7, Kimberley surface; 8, Kimberley subsoil; 9, Ruthven surface; 10, Ruthven subsoil.

determining the predominant plate separation from nitrogen desorption data involves the selection of the plate separation at which the differential peak occurs. As the nitrogen desorption results only determine pores below 30 nm, pores which do not contribute significantly to surface area will not be included. The soils used here appear in Fig. 5 as dots, numbered as in Table 1, and with the exception of the Ruthven krasnozems all possess very similar plate separations ($\simeq$ 3 nm). These soils have lower plate separations than those found for the illite–kaolinite mixtures, and this may result from overconsolidation following repeated wetting and drying cycles.

The two dots (numbered 9 and 10) above the curve in Fig. 5 represent the Ruthven soils and indicate how different these are from the other clay soils examined which all fall below the curve. Although the Ruthven soils have similar physical compositions, they have principal plate separations of about 6 nm, approximately double the 3 nm plate separation of the other soils.

The reason for wide differences in pore size distributions between the krasnozem and other clay soils is not clear. Two differences in mineralogy between the Ruthven and the other clay soils are apparent. The Ruthven krasnozems are the only soils

in which kaolinite is not accompanied by significant proportions of other clay minerals, viz. illite or montmorillonite. The kaolinite in the Ruthven soil appears to be as finely divided as the clays forming the mixtures in the other soils, and the effects of these differences in the mineralogy on pore structure would require further investigation. The presence in the Ruthven soil of sesquioxides which are largely absent in the other soils, in this case oxides of iron, may contribute to the textural and structural differences. Many workers have suspected these materials of acting in the role of cementing agents. Evidence was presented by McIntyre (1956) of the relationship between macroporosity and free iron oxide content in the $< 2\ \mu m$ fraction of some terra rossa and renzina soils. Proof of this is difficult to demonstrate, as the treatment of soils with iron dissolving agents is often drastic and causes problems in interpreting results. If the cementing agents act through some mechanism like chloritization, the plate separations affected would be of the order of 0·5 nm and so are too small to be detected by the methods used. On the other hand, pores greater than 15 μm, which have been shown by Quirk and Panabokke (1962) and Quirk and Williams (1974) to be implicated in the stabilization of soils by the sorption of stabilizing agents, are largely outside the range of the apparatus used in this study. Examination of pores in this range, that is, those at the level of 'macroporosity', may best be carried out using other techniques such as light microscopy of thin sections. However, the need for an examination of a large number of sections to obtain a statistically meaningful picture does not make this method attractive.

Conclusions

It is clear that clay soils which undergo changes in texture during prolonged manipulation, e.g. subplastic, superplastic and self-mulching soils, do not differ significantly in pore structure in the range of pore sizes 2 nm to 50 μm from normal labile clay. With the exception of the krasnozems the clay soils examined have the majority of their pore volume in a narrow range of pore sizes centred around 3 nm plate separation. Above approximately 10 nm the remaining pore volume is distributed over a wide range of pore sizes.

In the case of the krasnozem, the particle size analysis does not correspond to the texture assessment as a clay loam. The pore size distributions of the surface and subsoils differ from the other clay soils examined in that the clay pore peak is centred around 6 nm, and in the case of the surface soil only a small proportion of the rather high pore volume is in pores smaller than 10 nm plate separation. Reasons for these differences are not clear, but the answer may lie in the high sesquioxide content of the krasnozems, and this question is under further investigation.

References

Aylmore, L. A. G., and **Quirk, J. P.** (1967). The micropore size distribution of clay mineral systems *J. Soil Sci.* **18**, 1–17.

de Boer, J. H., van den Heuval, A., and **Linsen, B. G.** (1964). Studies on pore systems in catalysts. IV. The two causes of reversible hysteresis. *J. Catalysis* **3**, 268–73.

Butler, B. E. (1955). A system for the description of soil structure and consistence in the field. *J. Aust. Inst. agric. Sci.* **21**, 239–49.

Churchward, H. M., and **Flint, S. F.** (1956). Soils and land use of Jernargo extension of the Berriquin Irrigation district, New South Wales. CSIRO Aust. Soils and Land Use Ser. No. 18.

Diamond, Sidney. (1970). Pore size distributions in clays. *Clays Clay Miner.* **18**, 7–23.

Hutton, J. T. (1955). A method of particle size analysis of soils. CSIRO Aust. Div. Soils, Divl. Rep. No. 11/55.
Ingles, O. G. (1958). Design and operation of a high pressure mercury porosimeter. *Aust. J. appl. Sci.* **9**, 120–6.
Innes, W. B. (1957). Use of a parallel plate model in calculation of pore size distribution. *Analyt. Chem.* **29**, 1069–73.
McIntyre, D. S. (1956). The effect of free ferric oxide on the structure of some terra rossa and renzina soils. *J. Soil Sci.* **7**, 302–6.
Nagpal, N. K., Boersma, L., and **De Backer, L. W.** (1972). Pore size distributions of soils from mercury injection porosimeter data. *Proc. Soil Sci. Soc. Am.* **36**, 264–7.
Quirk, J. P., and **Panabokke, C. R.** (1962). Incipient failure of soil aggregates. *J. Soil Sci.* **13**, 60–70.
Quirk, J. P., and **Williams, B. G.** (1974). The disposition of organic materials in relation to stable aggregation. 10th int. Congr. Soil Sci., Moscow, 1, 165–71.
Ritter, H. L., and **Drake, D. L.** (1945). Pore size distribution in porous materials. *Ind. Engng Chem., analyt. Edn* **17**, 782–91.
Sills, I. D. (1972). Distribution of pore sizes—soil and clay materials. M.Sc. Thesis, Univ. of Western Australia.
Sills, I. D., Aylmore, L. A. G., and **Quirk, J. P.** (1973). An analysis of pore size in illite–kaolinite mixtures. *J. Soil Sci.* **24**, 480–90.
Smith, R. (1945). Soils of the Berriquin Irrigation district, New South Wales. Bull. Coun. Scient. ind. Res. Aust. No. 189.
Stace, H. C. T. *et al.* (1968). 'A Handbook of Australian Soils.' (Rellim Technical Publications: Glenside, S.A.)
Taylor, J. K., and **Hooper, P. D.** (1938). A soil survey of horticultural soils in the Murrumbidgee Irrigation areas, New South Wales. Bull. Coun. scient. ind. Res. Aust. No. 118.
Winslow, N. M., and **Shapiro, J. J.** (1959). An instrument for the measurement of pore-sized distribution by mercury penetration. *Bull. Am. Soc. Test. Mater.* **236**, 39–54.

Manuscript received 29 May 1974

Plant and Soil **45**, 577–594 (1976) Ms. 2717

MEASUREMENT OF WATER FLUXES AND POTENTIALS IN A SINGLE ROOT-SOIL SYSTEM

I. THE TENSIOMETER—POTOMETER SYSTEM

by H. B. SO, L. A. G. AYLMORE and J. P. QUIRK*

SUMMARY

The construction and operation of a novel tensiometer-potometer system capable of measuring the xylem water potential and flux of water into the root is described. The validity of its measurements has been illustrated and it was shown that a unique linear relationship exists between the resistance to water flow and the water status of the root tissues.

INTRODUCTION

The flow of water to plant roots is part of a catenary process of water transport from the soil through the plant and into the atmosphere[8]. A considerable amount of investigation has been carried out on the various sections of the water flow pathway. However, the region that has received the least attention is that of the root and the soil immediately around it. Progress in this area has been limited largely because of the difficulties associated with direct experimental measurements in this region. The root—soil interface is very complicated in its geometry and furthermore changes with time.

It has long been recognised that the water potential at the root-soil interface is an important parameter as it determines to a large extent the availability of the soil water[16] and at the same time it has a large influence on the distribution of water potentials throughout the plant[14].

* Lecturer, Department of Agronomy and Soil Science, University of New England, Armidale, N.S.W.; Senior Lecturer, and Professor, Department of Soil Science and Plant Nutrition, University of Western Australia, Nedlands, W.A.

Recently increasing attention has been directed towards measurements of water potential gradients in the root-soil system and the associated root and soil resistances[3 4 5], the relative magnitudes of which have become a matter of dispute[12 13]. Except for the root psychrometer all others are destructive methods. However, it is not clear to which part of the root the potential, measured by the root psychrometer, relates.

This paper describes the construction and operation of a tensiometer—potometer capable of measuring *in situ* and simultaneously the xylem water potential, the root-soil interface water potential and the flux of water into a single root growing in soil. The use and applications of this tensiometer will be described in a second paper of this series.

METHODS AND MATERIALS

It was considered that a tensiometer could be used for measuring the root water potential if a material could be found that provides essentially immediate contact between the tensiometer and root surface. The requirement for such a material is that it should have as small a specific moisture capacity ($d\theta/d\psi$) as possible while providing a reasonably high and relatively constant conductivity, such that any disturbance by the root is transmitted almost instantaneously to the tensiometer. Hence it should act essentially as an extension of the ceramic wall of the tensiometer. It was felt that good contact between the root and this material would be obtained by growing the root into that material. With these requirements in mind the tensiometer collar was constructed as outlined below.

Construction of the tensiometer and flow collars

The construction of the collar tensiometers of 0.6 cm internal diameter is shown in the diagram of Fig. 1. Ceramic cylinders* 0.6 cm I.D., 1.2 or 2 cm long and a wall thickness of 0.2 cm were cemented with panel-metal epoxy cement** at the ends inside perspex cylinders leaving a gap between the ceramic and perspex to act as a water reservoir. This reservoir was connected to the pressure transducer system by means of $\frac{1}{8}''$ O.D. copper tubing and 'Gra-tec'*** vacuum connectors. The pressure transducer used is a Dynisco**** model PT 25-30, 0 to $\pm$ 15 psig, excited at 4 V giving an output of 1.12 μv/m bar. This was amplified with a John Fluke (Model 845 AB) microvoltmeter and recorded on a Smith's Servoscribe recorder (Fig. 2).

* Al-4, 1300°C ceramic tubes supplied by Gallard and Robinson, Sydney, N.S.W.
** Shelley's product.
*** Gra-tec Inc., Los Altos, Calif. U.S.A.
**** Dynisco Inc., Mass. U.S.A.

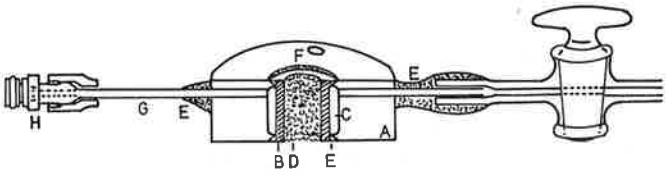

Fig. 1. Diagram of a tensiometer or flow collar.
A. Perspex cylinder; **B.** Ceramic cylinder; **C.** Water reservoir; **D.** Ceramic particles; **E.** Panel metal cement; **F.** Hole for bolt; **G.** Copper tube; **H.** Gra-tec vacuum connector.

The tensiometer's water reservoir is at the same time connected to a water supply bottle under controlled suction through a 3-way high vacuum glass tap and a calibrated glass capillary tube. When the 3-way tap is closed, the system operates as a tensiometer. However, when the 3-way tap is open to the capillary tube the system operates as a flow cell where the flux of water into the root is measured by the movement of an air bubble in the capillary tube. In such a situation the pressure transducer measures the potential of the water in the reservoir.

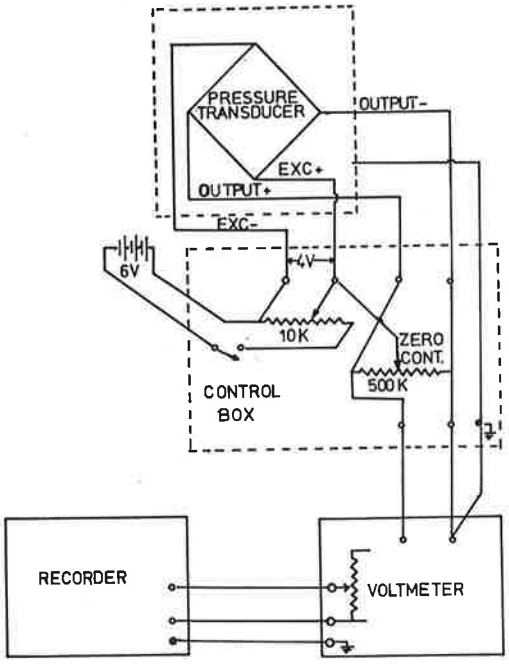

Fig. 2. Circuit diagram of the pressure transducer system.

TABLE 1

Flow parameters of the ceramic particles
$\overline{\Psi}$ = average water potential; R = resistance to water flow of ceramic particle column 1.2 cm long, 0.6 O.D. and 0.16 cm I.D.; k = conductivity for water

$\overline{\Psi}$ (cm H_2O)	*Alundum particles*		*Al-4 particles* (G. & R.)	
	R (HR cm^{-2})	k (cm HR^{-1})	R (HR cm^{-2})	k (cm HR^{-1})
− 5	1.7	1.10×10^{-1}	50	3.68×10^{-3}
−100	131	1.4×10^{-3}	73	2.54×10^{-3}
−200	602	3.03×10^{-4}	76	2.42×10^{-3}
−305	1913	9.6×10^{-5}	88	2.08×10^{-3}
−405	3348	5.5×10^{-5}	120	1.52×10^{-3}
−505	6648	2.8×10^{-5}	—	
−600			152	1.21×10^{-3}
700			264	6.95×10^{-4}

The Flow Collars are constructed in exactly the same way as the tensiometer collars but are connected directly to the water supply bottle under controlled suction through a calibrated glass capillary tubing. These collars measure the flux of water into the root under controlled suctions.

The tensiometer collar was packed with ground ceramic particles (0.25–0.5 mm). The most satisfactory materials were Alundum (Coors Porcelain, Colorado, U.S.A.) which were used for the initial experiments and Al-4, 1300°C (Gallard and Robinson, Sydney, N.S.W.) which were used for the later experiments. These materials fulfil the requirements of a very small specific moisture capacity ($d\theta/d\psi$) as shown in Figure 3 and have a relatively high and constant conductivity as shown in Table 1. The pore size distribution of Al-4 is much more uniform than that of the Alundum, hence a more constant conductivity is observed with changes in moisture potential (Fig. 4). The ceramic material was ground with a rubber pestle and the particle size 0.25–0.5 mm was found the most satisfactory.

The flow collars were packed with the same ceramic particles or soil as desired.

A series of tensiometer and flow collars make up the tensiometer-potometer system. A long thin hypodermic needle smaller than the selected root by approximately 0.1 mm, was positioned in the centre of the collars during packing and its removal provided an access hole for the root to grow through. The collars were separated by a brass washer filled with a soft mixture of paraffin oil and wax (melting point 45°C) sandwiched between two lens tissue paper smeared with the same mixture. This was necessary to prevent leakage of water between collars. A schematic diagram of the tensiometer-potometer system is shown in Fig. 5.

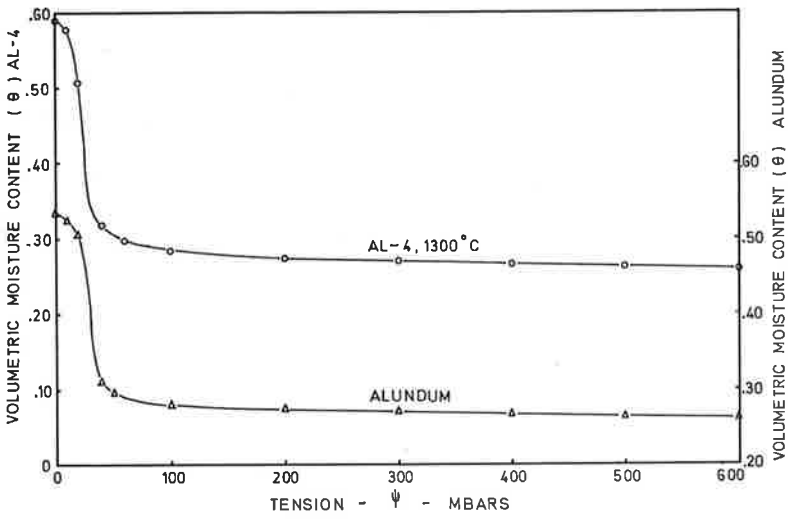

Fig. 3. Moisture characteristic curve of the ceramic particles.

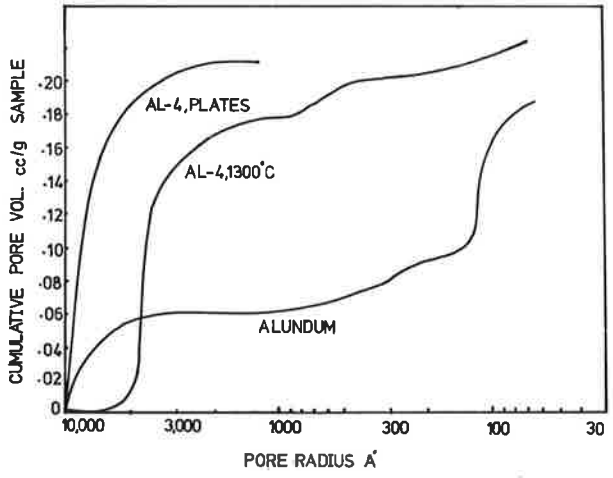

Fig. 4. Pore-size distribution of the ceramic materials used.

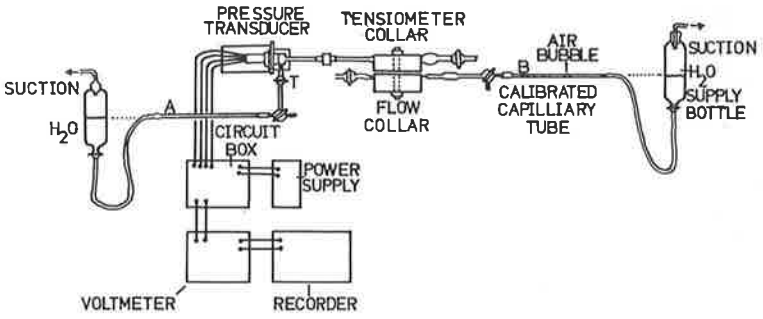

Fig. 5. Schematic diagram of the tensiometer-pressure transducer and flow collar systems in the experimental set-up.

Environmental control of the plant

A schematic diagram of the environmental control of the experimental plant is shown in Fig. 6. The aerial part of the plant is grown in a perspex cabinet ($20 \times 20 \times 30$ cm^3). Light was supplied by a bank of eight 40 W fluorescent tubes and two 200 W incandescent bulbs, at an intensity of 3500 ft. candles halfway up the cabinet for 14 hours/day. A fan driven by a toy electric motor keeps the air constantly stirred to maintain uniform conditions. Dry air was supplied at a rate of $\frac{1}{2}$ to 2 l/min and transpiration rates were measured by the increase in weight of the Si-gel trap.

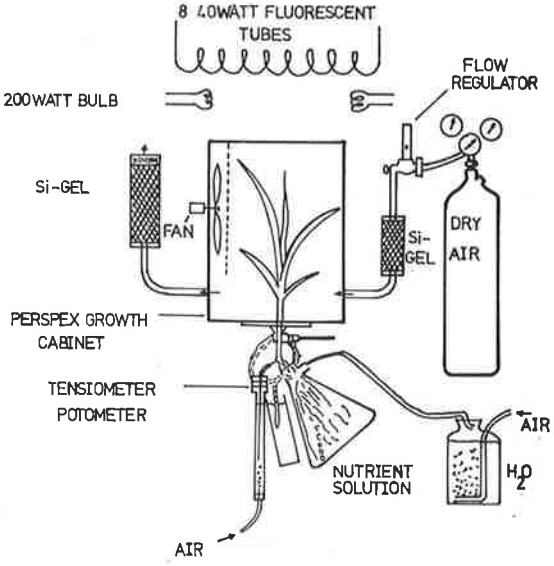

Fig. 6. Schematic diagram of the environmental control system.

TABLE 2

Composition of standard nutrient solution used

Compound	Conc. of nutrients/litre
$CaCl_2.2H_2O$	2000 μM
KNO_3	200 μM
$MgSO_4.7H_2O$	100 μM
NH_4NO_3	100 μM
$NaH_2PO_4.7H_2O$	50 μM
Fe-sequestrian	9 μM
$NaSiO_3$	100 μM
$ZnSO_4.7H_2O$	.475 μM
$(NH_4)_6Mo_7O_{24}.4H_2O$	.02 μM
H_3BO_3	.3 μM
$CuSO_4.5H_2O$	.1 μM
$CoSO_4.7H_2O$	.045 μM
$MuSO_4.H_2O$	.50 μM

The day temperature in this growth cabinet was 32.5 $\pm$ 0.5°C whereas the night temperature was equal to the room temperature of 22° $\pm$ 0.5°C.

With the exception of a preselected root, the root system was grown into a 600-ml suction flask containing aerated nutrient solution at standard or $2\frac{1}{2}$ times that of standard strength providing osmotic pressures of -106 and -266 m bars (measured on a commercial osmometer). Composition of the standard nutrient solution is given in Table 2. This solution was renewed every morning and evening to prevent significant changes in concentration. The selected root was directed vertically into the access hole by means of a curved thin polythene tube. The top of the root system and the selected root were kept moist by wrapping wet kleenex tissues around it without actually touching the roots.

Thus steady state flow of water through the plant was approximated by maintaining constant conditions throughout the day.

Plant material

The plant used was hybrid maize (supplied by Wesfarmers Tutt Bryant Pty. Ltd.) and the same batch of seeds was used for all experiments. The seeds were soaked in aerated water for 4 hours and germinated on a plastic tray containing a thick layer of kleenex wetted with 2000 μM $CaCl_2$. The tray was then covered with 'gladwrap' and kept in the dark at room temperature for 4 days after germination. This produced seedlings with $1\frac{1}{2}$–2 inches of Hypocotyl. 6 uniform seedlings with well developed root systems were selected and transferred into a gallon plastic bucket containing standard nutrient solution. The seedlings were supported by plastic foam pieces inside 1″ holes made in the top of the buckets, hence the need for long

hypocotyls. These were then grown under identical conditions of light, temperature and daylength as those grown in the growth cabinet during the actual experiments. The roots were kept at 21°C. A suitable plant was selected at the age of 20–21 days when the second crown of nodal roots were 3–5 cm long. A suitable root to use is one that has a constant diameter over its length (in contrast to some that are tapered). A plant would be selected with such a root growing in the opposite direction from the hypocotyl (which is now the section between first node and seed) since this facilitated its assembly into the experimental system.

Experiment 1: The tensiometer response time.

The response time of the tensiometer-pressure transducer system without the ceramic particles was measured by enclosing the collar in an airtight water system onto which controlled suctions can be applied. The response time with ceramic particles packed into the collar was measured by using an Alundum tube (1.6 mm O.D.) as an artificial root. A supply bottle was connected to this tube and controlled suctions can be applied to the water in this bottle.

Experiment 2: The response of the tensiometer to root water potential changes.

The tensiometer collar was embedded 3 cm down in a column of soil and a selected single root was grown into an access hole in the soil such that it grew into the center of the tensiometer. The tensiometer was drained to a 60 m bar suction to assist the root in removing the water in the interparticle pores of the ceramic bed and its response was then monitored over a period of 6 days. The main root system was grown in nutrient solution. The air supply used for this experiment involved humidity towers* with relative humidities of 33% and 76%.

Experiment 3: 2 series of 3 experiments were carried out with the potometer (tensiometer and 1 flow collar in series) packed with ceramic particles to check the validity of the tensiometer measurements. The first series was carried out with the plant in darkness to reduce transpiration to a minimum. The growth cabinet was completely covered with Al-foil for this purpose. The second series was carried out with the plants transpiring.

The tensiometer was used to monitor the xylem tensions and the flow collar or tensiometer collar was used to measure the flux of water into the root under different suctions applied to the supply bottle.

* Madden, J. J. and Nordon, P. Air supply of constant humidity. Rev. Sci. Instr. **58**, 561 (1967).

TABLE 3

Response times of the tensiometer-pressure transducer system

Change in applied suctions (S) (cm H_2O)	Response time for		
	.63 ΔS	.95 ΔS	.99 ΔS
0 to 10	1.9 sec	2.9 sec	4 sec
500 to 525*	1.6 sec	2.2 sec	4.5 sec
525 to 500*	1.4 sec	3.0 sec	5.8 sec
Exponential response	T_R	$3T_R$	$4.6T_R$

* Results are averages of three replicates.

RESULTS AND DISCUSSION

Response of the tensiometer-pressure transducer system

The tensiometer—pressure transducer system without the ceramic particles showed a very fast response to suction changes at the ceramic surface as shown in Table 3.

When packed with ceramic particles (Alundum) these particles formed essentially an extension of the tensiometer cup itself. However the response time is slower (Table 4) and a typical response curve is shown in Figure 7. These response curves are not exponential and for that reason the response time for 0.99 ΔS was used. These were less than 5 min. for the tensiometer with ceramic

TABLE 4

Response times of tensiometer and Alundum particles

S initial (cm H_2O)	S final (cm H_2O)	Response time for .99 ΔS (minutes)
20	30	4.0
30	40	2.0
0	40	3.6
40	0	3.4
0	100	1.75
100	0	4.50
100	110	0.95
100	200	2.50
200	300	1.75
400	425	1.33
500	525	4.50

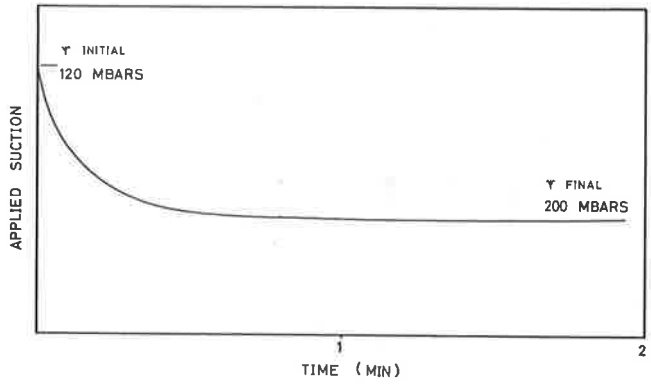

Fig. 7. Response curve of tensiometer.

particles packed into them, which was considered small enough compared to the expected slow rate of change of the root water potentials.

However, the artificial root used in this experiment has an infinite capacity to absorb or supply water to the tensiometer system and hence the tensiometer response time was determined only by the flow properties of its components as defined by the equation[7 15]:

$$T_R = 1/KS$$

where T_R = tensiometer response time
K = conductance of the tensiometer cup
S = sensitivity of the pressure gauge

A real plant root, however, does not have an infinite capacity to absorb water and therefore the rate of water uptake will tend to determine the overall response of the tensiometer-root system.

Response of the tensiometer to root water potential changes

The result of Experiment 2, presented in Figure 8, is plotted as root water tensions versus time. On the third day the tension suddenly increased sharply and continued to do so at a rate of approximately 9 mbars hour. This was due to the active portion of the root growing through the tensiometer. Since the tensiometer was approximately 3 cm away from the root tip initially, this would correspond to a root growth rate of about 1/cm day. Previously measured rates ranged from $1\frac{1}{2}$ to $2\frac{1}{2}$/cm day under similar conditions. However, the abrasive ceramic particles of the tensiometer

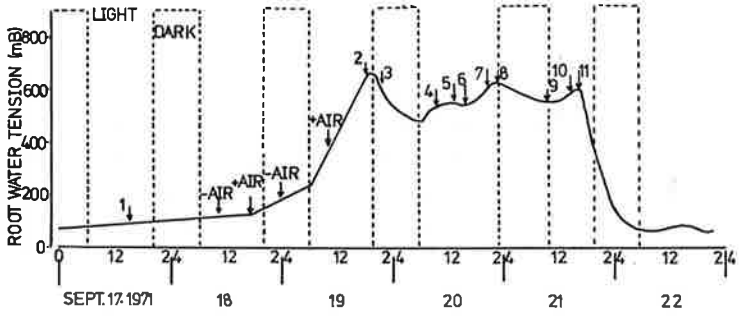

Fig. 8. Response of the tensiometer to root tension changes induced by various treatments.

offer a high resistance to deformation and would have reduced the growth rate of the root. When the lights and fan were switched on that morning the tension increased even more rapidly at approximately 23 mbars/hour, and this rate was maintained throughout the day. When the lights and fan were switched off at night the tension dropped rapidly. This did not happen on the previous night as the tensiometer was in the process of coming to equilibrium with the root water potential. A time lag of approximately $\frac{1}{2}$ hour exists between the switching off of the lights and the rapid decrease in tension. The largest effect on the root tension was that of light which was expected since light controls the stomates, a major factor in transpiration. Relatively minor effects were noticed from changing the humidity of the air. The tension dropped rapidly on the sixth day when the soil column was wetted from the bottom and it appears that free water leaked into the tensiometer, hence the rapid decrease to almost zero tension.

This preliminary experiment showed that the tensiometer did in fact respond to root water potential changes, the largest changes being associated with changes in transpiration due to opening and closing of the stomata stimulated by light. As water could only move into or out of the tensiometer through the root itself, water vapour transfer being negligible, the tensions measured must be related to those of the root. The question arises as to which part of the root was involved, the root-soil interface, the cortex or the xylem? Also, how efficient is the tensiometer in reacting to root water potential changes?

The root water potential (Experiment 3)

The tensiometer will only measure the water potential at the root surface if the epidermis is a perfect semi-permeable membrane. Although the epidermis of maize is known to have a higher resistance to water flow than the cortex[17], the existence of the root free space[1 9] proces that it is not a semi-permeable membrane. Hence it eliminates the possibility of the tensiometer measuring the root-soil water potential.

At equilibrium the tensiometer will measure the xylem water potential only if no longitudinal movement of water occurs in the cortex of the root. There is no *a priori* reason why such movement will not occur and if it occurs to a significant magnitude, then the tensiometer would measure the water potential of a point in the cortex region.

The results of the first series of tensiometer-potometer experiments are presented in Figure 9 where the tension measured by the tensiometer was plotted against time. It is obvious that it varied with light and darkness although on curves B and C the changes were relatively small. When a change in suction was applied to the flow collar adjacent to the tensiometer, no systematic or significant

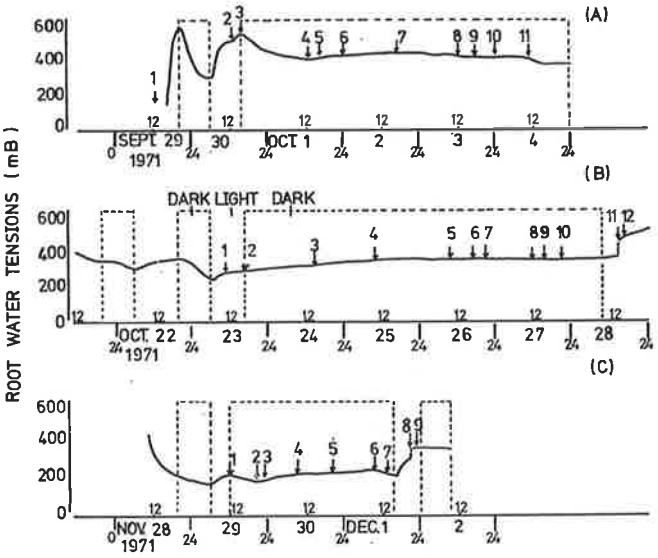

Fig. 9. Tensiometer readings with time for experimental series 1.

changes occurred in the tensiometer readings. If longitudinal movement in the cortex was significant then a change in suctions on the flow collar should be reflected by the tensiometer. The amount of water necessary to bring about such a change is very small as the volume displacement of the pressure transducer is approximately 10^{-3} cc for a full scale deflection of 1000 m bars. Therefore it was concluded that the tensiometer readings must be associated with the xylem water potential.

This conclusion can be supported by a simplified calculation of the ratio of the longitudinal and radial resistances involved. Assume a root radius r_0 of 0.5 mm. Microscopic examinations revealed that the inner radius r_i of the endodermal ring was approximately 0.2 mm. If K is the conductivity of the parenchyma cells in any direction, the longitudinal resistance R_L can be obtained from the expression of Flux $F = \Delta\psi/R_L = \pi(r_0^2 - r_i^2)K \cdot (\Delta\psi/l)$ where l is the length of the root section involved (1.2 cm for tensiometer). Thus $R_L = 18.2/K$. Similarly the radial resistance R_R can be obtained from the solution to the flow equation given by Gardner[6] as $\Delta\psi = (Q/4\pi K) \ln (r_0/r_i)^2$. Thus R_R when calculated equals 0.145/K. Therefore the ratio $R_L/R_R = 126$. Although admittedly

---

Legend to Fig. 9

CURVE A.	*CURVE B.*	*CURVE C.*
1. ⅔ of root system cut off.	1. ½ of root system cut off.	1. Lights and fan turned off.
2. Suction increased: 80 to 220 mbars	2. Lights and fan turned off.	2. S increased: 80 to 120
3. Lights and fan turned off.	3. S increased: 100 to 200	3. All roots except tested cut off.
4. All roots except tested cut off.	4. S increased: 200 to 300	4. S increased: 120 to 160
5. S decreased: 220 to 120	5. S decreased: 300 to 100	5. S increased: 160 to 208
6. S increased: 120 to 320	6. S increased: 100 to 200	6. S increased: 208 to 280
7. S decreased: 320 to 220	7. S increased: 200 to 500	7. S decreased: 280 to 120
8. S increased: 220 to 320	8. S decreased: 500 to 300	8. Tensiometer flushed and readjusted.
9. S decreased: 320 to 220	9. S decreased: 300 to 200	9. S increased: 120 to 368
10. S increased: 220 to 407	10. S decreased: 200 to 100	
11. S increased: 407 to 520	11. Tensiometer flushed and readjusted	
	12. S increased: 100 to 300	

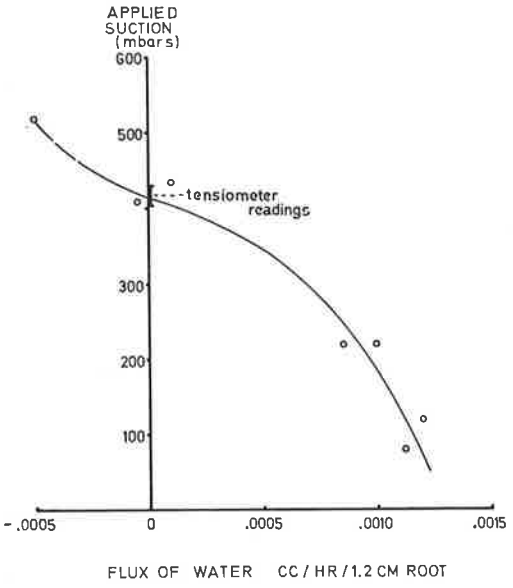

Fig. 10. Flux *vs* suction applied to the flow collar (Exp. 1).

an oversimplification, this indicates that leakage of water from adjacent collars through the cortex amounts to less than 1%.

This conclusion is further supported when the flux of water measured by the flow collar is plotted against the suction applied on that collar (Fig. 10) producing a curvilinear relationship. The tensiometer readings agree well with the suction that produced zero flux. The other two experiments were not plotted in this fashion as the fluxes were too small. It is interesting to note from Fig. 10 that when the suction applied was greater than the xylem tension, water moved out of the root, a phenomena which has been previously observed[11]. This indicates that the tensiometer should react to a decreasing as well as an increasing xylem tension.

The second series of experiments with the plants transpiring was more concerned with the flux-suction relationship. No continuous recording of the tensiometer was attempted mainly because the flow collar was not operating satisfactorily during these experiments and flux measurements were carried out on the tensiometer collar.

The results of the first two experiments were presented in Fig. 11. The horizontal lines are estimates of the errors in measurements. Here again the flux-section relationships are curvilinear and the

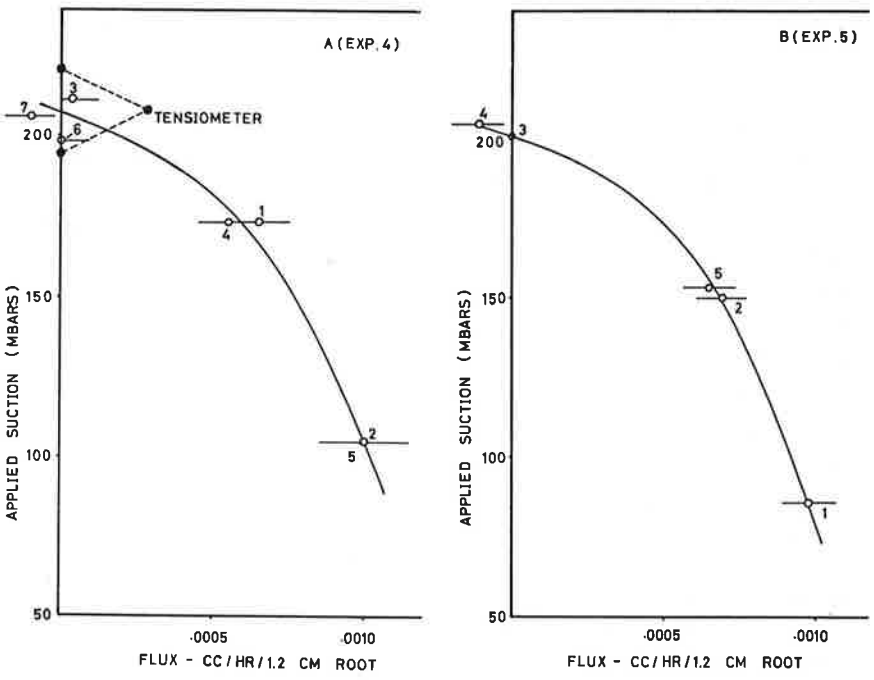

Fig. 11. Flux-suction relationships for the roots of experimental series 2.

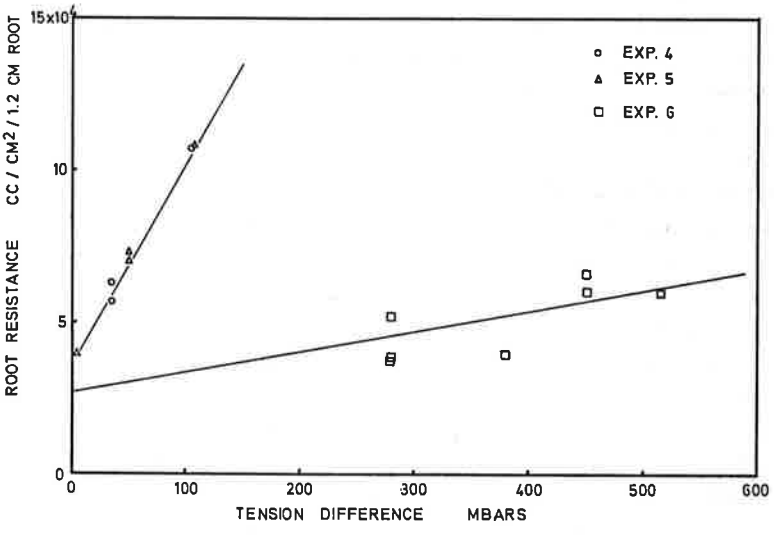

Fig. 12. Root resistance plotted against tension difference for experimental series 2.

tensiometer readings agree well with the suction producing zero flux of water.

It is obvious from Fig. 10 and 11 that within the conditions of these experiments the root tissues show a similar flux-suction relationship regardless of whether the driving force is predominantly osmotic (in the absence of transpiration) or transpirational in origin.

Curves A and B of Fig. 11 are almost identical and subsequent measurement indicates that this replication was undoubtedly fortuitous. However, each curve was in itself reproducible and did not exhibit any significant hysteresis effect, indicating the uniqueness of the flux-suction relationship. Hence a unique relationship must exist between the resistance of the root to water flow and the suction gradients across the tissues. This is a direct proof that the analogy with Ohm's law is valid for the steady state flow of water through the plant root.

When this resistance was calculated and plotted against the suction difference across the root tissue, a linear relationship is obtained as shown in Fig. 12. The correlation coefficient for each line was highly significant. The root resistance is the total resistance of the tissues of 1.2 cm of root to the radial flow of water, hence the unusual dimensions used.

Since the xylem potential remained constant, the linear relationship could also be interpreted as the resistance decreasing proportionally with increasing average tension of the root tissues. This is in agreement with observations by earlier investigators[2 10]. However, the mechanism of this reduction is not known.

The tensiometers response time

As previously discussed, the response time of the tensiometer-root system will depend largely on the flux of water into the root. This was measured at the end of the first experiment of the second series. The tensiometer was equilibrated with a suction of 100 m bars. The xylem tension was approximately 200 m bars. The capillary flow system was then cut off and the tensiometer allowed to equilibrate with the xylem tension. After 10 hours, the tensiometer finally equilibrated at 244 m bars. The amount of water drained from the ceramic particles between 100 and 224 m bars was approximately 0.007 cc estimated from its moisture characteristic curve. Thus the average rate of water uptake was roughly 0.0007 cc

h^{-1} agreeing favourably with the observed rates of uptake of curve A in Figure 11, which ranged from 0 at 206 m bars to 0.001 cc h^{-1} at 100 m bars suction.

The above calculations clearly show the dependence of response times on the ability of the root to absorb water. With higher uptake rates such as that in the last experiment of the second series (range: 0–0.01 cc h^{-1}) the response time could be reduced considerably to the order of 1 to 2 hours for 0.99 ΔS.

It is clear that with response times of this order, the tensiometer is more suitable for steady state rather than transient conditions.

In conclusion, it has been shown that the root tensiometer described in this paper is capable of measuring the xylem water potential of a plant root subjected to steady state conditions with respect to water flow. It has also been shown, that under the condition of this experiment a unique linear relationship exists between the flux of water or the root resistance to water flow and the water status of the root tissues.

ACKNOWLEDGEMENT

This work was financed by grants from the Western Australian Wheat Industry Research Committee whose support is gratefully acknowledged.

Received 30 December 1974

REFERENCES

1 Briggs, G. E. and Robertson, R. N. Apparent free space. Ann. Rev. Plant Physiol. **8**, 11–30 (1957).
2 Brouwer, R., Water absorption by the roots of *Vicia faba* at various transpiration strengths. III. Changes in water conductivity artificially obtained. Proc. Kon. Ned. Akad. Wet. **C57**, 68–80 (1954).
3 Cary, J. W. and Fischer, H. D., Plant water potential gradients measured in the field by freezing point. Physiol. Plantarum **24**, 397–402 (1971).
4 De Roo, H. C., Water stress gradients in plant and soil root systems. Agron. J. **61**, 511–515 (1969).
5 Fiscus, E. L., In situ measurements of root-water potentials. Plant. Physiol. **50**, 191–193 (1972).
6 Gardner, W. R., Dynamic aspects of water availability to plants. Soil Sci. **89**, 63–73 (1960).
7 Klute, A. and Gardner, W. R., Tensiometer response time. Soil Sci. **93**, 204–206 (1962).
8 Honert, T. H. van der, Water transport in plants as a catenary process. Dis. Faraday Soc. **3**, 145–153 (1948).

9 Kramer, P. J., Outer space in plants. Science **125**, 633–635 (1957).
10 Kuiper, P. J. C., Water transport across membranes. Ann. Rev. Plant Physiol. **23**, 157–172 (1972).
11 Müller-Stohl, W. R., The problem of water outflow from roots, *in* B. Slavik (Ed.), Water stress in plants, pp. 21–29. Czech. Acad. Sci. Prague (1965).
12 Newman, E. I., Resistance to water flow in soil and plant. I. Soil resistance in relation to amounts of root. Theoretical estimates. J. Appl. Ecol. **6**, 1–12 (1969).
13 Newman, E. I., Resistance to water flow in soil and plant. II. A review of experimental evidence on the rhizosphere resistance. J. Appl. Ecol. **6**, 261–272 (1969).
14 Philip, J. R., Plant water relation – some physical aspects. Ann. Rev. Plant Physiol. **17**, 245–268 (1966).
15 Richards, L. A., Methods of measuring soil moisture tensions. Soil Sci. **68**, 95–112 (1949).
16 Slatyer, R. O., Plant water relationships. Academic Press, London & N.Y. (1967).
17 Woolley, J. T., Radical exchange of labelled water in intact maize roots. Plant Physiol. **40**, 711–717 (1965).

Reprinted from the *Soil Science Society of America Journal*
Volume 40, no. 2, March–April 1976
677 South Segoe Rd., Madison, WI 53711 USA

The Resistance of Intact Maize Roots to Water Flow[1]

H. B. So,[2] L. A. G. Aylmore,[3] and J. P. Quirk[4]

ABSTRACT

Using a novel tensiometer-potometer system the relationship between the root resistance to water flow of maize and the water potential of the root tissue has been examined. Over the range of water potentials used a linear relation has been observed in contrast to previous observations. Calculations using published data indicate that the rhizosphere resistance is of the same order of magnitude as the root resistance when the soil moisture potential of the rhizosphere is about −1 to −2 bars.

Additional Index Words: **root resistance, xylem potential, rhizosphere resistance.**

Under steady rates of transpiration, the radial flow of water across the root tissues can be described by the relationship

$$F = \Delta\phi / R$$

where F is the radial volume flux of water per unit length of root (cm^2 hour^{-1}), $\Delta\phi$ is the difference in total water potential between xylem and external medium (mbars), and R is the radial resistance of the root tissue between xylem and external surface as a unit length of root (mbar hour cm^{-2}).

The relative magnitudes of the soil and plant resistances have been a matter of some dispute (7). However, it has not been possible to resolve this matter since the root and rhizosphere resistances could not be measured directly. Recently, we have been successful in developing a tensiometer-potometer capable of measuring in situ and simultaneously the flux of water into the root and the water potentials at the root soil interface and in the xylem of a root growing in soil. The details of the construction and operation of this equipment are described elsewhere (9). This paper briefly describes the interesting relationship observed between the root resistance to water flow and the water potential of the root tissue.

PROCEDURE

The tensiometer is based on the principle that if the tensiometer cup (in the form of a hollow cylinder, hereafter referred to as the tensiometer collar) is connected to the root surface by means of a material that has a very small specific moisture capacity ($d\theta/d\phi$) and at the same time allows a high water conductivity then this material will transmit any disturbances almost instantaneously and act sentially as an extension of the tensiometer collar itself. Ceramic aterials with uniform pores, ground to 0.25 to 0.5-mm particles ere successfully used for this purpose. The root was allowed to grow through an access channel to establish proper contact with this material. The pressure sensing device used was a sensitive strain-gauge pressure transducer (Dynisco PT 25-30, 0 to ± 15 psig). The tensiometer was filled with deaerated 100 μM $CaCl_2$ solution. Preliminary trials did not show differences in flux of water into the root when deionized water or 2000 μM $CaCl_2$ solution was used in the tensiometer.

This root tensiometer was used on the nodal roots (second crown) of 20–21 days old maize plants enabling the measurement of the root resistances as a function of root potential to be made. The aerial part of the plant was exposed to constant transpirational conditions in a small perspex cabinet of 20 by 20 by 30 cm^3. Light was supplied at an intensity of 37,800 lux (3,500 ft candles) halfway up the cabinet for 14 hours/day. A fan kept the air constantly stirred to maintain uniform conditions and dry air was supplied to the cabinet at a constant rate (0.5 to 2 liters/min). The transpiration rates were measured periodically by the increase in weight of a Si-gel trap positioned at the air outlet of the cabinet. The day temperature in the cabinet was 32.5 ± 0.5°C whereas night temperature was 22 ± 0.5°C.

The root system with the exception of a selected nodal root, was maintained in aerated nutrient solution of a standard strength in a 600-ml flask providing an osmotic potential of −106 mbars. This solution was changed twice daily. An approximately steady-state flow of water through the plant was maintained throughout the day and it was found that an essentially constant xylem potential (ϕ_x) was maintained in the selected root and this was little affected by changes in suction in the tensiometer collar. This root was grown into a tube containing the same nutrient solution after it passed the tensiometer. The tensiometer was isolated from the nutrient solution by a paraffin wax seal around the root and a small air gap to allow air (used to aerate the solution) to escape. Measurements were not made until the root had penetrated the tensiometer by approximately 4–5 cm. Later measurements showed a gradual increase in resistance with distance from the tip after this point.

Xylem Water Potential Measurement It was shown that water moves principally in the radial direction through the root tissues into the zylem and that no longitudinal flow could be detected to affect the tensiometer readings (9). Therefore, when the tensiometer is at equilibrium with the root, it measures the total water potential of the zylem vessel (ϕ_x).

Flux Measurements The tensiometer collar was also connected to a supply bottle under controlled suctions through a calibrated glass capillary tube. The flux of water could be measured by the rate of movement of an air bubble in this capillary tube. However, this system could be disconnected when the measurement of the xylem potential was desired. The suction applied

[1]Contribution from the Department of Soil Science & Plant Nutrition, University of Western Australia, Nedlands, Western Australia 6009. Received 8 May 1975. Approved 22 Dec. 1975.

[2]Lecturer, Department of Agronomy & Soil Science, Univ.of New England, Armidale, N.S.W., Aust.

[3]Senior Lecturer, Department of Soil Science & Plant Nutrition, Univ. of Western Australia, Nedlands, Western Australia 6009.

[4]Professor, Waite Agricultural Research Inst., Univ. of Adelaide, South Australia.

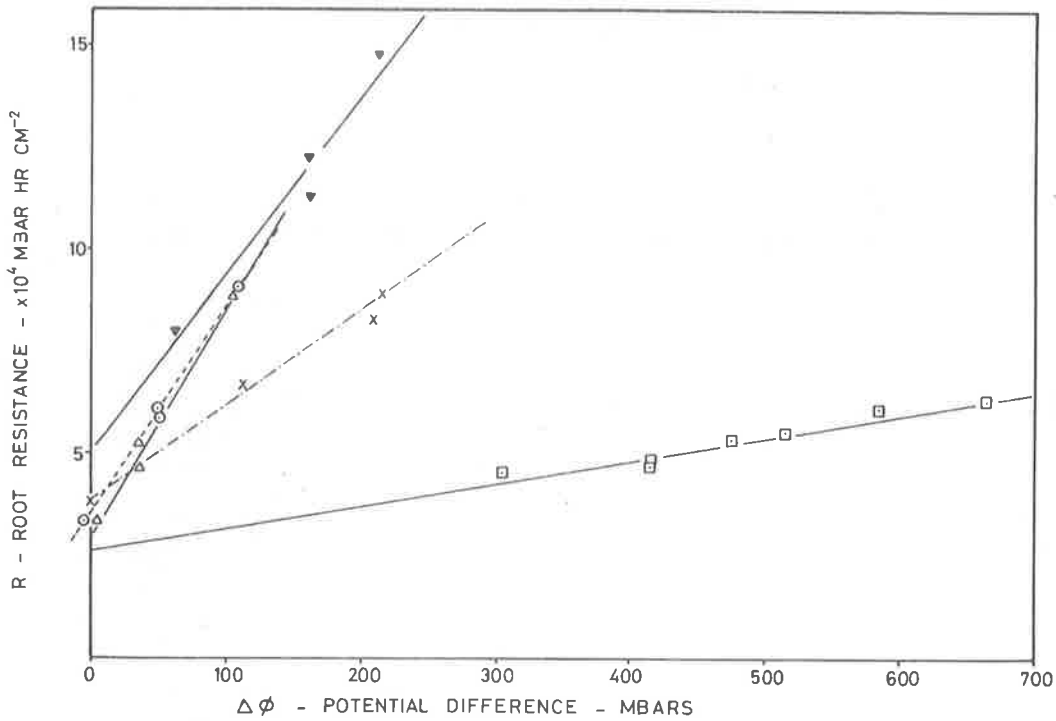

Fig. 1—Root resistance as a function of potential difference for maize roots: Plant no. 1, 0: no. 2, Δ; no. 3, □; no. 4, X; no. 5, ▼.

to the water in the supply bottle was essentially equal to the potential at the root surface (ϕ_r) since the ceramic particles offer negligible resistance relative to the root resistance. Thus the flux (F) of water into the root and the potential difference ($\Delta\phi = \phi_r - \phi_x$) between the xylem and root surface could be measured by the root tensiometer. This tensiometer has the same limitations as conventional soil tensiometers with a potential range of approximately 0 to −0.85 bars.

RESULTS AND DISCUSSIONS

The results of measurements made on roots of five different plants are shown in Fig. 1 where the radial resistance R of 1 cm of root is plotted against the potential difference $\Delta\phi$. A linear regression analysis was carried out on each set of data and the results are presented in Table 1. With the exception of root no. 5, all correlation coefficients were highly significant.

With the exception of plant no. 3, other plants were grown under identical conditions in the laboratory. However, each root has a different linear relationship between R and $\Delta\phi$. Plant no. 3 was grown in the glasshouse during the hot summer months and produced roots of the same size and features (2nd crown nodal roots) after 2 weeks as compared to 3 weeks for plants grown in the laboratory. The laboratory plants were slightly taller. During the experiments, plant no. 3 was stripped of all its roots except for the selected root which had to supply the transpirational demand of the plant. Although this demand was kept low, the plant was under stress and appeared slightly wilted during the daytime, in contrast to the other plants which remained turgid at all times. It is not clear whether the different $R - \Delta\phi$ relationship of root 3 was the result of the different growing conditions, the water stress conditions or a combination of both.

A comparison with resistances of maize roots calculated from published data is presented in Table 2. All the resistances were calculated as radial resistance (mbar hour cm^{-2}) for 1 cm of root. The values of R as measured with

Table 1—Regression equations and correlation coefficients for five maize roots.

Plant root no.	Regression equation†	Correlation coefficients	Level of significance
1	$Y = (0.0663\ X + 3.565)\ 10^4$	0.9961	$P < 0.01$
2	$Y = (0.0607\ X + 4.206)\ 10^4$	0.9988	$P < 0.01$
3	$Y = (0.0068\ X + 3.1053)\ 10^4$	0.9640	$P < 0.01$
4	$Y = (0.0273\ X + 4.64)\ 10^4$	0.9927	$P < 0.01$
5	$Y = (0.0524\ X + 6.013)\ 10^4$	0.9786	$P < 0.05$

† Y = root resistance (mbars hour cm^{-2}) and X = the potential difference across the root cortex (mbars).

Table 2— Radial root resistances of maize roots calculated from published data.

Radial root resistance, 10^4 mbar hour cm^{-2}	Type of root used	Age or size of plant	Method of measurement	Reference
1,170	Whole root system	3–4 weeks	Exudation	Newman (1973)
330	Primary root	7 days	Exudation on pre-conditioned roots	Klepper (1967)
75	Primary root	7 days	Exudation on non-conditioned roots	House & Findlay (1966)
75	Nodal root	25–30 cm tall	Potometer on transpiraing plant with all roots trimmed.	Hayward & Spurr (1944)
105	Primary root		Fluxes of water measured across a hollow segment of root with its stele removed.	Ginsburg & Ginsburg (1970)
5–15	Nodal roots	3 weeks	Tensiometer–potometer on transpiring plant	This work.

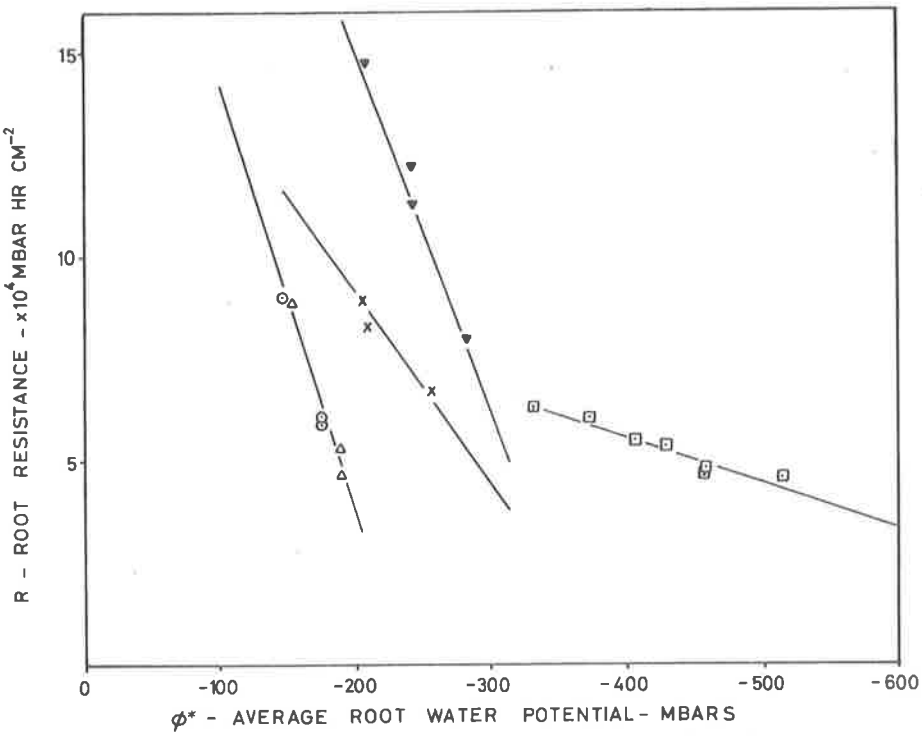

Fig. 2—Root resistance as a function of average root potential for maize roots.

the tensiometer-potometer is lower by one or two orders of magnitude to those calculated from published data. However, most of these values were obtained from exudation experiments on excised primary roots or root systems. Newman (8) used a detopped root system with a piece of the stem which may offer a large resistance to water flow. In addition, his findings include the resistance of the fine seminal root system. Hence they are not comparable to the resistance of a large single nodal root.

The measurement made by Hayward and Spurr (4) is comparable to that of the present work as the plants used were of similar size (25–30 cm high) and measurements were made with the plant transpiring and growing in a nutrient solution. Plant no. 3 in the present work had only one nodal root supporting the plant during measurement. They found that under the condition of their experiments, the xylem osmotic potential was 5.7 atm giving a very high flux of 6.6×10^{-3} cm³/hour at osmotic potentials of 0.8 atm. The resistance R calculated from their data is one order of magnitude higher than from this work. However, the plants used by Hayward and Spurr were of high salt status in contrast to the low salt status of the plants used in the present work.

Since the xylem water potential ϕ_x remained constant, a zero potential difference means that the root tissue is at a potential equal to ϕ_x, while an increasing potential difference corresponds to an increasing average root potential (ϕ_r^*).

Figure 2 shows the root resistance plotted against the average root potential. It is obvious that the linearity of the $R - \phi_x^*$ relationship cannot hold much beyond the range of the present experiments as R would soon become zero at unrealistically high values of root potentials. Obviously, zero resistance is not possible. Thus at lower potentials the root resistance should tend to level off, perhaps in a similar fashion as that of root 3 in which the change in resistance with water potential becomes much smaller. To the authors' knowledge this type of relationship has not been previously observed. The data presented suggests that different mechanisms operate in the low and high potential ranges in controlling the root resistance.

The decrease in root resistance with decreasing ϕ_{root}^* is contrary to the findings of Klepper (6) who found an increasing resistance in excised maize roots with decreasing osmotic potential of the growth medium of a decreasing ϕ_{root}^*. However, Brouwer (1) found a decreasing resistance

Table 3—The rhizosphere resistance R (mbar hour^{-1} cm^{-2}) calculated in three different soils.†

Soil moisture potential	Chino clay		Pachappa sandy loam		Superstition sand	
	Conductivity, K	Resistance, R	K	R	K	R
bars	cm hour^{-1}					
		$\times 10^4$		$\times 10^4$		$\times 10^4$
-0.2 to -0.3	1.25×10^{-4}	0.17	4.7×10^{-4}	0.05	0.84×10^{-4}	0.25
-0.5 to -0.6	1.83×10^{-5}	1.15	3.5×10^{-5}	0.60	2.1×10^{-5}	1.00
-0.8 to -1.0	0.71×10^{-5}	2.96	1.4×10^{-5}	1.50	6.25×10^{-6}	3.36
-2.0 to -4.0	3.04×10^{-6}	6.90	1.96×10^{-6}	10.70	-	
-4.0 to -8.0	1.04×10^{-6}	20.2	5.84×10^{-7}	36.00	-	

† Cylinder dimensions are 0.6 cm OD and 0.16 cm ID. Conductivity values after Gardner (1956).

in intact broad bean roots when the osmotic potential of the growth medium is decreased.

The radial resistances of rhizospheres of the same dimensions as the ceramic particle bed in the tensiometer collar were calculated using published data (2) for 3 soils with different textures. The results are presented in Table 3. It is clear that under the conditions of the present experiments the rhizosphere resistance is of the same order of magnitude as the root resistance when the soil moisture potential of the rhizosphere is about -1 to -2 bars. However, if root density is very high, the rhizosphere resistance will not become significant until the soil moisture potential becomes relatively low.

LITERATURE CITED

1. Brouwer, R. 1954. The regulating influence of transpiration and suction tension in the water and salt uptake by the roots of intact vicia faba plants. Acta. Botanica Neerl. 3:264–312.
2. Gardner, W. R. 1956. Calculation of capillary conductivity from pressure plate outflow data. Soil Sci. Soc. Am. Proc. 20:317–320.
3. Ginsburg, H., and Ginsburg, B. Z. 1970. Radial water and solute flows in roots of *Zea mays*. II. Ion fluxes across the root cortex. J. Exp. Botany. 21:593–604.
4. Hayward, H. E., and Spurr, W. B. 1944. Effects of isosmotic concentrations of inorganic and organic substrates on entry of water into corn roots. Bot. Gazette 106:131–139.
5. House, C. R., and Findlay, N. 1966. Analysis of transient changes in fluid exudation from isolated maize roots. J. Exp. Botany. 17:627–640.
6. Klepper, Betty. 1967. Effects of osmotic pressure on exudation from corn roots. Aust. J. Biol. Sci. 20:723–735.
7. Newman, E. I. 1969. Resistance to water flow in soil and plant. II. A review of experimental evidence on the rhizosphere resistance. J. Applied Ecol. 6:261–272.
8. Newman, E. I. 1973. Permeability to water of the roots of five herbaceous species. New Phytol. 72:547–555.
9. So, H. B., L. A. G. Aylmore, and J. P. Quirk. 1976. Measurement of water fluxes and potentials in a single root-soil system. I. The tensiometer-potometer system. Plant and Soil (in press).

Clays and Clay Minerals, Vol. 25, pp. 148–154. Pergamon Press 1977. Printed in Great Britain

MICROPOROSITY IN MONTMORILLONITE FROM NITROGEN AND CARBON DIOXIDE SORPTION

L. A. G. AYLMORE

Department of Soil Science and Plant Nutrition, Institute of Agriculture,
University of Western Australia, Nedlands, W.A. 6009

(*Received* 15 *August* 1976)

Abstract—Nitrogen adsorption at 78°K and carbon dioxide sorption at 195°K on homoionic lithium, sodium, caesium, calcium, lanthanum and hexane diammonium saturated montmorillonites have been examined by means of *V–n* plots. In the case of carbon dioxide, sorption on the lithium saturated clay was used as a standard for comparison of the other samples.

The nitrogen plots indicate that most of the surface area lies in super-micropores of approximately 10 Å equivalent plate separation. Variations between cations are attributed to differences in the structure of the porous matrix formed on drying rather than differences in the degree of entry into quasi-crystalline regions. While the initial sorption of carbon dioxide clearly is influenced by the solvation properties of the cations, the subsequent reversibility of the isotherms and linearity of the *V–n* plots indicates that for all but the largest cations the same sorption process is occurring on surfaces external to the quasi-crystalline regions

INTRODUCTION

Gas sorption studies on the layer lattice alumino-silicate clay minerals have provided valuable information on the surface properties of these materials and on the mechanisms of sorption processes in micro-porous systems. The montmorillonite clays are of particular interest since polar water molecules are able, in certain circumstances, to penetrate between and separate the individual alumino-silicate sheets. The extent of this swelling process varies with the nature of the exchangeable cation ranging from near complete dispersion for the sodium saturated clay to the restricted sorption of one or two layers of water molecules for clays saturated with polyvalent cations.

While the nature of the exchangeable cation has relatively little influence on the specific surface area obtained for fixed lattice clays such as illite and kaolinite, using standard gas sorption procedures (Aylmore, 1974a), wide variations in the area measured are obtained for the same montmorillonite saturated with different cations.

Aylmore and Quirk (1967, 1971) attributed this variation in area of the dry clay accessible to gas sorption to changes in the orderlinesss of packing of the montmorillonite lamellae consequent to a large extent on the degree of dispersion of the lamellae in suspension. On the other hand, Thomas and Bohor (1968) believed that essentially the same matrix structure is formed on drying regardless of the cation present but that carbon dioxide and, to a lesser extent, nitrogen, penetrate the interlamellar space to an extent determined primarily by the size and charge of the interlayer cation. Subsequently, Aylmore *et al.* (1970) have shown that the nitrogen and carbon dioxide areas obtained for montmorillonite depend markedly on the outgassing procedure used and suggested that residual water molecules facilitating the entry of sorbent molecules could explain the greater penetration observed by Thomas and Bohor (1968).

More recently, Fripiat *et al.* (1974) have presented X-ray powder diffraction and i.r. evidence supporting the interlamellar penetration of carbon dioxide in homoionic smectites although, once again, using a relatively mild outgassing procedure.

Knudson and McAtee (1974) by classifying nitrogen sorption isotherms on homoionic montmorillonite into Type I or Type II plots of the Brunauer classification, concluded that no significant interlamellar sorption occurred in the case of the sodium, barium and caesium clays. Significant interlamellar sorption of nitrogen occurred only for a narrow size range of larger exchangeable cations such as the dimethyl-ammonium and $Co(en)_3^{3+}$ ions.

In a previous paper, the author (Aylmore, 1974a) used *V–n* plots to examine the sorption of nitrogen, argon and carbon dioxide on illite and kaolinite clays and sesquioxides. In these "reduced" isotherms the volume sorbed is plotted against the number of statistical layers which would be sorbed on a non-porous material at the same relative vapor pressure, thus allowing any variation from normal multilayer adsorption to be observed. A similar approach is used here to analyse sorption isotherms for nitrogen and carbon dioxide on homoionic montmorillonites.

EXPERIMENTAL

Sorption isotherms were determined on homoionic samples prepared from the following natural montmorillonite deposits:

Wyoming bentonite–montmorillonite from the John C. Lane Tract, Upton, Wyoming. Standard clay

as an index mineral that links the Al-Hasa region with neighbouring regions having geological and mineralogical similarities.

Eastern Saudi Arabia is geologically linked, in terms of parent material and age, with the arid and semi-arid regions of Iraq, Syria and east of the Mediterranean. Attapulgite, in association with kaolinite, chlorite and mica, is of common occurrence in Syrian desert soils and is believed to originate, with little alteration, from the underlying limestone parent material (Muir, 1951). Montmorillonite without attapulgite was found on basaltic soils. Jordanian and north Lebanese soils along the Syrian border contain attapugite.* It is then evident that attapulgite occurs in association with limestone parent material over a large arid or semi-arid region extending from east of the Mediterranean through Syria, Iraq, and eastern Saudi Arabia. The mineral may be formed from lagoonal deposits or pyroxenes and amphiboles through hydrothermal action (Caillere and Hein, 1961), derived from the underlying limestone with no alteration (Muir, 1951) and in lagoonal deposits and dry desert lakes (Grim, 1968; McLean *et al.*, 1972). Although pedogenic origin of attapulgite has been reported (Vanden Heuvel, 1966) more evidence indicates lacustrine or alluvial origin (McLean *et al.*, 1972; Millot, 1970; Parry and Reaves, 1968). In Al-Hasa, extensive large gravels consisting of quartz, various types of igneous and metamorphic rocks and limestone boulders derived from Tuwayq mountains 400 km inland, suggest rapid erosion of the interior in the Miocene age as a result of eastward tilting of the Arabian foreland (Powers *et al.*, 1963). Al-Hasa shows some distinguishing criteria of lacustrine deposits, but in the light of the wide occurrence of attapulgite in areas most commonly related by parent material, an alluvial origin is more likely.

Some clay samples from the bottom of the soil profiles and the beds in the outcrop were found to be rich in montmorillonite, with varying amounts of attapulgite. Although evidence suggests the weathering of attapulgite to montmorillonite (Jackson, 1964; Mumpton and Roy, 1958; Millot, 1972) no trace of montmorillonite was found in the desert calcareous attapulgite rich soils of Syria (Muir, 1951) where rainfall is about three times that of Al-Hasa. It seems likely that the predominance of a certain mineral or mineral group in the beds and the clay layers underlying the soils reflect a particular sediment source and that since deposition minimum alteration has taken place in this area of extreme aridity.

* A. H. Sayegh, unpublished data.

REFERENCES

Caillere, S. and Henin, S. (1961) Sepiolite and palygorskite: in *X-ray Identification and Crystal Structure of Clay Minerals* (Edited by G. Brown). Mineralogical Society, London.

Grim, R. W. (1968) *Clay Mineralogy*: McGraw-Hill, New York.

Jackson, M. L. (1956) *Soil Chemical Analysis—Advanced Course*: Published by the author, Dept of Soil Science, University of Wisconsin, Madison.

Jackson, M. L. (1964) Soil clay mineralogical analysis: in *Soil Clay Mineralogy* (Edited by C. I. Rich and G. W. Kunze). The University of North Carolina Press, Chapel Hill.

McLean, S. A., Allen, B. L. and Craig, J. R. (1972) The occurrence of sepiolite and attapulgite on the Southern High Plains: *Clays & Clay Minerals* **20,** 143–149.

Millot, G. (1970) *Geology of Clays*: Springer Verlag, New York.

Mitchel, R. C. (1957) Notes on the geology of Western Iraq and Northern Saudi Arabia: *Geol. Rundschau* **46**(2), 476–493.

Muir, A. (1951) Notes of Syrian soils: *J. Soil. Sci.* **2.** 163–183.

Mumpton, F. A. and Roy, R. (1958) New data on sepiolite and attapulgite: *Clays and Clay Minerals*, National Academy of Science. National Research Council, **566.** 136–143.

Parry, W. T. and Reeves, C. C. (1968) Clay mineralogy of pluvial lake sediments, Southern High Plains, Texas: *J. Sediment. Petrol.* **38.** 516–519.

Powers, R. W., Ramirez, L. F., Redmond, C. D. and Elberg, E. L. (1963) Geology of the Arabian Peninsula: sedimentary geology of Suadi Arabia. *Geol. Survey Professional Paper 560D* pp. D93–D94.

Sayegh, A. H., Alban, L. A. and Paterson, R. C. (1958) A sampling study in a saline and alkali area: *Soil Sci. Soc. Am. Proc.* **22** (3), 252–254.

Saxon, A. (1968) *Situation of the Irrigated Agriculture in the Eastern Province of Saudi Arabia*: Saudi German Research, Publication No. 1, Riyadh.

Stewart, D. and The Editors of Life (1962) *The Arab World*: Time Inc., New York.

Theisen, A. A. and Harward, M. E. (1962) A paste method for the preparation of slides for clay mineral identification by X-ray diffraction: *Soil Sci. Soc. Am. Proc.* **26.** 90–91.

Vanden Heuvel, R. C. (1966) The occurrence of sepiolite and attapulgite in the calcareous zone of a soil near Las Cruses, New Mexico: *Clays & Clay Minerals* **13,** 193–207.

mineral No. 25b of the American Petroleum Institute Research Project No. 49.

Redhill montmorillonite—from Redhill, Surrey, England: supplied by Fullers Earth Company.

Homoionic samples of the $< 2\,\mu m$ fractions were prepared as previously described (Aylmore, 1974a) and compressed into 200 mg cores to facilitate experimental handling.

Gas sorption isotherms were determined by the usual doser technique after outgassing the samples overnight, usually at 250°C and 10^{-6} mm mercury pressure. Previous studies (Aylmore, 1960) have shown that this procedure has no significant effect on the swelling behavior of the montmorillonites. The sample saturated with hexane diammonium ions was outgassed initially for 2 days at 50°C to prevent the destruction of the organic cation and then at increasing temperatures to 250°C causing the gradual destruction of the large organic cations.

Sorption isotherms were determined with the sample bulb immersed in a liquid nitrogen bath for nitrogen sorption and in a gently stirred solid carbon dioxide–ethanol slush for carbon dioxide sorption.

RESULTS AND DISCUSSION

Nitrogen sorption

V–n plots for nitrogen adsorption on lithium, sodium, caesium, calcium and lanthanum saturated Wyoming bentonite and on sodium, calcium and caesium saturated Redhill montmorillonite are shown in Figures 1 and 2, respectively. Values of *n* were calculated using a standard isotherm constructed from a combination of the data provided by Shull (1948) for

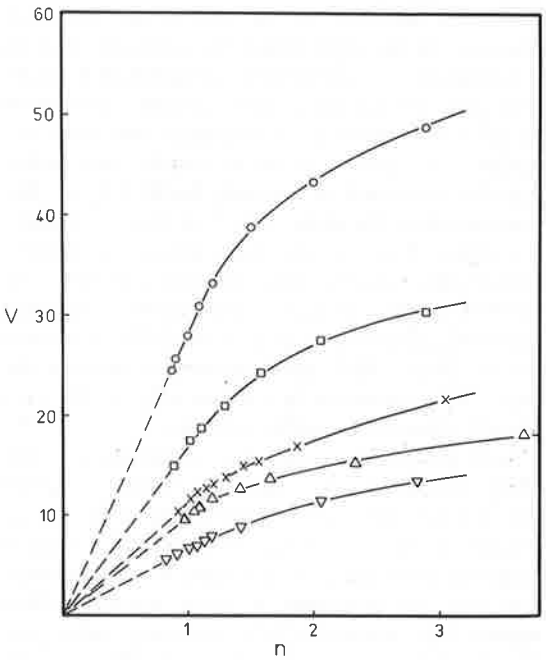

Figure 1. *V–n* plots for nitrogen adsorption on homoionic Wyoming bentonite: × sodium, □ lithium, ○ caesium, △ calcium, ▽ lanthanum.

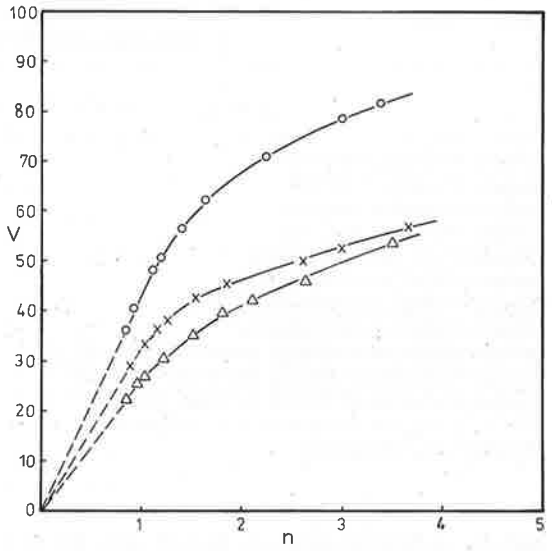

Figure 2. *V–n* plots for nitrogen adsorption on homoionic Redhill montmorillonite: × sodium, ○ caesium, △ calcium.

nitrogen adsorption on crystalline materials of large crystal size and similar measurements obtained in these laboratories.

For systems such as these clay minerals, containing essentially slit-shaped pores, linear regions in *V–n* plots indicate that within these regions the shape of the isotherm is essentially the same as that obtained on the non-porous reference solids and that unrestricted physical adsorption is occurring on the flat surfaces of the clay plates. A negative curvature occurs when the area available for sorption is reduced as a result of the filling of smaller pores by the merging of sorbate layers. Conversely, enhanced sorption as a result of capillary condensation will result in a positive curvature of the *V–n* plot.

In each case, the plots extrapolate readily through the origin and the specific surface areas calculated from the slope of the initial linear regions agree well with, although generally slightly higher than, those obtained by application of the BET theory (Table 1). Following this initial linear region, there is a gradual reduction in slope commencing in each case at approximately $n = 1.2$. Thus at $n = 1$ all the surface area accessible to nitrogen should be covered with a complete layer of nitrogen molecules. Assuming a value of some 4 Å for the thickness of a single layer of adsorbed molecules, a negative deviation in slope at $n = 1.2$ would, in a system containing essentially only slit-shaped pores, suggest that the smallest pores present were of some 10 Å plate separation.

Comparative plots of the data in the linear forms of the Brunauer Type I (or Langmuir) and Type II (or BET) equations [e.g. Figure 4(a) for Cs^+ Wyoming bentonite] support the consistent agreement of the sorption process for nitrogen on these homoionic montmorillonites with the multilayer theory, as observed by Knudson and McAtee (1974), rather than

Table 1. Specific surface areas obtained by application of BET theory and from slope of V–n plots for gas sorption on homoionic montmorillonites. Surface area (m^2/g)

Clay	N_2		CO_2	
	BET	(V–n)	BET	(V–n)
Lithium Wyoming bentonite	63	72	87	—
Sodium Wyoming bentonite	42	49	59	44
Caesium Wyoming bentonite	112	122	249	—
Calcium Wyoming bentonite	45	42	54	39
Lanthanum Wyoming bentonite	30	28	48	32
Sodium Redhill montmorillonite	120	141	150	142
Caesium Redhill montmorillonite	170	189	220	—
Calcium Redhill montmorillonite	99	114	115	101
Hexane diammonium Redhill montmorillonite (50°C)*	240	283	298	—
Hexane diammonium Redhill montmorillonite (200°C)	104	128	—	—
Hexane diammonium Redhill montmorillonite (250°C)	50	56	—	—

* Outgassing temperature.

with the monolayer equation. In each case, the BET plots provide good straight lines whilst the Langmuir plots show marked negative curvature, indicating that considerably more sorption is occurring than corresponds to monolayer formation. Such plots are not particularly sensitive to small variations but should be adequate to judge the predominant process.

Knudson and McAtee (1974) reported that for montmorillonite saturated with large dimethylammonium or $Co(en)_3^{3+}$ ions, comparative plots of the BET and Langmuir functions indicated that significant interlamellar sorption of nitrogen did occur. In Figure 3, V–n plots for nitrogen sorption on Redhill montmorillonite saturated with hexane diammonium ions and outgassed at temperatures of 50°C, 100°C and 250°C, respectively, are given. The high surface area estimated for the clay outgassed at 50°C clearly arises largely from adsorption in micropores. Whether this occurs by volume filling within regions where the lamellae are already sufficiently separated

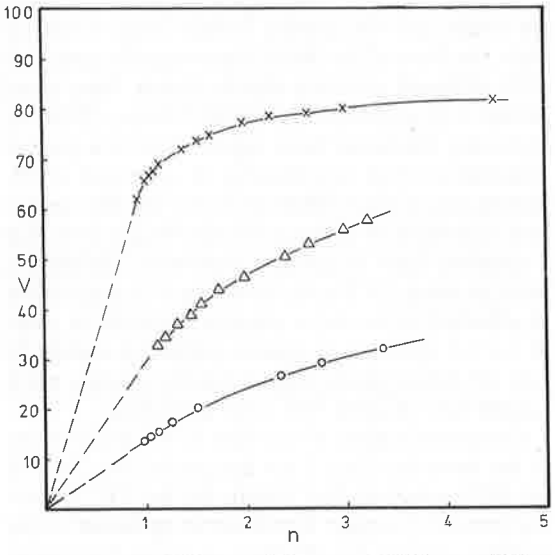

Figure 3. V–n plots for nitrogen adsorption on hexane diammonium Redhill montmorillonite after outgassing at × 50°C, △ 100°C and ○ 250°C, respectively.

to allow the sorption of one or more layers of nitrogen molecules or by nitrogen expanding the already partly expanded quasi-crystals, is not clear. Although the plot has been extrapolated to the origin to provide an estimate of specific surface area, the V–n plot does not allow a distinction between the mechanisms to be made. Because of the complex interleaving of lamellae evident in the montmorillonite matrix it is probable that in many regions there is no sharp transition between intra-crystalline and inter-crystalline surfaces.

From the comparative plots in Figure 4(b) it is clear that after outgassing at 50°C the sorption data do not conform satisfactorily to either the BET or Langmuir equation. The increase in sorption with increasing pressure is greater than that corresponding to Langmuir-type sorption, causing a significant downward curvature in the plot of the Langmuir function. On the other hand, the enhanced sorption is inadequate to correspond to predominantly multilayer sorption causing a slight upward curvature in the BET plot. In these circumstances, the actual accessible surface area could be considerably higher than that calculated by assuming the BET V_m, or that calculated from the slope of the V–n plot, to represent a complete layer on separate surfaces. An extreme case of such intra-crystalline sorption is illustrated by the BET analysis of water vapor sorption on montmorillonite given by Mooney *et al.* (1952). As pointed out by Sing (1967), good agreement between the values of V_m calculated by the two methods does not in itself confirm the validity of either.

With the gradual destruction of the large hexane diammonium ions by progressive heating to higher temperatures, there is clearly a collapse in the internal volume of the clay matrix resulting in a marked reduction in surface area accessible to nitrogen sorption with the formation of larger quasi-crystalline regions. After heating to 250°C, the comparative plots [Figure 4(c)] suggest that subsequent nitrogen sorption is predominantly multilayer in line with that observed for the inorganic cations.

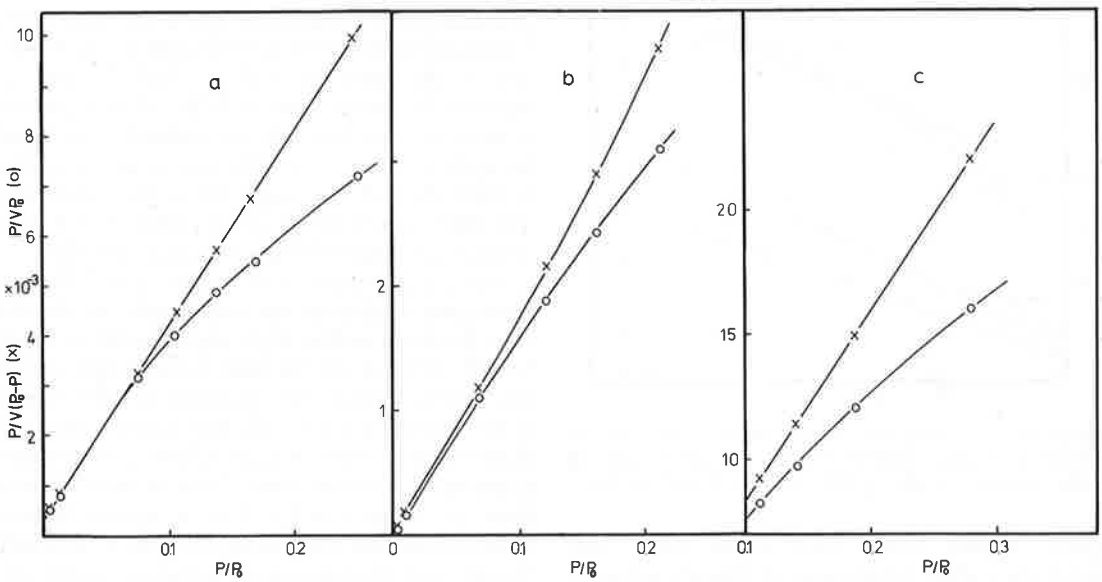

Figure 4. Comparative plots of Type I and Type II functions of Brunauer classification for nitrogen adsorption on (a) caesium Wyoming bentonite, (b) hexane diammonium Redhill montmorillonite outgassed at 50°C and (c) hexane diammonium Redhill montmorillonite outgassed at 250°C.

Carbon dioxide sorption

The interpretation of carbon dioxide sorption isotherms at 195°K on clay mineral systems is beset by several problems which are of no real significance in nitrogen sorption. The assumption that carbon dioxide adsorbed at 195°K behaves like a supercooled liquid with the corresponding saturation vapor pressure (approx. 1.86 atm), has been made by most workers dealing with coal and charcoal systems (Anderson *et al.*, 1965; Walker and Kini, 1965). However, in calculating surface areas from BET plots, molecular areas much larger than that calculated from the liquid density (approx. 17 Å) frequently have had to be assumed to give values consistent with nitrogen areas. In addition, there is clearly a marked dependence of the packing density on the crystalline nature of the substrate with values for molecular area ranging from 16.3 Å to 22 Å.

In dealing with clay mineral systems the problem is further complicated by the significant dependence of carbon dioxide sorption on the nature of the exchangeable cation. Aylmore (1974a) showed that for homoionic kaolinite and illite clays the sorption of carbon dioxide increased in the order $La^{3+} < Ca^{2+} < Na^{+} < Cs^{+}$.

The previous factors make it difficult to construct a suitable calibration curve for carbon dioxide sorption against which comparison by means of *V–n* plots can be made for other sorbents. However, in the present study, the same crystalline surface is involved and variations in sorption can be attributed either to the nature of the exchangeable cation or variations in porous structure. By the suitable choice of one isotherm as standard, several interesting comparisons can be made.

A number of workers have demonstrated that, on heating, the small size of the dehydrated lithium ion enables it to migrate into the crystal structure of clays with consequent neutralization of the charge originating from isomorphous replacement. Keenan *et al.*

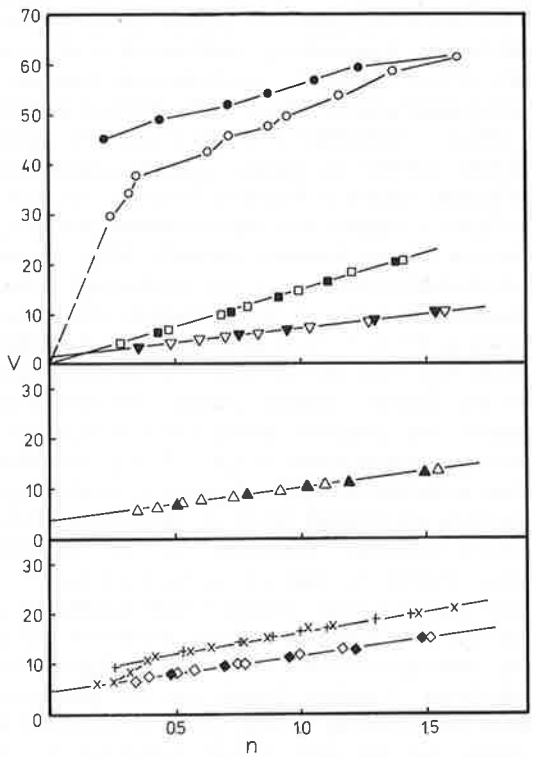

Figure 5. *V–n* plots for carbon dioxide adsorption on homoionic Wyoming bentonite: sodium ◇, × ads., ◆, + des.; lithium □ ads., ■ des.; caesium ○ ads., ● des.; calcium △ ads., ▲ des.; lanthanum ▽ ads., ▼ des.

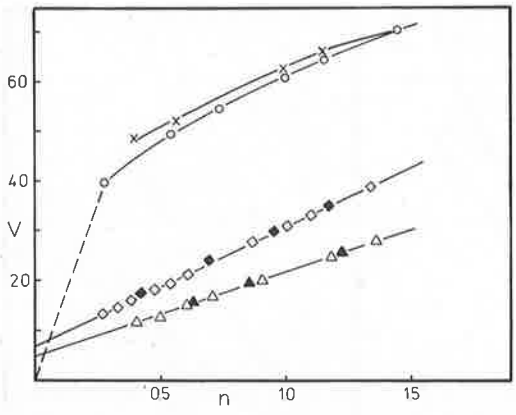

Figure 6. *V–n* plots for carbon dioxide sorption on homoionic Redhill montmorillonite: sodium ◇ ads., ◆ des.; caesium ○ ads., × des.; calcium △ ads.; ▲ des.

(1931), Jurinak (1961) and others have concluded that after dehydration of lithium saturated kaolinite, the adsorbed lithium ions are stearically hindered from hydrating and have no apparent effect on subsequent water adsorption. Similarly, the water sorption and cation exchange capacity of lithium montmorillonite is markedly reduced by heating (Quirk and Theng, 1960). Since the outgassing procedure employed here involves heating the clay to 250°C under vacuum it seems reasonable to adopt the sorption isotherm for carbon dioxide on the lithium saturated clay as a standard with which to compare the sorption on the other homoionic samples. While it may not follow that carbon dioxide sorption on this clay is completely uninfluenced by the presence of the Li^+ ions, the experience with water sorption suggests that it is likely to be the least affected.

The *V–n* plots obtained in this manner for carbon dioxide sorption on sodium, caesium, calcium and lanthanum saturated Wyoming bentonite are shown in Figure 5 together with the calibration plot calculated for lithium Wyoming bentonite. Plots for carbon dioxide sorption on sodium, calcium and hexane diammonium saturated Redhill montmorillonite are shown in Figure 6. Both adsorption and desorption points have been plotted, since it is significant that for the lithium, sodium, calcium and lanthanum cations the complete adsorption–desorption isotherms to condensation at $p/p_0 \simeq 0.53$ proved effectively reversible. In each of these cases, good straight line plots are obtained. While the calibration plot for lithium saturated Wyoming bentonite naturally passes through the origin, those for the sodium, calcium and lanthanum cations exhibit positive intercepts on the volume axis. Although it could be argued that these intercepts result from varying degree of intercalation of carbon dioxide into the montmorillonite quasi-crystals, the reversibility of the isotherms suggest that the most logical explanation lies in enhanced sorption resulting from interaction of the carbon dioxide with the surface cations, as observed by Aylmore (1974a) for carbon dioxide sorption on homoionic illite and kaolinite clays. The order of enhancement indicated by the intercepts on the volume axis is the same, i.e. $La^{3+} < Ca^{2+} < Na^+$ as observed on the kaolinite and illite clays. Variations in microporosity with different packing of the lamellae in the presence of different cations also may have a small effect on the magnitude of these intercepts. The differences in energy of interaction of the initial sorption are reflected in the C values obtained.

Previous arguments with respect to the effects of inadequate outgassing are highlighted by the two plots shown for sodium Wyoming bentonite in Figure 5, both obtained on the same sample. This sample was initially inadvertently outgassed at 100°C instead of the customary 250°C. The first isotherm obtained, shown by the crosses, initially follows a slope corresponding to a specific surface area of some 44 m^2/g. Over the range $n \simeq 0.35$–0.45, a sudden increase in the volume adsorbed occurs, followed by a straight line plot corresponding to an enhanced specific surface area of 50 m^2/g. On desorption, the adsorption isotherm is retraced to the point of this step after which there is a substantial hysteresis corresponding to the volume of carbon dioxide intercalated. On subsequent outgassing at 250°C, a completely reversible isotherm corresponding to a slope of 44 m^2/g was obtained. Almost certainly, the step in the first sorption isotherm can be attributed to the sudden entry of carbon dioxide into interlamellar regions propped apart by residual water molecules.

Significantly, the adsorption isotherm for carbon dioxide on Cs^+ saturated Wyoming bentonite is characterized by a number of similar steps followed by a marked hysteresis in the desorption process. The author has previously discussed (Aylmore *et al.*, 1970) the fact that for the caesium cation the *d* (001) spacing in the dry clay is approximately 11.8 Å, leaving roughly 2.3 Å between the lamellae. In this case, much of the work of expansion already has been accomplished and some intercalation of carbon dioxide clearly occurs. For the Redhill montmorillonite saturated with hexane diammonium ions (Figure 6) the *d* (001) spacing in the dry state was 13.8 Å. The enhanced carbon dioxide sorption exhibited by this clay exhibits much less hysteresis, presumably as a result of the greater accessibility of the interlayer area.

Microporosity in montmorillonite

Much of the controversy surrounding the question of the possible penetration of gases into quasi-crystalline regions of the montmorillonite structure, arises from the somewhat unrealistic tendency to regard the structure as being composed of neat stacks or booklets. This concept leads to the assumption that the surfaces of the lamellae are either internal, i.e. perfectly aligned with their neighbors, or external and thus able to accommodate unrestricted multilayer adsorption. In reality, variations in the lateral dimensions of individual lamellae, their juxtaposition with respect to their neighbors and interleaving of lamellae

on drying from suspension, will undoubtedly lead to a much more complex structure. This complexity has been emphasized by the author in a number of previous publications (Aylmore and Quirk, 1967, 1971; Aylmore *et al.*, 1970b; Aylmore, 1974).

Almost certainly there will be many regions in which the interleaving of individual lamellae, the buckling of lamellae, frequently observed in electron micrographs, and discontinuities of one lamellae with respect to its neighbors, even when in perfect parallel alignment, will lead to the formation of slit-shaped pores of corresponding dimensions. Such pores of the order of 10 Å plate separation would provide a satisfactory explanation of the behavior observed in the nitrogen *V–n* plots, i.e. by accommodating little more than a single layer of sorbate molecules on opposite surfaces before filling of the pores occurs. Pores of these dimensions have been designated 'super-micropores' (Dubinin, 1974) to distinguish their sorptive behavior as intermediate between ultra-micropores in which surface interactions dominate and mesopores in which capillary condensation occurs.

When thoroughly outgassed, the nitrogen surface area for a given sample is accurately reproducible and shows no significant increase on prolonged exposure to the sorbate. The surface areas accessible to nitrogen sorption represent a small proportion of the total lamellar area and, as has been shown by various workers (Greene-Kelly, 1954; Knudson and McAtee, 1974), this area for sodium montmorillonite can be reduced to less than $5\,m^2/g$ by careful manipulation of the packing during the drying process. In these circumstances, the most logical interpretation of the *V–n* plots is that nitrogen sorption occurs essentially only on surfaces external to the quasi-crystalline regions of parallel alignment and in pores able to accommodate generally one complete layer on opposing surfaces. The extent of nitrogen penetration into wedge-shaped pores, e.g. where two lamellae diverge, will depend on the nature of the packing and in particular on the influence of the exchangeable cation. However, this clearly does not progress to allow significant further expansion of the matrix for the inorganic cations studied.

Nitrogen sorption isotherms on clay minerals generally exhibit considerable hysteresis at relative vapor pressures above about 0.4 which can be related to irreversibility in the processes of capillary condensation and evaporation dependent on the porous structure of the matrix (Aylmore and Quirk, 1967; Alymore, 1974b). In most cases, when thoroughly outgassed, the hysteresis loops close on desorption at $p/p_0 \simeq 0.4$, as would be expected in the absence of interlamellar sorption. The exceptions to this occur when the expanding clays such as montmorillonite have been incompletely outgassed (Brooks, 1955) or in the presence of some large exchangeable cations (Barrer and McLeod, 1955).

In contrast, carbon dioxide sorption isotherms at 195°K on clay minerals are, in most cases, essentially reversible up to the maximum pressure which can be obtained before condensation of the solid carbon dioxide occurs. For these samples, there is no evidence of capillary condensation of carbon dioxide in the pores. Once again, the hysteresis which occurs does so either as a result of incomplete outgassing of the clay or the presence of certain of the largest exchangeable cations, In these cases, the hysteresis increases with desorption and persists to low relative vapour pressures, almost certainly indicating that it results from intracrystalline sorption.

Because of the differences in size, polarity, etc. of the molecules of different gases, the distinction between internal and external surfaces of a montmorillonite matrix becomes largely a matter of definition in terms of their accessibility to a given gas. In view of the previous consideration, it seems reasonable to conclude that the variations in nitrogen surface area with exchangeable cation result essentially from real differences in matrix structure consequent on the degree of dispersion in suspension. While the initial sorption of carbon dioxide clearly is influenced by the solvation properties of the cations, the subsequent reversibility of the isotherms and linearity of the *V–n* plots indicates that for all but the largest cations the same sorption process is occurring on surfaces external to the quasi-crystalline regions.

REFERENCES

Anderson, R. B., Bayer, J. and Hofer, L. J. E. (1965) Determining surface areas from CO_2 iosotherms: *Fuel* **44,** 443–452.

Aylmore, L. A. G. (1960) Ph.D. thesis, University of Adelaide.

Aylmore, L. A. G. (1974a) Gas sorption in clay mineral systems: *Clays and Clay Minerals* **22,** 175–183.

Aylmore, L. A. G. (1974b) Hysteresis in gas sorption isotherms: *J. Colloid Interface Sci.* **46,** 410–416.

Aylmore, L. A. G. and Quirk, J. P. (1967) The micropore size distributions of clay mineral systems: *J. Soil. Sci.* **18,** 1–17.

Aylmore, L. A. G. and Quirk, J. P. (1971). Domains and quasi-crystalline regions in clay systems: *Proc. Am. Soil Sci. Soc.* **35,** 652–654.

Aylmore, L. A. G., Sills, I. D. and Quirk, J. P. (1970a). Surface area of homoionic illite and montmorillonite clay minerals as measured by the sorption of nitrogen and carbon dioxide: *Clays and Clay Minerals* **18,** 91–96.

Aylmore, L. A. G., Sills, I. D. and Quirk, J. P. (1970b). Reply to comments of Thomas, Bohor and Frost on Aylmore, L. A. G., Sills, I. D. and Quirk, J. P. (1971). The surface area of homoionic illite and montmorillonite clay minerals as measured by the sorption of nitrogen and carbon dioxide: *Clays and Clay Minerals* **18,** 407–409.

Barrer, R. M. and MacLeod, D. M. (1955) Activation of montmorillonite by ion exchange and sorption complexes of tetra-alkylammonium montmorillonite: *Trans. Faraday Soc.* **51,** 1290–1300.

Brooks, C. S. (1955) *Soil Sci.* **79,** 331.

Dubinin, M. M. (1974) On physical feasibility of Brunauer's Micropore Analysis Method: *J. Colloid Interface Sci.* **46,** 351–356.

Fripiat, J. J., Cruz, M. I., Bohor, B. F. and Thomas, J., Jr. (1974) Interlamellar adsorption of carbon dioxide by smectites: *Clays and Clay Minerals* **22,** 23.

Greene-Kelly, R. (1964) The specific surface areas of montmorillonite: *Clay Miner. Bull.* **5**, 392–400.

Jurinak, J. J. (1961) The effect of pretreatment on the adsorption and desorption of water vapor by lithium and calcium kaolinite: *J. Phys. Chem.* **65**, 62.

Knudson, M. I. and McAtee, J. L., Jr. (1974) Interlamellar and multilayer nitrogen sorption by homoionic montmorillonites: *Clays and Clay Minerals* **22**, 59.

Mooney, R. W., Keenan, A. G. and Wood, L. A. (1952) Adsorption of water vapour by montmorillonite II. Effect of exchangeable ions and lattice swelling as measured by X-ray diffraction: *J. Am. Chem. Soc.* **74**, 1371–1374.

Quirk, J. P. and Theng, B. K. G. (1960) Effect of surface density of charge on the physical swelling of lithium and montmorillonite: *Nature* **187**, 967–968.

Shull, C. G. (1948) The determination of pore size distribution from gas adsorption data: *J. Am. Chem. Soc.* **70**, 1405–1414.

Sing, K. S. W. (1967) Assessment of microporosity: *Chem. Ind.* 829–830.

Thomas, J., Jr. and Bohor, B. F. (1968) Surface area of montmorillonite from the dynamic sorption of nitrogen and carbon dioxide: *Clays and Clay Minerals* **16**, 83–91.

Walker, P. L., Jr. and Kini, K. A. (1965) Measurement of ultrafine surface area of coals: *Fuel* **44**, 453–459.

Reprinted from the *Soil Science Society of America Journal*
Volume 41, no. 3, May–June 1977
677 South Segoe Rd., Madison, WI 53711 USA

Water and Salt Flow Through Compacted Clays: I. Permeability of Compacted Illite and Montmorillonite[1]

P. F. ROLFE[2] AND L. A. G. AYLMORE[3]

ABSTRACT

Studies have been made of the pressure-induced flow of the chloride solutions of various monovalent, divalent and trivalent cations, at various concentrations, through compressed Wyoming bentonite and Willalooka illite cores.

The majority of the measurements were carried out on the Willalooka illite core and its permeability has been shown to depend markedly on the nature and concentration of the cations present, with three- to fourfold variations being observed in some instances. At the lower electrolyte concentrations permeability increases in the order Na < Ca < Ba < La < Cs at a given concentration. In addition the permeability increases linearly with flow pressure to an extent ranging from some 15% for the Na systems to 97% for the 3.0*M* $LaCl_3$ system over the pressure range examined.

The contributions to the permeability changes arising from mechanical expansion of the flow cell, particle rearrangements and the electroviscous effect have been shown to be quite inadequate to account for the major changes observed. It is suggested that the most significant effects arise as a result of the influence of cationic size, charge, and concentration on the viscosity of the several layers of coerced water which form adjacent to the clay surfaces. Coercion of water may arise partly through its association with the exchangeable cations adsorbed on the surface or forming diffuse double layers, but mainly from the preferred or unique water structure developed in proximity to the clay surface. In particular increasing concentrations of Cs, Ca and La cations appear to cause a pronounced breakdown in water structure within the pores.

Additional Index Words: **clay permeability, water structure, hydraulic pressure, cationic hydration, bentonite, illite.**

THE MOVEMENT of water and electrolyte solutions through saturated porous media is of considerable interest in a variety of disciplines. In agriculture the hydrology of a particular area can be very dependent on the permeability of clay subsoils and at present little is known of the extent to which subsoil permeability can be modified. Similarly the uptake of water and nutrient ions by plants takes place by their movement through the porous soil structure under the influence of both pressure and concentration gradients. Modern solution mining technology also depends upon the permeability of hard rock structures to appropriate leaching solutions (Lackey, 1975). Furthermore the increasingly urgent necessity to improve methods for the desalination of water and in the development of dialyzing membranes for artificial organs, has led to an increase in activity to understand the processes of importance in reverse osmosis, electrodialysis and membrane technology in general.

The laminar flow of water through inert rigid materials is in general adequately described by the empirical equation derived by Darcy in 1856 and this description remains satisfactory as a first approximation for many other systems. However, in many circumstances the requirements of Darcy's Law that flow velocity be proportional to hydraulic gradient is not satisfied, with both less than and greater than proportional increases being observed (Lutz and Kemper, 1959; Miller and Low, 1963; Swartzendruber, 1962; Gairon and Swartzendruber, 1975). A variety of explanations have been proffered for these deviations including experimental artifacts (Olsen, 1965), the development of modified water structure in proximity to clay surfaces (Low, 1960), particle rearrangements during the flow process (Mitchell and Younger, 1967; Russel and Swartzendruber, 1971) and in particular in reactive systems, to electrokinetic phenomena associated with the ionic distribution within the porous media.

Depending on the reactivity of the media the flow process may be accompanied by a number of electrochemical phenomena of considerable practical importance. Numerous

[1]Contribution from the Dep. of Soil Science and Plant Nutrition, University of Western Australia, Nedlands, Western Australia, 6009. Received 11 June 1976. Approved 1 Feb. 1977.

[2]Extension Officer, Extension Service, Univ. of Western Australia, Nedlands, Western Australia, 6009.

[3]Senior Lecturer, Dep. of Soil Science and Plant Nutrition, Univ. of Western Australia, Nedlands, Western Australia, 6009.

workers (McKelvey et al. 1959, 1962; Kemper, 1960; Kemper and Maasland, 1964) have demonstrated that certain compacted ion-exchange membranes, including natural clays, permit the passage of water under a hydraulic pressure gradient, while partially restricting the movement of dissolved salts. Thus, solutions of reduced concentration pass out of the porous media, and accumulation of salts occurs at the high pressure, input face (Jacazio et al., 1972; Simons and Kedem, 1973; Dresner and Johnson, 1974). At the same time the liquid flow rate through the porous media may be reduced as a result of an electroviscous retardation arising from the development of a streaming potential (Kemper, 1960; Burgreen and Nakache, 1964; Churaev and Derjaguin, 1966; Levine et al., 1975).

The aim of this investigation was to examine the changes in permeability and salt sieving which accompany the flow of different types of metallic chloride salts at varying solution concentrations, through saturated, compacted illite and montmorillonite clay media. In the present paper an attempt has been made to relate the observed changes in permeability to the mechanical and physicochemical properties of the clay system. A particular feature of this study is that in the permeameter used (based on that described by McKelvey and Milne, 1962), the clay media is so compacted and confined that permeability variations as a result of particle rearrangements should be minimal.

MATERIALS

The clays studied were Wyoming bentonite montmorillonite and Willalooka illite. The bentonite originated from the John C. Lane Tract, Upton, Wyoming and was a sample of standard clay mineral, no. 256, of the American Petroleum Institute, project 49. The illite was obtained from the "hundred of Laffer" in South Australia, and contained a small percentage of kaolinite. Sodium saturated, < 2 μm fractions of both clays were prepared using the method described by Posner and Quirk (1964). After P_2O_5 drying, samples of these clays were equilibrated with a 75% RH atmosphere which brought the water content of both clays to something in excess of 15% by weight.

APPARATUS

The apparatus used in these studies is essentially similar to that described by McKelvey and Milne (1962), consisting of a cylindrical flow cell of 5.08 cm internal diameter in which a clay bed is compacted between two porous end pistons. Compaction of the clay samples into the flow cell was carried out with the aid of an hydraulic press and was maintained using steel end plates bolted together. However, the nylon liner fitting within the confining steel cylinder of the flow cell as used by McKelvey and Milne was replaced with Delrin, an opaque white polyacetal possessing good electrical insulting and frictional properties. Delrin absorbs less moisture and swells less than nylon, which, when swollen rendered dismantling of the flow cell very difficult. The metallic filters, fitted into the pistons of McKelvey and Milne's apparatus to allow passage of saline solutions into and out of the compacted clay samples, were replaced with more easily obtainable porous ceramic discs. The pore diameter of this ceramic was approximately 50 mm. Stainless steel of 316 grade was used for the manufacture of the pistons and associated input and output line couplings and the bypass control to prevent salt corrosion.

The construction of the flow cell was made as rigid as possible to minimize changes in the degree of compaction of samples which might be caused by changes in the applied hydraulic pressure. Thus Novasteen, a fabric reinforced phenolic material, possessing very good insulating properties and high compressive strength, was used as the electrical insulators inserted in the flow cell end-plates. The flow cell end-plates were constructed from 3.8-cm thick mild steel, and the bolts were 3.2-cm diam hardened steel. Calculations based on measurements of the compressibility of the Novasteen inserts, elastic bending of the steel end-plates and the extension of the flow cell bolts, indicated that the porosity of compacted clay samples changed by $< 0.4\%$ over the chosen hydraulic pressure range up to 20.7 MegaPascals (MPa).

Approximately 20 g of hydrated clay was weighed accurately and then compressed between the pistons of the flow cell for 24 hours using a hydraulic ram at a compaction pressure of 34.5 MPa. The end-plates of the cell were bolted together during compaction, the strain in the bolts being adjusted to maintain the load on removal from the press. The cores obtained were approximately 0.7 cm in thickness and generally permitted the flow of several ml of salt solution per day depending on the applied hydraulic pressure and salt solution.

An asbestos packed bypass control (filter) was used to ensure that the input face of the compacted clay core was continuously flushed free of any rejected salt, which would otherwise have accumulated at this interface. Flow rates through the bypass filter line were adjusted to the same magnitude as those through the clay cores.

Fluid flowing through the compacted clay cores was collected in a burette graduated in 0.01-ml divisions and considerable precautions were taken to prevent evaporation. Fluid which passed through the bypass flow system after flushing the input faces of the clay cores was also collected in the same fashion.

The experiments were carried out in a constant temperature laboratory (20°C ± 1°C) to ensure that thermally-induced variations in aqueous properties (e.g. Korson et al., 1969; Drost-Hansen, 1969; Vnuk, 1976) as well as the expansion and contraction of the metal flow cell should be reduced to a minimum.

A preliminary series of measurements was conducted on sodium saturated Wyoming bentonite using 0.1 normal sodium chloride solution and hydraulic flow pressures ranging from 34.5 MPa to 69.0 MPa. However, the majority of experiments were carried out on Willalooka illite using various exchangeable cations and chloride solution concentrations. Cation exchange in the compressed core was carried out by passing concentrated chloride solutions of the appropriate cation and monitoring the outgoing solution using atomic absorption spectroscopy.

Table 1—Comparison of specific permeabilities (K) and average effective thicknesses ($2b_e$) for sodium chloride solutions in Na-Wyoming Bentonite cores.

Authors	Compaction pressure	Flow pressure	Solution concentration	$K \times 10^{16}$	$2b_e$
	MPa		M	cm^2	nm
Rolfe and Aylmore	34.5	34.5	0.10	0.30	1.90
Rolfe and Aylmore	34.5	47.0	0.10	0.31	1.93
McKelvey and Milne	69.0	34.5	0.15	0.12	1.20

RESULTS AND DISCUSSIONS

The results of the preliminary experiments in which a 0.1M NaCl solution was passed through the Na-saturated Wyoming bentonite core are summarized in Table 1 and compared with those obtained by McKelvey and Milne (1962). The permeability and hence the average effective film thickness within the clay pores (as defined by Kemper, 1961a, 1961b) is considerably greater in the present work as would be expected from the lower compaction pressure used. An increase in hydraulic flow pressure caused both the specific permeability and average effective film

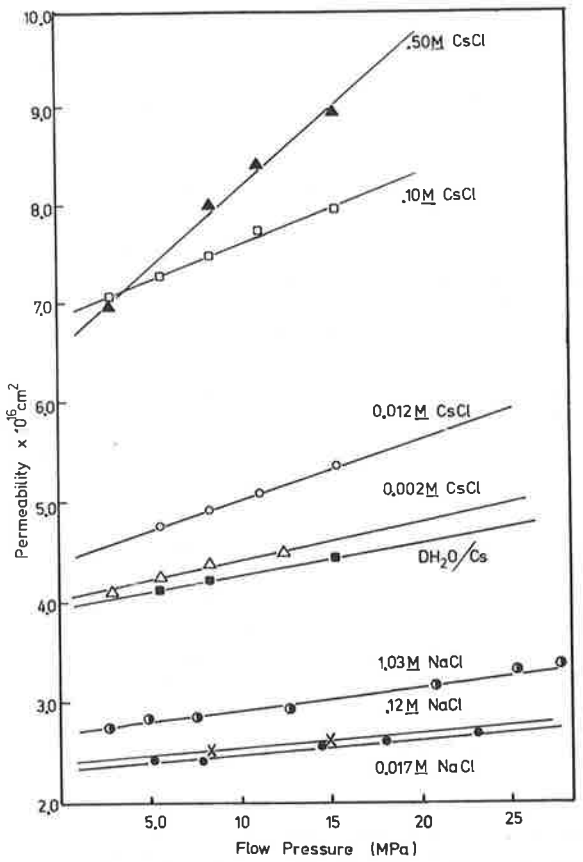

Fig. 1—Changes in the specific permeability of the Willalooka illite core, against applied hydraulic pressure, for a series of concentrations of sodium and cesium chloride.

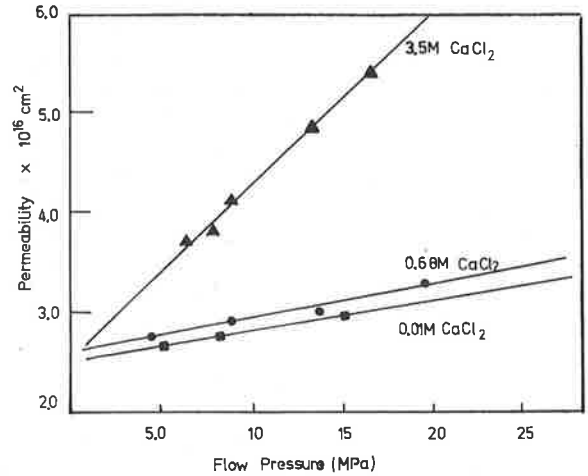

Fig. 2—Changes in the specific permeability of the Willalooka illite core, against applied hydraulic pressure, for a series of concentrations of CaCl.

thickness to increase slightly. A similar trend was also noted by McKelvey and Milne.

In Fig. 1, 2, and 3 the changes in permeability of the Willalooka illite core with applied hydraulic flow pressure are shown for a series of concentrations of sodium, cesium, calcium, barium and lanthanium chloride solutions. The time required to establish a new equilibrium flow rate on changing the flow pressure varied slightly with both flow

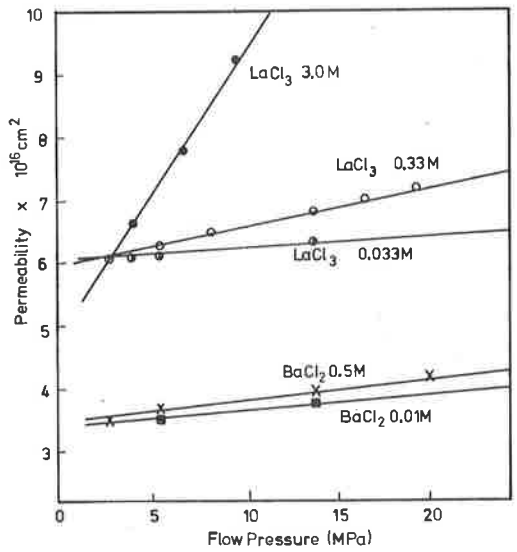

Fig. 3—Changes in the specific permeability of the Willalooka illite core, against applied hydraulic pressure, for a series of concentrations of barium and lanthanum chloride.

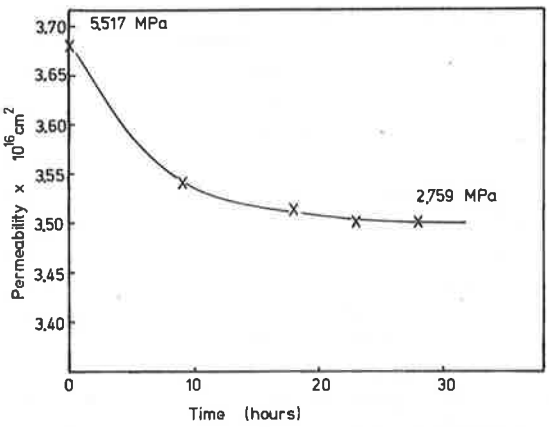

Fig. 4—Change in the specific permeability of the Willalooka illite core, against time, for the flow of a 0.5*M* BaCl solution during equilibration from 5.517 MPa to 2.759 MPa hydraulic pressure.

pressure and the exchangeable cation present, but was usually <24 hours as illustrated in Fig. 4.

The marked dependence of permeability on both the nature of the exchangeable cation and the electrolyte concentration is immediately apparent. In addition, in each case the permeability of the core increases in a linear fasion with flow pressure. At the lower electrolyte concentrations this increase in permeability with flow pressure appears similar for all cations (some 15% for the Na clay over the pressure range up to 27.6 MPa) and permeability increases in the order Na < Ca < Ba < La < Cs. However at the highest concentrations permeability increases much more rapidly with hydraulic pressure, e.g., some 97% for 3*M* LaCl over the pressure range measured (Fig. 3).

In view of the similarity in the change in permeability of the core with pressure for all cations at all, but the highest concentrations, it could be argued that the changes in these cases are related to mechanical changes in the porous structure of the clay core with increasing pressure. This would have to occur as a result of an overall expansion of the ma-

Table 2—Comparison of specific permeability-pressure gradients for five cations against increasing solution concentrations.

Cation	Solution concentration, *M*	Gradient (10^{-20} cm^2/6.89$_5$kPa)
Na^+	0.017	1.06
	0.12	1.10
	1.03	1.60
Ca^{2+}	0.011	2.00
	0.68	2.30
	3.50	11.98
Ba^{2+}	0.010	1.75
	0.50	2.15
Cs^+	"Distilled H_2O"	2.28
	0.002	2.65
	0.012	4.32
	0.10	5.12
	0.50	11.74
La^{3+}	0.033	1.30
	0.33	4.05
	3.00	30.75

trix or by an internal rearrangement of the structural configuration with increasing flow pressure. Both possibilities seem unlikely. Firstly, expansion of the cell was monitored with strain gauges and it can be demonstrated that the maximum possible expansion of the compacted clay matrix with increasing pressure up to 27.6 MPa, resulting from lengthwise and lateral expansion of the cell, could only account for $< 2\%$ increase in permeability compared with the smallest change of some 15% observed for 0.017*M* NaCl. Secondly, while electron microscopic examination indicates that the illite clay particles are, on the average, some 4 to 5 nm thick and some 100 nm across the planar surfaces, dividing the pore volume by the specific surface area indicates that in the compacted state in the flow cell, the average separation between crystal surfaces is only of the order of 4 nm. In these circumstances and bearing in mind the complex interleaving generally present in the domain structure of such a clay matrix (Aylmore and Quirk, 1960), it seems reasonable to assume that any rearrangement of the configuration of the matrix would be minimal. Also measurements using various sequences of flow pressure indicated that, within the limits of experimental error, changes in permeability of the core were essentially reversible with respect to flow pressure. Thus, there were no indications that hydraulically induced permanent structural changes occurred.

The possibility that internal flexing of the clay matrix with increasing flow pressure, results in the production of some larger pores at the expense of smaller flow paths cannot be overlooked. Although the relatively small hydraulic pressure gradients across any given clay plate would seem inadequate to produce this type of flexing, the increase in mechanical load throughout the matrix due to an increased hydraulic pressure at the ingoing face may make some small contribution.

A detailed examination of the permeability — pressure gradients at the lower concentrations indicates that although similar, the gradients in fact show a significant dependence on electrolyte concentration over the whole concentration range, e.g. Table 2. Thus with the structural configuration of the clay matrix essentially fixed, it seems likely that the increases in permeability with flow pressure are at least partly if not mainly, electrochemical in origin.

It is clear that the major changes in permeability arise from the changes in ionic distribution associated with changes in exchangeable cation and electrolyte concentration. In the present system several mechanisms may contribute to these changes:

1) Alterations in the distribution of pore dimensions as a result of changes in swelling forces within the clay matrix.

2) Variations in the magnitude of the electroviscous retardation of flow arising from the development of a streaming potential across the flow cell.

3) Variations in the mobility of water molecules associated with exchangeable cations absorbed on the surfaces or forming diffuse double layers, and

4) Alterations in the actual viscous behaviour of the water structure as a result of the disruptive action of the cations.

Changes in ionic distribution or the development of the diffuse double layer will have significant effects on the internal swelling pressures between individual pairs of plates. Under the mechanical load resulting from the initial compaction, there could be some degree of distortion of the plates giving rise to irregularities in plate spacings with some regions of the generally parallel crystals being compacted to closer proximity i.e. concertinaed, more than others. With high swelling pressures (e.g. in 0.017*M* NaCl system) there would be a tendency for the separation between the plates to be equalized throughout the matrix. This in turn could be expected to reduce the permeability by the replacement of the larger flow channels, which contribute disproportionately to flow, by several smaller channels. At first sight, the experimental observations do in general conform with this expectation of decreasing permeability in the order of increasing development of diffuse double layers with decreasing electrolyte concentration and valency of the cation. Also, increasing the flow pressure and hence the mechanical load could be expected to counteract to some extent this regularization of the structure and to cause slight increases in permeability as observed.

The extent of the contribution of such swelling forces to a possible regularization of the structure can be estimated from simple calculations. For example, the swelling pressure associated with a 0.017*M* NaCl solution between illite plates separated by 4 nm is of the order of 0.1 MPa. Use of the usual formula to calculate the maximum bending at the center of a plate of 10^4 nm^2 pinned at opposite ends (Timoshenko and Woinowsky-Krieger, 1959) indicates a possible flexing of approximately 1 nm. Similar calculation for the 0.12*N* NaCl system indicates a bending at the center of the plate of <0.4 nm. When the slight increase in permeability observed over this concentration range is compared with that for the change to 1.0*M* NaCl, or to the Ca systems, for both of which the bending due to swelling pressures would be negligible, it seems unlikely that the further reduction in swelling pressures would account for this large change. The Cs systems would again be devoid of significant swelling pressure and yet their permeabilities are markedly increased with respect to the 1.0*M* Na and the Ca systems. Since in general the plates constituting the clay matrix are likely to be subject to greater constraints than a simple pinning at two ends, it must be concluded that this mechanism is inadequate to explain the experimental observations.

The electroviscous effect arises essentially as a result of

the difference in cation and anion concentrations in proximity to a charged surface. Within the region of the double layer there is an excess of cations and if a pressure gradient is applied to make the salt solution flow through the pore then because of this excess of charge of one sign within the pore liquid, there results a net transfer of charge and the build-up of a streaming potential. The potential becomes increasingly positive at the outflow end and increasingly negative at the inflow end. The effect of this electric field parallel to the surface is to increase the transport of the anions and to reduce that of the cations until there is an equal steady-state transport of positive and negative ions (provided the feed and effluent solutions are electrically insulated from each other so that there is no current flow). In this steady-state salt and water are transported through the capillaries but not charge.

Two principal effects can arise as a result of the distribution of potential within the capillaries. First, under the appropriate conditions the net effect of the anion exclusion and the axial field may be such as to cause the ratio of the molar salt flux to the volume flux of water to be less than the molar salt concentration on the high pressure, input face of the membrane, i.e. the membrane tends to reject salt. This aspect will be considered in detail in a subsequent paper. Secondly, since there are more cations than anions the net effect of the streaming potential gradient is to retard the forward movement of the water, i.e. the liquid flow rate through the pore will be reduced as a result of this electroviscous retardation on the normal Poiseuille flow; an effective reduction in permeability or increase in apparent viscosity. The magnitude of this effect will of course depend largely on the extent of the anion exclusion from the pore volume and will therefore be of most significance at low electrolyte concentration and for those cations which form appreciable double layers.

Analytical solutions of the general equation of electrokinetic flow through narrow parallel-plate channels, taking into account both hydrodynamic and electro-osmotic contributions, have recently been provided in several publications (Burgreen and Nakache, 1964; Levine et al., 1975; Churaev and Derjagnin, 1966). These show that when diffuse double layers constitute a significant part of the pore volume or in fact overlap (e.g., in very fine capillaries or at high surface potentials) the apparent viscosity in the channel (η_a) exceeds the viscosity of the bulk electrolyte (η). In addition, the ratio of the two viscosities has a maximum with respect to the electrokinetic radius (given by κh where $1/\kappa$ is the Debye length and h is the half-plate separation) at fixed zeta potential ζ (usually at about $\kappa h = 1$) and also a maximum with respect to ζ at fixed κh.

Applying this approach to the Willalooka illite clay system, for example, for 0.017M NaCl, the predictions of Levine et al. (1975) indicate that the ratio of apparent to real viscosities η_a/η would be approximately 1.20. If it is assumed that at a concentration of 1.03M NaCl the electroviscous retardation of flow is extremely small if not negligible, the observed decrease in permeability from 1.03 to 0.017M CaCl is (using the intrinsic values obtained by extrapolating to zero flow pressure) from approximately 2.7×10^{-16}cm^2 to 2.3×10^{-16}cm^2, that is, an apparent increase in viscosity of 1.17 times. Similarly if the intrinsic permeability for 0.01M $CaCl_2$ is compared with that for 1.03M NaCl (or for 0.68M $CaCl_2$ which has a similar value) the ratio η_a/η observed is 1.08 compared with a predicted increase for 0.01M $CaCl_2$ of approximately 1.06.

In view of the assumptions inherent in these calculations the excellence of the agreement is undoubtedly somewhat fortuitous. In particular the effects of the tortuosity of the flow paths through real porous media has been neglected and this would reduce the predicted values. However it is clear that in these cases the effects predicted are at least of the right magnitude to explain the variation in apparent viscosity with electrolyte concentration.

On the other hand it is equally clear that this electrokinetic braking is quite inadequate to account for the major changes in permeability observed. The maximum ratio η_a/η predicted from the electroviscous effect under the most favorable conditions for a membrane such as the Willalooka illite core is approximately 1.3. This has to be compared with the three- to four fold variation observed for different cations and in particular the marked variation with electrolyte concentration for the Cs saturated clay. Cesium is generally regarded as an ion which forms little if any significant diffuse double layer (Edwards et al., 1965). Its large ionic radius and single charge mean that it is poorly hydrated and consequently strongly bound to the clay surface. Although the streaming potential measurements and salt-sieving data to be presented in a subsequent paper, indicate that some development of a diffuse double layer does occur in very dilute Cs systems, nevertheless this will be small compared with the dilute Na system. In spite of this the ratio of the apparent viscosities observed in changing from 0.012M CsCl to 0.1M CsCl is of the order of 1.6, appreciably higher than that (of approximately 1.1) predicted by the theory for 0.012M CsCl. Furthermore it will be shown (Rolfe and Aylmore, in preparation) that with increasing flow pressure in the present system, the salt sieving and the streaming potential-pressure gradient present at low concentrations are progressively reduced until at the highest flow pressures used the electroviscous retardation arising from the back diffusion of cations will be negligible. Although this might seem to provide at least in part, an explanation for the small increases in permeability observed with flow pressure at the lower concentrations, this origin for the differences in permeability at low concentrations is contradicted by their persistence even at the highest flow pressures.

Thus it seems most likely that the effects observed are associated with the influence of the cations on the flow properties of the fluid itself, either through the degree of reduction in mobility of water molecules associated with cations adsorbed on the surface or forming diffuse double layers, or by the degree to which they alter the actual viscous behavior of the water itself (i.e., the extent of the breaking-up of the preferred water structure by the cations). Both effects are dependent on the size, charge, and concentration of the cations.

Kemper et al. (1964) using measurements of D_2O diffusion have shown that the first molecular layer of adsorbed water on Na and Ca saturated montmorillonite had mobilities which were 30% and 5% respectively of the mobility of water molecules in bulk water. The very low mobilities in the Ca clay were attributed to the strong associations be-

tween the water molecules and the adsorbed Ca ions. Similarly Gargallo et al. (1969) have suggested that the effect of more strongly hydrated cations in the double layer would be to trap a greater part of the double layer during displacement and therefore to increase the distance of the plane of shear from the surface. For concentrations of less than some 0.5*M* NaCl, interacting double layers from opposing surfaces would occupy the full width of the average-sized pores in the Willalooka illite core (some 4-mm plate separation) (Kemper and Quirk, 1970). Similarly for the 0.01*M* CaCl solution the extent of the double layer from each surface (approximately 6 nm) would again occupy the entire width of the average-sized pores, but at 0.68*M* the diffuse double layer can be neglected. Thus at the lower electrolyte concentrations the development of interacting double layers may contribute further to the observed reductions in permeability by the restrictions to the mobility of the water forming hydration shells around the cations.

Normal bulk water has frequently been described as possessing a diffuse (or quasi-) crystalline structure (Wong et al., 1952; Kell, 1972; Davis and Jauzyorski, 1972). Furthermore there is evidence to suggest that in proximity to clay surfaces *pseudomorphism* may occur between the water structure and the crystalline structure of the clay (Ravina and Low, 1972). Thus the development of a unique water structure bonded to and propagated away from the surface, together with the polarizing influence of surface electrostatic fields, may result in an appreciable layer of strongly coerced water. The existence of such boundary layers has been involked to explain differences between theoretical diffuse double layer repulsive forces and experimental observations in close proximity to clay surfaces (Barclay and Ottewill, 1970). In these circumstances the role of the exchangeable cation could become paramount in determining the mobility of the water in the pores.

The role of a particular cation in determining the development of coerced water layers will depend partly on the extent to which it forms diffuse double layers and partly on its polarizing influence on the surrounding water molecules. The greater the ionic potential (ϕ = [cationic charge (q)]/[cationic radius (r)] of a given cation the greater will be its polarizing influence on the surrounding water molecules (Moeller, 1952). However the extent of double layer development will depend on the Stern layer potential consequent on the specific adsorption of the cations, which in turn depends essentially on the ionic potential of the hydrated cation. Thus at the lower concentration levels although the divalent Ca ions are more strongly adsorbed, their greater polarizing influence results in permeabilities only slightly higher than the twice as numerous (but less strongly hydrated) monovalent Na ions with their more extensive diffuse double layer development.

Conversely ions which are poorly hydrated and strongly adsorbed will provide far less hinderance to the movement of water molecules. In particular large ions such as Cs^+ have for some time been regarded as structure breaking ions; because of their particular combination of size and charge they do not appear to fit in, as it were, with the normal bulk water arrangement as do the smaller or more strongly hydrated ions (Frank and Evans, 1945; Millero, 1972). In these circumstances any tendency for the water to develop a unique structure bonded to and propagated away from the surface, would be increasingly disrupted by increasing concentration of the Cs ions. Thus in addition to the removal of any electroviscous retardation which might arise from the apparent development of diffuse layers at the lowest concentrations, increasing concentration would further enhance permeability by making the coerced boundary layers more mobile.

Kemper et al. (1964) observations would suggest that significant reduction in mobility of the water occurs only in the most severely coerced regions of the double layer near the surface. Thus, while relatively small increases in permeability may occur as a result of the contraction of diffuse double layers with increasing concentration or valency of the cation, for significant changes in the permeability to occur these strongly coerced layers must be broken down, that is, their viscosity must be reduced. From the present data this is clearly achieved by certain combinations of cationic size, charge, and concentration.

The dramatic increase in permeability of even the most dilute Cs system (distilled water) compared with the Na and Ca systems, clearly indicates that the disruptive effects of this cation on water structure produces far greater effects on permeability than those associated with any effects of diffuse double layer formation or pressure increase. The effect of increasing concentration of the structure breaking Cs ions (Kavanau, 1964; Kijne, 1969) on the flow properties of the solution is perhaps the most striking phenomenon in the present data. While a 10-fold change in concentration (from 0.017*M* to 0.1*M*) of NaCl produces an insignificant change in the permeability of the illite core, the same change in concentration of CsCl almost doubles an already greatly enhanced permeability (see Fig. 1).

Similar arguments may help to explain the greatly increased permeabilities at high concentrations for Ca and La and also the marked sensitivity to flow pressure at the higher concentrations. At high concentrations these cations would compete vigorously with the original water structure in order to satisfy their separate hydration shell requirements and in this sense large concentrations could cause a special type of water structure breakdown. Furthermore although the flow pressures used could only contribute a very small percentage of the energy required to break average strength hydrogen bonds between water molecules, (International Critical Tables, 1929), the possibility exists that they might be sufficient to disrupt some of the, perhaps peculiar, bonds present in any bound water layers (particularly in the presence of high cation concentrations) and this could explain the rapid increases in permeability with flow pressure (Low, 1961). Lanthanum may be a special case, since reasonable doubt now exists (Kepert, 1973) about the status of La^{3+} in solutions of concentrations in excess of 0.01*M*. Species of the type $(La(OH)^{2+})_n$, with unit radii of about 2.8Å, are considered to be present as polymers in coexistence with La^{3+}. These polymeric species may be even less polarizing to water structure than Cs^+.

Table 3 contains details relating the intrinsic permeability *(Ki)* (obtained by extrapolating the permeability-pressure plots back to the y-axis), to the cationic radii (r_x) at the concentration of approximately 0.02*N*. A plot of Ki vs. $1/r_x$ gives a straight line of negative gradient illustrating the

Table 3—Intrinsic permeabilities for 0.02*N* solution related to cationic crystallographic radii.

Cation	Intrinsic permeability ($\times 10^{-16}$ cm^2)	Radius (Å)	1/Radius
Na^+	2.30	0.97	1.032
Ca^{2+}	2.50	0.99	1.010
Ba^{2+}	3.40	1.34	0.746
Cs^+	4.40	1.67	0.598

prime importance of cationic radius in modifying water structure.

LITERATURE CITED

1. Aylmore, L. A. G., and J. P. Quirk. 1960. Domain or turbostratic structure of clays. Nature (London) 187:1046–1048.
2. Barclay, L. M., and R. H. Ottewill. 1970. Measurement of forces between colloidal particles. Spec. Dis. Faraday Soc. 1:138–147.
3. Drost-Hansen, W. 1969. Structure of water near solid interfaces and the possible existence of long-range order. Ind. Eng. Chem. 61:10–47.
4. Burgreen, D., and F. R. Nakache. 1964. Electrokinetic Flow in ultrafine capillary slits. J. Phys. Chem. 68:1084–1091.
5. Churaev, N. V., and B. V. Derjaguin. 1966. Influence of overlapping of diffuse ionic layers on electrokinetic effects in thin films and pores. Kolloid Z. 28:751–757.
6. Davis, C. M., and J. Jauzyorski. 1972. Mixture models of water, p. 377–423. *In* R. A. Horne (ed.) Water and aqueous solutions: Structure, thermodynamics and transport processes. Wiley — Interscience, New York.
7. Dresner, L., and J. S. Johnson Jr. 1974. Hyperfiltration (reverse osmosis) p. 346–433. *In* K. S. Spiegler and U. D. K. Laird (eds.) Principles of desalination, 2nd ed. Academic Press, New York.
8. Edwards, D. G., A. M. Posner, and J. P. Quirk. 1965. Repulsion of chloride ions by negatively charged clay surfaces. Part I - Monovalent cation fithian illites. Trans. Faraday Soc., 61:2808–2815.
9. Franks, H. S., and M. W. Evans. 1945. Free volume and entropy in condensed systems: III. Entropy in binary liquid mixtures. Partial molal entropy in dilute solutions, Structure and thermodynamics in aqueous electrolytes. J. Chem. Physics 13:507–532.
10. Gairon, S., and D. Swartzendruber. 1973. Water Flux and electrical potentials in water saturated bentonite. Soil Sci. Soc. Am. Proc. 39:811–817.
11. Gargallo, L., L. Sepulveda, and J. Goldfarb. 1968. Effect of the nature of ions on the electrophoretic mobility of model particles. Kolloid Z. Z. Poly. 229:51–54.
12. International Critical Tables of Numerical Data, Physics, Chemistry and Technology. 1929. E. W. Washburn (ed.) 5, 10. McGraw-Hill, New York.
13. Jacazio, G., R. F. Probstein, A. A. Sonin, and D. Yung 1972. Electrokinetic salt rejection in hyperfiltration through porous materials. Theory and experiment. J. Phys. Chem. 70:4015–4023.
14. Kavanau, J. L. 1964. Water and solute-water interactions. Holden-Day, Inc., San Francisco.
15. Kell, G. S. 1972. Continuum theories of liquid water. p. 331–376. *In* R. A. Horne, (ed.) Water and aqueous solutions: Structure, thermodynamics and transport processes; Wiley — Interscience, New Qork.
16. Kemper, W. D. 1960. Water and ion movement in thin films as influenced by the electrostatic charge and diffuse layer of cations associated with clay mineral surfaces. Soil Sci. Soc. Am. Proc. 24:10–16.
17. Kemper, W. D. 1961a. Movement of water as effected by free energy and pressure gradients: I. Application of classic equations for viscous and diffusive movements to the liquid phase in finely porous media. Soil Sci. Soc. Am. Proc. 25:255–260.
18. Kemper, W. D. 1961b. Movement of water as effected by free energy and pressure gradients: II. Experimental analysis of porous systems in which free energy and pressure gradients act in opposite directions. Soil Sci. Soc. Am. Proc. 25:260–265.
19. Kemper, W. D., and D. E. L. Maasland. 1964. Reduction in salt content on passing through thin films adjacent to charged surfaces. Soil Sci. Soc. Am. Proc. 28:318–323.
20. Kemper, W. D., D. E. L. Maasland, and L. K. Porter. 1964. Mobility of water adjacent to mineral surfaces. Soil Sci. Soc. Am. Proc. 28:164–167.
21. Kemper, W. D., and J. P. Quirk. 1970. Graphic presentation of a mathematical solution for interacting diffuse layers. Soil Sci. Soc. Am. Proc. 34:347–351.
22. Kepert, D. L. 1973. Isopolyanions and heteropolyanions. Vol. 4:607–672. *In* J. C. Bailar, H. J. Emeleus, R. S. Nyholm, and A. F. Trotman-Dickensen (eds.) Comprehensive inorganic chemistry: Pergamon Press, Oxford, England.
23. Kijne, J. W. 1969. On the interaction of water molecules and montmorillonite surfaces. Soil Sci. Soc. Am. Proc. 33:539–543.
24. Korson, L., W. Drost-Hansen, and F. J. Millero. 1969. Viscosity of water at various temperatures. J. Phys. Chem., 73:34–39.
25. Kraus, K. A., H. O. Phillips, A. E. Marcinkowsky, J. S. Johnson and A. J. Shor. 1966. Hyperfiltration studies VI. Salt rejection by dynamically-formed polyelectrolyte membranes. Desalination 1:225–230.
26. Kraus, K. A., A. J. Shor, and J. S. Johnson. 1967. Hyperfiltration studies X. Hyperfiltration with dynamically-formed membranes. Desalination 2:243–266.
27. Lackey, J. A. 1975. Solution mining (in situ leaching). A literature survey. AMDEL Bull. 19:40–61.
28. Levine, S., J. R. Marriott, and K. Robinson. 1975. Theory of electrokinetic flow in a narrow parallel-plate channel. J. Chem. Soc., Faraday Trans. 2:1–11.
29. Low, P. F. 1960. Viscosity of water in clay systems. Clays Clay Miner. 8:170–172.
30. Low, P. F. 1961. Physical chemistry of clay-water interaction. Adv. Agron. 13:269–327.
31. Lutz, J. F., and W. D. Kemper. 1969. Intrinsic permeability of clay as affected by clay-water interaction. Soil Sci. 88:83–90.
32. McKelvey, J. G., Jr., and I. H. Milne. 1962. The flow of salt solutions through compacted clay. Clays Clay Miner. 9:248–259.
33. McKelvey, J. F., Jr., K. S. Spiegler, and M. R. J. Wyllie. 1959. Ultrafiltration of salt solutions through ion-exchange membranes. Chem. Eng. Prog. Symp. Ser. 5:199–208.
34. Miller, R. J., and P. F. Low. 1963. Threshold gradient for water flow in clay systems. Soil Sci. Soc. Am. Proc. 27:605–609.
35. Millero, F. J. 1972. The partial molal volumes of electrolytes in aqueous solutions. p. 519–564. *In* R. A. Horne (ed.) Water and aqueous solutions: Structure, thermodynamics and transport processes. Wiley-Interscience, New York.
36. Mitchell, J. K., and J. S. Younger. 1967. Abnormalities in hydraulic flow through fine-grained soils in permeability and capillarity of soils. ASTM Data Ser. 417.
37. Moeller, T. 1952. p. 210 In Inorganic chemistry — An advanced textbook. John Wiley & Sons, New York.
38. Olsen, H. W. 1965. Deviations from Darcy's law in saturated clays. Soil Sci. Soc. Am. Proc. 29:135–140.
39. Posner, A. M., and J. P. Quirk. 1964. The adsorption of water from concentrated electrolyte solutions by montmorillonites and illite. Proc. Roy. Soc. London, 278:35–56.
40. Ravina Israela, and P. F. Low. 1972. Relation between swelling, water properties and b-dimension in montmorillonite-water systems. Clays Clay Miner. 20:10–123.
41. Russel, D. A., and D. Swartzendruber. 1971. Flux-gradient relationships for saturated flow of water through mixtures of sand, silt and clay. Soil Sci. Soc. Am. Proc. 35:21–26.
42. Shor, A. J., K. A. Kraus, W. T. Smith, and J. S. Johnson. 1968. Hyperfiltration studies XI. Salt rejection properties of dynamically-formed hydrous zirconium (IV) oxide membranes. J. Phys. Chem. 72:2200–2209.
43. Simons, R., and O. Kedem. 1973. Hyperfiltration in porous fixed charge membranes. Desalination 13:1–16.
44. Swartzendruber, D. 1962. Non-Darcy flow behaviour in liquid saturated porous media J. Geophys. Res. 67:5205–5213.
45. Timoshenko, S. P., and S. E. Woinowsky-Krieger. 1959. Theory of plates and shells, 2nd ed. McGraw-Hill, New York.
46. Vnuk, F. 1976. Water — an anomalous solvent. R. Aust. Chem. Inst. (4th Aust. Electrochem. Conf., Adelaide, Aust.)
47. Wong, J. H., C. V. Robinson, and I. S. Edelman. 1952. Self-diffusion and structure of liquid water III. Measurement of the self-diffusion of liquid water with H^2, H^3 and O^{18} as tracers J. Am. Chem Soc. 75:466–470.

CHAPTER 8

Pore Structure and Mechanical Strength of Soils in Relation to Their Constitution

L. A. G. AYLMORE and I. D. SILLS

Abstract

A number of soils possessing a range of textures, and some of which exhibit hard-setting characteristics, have been examined with respect to their physical properties, including pore size distribution, mechanical strength and water stability. In many cases, two pore classes dominate, those corresponding to the packing of clay-sized particles (< 30 nm equivalent plate separation) and those corresponding to the packing of sand-sized particles (> 3 μm equivalent cylindrical radius).

Comparisons between the natural soils and corresponding homogeneous sand–clay mixtures show that many of the soils possess considerably higher proportions of intra-aggregate pores of > 3 μm equivalent cylindrical radius than would be anticipated on the basis of their constituent primary particles. This is particularly noticeable in those soils containing high sesquioxide contents. Disruption of the structure of the aggregates, by puddling or dispersion, and reconstitution generally removes most of the enhanced macro-porosity compared with the sand-clay mixtures.

Introduction

This paper starts from the premise that the pore size distribution of a soil depends, in the first instance, on the particle size distribution and that deviations from this basic relationship may be related to the ordering (or structuring) influences of various factors. It is not difficult to show that the pore sizes between compacted particles of a given size bear, in general, a direct relation to the size of the constituent particles within certain limits determined by the nature of the packing (Childs 1969, Wade 1965). Thus, in the absence of additional structure controlling influences, e.g. specific bonding mechanisms arising from the presence of organic matter, sesquioxides and so on, the pore size distribution of a soil in which the constituent particles are homogeneously mixed could be expected to bear a direct relation to the particle size distribution.

Obviously, the previous history of wetting and drying will affect particle arrangements in natural soils. However, after a number of such wetting and drying cycles, there will be a tendency for the particles to adopt positions of minimum potential energy (Croney and Coleman 1954, Aylmore and Quirk 1960).

Even in the simplest systems, such as packed uniform spheres, the exact prediction of pore sizes poses appreciable mathematical problems (Venable and Wade 1965). In soils, the multiplicity of particle shapes and sizes present makes the possibility of predicting unique standard relationships remote indeed. On the other hand, it is likely that useful information on the manner in which structure formation occurs and the processes contributing to it may be provided by experimental comparisons between the physical properties of natural soils and those exhibited by homogeneous mixtures of the basic primary particles.

In this paper, physical properties of some W.A. wheat-belt soils, mostly hard-setting, and some sesquioxide soils exhibiting no structural problems are compared with those of the reconstituted soils and with artificial clay–sand mixtures. Differences between the properties of the natural aggregates and the homogeneous mixtures are related to the degree of structural ordering and to particle bonding in the natural aggregates.

Materials and Methods

Soils

Samples designated 1–22 and N1–N22 were from soils described by farmers as hard-setting whereas those numbered 31–34 were not. Properties of some of these samples are given in Table 1.

For comparison, samples designated S1–S13 were obtained from sesquioxide soils with good structural properties. Details of samples from 5 of these are also given in Table 1. The soils were euchrozems from the Darling Downs, Qld. (site B177, Stace *et al.* 1968), Armidale, N.S.W. and Kununurra, W.A., samples, S5, S6–S8 and S10–S11 respectively; krasnozems from Ruthven, Qld. (Reeve *et al.* 1960) and Dorrigo, N.S.W., samples S9 and S12–S13, respectively.

The clay fractions of all soils sampled were dominantly kaolin.

A few soils were puddled using a method similar to that used to obtain a saturated soil paste (Richards 1954). They were then dried on a porous plate at 700 mbar suction prior to air-drying, followed by drying at 60 °C.

In selected cases, soil samples were first separated into primary particles and then reconstituted in their original proportions. Dispersion was effected by saturating the exchange sites with Na and then increasing the pH of the salt-free suspension to between 8 and 9. Clay and silt were separated by sedimentation and portions of the clay saturated with Ca before drying. Subsequently, samples of the homoionic clay, silt and sand fractions were recombined in various proportions as described below for the artifical soils.

Artificial soils

Artificial mixtures of clay and sand were prepared using the following materials: (a) Rocky Gully kaolin, $< 2\ \mu m$ fraction of Kent sand from Rocky Gully, W.A.; this is a fine soil kaolinite having a specific surface area of 36 $m^2 g^{-1}$ measured by

Table 1. Physical and chemical properties of soils used.

Sample	Source	Depth (cm)	Composition (%)			ESP (%)	Organic matter (%)	Modulus of rupture (mbar)	Aggregate stability (%)	Extractable	
			Sand	Silt	Clay					Fe (mg/100 g)	Al (mg/100 g)
1	Katanning	5–10	53	5	42	29	2.0	4570	22		
3	Katanning	0–5	61	7	32	–	2.8	1940	37		
4	Katanning	10–20	38	7	55	26	1.3	8700	18		
6	Katanning	0–10	53	11	36	11	1.8	4320	88		
8	Katanning	2–10	72	9	19	11	2.7	2390	67		
9	Katanning	0–2	67	12	21	8	3.4	1100	–	21	15
11	Lake Grace	0–3	75	5	20	12	1.5	2800	47		
12	Lake Grace	3–8	79	4	17	23	1.4	2830	19		
13	Lake Grace	10–20	64	4	32	15	1.0	1820	5		
14	Lake Grace	0–10	72	4	24	4	1.5	1960	75		
17	Lake Grace	0–5	88	3	9	10	1.8	947	81		
19	Kukerin	0–5	76	5	19	8	2.5	609	100	10	19
22	Kukerin	0–5	64	5	31	11	1.9	580	85	17	36
33	Toodyay	0–10	65	13	22	3	2.1	248	85	20	21
N6	Tincurrin	0–10	83	9	8	6	2.5	300	–		
N12	Moulyinning	0–15	81	10	9	0.2	1.0	1500	–		
N18	W. Kulin	0–10	65	17	18	5	2.6	893	–		
S5	Darling Downs	27–45	33	18	49	–	2.5	–	99	160	76
S6	Armidale	0–10	46	25	29	–	8.3	–	98	61	105
S7	Armidale	10–25	39	25	36	–	6.4	–	100	79	154
S8	Armidale	35	20	11	69	–	1.3	–	100	94	191
S9	Dorrigo		30	26	44	–	12.9	–	100	190	153
S10	Kununurra	10–20	23	20	57	–	2.7	–	96	39	37
S11	Kununurra	20–30	29	22	49	–	1.9	–	97	43	42
S12	Ruthven	0–10	17	18	46	–	8.5	0	97	230	175
S13	Ruthven	22–40	13	14	69	–	0.5	0	97	–	–

N_2 sorption. (b) 63–180 μm and 250–500 μm fractions of sand obtained by sieving washed silica sand.

Various proportions of these materials were slurried with water at sufficient consistency to prevent problems of sedimentation of the coarser fractions. A portion of each mixture was immediately dried in an oven at 60 °C whilst the remainder was placed on a ceramic suction plate and taken through wetting and drying cycles between 5 mbar and 700 mbar suction before oven-drying as before. This procedure was followed to observe any natural rearrangement of the particles which might occur.

Methods

Particle size distributions of the soils were measured by the pipette method (Day 1965). Pore size distributions (< 60 μm) were determined using oven-dry soil and a standard mercury injection technique (Ingles 1958, Sills, Aylmore and Quirk 1974). Modulus of rupture determinations were carried out using a method based on that described by Richards (1954) and aggregate stability was determined by the method of Kemper (1965).

Results and Discussion

3 μm volume ratio

Examples of pore size distributions obtained by the combination of Hg injection and N_2 sorption on soils of loamy to clay texture are shown in Fig. 1. A significant feature of the large numbers of soils from the W.A. wheat-belt examined is that two pore classes frequently dominate the internal pore size distributions of the soil aggregates, those < about 30 nm equivalent plate separation generally corresponding to the packing of clay-sized particles (Sills *et al.* 1973) and those > about 3 μm equivalent cylindrical radius corresponding to those generally observed in the packing of sand-sized particles. While the plateau in the curves may be related to the comparatively low silt content of many of these soils, subsequent studies on the effects of puddling or reconstitution of the soils indicate that this is not necessarily the case.

In Fig. 2, the results obtained for the Rocky Gully kaolinite–sand mixtures have been presented in terms of the 3 μm volume ratio, defined as the ratio of the volume of pores of equivalent cylindrical radii between 3 and 60 μm (determined by Hg injection) to the total measured pore volume (determined by the kerosene method with excess liquid being removed with blotting paper), plotted against the % sand. The reproducibility of the data, regardless of the pretreatment used, suggests that such short-term wetting and drying is of little, if any, significance in determining the 3 μm ratio in these materials.

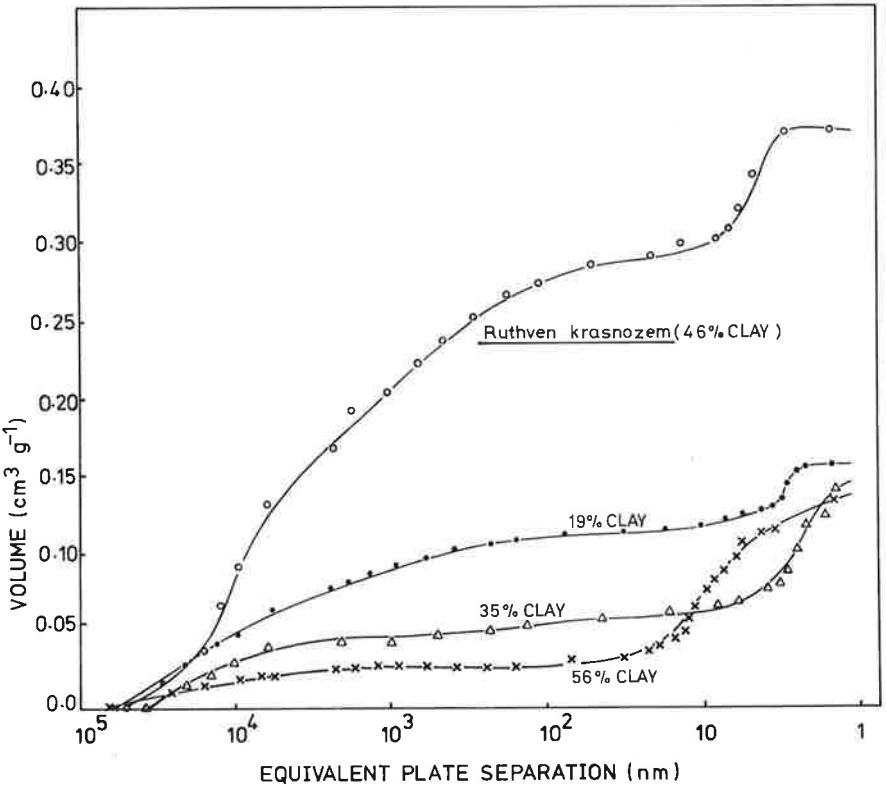

Fig. 1. Distributions of sizes of pores smaller than about 60 μm in natural aggregates from a krasnozem and three typical W.A. wheat-belt soils

Particle ordering

For constituent primary particles of similar dimensions, it seems reasonable to consider a line through these data as a rough standard to assess the extent to which the pore structure of a given soil is different from that corresponding to a homogeneous mixing of the constituent particles. Use of a coarser sand fraction (250–500 μm shown by the triangles) displaces the 3 μm ratio to higher values at high sand contents, presumably because there is insufficient clay to fill in the larger intervening voids compared with those formed by the finer sand fraction. Thus, while the validity of this standard curve will vary with variations in the dimensions of the primary particles within each textural class, displacements produced by such variations in particle dimensions should be readily interpretable. A sieve analysis of a number of the wheat-belt soils indicate that the size of the sand particles range between 63 and 1000 μm. However, in most of the soils examined, the 63–180 μm fraction dominates and consequently, this was considered the most practical for setting the initial standard. Mixtures of the clay and 250–500 μm sand had

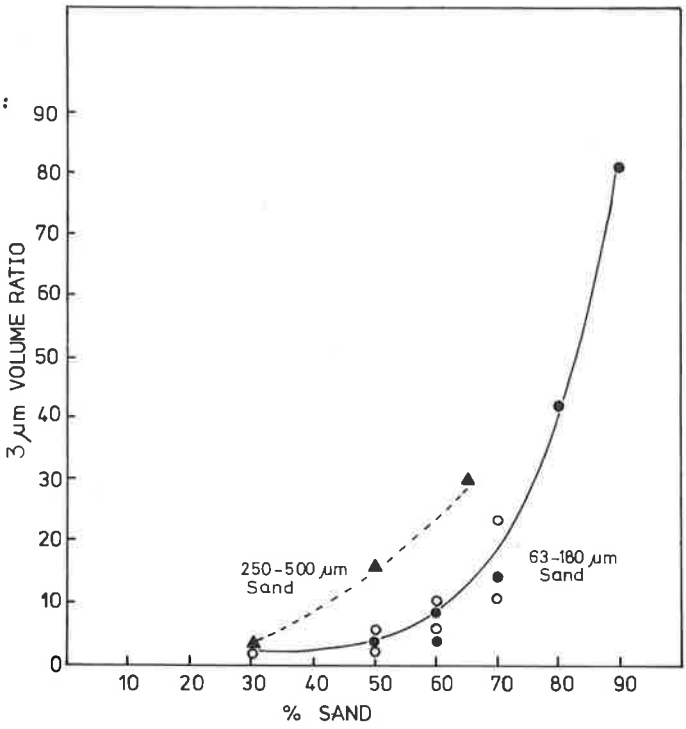

Fig. 2. 3 μm volume ratio as a function of the composition of sand-Rocky Gully kaolinite mixtures. Circles represent mixtures containing 63–180 μm sand. Open symbols refer to slurries dried at 60 °C, closed symbols to slurries cycled between 5 mbar and 700 mbar suction before drying at 60 °C

insufficient coherence on drying to enable satisfactory porosity measurements to be obtained once the sand content was $> 65\%$.

In Fig. 3, the data obtained for the soil samples have been plotted and compared with the standard kaolin–sand mixture curve. It is immediately apparent that most of the soils examined have significantly larger proportions of their pore volumes in pores > 3 μm equivalent cylindrical radius than would be anticipated on the basis of their constituent primary particles. In some cases satisfactory explanation for small deviations can be proffered in terms of the presence of primary sand particles of larger dimensions than those used in obtaining the standard curve or the presence of appreciable quantities of silt. However, in most cases deviations can only reflect an ordering of the primary particles to provide an increase in macro-porosity with presumably some decrease in meso- and micro-porosity. (The terminology adopted here is that generally accepted in current literature on sorption in porous materials, Dubinin 1968).

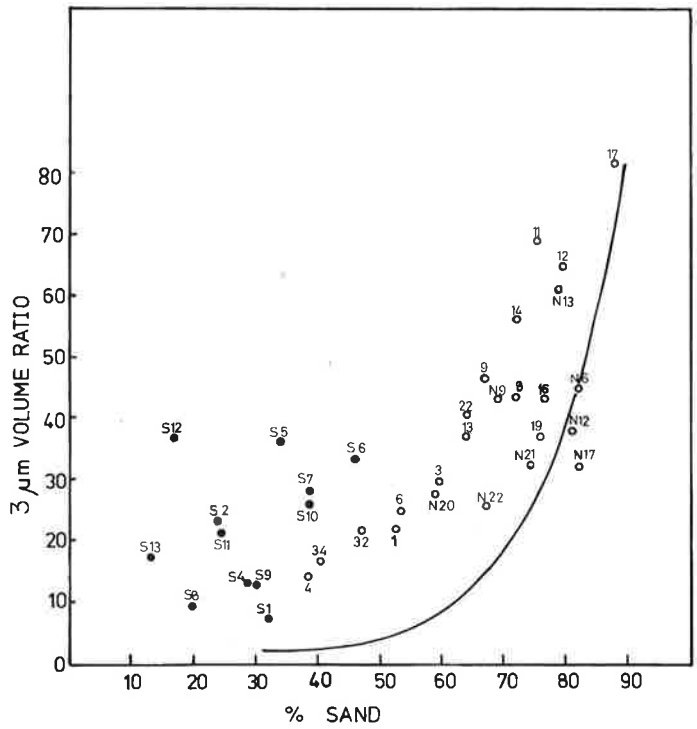

Fig. 3. 3 μm volume ratio as a function of sand content of natural soil aggregates compared with the artificial sand–kaolinite mixtures (solid line). ○ W.A. wheat-belt soils ● sesquioxide soils

Particle bonding

Large deviations (corresponding to nearly 40% of the total porosity) were observed for a number of the soils of higher clay content, in particular the Ruthven krasnozem and Darling Downs euchrozem, S5 and S12 respectively. A significant feature of these soils is that they are all characterized by high sesquioxide contents. This lends support to the suggestion that the presence of these specific bonding constituents enhances the development of a more ordered, open structure. Edwards and Bremner (1967) proposed the linking of organic matter and clay with polyvalent cations in the formation and stabilization of micro-aggregates and later (Giovannini and Sequi 1976) attempted to selectively extract the Fe and Al which they postulated were involved in such a linking role. This method involves the use of acetylacetone in benzene to remove Fe and Al but not organic matter. The results of extractions performed on the sesquioxide dominated soils and on several W.A. wheat-belt soils using this technique appear in Table 1 and show that, on the whole, there is a far greater concentration of extractable Fe and Al in the former group of soils than in the wheat-belt soils. This is consistent with the proposal that bonding

forces resulting from polyvalent cations may cause structuring of the soil particles and hence a displacement above the standard curve. While no significant correlations between the magnitudes of the displacements from the standard curve and the amounts of Fe, Al or organic matter within the sesquioxide dominated soils are evident, it is likely that successful structure formation may depend on the particular form and combinations of these constituents required to effect bonding.

Puddled soils and reconstituted soils

In Fig. 4 is shown the effects of structure disruption by puddling on the 3 μm volume ratio of a number of soils which exhibit large deviations from the standard curve. In most cases, the ratio was reduced to the immediate vicinity of the standard curve. The deviation remaining in soil S12 presumably reflects the incomplete disruption of structure during puddling or basic differences in primary particle size from that of the clay–sand mixtures used to determine the standard curve. The fact that the 3 μm volume ratio of soil N18 increased slightly after puddling indicates that the natural soil already possesses minimal structure. Results for two reconstituted, typical hard-setting soils, (N18 from W. Kulin and 6 from Katanning) are also shown in Fig. 4. In both cases, reconstitution of the soils produced values close to the standard curve which were little different from those

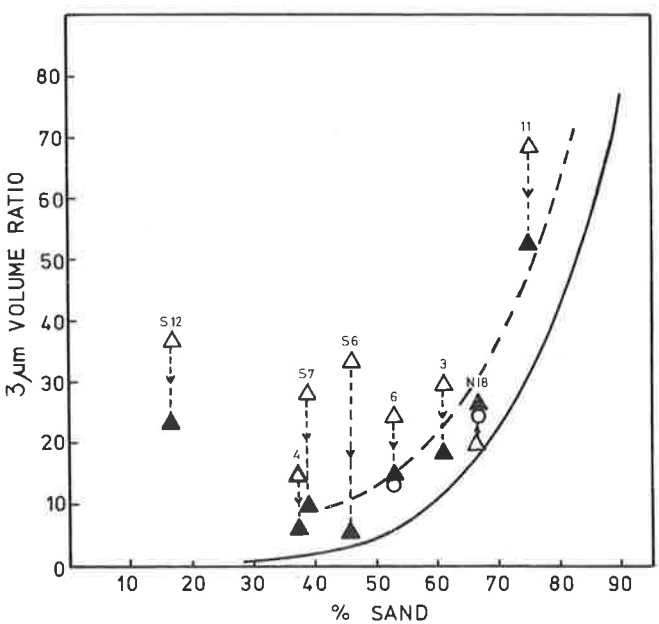

Fig. 4. Effect on 3 μm volume ratio of mixing components of soils (reconstituted soil, ○; sand-clay mixtures, – – –) and of puddling soils (natural, △; puddled, ▲) compared with the sand-Rocky Gully kaolinite mixtures (———)

obtained for the natural soils after puddling. The results for mixtures of sand and clays derived from soils 6 and N18 (presented as the dashed line in Fig. 4) follow the curve closely. The fact that the puddled and wholly reconstituted soils (including the silt content) also fall close to this line indicates that, in these cases at least, ignoring the silt content detracts little, if any, from the validity of the standard curve.

Aggregate stability

In view of the multiplicity of factors which may affect development and stability of structure in soils, it is difficult to evaluate correlation coefficients on such a relatively small number of soils. However, the deleterious effects of exchangeable sodium on structure are illustrated by significant negative correlations between aggregate stability and ESP ($r = -0.7$) and between the displacement ratio and ESP ($r = -0.6$). The displacement ratio is the displacement from the standard curve divided by the standard 3 μm volume at that sand content.

Most of the wheat-belt soils provided relatively high values to the modulus of rupture test (Table 1), particularly those in which there is a very high ESP. In striking contrast, despite their generally higher clay contents, the sesquioxide-dominated soil aggregates had almost total stability under the conditions of the test and either would not form wafers necessary for the test or yielded insignificant readings. This together with the porosity comparisons, clearly illustrates the basic difference in internal structure of the aggregates between the two groups of soils. In the hard-setting soils, the packing of the clay particles to form a more extensive interleaving of domains gives rise to a massive structure with a minimum of porosity other than that between neighbouring clay plates (Aylmore and Quirk 1967). The action of intra-aggregate structure forming agencies is obviously to reduce this natural packing of the clay particles presumably by either enhancing the precipitation and cementation of micro-aggregates prior to packing or by crosslinking with larger primary particles.

It is suggested that a satisfactory understanding of the level at which various bonding agents operate will inevitably necessitate a systematic dissection of the particle size-pore size relationship similar to that attempted here.

References

Aylmore, L. A. G., and Quirk, J. P. (1960). *Nature*, **187**, 1046–1048.

Childs, E. C. (1969). *An Introduction to the Physical Basis of Soil Water Phenomena*. John Wiley, London.

Croney, D., and Coleman, J. D. (1954). *J. Soil Sci.*, **5**, 75–84.

Day, P. R. (1965). *In* Black, C. A. (Ed.) *Methods of Soil Analysis, Part 1*, 545–567, Am. Soc. Agron., Wisconsin.

Dubinin, M. M. (1968). *Adv. Coll. and Interface Sci.*, **2**, 217–235.

Edwards, A. P., and Bremner, J. M. (1967). *J. Soil Sci.*, **18**, 47–63.

Giovannini, G., and Sequi, P. (1976). *J. Soil Sci.*, **27**, 140–153.

Ingles, O. G. (1958). *Aust. J. Appl. Sci.*, **9**, 120–126.

Kemper, W. D. (1965). *In* Black, C. A. (Ed.) *Methods of Soil Analysis, Part 1*, 511–519, Am. Soc. Agron., Wisconsin.

Reeve, R., Thompson, C. H., and Beckmann, G. G. (1960). *CSIRO Div. Soils*, Div. Rep. 1/60.

Richards, L. A. (Ed.) (1954). *Diagnosis and Improvement of Saline and Alkali Soils*. USDA Agric. Hdbk. 60.

Sills, I. D., Aylmore, L. A. G., and Quirk, J. P. (1973). *J. Soil Sci.*, **24** , 480–490.

Sills, I. D., Aylmore, L. A. G., and Quirk, J. P. (1974). *Aust. J. Soil Res.*, **12**, 107–117.

Stace, H. C. T., Hubble, G. D., Brewer, R., Northcote, K. H., Sleeman, J. R., Mulcahy, M. J., and Hallsworth, E. G. (1968). *A Handbook of Australian Soils*. Rellim, Glenside, S. A.

Venable, R., and Wade, W. H. (1965). *J. Phys. Chem.*, **69**, 1395–1401.

Wade, W. H. (1965). *J. Phys. Chem.*, **69**, 323–326.

Plant and Soil **49**, 461–475 (1978) Ms. 3376

MEASUREMENT OF WATER FLUXES AND POTENTIALS IN A SINGLE ROOT–SOIL SYSTEM

II. APPLICATIONS OF TENSIOMETER-POTOMETER SYSTEM*

by H. B. SO, L. A. G. AYLMORE and J. P. QUIRK**

SUMMARY

The usefulness of a tensiometer–potometer system in investigations of water flow in the vicinity of a plant root has been demonstrated. Measurements were made of the root–soil interface water potential, xylem potential and the distribution of water fluxes and root resistance along the length of a maize root. For a root growing in sand, the rhizosphere resistance was 3.5 to 8 times the radial resistance of the root at average rhizosphere potentials of −250 m bars. For a root growing in sandy loam such rhizosphere resistance was not achieved until the average rhizosphere potential is approximately −2 bars.

INTRODUCTION

The importance of obtaining direct experimental measurements of the water potentials and fluxes in the vicinity of plant roots growing in soil has recently been emphasised[11 12]. At present most of the information available has been derived from indirect measurements or from mathematical models based on various assumptions.

Of particular interest is the relative magnitude of the resistance to flow provided by the soil and plant pathways respectively. While numerous workers have presented evidence to suggest that the rhi-

* Contribution from the Department of Soil Science and Plant Nutrition, University of Western Australia, Nedlands, Western Australia 6009.

** Present affiliations; Lecturer, Department of Agronomy and Soil Science, University of New England, Armidale, N.S.W. Australia; Senior Lecturer, Department of Soil Science and Plant Nutrition, University of Western Australia, Nedlands, Western Australia 6009 and Director, Waite Agricultural Research Institute, Glen Osmond, South Australia.

zosphere resistance can be appreciable in relation to the resistance in the plant even at very high matric potentials[3 5 6 7 8], Newman has questioned the validity of many of the assumptions and interpretations used in previous work and has concluded that appreciable rhizosphere resistances generally only occur when the soil is near or beyond the permanent wilting point.

Much of the difficulty in resolving this question arises from the lack of a suitable method of measuring the water potential at the root-soil interface. In the preceding paper of this series[15] the construction and operation of a tensiometer-potometer system capable of measuring *in situ* and simultaneously the xylem water potential, the root-soil interface water potential and the flux of water into a single root growing in a soil was described. This paper presents three series of experiments carried out to evaluate the possible applications of this tensiometer-potometer system.

MATERIALS AND METHODS

The construction and operation of the tensiometer-potometer system was described in the previous paper of this series[15]. Briefly, this apparatus consists of a tensiometer collar in series with one or more flow collars to make up a potometer system, in which a single plant root can be grown. The tensiometer consists of a ceramic cylinder of 0.6 cm ID cemented at its ends inside a perspex cylinder leaving a gap between the two materials which acts as a water reservoir. This reservoir is connected to a pressure transducer system and a calibrated capillary through a 3-way vacuum tap, such that it can be operated as a tensiometer or a flow collar for measuring the flux of water into the root. The inside of the ceramic cylinder of the tensiometer is packed with ceramic particles of 0.25–0.5 mm size, leaving a small channel in the centre for the root to grow through. The expectation is that the ceramic particles will act essentially as an extension of the ceramic wall of the tensiometer. The flow collars which are similar in construction (with the exception that they are not connected to a pressure transducer system) were similarly packed with either ceramic particles or soil.

At equilibrium the tensiometer will measure the xylem water potential of the root. The flow collars are used to measure the flux of water into the root under various suctions applied to the collar to simulate various soil suctions.

The soils used were a silicious sand from Jandakot, Perth, W. A. and a sandy loam from Harvey, W. A. Plants used were hybrid maize seedlings described in the first paper[15]. The transpirational demand on the plant was varied by controlling the environmental conditions of the aerial part of the plant within a perspex cabinet.

Measurement of the xylem water potential using the flux-estimation method

As the tensiometer is limited in the range of measurement to −0.85 bars, it was hoped that xylem water potentials below −0.85 bars could be estimated by the flux estimation method, similar to the method employed by Brouwer[2] with his potometers containing nutrient solutions with various concentrations of an osmoticum. This would greatly enhance the range of usefulness of the equipment.

The resistance of the root tissues to water flow is known to change with the suctions applied to the root[2 10 13] but this change takes some time to complete. The flux immediately after a change in applied suctions will consequently be subject to the original root resistance before the change. An estimate of the xylem water potential can therefore be obtained by linear extrapolation to zero flux of the flux-suction relationship given by the fluxes measured before and immediately after the change in suction. For given environmental conditions including a constant root environment the xylem water potential will remain essentially constant and unaffected by the suctions imposed on a single root.

Two experiments were conducted using a two-collar arrangement (Exp. 1 and 2) to investigate the accuracy of this method. One collar was used as a flow collar whereas the other was used as a tensiometer collar to check the accuracy of the flux estimation method.

Measurement of the water potential at the root-soil interface and the root-soil resistance to water flow

These measurements were conducted using three collar arrangements consisting of a 2 cm flow collar packed with Jandakot sand (sand collar), a tensiometer and a flow collar packed with ceramic particles (ceramic collar).

The fluxes of water through the sand collar were measured with various suctions applied to the collar. These valves thus constitute the suctions of the soil water at the outer boundary of the soil cylinder. Simultaneously the flux-suction curve for the same root was measured using the tensiometer and ceramic flow collar which was subjected to various applied suctions. As the resistance of the ceramic particle bed (10^2 mbar HR cm^{-2}) was very small relative to the root resistance (10^4 mbar HR cm^{-2}) the flux-suction curve essentially relates to the flow properties of the root only and the applied suction is essentially the inverse of the water potential at the root surface.

The water potential at the root surface that results in a flux similar to the flux of water through the sand collar can thus be found from the flux-suction curve. Once this was determined, it becomes a simple matter to calculate the root and soil (or sand) resistances.

Three experiments were carried out in this series (Exp. 3, 4 and 5).

Measurement of the distribution of fluxes and resistances along the length of a root

These measurements were conducted using a three-collar arrangement consisting of a tensiometer collar (ceramic) sandwiched between two soil

collars packed with a sandy loam from the Harvey region in W. A. Flux measurements were taken at the soil collars under a constant suction of 100 mbars and the xylem potential was monitored with the tensiometer. The soil resistance at this suction was very small relative to the root resistance and hence the root-soil interface potential measurements were not considered necessary. The length of root that had grown through the potometer was monitored with time so that any flux measured could be associated with a particular position on the root.

The sandy loam was used instead of the sand because its resistance to water flow is smaller, its resistance to root penetration is smaller and it appears that the root made better contact with the sandy loam than with the sand. Two experiments were conducted for this series (Exp. 6 and 7).

RESULTS AND DISCUSSION

The flux estimation method

A typical result of this method is shown in Fig. 1. The numbers on the points refer to the sequence of operation. For Exp. 1 the number

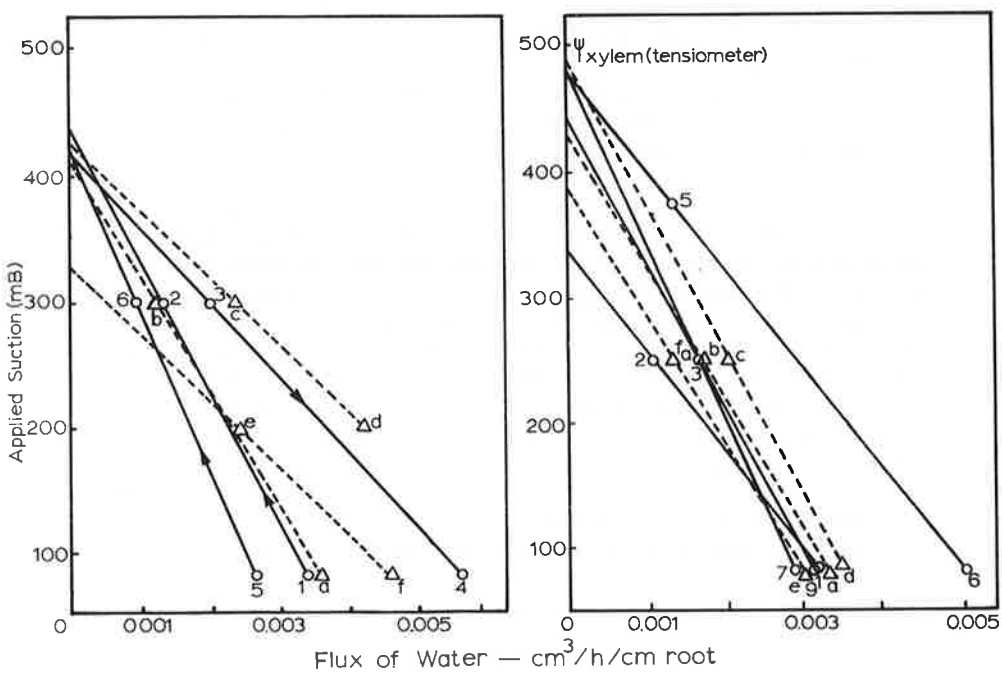

Fig. 1. Xylem tension estimated using the flux estimation method.

TABLE 1

Accuracy of the flux estimation method

Exp.	Tensiometer	Xylem potential (mbars) measured by flux estimation method*
1	—	−410, −416, −420, −426, −436
2	−493	−340(69), −483(98), −480(97½), −440(89½) −340(69), −385(78), −430(87), −485(98½)
3	−312	−290(93), −360(115), −315(101)
4	−312	−291(93), −287(92)
5	−465	−386(83), −394(85), −290(62½)

* Numbers in brackets are the percentages of the tensiometer readings.

1 is the equilibrium flux at a suction of 80 mbars, 2 is transient flux immediately after the suction was changed to 300 mbars (after allowing 5 min for a drainage equilibrium to be achieved for the ceramic particles). 3 is the equilibrium flux at 300 mbars suction whereas 4 is the transient flux immediately after the suction was changed to 80 mbars. The intercept of line 1–2 or 3–4 with the Y-axis should give an estimate of the xylem water potential as measured by the tensiometer. The accuracy of these estimations varies widely as shown in Table 1. In this table this method was extended to include other experimental runs. It is obvious that the accuracy of this method was not satisfactory as the estimates range from 60–115% of the true value (tensiometer reading) with the majority being below 100%. Thus the method tends to over-estimate the xylem water potential. The poor precision and accuracy of this method was probably the result of the lack of accuracy of the flux measurements immediately after the suction change. Such a change was always accompanied by a change in water content of the ceramic particles which was completed within 5 minutes when no plant was present, and hence the 5 minutes delay before the first flux measurement was made. However, the change in root resistance caused by a change in suction was usually completed in about 30 minutes for maize which is in agreement with the findings of Hayward and Spurr[9]. This allowed only one or two transient flux measurements before the change in resistance was complete (approximately 25 minutes) which was not enough to make corrections for the first 5 minutes period after the change.

Brouwer[1] found that the change in resistance of broad bean

roots associated with a suction change was completed in 3 hours which allows adequate time for reasonably accurate measurements.

It was concluded that the flux estimation method does not provide sufficient accurate estimates of the xylem tension of a maize root.

The root–soil interface water potential

The results of three experiments are presented in Fig. 2 where the

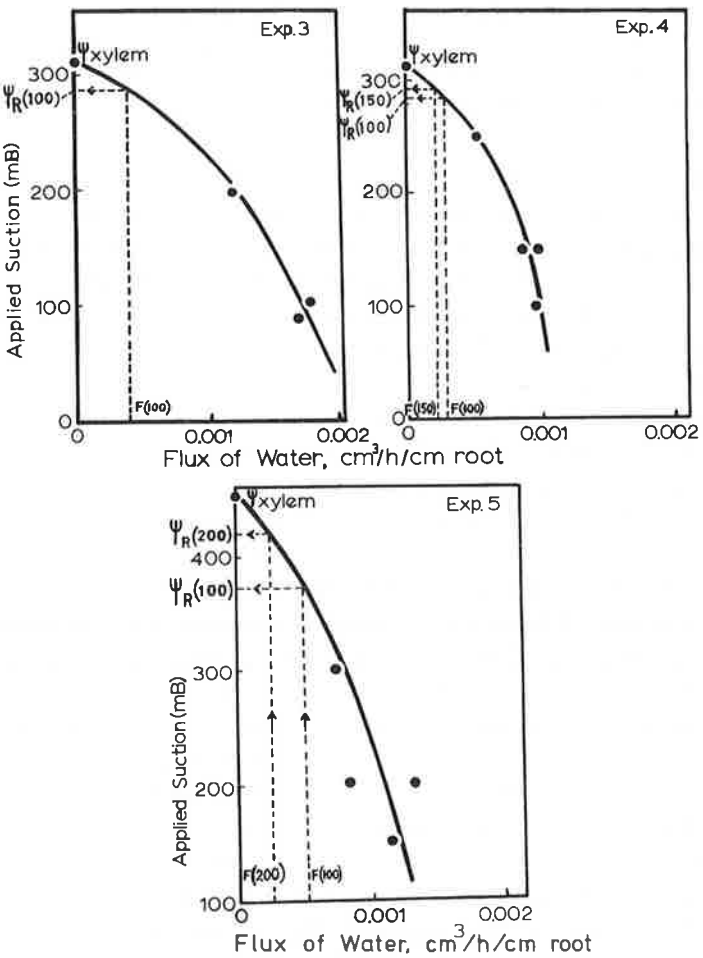

Fig. 2. Flux-suction relationships for the roots of Expts. 3, 4 and 5. Dotted lines with arrows show the method used for obtaining Ψ root from the flux of water through the sand column. $F_{(100)}$ = flux of water through sand at 100 mbars suction. $R_{(100)}$ = Tension at the root surface at soil tension of 100 mbars.

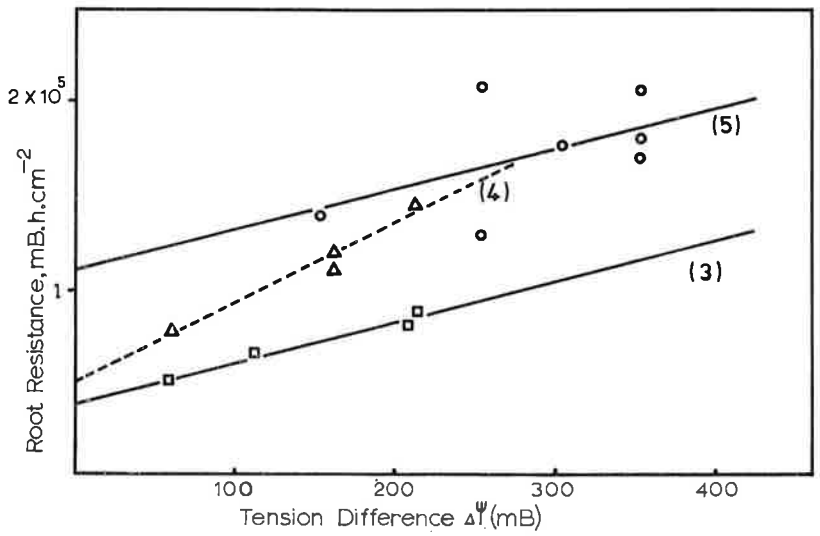

Fig. 3. Root resistance *versus* tension difference for roots in Expts. 3, 4 and 5.

flux was plotted against applied suction at the root surface. The solid curves were replotted from the regression lines in Fig. 3 which shows the root resistance plotted against the suction differences between the xylem and root surface[15].

The flux through the soil collar under applied suctions of 100 and 150 mbars (F100 and F150) were superimposed on this curve and the root-soil-interface tensions were found as shown by the dotted lines (100 and 150 respectively).

This allows the root and sand resistances (R_R and R_S) to be calculated from the Ohm's law analogue

$$\text{Flux} = -\frac{\Psi_X - \Psi_R}{R_R} = -\frac{\Psi_R - \Psi_S}{R_S} \qquad (1)$$

where Ψ_X, Ψ_R and Ψ_S are the water potentials of the xylem, root-soil-interface and the soil respectively.
Therefore the ratio

$$\frac{R_R}{R_S} = \frac{\Delta\Psi_{root}}{\Delta\Psi_{soil}} \qquad (2)$$

The results of the 3 experiments in this series are presented in Table

TABLE 2

Water potentials and resistances to water flow observed during experiments on Jandakot sand

(1)	(2)	(3)	(4)	(5)	(6)	(7)	(8)	(9)	(10)	(11)
Exp.	Ψxylem	Ψsoil (at r = 0.3 cm)	Ψroot surface	Flux of water per cm of root cc HR^{-1}	R_S calculated from R_R				R_S calculated from $\Delta\Psi$soil	
					$\Delta\Psi_{root}$	$R_{root} \times 10^4 HR\ cm^{-2}$	R_S/R_R	$R_S \times 10^4 HR\ cm^{-2}$	$\Delta\Psi_{soil}$	$R_S \times 10^4 HR\ cm^{-2}$
3	−312	−100	−288	4.8×10^{-4}	24	5.35	7.85	41.9	188	39.2
4	−312	−100	−285	3.6×10^{-4}	27	7.20	6.85	49.3	185	51.4
		−150	−294	2.7×10^{-4}	18	6.85	8.00	54.9	144	53.4
5	−452	−100	−372	6.0×10^{-4}	80	15.4	3.40	52.4	272	45.4
		−200	−421	3.0×10^{-4}	31	14.1	7.21	100.4	221	74.0

2. R_S was calculated from R_R taken from Fig. 3 and multiplied by the factor R_S/R_R (Column 9) and also directly using the Ohm's law analogue (Column 11). The agreement between the two R_S values was good, indicating that the values of Ψ_R were valid and accurate.

A comparison was made between these experimental values of R_S with those calculated from conductivity (K) data of the Jandakot sand measured separately[15]. As K is a sensitive function of matric potential, it was averaged by the formula given by Crank[4].

$$\overline{K} = \frac{1}{\Psi_2 - \Psi_1} \int_{\Psi 1}^{\Psi 2} K d\Psi \qquad (3)$$

The geometry of the root is not a simple cylinder, as root hairs protrude out of the main cylinder. However, as the effective root radius is not known, maximum and minimum possible values of the average soil cylinder resistances can be calculated from $\overline{K}$ values of Equation (3). The maximum average soil cylinders resistances $\overline{R}_s$ were calculated using the dimensions of 0.6 cm O.D. and 0.16 cm I.D. which are the diameters of the root cylinders whereas the minimum average soil resistance $\overline{R}_s$* were calculated using 0.6 cm O.D. and 0.31 cm I.D. which is the diameter of the cylinder at the tip of the root hairs.

The agreement of the R_s values of Table 2 being the resistance of the effective soil cylinder, with the values of $\overline{R}_s$ and $\overline{R}_s$* (Table 3)

TABLE 3

Calculated resistance of sand collar

Exp.	Soil tensions (mbars)	k (10^{-7} cmHR^{-1})	Ψ (mbars)	R_s (.16cm ID) (10^4HRcm^{-2})	R_s* (.31cm ID) (10^4HRcm^{-2})
3	100–288	8.1	243	65	32.5
4	100–285	8.1	243	65	32.5
	150–294	4.3	254	80	40
5	100–372	5.7	285	130	65
	200–421	—	—	—	—

was good. With the exception of experiment 5, the values of R_s were all between the maximum $\overline{R}_s$ and the minimum $\overline{R}_s$*. The root of experiment 5 appeared to be diseased (brown spots were visible on the root when dismantling) and this may be the cause of the poor correlation between root resistance and suction difference (Fig. 3) and the poor agreement between the various soil resistance values.

It must be concluded that with the agreement between the two experimental values of R_s and the calculated values of $\overline{R}_s$ and $\overline{R}_s$*, that the accuracy of the measurement of the root–soil interface water potential must be good.

Higher suctions were not used on the sand collar as the fluxes became too small for accurate measurements due to the rapid reduction of the conductivity K.

The values of R_s/R_R ranged from 3.5 to 8 for Jandakot sand under suctions of 100 to 200 mbars applied at a distance of 0.3 cm from the root axis. The sand within this area is considered as the rhizosphere[14]. Thus the resistance of the sand rhizosphere was much higher than the root resistance. The rhizosphere in these experiments is equivalent to that of a root system with a density of 3.5 cm root /cm^3 of soil, ($= 1/\pi R^2$, R = inner radius of tensiometer cylinder) where the root system is assumed to be an array of parallel roots.

Newman[11,12] developed Gardner's model further and predicted that the development of an appreciable rhizosphere resistance was rare at soil suctions as low as 1 bar and claims that such a high rhizosphere resistance is only possible with very low root densities such as those used by Cowan[3] which ranged from 0.125 to 0.5 cm/cm^3. In his treatment of the radial flow of water to a single root, Gardner[7] gives the solution of the steady state flow of water in a hollow

cylinder as

$$\Delta\Psi = \Psi_a - \Psi_b = \frac{\Phi}{4\pi K} \ln \frac{(b^2)}{a^2} \quad (4)$$

where: Ψ_a and Ψ_b are the water potentials at r = a (root radius) and r = b (outer radius of soil cylinder), Φ = volume flux of water (radial flow) and K = soil's conductivity.

Using this solution and extrapolating to a soil–plant system, Newman obtained an expression for the soil conductivity K when the rhizosphere resistance becomes appreciable or when the soil resistance (R_S) equals the plant resistance (R_p):

$$K = \frac{1}{2\pi L_A R_P} \ln \frac{b}{a} = \frac{E}{2\pi L_A(\Psi_R - \Psi_e)} \ln \frac{b}{a} \quad (5)$$

Where E = transpiration rate, Ψ_R and Ψ_e are the water potentials at the root surface and evaporating sites in the leaves respectively and L_A = length of root per unit ground surface area. Therefore, the value of K is dependent on L_A. From his examination of observed L_A values Newman concluded that the rhizosphere resistance rarely becomes appreciable until the soil moisture potential is near wilting point except at very low values of L_A.

If we assume a rooting depth of 15 cm for a 3 week old maize (actual root lengths range from 0 to 50 cm) this will give a value for L_A of approximately 50 (15 cm $\times$ 3.5 cm/cm^3) which is within the range of observed L_A values[12] (5 to 4000 cm/cm^2). The values of ln (b/a) in this experiment range from 0.66, if the tip of the root hairs is considered as the root cylinder, to 1.40 if the root cylinder itself is used. Therefore a value of 1.00 was used. The value of R_p of 5×10^3 days used by Newman was used, considering the leaf water potential under the experimental conditions was approximately 3 bars and the potential transpiration rate of 0.6 cm/day which gives an R_P of 5×10^3 days. Using Equation (5) K was calculated to be 2.7×10^{-8} cm h^{-1} which corresponds to a suction of 260 mbars in the Jandakot sand and approximately 2 bars in the Harvey sandy loam.

The experimental results show that at average rhizosphere suctions of 240 to 285 mbars (Table 3) the rhizosphere resistance is several times the root resistance. The ratio R_s/R_R would remain the same for a whole root system as well as a single root assuming water

flows predominantly in the radial direction. However, the plant resistance would be 2 to 3 times the root resistance. Hence, the results show that appreciable rhizosphere resistance can develop at suctions well before wilting point is approached and this will depend on the conductivity – water potential relationship of the soil used.

The uncertainties in the calculations are the values of L_A and R_P which are inversely related to K. However the magnitude of the average soil potential is insensitive to changes in the magnitude of K. A change in K by factor of 10^3 will produce a change in soil potential of approximately 100 mbars in the sand and 0.9 to 1 bar in sandy loam[15]. Therefore unless L_A and R_P are in error by several orders of magnitude the above conclusion will not be significantly affected.

Thus Newman's generalisation should be viewed with caution and a consideration of the soil type should be included.

Distribution of the flux and resistance along the root

The results of the 2 experiments are presented in Fig. 4 where the flux of water is plotted against distance from the root tip. These fluxes were measured subject to a constant suction of 100 mbars. The xylem potentials were not constant, decreasing progressively from —645 to —690 mbars for the first experiment and from —700 to —710 mbars for the second experiment over the 3 days of the measurements. As the flux varied with xylem potentials, the data had to be standardized assuming that R_R remained constant over the relatively small changes of xylem potentials. This was achieved by using the equation:

$$R_R = \frac{-\Psi_X^S - 100}{F_S} = \frac{-\Psi_X^i - 100}{F_i} \qquad (6)$$

where:

F_i, F_S = measured and standardized fluxes of water,
Ψ_X^i, Ψ_X^S = measured and standard xylem potentials, and the number 100 refers to the suction applied to the collars.

Thus:

$$F_S = F_i \frac{\Psi_X^S - 100}{\Psi_X^i - 100} \qquad (7)$$

The fluxes of the first experiment were standardized to a xylem

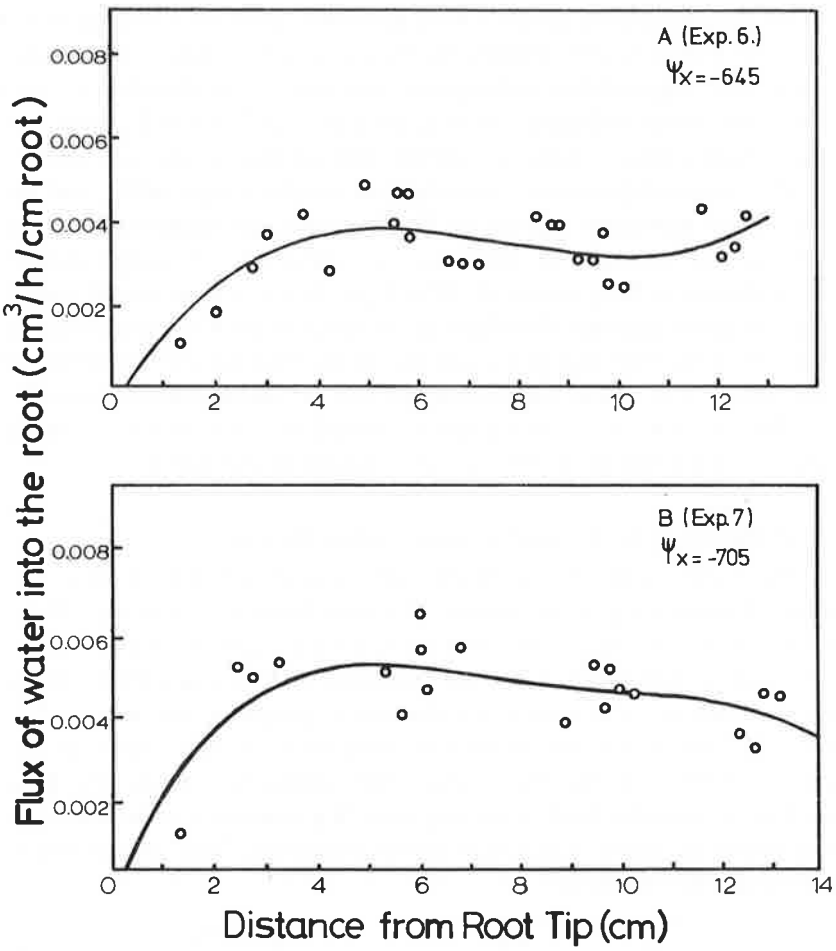

Fig. 4. Distribution of water fluxes along the root.

potential of −645 mbars whereas an average xylem potential of −705 mbars was used in the second experiment as the range was small and therefore the fluxes were not corrected. The curves were fitted to the data using the polynomials of the type $Y = a_0 + a_1X + a_2X^2 + \ldots\ldots$ etc. The best fitting curve was considered the polynomial with the minimum order that had the following characteristics: (a) A negative intercept with the Y-axis and consequently a positive intercept with the X-axis as the root tip would most probably show very little water uptake, and (b) The mean square of the

residuals should not change significantly with an additional increase in the order of the polynomial.

The polynomials for the two curves are:

1st exp: $Y = -0.000475 + 0.0019\,X - 0.000275\,X^2 + 0.000012\,X^3$

2nd exp: $Y = -0.00028 + 0.0028\,X - 0.00053\,X^2 + 0.000041\,X^3 - 0.0000012\,X^4$

where Y is the flux of water into the root in cm^3/HR cm root and X is the distance from the root tip in cm.

It is interesting to note that although the data show a considerable amount of scatter, both curves have the same shape except for the increasing uptake rate at the base of the root of curve A. This was undoubtedly a result of the branching of the root at the top collar which was observed when dismantling the potometer at the end of the experiment. Although the absolute values of the fluxes were different, the distribution patterns along the roots were very similar with a maximum uptake rate at 5 to $5\frac{1}{2}$ cm from the root tip. The rate of uptake increased sharply from the tip to the maximum and decreased slowly thereafter. When the root resistances were calculated using the Ohm's law analogue, two similar distributions of root resistances were obtained for both experiments (Fig. 5). Thus the

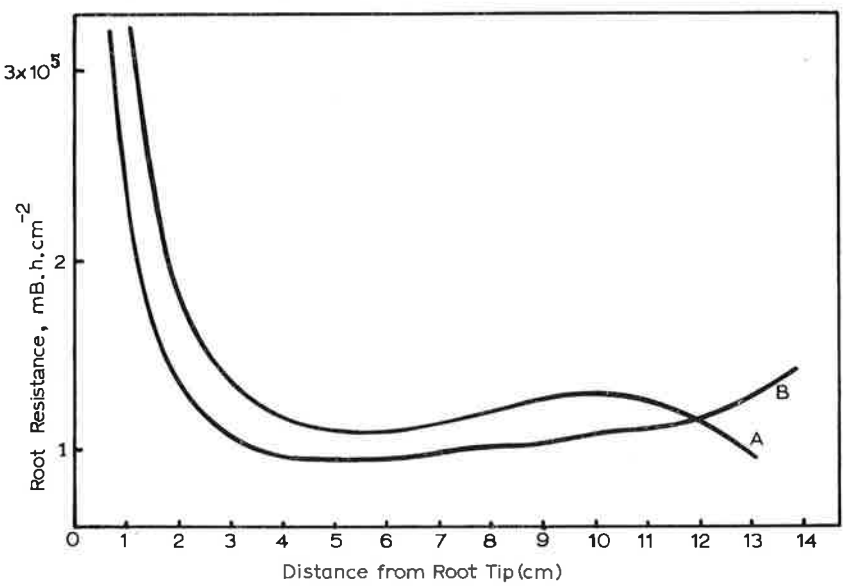

Fig. 5. Distribution of root resistances along the root.

differences in uptake rates resulted from differences in root resistance as well as observed differences in xylem potentials. These resistances are lower than those found by other workers on maize roots[16].

The assumption used that the rates of uptake or root resistances were uniform along the root is acceptable if measurements were taken some 4 cm or more away from the root tip. In the preceding experiments measurements were not started until the root has penetrated past the potometer by some 3 to 4 cm.

In conclusion, it has been shown that the tensiometer-potometer, described in a preceding paper[15] will be a useful research tool in plant soil water relationships. It is limited in the range of root xylem potentials that can be measured with this instrument. However, it may be possible to extend this range by using the flux estimation method on a root that requires a longer period than maize to change its resistance when subjected to a sudden change in applied suction, such as a broad bean root[1]. This instrument is capable of measuring the root-soil-interface water potential, the xylem potential and the flux of water simultaneously under various applied soil water potentials. Therefore it makes possible the direct measurement of root and rhizosphere resistances. Note that in these experiments good root–soil contact was maintained. It is also a useful tool for measuring the distribution of water flux or root resistances to water flow along the root length. If the variation of the tensiometer readings during the last experiments can be taken to be the result of xylem resistance, then it must be concluded that the xylem resistance of the nodal roots of maize is relatively small compared to its radial resistance.

ACKNOWLEDGEMENT

This work was financed by grants from the Western Australian Wheat Industry Research Committee whose support is gratefully acknowledged.

Received 28 January 1977

REFERENCES

1 Brouwer, R., Water absorption by the roots of *Vicia faba* at various transpiration strengths. II. Causal relation between suction tension, resistance and uptake. Proc. K. Ned. Akad. Wet C **56**, 129–136 (1953).

2 Brouwer, R., The regulating influence of transpiration and suction tension on the water and salt uptake by the roots of intact *Vicia faba* plants. Acta Bot. Neerl. **3**, 264–312 (1954).
3 Cowan, I. R., Transport of water in the soil-plant-atmosphere system. J. Appl. Ecol. **2**, 221–339 (1965).
4 Crank, J., Mathematics of Diffusion. Oxford University Press, London. (1956).
5 Denmead, O. T. and Shaw, R. H., Availability of soil water to plants as affected by soil moisture content and meteorological conditions. Agron. J. **54**, 385–390 (1962).
6 Etherington, J. R., Soil water and growth of grasses II. Effects of soil water potential on growth and photosynthesis of *Alopecurus pratensis*. J. Ecol. **55**, 373–380 (1967).
7 Gardner, W. R., Dynamic aspects of water availability to plants. Soil Sci. **89**, 63–73 (1960).
8 Gardner, W. R. and Ehlig, C. F., Some observations on the movement of water to plant roots. Agron. J. **54**, 453–456 (1962).
9 Hayward, H. E. and Spurr, W. B., Effects of isosmotic concentrations of inorganic and organic substances on entry of water into corn roots. Bot. Gaz. **106**, 131–139 (1944).
10 Kramer, P. J., Plant and Soil Water Relationships. A modern synthesis. McGraw Hill Book Co., N.Y. (1969).
11 Newman, E. I., Resistance to water flow in soil and plant. I. Soil resistance in relation to amounts of roots: Theoretical estimates. J. Appl. Ecol. **6**, 1–12 (1969).
12 Newman, E. I., Resistance to water flow in soil and plant. II. A review of experimental evidence on the rhizosphere resistance. J. Appl. Ecol. **6**, 261–272 (1969).
13 Rawlins, S. L., Resistance to water flow in the transpiration stream; *In* Israel Zelitch (Ed.). Stomata and Water Relations in plants; Advanced Seminar on the Physiol. and Biochem. of Leaf Stomata (1963).
14 Rovira, A. D., Studies of the interactions between Plant Roots and Micro-Organisms. J. Aust. Inst. Agric. Sci. **36**, 91–95 (1972).
15 So, H. B., Aylmore, L. A. G. and Quirk, J. P., Measurements of water fluxes and potentials in a single root-soil system. I. The tensiometer-potometer system. Plant and Soil **45**, 577–594 (1976).
16 So, H.B., Aylmore, L. A. G. and Quirk, J. P., The resistance of intact maize roots to water flow. Soil Sci. Soc. Am. Proc. **40**, 222–225 (1976).

Predicting the Movement of Solutes in Soil Profiles.

Proc. Hydrology and Water Resources Symposium, Perth: 210-215. (1979)

V. Murali and L.A.G. Aylmore.

Predicting the Movement of Solutes in Soil Profiles

V. MURALI

Post Doctoral Research Fellow, Department of Soil Science and Plant Nutrition, University of Western Australia

L.A.G. AYLMORE

Professor of Soil Science, Department of Soil Science and Plant Nutrition, University of Western Australia

SUMMARY It has been shown by means of computer simulations using numerical methods and by experimental observations that the complexities of adsorption kinetics, intermittent flow and residual and competitive adsorption can be extremely important in determining the movement of solutes through soil. Current analytical approaches generally involve simplifying assumptions which ignore these complexities.

1 INTRODUCTION

The quality of water percolating through the soil profile to groundwater is of great importance in groundwater recharge. This is adversely affected by natural salinity, agricultural pollutants, industrial and domestic effluents and landfill leachates. Methods for predicting changes in the chemical composition of water as it moves through the soil must be able to take into account both the physical and chemical characteristics of the system.

The movement of non-interacting solutes in uniform soil profiles under saturated conditions can be predicted with reasonable accuracy using analytical procedures taking into account the effects of convective flow velocity, hydrodynamic dispersion and molecular diffusion (Selim & Mansell, 1976; Cleary and Adrian, 1973; Marino 1974; Lindstrom *et al.*, 1967). In the presence of solute-soil interaction however, such analytical procedures have been largely limited to the assumptions of linear adsorption isotherms and instantaneous equilibria because of the difficulty in coping with the non-linear partial differential equations which arise for more complex isotherms or rate dependent processes. Such assumptions are frequently unrealistic and the solutions obtained are limited to the description of highly specific cases where the different sets of simplifying assumptions apply. They are generally quite inadequate to describe most of the systems of practical interest, for example, the transport of phosphate, sulphate, heavy metal ions etc. through soil profiles where the adsorbing materials may include clay minerals, iron and aluminium oxides, organic matter and so on. In this respect, it would be most advantageous to utilize Langmuir type isotherms which despite their limitation, have been used successfully in describing sorption kinetics and equilibrium isotherms for a wide range of adsorbates and adsorbents including the above (Aylmore *et al.*, 1967; Hingston *et al.*, 1971).

Furthermore the complexities of soil structure and varying water content and the difficulties which arise through the presence of adsorption-desorption hysteresis and competition between adsorbing species, effectively preclude the development of a universal and rigorous analytical approach capable of handling the many variations possible. The increasing accessibility of computing facilities and the development of numerical procedures have however provided a practical method of simulation and prediction capable of handling most of these complexities. In this paper we briefly review the limitations inherent in previous analytical approaches and illustrate the ability of numerical methods to describe the experimental results obtained from practical systems.

2 THEORY

From considerations of the conservation of mass and continuity equations, the partial differential equation describing the transport of a non-interacting solute in a soil profile

$$\frac{\partial C}{\partial t} = \frac{\partial}{\partial z}\left[(D_d + D_m)\frac{\partial C}{\partial z}\right] - \frac{\partial}{\partial z}(VC) \qquad \ldots\ldots(1)$$

can be readily obtained (Boast, 1973), where

C is the solution phase concentration

D_d is the dispersion coefficient (mechanical or hydrodynamic),

D_m is the molecular diffusion coefficient,

V is the flow velocity,

and z and t are depth and time variables.

For a uniform homogeneous soil, when flow velocity is independent of depth and the combined dispersion coefficient D ($= D_d + D_m$) is independent of concentration, equation (1) simplifies to

$$\frac{\partial C}{\partial t} = D\frac{\partial^2 C}{\partial z^2} - V\frac{\partial C}{\partial z} \qquad \ldots\ldots(2)$$

Equation (2) has been solved analytically by numerous workers for particular initial and boundary conditions (Selim & Mansell, 1976; Cleary & Adrian, 1973; Lindstrom *et al.*, 1967, Marino, 1974). It can be extended (Boast, 1973) to describe the case where solute interacts with the soil, e.g. adsorption, exchange, precipitation, transformation etc. by the inclusion of a source-sink term thus

$$\frac{\partial S}{\partial t} + \frac{\partial C}{\partial t} = D\frac{\partial^2 C}{\partial z^2} - V\frac{\partial C}{\partial z} \qquad \ldots\ldots(3)$$

together with the appropriate expression describing the adsorption-desorption kinetics

$$\frac{\partial S}{\partial t} = f\ (C,S,\ \frac{\partial C}{\partial t}\ ,\ \text{--------}) \qquad \text{.....(3b)}$$

where S is the amount of adsorbed material.

The two equations have to be solved simultaneously for appropriate initial and boundary conditions in order to predict the solute concentration as a function of time and depth.

Previous exact analytical solutions have generally depended on the assumption of simple relationships for equation (3b) for example

$$\frac{\partial S}{\partial t} = K_e \frac{\partial C}{\partial t} \qquad \text{.....(4a)}$$

which assumes instantaneous equilibrium between solution and adsorbed phases and a linear relationship between them, or

$$\frac{\partial S}{\partial t} = K_a C \qquad \text{.....(4b)}$$

in which adsorption is considered irreversible and the rate of adsorption is proportional to solution concentration. Here K_e and K_a are respectively the equilibrium distribution and adsorption rate coefficients. For these simple cases equation (3a) can be reduced to a form similar to equation (2) and solved analytically (see, for example, Kirkham & Powers, 1972).

To be more realistic the expressions need to be able to handle more complex interactions such as non-instantaneous equilibria which may involve different rates of adsorption and desorption or non-linear isotherm shapes. The simplest case of adsorption-desorption kinetics is for a linear type isotherm given by the equation

$$\frac{\partial S}{\partial t} = K_a C - K_d S \qquad \text{.....(5a)}$$

which under equilibrium conditions reduces to

$$S = K_e C \qquad \text{.....(5b)}$$

where K_a, K_d and K_e are respectively the rates of adsorption and desorption and equilibrium distribution coefficients such that $K_e = K_a/K_d$.

In practice, however, many interactions conform to the Langmuir type isotherm for which the equilibrium expression ($\partial S/\partial t \rightarrow 0$) is

$$S = \frac{Q K_e C}{1 + K_e C} \qquad \text{.....(6a)}$$

where Q is the adsorption capacity of the soil.

For instantaneous adsorption-desorption equilibria the equation describing the rate of change of adsorbed phase concentration with changing solution concentration as the solute moves through the soil can be obtained by differentiating equation (6a) with respect to time, i.e.

$$\frac{\partial S}{\partial t} = \frac{K_e Q}{(1 + K_e C)^2} \cdot \frac{\partial C}{\partial t} \qquad \text{.....(6b)}$$

For non-instantaneous interaction the rate equation describing the approach to adsorption equilibrium takes the form

$$\frac{\partial S}{\partial t} = K_a C\ (Q - S) - K_d S \qquad \text{.....(6c)}$$

In practice interactions involving non-instantaneous equilibration and non-linear isotherms are the rule rather than the exception. In the following section we illustrate the magnitude of the errors introduced by neglecting such realities.

3 SIMULATIONS OF THE EFFECTS OF ADSORPTION-DESORPTION KINETICS AND ISOTHERM SHAPE ON SOLUTE MOVEMENT

The consequences of the simplifying assumptions used to facilitate analytical solutions to the continuity equations, on the time distribution of solute predicted, can be readily demonstrated by computer simulations of the breakthrough curves or profile distributions obtained under the different assumptions. The use of fast computers makes it possible to obtain solutions of partial differential equations with non-uniform initial and boundary conditions, coupled differential equations and certain partial differential equations with non-constant coefficients. These solutions involve the use of appropriate finite difference analogs to compute the progressive change in required quantities with time or distance. A number of different procedures can be used for example, explicit (or forward difference), implicit (backward difference) or explicit-implicit depending on programming experience, computer memory available and the complexity of the problem to be solved. Detailed texts on this technique are readily available (e.g. Richtmyer and Morton, 1967).

The assumption of instantaneous equilibria means that should two ionic species have the same equilibrium isotherm then identically shaped and positioned breakthrough curves will be predicted for the passage of their pulses through a soil column. (For a simple linear isotherm curve A in Figure 1 is obtained using equations (3a) and (4a) for the parameters given). However the rate of approach to adsorption equilibrium may vary considerably between different species and this will result in a range of markedly different breakthrough curves depending on the rate coefficients (equation 5a) applicable, even for a simple linear isotherm (for example curves B,C,D, and E in Figure 1).

Furthermore for many of the chemicals of interest there are significant differences in the rates of adsorption (K_a) and desorption (K_d). The assumption of instantaneous equilibria invariably results in the prediction that peak adsorption coincides with peak solution concentration (Figure 2) and this is not necessarily so when kinetic

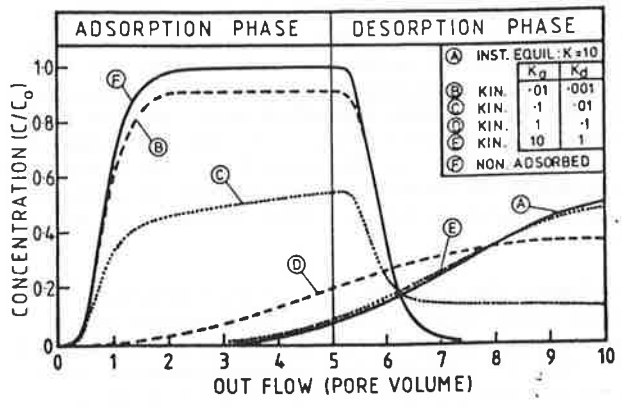

Figure 1 Simulation of adsorption-desorption breakthrough curve for instantaneous equilibrium (curve A), kinetic models (B,C,D,E) and non-interacting solute (F)

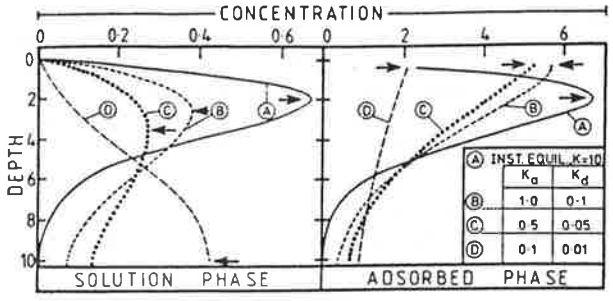

Figure 2 Simulations of profile distributions of solution (a) and adsorbed phase (b) concentrations for instantaneous equilibrium and kinetic models

processes are involved. Depending on the rate coefficients applicable the movement of peak solution and sorbed concentrations may be either grossly overestimated or underestimated by the assumption of instantaneous equilibrium. (Figure 2)

Differences between adsorption and desorption rates may also lead to other significant consequences. Where the rate of desorption is markedly slower than the rate of adsorption the net result may simulate the occurrence of an irreversible adsorption or "fixation" of the adsorbed species. The practical consequence of such an adsorbed "residual", remaining despite subsequent leaching with solute free water (e.g. rainfall), will be the enhanced transport or more rapid breakthrough of subsequent applications of solute as illustrated in Figure 3 for kinetic Langmuir adsorption. This may be of considerable importance where possible pollution of groundwaters is concerned.

In practice, vertical movement of water through soils rarely, if ever, occurs continuously or at uniform flow velocity for any length of time. The water content of the soil described as "field capacity" results from the much slower redistribution of water following infiltration. Consequently there is a period following infiltration when flow is negligible but adsorption/desorption processes may continue. Thus rather than being able to assume a constant or average pore water velocity, it is important to consider the effects of the "go-stop" nature of water movement where adsorption kinetics are concerned.

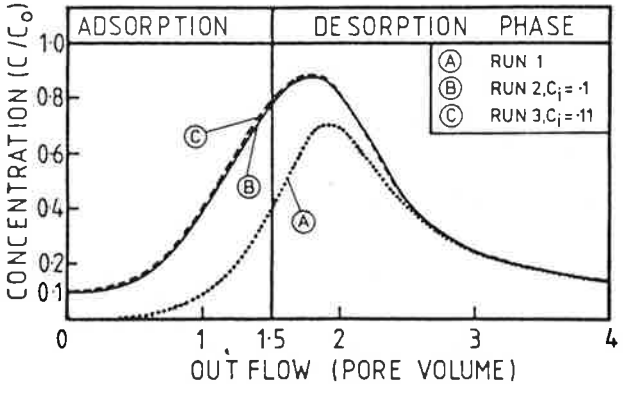

Figure 3 Simulations showing effects of residual adsorption on successive breakthrough curves

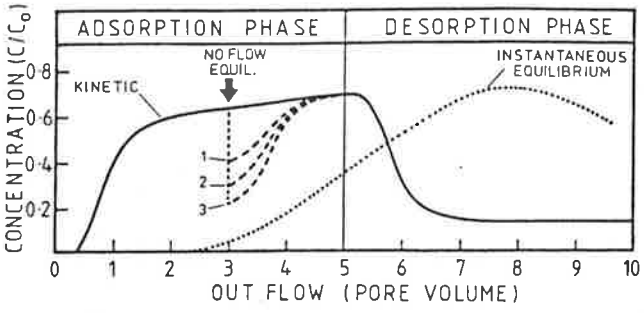

Figure 4 Simulations showing effects of no flow equilibrations on breakthrough curves using instantaneous equilibrium and kinetic models

Figure 4 shows the consequence of different "no-flow equilibration" periods on the breakthrough curves predicted by computer simulation for non-instantaneous equilibration using a simple linear isotherm (equation (5a)). The assumption of instantaneous equilibration will of course obscure these effects completely.

4 SIMULATION OF THE EFFECT OF COMPETITIVE ADSORPTION

One of the most important factors in determining the adsorption and hence susceptibility to leaching of a particular ionic species, which is difficult if not impossible to satisfactorily handle by analytical methods, is the influence of competitive ions in solution. The adsorption sites for different ions are frequently the same and the marked influence of the preferred adsorption of one ionic species on the transport of other ions, has been demonstrated for several ion pairs by different investigators (e.g. sulphate-phosphate, Aylmore & Karim 1968; arsenite-phosphate and selenite-phosphate, Hingston *et al.*, 1971).

Using numerical techniques it is possible to simulate a variety of conditions which may govern the competitive interactions and to assess their applicability to practical cases. A completely generalized model for transport under competitive conditions would need to be capable of handling a general adsorption rate equation including competition with, if pertinent, different adsorption maxima for different species and also be able to take into account any peculiar characteristics of the competitive interaction. For example whether competition is of significance over the full range of the adsorption isotherms or perhaps only when the sites are saturated. In practice however such a sophisticated and cumbersome treatment may not be necessary. For example when two adsorbing ions have different adsorption maxima and follow Langmuir type adsorption-desorption kinetics, the rate equations describing the approach to equilibrium for each species may be derived by differentiating the appropriate isotherm equation

$$S_A = \frac{Q_A K_A C_A}{1 + K_A C_A + K_B C_B} = \frac{Q_A K_{aA} C_A}{K_{dA} + K_{aA} C_A + K_B . K_{dA} C_B} \quad \ldots\ldots\ldots (7)$$

whence

$$\frac{\partial S_A}{\partial t} = K_{aA}\, C_A\, (Q_A - S_A) - K_{dA}\, S_A\, (1 + K_B\, C_B) \quad \ldots\ldots (8a)$$

and similarly

$$\frac{\partial S_B}{\partial t} = K_{aB}\, C_B\, (Q_B - S_B) - K_{dB}\, S_B\, (1 + K_A C_A) \quad \ldots\ldots (8b)$$

where Q_A and Q_B are adsorption maxima and the subscripts A and B refer to the ionic species A and B respectively. Equation (3a) may then be used to describe the dispersive-convective-adsorptive mass balance for each species. It is a relatively simple matter to extend this approach to include a number of the competing ions.

Models using this approach predict a number of interesting features for the breakthrough curves of competing ions which depend on their concentrations and the degree of preference of the adsorbent for each species as illustrated in Figure 5.

As expected the breakthrough curve for the least strongly adsorbed species will be progressively displaced towards that appropriate to a non-adsorbed species to an extent which will depend on both the concentrations and degree of preferential adsorption as determined by the respective equilibrium coefficients. Of particular interest however is the prediction that under appropriate conditions the outflow concentration of the less strongly adsorbed species may peak at a value considerably above that of the inflow concentration. Physically this would correspond to the displacement by the more slowly advancing front of the more strongly adsorbed species, of the preadsorbed less strongly adsorbed species.

5 EXPERIMENTAL RESULTS

The validity of the shapes and positions of breakthrough curves for adsorbed species under different conditions, predicted by numerical methods is illustrated by the data for phosphate and selenite ions presented in Figures 6 to 8. These were obtained by experimental methods essentially similar to those described by various workers (Aylmore & Karim, 1968; Elrick *et al.*, 1967) using radioactive tracers. Briefly this involved monitoring the outflow concentration from water (0.1M sodium chloride buffered) saturated soil columns when solute free input is replaced by a given concentration of a particular ion. The desorption or solute outflow process is followed by changing the input back to solute free water. The system is designed to enable flushing of the input chamber to ensure an essentially instantaneous change in concentration at the input face. The concomitant breakthrough for the water front was followed using tritiated water and represents the breakthrough for a non-adsorbed species.

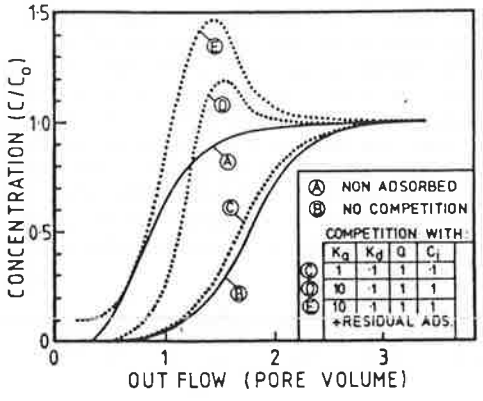

Figure 5 Simulations showing effects of competitive adsorption on breakthrough curves

Figure 6 showing the breakthrough curves obtained for phosphate ions in an artificial soil column containing sand plus 5% kaolinite clay demonstrates several features characteristic of a kinetic adsorption-desorption process. Whereas simulations using instantaneous equilibria invariably predict an essentially symmetrical breakthrough and outflow curve, that for phosphate (curve A) exhibits a comparatively early breakthrough and rapid rise in effluent concentrations followed by a slow approach to input concentration. The outflow curve exhibits the same characteristics leaving a substantial residual adsorption which is only slowly removed. The effort of such residual adsorption is to cause a more rapid breakthrough and rapid rise to higher concentration of a second solute front (curve B). Interestingly enough a subsequent solute front (curve C) follows closely the breakthrough exhibited by the second indicating that a comparatively constant amount of solute is strongly retained or "fixed" by this material. (cf. Figure 3).

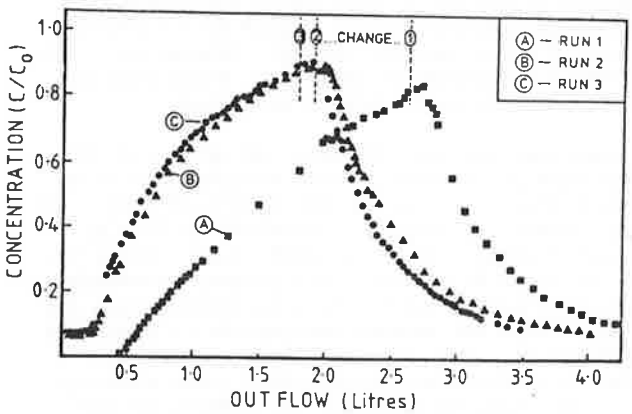

Figure 6 Successive experimental breakthrough curves for phosphate movement through Yalanbee sandy loam showing effects of residual adsorption

In Figure 7 breakthrough curves for selenite ions in a column containing a sandy loam from York W.A. demonstrate the effects of no-flow equilibrium periods on the effluent concentration analogous to those simulated in Figure 4. Again the breakthrough curve for a second solute front after flushing with solute free water is displaced to lower effluent volumes.

When both phosphate and selenite are introduced in a third front the preadsorbed selenite is rapidly displaced by the more strongly adsorbed phosphate and the breakthrough curve for the selenite is displaced to even lower effluent volumes and close to that obtained for the non-adsorbed tritium ion (Figure 8). Note that as simulated in Figure 5 the effluent concentration peaks at a value considerably higher than the input concentration.

6 CONCLUSIONS

Transport processes involving solute ions which interact with soil material exhibit a number of features which are extremely difficult if not impossible to satisfactorily describe using analytical methods. Some of these can be very important in determining how far and how fast a particular ion will move. These include the nature of the adsorption-desorption kinetics (e.g. non-instantaneous equilibria and non-linear isotherms), intermittent flow and residual and competitive adsorption. It has been shown that these complexities can be satisfactorily simulated using numerical methods.

7 REFERENCES

Aylmore, L.A.G. and Karim, M. (1968). Leaching of fertilizer ions in soil columns. 9th Intern. Soil Sci. Soc. Trans., Adelaide, Vol. I: 143-53.

Aylmore, L.A.G., Karim, M. and Quirk, J.P. (1967). Adsorption and desorption of sulphate ions by soil constituents. Soil Sci. 103: 10-15.

Boast, C.W. (1973). Modelling the movement of chemicals in soils by water. Soil Sci. 115: 224-230.

Cleary, R.W. and Adrian, D.D. (1973). Analytical solution of the convective-dispersive equation for cation adsorption. Soil Sci. Soc. Am. Proc. 37: 197-199.

Elrick, D.E., Erh, K.T. and Krupp, H.K. (1967). Applications of miscible displacement techniques to soils. Water Resources Res. 2: 717-727.

Hingston, F.J., Posner, A.M. and Quirk, J.P. (1971). Competitive adsorption of negatively charged ligands on oxide surfaces. Disc. Faraday Soc. 52: 334-342.

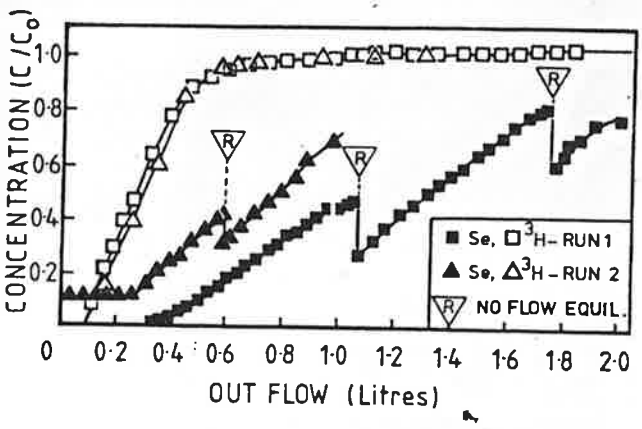

Figure 7 Experimental breakthrough curves for tritium and selenium movement through York loamy sand showing effects of no-flow equilibration and residual adsorption

Kirkham, D. and Powers, W.L. (1972). Advanced Soil Physics, Wiley-Interscience, New York.

Lindstrom, F.T., Haque, R., Freed, V.H. and Boersma, L. (1967). Theory on movement of some herbicides in soils. Environ. Sci. Technol. 1: 561-565.

Marion, M.A. (1974). Numerical and analytical solutions of dispersion in a finite, adsorbing porous medium. Water Resources Bull. 10: 80-90

Richtmyer, R.D. and Morton, K.W. (1967). Difference methods for initial value problems.

Selim, H.M. and Mansell, R.S. (1976). Analytical solution of the equation for transport of reactive solutes through soils. Water Resources Res. 12: 528-532.

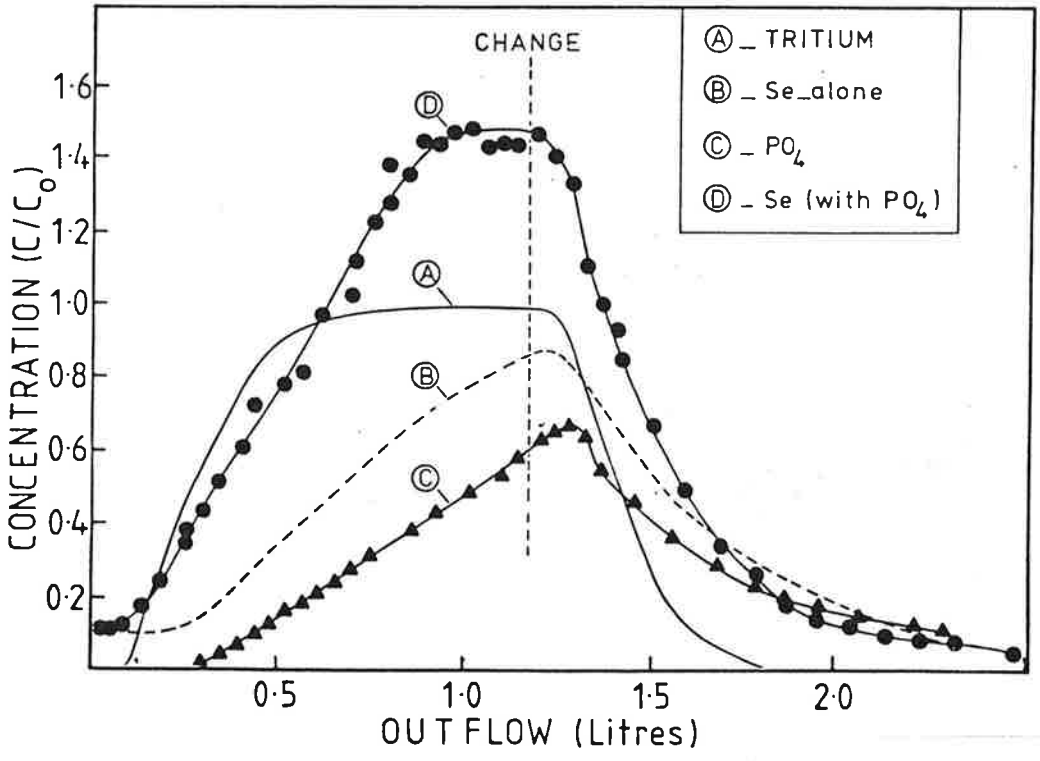

Figure 8 Experimental breakthrough curves showing the effects of competitive adsorption (with phosphate) on selenite breakthrough curves in York loamy sand.

No-flow equilibration and adsorption dynamics during ionic transport in soils

V. Murali & L. A. G. Aylmore

reprinted from
nature

Reprinted from Nature, Vol. 283, No. 5746, pp. 467-469, January 31 1980

No-flow equilibration and adsorption dynamics during ionic transport in soils

V. Murali & L. A. G. Aylmore

Department of Soil Science and Plant Nutrition, University of Western Australia, Nedlands, Western Australia 6009, Australia

Methods for predicting the movement of adsorbing chemicals such as fertilisers, pesticides, herbicides and heavy metals in soils have received increasing attention because of their importance in relation to the efficiency of fertiliser usage and in the control of agricultural and industrial pollutants[1]. Because of the difficulty in coping with the complex non-linear partial differential equations necessary to describe the dispersive–convective–adsorptive flow process, analytical solutions have been largely limited to the assumptions of instantaneous equilibrium and simple linear adsorption isotherms[2–5]. We demonstrate here the need to incorporate adsorption dynamics to describe adequately practical situations, particularly those involving intermittent flow.

In reality the movement of water through soils rarely, if ever, occurs continuously or at uniform flow velocity for any length of time. For example, the water content of the soil described as 'field capacity'[6] results from the much slower redistribution of water following infiltration. Consequently there is a period following infiltration when flow is negligible but adsorption/desorption processes may continue. Thus, rather than being able to assume a constant or average pore water velocity and instantaneous equilibration between solute and adsorbent, it is imperative to consider the effects of the 'go–stop' nature of water movement where adsorption dynamics are concerned.

The importance of this effect is illustrated by our recent studies of the influence of adsorption dynamics on the movement of adsorbing ions in soil columns. The term 'adsorption dynamics' is used here to include not only adsorption kinetics at solid surfaces, but also any intermediate steps which may influence the rate at which chemicals are exchanged between solution and adsorbed phases. In particular this includes diffusion from the centres to the walls of hydrodynamic pores (that is, pores responsible for hydrodynamic dispersion) but excludes intra-aggregate diffusion which can be viewed as a separate process.

A standard technique for studying the movement of ions in soil[7,8] is the measurement of 'breakthrough curves' which describe the change in the outgoing solution from a soil column with outflow volume following a change in input concentration.

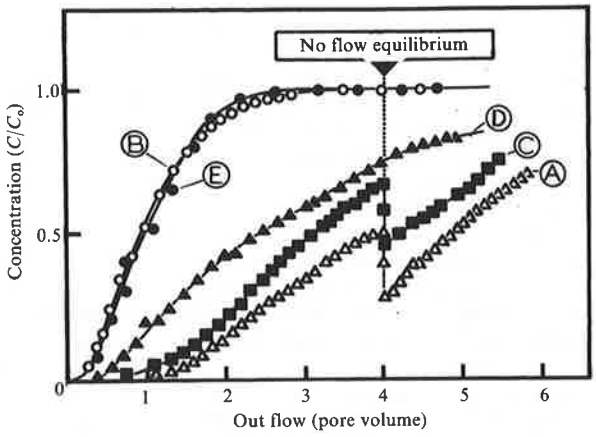

Fig. 2 Experimental breakthrough curves for phosphate (A) and tritium (B) movement through Yalanbee sandy loam and selenite (C), sulphate (D) and tritium (E) through York sandy loam showing effects of 24-h no-flow equilibration. Flow velocity equivalent to 0.3 pore volumes per hour.

Figure 1 contrasts the breakthrough curves, predicted by computer simulations using numerical methods, for non-instantaneous equilibration involving a range of different adsorption and desorption rates (k_a and k_d respectively), with that obtained for instantaneous equilibration (at the same equilibrium constant) using a simple linear isotherm. The simulations depict the passage of five pore volumes of solution containing the ion into a column of soil saturated with water (adsorption phase) followed by five pore volumes of ion free water (desorption phase). The value of the equilibrium constant K at relevant soil solution concentrations is generally greater than unity and $K = 10$ has been used as a suitable example.

The assumption of instantaneous equilibrium means that for two ionic species having the same or similar equilibrium isotherms, identically shaped and positioned breakthrough curves (curve A) will be predicted for the passage of their concentration pulses through a soil column. However, the rates of approach to adsorption and desorption equilibrium may vary considerably between different species and this will result in a range of markedly different breakthrough curves depending on the relevant rate coefficients (for example, curves B, C, D and E).

The consequence of different 'no-flow equilibration' periods on the breakthrough curves predicted in any case involving adsorption dynamics is particularly relevant. This is illustrated by the depressions in outgoing concentration for curve C corresponding to no-flow periods of increasing length. The

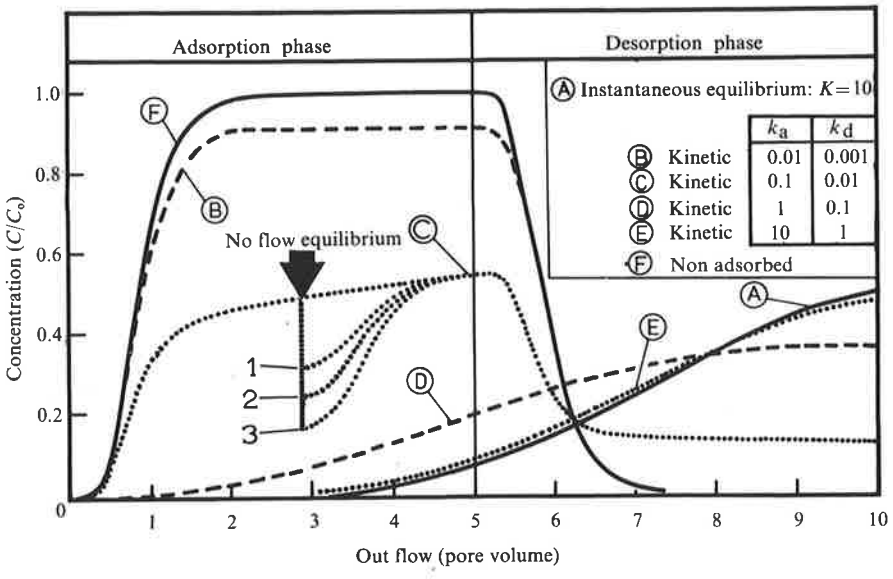

Fig. 1 Simulation of adsorption–desorption breakthrough curves for instantaneous equilibrium (curve A), kinetic models (B, C, D, E) and non-interacting solute (F). Effects of no-flow equilibrations are shown on curve C for increasing periods equivalent to the time taken for the outflow of 2, 4 and 10 pore volumes respectively.

assumption of instantaneous equilibration (curve A) will, of course, obscure this effect completely.

In the previous simulations simple linear adsorption kinetics were used to demonstrate the effects of time dependency of the adsorption/desorption processes. However, in other simulations we have shown that the same considerations are relevant regardless of the type of isotherm involved, for example, Freundlich and Langmuir.

The considerable practical significance of this effect is demonstrated by the breakthrough curves in Fig. 2 obtained for solutions of phosphate (2.5 mM), selenite (1.0 mM) and sulphate (1.0 mM) ions, and tritium labelled water including a 24 h no-flow equilibration period. The soils used were in a finely-ground state and the depressions in outgoing concentration for phosphate and selenite following no-flow periods cannot be attributed to intra-aggregate diffusion. This is verified by the absence of measurable depressions in the case of the sulphate despite the measurable adsorption of this ion and for the effectively non-adsorbed tritium ion. Thus it is clear that adsorption dynamics as previously defined, can be particularly important in controlling ionic transport in real conditions. The significant difference in the shapes of the breakthrough curves for sulphate and tritium, despite the absence of no-flow depressions for both, clearly demonstrates that adsorption kinetics form only part of the total adsorption dynamics influencing ionic movement. Other studies demonstrate that in aggregated systems the involvement of intra-aggregate diffusion before surface interactions, introduces no-flow depressions in outgoing concentrations for even non-adsorbed species and greatly enhances those for adsorbing species.

Such intermittent flow/no-flow measurements apparently provide a simple and convenient technique for checking the pertinence of adsorption dynamics for any particular ion–soil system, solution concentration and flow velocity, and we are not aware of any previous such demonstration in non-aggregated systems.

The nature of the rate determining steps in these studies will require further investigation. While studies on equilibrium distributions involving agitation and high solution-to-solid ratios generally indicate extremely fast ion–soil interactions[9], the present observations demonstrate that such measurements of adsorption kinetics may be of little relevance in relation to ionic transport. There is increasing evidence that considerably slower rates are involved in actual soil systems[10,11].

These observations form part of a much more detailed study of ionic transport through soil systems involving computer simulations using numerical methods and experimental determinations in soil columns being undertaken in this Department.

Received 20 September; accepted 29 November 1979.

1. Viets, F. G. *CRC Crit. Rev. Envir. Control* **5**, 423–453 (1975).
2. Marino, M. A. *Wat. Resour. Bull.* **10**, 80–90 (1974).
3. Lindstrom, F. T., Haque, R., Freed, V. H. & Boersma, L. *Envir. Sci. Technol.* **1**, 561–565 (1967).
4. Cleary, R. W. & Adrian, D. E. *Soil Sci. Soc. Am.* **37**, 197–199 (1973).
5. Murali, V. & Aylmore, L. A. G. *Hydrol. Wat. Resour. Sym. Perth* 210–214 (1979).
6. Richards, L. A. *J. Am. Soc. Agron.* **28**, 298–301 (1936).
7. Aylmore, L. A. G. & Karim, M. *9th int. Soil Sci. Soc. Trans. Adelaide* **1**, 143–153 (1968).
8. Elrick, D. E., Erh, K. T. & Krupp, N. K. *Wat. Resour. Res.* **2**, 717–727 (1967).
9. Madrid, L. & Posner, A. M. *J. Soil Sci.* (in the press).
10. Parfitt, R. L. *Adv. Agron.* **30**, 1–50 (1978).
11. Barrow, N. J. & Shaw, T. C. *J. Soil Sci.* **30**, 67–76 (1979).

Printed in Great Britain by Macmillan Production Ltd., Basingstoke, Hampshire

Water and Salt Flow through Compacted Clays

II. Electrokinetics and Salt Sieving

P. F. ROLFE AND L. A. G. AYLMORE

Department of Soil Science and Plant Nutrition, University of Western Australia, Nedlands 6009, Western Australia

Received December 23, 1978; accepted May 22, 1980

Studies have been made of the salt-sieving and electrokinetic effects associated with the pressure-induced flow of the chloride solutions of various monovalent, divalent, and trivalent cations, at various concentrations, through highly compacted Wyoming bentonite and Willalooka illite cores. The majority of the measurements were carried out on the Willalooka illite cores. Maximum salt-sieving coefficients were measured at the lowest flow pressures used (approximately 3 MPa) and salt sieving decreased rapidly with increasing flow pressure. Over the range of flow pressures used it is believed that convective flow overcomes the effects of diffusion which at lower flow pressures may partially compensate for the discrimination in transport between water and anions resulting from the excess negative potential in the core pore spaces. The rapid decrease in salt sieving with increasing flow pressure does not appear to be accompanied by any major alteration in the integrity of the double-layer distribution. The maximum salt-sieving coefficients agreed well with the maximum salt rejections predicted by electrokinetic theory and were also in good agreement with measured osmotic efficiency coefficients. Wall potentials calculated from the streaming potential–pressure gradients agreed well with the outer Stern layer potentials calculated using simple static diffuse-double-layer theory.

INTRODUCTION

When electrolytes flow through reactive porous media containing pores with sufficiently high surface potentials, the interaction between the ions and the charged surfaces can have significant effects on both the flow rate and the transport of salt through the system (9, 13, 18, 19). These factors of permeability and salt transport are of particular importance in soil science and in many other areas of the physical and life sciences; for example, water desalination and the development of dialyzing membranes for artificial organs.

In a previous paper (23) we examined the way in which the permeability of compacted clay mineral systems varied for a range of chloride solution concentrations of various cations for flow pressures ranging up to 28 MPa. In some instances three- to fourfold changes in permeability with the nature and concentration of the cations were observed. It was concluded that while significant variations in permeability could result from the electrokinetic effects arising in the systems examined, these were far outweighed by the effects of the size, charge, and concentration of the cations on the viscosity of coerced water layers in proximity to the clay surfaces. At high cationic concentrations the disruption of the coerced water layers resulted in rapid increases in permeability with increasing flow pressure. However, at lower electrolyte concentrations, where the electrokinetic effects arising from the development of diffuse double layers will be of most significance, only relatively small increases in permeability with flow pressure were observed.

This paper presents the corresponding results obtained from these studies of the

0021-9797/81/020301-07$02.00/0

salt exclusion and electrokinetic properties of the system.

MATERIALS AND METHODS

The flow equipment and materials used have been described in detail in Part I (23). Briefly, the clay was compacted in a stainless-steel cell under high pressure to prevent structural rearrangements during the subsequent flow at various pressures of various concentrations of selected metallic chloride solutions.

Fluid flowing through the compacted clay cores was collected in a burette graduated in 0.01-ml divisions and considerable precautions were taken to prevent evaporation. Fluid which passes through a bypass flow system after flushing the input faces of the clay cores was also collected in the same fashion. Flushing of the input faces was maintained at sufficiently high rates to ensure that no significant increase in concentration occurred as a result of salt sieving.

Analysis of the saline solutions was performed by determination of the chloride ion concentration using electrometric titration against silver nitrate (17). The determination of cation concentrations using atomic absorption spectroscopy provided a useful check on the accuracy of the chloride analyses.

Streaming potential measurements were made when both the hydraulic conductivity and the electrolyte concentration determinations indicated that equilibrium had been reached during each flow experiment. The construction of the cell was such as to ensure that the stainless-steel pistons were electrically insulated from one another. They thus served in place of reversible electrodes since the instruments used for measuring the streaming potentials (initially a radiometer, Model 28b pH/mV-meter, and subsequently a Smiths Model R.E. 511.20 Servoscribe Potentiometric Recorder) possessed very high input impedances and this minimized electrode reactions. Streaming potential measurements were made very rapidly to avoid electrode depolarization (6). As experienced by other workers (3, 18) the determination of streaming potentials was complicated by the presence of significant asymmetric or rest potentials (i.e., potentials at no flow). To avoid the problems of such spurious potentials, streaming potential–flow pressure gradients were determined over ranges of some 3.5 MPa, pressures being chosen both below and above the major operating pressure. It is this differential which can be related to the ζ potential (9, 20). The streaming potential–flow pressure gradients were measured as the millivolt change per megapascal of flow pressure. In general, plots of streaming potential against pressure over this small range were essentially linear. Plots extending over wider ranges of approximately 10 MPa were also essentially linear and possessed similar streaming potential–flow pressure gradients (Fig. 2).

RESULTS AND DISCUSSION

The results of the preliminary experiments in which a 0.1 M sodium chloride solution was passed through a sodium-saturated Wyoming bentonite core are summarized in Table I and compared with those obtained by McKelvey and Milne (18) on a similar core. The salt-sieving coefficients were calculated as the ratio

$$\beta_{\text{obsd}} = \frac{C_0 - C}{C_0} \quad (0 < \beta < 1),$$

where C_0 is the equilibrium bypass fluid concentration (which represents the equilibrium input concentration to the core) and C is the equilibrium outflow concentration.

In both studies the salt-sieving coefficient decreased significantly with increasing hydraulic gradient. Such a decrease in the salt-sieving coefficient with an increase in effective film thickness ($2b_e$) can be qualitatively prediced by using the diffuse-double-layer theory, as shown by Kemper (11). However, the salt-sieving results obtained

TABLE I

Flow of NaCl Solutions through Na Wyoming Bentonite Cores

Researchers	Inflow concn (M)	Compaction pressure (MPa)	Hydraulic pressure (MPa)	β_{obsd}	β_{theory}	$2b_e$ (Å)
Rolfe and Aylmore	0.10	34.5	34.5	0.42	0.83	19.0
	0.10	34.5	47.0	0.26	0.83	19.3
McKelvey and Milne	0.16	68.9	34.5	0.88	0.92	12.0
	0.15	68.9	68.9	0.70	0.92	13.0

here do not agree closely with the values calculated from theory, all being somewhat lower. Furthermore the decrease in β with increasing hydraulic gradient observed contrasts with the increase predicted by this theoretical analysis.

In Fig. 1, the most significant salt-sieving coefficients obtained in the Willalooka illite system are plotted against flow pressure. Salt sieving is clearly at a maximum for the lower concentrations and in each case there is a rapid decrease in the coefficient with flow pressure. This result may be contrasted with the observations in Part I (23) with respect to hydraulic conductivity, where the most dramatic effects of flow pressure were observed at the higher electrolyte concentrations.

Previous theoretical models (9, 13) have predicted that, with increasing flow pressures, convective flow would increasingly overcome the ability of diffusion to compensate for the discrimination of transport between water and anions resulting from the excess negative potential in the pore space. Thus salt sieving would increase with flow pressure and asymptote to a maximum value determined by the anion distribution within the pore volume, provided there was no change in the potential distribution within the pore volume at higher flow pressures. In the work carried out by Jacazio *et al.* (9), the maximum salt sieving was reached for Peclet numbers in the range 1 to 2. In the present work the Peclet numbers, which indicate the ratio of convective to diffusive flow rates, calculated using the same assumptions with respect to tortuosity of flow paths for the sodium-saturated Willalooka illite, cover a similar range from 0.24 to 2.40. It is probable that the flow paths between the larger Willalooka illite crystals forming domains, would be less tortuous than those between the montmorillonite lamellae forming quasi-crystals in the system studied by Jacazio *et al.* (9). Thus the Peclet numbers could in fact be considerably higher for the illite system. This is clearly not the only

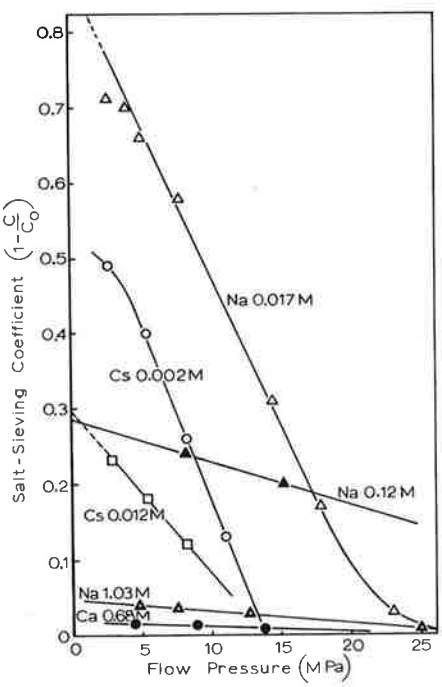

FIG. 1. Changes in the salt-sieving coefficient of the Willalooka illite core, against applied hydraulic pressure, for a series of concentrations of sodium, cesium, and calcium chloride.

criterion, however, since in the studies carried out by McKelvey and Milne (18) and in the preliminary work here on sodium montmorillonite, a decrease in salt sieving with increasing flow pressure was also observed. Presumably, the explanation for the contrasting salt-sieving behavior lies in differences in the electrokinetic properties of the systems under the particular conditions of the experiments, e.g., plate separation, electrolyte type and concentration, etc. Of some pertinence in this respect may be the differences in electrokinetic behavior between the potassium cation in the studies of Jacazio *et al.*, and the sodium cation in this study and in that of McKelvey and Milne (18). For example, potassium and chloride ions have similar diffusion coefficients, whereas that of sodium is much lower. The difference between the cation and the anion diffusivities is quite important in hyperfiltration (4).

It seems clear that the majority of the measurements of salt sieving presented here relate to flow pressures above the region where the effects of molecular diffusion on salt sieving are significant. Thus it is likely that the maximum β predicted by Kemper (11) and Jacazio *et al.* (9) occurs below this flow pressure range. There is some indication in the results (Fig. 1) at the lowest flow pressures used that the increase in salt sieving with decrease in flow pressure is beginning to level out. That is, the maximum values observed at the lower flow pressures could be expected to result, at least at the lowest concentrations, from an outgoing concentration of chloride ions approximately equal to that in the internal double layers. If it is assumed that the average anion concentration in the pores is approximated by the average between the concentration near the pore surface (essentially zero) and the concentration of the midplane, it is a simple exercise, using diffuse-double-layer theory, to show that the salt-sieving coefficient should be given by

$$\beta_{\mathrm{ddl}} = \{1 - (1/2)e^{(-Y_b)}\}$$

for a 1:1 electrolyte, where the valency $Z_a = Z_c = 1$ and Y_b is the dimensionless potential at the pore midplane.

In practice, the parabolic nature of the distribution of flow velocity with respect to distance from the shear plane would bias mass flow to the center of the pore (11) where anion exclusion from the clay surfaces would result in a higher concentration of anions. Furthermore, as shown in Part I, it is likely that little flow occurs in the coerced layers in proximity to the clay surfaces. In these circumstances, a more valid estimate of the salt-sieving coefficient might be given by

$$\beta_{\mathrm{midplane}} = \{1 - e^{(-Y_b)}\}.$$

Apparently, the measured salt-sieving coefficients should be between these theoretical estimates, but closer to $\beta_{\mathrm{midplane}}$.

In Table II comparisons are given between the maximum measured salt-sieving coefficients (Fig. 1) for different ingoing concentration, and the values predicted by these formulas.

The scaled potential at the midplane, Y_b, has been calculated using the information presented by Kemper and Quirk (15) designed to give fairly rapid yet accurate estimates. The gross surface density of charge of the Willalooka illite is 6.12×10^4 esu/cm^2. b, the distance from the midplane to the Stern layer, has been calculated to be 18 Å using data presented in Part I.

The calculations have been carried out using feasible values for percentage free sites (14) (i.e., available surface density of charge) under conditions of the close proximity of the clay plates at 20°C.

Table II shows that close approximation for the observed values for the maximum salt-sieving coefficient can be obtained using the simple static diffuse-double-layer approximation and reasonable values for percentage free sites. For example, for the 0.0174 M NaCl case the assumption of 8% free sites gives a value of 0.75 for $\beta_{\mathrm{midplane}}$ which agrees closely with the observed value of 0.73. Similarly, for the 0.0021 M CsCl

TABLE II

Comparison of Salt-Sieving Maxima $\beta_{obsd,\,max}$ and Theoretical Results

Ion	Assumed % free sites	C_0 (M)	Available SDC (esu/cm²)	Y_s	Y_b	e^{-Y_b}	β_{ddl}	$\beta_{midplane}$	$\beta_{obsd,\,max}$
Na^+	10	0.0174	6.12×10^3	2.4	1.58	0.20	0.90	0.80	0.73
	8		4.90×10^3	2.15	1.40	0.25	0.88	0.75	0.73
	5		3.06×10^3	1.50	1.05	0.35	0.82	0.65	0.73
	10	0.125	6.12×10^3	0.88	0.18	0.84	0.58	0.16	0.26
	8		4.90×10^3	0.72	0.17	0.84	0.58	0.16	0.26
	5		3.06×10^3	0.42	0.09	0.92	0.54	0.08	0.26
	8	1.03	4.90×10^3	≃0.01	≃0.01	≃0.99	≃0.50	≃0.01	0.04
Cs^+	0.4	0.0021	2.45×10^2	0.42	0.40	0.67	0.66	0.33	0.48
	0.5		3.06×10^2	0.65	0.62	0.54	0.73	0.46	0.48
	0.4	0.0125	2.45×10^2	0.10	0.08	0.92	0.54	0.08	0.23
	0.5		3.06×10^2	0.12	0.09	0.91	0.54	0.08	0.23
	0.5	0.100	3.06×10^2	<0.05	<0.01	>0.99	≃0.50	<0.01	0.01
Ca^{2+}	3.0	0.011	1.84×10^3	0.95	0.43	0.80	0.60	0.20	0.24
		0.100		0.50	0.015	0.99	0.50	0.01	0.03
		0.68		<0.20	<0.01	>0.99	≃0.50	<0.01	0.02

case 0.5% free site predicts a value of $\beta_{midplane}$ of 0.46 compared with the 0.48 observed.

These agreements suggest that the flow pressure at these points is sufficient to push the concentration of anions in the diffuse layer through the pores, flow being too rapid for diffusion to compensate for the discrimination of transport between water and anions. Also, the salt-sieving values agree with the maximum salt rejections predicted by the electrokinetic approach of Jacazio *et al.* (9), for acceptable ratios of the Debye length to pore radius. In fact the value for the maximum salt rejection coefficient for 0.0174 M NaCl obtained using this approach is 0.72 (cf. $\beta_{obsd} = 0.73$).

Furthermore, from the data presented in Table II, the 8% free sites choice for 0.0174 M NaCl suggests that 2.15 is a reasonable estimate of the nondimensional potential (Y_s) just outside the Stern layer (or 55 mV); i.e., an approximation to the ζ potential at the slip plane. This agrees well with the value, 2.0, obtained from calculations using the streaming potential–pressure gradient (9, 20). This wall potential compares well with illite ζ potentials of about 65 mV measured in electrophoretic experiments (21).

Measurements were also made of the osmotic efficiency coefficients (16). Use of the theory of the thermodynamics of irreversible processes combined with the Onsager reciprocal relationship as outlined by Kemper and Letey (12) leads to the hypothesis that the osmotic efficiency coefficient should equal the maximum salt-sieving coefficient. In fact, agreement was good as shown in Table III.

Over the flow pressure range examined here, transport of the chloride anion through the porous system is progressively enhanced compared with water transport (Fig. 1). Surprisingly, this does not appear to be accompanied by any major alteration in the integrity of the double-layer distribution since the streaming potential–distance gradient continues to increase in an essen-

TABLE III

Comparison of Osmotic Efficiency (σ) and Salt-Sieving (β) Coefficients

Ion	Percentage free sites	Inflow concn (M)	β_{max} (calc) (midplane)	β_{max}[a] (expt.)	σ (expt.)
Na^+	10	0.055	0.44	0.46	0.48
Ca^{2+}	3	0.075	0.02	0.04	0.04
Cs^+	0.4	0.0055	0.32	0.39	0.37
		0.055	0.02	0.06	0.09
		0.300	<0.01	<0.01	0.02

[a] β_{max} (expt.) estimated from β_{max} vs concn graphs.

tially linear fashion with flow pressure (Fig. 2).

In studies designed to illustrate the effects of diffusion in counteracting salt sieving, Kemper and Maasland (13) demonstrated an increase in β with increasing flow pressure. The work was carried out on greatly expanded montmorillonite systems and at very much lower flow pressures than those used here. In commenting on McKelvey and Milne's (18) earlier observations of a decrease in salt sieving with increasing flow pressure, they suggested that the development of high streaming potentials at the higher flow rates tended to cancel the sharp negative gradient in potential that exists where the solution enters the clay. However, the streaming potential–distance gradient across the core (approximately 31 mV/cm) would be very small in comparison with the potential gradient across the pores (some 55 mV/18 Å) and more recent studies (Thornton and Aylmore, in preparation) have shown that shorting out of the streaming potential has little or no effect on salt sieving.

It could be argued that at higher flow rates the potential distribution in proximity to the clay surfaces may be altered by the forced entry of feed solution (i.e., that convection so outweighs thermal diffusion as to markedly alter the equilibrium distribution of charge close to some surfaces). However, if this were to occur, it is surprising that the linear relationship between streaming potential and flow pressure is maintained (Fig. 2) particularly in view of the fact that

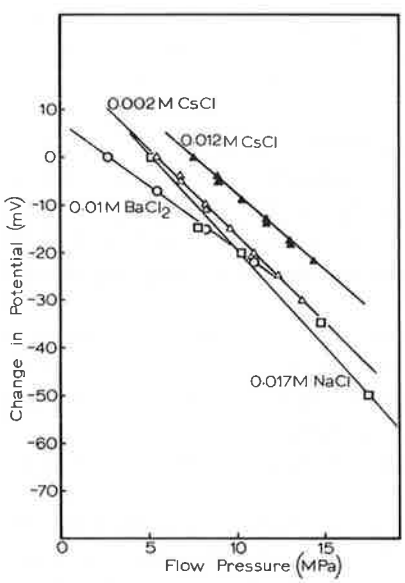

FIG. 2. Changes in potential, measured across stainless-steel electrodes confining the Willalooka illite core, against applied hydraulic pressure, for a series of concentrations of sodium, cesium, and barium chloride.

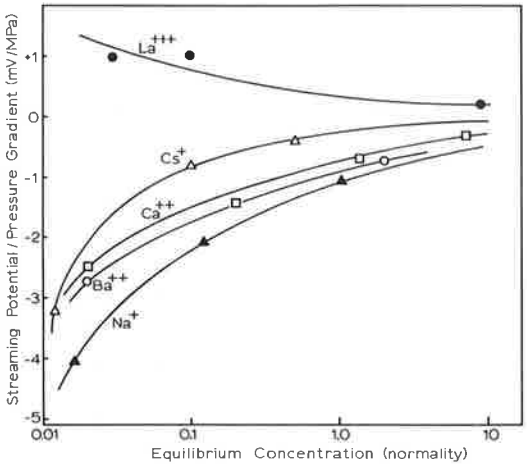

FIG. 3. Streaming potential–pressure gradients measured for the Willalooka core against the equilibrium input concentrations of sodium, cesium, barium, and lanthanum chloride solutions.

the attendant salt sieving is effectively annihilated at the highest flow pressures. If solutions of higher concentration were to progressively invade the total pore volume, one would expect the streaming potential–pressure gradient to be reduced as occurs at higher ingoing concentrations in Fig. 3, which shows the values obtained at different electrolyte concentrations for the different ions.

Reference to Fig. 1 also reveals the persistence of small salt-sieving coefficients for the approximately 1 *M* concentration NaCl and $CaCl_2$ solutions. This probably indicates that the cores exhibit some geometric exclusion to both cations and anions, in the absence of any significant exclusion arising from the charged surfaces.

REFERENCES

1. Bockris, J. O'M., and Reddy, A. K. N., "Modern Electrochemistry," Vol. 1, pp. 379–381. Plenum, New York, 1970.
2. Breslau, B. R., and Miller, I. F., *Ind. Eng. Chem. Fundam.* **10,** 554 (1971).
3. Broz, Z., and Epstein, N., *J. Colloid Interface Sci.* **56,** 605 (1976).
4. Dresner, L., *Desalination* **15,** 109 (1974).
5. Dukhin, S. S., and Derjaguin, B. V., *in* "Surface and Colloid Science" (E. Matijevic, Ed.), Vol. 7, Chap. 2, pp. 68–69. Wiley–Interscience, New York, 1974.
6. Gairon, S., and Swartzendruber, D., *in* "Ecological Studies 4. Physical Aspects of Soil Water and Salts in Ecosystems" (A. Hadas, Ed.), Springer-Verlag, Heidelberg, 1973.
7. Hildreth, D., *J. Phys. Chem.* **74,** 2006 (1970).
8. Horne, R. A., *Water Resour. Res.* **1,** 263 (1965).
9. Jacazio, G., Probstein, R. F., Sonin, A. A., and Yung, D., *J. Phys. Chem.* **70,** 4015 (1972).
10. Kedem, O., *Ber. Bunsenges. Phys. Chem.* **71,** 775 (1967).
11. Kemper, W. D., *Soil Sci. Soc. Amer. Proc.* **24,** 10 (1960).
12. Kemper, W. D., and Letey, J., *Trans. 9th Int. Congr. Soil Sci. Adelaide* **1,** 233 (1968).
13. Kemper, W. D., and Maasland, D. E. L., *Soil Sci. Soc. Amer. Proc.* **28,** 318 (1964).
14. Kemper, W. D., and Quirk, J. P., *Soil Sci. Soc. Amer. Proc.* **36,** 426 (1972).
15. Kemper, W. D., and Quirk, J. P., *Soil Sci. Soc. Amer. Proc.* **34,** 347 (1970).
16. Kemper, W. D., and Rollins, J. B., *Soil Sci. Soc. Amer. Proc.* **30,** 529 (1966).
17. Kolthoff, M., and Kuroda, P. K., *Anal. Chem.* **23,** 1304 (1951).
18. McKelvey, J. G., Jr., and Milne, I. H., *Clays Clay Miner.* **9,** 248 (1962).
19. McKelvey, J. G., Jr., Spiegler, K. S., and Wyllie, M. R. J., *Chem. Eng. Progr. Symp. Ser.* **5,** 199 (1959).
20. Oldham, I. B., Young, F. J., and Osterle, J. F., *J. Colloid Sci.* **18,** 328 (1963).
21. Petkanchin, I. B., Sokerov, S. K., and Stoylov, S. P., *Chemie, Physik-Chemie und Anwendungstechnik der Grenzflaechen Aktwen Stoffe Ber., Vom. 6, Int. Kongr.* **2,** 671 (1972).
22. Raridon, R. J., Dresner, L., and Kruns, K. A., *Desalination* **1,** 210 (1966).
23. Rolfe, P. F., and Aylmore, L. A. G., *Soil Sci. Soc. Amer. J.* **41,** 489 (1977).
24. Wiese, G. R., James, R. O., Yates, D. E., and Healy, T. W., *in* "Electrochemistry," Physical Chemistry Series 2 (J. O'M. Bockris, Ed.), Vol. 6, pp. 71–72. Butterworths, London, 1976.

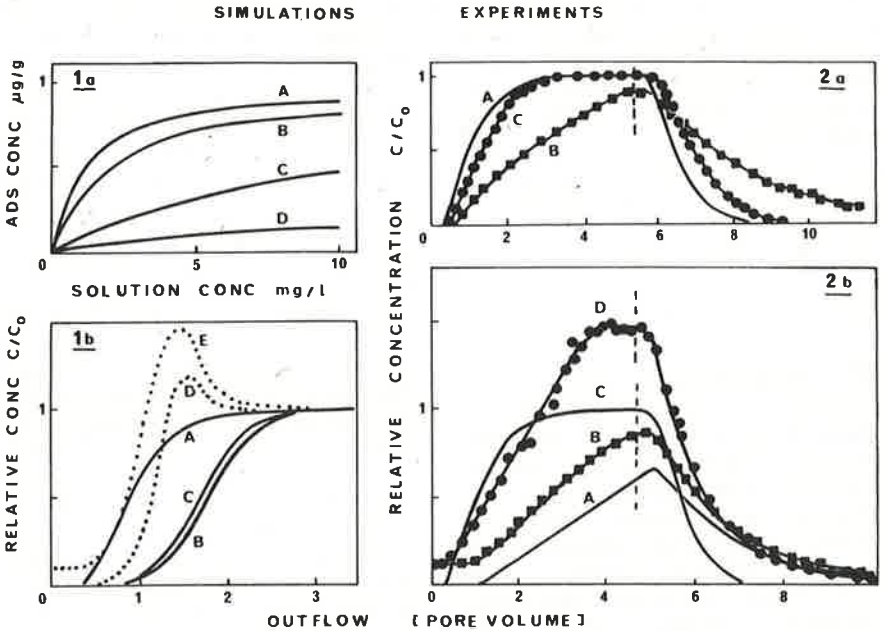

FIGURE 1

(a) Equilibrium adsorption isotherms simulated to show the influence of different degrees of competition.

Values of KC (K is the equilibrium distribution coefficient of the Langmuir isotherm and C is the solution phase concentration) for the second species of curves A, B, C and D are 0, 1, 10 and 50 respectively.

(b) Simulated breakthrough curves (BTC) showing the effect of competitive adsorption.

A and B are breakthrough curves for non-interacting species, and that of an adsorbing species in the absence of competition, respectively. Curves C and D simulate small and large degrees of competition while E demonstrates the impact of residual adsorption of a less preferred species when a mixture of the less preferred and a highly preferred species is infiltrated. BTC for a moderate degree of competition will be between curves A and B.

FIGURE 2

Experimental breakthrough curves
(a) Sulphate-phosphate system
(b) Selenite-phosphate system

Vertical broken lines indicate the start of the desorption phase (inlet concentration changed from C_0 to zero). Various curves are described in the text.

Competitive Adsorption: Its Importance in Ionic Transport in Soils

V. MURALI* and L. A. G. AYLMORE*

Transport of ions in soils is influenced by adsorption; adsorbing chemicals are less mobile than non-interacting species. The results of computer simulations and laboratory experiments presented here for multi-component systems, where two (or more) ions exist simultaneously and compete for adsorption sites, show that the mobility of ions, such as sulphate, selenite and phosphate, can increase depending on the relative preference soils have for the species. Pollution hazards of chemicals in soils should thus be assessed in realistic multi-component systems similar to those which occur in field situations.

Studies on the movement of chemicals, such as fertilisers, pesticides, herbicides, heavy metal ions and radioactive isotopes, in soil have received considerable attention from soil scientists and environmentalists because of their importance in the efficiency of fertiliser use and the disposal of industrial and agricultural pollutants (Murali and Aylmore, 1979, 1980; Viets, 1975; Letey and Farmer, 1974; Siddle *et al.*, 1977; Starr and Parlange, 1979). Inert or non-interacting solutes move with greater ease and over longer distances than adsorbing species because of the retardation through loss from solution phase of the latter. Amount and rates of adsorption and desorption, hydrodynamic dispersion (mixing caused by the dynamics of water movement in a porous soil matrix), molecular diffusion and convective or mass flow (of water) are some of the important factors governing the transport of chemicals in soil. In practical field situations, co-existence of two or more chemical species is often the rule rather than the exception. However, the effects of competitive adsorption among anions, such as phosphate, sulphate and selenite on solute transport are seldom accounted for in the mathematical models used to predict the movement. The present findings based on computer simulations and laboratory experiments demonstrate the extreme importance of competitive adsorption during solute movement in soils.

Prediction of solute transport in soil, particularly for adsorbing species, is increasingly based on computer-aided numerical solution of the appropriate partial differential equations. The type of adsorption, the form of the adsorption isotherm and dynamic aspects of the adsorption-desorption process are extremely critical in making reliable predictions (Murali and Aylmore, 1979 and 1980).

The results presented and discussed here are for a system of two adsorbing species (distinguished by subscripts A and B). This approach may readily be extended to three or more species. Our model for competition between two ionic species consists of four simultaneous equations, describing conser-

*Department of Soil Science and Plant Nutrition,
University of Western Australia,
Nedlands, WA 6009.

vation of mass during dispersive-convective-adsorptive flow for each species separately (equations 1 and 2) and two equations describing the rates of adsorption for the two species. These equations are:

$$\frac{\partial C_A}{\partial t} + \frac{\beta}{\theta} \cdot \frac{\partial S_A}{\partial t} = D \frac{\partial^2 C_A}{\partial Z^2} - \frac{V}{\theta} \frac{\partial C_A}{\partial Z} \quad (1)$$

$$\frac{\partial C_B}{\partial t} + \frac{\beta}{\theta} \cdot \frac{\partial S_B}{\partial t} = D \frac{\partial^2 C_B}{\partial Z^2} - \frac{V}{\theta} \frac{\partial C_B}{\partial Z} \quad (2)$$

$$\frac{\partial S_A}{\partial t} = f(C_A, S_A, C_B, S_B) \quad (3)$$

$$\frac{\partial S_B}{\partial t} = f(C_B, S_B, C_A, S_A) \quad (4)$$

where β, θ, V and D are soil bulk density, volumetric moisture content, convective flow velocity of water and effective hydrodynamic dispersion coefficient (mechanical dispersion and molecular diffusion) respectively, and C, S, Z and t are solution phase concentration, adsorbed phase concentration and depth and time variables respectively.

The dynamic (time-dependent) nature of solute adsorption in soils, particularly under flow conditions, is well established (Murali and Aylmore, 1979; 1980; van Genuchten *et al.*, 1974; Rao *et al.*, 1979). We have therefore used as the basis of our model a dynamic version of competitive Langmuir-type adsorption, with modifications to include different adsorption capacities for different species. Other types of adsorption, e.g. Freundlich, can readily be used in the model, but computer simulations (not presented here) have shown that the results presented here are valid and that they are a consequence of competitive adsorption. Complete derivation of the model and details of the computer programs are beyond the scope of this communication and will be published elsewhere in due course. Initial and boundary conditions used conform to the laboratory experiments described below.

The equilibrium adsorption isotherm, which describes the distribution of a chemical species between solution and solid (adsorbed) phases under equilibrium conditions ($\partial S/\partial t \rightarrow 0$) at various concentration levels, is the most general description of the ion-soil interaction which can be determined experimentally. Figure 1a depicts equilibrium adsorption isotherms simulated by this model, exemplifying the influence of increasing solution concentrations of competing ionic species. Similar results were obtained from laboratory experiments for competition between phosphate and citrate (Nagarajah, 1969), as well as for phosphate/selenite and phosphate/arsenite systems (Hingston *et al.*, 1971).

The transport component of the model (equation 1 or 2) has been found adequate, experimentally, in the absence of adsorption, and for single adsorbing species (Boast, 1973; Elrick *et al.*, 1967; Aylmore and Karim, 1968).

Some of our recent computer simulations on the transport of competing ions in soils, in the form of breakthrough curves, are presented in Figure 1b. These breakthrough curves (BTC) describe the change in effluent concentration as a function of cumulative outflow volume, following a step-change of inlet concentration. The simulations show a wide range in the degree of influence of ionic competition on solute transport. This effect is small (curve B) for strongly preferred ions (where the BTC position is almost unaffected by the presence of competing species), or moderate (positioned between A and B) when the position of BTC shifts significantly towards that of non-interacting species. The effect can, however, be large (curve D) where a less preferred species, in the presence of a highly adsorbing ion, moves in a manner not dissimilar to that of an inert chemical. Indeed, in this case the effluent concentration may even exceed the inlet concentration for some period. Further, if a less preferred ion is initially adsorbed ($C_i \neq 0$) prior to the infiltration of a mixture containing the less preferred and highly preferred ions, the less preferred species may be desorbed from the solid and carried forward by the influx. Under such conditions (residual adsorption of less preferred species) the effluent concentratons of the less preferred species may exceed the input concentration by a large proportion, during some stages of flow (curve E). Still further, if a highly preferred species is initially adsorbed and a less preferred species passed subsequently, the latter will move almost like an inert species. Other simulations also demonstrated that several factors, such as concentration of individual chemicals, have an important role in determining the actual extent of the competitive influence on solute transport in soils.

Experimental

Experiments on ionic movement were conducted with finely ground and sieved (<2 mm) soils packed in acrylic columns. A constant-head reservoir of required solution was connected to the inlet of the soil column and the effluent was collected with a fraction collector. Constant flow velocity was maintained by a peristaltic pump positioned between the column outlet and the fraction collector. All chemical solutions were prepared in decimolar sodium chloride (instead of deionised water) to avoid soil dispersion, and labelled with appropriate radioactive isotopes — ^{32}P for phosphate, ^{35}S for sulphate, ^{75}Se for selenite and ^{3}H for water (representing non-interacting solute). The concentration of different species in the effluent samples was determined by appropriate beta or gamma counting techniques.

Experimental breakthrough curves (BTC) of the sulphate-phosphate system are given in Figure 2a. Curve A is the BTC for tritiated water (non-reactive species) and curve B is that of sulphate breakthrough in the absence of any competitive adsorption (single-species system) while curve C is the BTC of sulphate when a solution containing both sulphate and phosphate was percolated (transport in the presence of competitive adsorption). The significant influence of competition on sulphate movement can be observed from the large shift in the breakthrough position towards that of tritium. In the presence of residual phosphate, the sulphate breakthrough was identical to that for the tritium. Results of selenite-phosphate experiments are presented in Figure 2b. Curve A is the BTC for tritium and curve B is that of selenite in the absence of competition, while curve D shows the breakthrough of selenite when a solution containing both selenite and phosphate was passed. There was, however, residual selenite adsorbed ($C_i/C_o = 0.1$) before the start of infiltration of selenite in both cases (curves B and D). Effluent concentrations exceeded input concentration during a significant period of flow, much as simulated by curve E of Figure 1b. Phosphate breakthrough curves had the same shape and position in single- (phosphate alone) and multi-component (selenite-phosphate) systems. Thus, in the soils studied, phosphate ion behaved as a highly preferred species while the movement of sulphate and selenite ions was susceptible to competitive adsorption by phosphate.

These findings have considerable consequences in relation to a number of important practical problems in agriculture and environmental conservation. While quantitative verification of the simulation model used here in relation to field observations is still necessary, the results obtained so far are very encouraging. Pollution hazards in a particular field situation should therefore be assessed in a system consisting of the relevant competing species because single species investigations could yield unreliable conclusions.

References

AYLMORE, L. A. G. and KARIM, M. (1968) Leaching fertiliser ions in soil columns. *9th Int. Soil Sci. Soc. Trans.* (Adelaide) **1**, 143-153.

BOAST, C. W. (1973) Modelling the movement of chemicals in soils by water. *Soil Sci.* **115**, 224-230.

ELRICK, D. E., ERH, K. T. and KRUPP, H. K. (1967) Application of miscible displacement techniques to soils. *Water Resource Res.* **2**, 717-727.

HINGSTON, F. J., POSNER, A. M. and QUIRK, J. P. (1971) Competitive adsorption of negatively charged ligands on oxide surfaces. *Disc. Faraday Soc.* **52**, 334-342.

LETLEY, J. and FARMER, W. J. (1974) Movement of pesticides in soil, in *Pesticides in Soil and Water*, ed. W. D. Guenzi. Soil Sci. Soc. Am. Inc. Publ., Wisconsin, 67-98.

MURALI, V. and AYLMORE, L. A. G. (1979) Predicting the movement of solutes in soil profiles. *Proc. Nat. Symp. Hydrol. Water Resources* (Perth) 210-215.

MURALI, V. and AYLMORE, L. A. G. (1980) No-flow equilibration and adsorption dynamics during ionic transport in soils. *Nature* **283**, 467-469.

NAGARAJAH, S. (1969) *Desorption of phosphate from kaolinite and oxide surfaces.* PhD Thesis, University of Western Australia, Perth, Australia.

RAO, P. S. C., DAVIDSON, J. M., JESSUP, R. E. and SELIM, H. M. (1979) Evaluation of conceptual models for describing non-equilibrium adsorption-desorption of pesticide during steady flow in soils. *Soil Sci. Soc. Am. J.* **43**, 22-28.

SIDDLE, R. C., KARDOS, L. T. nd van GENUCHTEN, M.Th. (1977) Heavy metal transport model in a sludge-treated soil. *J. Environ. Qual.* **6**, 438-443.

STARR, J. L. and PARLANGE, J. Y. (1979) Dispersion in soil columns: The snow-plow effect. *Soil Sci. Soc. Am. J.* **43**, 448-450.

van GENUCHTEN, M. Th., DAVIDSON, J. M. and WIERENGA, P. J. (1974) An evaluation of kinetic and equilibrium equations for the prediction of pesticide movement through porous media. *Soil Sci. Soc. Am. Proc.* **38**, 29-35.

VIETS, F. G. (1975) The environmental impact of fertilisers. *C. R. C. Critical Reviews of Environmental Control*, **5**, 423-453.

Submitted 9 October 1980
Accepted 9 December 1980

0038-075X/81/1312-0076$02.00/0
SOIL SCIENCE

February 1981
Vol. 131, No. 2
Printed in U.S.A.

MODELING ADSORPTION IN SOLUTE FLOW SIMULATIONS: DIFFUSE DOUBLE LAYER VERSUS GAS-SOLID INTERACTION APPROACHES

V. MURALI AND L. A. G. AYLMORE

Department of Soil Science and Plant Nutrition, University of Western Australia, Nedlands, Western Australia, 6009

Received for publication 4 March 1980; revised 29 May 1980

ABSTRACT

Ionic transport in soils is commonly described by equations representing mass conservation and the rates of ion-soil interactions. The type of adsorption equation used is an important factor in solute flow predictions. Adsorption is most commonly described by either the diffuse double layer (DDL) theory, or approaches based on gas-solid interactions (GSI). Computer simulations, in the form of breakthrough curves for a goethite system, showed that DDL and GSI model predictions were similar. The GSI approach is readily adaptable to adsorption-desorption dynamics, however, and was found to be more convenient than DDL models for the simulation of ionic transport in soils.

INTRODUCTION

Movement of solutes in soils can be described by a mass conservation equation of the form (Boast 1973)

$$\frac{\beta}{\theta}\frac{\partial S}{\partial t} + \frac{\partial C}{\partial t} = D\frac{d^2C}{dx^2} - \frac{V}{\theta}\cdot\frac{dC}{dx} \qquad (1)$$

where

C is solution phase concentration (M cm^{-3})
S is adsorption phase concentration (M g^{-1})
β is soil bulk density (g cm^{-3})
θ is volumetric moisture content (cm^3 cm^{-3})
D is effective diffusion-dispersion coefficient (cm^2 h^{-1})
V is convective flow velocity (cm h^{-1}) and
x and t are distance (cm) and time (h) variables

To solve Eq. (1), $\partial S/\partial t$ needs to be expressed as a function of other variables and has a general form

$$\frac{\partial S}{\partial t} = f\left(C, S, \frac{\partial C}{\partial t}, \cdots\right) \qquad (2)$$

The form of f depends on the nature of the adsorption-desorption process.

In recent decades, various approaches have been used to describe solute-soil interactions. Considerable attention has been given to adsorption models based on gas-solid interactions (GSI) that lead to Langmuir and Freundlich type equations. These have sometimes been criticized for neglecting the generally electrostatic nature of the ion-soil interactions and for ignoring the heterogeneity of the surface adsorption energy. Preference has often been given to models based on the diffuse double layer (DDL) theories (Bowden et al. 1980).

Until recently, these details were of little significance in relation to the modeling of solute flow in soils, since mathematical limitations largely restricted the attempts to solve Eqs. (1) and (2) to invariably unrealistic assumptions, such as linear adsorption isotherms, instantaneous equilibria, and constant convective flow velocities. As can be expected, such models are of limited applicability, because adsorption-desorption processes are often time dependent, particularly under flow conditions, and also because of the intermittent nature of flow in field situations. Now, however, the increasing accessibility of computers has greatly facilitated the use of numerical methods for solving the equations describing mass balance and sorption dynamics (Murali and Aylmore 1979, 1980) and has provided good prospects for developing a comprehensive model capable of accurately and realistically describing these processes. Success in this direction will depend on the use of functions in Eq. (2) that adequately describe the sorption processes and are, at the same time, sufficiently uncomplicated to provide an efficient and viable computer simulation model. GSI models have been frequently used for this

purpose in conjunction with Eq. (*1*) (Selim et al. 1976; de Camargo et al. 1979; Selim 1978). The purpose of this paper is to compare the suitability of the two types of sorption models, GSI and DDL, for computer simulation of solute transport in soils.

Adsorption models based on gas-solid interaction

The adsorption isotherms for most such anions as phosphate, sulfate, and selenite, under equilibrium conditions, are typically characterized (Hingston et al. 1970, 1971) by large values of $\partial S/\partial C$ (slope) at low concentrations, with a decrease in the slope as concentration increases. In addition, the slope often tends to 0 as the amount adsorbed (S) approaches the "adsorption maximum." The Langmuir type adsorption isotherm, which was initially developed for gas-solid interactions (GSI), is often used to fit such observations. For example, see the data for phosphate adsorption on goethite in Fig. 2 (Nagarajah 1969). The dynamic form of the Langmuir type isotherm is given by

$$\frac{\partial S}{\partial t} = k_a \cdot C \cdot (Q - S) - k_d \cdot S \qquad (3)$$

Equation (*3*) reduces, for equilibrium conditions ($\partial S/\partial t \rightarrow 0$) to Eq. (*4*)

$$S = \frac{K_L \cdot C \cdot Q}{1 + K_L C} \qquad (4)$$

Additional symbols are

k_a = adsorption rate coefficient
k_d = desorption rate coefficient
$K_L = k_a/k_d$ = equilibrium distribution coefficient and
Q = adsorption maximum

For phosphate adsorption for most solid surfaces, including soils, both Q and K_L are usually pH dependent.

An important criticism of the Langmuir type approach has been its implicit assumption of a constant adsorption energy over the entire range of adsorption. For soils, however, it is more realistic to assume heterogeneous adsorption energies.

Crickmore and Wojciechowski (1977) have modified the Langmuir type isotherm by allowing the adsorption energy to vary with the amount adsorbed. The resulting equation in the present notation is

$$\frac{\partial S}{\partial t} = k_a \cdot C \cdot N_c \cdot \left(1 - \frac{S}{N_c}\right)^{1/M} - k_d \cdot N_c \cdot \left(\frac{S}{N_c}\right)^{1/M} \qquad (5)$$

Under equilibrium conditions ($\partial S/\partial t \rightarrow 0$), Eq. (*5*) reduces to

$$S = \frac{K_C \cdot N_c \cdot C^M}{1 + K_C \cdot C^M} \qquad (6)$$

where M and K_C are isotherm parameters. We have assumed N_c to be the potential maximum adsorption (independent of pH). M and K_C are pH dependent. Equations (*5*) and (*6*) describe dynamic and equilibrium forms of the Crickmore model.

Adsorption model based on diffuse double layer hypothesis

The adsorption model of Bowden et al. (1974) is used as an example of the diffuse double layer (DDL) approach. In its complete form, the DDL model requires five simultaneous equations that have to be solved by iterative procedures to estimate the equilibrium distribution of ions between solution and solid (adsorbed) phases. The equations are

a. the surface charging equation

$$\sigma_s = \frac{N_S\left[K_H \cdot a_H \cdot \exp\left[\frac{-F\psi_s}{RT}\right] - K_{OH} \cdot a_{OH} \cdot \exp\left[\frac{F\psi_s}{RT}\right]\right]}{1 + K_H \cdot a_H \cdot \exp\left[\frac{-F\psi_s}{RT}\right] + K_{OH} \cdot a_{OH} \cdot \exp\left[\frac{F\psi_s}{RT}\right]} \qquad (7a)$$

b. charge in the diffuse double layer

$$\sigma_d = -1.22\ 10^{-10} C_{el}^{0.5} \cdot \sinh\ (0.0195\ \psi_d) \qquad (7b)$$

c. potential difference between the surface layer and the Stern layer

$$\psi_s - \psi_d = \sigma_s \cdot G \qquad (7c)$$

d. charge in the Stern layer

$$\sigma_t = \frac{N_t \cdot Z \cdot K \cdot C \cdot \exp(-Z \cdot F \cdot \psi_d/RT)}{1 + K \cdot C \cdot \exp(-Z \cdot F \cdot \psi_d/RT)} \qquad (7d)$$

e. the charge conservation equation

$$\sigma_s + \sigma_d + \sigma_t = 0 \qquad (7e)$$

Adsorbed phase concentration is then given by

$$S = \frac{\sigma_t}{Z} \qquad (7f)$$

The symbols used are

σ_s—charge in the surface layer, eq cm^{-2}
σ_t—charge in the Stern layer, eq cm^{-2}
σ_d—charge in the diffuse layer, eq cm^{-2}
N_S—number of possible sites for H_3O^+ and OH^-, cm^{-2}
N_t—number of possible sites for phosphate ions in Stern layer, cm^{-2}
K_H—distribution coefficient of H^+ ions
a_H—activity of H^+ ions in solution
K_{OH}—distribution coefficient of OH^- ions
a_{OH}—activity of OH^- ions in solution
ψ_s—electric potential of surface, mV
ψ_d—electric potential of Stern layer, mV
G—capacity of the region between surface and Stern layers, eq $V^{-1}cm^{-2}$
C—equilibrium (P) concentration, M/liter
C_{el}—concentration of the indifferent electrolyte, M/liter
Z—valency (including charge) of the adsorbing ion
K—distribution coefficient of the adsorbing ion
F—Faraday constant, C/M
R—gas constant, J/M°K
T—temperature, °K

Bowden et al. (1977) found it convenient to use the Nernst equation to compute the surface potential (assumed constant at any given pH) without losing accuracy, thus eliminating the need for Eq (*7a*). The Nernst equation with ψ_s in millivolts is

$$\psi_s = 59\left[\log\frac{K_H \cdot 10^{14}}{K_{OH}} - \text{pH}\right] \qquad (7g)$$

Application of the DDL approach in ion transport simulations involves Eq. (*1*) along with the DDL equations (*7b* to *7g*) for each time step and distance node. As the DDL equations have to be solved by an iterative procedure, this approach would involve enormous computation time. Thus, in its present form the DDL adsorption model is of severely limited use in solute transport simulations. We have observed, however, that plots of ψ_d versus ln C, in the data of Nagarajah (1969) for phosphate adsorption on goethite were effectively linear over a wide range

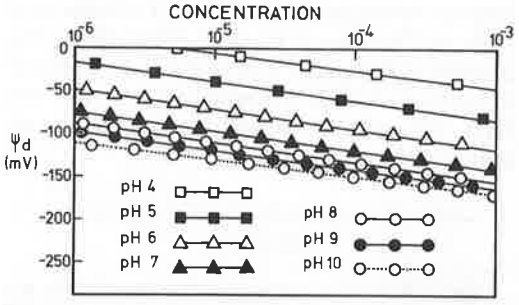

FIG. 1. Plots of ψ versus ln C for different pH values, using the phosphate adsorption data (Fig. 2) of Nagarajah (1969).

of pH values (Fig. 1). Statistical analysis showed that equations of the form $\psi_d = \alpha + \beta \ln C$, where α and β are constants, were significant at the 0.1% level for all pH values of interest. Therefore, for any ion-soil system for which this relationship holds, incorporating such a linear relationship in the DDL equations simplifies the adsorption model significantly and results in equations of the form

$$S = \frac{\sigma_t}{Z} = \frac{N_t \cdot K_B \cdot C^N}{1 + K_B \cdot C^N} \qquad (8)$$

where

$$K_B = K \cdot \exp(-0.039 \cdot Z \cdot \alpha) \qquad (8a)$$

$$N = (1 - 0.039 \cdot Z \cdot \beta) \qquad (8b)$$

Equation (*8*) is the simplified DDL model.

Similarity in the forms of the GSI and the simplified DDL models makes it possible to attach physical meaning to the Langmuir and Crickmore model parameters. For example, K_c may be considered as the effective distribution coefficient, which also accounts for the concentration dependence of the Stern potential. Whereas the DDL model was developed for equilibrium systems and thus has no dynamic form, GSI models have their time-dependent versions, and this is of considerable importance in modeling solute transport.

Simulations on the use of GSI and DDL adsorption approaches in solute transport models

Langmuir, Crickmore, and the DDL model parameters characterizing phosphate adsorption on goethite are presented in Table 1. Figure 2 compares the computed equilibrium isotherms and the experimental data. Although all three adsorption models provide a good approxima-

TABLE 1

Estimated adsorption model parameters for the isotherms in Fig. 2

Model and parameters	pH			
	4	6	8	10
Crickmore				
N_c	3.0	3.0	3.0	3.0
K_C	9.7	3.6	1.4	0.5
M	0.33	0.26	0.31	0.24
Langmuir				
Q	2.9	2.65	2.2	1.3
K_L	20	10	4	4
DDL				
N_T	3.0	3.0	3.0	3.0
K_B	9.3	3.5	1.4	0.4
N	0.37	0.23	0.22	0.33

tion to the experimental data, the most accurate representation is provided at all pH values by the Crickmore model.

Computer simulations of ionic transport were performed in the form of breakthrough curves (BTC). Instantaneous equilibrium of solute sorption processes was assumed for all three adsorption models—Langmuir, Crickmore, and DDL—as one of them (DDL) is valid only for such conditions. The solute transport model and boundary conditions in this case can be simplified to

$$\frac{\partial C}{\partial t} = \frac{D}{R}\cdot\frac{\partial^2 C}{\partial x^2} - \frac{V}{\theta R}\cdot\frac{\partial C}{\partial x}$$

where $R = 1 + (\beta/\theta)\cdot(\partial S/\partial C)$ is the retardation function.

$$C(x, t) = 0 \qquad \text{for } t < 0$$

$$C(0, t) = C_0 \qquad \text{for } 0 \le t \le T$$

$$C(0, t) = 0 \qquad \text{for } t > T \text{ and}$$

$$dC/dx = 0 \qquad \text{at } x = L$$

where T and L are the infiltration time and the length of the soil column, respectively.

Examples of the breakthrough curves simulated to compare phosphate movement through hypothetical soil columns composed of Nagarajah's goethite, at different pH levels, using the different adsorption models, are presented in Fig. 3. Other parameters used for these simulations are given in Table 2.

The simulated BTCs indicate that the three adsorption models differ only marginally in their predicted results. The steep rise in the breakthrough curve during the adsorption phase is perhaps indicative of the instantaneous reaction and the shape of the isotherms. In the desorption phase, however, the Langmuir model predicted a more gradual change in the effluent concentration than the other two models.

Use of three parameter adsorption equations, such as provided by the Crickmore and DDL theories for the instantaneous reaction in numerical simulations, requires caution because of a convergence problem. The factor responsible for this problem appears to be the discontinuity in $\partial S/\partial C$ at $C = 0$. Whereas the slope $(\partial S/\partial C)$ increases steeply as C approaches 0 from the positive side, it is 0 at $C = 0$. Such convergence problems were not encountered with the Langmuir type isotherm nor with the dynamic form of the GSI models. The predictions based on the dynamic form of the GSI models were found to approach the corresponding instantaneous model predictions for large values of the rate coefficients. In addition, since adsorption in soils is often time dependent, particularly under flow conditions (Murali and Aylmore 1980), and because of the generally intermittent nature of

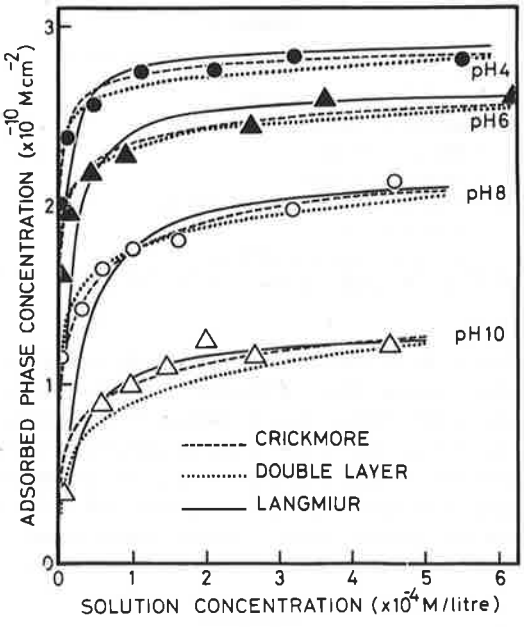

FIG. 2. Phosphate adsorption isotherms for goethite. Data points are from Nagarajah (1969), and isotherms are estimated from Langmuir, Crickmore, and DDL adsorption models.

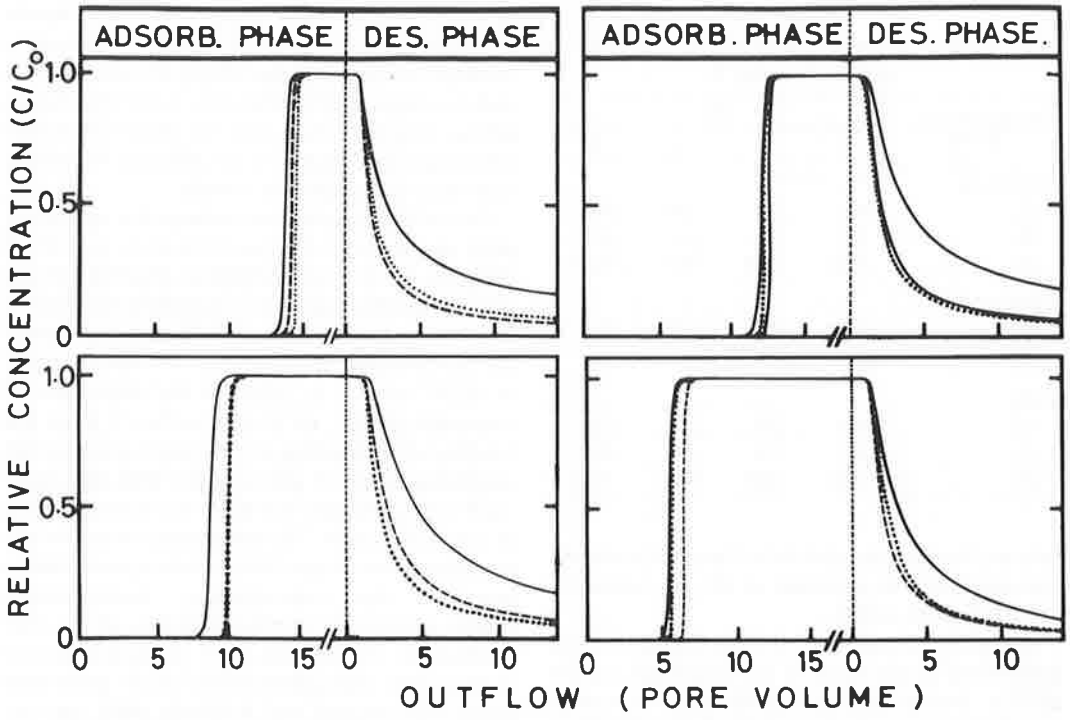

FIG. 3. Breakthrough curves simulated to compare phosphate movement through hypothetical columns composed of goethite.

TABLE 2

Model parameters used in the simulations

β	= bulk density = 1.6 g cm^{-3}
θ	= moisture content = .35 cm^3 cm^{-3}
L	= length = 10 cm
V	= velocity = 5 cm h^{-1}
D	= dispersion coefficient = 5 cm^2 h^{-1}
	area = 80 cm^2
	one pore volume = 280 cm^3
C_o	= concentration (input) = 1×10^{-4} M/liter

flow in field situations, it is advisable to employ the dynamic form of the GSI models in ionic transport studies. The limitation of instantaneous interaction of the DDL model restricts its practical utility. The closeness of the predicted ionic transport between DDL and GSI models for the present data, however, offers promise, and GSI models may be used with confidence.

SUMMARY

Ionic transport in soils can be described by the convective-dispersive-adsorptive flow equation. Adsorption of ions by soils is most commonly interpreted in terms of two approaches—the diffuse double layer (DDL) theory and developments based on gas-solid interaction (GSI) theories. A variable adsorption energy version of the GSI models has the form similar to the simplified DDL adsorption model. This enables practical significance to be given to the experimentally determined parameters of the GSI models instead of treating them as purely empirical constants. Comparison of DDL and GSI models for their usefulness in ionic transport was carried out using computer simulation of breakthrough curves (BTC) of phosphate ions through a goethite column for the phosphate adsorption data of Nagarajah (1969). In its standard form, the DDL approach is of limited use in numerical modeling because of the large computation time it would involve. The simplified form of DDL and two examples of GSI (Langmuir and Crickmore) adsorption models gave comparable simulated BTCs in the adsorption phase, and the desorption phase, Langmuir isotherms resulted in a relatively more gradual change of the effluent concentration. A convergence problem was encountered while using the instantaneous interaction form, which is necessary for a DDL type model. Such problems do

not arise for the dynamic form of GSI models. Since in practice one often encounters such problems as intermittent flow, it is concluded that GSI models are more adaptable to ionic transport studies than DDL models.

REFERENCES

Boast, C. W. 1973. Modeling the movement of chemicals in soils by water. Soil Sci. 115:224–230.

Bowden, J. W., A. M. Posner, and J. P. Quirk. 1974. A model for ion adsorption on variable charge surfaces. Trans. Intern. Congr. Soil Sci. 10th Congr. Moscow 2:29–36.

Bowden, J. W., A. M. Posner, and J. P. Quirk. 1977. Ionic adsorption on variable charge mineral surfaces: Theoretical charge development and titration curves. Aust. J. Soil Res. 15:121–136.

Bowden, J. W., S. Nagarajah, N. J. Barrow, A. M. Posner, and J. P. Quirk. 1980. Describing the adsorption of phosphate, citrate and selenite on a variable-charge mineral surface. Aust. J. Soil Res. 18:49–60.

Crickmore, P. J., and B. W. Wojciechowski. 1977. Kinetics of adsorption on energetically heterogeneous surfaces. J. Chem. Soc. Faraday Trans. 1 73:1216–1223.

de Camargo, O. A., J. W. Biggar, and D. R. Nielsen. 1979. Transport of inorganic phosphorus in an Alfisol. Soil Sci. Soc. Am. J. 43:884–890.

Hingston, F. J., A. M. Posner, and J. P. Quirk. 1970. Adsorption of selenite by goethite. *In* Adsorption from Aqueous Solutions. Adv. Chem. Sci. 79:82–90.

Hingston, F. J., A. M. Posner, and J. P. Quirk. 1971. Competitive adsorption of negatively charged ligands on oxide surfaces. Discuss. Faraday Soc. 52: 334–342.

Murali, V., and L. A. G. Aylmore. 1979. Predicting the movement of solutes in soil profiles. Proc. Natl. Symp. Hydrol. Water Resources. Perth, pp. 210–215.

Murali, V., and L. A. G. Aylmore. 1980. No-flow equilibration and adsorption dynamics during ionic transport in soils. Nature 238:467–469.

Nagarajah, S. 1969. Desorption of phosphate from kaolinite and oxide surfaces. Ph.D. thesis. University of Western Australia, Perth, Australia.

Selim, H. M. 1978. Transport of reactive solutes during transient unsaturated water flow in multilayered soils. Soil Sci. 126: 127–135.

Selim, H. M., R. S. Mansell, and A. A. Elzeftawy. 1976. Distribution of 2,4-D and water in soil during infiltration and redistribution. Soil Sci. 121:176–183.

A Convective-Dispersive-Adsorptive Flow Model for Solute Transport in Soils. I Model Description and some Simulations

V. Murali and L. A. G. Aylmore

Department of Soil Science and Plant Nutrition,
University of Western Australia,
Nedlands, W.A. 6009.

Abstract

Solute transport predictions are usually based on mathematical (analytical and numerical) solutions of partial differential equations describing convective-dispersive-adsorptive flow and ion-soil interactions. In this paper computer simulations based on a numerical model of solute transport in soil columns have been used to illustrate the significance of flow dynamics and adsorption-desorption parameters in determining the shape and position of solute breakthrough curves.

Approximating non-linear isotherms of the form $S = KC^M$, where S is adsorption phase concentration, C is solution phase concentration, and K and M are constants, by linear isotherms of the form $S = KC + \varepsilon$, where ε is the intercept, to facilitate the use of analytical solutions, has been shown to result in significant errors when the retardation factor fails to account for the intercept ε (when ε is zero, the retardation factor equals $1 + \beta K/\theta$, where β is the bulk density and θ is water content). Using the dynamic form of Freundlich adsorption, the importance of non-linearity in the equilibrium isotherms is demonstrated. Computer simulations have also been used to demonstrate the extreme importance of intermittent flow, the simultaneous occurrence of adsorption dynamics, ionic fixation and hysteresis during instantaneous adsorption and desorption in determining the transport of solutes in soils.

Introduction

Methods for predicting the movement of adsorbing chemicals such as fertilizers, pesticides, herbicides and heavy metals in soils have received increasing attention in recent years, because of their importance in relation to the efficiency of fertilizer usage and in the control of agricultural and industrial pollutants. A variety of models have evolved through attempts to quantitatively describe these transport processes. However, the multiplicity of factors which may be involved in determining the transport of any given solute through a soil profile makes the task of deriving a comprehensive model capable of handling the many possible variations in mechanisms, boundary conditions and so on, which are possible, extremely difficult. Consequently success in previous work has varied depending on the closeness of approximation of a particular model to the processes actually involved.

The approaches used to predict solute movement can be broadly distinguished into three classes – (*a*) empirical models based on simple concepts which often fail to account explicitly for certain important processes such as hydrodynamic dispersion

(e.g. Tanji *et al.* 1967; Tarkaltoub and Babcock 1971; Addiscott 1977), (*b*) analytical solutions of the differential equations describing dispersive-convective-adsorptive flow, which have generally been obliged by mathematical complexities to ignore either the dynamic or the non-linear aspects of adsorption (e.g. Lapidus and Amundson 1954; Lindstrom *et al.* 1967; Cleary and Adrian 1973; Marino 1974; Selim and Mansell 1976), and (*c*) computer simulation models which solve the pertinent flow and sorption equations by numerical techniques (e.g. van Genuchten *et al.* 1974; Selim *et al.* 1977; Murali and Aylmore 1979, 1980; Gureghian *et al.* 1979; Scotter 1979). Of these approaches, the computer-based numerical modelling is the only one which seems likely to achieve a comprehensive description of solute transport in soils, particularly for adsorbing species.

The purpose of this and subsequent papers will be to describe by means of computer simulations, the effects of various dispersive mechanisms, including in particular solute-soil interactions, occurring in isolation or simultaneously, on ionic transport in soils. A particular virtue of this approach is that it not only permits the accurate prediction of solute distributions, but also facilitates the interpretation of measured solute distributions in terms of the specific mechanisms involved. In this paper we illustrate the role of adsorption-desorption-fixation processes on solute transport under different conditions governing the flow processes.

Physics of the System

Ionic transport in soil profiles is best described by simultaneous differential equations which are based on material conservation and on ion-soil interaction. As a basis for subsequent development, the system which is considered in the present work includes the following processes and conditions:

(*a*) intermittent convective flow in one dimension with constant moisture content;
(*b*) hydrodynamic dispersion (molecular diffusion in conjunction with mechanical dispersion);
(*c*) sorption processes, including sorption dynamics, instantaneous adsorption and desorption, and fixation;
(*d*) transient solute dynamics.

Water flow in soils which gives rise to dispersive-convective flow of solutes, rarely, if ever, occurs continuously or at uniform flow velocity for any length of time, i.e. during infiltration, redistribution or ground water movement. Generally the movement of water occurs in two stages – a relatively fast transport phase, during and immediately after rainfall or irrigation followed by a second stage in which flow may be essentially negligible but during which adsorption/desorption, intra-aggregate diffusion and other equilibration processes may continue. The assumption of a constant 'average' flow velocity during solute movement can lead to quite erroneous predictions when such time-dependent equilibrations are involved. It is thus important that the intermittent character of water flow be included as a basic component in any model. While analytical approaches are unable to handle this intermittent nature of the flow process, it can be readily incorporated into numerical models (Murali and Aylmore 1979, 1980). Intermittent flow is used here as a first approximation of field situations, to demonstrate the inadequacies of the unrealistic

assumption of constant convective flow when other equilibrations are involved. Constant moisture content and one-dimensional flow are assumed here in order to limit the complexities of the model while illustrating the effects of adsorption–desorption parameters. Continuously changing flow velocity and moisture content profiles can be readily incorporated into more sophisticated simulations.

The hydrodynamic dispersion coefficient, which represents the sum of molecular diffusion and mechanical dispersion components, has been investigated by numerous workers under laboratory and field conditions (Gupta and Greenkorn 1974; Biggar and Nielsen 1976; Klotz *et al.* 1980). The results indicate that the hydrodynamic dispersion coefficient is a function of convective flow velocity, which decreases with decreasing velocity to approach the molecular diffusion coefficient when flow ceases. That is, the diffusion coefficient is much smaller in magnitude than the dispersion coefficient at all but very low flow velocities. We have, following Bresler (1973), ignored the molecular diffusion component, thus leading to a finite value of dispersion during flow and a zero value during no-flow periods.

The importance of adsorption/desorption processes in determining solute transport has been clearly demonstrated in previous models (van Genuchten *et al.* 1974, 1977; Selim *et al.* 1977; Gureghian *et al.* 1979; Murali and Aylmore 1979). Such models which utilize adsorption components are generally limited to considerations in terms of either an instantaneous interaction or dynamic interaction alone. It is evident, however, from ionic adsorption studies (e.g. Parfitt 1979; Barrow and Shaw 1979) that several processes, including adsorption–desorption hysteresis and fixation involving both instantaneous and dynamic interactions, may occur simultaneously. A satisfactory model should thus be able to handle all such possibilities for both linear and non-linear isotherms.

Theoretical Treatment

Fig. 1 depicts the solute flow and ion-soil interactions involved.

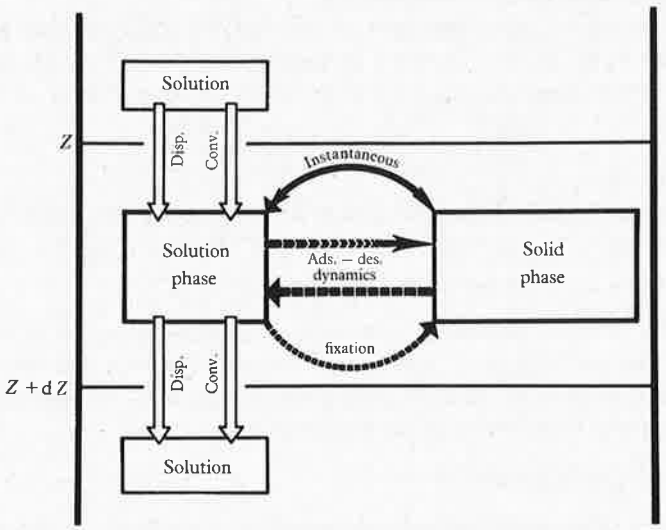

Fig. 1. Compartmentalized representation of the various processes involved in the solute transport model.

Consider a small section of soil between depths Z and $(Z + dZ)$. The quantity of ions entering this layer due to the dispersion–diffusion process per unit area and unit time (J_D) is

$$J_D = -D \cdot \frac{dC}{dZ} \cdot \theta \tag{1}$$

where J_D is the dispersive flux, D is the hydrodynamic dispersion coefficient, dC/dZ is the concentration gradient at Z, and θ is the volumetric water content. The negative sign indicates that the flow is from higher concentration to lower concentration. The factor θ is included at this stage to account for the fact that flow occurs only in water-filled pores. For details of symbols used, see Appendix 1.

Similarly, convective flux, J_C, is given by

$$J_C = V_p C\theta, \tag{2}$$

where V_p is the pore water velocity, C is the concentration of ions within the solution phase. As before θ accounts for water-filled pores.

The total convective–dispersive flux (over unit area of whole soil matrix) J_T can therefore be written as

$$J_T = J_D + J_C = -D\theta(dC/dZ) + VC, \tag{3}$$

where V is the matrix flow velocity ($V = V_p\theta$). The principle of mass conservation is now applied, i.e. the rate of change of this flux J_T results in a change in the rate of accumulation (or depletion) of the ions, at any given depth. In the case of interacting species, accumulation or depletion occurs in both solution and adsorbed phases. The proportion of the solid phase per unit volume is given by β, the bulk density, and the corresponding proportion of solution phase is given by θ, the volumetric water content. The conservation equation for this two 'phase' system is therefore

$$\frac{\partial}{\partial t}\left[\theta C + \beta S\right] = -\frac{dJ_T}{dZ}, \tag{4}$$

where S is adsorption phase concentration.

The negative on the right-hand side of the equality indicates that an increase in the accumulations results in a decrease in the solution phase flux. On expanding the equation on the assumption that θ is independent of both t and Z, we obtain

$$\frac{\partial C}{\partial t} = D\frac{d^2C}{dZ^2} - \frac{V}{\theta}\frac{dC}{dZ} - \frac{\beta}{\theta}\frac{\partial S}{\partial t}, \tag{5}$$

which is the most common form of solute flow equation. To solve this equation, however, we have to express $\partial S/\partial t$ as a function of other variables. Thus,

$$\partial S/\partial t = f(C, S, \partial C/\partial t, \ldots). \tag{6}$$

Conventionally, $\partial S/\partial t$ is positive for adsorption and negative for desorption. There are, however, different types of interactions between the ions and the soil particles, and the simplest of these are dealt with in the following section. Appendix 2 outlines numerical methods used and column dimensions.

Adsorption–Desorption Dynamics

Ion–solid interactions are generally modelled by using either of two approaches – (*a*) an analogy to gas–solid interactions, or (*b*) diffuse double layer theory. The use

of the diffuse double layer approach in solute transport simulations, however, involves a number of inherent difficulties (Murali and Aylmore 1981), and for convenience in the present work we have chosen to use the formulations derived from the gas–solid interaction approach.

Interactions between ions and solids may be roughly grouped in terms of the type of interaction occurring, and the most common formulations, using the terminology of Lapidus and Amundson (1952), are presented below. In these equations k_a, k_d, k_a', k_d', M and N are constants, while Q is the adsorption maximum.

(i) First order–first order kinetics:

$$\partial S/\partial t = k_a' C Q - k_d' C_i S = k_a C - k_d S. \tag{7}$$

This is the linear adsorption kinetics most commonly used in solute transport studies.

(ii) Second order–zero order kinetics:

$$\partial S/\partial t = k_a C (Q - S). \tag{8}$$

(iii) Second order–first order kinetics:

$$\partial S/\partial t = k_a C(Q - S) - k_d S. \tag{9}$$

This is also known as Langmuir kinetics.

(iv) Second order–second order kinetics:

$$\partial S/\partial t = k_a C(Q - S) - k_d S(C - C_1). \tag{10}$$

Many soil–anion interactions (Barrow and Shaw 1979) are better approximated by a power function or Freundlich type equations. Thus

$$\partial S/\partial t = k_a C^M - k_d S^N. \tag{11}$$

However, from a practical point of view, equilibrium adsorption studies only show the estimation of the ratio M/N and the estimation of M and N individually can be extremely laborious. For this reason, a value of unity for N has often been assumed. This results in

$$\partial S/\partial t = k_a C^M - k_d S, \quad K = k_a/k_d. \tag{12}$$

Adsorption–Desorption Hysteresis and Instantaneous Components

It is often observed that the experimental equilibrium adsorption and equilibrium desorption isotherms do not coincide. Further, this observation is not necessarily attributable to the dynamics alone, and the difference may not be spurious or simply the result of an inadequate equilibration period. In terms of theoretical treatment there are a number of considerations that may be relevant in attempting to model this result. Firstly, the kinetic parameters k_a and k_d, and perhaps the coefficient M may be different for the adsorption and desorption processes. In this situation three additional parameters would be required to describe hysteresis. On the other hand, the presence of an instantaneous component in the adsorption–desorption process for which the rates are different during adsorption and desorption would lead to a similar result. Since separate instantaneous components have been observed in many ion–soil interactions and should thus be included as part of the model, we have chosen in the first instance to treat hysteresis in terms of an instantaneous linear component for which the distribution coefficients in adsorption and desorption are different. The inclusion of hysteresis in this fashion requires only one additional

parameter. van Genuchten *et al.* (1974) used a non-linear instantaneous interaction with different adsorption and desorption coefficients to model the hysteresis observed during pesticide transport in soils, but did not incorporate a kinetic component. In the present treatment, for simplicity, we incorporate the non-linearity in the adsorption dynamics and hysteresis in an associated instantaneous linear interaction. Extension to include non-linear instantaneous components can readily be achieved if required.

The form of the instantaneous component is:

$$\partial S/\partial t = K_a \, \partial C/\partial t \tag{13}$$

during adsorption (i.e. $\partial S/\partial t > 0$) and

$$\partial S/\partial t = K_d \, \partial C/\partial t \tag{14}$$

during desorption. For most ions, adsorption is faster than desorption, and thus $K_a \geqslant K_d$. When we are not dealing with hysteresis the subscript is dropped.

From qualitative considerations, the instantaneous interaction has the following forms

(*a*) reversible when $K_a = K_d$;
(*b*) irreversible when $K_d = 0$;
(*c*) hysteretic when $K_a > K_d > 0$.

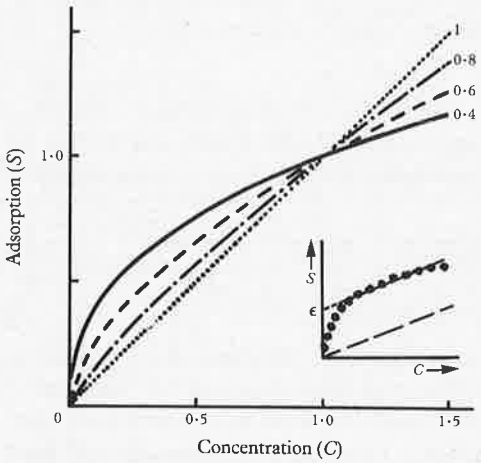

Fig. 2. Simulated equilibrium adsorption isotherms for the Freundlich model using $K = 1$, with various values of M. Inset: Fitting $S = KC + \varepsilon$ to a limited portion of the isotherm (curve A) and the corresponding curve (B) with zero intercept (ε) but having the same slope ($\partial S/\partial C$).

Ion Fixation

Ion fixation is commonly described as a continuous process, its rate being governed by solution phase concentration. Further, fixation is invariably considered to be irreversible. This reaction can be linear or nonlinear, but for the present a linear component is again only considered to keep the model parameters to a minimum, and also because the non-linearity has already been introduced into the dynamics. The mathematical form of the simplest case is

$$\partial S/\partial t = k_f C. \tag{15}$$

It can be noted that single step radioisotopic decay follows the same mechanism.

Computer Simulations

Freundlich adsorption dynamics was used in the solute flow simulations presented in this paper. Fig. 2 shows the change in the equilibrium isotherm shape for different values of M in the isotherm $S = KC^M$. The value of M for different ion–soil interactions is almost always less than unity, and hence we have not presented the shapes for M values higher than unity. On the basis of shape, the equilibrium isotherm can be divided into three regions, with respect to solution concentration. These are: (*a*) $C < 1$, (*b*) $C \simeq 1$ and (*c*) $C > 1$. When $C \simeq 1$ there is a narrow region in which S is almost independent of M. For $C < 1$, S at any given value of C increases as M decreases. This effect is reversed in the region $C > 1$, where S decreases as M decreases. An important feature of the isotherms which is sometimes misinterpreted is that in limited regions all the isotherms can be approximated to straight lines or linear isotherms. However, except when $M = 1$, such approximations will yield positive intercepts (ϵ), e.g. $S = KC + \epsilon$, which physically interpreted means that even in the absence of solute in the solution phase, the amount adsorbed is finite (see inset of Fig. 2). The predictions from isotherms of the type $S = KC + \epsilon$, particularly if one assumes instantaneous interaction and then uses a retardation factor $[= 1 + (\beta/\theta).\ \partial S/\partial C]$ approach, will be for a ficticious isotherm parallel to the one required, which passes through $C = 0$, $S = 0$ (see inset of Fig. 2).

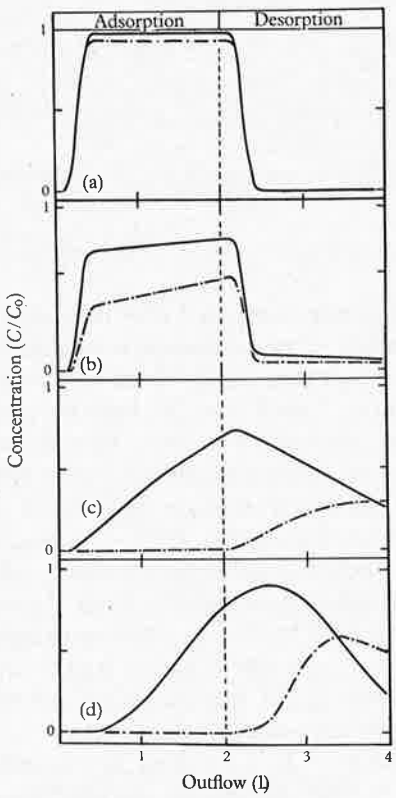

Fig. 3. Simulated breakthrough curves showing the effect of isotherm non-linearity (M of the isotherm $S = KC^M$) for different rates of interaction.
$K = 1$, $C_0 = 0{\cdot}25$.
One pore volume = 280 ml.
— $M = 1$. ·—· $M = 0{\cdot}4$.
(*a*) $k_a = k_d = 0{\cdot}01$.
(*b*) $k_a = k_d = 0{\cdot}1$.
(*c*) $k_a = k_d = 1{\cdot}0$.
(*d*) $k_a = k_d = 5{\cdot}0$

The difference between solute transport predictions based on linear ($M = 1$) and non-linear isotherms ($M \neq 1$) depends, among other things, upon C_0, the input

concentration. This is demonstrated by computer simulations in the form of solute breakthrough curves (BTC) with $K = 1$ in Figs 3 and 4. For solute input concentrations less than unity (Fig. 3), use of a linear model for adsorption predicts higher

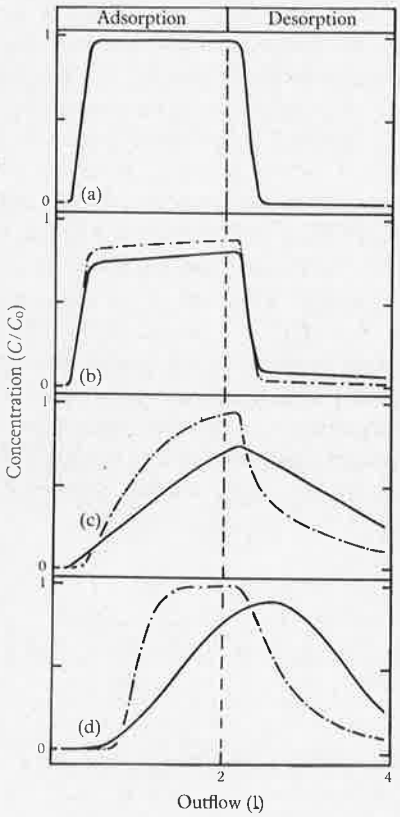

Fig. 4. Simulated breakthrough curves showing the effect of isotherm non-linearity (M of the isotherm $S = KC^M$) for different rates of interaction, $K = 1$, $C_0 = 2{\cdot}5$. One pore volume = 280 ml. Curves, as for Fig. 3. $k_a = k_d$, as for Fig. 3.

outflow concentrations or an earlier breakthrough, as compared with the predictions of the non-linear adsorption model. The effect of non-linearity is negligible for extremely slow rates (Fig. 3*a*), but becomes prominent as the rates become faster (Figs 3*b*, *c* and *d*). For faster rates of interactions (Figs 3*c* and 3*d*) both the position and shape of the breakthrough curves can be markedly different. Comparison of Figs 3 (for $C_0 = 0{\cdot}25$) and 4 (for $C_0 = 2{\cdot}5$, taken as an example of $C_0 > 1$) demonstrates the discrepancy which may arise from the use of an incorrect isotherm shape (i.e. in terms of linearity). In contrast to the predictions in Fig. 3 ($C_0 < 1$), the linear model ($M = 1$) for $C_0 > 1$ predicts lower outflow concentrations and a delayed breakthrough, compared to the non-linear adsorption flow model (Fig. 4). Again, for extremely slow rates of interaction (Fig. 4*a*), even for $C_0 > 1$, the difference between linear and non-linear models is negligible but becomes significant for higher rates of interaction (Figs 4*b*, 4*c* and 4*d*). For values of $C_0 > 2{\cdot}5$, the discrepancies between the predictions of the linear and non-linear models become even greater.

Effects of equilibrium distribution coefficient $K (= k_a/k_d)$ and the rate coefficients on solute breakthrough are presented in Fig. 5. The effect of the rate coefficients k_a and k_d is only marginal when the equilibrium distribution coefficient is small, for example $K = 0{\cdot}1$ (Fig. 5*a*), presumably because the actual amount adsorbed is

quite small. However, the influence of k_a and k_d becomes very significant for higher values of K. For extremely small rates of interaction the solute flow is not dissimilar to that of a non-interacting species. (Note that the relative outflow concentration (C/C_0) of 0·5 occurs at an outflow of one pore volume ($\simeq$280 ml)). As the rate of adsorption increases, the breakthrough position shifts to higher outflow volumes to the breakthrough curve position and shape converge with that for an instantaneous interaction. For a given value of k_a, changing k_d will alter K and hence the predicted shape and position of the BTC will be different. The same is also true for different values of k_a for a fixed k_d. The effect of changing k_d (0·01, 0·1 and 1) for a fixed value of k_a (0·1) on the shape and position of BTC's is shown in Fig. 6. Evidently, the shape and position of the breakthrough curves are extremely sensitive to the rate coefficients.

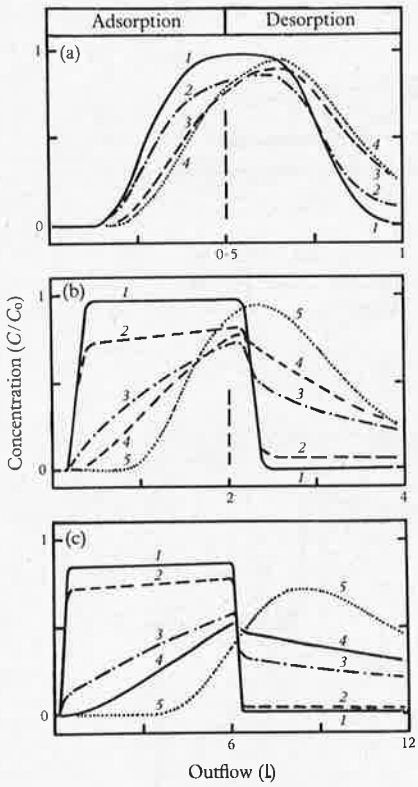

Fig. 5. Simulated breakthrough curves showing the effect of adsorption and desorption rates (k_a and k_d) and equilibrium distribution coefficient (k). The value of k in (*a*), (*b*) and (*c*) is 0·1, 1 and 5 respectively. In (*b*) the curves *1* to *5* are for k_a values of 0·01, 0·1, 0·5, *1* and *5*, while in (*c*) the corresponding k_a values are 0·05, 0·1, 0·5, 1 and 5.

The effect of input concentration, C_0, on solute breakthrough is depicted in Fig. 7. As mentioned earlier, three regions of Freundlich isotherms can be distinguished based on solution concentration, viz $C < 1$, $C \simeq 1$ and $C > 1$ for $K = 1$ and to represent these regions in the simulation, three values of C_0 (0·1, 1, and 10) were used. A value of $M = 0{\cdot}7$ providing a reasonable degree of non-linearity was used for these simulations. As in the earlier cases, extremely slow interactions produce identical BTC's for all three concentration levels (Fig. 7*a*), presumably because of the negligible amounts of adsorption. However, at moderate and high rates of adsorption C_0 has a very pronounced influence on solute transport. Breakthrough occurs earlier or faster at high concentrations (e.g. $C_0 = 10$), and slower for low concentrations

(C_0 = 0·1) when compared to C_0 = 1 (for continuous flow systems outflow volume and time are directly related). This effect becomes more significant for higher rates

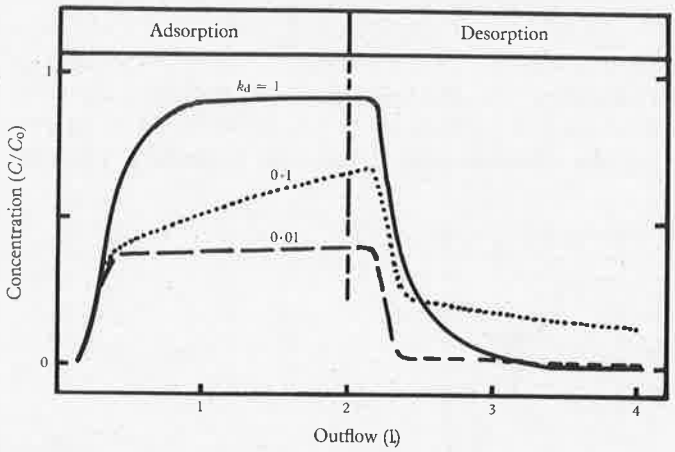

Fig. 6. Simulated breakthrough curves showing the effect of desorption rate (values of k_d are given on curves) for a fixed rate of adsorption (k_a = 0·1). One pore volume = 280 ml.

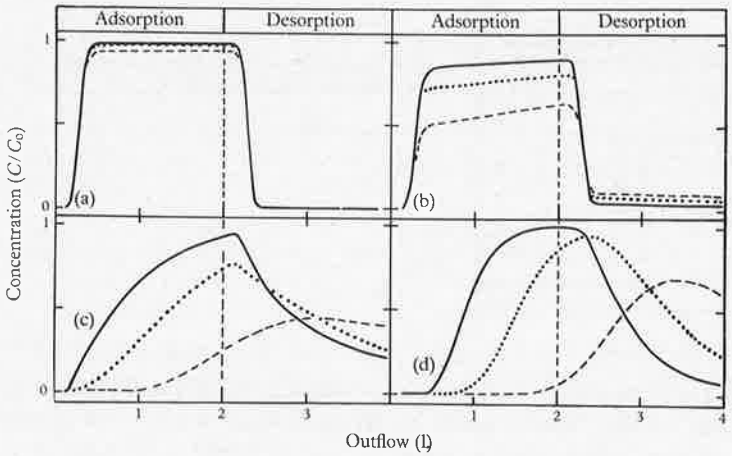

Fig. 7. Simulated breakthrough curves demonstrating the effect of input concentration C_0 on solute transport, for different rates of interaction. K = 1 and M = 0·7 were used. One pore volume, 280 ml. — C_0 = 10. . . . C_0 = 1. - - - - C_0 = 0·1. k_a = k_d: As for Fig. 3.

of interaction. It is worth emphasizing at this point that for linear adsorption models the solution breakthrough would be independent of input concentration, and these effects would be obscured by such an assumption.

The effect of the initial solution concentration in the soil, C_i, on solute breakthrough curves is presented in Fig. 8. Again the effect is minimal for extremely

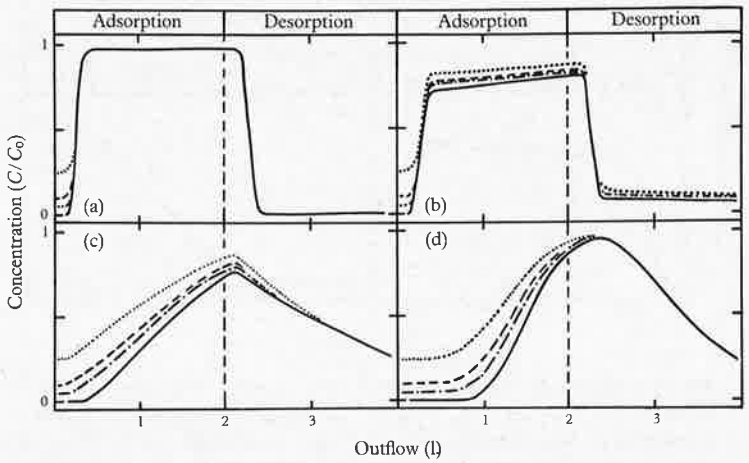

Fig. 8. Computer simulation of the effect of initial concentration, C_i, on solute breakthrough curves. $K = 1$ and $M = 0{\cdot}7$ were used. One pore volume = 280 ml. — $C_i = 0$. –·– $C_i = 0{\cdot}05$. – – – $C_2 = 0{\cdot}2$. . . . . $C_i = 0{\cdot}25$. $k_a = k_d$: As for Fig. 3.

small rates of interactions but dominates at higher rates.

The rate of adsorption $\partial S/\partial t$ decreases with increasing S, and hence at higher initial concentrations (which is synonomous to higher initial S) the slope of the solute breakthrough curve is smaller. After several pore volumes, however, the amount adsorbed approaches the same value, despite the different levels of C_i. Thus the curves converge.

Intermittent flow or no-flow equilibration is an extremely important factor in the dynamic adsorption model. It is completely obscured if an instantaneous adsorption model is used. This factor, which causes a depression in the outflow concentration following a no-flow equilibration, has recently been demonstrated by laboratory experiments and also by computer simulations (Murali and Aylmore 1980). Fig. 9 depicts the influence of the rates of interaction on the effect of different durations of no-flow equilibration on solute transport. For extremely slow interactions, e.g. $k_a = k_d = 0{\cdot}01$ (Fig. 9*a*), an increase in the no-flow equilibration period increases the extent of the no-flow depression. However, for moderate rates of interaction, $k_a = k_d = 0{\cdot}1$ (Fig. 9*b*), the adsorption process reaches equilibrium sooner and hence an increase in the period of equilibration has progressively less influence. For higher rates of interaction (for $k_a = k_d = 1$ and 5) (Figs 9*c* and 9*d*), the adsorption equilibrium is reached very rapidly and thus the BTC's for the three equilibration periods 2, 5 and 10 are similar for all practical purposes. Consequently in the case of instantaneous interactions, no-flow depressions are absent, and similarly, when interactions are extremely slow, a short period of equilibration may fail to produce a measurable no-flow depression. No-flow depressions are caused by time-dependent interactions and are not solely due to dynamics. Interactions such as fixation can also produce similar effects.

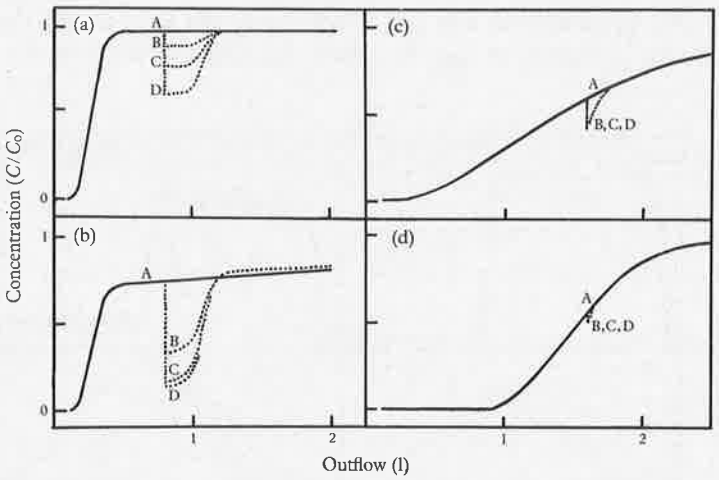

Fig. 9. Simulated breakthrough curves showing the influence of intermittent flow for the duration of no-flow periods on solute breakthrough for different rates solute–soil interaction. $K = 1$ and $M = 0{\cdot}7$ were used. The duration of no-flow periods for curves A, B, C and D are 0, 2, 5 and 10 units respectively. The time units are arbitrary and will be consistent with D and V units. $D = V = 2$ was used. Thus if the flow velocity was 2 cm/h, the no-flow periods will be in hours. $k_a = k_d$: (*a*) 0·01; (*b*) 1; (*c*) 0·1; (*d*) 5.

As briefly discussed earlier, fixation is a common ion–soil interaction and has a similar mathematical form to radioisotopic decay. The effect of fixation modelled as a linear decay, with superimposed sorption dynamics on solute transport, is

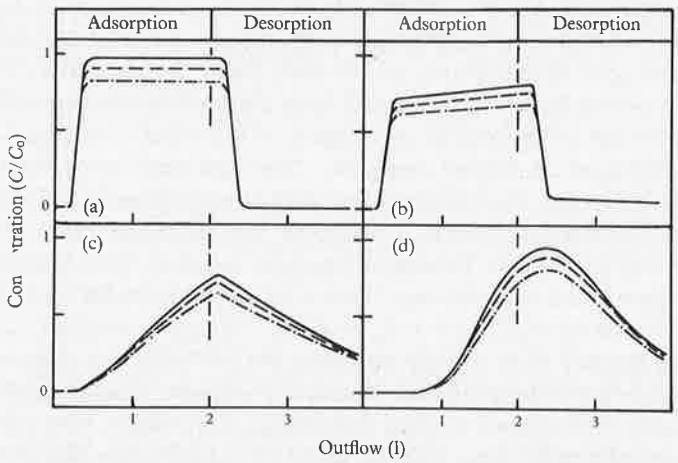

Fig. 10. Simulations showing the combined influence of fixation and adsorption–desorption dynamics on solute flow. K_f values: — 0; - - - 0·1; – · – · 0·25. $k_a = k_d$: As for Fig. 3.

demonstrated by the computer simulations presented in Fig. 10. The effect, for all rates of interaction, is to lower the maximum outflow concentration. As the rate of fixation increases there is a progressive reduction in the maximum outflow concentration. Instead of a tendency for the BTC to asymptote to input concentration, which is the case in the absence of fixation, the outflow concentration tends to level off at a concentration lower than the input concentration, and this reduction is directly related to the rate of fixation. This effect could have important implications in the land disposal of radioactive chemicals, because the amount of activity will always be lower than that predicted for the non-radioactive nuclide of the same element. It is worth noting here, however, that this conclusion is strictly applicable only to this model and for the type of boundary conditions used here. Other studies which account for competitive adsorption between two chemical species (Murali and Aylmore 1979) and between two nuclides of the same species (Starr and Parlange 1979), however, have shown that higher activities of radioisotopes in the outflow than the input concentration can occur at any particular depth, as a pulse, depending on the relative concentrations and adsorption affinities of the two species (or nuclides).

Apart from a dynamic component, ion–soil interactions can, as previously discussed, also have an instantaneous component. The combined effect of a linear instantaneous component and a non-linear dynamic component on solute BTC's is presented in Figs 11 and 12. Fig. 11 shows the effect of progressively increasing the instantaneous component (K = 0, 1, 2 and 3) for two different values of sorption

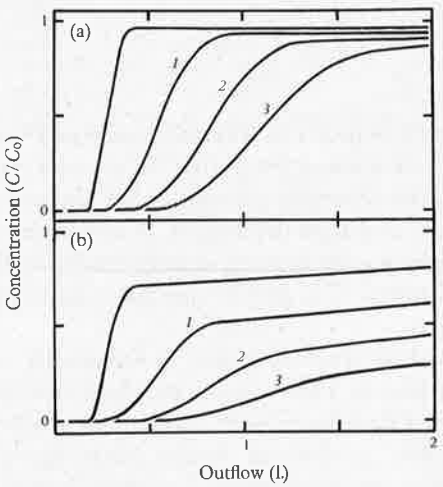

Fig. 11. Simulations showing the combined influence of instantaneous and dynamic components of adsorption on solute breakthrough.
Figures on curves are K_i values.
(*a*) $k_a = k_d = 0{\cdot}01$.
(*b*) $k_a = k_d = 0{\cdot}1$.

dynamics ($k_a = k_d = 0{\cdot}01$ in Fig. 11*a* and 0·1 in Fig. 11*b*). As the instantaneous component becomes larger the solute breakthrough becomes slower and more gradual. Comparing corresponding curves of Figs 11*a* and 11*b*, it is apparent that for any given value of instantaneous interaction, increasing the sorption rate delays the breakthrough and makes it more gradual. Fig. 12 shows the effect of hysteresis in the instantaneous component. The instantaneous component during the adsorption phase for all the simulated curves in Fig. 12 is the same ($K_a = 2$), but the dynamic components are different for Figs 12*a* and 12*b*. During the desorption phase, the effect of hysteresis becomes evident. Irreversible instantaneous interaction ($K_d = 0$) results in an early breakthrough in the desorption phase, while a reversible

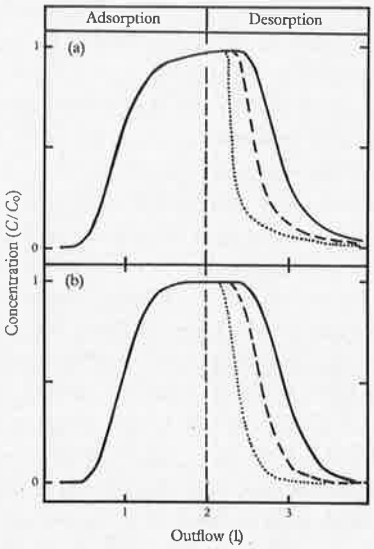

Fig. 12. Simulations showing the effect of hysteresis in the instantaneous component of a combined instantaneous and dynamic adsorption system on solute breakthrough. K_d values: — 2; - - - 1; .... 0. $K_a = 2$. (*a*) $k_a = 0{\cdot}1$, $k_d = 1$. (*b*) $k_a = 1$, $k_d = 10$.

instantaneous interaction ($K_a = K_d = 2$) results in a delayed breakthrough. In the case of instantaneous hysteresis, the breakthrough is intermediate to the completely reversible and the irreversible cases.

Summary and Conclusions

Predictions of the movement of adsorbing chemicals in soils are commonly based on mathematical solutions (numerical or analytical) of the partial differential equation governing the conservation of mass and the adsorption rate equation. In practice solute–soil interactions are usually non-linear and time dependent. Further, several types of interactions can occur simultaneously, e.g. adsorption–desorption dynamics, fixation, hysteresis and instantaneous interactions. The physics of such systems have been briefly discussed in this paper.

Equation (5) refers to solute transport when convective flow is essentially unidirectional. It can be readily extended to two or three-directional flow systems. However, in aggregated systems or others where mass flow occurs essentially in macropores (e.g. soil cracks, root channels, earthworm holes) intra-aggregate diffusion and diffusive transfer between macro- and micro-pores becomes important. For such systems, equation (5) is not valid in its present form, but has to be modified accordingly. These aspects are being examined both theoretically and experimentally, and will be discussed in subsequent papers.

Computer simulations based on a numerical model of solute transport in soil columns have been used to illustrate the significance of adsorption–desorption parameters and flow dynamics in determining the shape and position of solution breakthrough curves. In particular, it has been shown that approximating a non-linear isotherm of the Freundlich type by a simple linear isotherm ($S = KC + \epsilon$), to facilitate analytical solutions of the mass flow equation, can lead to significant errors in solute flow predictions. While predictions based on linear isotherms are

independent of input solution concentration, the predictions based on a non-linear Freundlich isotherm are sensitive to input concentration. For instance, when $K = 1$, the difference between linear and Freundlich based predictions are large except when $C_0 \simeq 1$. Compared with the predictions based on a non-lineare adsorption model, use of a linear adsorption model underpredicts the outflow concentrations when $C_0 < 1$ and overpredicts them when $C_0 > 1$.

Adsorption parameters used in the present simulations cover a wide range for slow, moderate and fast rate coefficients (k_a, k_d) as well as for small, moderate and large adsorption equilibrium constants (K), and thus should cover a variety of ion–soil systems. The qualitative shapes of the simulated breakthrough curves are essentially similar to those obtained from experiments with selenite, sulfate and phosphate in laboratory studies, and also those found in published works for other chemical species including pesticides, herbicides and heavy metal ions.

The effect of the rate coefficients k_a and k_d on solute breakthrough curves is only marginal when the equilibrium distribution coefficient K ($=k_a/k_d$) is small. However, the influence of k_a and k_d becomes very significant for higher values of K.

At extremely small rates of interaction, the effect of the initial solution concentration in the soil is minimal, but with increasing rates of interaction the BTC is considerably affected. This effect is of most importance for small times or flow volumes, with the curves converging as column saturation occurs.

Intermittent flow has a profound influence on solute transport when sorption processes are time dependent. Computer simulations show that adsorption dynamics produce a dip in the breakthrough curve following a no-flow equilibration, and that the magnitude of this effect depends upon the duration of the equilibrium, and the rate coefficients of adsorption and desorption. Use of instantaneous equilibrium adsorption models would completely obscure this effect.

Ion–soil interactions may involve both time-dependent and instantaneous components. It has been shown that as the instantaneous component is increased, solute breakthrough is delayed and becomes more gradual. The presence of hysteresis in the instantaneous component results in a delayed release of solute during the desorption phase to an extent dependent on the desorption rate coefficient (K_d). Simulation of fixation processes by the inclusion of a linear decay type interaction shows that the maximum outflow concentration is lowered as a result.

While the present simulations cover only a limited number of the combinations of boundary conditions and interactions possible, it is clear that this approach is extremely valuable in understanding the relative importance of the various mechanisms involved in solute transport.

References

Addiscott, T. M. (1977). A simple computer model for leaching in structural soils. *J. Soil Sci.* **28**, 554–63.

Barrow, N. J., and **Shaw, T. C.** (1979). Effects of solution : soil ratio and vigour of shaking on the rate of phosphate adsorption by soil. *J. Soil Sci.* **30**, 67–76.

Biggar, J. W., and **Nielsen, D. R.** (1976). Spatial variability of the leaching characteristics of a field soil. *Water Resour. Res.* **12**, 78–84.

Bresler, E. (1973). Simultaneous transport of solutes and water under transient unsaturated flow conditions. *Water Resour. Res.* **9**, 975–86.

Cleary, R. W., and **Adrian, D. D.** (1973). Analytical solution of the convective-dispersive equation for cation adsorption. *Soil Sci. Soc. Am. Proc.* **37**, 197–9.

van Genuchten, M. Th., Davidson, J. M., and **Wierenga, P. J.** (1974). An evaluation of kinetic and equilibrium equations for the prediction of pesticide movement through porous media. *Soil Sci. Soc. Am. Proc.* **38**, 29–35.

van Genuchten, M. Th., Wierenga, P. J., and **O'Connor, G. A.** (1977). Mass transport studies in sorbing porous media. III. Experimental evaluation with 2,4,5-T. *Soil Sci. Soc. Am. J.* **41**, 278–85.

Gupta, S. P., and **Greenkorn, R. A.** (1974). Determination of dispersion and nonlinear adsorption parameters for flow in porous media. *Water Resour. Res.* **10**, 839–46.

Gureghian, A. B., Ward, D. S., and **Cleary, R. W.** (1979). Simultaneous transport of water and reacting solutes through multilayered soils under transient unsaturated flow conditions. *J. Hydrol.* **41**, 253–78.

Klotz, D., Seiler, K. P., Moser, H., and **Neumaier, F.** (1980). Dispersity and velocity relationship from laboratory and field experiments. *J. Hydrol.* **45**, 169–84.

Lapidus, L., and **Amundson, N. R.** (1952). Mathematics of adsorption in beds. VI. The effect of longitudinal diffusion in ion-exchange and chromatographic columns. *J. Phys. Chem.* **56**, 984–8.

Lindstrom, F. T., Haque, R., Freed, V. H., and **Boersma, L.** (1967). Theory on movement of some herbicides in soils. *Environ. Sci. Technol.* **1**, 561–5.

Marino, M. A. (1974). Numerical and analytical solutions of dispersion in a finite, adsorbing porous medium. *Water Resour. Bull.* **10**, 81–90.

Murali, V., and **Aylmore, L. A. G.** (1979). Predicting the movement of solutes in soil profiles. Proc. Natl Symp. Hydrol. Water Resour. Perth, pp. 210–15.

Murali, V., and **Aylmore, L. A. G.** (1980). No-flow equilibration and adsorption dynamics during ionic transport in soils. *Nature (London)* **283**, 467–9.

Murali, V., and **Aylmore, L. A. G.** (1981). Modelling adsorption in solute flow simulations: diffuse double layer vs. gas solid interaction approaches. *Soil Sci.* **131** (2), in press.

Parfitt, R. L. (1979). Anion adsorption by soils and soil materials. *Adv. Agron.* **30**, 1–50.

Scotter, D. R. (1979). Preferential solute movement through large soil voids. I. Some computations using simple theory. *Aust. J. Soil Res.* **16**, 257–67.

Selim, H. M., Davidson, J. M., and **Rao, P. S. C.** (1977). Transport of reactive solutes through multilayered soils. *Soil Sci. Soc. Am. J.* **41**, 1–10.

Selim, H. M. and **Mansell, R. S.** (1976). Analytical solution of the equation for transport of reactive solutes through soils. *Water Resour. Res.* **12**, 528–32.

Starr, J. L., and **Parlange, J. Y.** (1979). Dispersion in soil columns: the snow-plow effect. *Soil Sci. Soc. Am. J.* **43**, 448–50.

Tanji, K. K., Dutt, G. R., Paul, J. L., and **Doneen, L. D.** (1967). Quality of percolating waters. II. A computer method for predicting salt concentrations in soils at variable moisture contents. *Hilgardia* **38**, 307–18.

Tarkeltoub, R. W., and **Babcock, K. L.** (1971). A simple method for predicting salt movement through soil. *Soil Sci.* **111**, 182–7.

Manuscript received 11 August 1980

Appendix 1. List of Symbols (dimensions in parantheses)

Notation

C concentration in solution phase (ml^{-3})
D hydrodynamic dispersion coefficient ($l^2\ t^{-1}$)
J flux ($ml^{-2}\ t^{-1}$)
K equilibrium distribution coefficient (Depends on the equation)
k rate coefficient of interaction
M, N parameters in the Freundlich adsorption model (dimensionless)
Q adsorption capacity (mm^{-1})
S adsorption phase concentration (mm^{-1})
t time variable (t)
V flow velocity ($l\ t^{-1}$)
Z distance variable (l)
β bulk density (ml^{-3})
θ volumetric water content ($l^3\ l^{-3}$)
ϵ intercept of linear adsorption model (mm^{-1})

Subscripts

i initial level
o input level
a adsorption (e.g. k_a)
d desorption (e.g. k_d)
f fixation
C convection
D dispersion + diffusion
p pore level (e.g. V_p – velocity inside pores)

Appendix 2. Numerical Methods and Column Dimensions

Most of the computer simulations presented in the paper were performed on the HEATHKIT microcomputer facility available in the Department of Soil Science and Plant Nutrition, using Benton Harbor Extended BASIC and FORTRAN languages, while some of the simulations were also done on DEC10 and CYBER computers available at the Regional Computer Centre of the University of Western Australia, using FORTRAN IV language. Standard finite difference analogues were used to discretize time and distance variables. Length of the column was assumed to be 10 arbitrary units, each divided into 10 to 20 intervals. Convergence and stability were achieved by using suitable time increments. In the presence of adsorption, it was found useful to utilize smaller time steps in the initial time values of the simulations and gradually increase the step size to a predetermined value. These simulations were performed with a Peclet number (VL/D) of 10. Thus V and D were numerically equal. The pore water velocity (V/θ) was determined by volumetric water content for which a value of 0·35 was used. The column was assumed to have an area of 80 units, thus one pore volume, in the c.g.s. system, had 280 ml. The outflow volumes of the BTC's were plotted in litres.

A Convective-Dispersive-Adsorptive Flow Model for Solute Transport in Soils. II* Evaluation of Single and two-Component Adsorption Models for Phosphate Movement in Soils

L. A. G. Aylmore and V. Murali

Department of Soil Science and Plant Nutrition,
University of Western Australia, Nedlands, W.A. 6009.

Abstract

Comparisons have been made between experimental breakthrough curves for phosphate ions in soil columns and computer simulations of solute transport based on a number of different adsorption models. These include single component linear and non-linear, instantaneous and dynamic adsorption models; as well as the model incorporating a combination of instantaneous and time-dependent components suggested in Part I.

While certain portions of the complete breakthrough curves for phosphate could be reasonably approximated using simple one-component models, these generally failed badly to describe the shape and position of the experimental data over the complete range of the breakthrough curve. This was even more evident when both adsorption and desorption phases were considered.

On the other hand, the model described in Part I combining instantaneous linear and a simultaneous time-dependent (dynamic) Freundlich-type adsorption components provided a good simulation of the experimental data over the full range of the breakthrough curves for both adsorption and desorption phases. Of particular significance is the ability of the model to handle successive experimental breakthrough curves with different amounts of residual adsorption.

A method for 'normalizing' the solute transport equations to facilitate computer simulations is presented.

Introduction

Miscible displacement experiments and computer modelling have been widely used to investigate the transport of both non-reactive and reactive chemicals in soils. The major areas of research in which these techniques have found application include studies on the leaching of fertilizer ions, pesticide and herbicide movement, the development and reclamation of saline and sodic soils, and the transport of industrial pollutants such as heavy metals.

A number of modelling approaches have proved successful in handling simple, non-reactive systems (Rose and Passioura 1972; Biggar and Nielsen 1976). On the other hand, the complexities which arise when it is necessary to incorporate the effects arising from solute–soil interactions, with all their variability, into the modelling process have proved considerably more difficult to handle. Even for single species systems, it is necessary to describe accurately the shape of the relevant equilibrium adsorption isotherm and also, in particular, the kinetics of the rate processes leading to that isotherm (Barrow 1978; Parfitt 1979; Murali and Aylmore 1980). In few cases will the equilibrium isotherms be adequate on their own, and the presence of hysteresis between adsorption and desorption isotherms, fixation and reversion processes, will further complicate the transport process. Frequently, attempts to extend models which have been successful in describing non-interacting

* Part I, *Aust. J. Soil Res.*, 1981, **19**, 23.

solute transport in soils to interacting systems, have failed because of the inadequacy of the adsorption models used. For example, the assumption of an instantaneous linear adsorption model has proved unsatisfactory in attempts to describe the transport of pesticides and herbicides (Elrick *et al.* 1967; Letey and Farmer 1974) and in predicting phosphate movement in soil columns (Selim *et al.* 1975; Kanchanasut *et al.* 1978). Similarly, van Genuchten *et al.* (1974) demonstrated that pesticide movement in soils could not be accurately described by the use of either an instantaneous adsorption model or a kinetic adsorption model alone. While it is frequently possible to match portions of theoretical and experimental breakthrough curves, a model has little validity unless matching can be achieved for both adsorption and desorption cycles and on repeated cycles.

One major difficulty in incorporating adsorption-desorption dynamics into models of the transport process lies in the difficulty in obtaining the rate coefficients of the adsorption and desorption processes applicable during solute transport in soils. Whereas adsorption experiments are normally conducted at high solution:soil ratios with continuous shaking or stirring, solute flow studies are characterized by solution:soil ratios which are small (unity or less) and by the absence of physical agitation. As a consequence, the adsorption rate parameters as well as the shape of the isotherms estimated from miscible displacement experiments can differ markedly from those obtained from the usual adsorption experiments, e.g. Gupta and Greenkorn (1974) and Mansell *et al.* (1977).

In the previous paper (Murali and Aylmore 1981) the authors demonstrated the effects of changes in the adsorption parameters on computer simulations of solute breakthrough curves and presented a model (equations 5, 6), incorporating a combination of instantaneous linear (equations 13, 14) and time-dependent (dynamic) Freundlich- and Langmuir-type components (equations 12 and 9 respectively). While it is clearly possible to statistically fit almost every shape of breakthrough curve if sufficient adjustable parameters are used, for practical purposes, the number of such parameters should be minimal, and these should be physically meaningful. In the present paper the ability of this approach to describe experimental breakthrough curves for phosphate in soil columns is compared with that of simple linear and non-linear, instantaneous and dynamic adsorption models.

Experimental

The experimental system used for the miscible displacement studies, showing details of the column construction, is illustrated in Fig. 1. Two soils were used in this study: a mixture of sand and kaolin clay (approximately 10% clay) and a sandy loam from Yalanbee series, Western Australia. Soils were lightly ground and sieved (<2 mm) and then packed uniformly into acrylic columns. A filter paper, a stainless steel wire mesh and a stainless steel support screen were used at either end of the column to confine the soil. The column was held together by PVC end-pieces. The inlet end of the column was connected to a reservoir of the required solution. The effluent (outlet) end was connected to a peristaltic pump to maintain the required flow velocity. Effluent was collected at regular intervals using a fraction collector. The system was designed to enable a rapid change of inlet solution from one concentration to another. This change-over process was normally achieved in a minute or less. Solutions of the required ion (e.g. phosphate) were prepared in decimolar sodium chloride to prevent soil dispersion, which can occur if distilled water is used and labelled with the appropriate radioactive isotope (phosphorus-32) and tritiated

water. A few drops of chloroform were added to all solutions to minimize microbial transformations of the ions and blocking of pores. Every fresh soil column was leached for several pore volumes with decimolar sodium chloride prior to the start of an experiment in order to achieve the initial conditions [$C(z) = 0$ at $t = 0$].

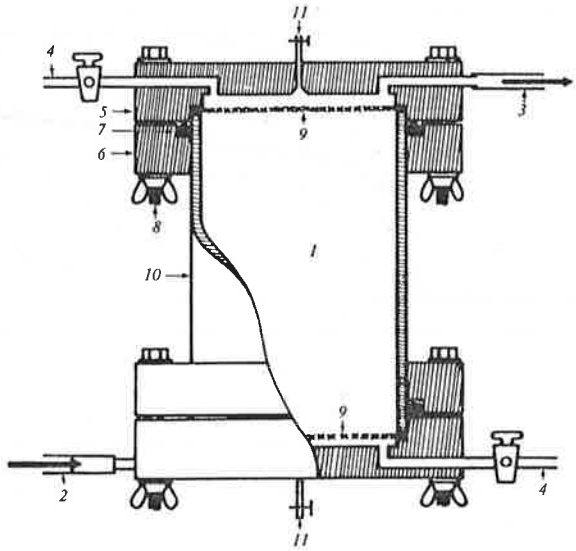

Fig. 1. Experimental system used for miscible displacement studies showing details of column construction. *1*, Soil. *2*, Solution input tube. Connected to tracer (or tracer-free) reservoir. *3*, Solution outflow connection. Goes to a fraction collector via a peristaltic pump. *4*, Connection to aid rapid change-over of concentration at input and for flushing of the inlet and outlet chambers. *5*, Confining lids (one each on top and bottom) made of PVC or acrylic, machined to ensure proper mixing in the inlet and outlet chambers and to maintain uniform flow across the whole cross-sectional area. *6*, Collar (PVC or acrylic) to hold the confining lid (5). *7*, *O*-ring seal. *8*, Screw, washers, bolt. Four on each end. *9*, Wire-gauze, wire-mesh, and filter paper to hold the soil and define the boundaries. *10*, Hollow acrylic cylinder. (This set up has been designed to use columns of different length). *11*, Narrow outlet, to prevent the entrapped air from choking the system.

For several miscible displacement experiments on each column, tritium breakthrough curves were identical, which indicated that throughout the duration of the experiments, the soil columns were stable and that no significant physical deformation or structural changes were taking place. Thus, the differences in the position of consecutive breakthrough curves for phosphate (to be described later) cannot be attributed to any physical damage or structural alterations in the soil columns.

Results and Discussion

Breakthrough curves (BTC) are usually drawn as C/C_0 *v.* cumulative outflow. With a pulse input an adsorption phase is followed by a desorption phase. In the case of an essentially non-adsorbing species, such as tritiated water, when the input pulse is large (i.e. in excess of about 2 pore volumes) the breakthrough curve is best plotted for relative concentration as $[(C - C_i)/(C_0 - C_i)]$ instead of C/C_0, where C_i is the initial concentration in the column. The advantage here is that at the commencement of the 'desorption phase', the relative tritium concentration is unity throughout (i.e. for all Z), whereas the input concentration is zero. Thus the 'break-back curve'

can be treated as a different independent breakthrough curve. The hydrodynamic dispersion coefficients were estimated from tritium breakthrough curves.

Breakthrough curves predicted by solute flow models based on an instantaneous linear adsorption model and on the dynamic Freundlich and Langmuir type models

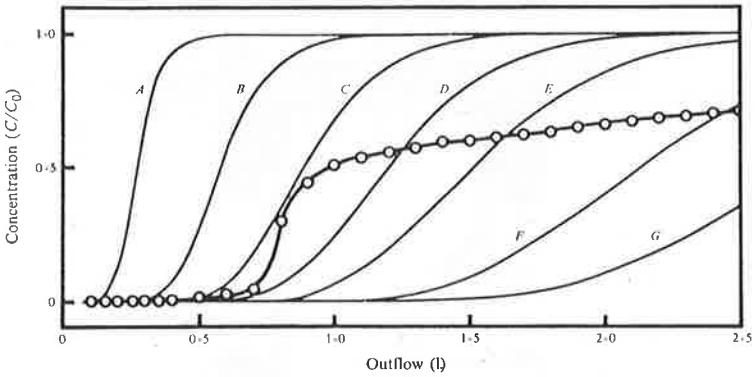

Fig. 2. Comparison of experimental phosphate BTC (open circles) for sand/kaolin column and theoretical BTC for different values of instantaneous linear adsorption (K) values. Curves A, B, C, D, E, F and G and for K values of 0, 0·25, 0·5, 0·75, 1, 1·5 and 2 respectively. (One pore volume = 280 ml.)

separately, for a range of parameter values, along with a typical phosphate breakthrough curve through the sand–kaolin system, are presented in Figs 2 and 3. Fig. 2 contrasts the predictions of the instantaneous linear adsorption model obtained from the analytical solution of Lapidus and Amundson (1952) for different

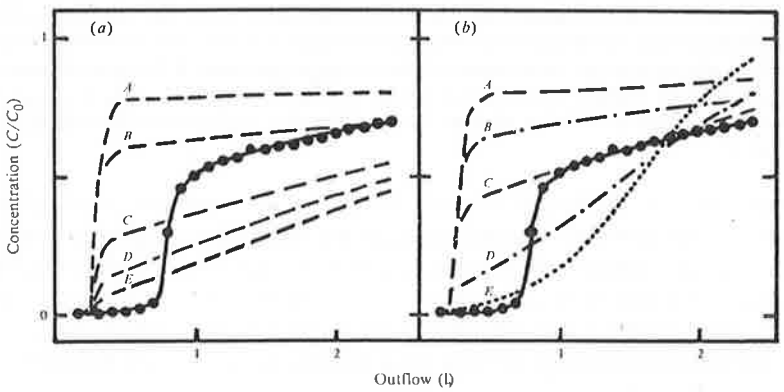

Fig. 3. Comparison of experimental phosphate BTC (closed circles) for sand/kaolin column and computer simulations (curves A to E) with Freundlich dynamic adsorption (a) and Langmuir dynamic adsorption (b). Model parameters are given in Table 1.

values of the equilibrium constant K, against the experimental phosphate breakthrough curve. There are several analytical solutions to instantaneous linear flow models available in the literature (e.g. Lindstrom *et al.* 1967; Cleary and Adrian 1973; Selim and Mansell 1976), but these differ only marginally as far as the shape of the predicted breakthrough curves is concerned. The shape of the

experimental breakthrough curve in Fig. 2 is quite unlike any of the predictions with the linear instantaneous models, when the complete range of the breakthrough is considered, even though a small initial portion bears some similarity. Similarly, non-linear instantaneous equilibrium models, based on the Langmuir or Freundlich

Table 1. Summary of the model parameters and other relevant information corresponding to the computer simulations presented in this paper

Fig. no. and data source	Model parameters for computer simulations										Remarks
				Instantaneous components		Dynamic component					
	C_0	C_i	Curve	K_a	K_d	Model[A]	M	k_n	k_d	Q	
2. Phosphate BTC in sand/kaolin column. Run 1. (Only adsorption phase of the BTC data presented)	5	0	*A*	0·0							Instantaneous linear adsorption isotherm only. No kinetic term
			B	0·25							
			C	0·5							
			D	0·75							
			E	1·0							
			F	1·5							
			G	2·0							
3. Data same as Fig. 2	5	0	*A*			Frd		0·84	0·1		No instantaneous interaction term. Freundlich type dynamic adsorption component. Experimental k_a/k_d = 7·34 was used
			B						0·2		
			C						0·5		
			D						0·75		
			E					1			
3*b*. Data same as in Figs 2 and 3*a*	5	0	*A*			Lang			0·005	14	No instantaneous interaction term. Langmuir type dynamic adsorption component. Experimental k_a/k_d = 1·4 was used
			B						0·01		
			C						0·02		
			D						0·05		
			E						0·01		
4*a*. Phosphate BTC in sand/kaolin column. Run 1	5	0	*A*	2	0	Frd	0·84	0·08	0·16		An instantaneous linear term and a dynamic Freundlich term were used
			B					0·09	0·18		
4*b*. Phosphate BTC in sand/kaolin column. Run 2	5	0·1	*A*	0	0	Frd	0·84	0·08	0·16		Compared with 4*a*, this has residual (or initial) adsorbed and solution phase phosphate. Instantaneous term was zero
			B					0·09	0·18		
5*a*. Phosphate BTC in Yalanbee soil column. Run 1	2·5	0	*A*	0·6	0	Frd	0·7	0·5	1		An instantaneous term and a dynamic Freundlich component were used
			B					0·8	1		
5*b*. Phosphate BTC in Yalanbee soil column. Run 2	2·5	0·16	*A*	0	0	Frd	0·7	0·5	1		Compared with 5*a*, this has residual (or initial) solution and adsorped phase phosphate. Instantaneous term was zero
			B					0·8	1		
5c. Yalanbee soil column. Run 3	2·5	0·19	*A*	0	0	Frd	0·7	0·5	1		Same remarks as for 5*b*
			B					0·8	1		
6*a*. Yalanbee soil column. Run 1	2·5	0	*A*	2	0	Frd	0·7	0·3	1		Instantaneous linear adsorption plus dynamic Freundlich component were used
			B					0·4	1		
6*b*. Yalanbee soil column. Run 3	2·5	0·19	*A*	0	0	Frd	0·7	0·3	1		Curves *C* and *D* are the same as curves *A* and *B* of Fig. 5c. Curves *A* and *B* of this figure correspond to the model parameters of Fig. 6*a* (*A* and *B*) with observed C_i. Instantaneous component is zero
			C					0·5	1		
			D					0·8	1		

[A] Frd, Freundlich; Lang, Langmuir.

isotherms, although not shown here, were equally unsatisfactory when compared with the entire range of the experimental breakthrough curve.

The same experimental phosphate breakthrough curve (as in Fig. 2) is compared with the predictions of the dynamic, Freundlich-based solute transport model in Fig. 3*a* and with the dynamic Langmuir (equations 5, 12 and 5, 9 of Part I) in Fig. 3*b*. Whereas the instantaneous linear adsorption model provided reasonable agreement with the experimental breakthrough curve during the initial stages, the situation is reversed in the dynamic case. Here, the model predictions were unsatisfactory in the initial stages, but approached the experimental curve asymptotically (for example, curves *B* of Fig. 3*a* and *C* of Fig. 3*b*). However, the overall prediction is quite inadequate. (Note that the same experimental data was used in the Figs 2, 3*a* and 3*b*.) Table 1 gives a summary of the model parameters corresponding to the different curves presented in this paper. For large values of the adsorption rate coefficients, the dynamic model predictions coincide with those of the instantaneous equilibrium model. Since the model predictions were unsatisfactory even for large adsorption rate coefficients (Fig. 3*a* and 3*b*), the earlier conclusion that the non-linear instantaneous adsorption-based solute transport models are unsatisfactory in predicting experimental breakthrough curves for phosphate is supported. As the model predictions, so far, were inadequate in the adsorption phase of the breakthrough curve, the desorption phases in Figs 2 and 3 have been omitted.

Experimental breakthrough curves and simulations for two sets of parameters of the model proposed in Part I (Murali and Aylmore 1981) are presented in Fig. 4. This model combines an instantaneous linear and simultaneous dynamic Freundlich-type adsorption components. The vertical broken line shows the position of the changeover from adsorption phase to the desorption phase (i.e. from $C = C_0$ at $Z = 0$ to $C = 0$ at $Z = 0$). The prediction in the adsorption phase has improved considerably when compared to the predictions in Figs 2 and 3. Model parameters used are given in Table 1. It was observed that successive experimental breakthrough curves in the desorption phase were very similar, and thus largely independent of residual adsorption. A linear instantaneous component was therefore incorporated as an irreversible interaction (i.e. $K_d = 0$). The parameter M, which is the power coefficient in the Freundlich adsorption used in these simulations, was the experimentally estimated value (using the usual 5:1 solution:solid ratio and a 24 h shaking). The basis of such usage is that the extent of non-linearity of adsorption is unaffected by shaking and dilution. As mentioned earlier, this assumption need not always be valid. The two simulated curves in Fig. 4*a* have adsorption and desorption rate coefficients of 0·08 and 0·16, and 0·09 and 0·18 respectively, which represents the order of magnitude of the range in the adsorption rates and illustrates the sensitivity of the model. The experimental breakthrough curve for a subsequent run, with some residual adsorption, is presented in Fig. 4*b*. The simulated breakthrough curves are for the same dynamic model but with no instantaneous interaction component. The experimental value for the initial concentration was used. Our experience with phosphate breakthrough curves on several soils has been similar in that successive experimental breakthrough curves with different residual adsorption could be fitted with the same dynamic adsorption model, but only the first run required a significant linear instantaneous interaction, while later runs needed much smaller values or zero for the instantaneous interaction parameter.

Fig. 5 (*a–c*) shows three consecutive experimental phosphate breakthrough curves on a soil column packed with sandy loam from Yalanbee, W.A., and simulated

breakthrough curves for two sets of parameters of the model (Murali and Aylmore 1981). As in the case of the sand–kaolin mixture (Fig. 4), the dynamic adsorption parameters used for all three consecutive breakthrough curves are identical (0·5/1 and 0·8/1 for the ratios of adsorption/desorption rate coefficients respectively). Again, the instantaneous (irreversible) equilibrium component was finite for run 1 and zero for the subsequent runs. For runs 2 and 3, the experimental initial concentration was used in the simulations. One of the simulated breakthrough curves (*B*)

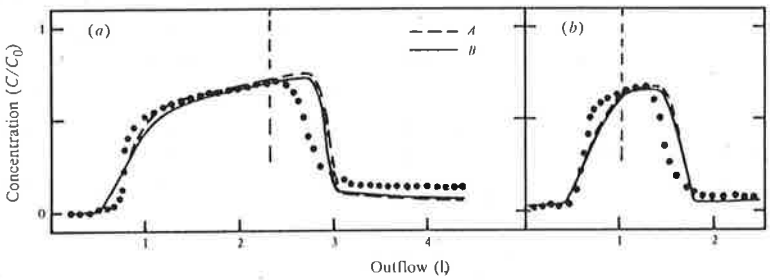

Fig. 4. Comparison of experimental phosphate BTC's (closed circles) for sand/kaolin column (*A*) and computer simulations (*B*). (*a*) is for run 1; (*b*) is for run 2. Model parameters are given in Table 1.

is close to the experimental curve during the adsorption phase, while the other simulated curve (*A*) is close in the desorption phase, for all the three runs (i.e. Fig. 5*a–c*). Since the range in the adsorption rate coefficients is small and since the same dynamic parameters were used for all three runs, the model predictions seem reasonable. One possible reason for the inability of a single set of parameters to

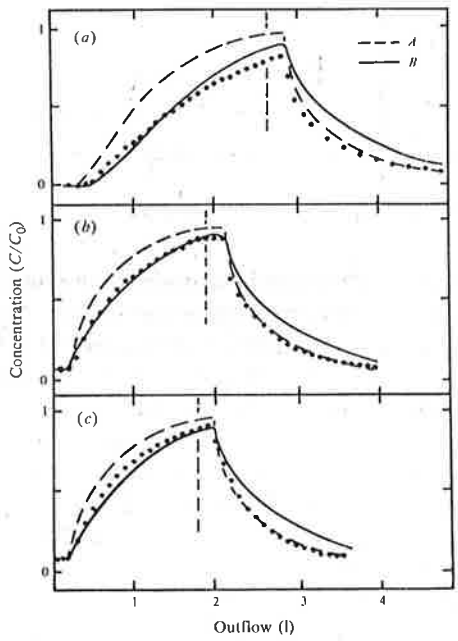

Fig. 5. Comparison of experimental phosphate BTC's (closed circles) for Yalanbee soil column (*A*) and computer simulations (*B*). (*a*), (*b*) and (*c*) are for runs 1, 2 and 3 respectively. Model parameters are given in Table 1.

accurately predict both the adsorption and the desorption phases of the breakthrough curves lies in the form of the Freundlich-type model used. As described in Part I, the equation used is of the form

$$\frac{\partial S}{\partial t} = k_a C^M - k_d S$$

instead of

$$\frac{\partial S}{\partial t} = k_a C^M - k_d S^N$$

in order to minimize the model's adjustable parameters (note: from equilibrium adsorption isotherms M/N can be estimated but not M and N individually). Use of the latter form will involve an additional adjustable parameter. Therefore, a compromise between the accuracy of the model predictions and the complexity of the model is required. However, until a simple experimental method for the determination of both M and N is found, it is preferable to keep the model parameters to a minimum (i.e. assuming $N = 1$), particularly since the range of the dynamic model parameters is small. If for some reason it is considered more appropriate to assume that $M = 1$ instead of $N = 1$, such a version can be used without increasing the complexity.

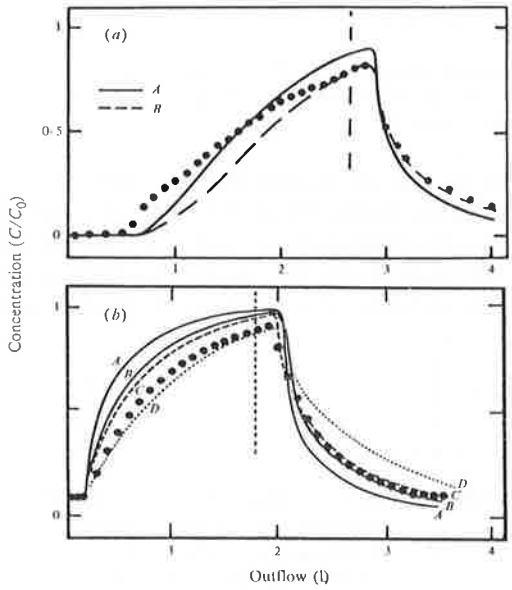

Fig. 6. Comparison of experimental phosphate BTC's (closed circles) for Yalanbee soil column (*A*) and computer simulations (*B*). (*a*) is for run 1; (*b*) is for run 3. Model parameters are given in Table 1 and discussed in the text.

As demonstrated earlier, it is possible to 'fit' a seemingly reasonable simulation to one breakthrough curve by adjusting the parameters for a variety of models, but the value of the present model lies in predicting more than one breakthrough curve for a given soil-solute system, with a given set of parameters. This is illustrated by the two simulated breakthrough curves for run no. 1 on Yalanbee sandy loam (same experimental data as in Fig. 5*a*) presented in Fig. 6*a*. Curve *A* is reasonable in the desorption phase and asymptotes to the experimental values in the adsorption phase, while curve *B* predictions differ only marginally from the experimental values. Fig. 6*b* shows the experimental data of run 3 (same as in Fig. 5*c*), and breakthrough curves predicted by the dynamic parameters used in Fig. 6*a*, and a zero value instantaneous linear component. For comparison, the earlier predictions (Fig. 5*c*) are also included. Obviously the latter estimates (Fig. 6*a*) are less satisfactory for predicting the adsorption phase of the third run. Similar disparities were encountered in attempts to predict the second run on Yalanbee soil. (A run refers to one complete breakthrough curve with one adsorption phase followed by a desorption phase.)

In the absence of independent methods of measuring parameters such as the individual values of M and N, it is clear that useful modelling of solute transport requires a compromise between oversimplification on the one hand and a multiplicity of parameters on the other. Valid assessment of a given model effectively requires that model parameters estimated from one set of experimental data should enable the computer model to satisfactorily describe a separate or subsequent set of experimental data. For example, in this study only one of the sets of model parameters giving a reasonable description of the data or run No. 1, provides reasonable simulations of runs 2 and 3. While over-simplified models are clearly inadequate, the use of too many adjustable parameters is likely to result in considerable difficulties in matching subsequent breakthrough curves.

Normalised System of Equations for Solute Transport

Finite difference techniques are simple and convenient for the simulation of transport processes in soils and are therefore quite widely used. However, when the hydrodynamic dispersion coefficient (D) is small, numerical instability is sometimes encountered at the solute dispersion front. When an instantaneous interaction term (K) is present, it is convenient to treat it as a retardation factor as described in Part I, i.e. to use a reduced dispersion coefficient which equals $D/(1+\beta K/\theta)$, which is smaller in magnitude than D. In such cases where D is small, the problem of instability can be overcome using an upstream weighted difference scheme (Gray and Pinder 1976). However, such a scheme creates numerical dispersion (Gray and Pinder 1976). The estimation of adsorption parameters by matching computer simulations with experimental breakthrough curves can, however, frequently be achieved using a larger value of D such that the normalized parameters are unaltered. Adsorption parameters estimated in this manner can be related back to real situation by using the relationships between the real and normalized parameters. A set of normalized equations together with the relationships between the normalized and the real parameters are presented below.

The notation for the real parameters is:

C = solution phase concentration;
S = adsorbed phase concentration;
D = hydrodynamic dispersion coefficient;
V = pore water velocity,
θ = volumetric water content;
β = bulk density of the soil;
Z, t = depth (distance) and time variables;
k_a, k_d = adsorption and desorption rate coefficients;
$K_L = k_a/k_d$ = the equilibrium distribution coefficient in the Langmuir model;
L = length of the column;
Q = adsorption capacity in the Langmuir model;
M = non-linearity parameter (power) in the Freundlich model;
K = instantaneous (linear) equilibrium model parameter.

Generalized Case with Freundlich Model

Regular equations for the generalized case are:

$$\frac{\beta}{\theta}\frac{\partial S}{\partial t}+\frac{\partial C}{\partial t}=\frac{D}{(1+K\beta/\theta)}\frac{\mathrm{d}^2C}{\mathrm{d}Z^2}-\frac{V}{(1+K\beta/\theta)}\frac{\mathrm{d}c}{\mathrm{d}Z}-k_fC$$

and

$$\frac{\partial S}{\partial t}=k_aC^M-k_dS.$$

The corresponding normalized equations are:

$$\frac{\partial S^*}{\partial T^*} + \frac{\partial C^*}{\partial T^*} = B^* \frac{\mathrm{d}^2 C^*}{\mathrm{d}Z^{*2}} - R^* \frac{\mathrm{d}C^*}{\mathrm{d}Z^*} - k_f^* C^*$$

and

$$\frac{\partial S^*}{\partial T^*} = k_a^* C^{*M} - k_d^* S^*,$$

where the normalized variables are related to the regular variables by the following relations:

$$\begin{aligned}
B^* &= \frac{D}{VL(1+\beta K/\theta)} = \frac{DR^*}{VL} \\
C^* &= C/C_0 \\
k_a^* &= k_a C_0^{(M-1)} L\beta/V \\
k_d^* &= k_d L/V \\
k_f^* &= k_f L/V \\
R^* &= 1/(1+\beta K/\theta) \\
S^* &= \beta S/\theta C_0 \\
T^* &= Vt/L \\
Z^* &= Z/L.
\end{aligned}$$

Langmuir Dynamics

Regular equations:

$$\frac{\beta}{\theta}\frac{\partial S}{\partial t} + \frac{\partial C}{\partial t} = D\frac{\mathrm{d}^2 C}{\mathrm{d}Z^2} - \frac{V}{\theta}\frac{\mathrm{d}C}{\mathrm{d}Z}$$

and

$$\frac{\partial S}{\partial t} = k_a C(Q-S) - k_d S = k_a CQ - k_d S(1+K_L C).$$

The corresponding normalized equations are:

$$\frac{\partial S^*}{\partial T^*} + \frac{\partial C^*}{\partial T^*} = B^* \frac{\mathrm{d}^2 C^*}{\mathrm{d}Z^2} - \frac{\mathrm{d}C}{\mathrm{d}Z}$$

and

$$\frac{\partial S^*}{\partial T^*} = k_a^* C^* - k_d^* S^*(1+K_L^* C^*)$$

where

$$\begin{aligned}
B^* &= D/VL \\
C^* &= C/C_0 \\
K_L &= k_a/kd \\
k_a^* &= \frac{k_a Q\beta L}{\theta V} \\
k_d^* &= k_d L/V \\
K_L^* &= K_L C_0 \\
S^* &= \beta S/\theta C_0 \\
T^* &= Vt/L \\
Z^* &= Z/L.
\end{aligned}$$

These equations can be readily extended to the generalized case where instantaneous interactions and fixation occur simultaneously with the Langmuir-type dynamics, in a way similar to the Freundlich case presented earlier.

Summary and Conclusions

Solute transport in soils is usually described by differential equations based on the dispersive-convective-adsorptive mass balance. For non-adsorbing species and for a few limited types of adsorption (e.g. linear instantaneous equilibrium) and for simple initial and boundary conditions, solute transport can be described by analytical procedures. Numerical methods are commonly used to study the transport of adsorbing species with non-linear adsorption. A model which deals with non-linear adsorption kinetics, instantaneous reversible, hysteretic and irreversible adsorption, and ion fixation has been described in Part I. Using computer simulations and analytical solutions, a typical experimental phosphate breakthrough curve was compared with some linear and non-linear, dynamic and instantaneous adsorption models. These comparisons showed that, while such models partially explained the experimental curve, they were unsatisfactory for the complete range of the breakthrough. Using the proposed model we have been able to describe the experimental curves more closely. An important feature of our model prediction was that the same dynamic model parameters explained successive breakthrough curves for a given ion-soil system. The range in the dynamic adsorption model parameters which explained both the adsorption and the desorption phases of consecutive breakthrough curves was quite small. A possible pitfall of using models with more adjustable parameters, which are estimated by the best-statistical-fit approach from limited amounts of experimental data was demonstrated with an example. In such cases the estimated adsorption model parameters may not accurately explain the subsequent breakthrough curves of the same ion-soil system. In view of the present state of the art of the procedures for solute transport prediction, the use of models which have a minimum number of adjustable parameters is recommended. Valid assessment of a given model in the absence of independent determinations of model parameters will generally require cross-checking with a number of sequential breakthrough curves.

References

Barrow, N. J. (1978). The description of phosphate adsorption curves. *J. Soil Sci.* **28**, 447–62.

Biggar, J. W., and **Nielsen, D. R.** (1976). Spatial variability of the leaching characteristics of a field soil. *Water Resour. Res.* **12**, 78–84.

Cleary, R. W., and **Adrian, D. D.** (1973). Analytical solution of the convective-dispersive equation for cation adsorption. *Soil Sci. Soc. Am. Proc.* **37**, 197–9.

Elrick, D. E., Erh, K. T., and **Krupp, H. K.** (1967). Applications of miscible displacement techniques to soils. *Water Resour. Res.* **2**, 717–27.

van Genuchten, M. Th., Davidson, J. M., and **Wierenga, P. J.** (1974). An evaluation of kinetic and equilibrium equations for the prediction of pesticide movement through porous media. *Soil Sci. Soc. Am. Proc.* **38**, 29–35.

Gray, W. G., and **Pinder, G. F.** (1976). An analysis of the numerical solution of the transport equation. *Water Resour. Res.* **12**, 547–55.

Gupta, S. P., and **Greenkorn, R. A.** (1974). Determination of dispersion and nonlinear adsorption parameters for flow in porous media. *Water Resour. Res.* **10**, 839–46.

Kanchanasut, P., Scotter, D. R., and **Tillman, R. W.** (1978). Preferential solute movement through larger soil voids. II. Experiments with saturated soil. *Aust. J. Soil Res.* **16**, 269–76.

Lapidus, L., and **Amundson, N. R.** (1952). Mathematics of adsorption in beds. VI. The effect of longitudinal diffusion in ion-exchange and chromatographic columns. *J. Phys. Chem.* **56**, 984–8.

Letey, J., and **Farmer, W. J.** (1974). Movement of pesticides in soil. *In* 'Pesticides in Soil and Water', ed. W. D. Guenzi. Soil Sci. Soc. Am. Inc. Publ., Wisconsin, pp. 67–98.

Lindstrom, F. T., Haque, R., Freed, V. H., and **Boersma, L.** (1967). Theory on the movement of some herbicides in soils: linear diffusion and convection of chemicals in soils. *Environ. Sci. Technol.* **1**, 561–5.

Mansell, R. S., Selim, H. M., Kanchanasut, P., Davidson, J. M., and **Fiskell, J. G.** (1977). Experimental and simulated transport of phosphorus through sandy soils. *Water Resour. Res.* **13**, 189–94.
Murali, V., and **Aylmore, L. A. G.** (1980). No-flow equilibration and adsorption dynamics during ionic transport in soils. *Nature* **238**, 467–9.
Murali, V., and **Aylmore, L. A. G.** (1981). A convective-dispersive-adsorptive flow model for solute transport in soils. I. Model description and some simulations. *Aust. J. Soil Res.* **19**, 23–39.
Parfitt, R. L. (1979). Anion adsorption by soils and soil materials. *Adv. Agron.* **30**, 1–50.
Rose, D. R., and **Passioura, J. B.** (1972). The analysis of experiments on hydrodynamic dispersion. *Soil Sci.* **111**, 252–7.
Selim, H. M., and **Mansell, R. S.** (1976). Analytical solution of the equation for transport of reactive solutes through soils. *Water Resour. Res.* **12**, 528–32.
Selim, H. M., Kanchanasut, P., Mansell, R. S., Zelazny, L. W., and **Davidson, J. M.** (1975). Phosphorus and chloride movement in a Spodosol. *Soil Crop Sci. Fla Proc.* **34**, 18–23.

Manuscript received 2 February 1981, accepted 6 May 1981

Characterization of Soil Structure and Stability Using Modulus of Rupture–Exchangeable Sodium Percentage Relationships

L. A. G. Aylmore and I. D. Sills

Department of Soil Science and Plant Nutrition,
University of Western Australia, Nedlands, W.A. 6009.

Abstract

Measurements of the modulus of rupture (MOR) and in particular of the way in which it changes for a given soil with change in exchangeable sodium percentage (ESP) from zero to 20, have been used to characterize the structural stability of a range of soils from the Western Australian wheat-belt. For convenience soils were categorized as hard-setting or non–hard-setting by an arbitrary choice of an MOR value of the natural soil of 60 kPa as the lower limit of the hard-setting behaviour. The most striking differences between the two soil categories are the higher soil strength at zero ESP (baseline MOR) and rapid increase in MOR with increasing ESP (sodium sensitivity) generally characteristic of the hard-setting soils compared with the non–hard-setting soils. The MOR values quantitatively evaluate the tendency of the soils to slake on wetting, and the sensitivity of the MOR to increasing ESP (as a result of increasing double layer swelling forces) illustrates the extent and permanency of the stabilizing bonds in the soil matrix.

The presence of exchangeable magnesium on the exchange sites has been shown to increase the MOR values compared with those for exchangeable calcium at all ESP values in line with previous evidence of the deleterious effects of this cation on soil structure.

Although more detailed studies are required, the value of this approach is illustrated by its apparent ability to differentiate clearly between the effects of different management techniques (e.g. continuous cultivation as against continuous cropping), and even between short term effects arising within 1/1 rotations.

The results from the 'paired' sites where soils, similar in most respects and having undergone identical management, exhibit significant differences in sodium sensitivity of their MOR, suggest that the strength and longevity of structural bonds may be related to the nature of the exchangeable cations present (in particular, whether sodium or calcium dominate) at the time of incorporation of organic matter in the soil.

Introduction

Despite the considerable amount of research which has been carried out, the ways in which the various soil constituents contribute to soil structure, and the mechanisms by which soil structure is stabilized under field conditions, are still far from understood. Certain general trends are well recognized (e.g. the value of organic matter, the preference for divalent exchangeable cations, etc.). However, because of the multiplicity of factors which, together with their interactions, can influence soil structural stability, attempts to correlate soil structure with the presence or absence of given soil constituents have had only limited success (Williams 1971). Similarly the direct addition or removal of given constituents to examine their specific effects is difficult to achieve without seriously disturbing the soil system in other ways (Deshpande *et al.* 1968; Blackmore 1973; Giovanni and Sequi 1976*a*, 1976*b*). In particular, there is a decided lack of any quantitative evaluation of the contributions to soil structural stability to be expected from specific particle size distributions, exchangeable cations, organic matter constitution, etc.

In the course of a detailed investigation into the susceptibility to waterlogging and hard-setting on drying, characteristic of many of the sandy loam soils of the Western Australian wheat-belt, we have found a combination of modulus of rupture (MOR) and hydraulic conductivity measurements useful in classifying soils in terms of their strength and structural stability.

Surface crusting and hard-setting arise when the structure of the soil is insufficiently stable to withstand the disruptive forces occurring on wetting (McIntyre 1958; Quirk and Panabokke 1962). The soil slakes and on drying a much more compact matrix is formed. Such compaction can present serious problems during tillage, and in particular in relation to the infiltration of water, burr setting, seed germination, root penetration, aeration etc. (Rose 1962; Arndt 1965; Domby and Kohnke 1956; Richards 1963; Barley 1976).

A major stumbling block in comparing the stability of different soils has always arisen from the natural variations in exchangeable sodium percentage (ESP) and hence different swelling pressures attendant on wetting. In the present work the effect of varying ESP on swelling pressure has been turned to advantage as a means of subjecting the soil matrix to a range of internal disruptive forces and hence as a measure of the inherent stability of the soil matrix to the wetting process. Subsequent measurements of the MOR on drying reflect the extent to which the soil structure has withstood or broken down under different levels of disruption. A particular virtue of this approach is that it facilitates the distinction between those soils whose physical behaviour is controlled essentially by textural considerations and the nature of the dominant cation, and those in which additional bonding or cementing materials are operative.

While a number of techniques have been used to classify soils in terms of their stability to disruptive forces, e.g. wet sieving (Yoder 1936; Quirk 1950), ultrasonics (North 1979) and immersion (Emerson 1967), these generally provide little help in directly identifying and quantifying soil management problems. The present approach would appear to have considerable potential in this respect, as well as for the quantitative evaluation by laboratory experiments of the contributions to soil structural stability arising from different sources.

Experimental

Soils were sampled from numerous sites spanning a wide area of the Western Australian wheat-belt. These were chosen to include variations in texture and natural severity of hard setting, as well as for their representation of particular areas. Of particular interest were eight soils taken from long-term rotation trials at the Chapman Valley and Merredin Research Stations of the Western Australian Department of Agriculture.

Soils were sampled at depths 0–10 cm, air-dried, gently crushed and sieved to pass through 2 mm, then thoroughly mixed.

Particle size analyses were carried out by the pipette method similar to Day (1965), except that dispersion was carried out by shaking the sample for 5 min in a Spex mill with alkaline sodium hexametaphosphate dispersant.

Modulus of rupture (MOR) determinations closely followed the method of Richards (1953), with the exception of the drying temperature being 45°C. Organic matter was estimated by the method of Walkley–Black (Allison 1965).

Exchangeable plus soluble cations were determined by washing with 0·025 M $SrCl_2$ and analysing the extract for Na^+, Ca^{2+} and Mg^{2+} by atomic absorption spectroscopy (AAS). Except in the cases noted (see Table 1), the contributions arising from cations in solution were negligible. Extraction of the adsorbed Sr^{2+} after washing the soil free of salt with 60% methanol and subsequent analysis by AAS enabled the cation exchange capacity to be estimated.

Where required, samples of the soils were brought to the required cation status by the following procedure. Approximately 170 g of soil was placed in Perspex permeameters 100 cm deep by 50 cm

diameter in three equal additions, tapping the column 20 times from a height of 1 cm after each addition. The soil column was wet slowly from below with 0·1 M $CaCl_2$ solution until saturated. Leaching of the soil column was carried out with 500 ml of 0·1 M $CaCl_2$, followed by 1 litre of 10 mM $CaCl_2$ and 500 ml of 1 mM $CaCl_2$. For the Na^+–Ca^{2+} soils NaCl was added to the 10 mM and 1 mM $CaCl_2$ solutions in the proportions necessary to achieve the desired sodium adsorption ratio (SAR). It was found that the electrical conductivity of the 1 mM $CaCl_2$ leachate reached that of the leachant after the passage of some 250 ml. Excess solution was removed by applying suction from a water pump to the bottom of the permeameter, the soil was removed from the permeameter, and the remaining solution content was estimated from the water content. The soil was dried in a forced draft drying cabinet at 45°C and gently crushed to pass through a 2 mm sieve.

Soils containing exchangeable Mg^{2+} instead of Ca^{2+} were prepared in the same way as for the Na^+–Ca^{2+} soils by replacing the $CaCl_2$ solutions with $MgCl_2$ solutions.

For a number of soils, exchangeable sodium, calcium and magnesium and the cation exchange capacities were determined after leaching, and the relationships between the SAR and exchangeable sodium percentage (ESP) were determined. The regression for the Na^+–Ca^{2+} exchange was:

$$ESP = 0{\cdot}867SAR + 0{\cdot}982,$$

while that for the Na–Mg exchange was:

$$ESP = 0{\cdot}915SAR + 1{\cdot}908.$$

These experimentally determined regressions were used to estimate the ESP of the remainder of the soils modified by leaching with solutions of known SAR. For these binary cation systems, this approach seemed more appropriate than the generalized Gapon relation (Richards 1954).

Electrical conductivities (EC's) on the 1 : 5 soil : solution ratio were determined on the soil after drying and ranged from about 30 μS cm^{-1} for the SAR 0 treatment to about 100 μS cm^{-1} for the SAR 20 treatment. This compares with the EC values of the natural soils of between 70 and 320 μS cm^{-1} for most, although there are a few which were considerably higher.

Relative hydraulic conductivities were determined on 100 g of soil packed and leached with solutions as before. However, instead of drying and removing the soils, excess solution was removed from the permeameter surface and deionized water passed through at constant head. In most cases the experiment ceased after some 200 min. The relative hydraulic conductivity was calculated by dividing the hydraulic conductivity at any given time by the initial hydraulic conductivity.

Results and Discussion

In Fig. 1, the MOR values obtained for the natural soils examined are plotted against their percentage clay contents. This figure serves to illustrate the wide variation in MOR observed and to demonstrate clearly that factors other than soil texture play a major role in determining soil strength and stability.

For convenience the soils were categorized as hard-setting or non-hard-setting by the somewhat arbitrary choice of a MOR value of 60 kPa as the lower limit of hard-setting behaviour. This criterion was based to some extent on farmers' opinions of what constituted a soil with a structure problem. The regional nature of hard-setting concepts is illustrated by the fact that soils falling in this category gave field penetrometer readings of greater than 5000 kPa when dry, an order of magnitude higher than that (500 kPa) cited in the Northcote criterion (Northcote 1974). In Table 1, the MOR values, ESP, EC, exchangeable cations, CEC, organic matter and clay contents for a number of soils representative of the two categories are given. These soils have clay contents which range from 13% to 48%, although most are between 18% and 27%. Previous surveys have indicated that most problem soils have loam or sandy loam textures. A feature of the hard-setting soils sampled here is the relatively high proportion with high EC's and consequently high ESP's. In these cases the estimation of the ions determined by the standard exchangeable cation technique exceeds the cation exchange capacity. Because of the variety of exchangeable cations likely to be present, ESP's were determined for these natural soils from the saturation extract using the calculation

$$\text{ESP} = \frac{100(-0{\cdot}0126 + 0{\cdot}01475x)}{1 + (-0{\cdot}0126 + 0{\cdot}01475x)},$$

where x is the SAR (Richards 1954).

MOR–ESP Relationships

The effect of ESP on the MOR has not been previously studied for these soils, and an understanding of the ways in which other factors contribute to structural stability requires an evaluation of this effect. Consequently, MOR values were obtained on a number of soils which had been leached in the laboratory to produce known ESP's. For a given soil an increasing ESP can be viewed as providing an increasing internal swelling pressure on wetting and hence as subjecting the soil structure to an increasing disruptive force. The more the soil slakes on wetting generally, the higher the MOR recorded for the wafers produced on drying.

In Fig. 2 the MOR–ESP relationships obtained for two soils representative of the hard-setting and non-hard-setting groups are shown. Each MOR value plotted represents the average of at least six measurements. The most striking differences

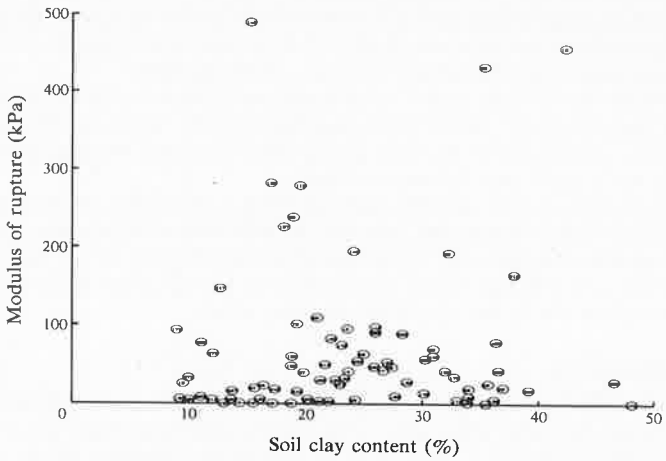

Fig. 1. Modulus of rupture versus clay content for a range of surface soils from the Western Australian wheat-belt. Numbering of the soils is immaterial for the purpose of the graph.

between the two soils are the higher soil strength at zero ESP and the rapid increase in MOR, with ESP generally characteristic of the hard-setting soils compared with the relative insensitivity of the non-hard-setting soils. The MOR–ESP relationships for all the soils are roughly linear, and this enables two parameters to be used to characterize their structural behaviour: (1) the sodium sensitivity, which is taken as the slope of the MOR–ESP relationship (kPa/%), and (2) the baseline MOR which is the strength value (or intercept) at zero ESP. These values for a number of the soils described in Table 1 are given in Table 2. The average values of baseline MOR and sodium sensitivity in the case of the hard-setting group (69·2 kPa and 7·3 kPa/% Na respectively) are substantially higher than the corresponding averages (8·7 kPa and 1·7 kPa/% Na respectively) for the 'soft' group (with calcium as the alternate cation). While there are individual variations and some overlap in either baseline MOR or sodium sensitivity between the two groups, it is interesting to note that a significant deviation from the average for one parameter is generally not matched by a similar deviation in the other. For example, non-hard-setting 3/77 has a higher

baseline MOR (37·9 kPa) than hard-setting 22/78 (19·9 kPa), but a far lower sodium sensitivity (1·9 kPa/% c.f. 8·6 kPa/%). These measurements thus quantitatively demonstrate the far greater tendency of the hard-setting soils to slake on wetting. This and their greater sensitivity to sodium on the exchange complex illustrates their lack of stabilizing bonding of whatever origin.

Table 1. Modulus of rupture and other characteristics of surface soils representative of hard-setting and non-hard-setting classifications

1, 2 and 3 are paired sites

Sample No.	MOR (kPa)	Clay content (%)	OM (%)	ESP (%)	EC (mS)	Na^+	Ca^{2+}	Mg^{2+}	CEC
						(m.e./100 g)			
				Hard-setting					
1/75	456·6	42	2·04	28·6	0·20	1·83	0·62	1·66	6·40
8/75	239·3	19	2·73	11·1	0·11	0·83	2·89	3·43	7·54
15/77	226·8	18	1·55	19·2	0·14	1·92	2·66	4·54	8·32
21/77[3]	131·7	13	1·38	9·3	0·08	0·80	3·98	2·24	6·76
3/78	63·7	25	2·31	12·8	0·18	1·53	5·70	4·48	12·00
4/78[1]	96·1	24	2·32	33·6[A]	2·5	10·74[B]	3·96	5·76	5·66
6/78	70·9	31	3·20	21·8[A]	1·17	3·92[B]	2·10	3·80	5·44
11/78[2]	98·1	26	3·52	14·5[A]	0·56	1·74[B]	3·32	4·10	5·96
19/78	83·4	22	2·87	16·1	0·48	1·34	4·80	2·35	8·30
21/78	165·8	38	3·33	41·8[A]	1·33	6·76[B]	1·00	1·12	4·58
22/78	91·4	26	2·95	9·0	0·17	0·76	3·80	2·14	8·44
				Non-Hard-setting					
54/76	15·1	19	2·36	3·5	0·06	0·20	3·80	1·20	5·52
69/76	32·2	18	2·57	6·8	0·25	0·42	4·12	1·60	6·84
3/77	37·0	19	2·35	3·8	—	0·28	5·90	1·50	7·33
20/77[3]	15·7	14	1·88	6·3	0·09	0·52	4·56	2·40	8·32
5/78[1]	0	19	4·83	11·1	0·32	0·88	5·80	2·70	7·94
7/78	0	15	3·50	12·1	0·31	0·86	5·76	2·32	7·10
10/78	5·2	16	3·52	8·4	0·12	0·70	5·78	2·64	8·30
15/78[2]	9·2	28	2·41	2·5	0·12	0·39	9·94	5·12	15·80
17/78	0	48	2·11	5·4	0·18	1·28	16·0	3·95	23·18
28/78	0	34	2·46	2·5	0·19	0·34	8·10	2·55	13·60

[A] ESP determined from saturation extract.

[B] High summation of exchangeable cations due to high salt content.

Effect of Exchangeable Magnesium

The effect of replacing exchangeable Ca^{2+} with exchangeable Mg^{2+} is apparent in Fig. 2 and from the values of the two parameters for 10 soils also given in Table 2. In all cases, the baseline strength of the soil saturated with exchangeable magnesium is higher than that saturated with exchangeable calcium. In most cases there is little difference between the sodium sensitivities of the sodium–calcium and the sodium–magnesium soils, so that within the range of ESP values studied (0–20%) the sodium–magnesium soils have higher strengths than the sodium–calcium soils. One exception is 21/77, where the sodium–magnesium soil has a higher strength at low ESP values, but this does not rise as sharply with increasing ESP as in the sodium–calcium systems. This effect of magnesium is similar to that reported by van der Merwe and Burger (1969), who obtained higher MOR values for Na^+–Mg^{2+} systems than for Na^+–Ca^{2+} systems. Similarly Bakker and Emerson (1973) observed a greater tendency for soils to slake when magnesium was the complementary cation rather than calcium. As most of the soils in the Western Australian wheat-belt have

significant proportions of exchangeable Mg^{2+}, the strength of these soils must be adversely affected by this cation.

Paired Sites

Of some particular interest were several locations where the particular farmer indicated a paddock in which areas of essentially the same soil, subject to the same

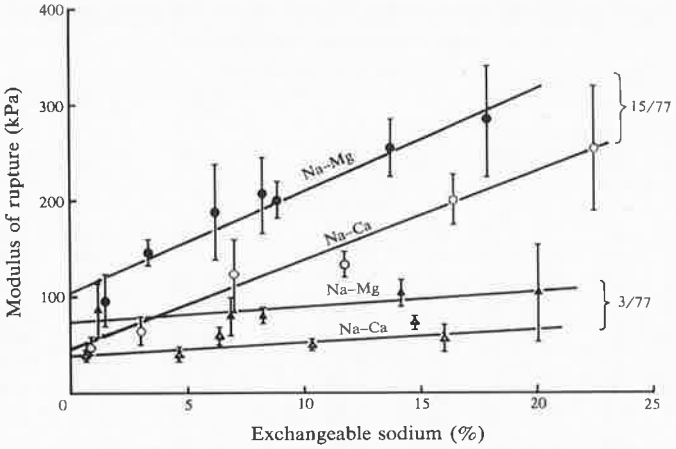

Fig. 2. Modulus of rupture versus exchangeable sodium percentage for a hard-setting (15/77) and non-hard-setting (3/77) soil with calcium or magnesium as a complementary cation.

management history, exhibited significantly different physical behaviour. Examples of such paired sites are given by soils 4/78 and 5/78 from Katanning, 11/78 and

Table 2. Baseline MOR and sodium sensitivity of MOR for hard-setting and non-hard-setting soils in presence of calcium and magnesium cations

Hard-setting				Non-hard-setting			
Sample No.	Other cations	Baseline MOR (kPa)	Sodium sensitivity (kPa/%)	Sample No.	Other cations	Baseline MOR (kPa)	Sodium sensitivity (kPa/%)
15/77	Ca^{2+}	47·2	9·8	33/75	Ca^{2+}	79·4	6·0
	Mg^{2+}	108·4	10·9		Mg^{2+}	156·9	3·0
21/77	Ca^{2+}	57·9	15·3	10/76	Ca^{2+}	0	3·6
	Mg^{2+}	129·4	7·2		Mg^{2+}	54·7	1·8
4/78	Ca^{2+}	136·2	5·0	40/76	Ca^{2+}	47·5	5·1
					Mg^{2+}	133·9	5·2
6/78	Ca^{2+}	65·1	1·3	54/76	Ca^{2+}	17·0	0·7
11/78	Ca^{2+}	68·3	7·9	69/76	Ca^{2+}	27·1	1·2
	Mg^{2+}	123·3	9·9		Mg^{2+}	40·4	2·8
19/78	Ca^{2+}	63·2	6·3	3/77	Ca^{2+}	37·9	1·9
					Mg^{2+}	78·7	1·4
21/78	Ca^{2+}	95·8	4·5	20/77	Ca^{2+}	9·6	4·6
22/78	Ca^{2+}	19·9	8·6	5/78	Ca^{2+}	0	0
3/78	Ca^{2+}	17·4	4·3	7/78	Ca^{2+}	4·3	0·7
	Mg^{2+}	57·3	10·7				
				10/78	Ca^{2+}	16·4	0
				15/78	Ca^{2+}	0	5·8
				17/78	Ca^{2+}	0	0
				28/78	Ca^{2+}	1·0	0·3

15/78 from Gnowangerup, and 20/77 and 21/77 from Moulyinning respectively (Table 1). The effects of ESP on the MOR values for these soils are shown in Fig. 3. At each location the 'paired' soils have similar textures, but in all cases the 'hard' soil has a considerably higher natural MOR, confirming the farmers' observations. While the higher ESP's and lower organic matter contents of the 'hard' soils undoubtedly

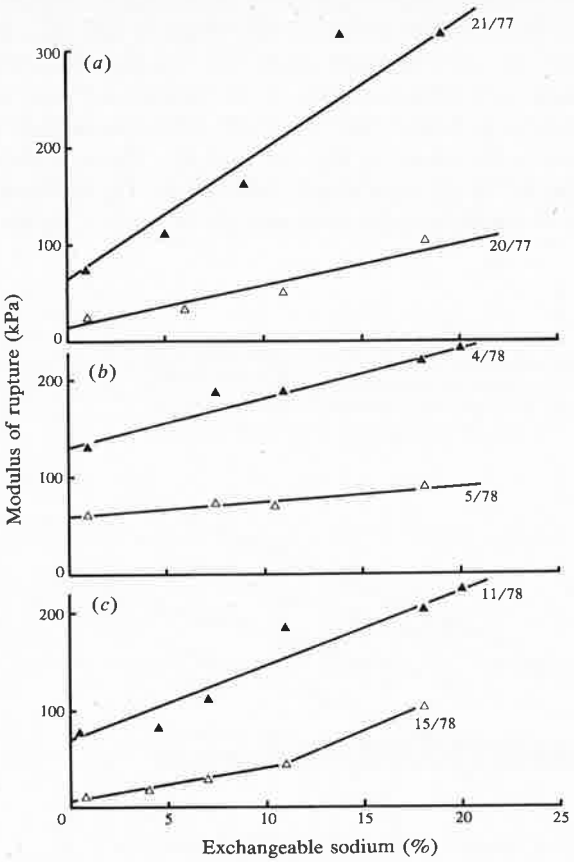

Fig. 3. Modulus of rupture versus exchangeable sodium percentage for soils from paired sites (Ca^{2+} as a complementary cation).

contribute to the poor physical behaviour of the natural samples, their higher baseline MOR's, and generally appreciably higher sodium sensitivities shown in Fig. 3, clearly indicate their lack of stabilizing bonds compared with their 'soft' counterparts. The simple correlation between the generally low organic matter contents of the soils examined (Table 1) and their stability to wetting as measured by the MOR test is not high. Furthermore those soils classified as non-hard-setting rarely showed high sodium sensitivities. Thus the origins of stability in these soils clearly involve more than simple considerations of quantity of organic matter and exchangeable sodium. One is led to speculate that this difference may be related to the specific interaction between the organic matter and the particular exchangeable cations present (e.g. Na^+ or Ca^{2+}) when the organic matter is laid down (Kononova 1966).

In most cases the MOR values for the natural soils agreed reasonably well with values which would be predicted from the MOR–ESP relationships obtained in the laboratory for the treated soils at the same ESP, the latter having been leached with calcium solutions and then adjusted to an appropriate ESP. This would suggest that the laboratory leaching treatment caused relatively little disruption of the natural

stability of the soils. In those instances where large differences occurred, these could generally be attributed to the high salt content of the natural soil, which would undoubtedly reduce the strength of the soil as a result of its flocculating effect.

Cultivation Effects

The MOR–ESP approach proved particularly sensitive in examining the effects of different management practices on the stabilization or otherwise of soil structure. The characteristics of a number of soils sampled from the Western Australian Department of Agriculture's long term rotation trials at its Chapman Valley and Merredin Research Stations are given in Table 3, and the MOR–ESP relationship obtained for the different trial plots are given in Figs 4*a* and 4*b*. These different treatments included plots subjected to (1) continuous cultivation, (2) continuous pasture, and (3) a 1/1 rotation of wheat/pasture over periods of up to 15 years.

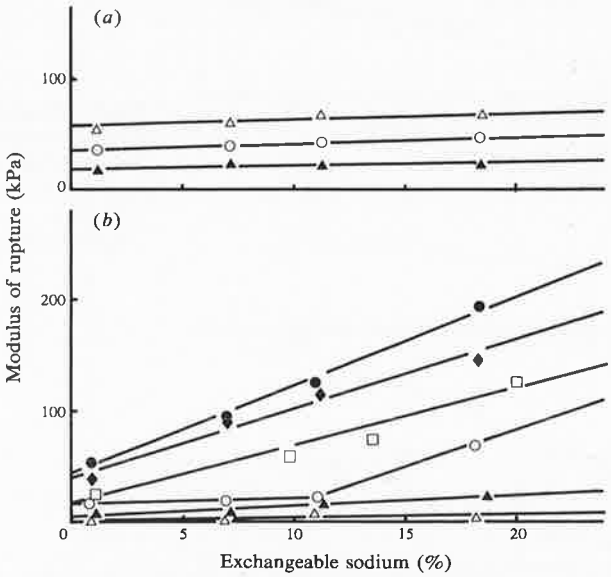

Fig. 4. Modulus of rupture versus exchangeable sodium percentage for soils from Western Australian Department of Agriculture long-term trials at (*a*) Chapman Valley and (*b*) Merredin Research Stations.
(*a*) △ Continuous cropping, 35/78; ○ 1/1 rotation (crop previous year), 34/78; ▲ continuous pasture, 32/78. (*b*) ● Continuous cultivation, 29/78; ◆ 1/1 rotation (crop previous year), 3/80; □ continuous cultivation, 26/78; ○ 1/1 rotation (pasture previous year), 2/80; ▲ continuous pasture, 27/78; △ continuous pasture, 28/78.

Although none of these soils fall into the hard-setting category, the influence of management practice on the structural stability of the soil is clearly differentiated by the MOR–ESP technique. The values for the natural soils subjected to continuous cultivation are appreciably higher than those for the parallel plots subjected to continuous pasture at both the Merredin and Chapman Valley stations (Table 3). While there is no appreciable change in the low sodium sensitivities of the Chapman Valley plots with different management (Fig. 4*a*), the Merredin plots show marked increases in sodium sensitivity with continuous cultivation (Fig. 4*b*). At Merredin, two

plots of each of the various treatments (continuous cultivation, etc.) were examined because of the changes in texture which were known to exist between some of the trial plots. Differences were more marked between the two continuous crop trials, and this can be attributed to the texture difference (39% and 26% clay respectively). Soils with higher clay content were generally observed to maintain better structure and hence a lower MOR.

The soils subjected to 1/1 rotations of wheat and pasture show MOR values generally intermediate between those obtained for continuous cultivation and continuous pasture. Of particular interest are the differences clearly indicated between the 1/1 rotation plots, with that subjected to crop in the previous year (3/80) having a substantially higher baseline MOR and sodium sensitivity to that (2/80) subjected

Table 3. Modulus of rupture and other characteristics of soils from Western Australian Department of Agriculture long-term trials at Merredin and Chapman Valley Research Stations

Sample No.	MOR (kPa)	Clay content (%)	OM	ESP	EC (mS)	Na^+	Ca^{2+}	Mg^{2+}	CEC
							(m.e./100 g)		
					Merredin Station				
					Continuous Cultivation				
26/78	28·0	39·3	1·48	2·9	0·07	0·42	9·3	2·5	14·3
29/78	47·3	25·9	1·35	5·7	0·09	0·5	4·4	1·8	8·8
					Continuous Pasture				
27/78	1·0	33·9	3·01	2·0	0·57	0·3	8·0	1·9	12·9
28/78	0	33·5	2·46	2·5	0·19	0·3	8·1	2·2	13·6
					1/1 Rotation (Pasture previous year)				
2/80	19·3	34·0	1·64						
					1/1 Rotation (Crop previous year)				
3/80	25·6	35·7	1·54						
					Chapman Valley Station				
					Continuous Cultivation				
35/78	42·7	7·0	0·83	3·8	0·08	0·08	1·13	0·19	2·12
					Continuous Pasture				
32/78	19·6	6·8	1·25	3·0	0·13	0·08	1·54	0·45	2·40
					1/1 Rotation (Pasture previous year)				
33/78	28·1	8·8	0·86	6·5	0·23	0·40	1·71	0·35	3·20
					1/1 Rotation (Crop previous year)				
34/78	31·6	6·9	0·93	8·9	0·08	0·18	1·17	0·29	2·02

to pasture in the previous year (despite their similar clay contents). More detailed and specific studies will of course be required to confirm the quantitative significance of these observations in indicating real structural changes with management history. These trials were designed and commenced long before the present measurements, and consequently no original or starting MOR values are available for the individual plots. However, the observations are sufficiently consistent and logical to strongly support the potential of the approach for the quantitative and sensitive evaluation of changes in soil structural stability. While in some instances the MOR values of the natural soils show no significant difference between soils, the baseline MOR's and sodium sensitivities reveal quite significant differences.

Hydraulic Conductivity and MOR

The significance of the MOR–ESP measurements in relation to the extent of physical disintegration of the soil on wetting, is illustrated by the changes in saturated hydraulic conductivity with time of leaching for representative hard-setting and non-hard-setting soils given in Figs 5*a* and 5*b*. With increasing ESP, the hydraulic conductivity of soil from Lake Grace (15/77) changes from being reasonably stable with time of leaching at ESP = 1·0, to a rapid slump to impermeability at higher ESP's (Fig. 5*a*). On the other hand, soil from Greenhills (3/77) maintains a reasonable permeability with time even at high ESP (Fig. 5*b*). These differences in physical stability on wetting are reflected in the MOR–ESP relationships for the two soils previously shown in Fig. 2.

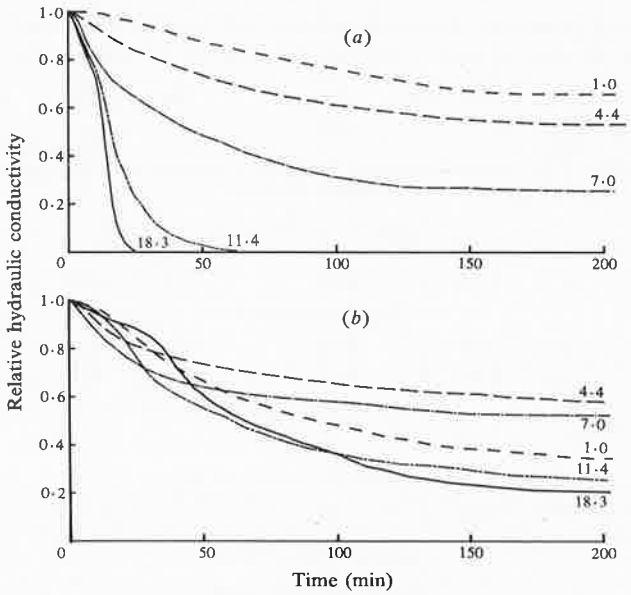

Fig. 5. Change in relative hydraulic conductivity with time of leaching for (*a*) hard-setting (15/77) and (*b*) non-hard-setting (3/77) soil with different exchangeable sodium percentages.

Causes of Hard-Setting

Some indications as to the cause of hard-setting may be obtained from the present data. The MOR of the natural soils was subjected to multiple linear regression analyses against the ESP of the natural soil, clay content, organic matter, exchangeable magnesium percentage and specific surface area of the clay fraction. The multiple correlation coefficient, R, was 0·855, and 54% of the variance was attributed to ESP, while nearly 18% was related to organic matter ($P<0·005$). No other factors were significantly correlated.

The baseline MOR of the soils was correlated against the ESP of natural soil, clay content, organic matter, exchangeable magnesium percentage, specific surface area of the clay fraction and MOR of natural soil. A multiple R of 0·90 was obtained; 67% of the variance was explained by the ESP of the natural soil ($P<0·001$), and nearly 14% by organic matter ($P<0·05$). Clearly the ESP of the natural soil can have no direct effect on the MOR of the soil which has undergone exchangeable cation

replacement in the laboratory. However, it may be possible that the ESP of the natural soil has some effect on the conversion of the dispersed solutions of ulmic and humic acids to cement. This conversion is described (Kononova 1966) as occurring through the supply of calcium from roots of legumes. If there are sufficient sodium ions present, this cementing process could be retarded, resulting in reduced bonding between soil particles. The net result of such weakened bonds could explain the higher MOR even at zero ESP in the present measurements.

The sodium sensitivity of the soils correlated with the ESP of the natural soil, organic matter, MOR of natural soil, and specific surface area of clay with a multiple regression coefficient R of 0·89 ($P<0·001$). Organic matter accounted for 44% of the variance ($P<0·20$), while a further 26% of the variance was accounted for by the MOR of the original soil ($P<0·001$). Organic matter is simply correlated with sodium sensitivity with R −0·625 ($P<0·01$). Clearly clay content and specific surface area of the clay fraction are not dominant effects in determining the MOR of these soils.

Field Applications

The classification of a soil as having a structure problem in terms of management practice obviously involves a consideration of both its natural MOR and its susceptibility to structural degradation as indicated by the sodium sensitivity. While there will inevitably be a continuous gradation in structural properties between good and bad categories, a value of natural MOR in the vicinity of 60 kPa using the present technique, appears to provide a useful delineation for practical purposes at least with this soil type. Bearing in mind the effects of moisture content on the MOR, some perspective on this value is given by the observation of Richards (1953), who found that an increase in the MOR of the soil crust on one soil from 10·8 to 27·3 kPa was sufficient to decrease the emergence of bean seedlings from 100 to 0%. Clearly a quantitative evaluation of the significance of the MOR value in relation to seedling emergence and pasture legume regeneration in these soils will be of considerable value, and these studies have commenced.

The results from the 'paired' sites, where soils similar in most respects and having undergone identical management, exhibit significant differences in sodium sensitivity of their MOR, suggest that the strength and longevity of structural bonds may be related to the nature of the exchangeable cations present (in particular, whether sodium or calcium dominate) at the time of incorporation of organic matter in the soil. Further studies are being conducted using the MOR–ESP approach to examine this hypothesis as well as the influence of other factors which may contribute to structural stability, e.g. microbial activity (Martin 1946; Tisdall *et al.* 1978); organic constitution (Posner 1979).

Currently the application of gypsum remains essentially the sole economic method of amelioration of hard-setting difficulties, although the results of such trials with these soils over recent decades have been markedly inconclusive. The use of the present techniques should assist considerably in the evaluation of the potential of a soil for amelioration by gypsum application.

Acknowledgment

This work forms part of a study funded by the Wheat Industry Research Committee of Western Australia, whose support is gratefully acknowledged.

References

Allison, L. E. (1965). Walkley-Black method. Agronomy 9. pp. 1372–6. Ed. C. A. Black. (Am. Soc. Agron.: Madison, Wis.)

Arndt, W. (1965). The impedance of soil seals and the forces of emerging seedlings. *Aust. J. Soil Res.* **3**, 55–68.

Bakker, A. C., and Emerson, W. S. (1973). The comparative effects of exchangeable calcium, magnesium, and sodium on some physical properties of red-brown earth subsoils. III. The permeability of Shepparton soil and comparison of methods. *Aust. J. Soil Res.* **11**, 159–65.

Barley, K. P. (1976). Mechanical resistance of the soil in relation to the growth of roots and emerging shoots. *Agrochimica* **20**, 173–82.

Blackmore, A. G. (1973). Aggregation of clay by the products of iron(III) hydrolysis. *Aust. J. Soil Res.* **11**, 75–82.

Day, P. R. (1965). Particle fractionation and particle size analysis. Agronomy 9. pp. 545–67. Ed. C. A. Black. (Am. Soc. Agron.: Madison, Wis.)

Despande, T. L., Greenland, D. J., and Quirk, J. P. (1968). Changes in soil properties associated with the removal of iron and aluminium oxides. *J. Soil Sci.* **19**, 108–22.

Domby, C. W., and Kohnke, H. (1956). The influence of soil crusts on gaseous diffusion. *Proc. Soil Sci. Soc. Am.* **20**, 1–5.

Emerson, W. W. (1967). A classification of soil aggregates based on their coherence in water. *Aust. J. Soil Res.* **7**, 47–57.

Giovanni, G., and Sequi, P. (1976*a*). Iron and aluminium as cementing substances of soil aggregates. I. Acetyl acetone in benzene as an extractant of fractions of soil iron and aluminium. *J. Soil Sci.* **27**, 140–7.

Giovanni, G., and Sequi, P. (1976*b*). Iron and aluminium as cementing substances of soil aggregates. II. Changes in stability of soil aggregates following extraction of iron and aluminium by acetyl acetone in a non-polar solvent. *J. Soil Soc.* **27**, 148–53.

Kononova, M. (1966). 'Soil Organic Matter, its Role in Soil Formation and Soil Fertility.' (Pergamon Press: New York.)

McIntyre, D. S. (1958). Soil splash and the formation of crusts by raindrop impact. *Soil Sci.* **85**, 261–6.

Martin, J. P. (1946). Microorganisms and soil aggregation. II. Influence of bacterial polysaccharides on soil structure. *Soil Sci.* **61**, 157–62.

van der Merwe, A. J., and Burger, R. D. (1969). The influence of exchangeable cations on certain physical properties of a saline-alkali soil. *Agrochemophysico* **1**, 63–6.

North, R. F. (1979). Rothamsted studies of soil structure. VI. Assessment of the ultrasonic method of determining soil structural stability in relation to soil management properties. *J. Soil Sci.* **30**, 463–72.

Northcote, K. H. (1974). 'A Factual Key for the Recognition of Australian Soils.' (Rellim Tech. Publ.: Glenside, S.A.)

Posner, A. M. (1979). Colloid properties of soil organic materials. *In* 'Colloids in Soils — Principles and Practice', Proc. R. Aust. Chem. Inst. Symposium on Colloids in Soils, Adelaide 1979.

Quirk, J. P. (1950). The measurement of stability of microaggregates in water. *Aust. J. Agric. Res.* **1**, 276–84.

Quirk, J. P., and Panabokke, C. R. (1962). Incipient failure of soil aggregates. *J. Soil Sci.*. **13**, 71–81.

Richards, L. A. (1953). Modulus of rupture as an index of crusting of soil. *Soil Sci. Soc. Am. Proc.* **17**, 321–3.

Richards, L. A. (1954). Diagnosis and improvement of saline and alkali soils. U.S. Dep. Agric. Handb. No. 60, p. 126.

Rose, C. W. (1962). Some effects of rainfall, radiant drying and soil factors on infiltration under rainfall into soils. *J. Soil Sci.* **13**, 286–98.

Tisdall, J. M., Cockcroft, B., and Uren, N. C. (1978). The stability of soil aggregates as affected by organic materials, microbial activity and physical distribution. *Aust. J. Soil Res.* **16**, 9–17.

Williams, R. J. B. (1971). Relationships between the composition of soils and physical measurements made on them. Rothamsted Exp. Stn. Rep. for 1970, Part 2, pp. 5–35.

Yoder, R. E. (1936). A direct method of aggregate analysis and a study of the physical nature of erosion losses. *J. Am. Soc. Agron.* **28**, 337–51.

Manuscript received 4 January 1982, accepted 31 March 1982

Transport of Non-Reactive and Reactive Solutes Through Soils.

Proc. Inter. Symposium on Salinity, Murdoch University, 24, 1-3. (1982).

L.A.G. Aylmore and V.K. Murali.

L.A.G. AYLMORE, B.Sc., Ph.D., A.R.A.C.I., Associate Professor of Soil Science, Department of Soil Science and Plant Nutrition, University of Western Australia.
V. MURALI, B.Sc., Ph.D., Post Doctoral Research Fellow, Department of Soil Science and Plant Nutrition, University of Western Australia.

Transport of Non-Reactive and Reactive Solutes through Soils.

Transport of Non-Reactive and Reactive Solutes Through Soils

L.A.G. AYLMORE

Associate Professor of Soil Science, Department of Soil Science and Plant Nutrition, University of Western Australia

V. MURALI

Post Doctoral Research Fellow, Department of Soil Science and Plant Nutrition, University of Western Australia

ABSTRACT Solute transport through soils is described using displays designed for ready comprehension by a wide variety of workers ranging from those with broad general interests to those concerned with specific aspects. Both theoretical and practical themes are developed around a compartmentalized approach in which the various physical and chemical factors of relevance such as convective mass flow, hydrodynamic dispersion, soil structure and soil-solute interactions will be outlined together with mutual interactions. Mathematical modelling and computer simulation techniques together with comparisons with experimental results will be illustrated. The use of gamma scanning and other studies on large undisturbed field cores to examine the applicability of the modelling approach to field situations is outlined. Information on spatial variability including anisotropy and heterogeneity under field conditions is similarly acquired.

1 INTRODUCTION

An essential and urgent prerequisite to the amelioration of land and stream salinity problems is an understanding of the mechanisms controlling the movement of solutes through soil profiles and the ability to accurately describe and predict the extent of such movement under given conditions. This ability requires solutions of the mass balance equations describing flow under the appropriate boundary conditions. It also requires a knowledge of the magnitudes and spatial variability of the soil characteristics controlling the relevant processes. However, when one considers the multiplicity of factors which may be involved in determining the transport of a solute through a soil profile, the task of deriving a comprehensive model capable of handling the many variations in mechanisms, boundary conditions and so on which are possible seems initially quite daunting.

2 NATURE OF TRANSPORT MECHANISMS

In Figure 1, the possible complexity in any given system is illustrated by the number of processes all of which have some basis in physical fact and which may all be involved at one time with a consequent compounding of the mathematical description by multiple interactions.

We are dealing with the convective or mass flow of water containing solute through the soil. This may take place in the saturated state if we are dealing with groundwater or during infiltration for short periods, but in most other cases we are dealing with unsaturated flow. Water flow may be continuous in some circumstances but most frequently we would be concerned with an intermittent flow process and this can be of marked significance in relation to solute concentration distribution with time (Murali and Aylmore, 1980). Steady-state solutions may be adequate under some circumstances but in others we would need to be able to handle the transient situation (Hillel, 1971).

Superimposed on this flow process we have as a result of molecular diffusion and the nature of the porous structure, a hydrodynamic dispersion process which gives rise to a spreading or increasing diffuseness of the solute concentration boundaries (Bear, 1961). In some circumstances we may only be concerned with, or it may only be necessary to handle, this effect in relation to one dimensional or longitudinal flow such as when we are dealing with movement from the surface to subsoil (or *vice versa*) of salt. In other cases such as in the movement of nutrients to plant roots or from placed fertilizers, salt transport into rivers from saline groundwaters etc., it will be necessary to describe both longitudinal and transverse components and the tensorial nature of the transport properties of soils (Nye and Tinker 1977; Bear, 1972).

Again, the nature of the soil structure will have a significant influence on solute concentration distribution with time. In few cases will we be dealing with an isotropic soil. Generally we need to take into account the diffusion into and out of aggregated material (van Genuchten *et al.* 1977), the presence of preferred flow channels arising from plant roots, soil cracking and so on (Scotter 1979, Hurle, pers. comm.). Similarly the layered nature of most soil profiles containing horizons of markedly different texture and structure will contribute to the complexity of describing solute distributions with time.

By far the greatest complexities arise however when we move from non-reactive to reactive solutes where we need to incorporate the effects arising from soil-solute interactions with all their variability, into our modelling process. Even for a single species system we need to be able to accurately describe the shape of the relevant equilibrium adsorption isotherm and also in particular, the kinetics of the rate processes leading to that isotherm (Barrow, 1978; Parfitt, 1979). In few cases will the equilibrium isotherms be adequate for our purposes and the presence of hysteresis between adsorption and desorption isotherms, fixation and reversion processes will further complicate the transport process (Murali and Aylmore, 1980).

Furthermore there will almost invariably be more than one adsorbing species present in the soil solution and the effects of competition for sorption sites on the individual isotherms can have drastic effects in relation to the mobility of a given species. In addition, cation exchange processes are important in understanding the dynamics of saline-

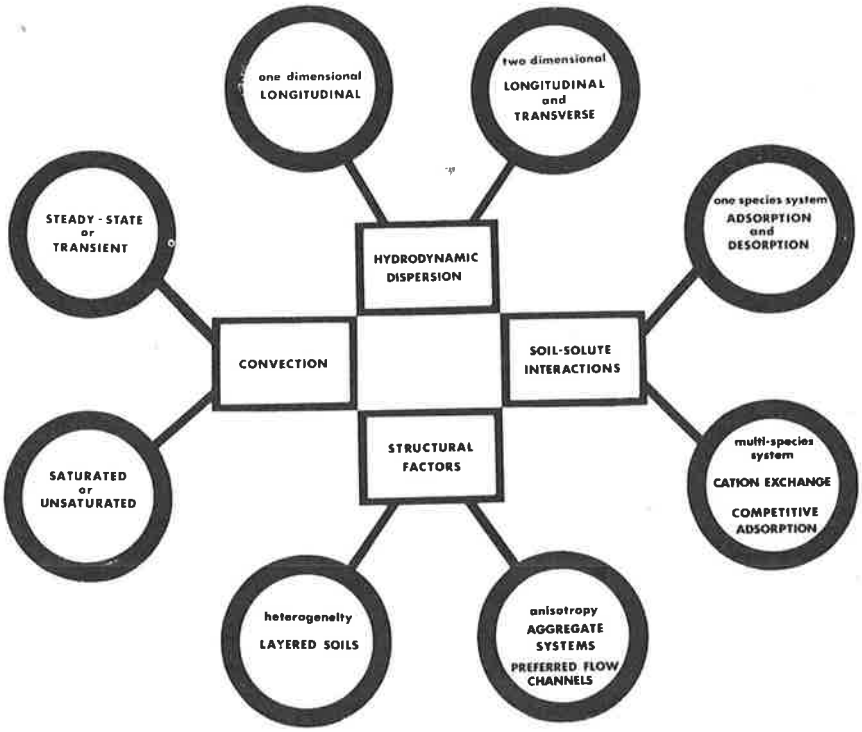

Figure 1 Conceptual basis for comprehensive modelling of solute transport in soils

alkaline soil development and thus need to be incorporated into solute transport models. Cation exchange is also important in the case of heavy metal ion pollution (de Wit and van Kuelin, 1972).

3 MODELLING APPROACHES

A truly comprehensive model would need to take into account and be able to handle the presence of all such factors and their interactions. While certain aspects of this overall system have been more or less satisfactorily described by analytical solutions of the relevant continuity equations describing the movement of solute, these are for various reasons invariably severely limited in applicability and almost always involve simplifying assumptions such as linearizing approximations, instantaneous equilibration, constant flow velocities and so on to simplify the mathematics. It can readily be shown that in most practical cases such assumptions generally lead to quite erroneous predictions.

Fortunately the increasing accessibility of computing facilities has greatly facilitated the use of numerical methods for modelling the various processes involved, and there seems no valid reason why ultimately, given adequate facilities, there should be any limit to our ability to accurately model such a system in its entirety and to satisfactorily describe and predict movement under any given circumstances. The real challenge however is to determine what particular processes are operative in any given system and that is frequently much more difficult than it may at first seem.

In recent years the authors have been developing computer sub-models to simulate the effects of the various mechanisms which influence solute movement in soils (Murali and Aylmore, 1980). The objective of this work has been to assess and illustrate the significance of changes in the various parameters on the shapes of breakthrough curves (i.e. measurements of the outgoing concentration from the bottom of a soil column following a change in ingoing concentration at the top) and hence on the time distribution of solution in soils.

Comparisons of these simulations with experimental measurements have been very encouraging and our future objective will be to gradually integrate these sub-models into a progressively more comprehensive model and to verify its applicability at laboratory and field level. One particular virtue of this approach is that it not only enables the accurate prediction of solute distributions but also facilitates the interpretation of measured solute distributions in terms of the specific mechanisms involved. It also illustrates the inadequacies and downright erroneous results obtained by accepting simplifying assumptions as an approximation to reality.

4 METHODOLOGY

Recent research on water and solute transport in soils has generally concentrated either on small scale laboratory experiments using artificially packed soil columns to examine the validity of various physical concepts or alternatively on

regional balances of salt and water which largely ignore the physical basis of transport processes. The present studies using gamma scanning and salinity measurements both on artificially packed soil columns and on large undisturbed cores sampled from the field seek to bridge this discontinuity between theoretical and applied aspects. In addition it is anticipated that this approach will provide information on the magnitudes and spatial variability (in particular anisotropy and heterogeneity) of those field soil characteristics which control solute movement in soils e.g. hydraulic conductivity, hydrodynamic dispersion coefficients etc. (Nielsen *et al.*, 1977; Peck *et al.*, 1977; Sharma *et al.*, 1980; Simmonds *et al.*, 1979).

5 REFERENCES

Barrow, N.J. (1978). The description of phosphate adsorption curves. *J. Soil Sci.* 29:447-462.

Bear, J. (1961). On the tensor form of dispersion in porous media. *J. Geophys. Res.* 66:1185-1197.

Bear, J. (1972). *Dynamics of Fluids in Porous Media.* Elsevier, New York. 764 pp.

de Wit, C.T. and van Kuelin, H. (1972). *Simulation of Transport Processes in Soils.* Pudoc, Wageningen.

Hillel, D. (1971). *Soil Water.* Academic Press, New York. 288 pp.

Hurle, D. (1979). Personal communication.

Murali, V. and Aylmore, L.A.G. (1980a). No-flow equilibration and adsorption dynamics during ionic transport in soils. *Nature* 238:467-469.

Murali, V. and Aylmore, L.A.G. (1980b). A convective-dispersive-adsorptive flow model for solute transport in soils: I. Model description and simulations. *Aust. J. Soil Res.* (Submitted).

Nielsen, D.R., Biggar, J.W. and Erh, K.T. (1973). Spatial variability of field measured soil water properties. *Hilgardia* 42:215-259.

Nye, P.H. and Tinker, P.B. (1977). *Solute Movement in the Soil-Root System.* Blackwell Scientific Publications. 342 pp.

Parfitt, R.L. (1979). Anion adsorption by soils and soil materials. *Advances in Agron.* 30:1-50.

Peck, A.J., Luxmoore, R.J. and Stolzy, J.L. (1977). Effect of spatial variability of soil hydraulic properties in water budget modelling. *Water Resources Res.* 13:348-354.

Scotter, D.R. (1979). Preferential solute movement through large soil voids. *Aust. J. Soil Res.* 16: 257-267.

Sharma, M.L., Gander, G.A. and Hunt, C.G. (1980). Hydrological variability of a water shed measured in terms of infiltration parameters. *J. Hydrol.* (in press).

Simmons, C.S., Nielsen, D.R. and Biggar, J.W. (1979). Scaling of field-measured soil properties. *Hilgardia* 47:77-174.

van Genuchten, M.Th., Wierenga, P.J. and O'Connor, G.A. (1977). Mass transport in sorbing porous media. III. Experimental evaluation with 2,4,5-T. *Soil Sci. Soc. Am. J.* 41:278-285.

0038-075X/83/1353-0143$02.00/0
SOIL SCIENCE

March 1983
Vol. 135, No. 3
Printed in U.S.A.

COMPETITIVE ADSORPTION DURING SOLUTE TRANSPORT IN SOILS: 1. MATHEMATICAL MODELS

V. MURALI AND L. A. G. AYLMORE

Department of Soil Science & Plant Nutrition, University of Western Australia, Nedlands, Western Australia 6009

Received for publication 11 August 1981; revised 23 November 1981

ABSTRACT

One-dimensional, convective-dispersive-adsorptive flow models, in Cartesian and polar coordinates, representing flow of chemicals in soils (e.g., leaching) and toward plant roots, are generalized to competitive multispecies systems. Langmuir-type competitive adsorption models suitable for equilibrium and dynamic interactions are presented, and a few special simplified cases are discussed. Freundlich-type equilibrium adsorption models are modified to multispecies situations. An empirical approach, capable of handling most general equilibrium adsorption isotherms, suitable for multispecies systems, is also described. The empirical approach is comparable to equilibrium Langmuir and Freundlich-type competition in binary systems. Isotopic exchange, which is a form of competition between isotopes of the species for adsorption or exchange sites, may be described through a simple McKay-type equation.

INTRODUCTION

Competition is a very common phenomenon in nature. In ecological and agronomic situations competition arises mainly due to limitations in such environment variables as food, light, nutrients, water, oxygen, etc. Competition among different species and among individuals of the same species (intra- and interspecific competition) is usually quite similar, and the differences are often only in degree (Frappell 1979). The term *competition* is also used in connection with adsorption of chemicals, e.g., ions, molecules, etc. Competitive adsorption is of interest in relation to solute transport in soils, because adsorption has a profound influence on the movement of chemicals.

A number of analogies can be drawn between competitive adsorption and agronomic competition. In interspecific competition, i.e., among individuals of the same species, increasing the population density (or seeding rate) produces initially a linear response in yield, but as the population density increases, the yield increase drops, until eventually a yield plateau is attained. In single-species adsorption, too, at low solution concentrations the adsorption isotherm is linear, but as the solution concentration increases, the isotherm becomes nonlinear until, as is often the case, an adsorption maximum is reached. Comparing the two systems of competition: solution concentration corresponds to the population density of a species; adsorbed phase concentration corresponds to yield; available adsorption sites correspond to food or an environmentally limiting factor. On desorption, once adsorbed chemicals can again compete for an adsorption site. There are sources and sinks in both systems. Simple Lotka-Volterra-type models are inadequate for both systems due to the nonlinear nature of the response functions. Whereas agronomic competition has been studied quite widely, the effects of competitive adsorption and isotopic exchange (competition among isotopes of the same species), particularly in relation to solute transport in soils and toward plant roots, need further investigation.

In this paper we generalize the single-species solute adsorption and transport models to multispecies systems. In subsequent parts of this series we will review the existing literature and compare the experimental observations with model simulations.

SINGLE-SPECIES SYSTEMS

Solute transport in soil profiles and toward plant roots are often described by convective-dispersive-diffusive-adsorptive flow equations, in appropriate coordinate systems (e.g., Cartesian and polar coordinates), with appropriate initial and boundary conditions. Boast (1973),

Anderson (1979), Murali and Aylmore (1981), and others have described the necessary partial differential equations and the underlying physics for solute transport in soil profiles, with the Cartesian coordinate system. Olsen and Kemper (1968), Nye and Marriott (1969), Drew et al. (1969), Barley (1970), Cushman (1979), Nye and Tinker (1977), and others have presented the theoretical foundations of solute transport toward plant roots in soils, using polar coordinates. The relevant partial differential equations are briefly discussed in this section.

Solute transport equations

The commonly used one-dimensional solute transport equation is given by Eq. (1)

$$\frac{\partial C}{\partial t} + \frac{\beta}{\theta}\cdot\frac{\partial S}{\partial t} = D\frac{\partial^2 C}{\partial Z^2} - \frac{V}{\theta}\cdot\frac{\partial C}{\partial z} \qquad (1)$$

Equations (2) and (3) describe solute transport to plant roots

$$\frac{\partial T}{\partial t} = \frac{1}{r}\frac{\partial}{\partial r}\left[rD\frac{\partial T}{\partial r} + rVC\right] \qquad (2)$$

$$\frac{\partial C}{\partial t} + \frac{\beta}{\theta}\frac{\partial S}{\partial t} = D\frac{\partial^2 C}{\partial r^2} + \left[\frac{D}{r} - \frac{V}{\theta}\right]\frac{\partial C}{\partial r} \qquad (3)$$

where

C is solution phase concentration, mL^{-3}
S is adsorbed phase concentration, mm^{-1}
β is soil bulk density, mL^{-3}
θ is volumetric water content, L^3L^{-3}
V is flow velocity, LT^{-1}
D is diffusion/dispersion coefficients, L^2T^{-1}
T is the total solute concentration (i.e., solution plus adsorbed phases), mL^{-3} and
Z, r, t are distance (vertical and radial) and time variables, L, L, T

Equations (1) and (3) can be used with most types of adsorption, e.g., instantaneous adsorption, dynamic (time-dependent) adsorption-desorption, fixation, exchange, etc., whereas Eq. (2) can be readily used only when soil-solute interactions are instantaneous. The transport equation is coupled with the appropriate adsorption model and solved for C and S or T, as the case may be. These adsorption models are described in the following sections.

The boundary conditions for plant uptake at the soil-root interface is usually based on the Epstein and Hagen (1952) equation (Eq. (4)) or its simplifications

$$F_{(r=a)} = QC/[K_p + C] \qquad (4)$$

where $F_{(r=a)}$ is the solute flux at the root surface (where a is root radius), and Q and K_p are constants. This equation is analogous to the Michelis-Menten equation. Simplifications of Eq. (4) sometimes used are

$$F_{(r=a)} = \alpha C \qquad (5)$$

and

$$F_{(r=a)} = F_0 \qquad (6)$$

The assumption underlying Eq. (5) is that at low solution concentrations, the flux is directly proportional to solution concentrations and α is treated as a constant; whereas at high concentrations, Eq. (4) approaches an uptake plateau representing a flux value independent of solution concentration (F_0 of Eq. (6)).

Semiinfinite or finite boundary conditions at one end and concentration or flux-based boundary conditions at the inlet end are commonly used in solute transport models in the Cartesian coordinate system.

Equilibrium adsorption models

In most solute transport studies related to vertical movement of chemicals, adsorption processes are characterized by equilibrium adsorption isotherms that describe the relationship between solution phase and solid phase distribution of the species, at equilibrium, for different solution concentrations. Commonly encountered adsorption models (the equations used to fit experimental adsorption isotherms) are the linear, Langmuir, and Freundlich-type equations. Linear adsorption isotherms are given by Eq. (7)

$$S = KC \qquad (7)$$

Equations (8) and (9) represent Freundlich-type and Langmuir-type adsorption models, respectively

$$S = K_F \cdot C^M \qquad (8)$$

$$S = K_L \cdot C \cdot Q/(1 + K_L \cdot C) \qquad (9)$$

In Eqs. (8) and (9), Q is the adsorption maximum (analogous to monolayer capacity in gas adsorption studies), and K_F, K_L, and M are model parameters usually assumed constant for a given solute-soil system.

Whereas Freundlich-type models yield linear plots between log S and log C, Langmuir-type isotherms can be linearized with plots of C/S versus C or $1/S$ versus $1/C$.

As analogs for adsorption isotherms, some plant nutritionists use equilibrium relationships between the total amount of a chemical, T, in

soil and the solution phase concentration, C. Such terms as buffering capacity, capacity factor, and buffer power are used in this context. For example, Nye and Tinker (1977) refer to $\partial T/\partial C$ as buffer power.

The total amount of solute in soil is related to the solution and adsorbed phase concentrations through Eq. (10)

$$T = \theta C + \beta S \tag{10}$$

Thus for linear adsorption models, a linear relationship also exists between T and C. However, if nonlinear adsorption models, such as Freundlich and Langmuir, are true representations of adsorption isotherms, such simple relationships between T and C do not hold. That is, if S and C are related through, say, a Freundlich-type model, T and C may not follow a Freundlich-type equation.

Dynamic adsorption-desorption models

Most adsorption studies in single-species systems are performed at high solution-to-solid ratios with continuous shaking or stirring. Such experiments usually yield reaction rates for adsorption that are almost instantaneous. Flow studies performed in columns, at realistic solution-to-solid ratios (usually unity or less), clearly indicate that for many chemical species of interest, such as phosphate and selenite, and even pesticides, the solute-solid interactions are much slower (e.g., van Genuchten et al. 1974; Murali and Aylmore 1980, 1981*a*). There is usually at least one time-dependent component in most solute-soil interactions.

Simple dynamic (time-dependent) adsorption models, which under equilibrium conditions yield the commonly used linear, Freundlich and Langmuir-type isotherms, are given by Eqs. (11) to (13). These will be referred to as the dynamic forms of linear, Freundlich, and Langmuir adsorption models, respectively. (Equations (13a) and (13b) are two different ways of expressing Langmuir-type dynamics)

$$\frac{\partial S}{\partial t} = k_a C - k_d S \tag{11}$$

$$\frac{\partial S}{\partial t} = k_a C^M - k_d S \tag{12}$$

$$\frac{\partial S}{\partial t} = k_a C \cdot (Q - S) - k_d S \tag{13a}$$

$$\frac{\partial S}{\partial t} = k_a C Q - k_d S \cdot (1 + K_L C) \tag{13b}$$

In these equations, k_a/k_d equals the equilibrium distribution coefficient (K) of the appropriate model, and k_a and k_d are the dynamic adsorption and desorption rate coefficients. At low levels of adsorption ($Q \gg S$), Langmuir-type dynamics are similar to linear adsorption dynamics.

MULTISPECIES SYSTEMS

Single-species solute transport models can be readily extended to multicomponent systems by using a few simplifying assumptions. The important assumption that makes the solute transport model very general is that the dispersion-diffusion coefficient of the soil depends on flow conditions, soil matrix properties, etc., but not on the solute. This assumption is implicit even in single adsorbing species models, in that the dispersion coefficient of soil is invariably estimated from the flow pattern of a noninteracting species and then used for the prediction of the transport of an adsorbing species. The generalized solute transport model (for the ith species, i ranging from 1 to N) in a system of N species, may be written, in one-dimensional Cartesian coordinates, as

$$\frac{\beta}{\theta} \cdot \frac{\partial S_i}{\partial t} = D \frac{\partial^2 C_i}{\partial z^2} - \frac{V}{\theta} \cdot \frac{\partial C_i}{\partial z} \tag{14}$$

$$\frac{\partial S_i}{\partial t} = f_i \left[C_j, S_j, \frac{\partial C_j}{\partial t}, \cdots (j = 1, N) \right] \tag{15}$$

Subscripts i and j refer to the ith and jth species, respectively. For example a two-species model (e.g., Murali and Aylmore, 1981*b*) would contain four equations, two describing transport (corresponding to Eq. (14)) and two describing the adsorption process. For one-dimension radial flow to roots, the generalized competitive ion transport equation (modified from Bar-Yosef et al. 1980) is

$$\frac{\partial C_i}{\partial t} + \frac{\beta}{\theta} \cdot \frac{\partial S_i}{\partial t} = D \frac{\partial^2 C_i}{\partial r^2} + \left[\frac{D}{r} - \frac{V}{\theta} \right] \cdot \frac{\partial C_i}{\partial r} \tag{16}$$

As in the previous case, the range of i covers the number of different species in the system. The adsorption equations are the same as for the Cartesian coordinate system (viz., Eq. (15)). Initial and boundary conditions depend upon the experimental setup used and are essentially similar to those encountered in single-species models.

Multicomponent adsorption models—Langmuir-type models

In most of the relevant literature, multicomponent adsorption has been quantified through Langmuir-type isotherms (e.g., Harter and Baker 1977). Invariably instantaneous equilibrium between solution and adsorbed ions has been assumed. The form of the equilibrium isotherm for multicomponent Langmuir-type adsorption is given by Eq. (17)

$$S_i = \frac{K_i C_i Q}{1 + \Sigma_j K_j C_j} \tag{17}$$

An important application of adsorption equations is to estimate adsorption parameters from experimental results. Further, experimental observations of multispecies adsorption could be used to verify and improve the models. Equation (17) is often too general for simple applications. A few simplifications, particularly for binary systems, are possible. Such cases are discused below.

Case 1. Extremely low effective concentrations

$$(\Sigma_j K_j C_j \ll 1 \; \Sigma_j S_j \ll Q)$$

When the effective solution concentrations or the levels of adsorption are extremely small, Eq. (17) simplifies to Eq. (18)

$$S_i = K_i C_i Q \tag{18}$$

This suggests that at low surface coverage, the effects of competition are insignificant.

Case 2. Binary systems, high concentration

$$(\sum_j^2 K_j C_j \gg 1 \text{ or } S_1 + S_2 \simeq Q)$$

Under the conditions of near total surface coverage, $K_1C_1 + K_2C_2 \gg 1$, we have (for species 1)

$$S_1 = \frac{K_1 C_1 Q}{K_1 C_1 + K_2 C_2} \tag{19}$$

which can be linearized by simple algebraic manipulation to Eq. (20)

$$\frac{C_1/C_2}{S_1} = \frac{1}{(K_1/K_2)Q} + \frac{C_1/C_2}{Q} \tag{20}$$

This suggests that the adsorption isotherm for species 1, in a binary system, may be linearized, when the solution concentration of species 2 is also known, by using the ratio C_1/C_2 instead of C, in the single-species model. (C/S versus C plots are linear in single-species Langmuir adsorption models.)

Case 3. Binary system, one species stronger than the other

$$K_1C_1 \sim 1; \qquad K_2C_2 \ll 1)$$

When one of the two competing species (e.g., species 2) has very low value of KC, while for the other species the product KC is comparable to unity, we obtain: $1 + K_1C_1 + K_2C_2 = 1 + K_1C_1$. Thus

$$S_1 = \frac{K_1 C_1 Q}{1 + K_1 C_1} \tag{21a}$$

$$S_2 = \frac{K_2 C_2 Q}{1 + K_1 C_1} \tag{21b}$$

From Eq. (21) it is evident that the less effective species (with low KC) has little influence on the more effective species, whereas the more effective species has a profound influence on the adsorption of the less effective species. Consequently, adsorption of species 2, which is only small amounts even without any competiton, is further depleted due to competition.

In this case linearization can be achieved as follows

$$\frac{C_1}{S_1} = \frac{1}{K_1 Q} + \frac{C_1}{Q} \tag{22a}$$

and

$$\frac{C_2}{S_2} = \frac{1}{K_2 Q} + \frac{K_1 C_1}{K_2 Q} \tag{22b}$$

Equation (22a) is the single-species form. Equation (22b) suggests that, in case 2, the plot of $|C_2/S_2|$ versus C_1 would be a straight line.

However, if such simplifications as those discussed above are not plausible, and simple linearization does not work, one can resort to statistical multiple linear regression methods to evaluate the parameters. The binary form of Eq. (17) can be written in multiple-linear form as follows

$$\frac{1}{S_1} = \frac{1}{Q} + \frac{1}{K_1 Q} \cdot \frac{1}{C_1} + \frac{K_2}{K_1 Q} \cdot \frac{C_2}{C_1} \tag{23}$$

The first two terms on the right-hand side of Eq. (23) correspond to single-species adsorption, and therefore the last term could be considered as the interaction term (note that while fitting such equations statistically, $C_1 \neq 0$).

Langmuir-type competitive adsorption dynamics

The dynamic form of Langmuir-type adsorption equations can be extended to multiple-species adsorption in the following two ways. The accuracy of these equations in representing adsorption dynamics in soils, however, needs verification.

Equation (13) can be generalized as

$$\frac{\partial S_i}{\partial t} = k_{ai} C_i Q - k_{di} S_i \cdot [1 + \sum_j K_j C_j] \quad (24)$$

The other form of generalizing Langmuir-type dynamics is as follows: consider the multispecies adsorption as a system of simultaneous reversible chemical reactions of the form

$$\boxed{X_i} + \boxed{\text{soil}} \rightleftharpoons \boxed{\text{soil} - X_i}$$

where

X_i is the solution phase of ith species
$\boxed{\text{soil}}$ is the available adsorption site and
$\boxed{\text{soil} - X_i}$ is the adsorbed phase of ith species

The corresponding concentrations for ith species are

C_i is solution phase concentration
$[Q - \sum_j S_j]$ is the available adsorption sites concentration and
S_i is the adsorbed phase concentration

Thus, a general Langmuir-type adsorption rate equation may be written as

$$\frac{\partial S_i}{\partial t} = k_{ai} \cdot C_i \cdot [Q - \sum_j S_j] - k_{di} \cdot S_i \quad (25)$$

It can readily be shown that Eqs. (24) and (25) reduce to Eq. (17) under equilibrium conditions.[1]

As in the case of equilibrium adsorption, dynamic Langmuir-type adsorption (Eqs. (24) and (25)) may be simplified to special cases.

Case 1. Extremely small effective concentrations or low surface coverage

$$\left[\sum_j K_j C_j \ll 1 \quad \text{or} \quad \sum S_j \ll Q\right]$$

Under such conditions we obtain

$$\frac{\partial S_i}{\partial t} = k_{ai} C_i Q - k_{di} S_i \quad (26)$$

Equation (26) suggests that, under the above conditions, Langmuir-type multiple adsorption dynamics simplifies to linear-type adsorption dynamics. Further, and more importantly, adsorption of any one species is independent of other species, i.e., no competition.

Case 2. Binary system

$$[K_1 C_1 \gg K_2 C_2 \quad \text{or} \quad S_1 \gg S_2]$$

When one of the two competing species is less effective compared with the other, we obtain

$$\frac{\partial S_1}{\partial t} = k_{a1} C_1 \cdot (Q - S_1) - k_{d1} S_1 \quad (27a)$$

$$\frac{\partial S_2}{\partial t} = k_{a2} C_2 \cdot (Q - S_1) - k_{d2} S_2 \quad (27b)$$

from Eq. (24). Under similar conditions, Eq. (25) simplifies to Eq. (28)

$$\frac{\partial S_1}{\partial t} = k_{a1} C_1 Q - k_{d1} S_1 \cdot (1 + K_1 C_1) \quad (28a)$$

$$\frac{\partial S_2}{\partial t} = k_{a2} C_2 Q - k_{d2} S_2 \cdot (1 + K_1 C_1) \quad (28b)$$

Equations (27) and (28) suggest that when one of the two competing species is much more strongly adsorbed than the other, the less reactive species has little or no influence on the adsorption dynamics of the more reactive species, while the dynamics of less strongly adsorbing species is further reduced by the presence of strongly adsorbing species. The preference, in Langmuir-type adsorption, appears to be related

---

[1] In Eq. (24) as $\partial S_i/\partial t \to 0$ (i.e., equilibrium), we obtain Eq. (17) straightaway, for $k_{ai}/k_{di} = K_i$.
In Eq. (25), as $\partial S_i/\partial t \to 0$

$$\frac{k_{ai}}{k_{di}} C_i = K_i C_i = \frac{S_i}{\left[Q - \sum_j S_j\right]} \quad (A.1)$$

Thence

$$1 + \sum_j K_j C_j = \frac{Q}{Q - \sum_j S_j} \quad (A.2)$$

From Eqs. (A.1) and (A.2)

$$[Q - \sum S_j] = \frac{Q}{\left[1 + \sum_j K_j C_j\right]} = \frac{S_i}{[K_i C_i]} \quad (A.3)$$

Rearranging the second equality of Eq. (A.3), we obtain

$$S_i = K_i C_i Q \Big/ \left[1 + \sum_j K_j C_j\right]$$

to the product KC, or the amount adsorbed S, of a particular species.

Case 3. High effective concentrations or near total surface coverage

$$[K_1C_1 + K_2C_2 \gg 1 \quad \text{or} \quad S_1 + S_2 = Q]$$

Under these conditions Langmuir-type adsorption dynamics simplifies to simple ion-exchange-type reactions (e.g., Bower et al. 1957)

$$\frac{\partial S_1}{\partial t} = k_{a1}C_1S_2 - k_{d1}K_2S_1C_2 \qquad (29a)$$

$$\frac{\partial S_2}{\partial t} = k_{a2}C_2S_1 - k_{d2}K_1S_2C_1 \qquad (29b)$$

Multispecies adsorption with Freundlich-like isotherms

Sheindorf et al. (1981) developed equilibrium isotherm equations for multispecies adsorption, where all the competing species followed Freundlich-type isotherms (Eq. (30)). The generalized adsorption equation for N-species competition is given by Eq. (31)

$$S_i = K_iC_i^{m_i} \qquad (30)$$

$$S_i = K_iC_i\cdot[\sum_j \alpha_{ij}C_j]^{m_i-1} \qquad (31)$$

In these equations α is a competition parameter, and $\alpha_{ij} = 1$.

Note that when $m_i = 1$, Eq. (31) reduces to Eq. (30), which seems to indicate that the model predicts the absence of competition when the single-species isotherm is linear. Fritz and Schlunder (1981) used competitive adsorption isotherms of the form of Eq. (32) for a two-species system whose single-species isotherms were Freundlich-type (i.e., Eq. (30))

$$S_1 = \frac{K_1C_1^{(m_1+m_{11})}}{[C_1^{m_{11}} + \alpha_{12}C_2^{m_{12}}]} \qquad (32a)$$

and

$$S_2 = \frac{K_2C_2^{(m_2+m_{22})}}{[C_2^{m_{22}} + \alpha_{21}\cdot C_1^{m_{21}}]} \qquad (32b)$$

Note that contrary to the equations of Sheindorf et al., Fritz-Schundler equations predict the possibility of competition even when single-species isotherms are linear.

An empirical approach for multispecies adsorption

An empirical approach has been developed by the authors (unpublished) that can be used in conjunction with any general equilibrium single-species isotherm, to account for competition. Suffix 0 in these equations refers to single-species values.

The method involves computing mobile or solution phase concentrations (C_{i0}) for all competing species ($i = 1$ to N). The single-species equilibrium adsorption concentrations (S_{i0}) are computed from the appropriate single-species isotherms. Competition is characterized by preferential adsorption coefficients (P_i) defined in such a way that

$$\sum_j P_j = 1 \qquad (33)$$

For example, a useful choice of defining P_i is $K_i/\sum_j K_j$, where K_j are the equilibrium adsorption parameters for Langmuir, linear, or Freundlich isotherms.

An empirical Eq. (34) is used to compute adsorption in multispecies situations (S_i)

$$S_i = S_{i0}\cdot P_iC_{i0}/\sum_j P_jC_{j0}) \qquad (34)$$

Resultant solution concentrations are computed from mass conservation equations (Eq. (35), for $i = 1$ to N)

$$\beta S_i + \theta C_i = \beta S_{i0} + \theta C_{i0} \qquad (35)$$

Simple iteration procedures may be required, sometimes, for improving the accuracy of the estimated values of C_i and S_i.

For example, in a binary system with Langmuir-type adsorption isotherms, this set of equations yields

$$S_1 = K_1C_1Q/|1 + K_1C_1 + K_2C_2 + (K_2C_2/K_1C_1)| \qquad (36a)$$

$$S_2 = K_2C_2Q/|1 + K_1C_1 + K_2C_2 + (K_1C_1/K_2C_2)| \qquad (36b)$$

Equation (36) illustrates the similarity between this approach and the Langmuir-type competition (Eq. (17)), except for an addition term in the denominator of the present equations. Thus, this empirical setup of computations slightly overestimates the effect of competition compared with Langmuir-type competition.

For Freundlich-type competition, Eq. (34) reduces to Eq. (37)

$$S_i = K_iC_i^{m_i+1}\Big/\left(\sum_j \alpha_{ji}C_j\right) \qquad (37)$$

where $\alpha_{ji} = K_j/K_i$.

Equation (37) is similar to those of Fritz and Schlunder (1981) and become identical if $m_{ij} = 1$. Thus, the empirical computation scheme could be considered as a special case of Fritz and Schlunder's more generalized scheme.

In this empirical setup even linear-type adsorption isotherms ($m_i = 1$) display competition.

ISOTOPIC EXCHANGE

Isotopic exchange can be considered as a form of competitive adsorption somewhat analogous to interspecific competition. Simple cases of isotopic exchange may be represented as a reversible chemical reaction

Reaction:	$\boxed{\text{soil} - X}$	+	$\boxed{BX^*}$	$\rightleftharpoons$	$\boxed{\text{soil} - X^*}$	+	$\boxed{BX}$
Concentrations:	$(a - x)$		y		x		$b - y$
Phase:	solid		fluid		solid		fluid

In the above reaction, X and X^* are the two isotopes (e.g., tracer and nontracer) in the form of solutions of BX and BX^* and adsorbed forms, soil-X and soil-X^*. The concentrations are usually (e.g., McKay 1938; Frost and Pearson 1961) expressed in total volume (solid plus fluid) basis. a is adsorption capacity per unit volume ($= \beta Q$), y equals $C^*\theta$, x corresponds to βS^*, and b is the initial solution phase concentration, i.e., $y = 0$ at $t = 0$. At any given time $b = \theta\ (C + C^*)$. The superscript asterisk denotes the tracer. Under such situations, in a closed system, the rate equation can be written as

$$-\frac{dy}{dt} = \frac{dx}{dt} = R\left(\frac{y}{b} - \frac{x}{a}\right) \tag{38a}$$

which, in the present notation, becomes

$$\frac{\partial S^*}{\partial t} = k_1 C^* - k_2 S^* \tag{38b}$$

In the above equations, R, k_1, and k_2 are constants. However, Eqs. (38a) and (38b) are valid for a closed conservative system, where b is a constant. Under more generalized conditions suitable for solute transport in soils, we obtain

$$\frac{\partial S^*}{\partial t} = k[C^* S - C S^*] \tag{39}$$

Under equilibration conditions ($\partial S/\partial t \rightarrow 0$), the familiar isotopic-dilution principle is satisfied (Eq. (40))

$$\frac{C}{C^*} = \frac{S}{S^*} \tag{40}$$

However, these equations assume homogenous adsorption energies for all adsorption sites. For heterogeneous adsorption energies, these equations need to be modified, and under certain conditions such generalizations lead to Elovich-type equations (e.g., Atkinson et al. 1971).

SUMMARY AND CONCLUSIONS

Adsorption of chemicals by soils has a profound influence on solute transport. Competitive adsorption, or adsorption in multispecies systems, is different from single-species adsorption. For accurate understanding of solute transport in soils under realistic multispecies systems, we need mathematical models capable of describing multispecies transport and solute-soil interactions. In this paper, we have presented some of the required models and discussed some of the special cases. Isotopic exchange has also been briefly described. In subsequent papers, we shall present a review of competitive adsorption in soils and its influence on solute transport. Computer simulations of some of the models presented will be used to qualitatively assess their validity and usefulness in predicting some of the experimental observations.

REFERENCES

Anderson, M. P. 1979. Using models to simulate the movement of contaminants through groundwater flow systems. Crit. Rev. Environ. Control 9:97–156.

Atkinson, R., A. M. Posner, and J. P. Quirk. 1971. Kinetics of heterogeneous isotopic exchange reactions: Derivation of an Elovich equation. Proc. R. Soc. London Ser. A. 324:247–256.

Barley, K. P. 1970. The configuration of the root system in relation to nutrient uptake. Adv. Agron. 22:159–201.

Bar-Yosef, B., S. Fishman, and H. Talpaz. 1980. A model for zinc movement to single roots in soils. Soil Sci. Soc. Am. J. 44:1272–1279.

Boast, C. W. 1973. Modeling the movement of chemicals in soils by water. Soil Sci. 115:224–230.

Bower, C. A., W. R. Gardner, and J. O. Goertzen. 1957. Dynamics of cation exchange in soil columns. Soil Sci. Soc. Am. Proc. 21:20–24.

Cushman, J. H. 1979. An analytical solution to solute transport near root surfaces for low initial concentration: 1. Equations development. 2. Applications. Soil Sci. Soc. Am. J. 43:1087–1090 and 1090–1095.

Drew, M. C., P. H. Nye, and L. C. Vaidyanathan. 1969. The supply of nutrient ions by diffusion to plant

roots in soils. 1. Absorption of potassium by cylindrical roots of onions and leek. Plant Soil 30:252–270.

Epstein, E., and C. E. Hagen. 1952. A kinetic study of the absorption of alkali cations by barley roots. Plant Physiol. 40:620–624.

Frappell, B. D. 1979. Competition in vegetable crop communities. J. Aust. Inst. Agric. Sci. 45:211–217.

Fritz, W., and E. U. Schlunder. 1981. Competitive adsorption of two dissolved organics onto activated carbon: 1. Adsorption equilibria. Chem. Eng. Sci. 36:721–730.

Frost, A. A., and R. G. Pearson. 1961. Kinetics and mechanisms. Wiley, New York.

Harter, R. D., and D. E. Baker. 1977. Applications and misapplications of the Langmuir equation to soil adsorption phenomena. Soil Sci. Soc. Am. J. 41:1077–1080.

Mackay, H. A. C. 1938. Kinetics of exchange reactions. Nature 142:997–998.

Murali, V., and L. A. G. Aylmore. 1980. No-flow equilibration and adsorption dynamics during ionic transport in soils. Nature 238:467–469.

Murali, V., and L. A. G. Aylmore. 1981*a*. A convective-dispersive-adsorptive flow model for solute transport in soils: 1. Model description and simulations. Aust. J. Soil Res. 19:23–39.

Murali, V., and L. A. G. Aylmore. 1981*b*. Competitive adsorption: Its importance in ionic transport in soils. Search 12:133–135.

Nye, P. H., and F. H. C. Marriott. 1969. Theoretical study of distribution of substances around roots resulting from simultaneous diffusion and mass flow. Plant Soil 3:459–472.

Nye, P. H., and P. B. Tinker. 1977. Solute movement in the soil-root system. Blackwell, London.

Olsen, S. R., and W. D. Kemper. 1968. Movement of nutrients to plant roots. Adv. Agron. 20:91–151.

Sheindorf, C. H., M. Rebhun, and M. Sheintuch. 1981. A Freundlich type multicomponent isotherm. J. Colloid. Interface Sci. 79:136–142.

van Genuchten, M. Th., J. M. Davidson, and P. J. Wierenga. 1974. An evaluation of kinetic and equilibrium equations for the prediction of pesticide movement through porous media. Soil Sci. Soc. Am. Proc. 38:29–35.

0038-075X/83/1354-0203$02.00/0
SOIL SCIENCE
April 1983
Vol. 135, No. 4
Printed in U.S.A.

COMPETITIVE ADSORPTION DURING SOLUTE TRANSPORT IN SOILS: 2. SIMULATIONS OF COMPETITIVE ADSORPTION

V. MURALI AND L. A. G. AYLMORE

Department of Soil Science and Plant Nutrition, University of Western Australia, Nedlands, W.A. 6009 Australia

Received for publication 27 August 1981; Revised 7 December 1981

ABSTRACT

Computer simulations of the effects of Langmuir and Freundlich-type competition, in binary systems under equilibrium and dynamic (time-dependent) conditions, have been presented and discussed.

These simulations indicate that during competitive adsorption (for both Langmuir and Freundlich-type competition), the presence of a competing species can have a marked effect in depressing (lowering) the equilibrium isotherm of an adsorbing species to an extent determined by the relative solution concentrations, distribution and selectivity coefficients, etc.

In Langmuir-type competitive dynamic (time-dependent) adsorption, the amount of adsorption can exceed the equilibrium value during some periods. In binary competition, the experimental conditions, such as solution-to-solid ratio, can have significant influence on the shape of the isotherm and thus on the isotherm parameters estimated.

Freundlich and Langmuir-type competitive adsorption isotherms in binary systems may resemble the isotherms in single-species systems. Thus, with limited experimental data, one may easily overlook the presence of competitive adsorption, even when it has significant influence on the equilibrium adsorption isotherms, and the adsorption parameters may change from one set of experimental conditions to another. Accounting for competition should allow the estimation of correct parameters.

INTRODUCTION

Competition between chemical species in solution for adsorption sites on soil surfaces can be of major significance in determining the effective mobility of any potentially adsorbing species. Part 1 of this series (Murali and Aylmore 1983) presented and discussed several mathematical models of competitive adsorption and multispecies solute transport in soils.

In this paper, we present simulations of some important effects of competition on equilibrium and dynamic (time-dependent) adsorption in binary systems. In a subsequent paper, we will examine experimental evidence from the literature to evaluate the relevance of the mathematical models used in these simulations.

SIMULATIONS

Simulations covering examples of single-species adsorption isotherms, Langmuir-type competitive adsorption under equilibrium and dynamic situations, equilibrium Freundlich-type competition, and an empirical approach to competition, are presented and discussed in the following sections. Although competition undoubtedly occurs commonly as a multispecies event, the present investigation has been confined to binary competition to facilitate subsequent experimental evaluations.

Simulation 1: Equilibrium Langmuir and Freundlich isotherms

An adsorption isotherm represents the functional relationship between adsorbed (S) phase concentrations and C, the solution concentration (i.e., $S = S\ (C)$} at constant temperature. For Langmuir and Freundlich-type isotherms the appropropriate equations are

$$\text{Langmuir} \quad S = K_L CQ/(1 + K_L C) \qquad (1)$$

$$\text{Freundlich} \quad S = K_F C^M \qquad (2)$$

In Eqs. (1) and (2), K_L and K_F are the equilibrium distribution coefficients for the Langmuir

and Freundlich adsorption models, respectively, Q is the adsorption capacity, and M is the Freundlich power coefficient.

Figure 1 demonstrates the effect of Langmuir and Freundlich model parameters on the shape of the equilibrium adsorption isotherms. In the equilibrium Langmuir adsorption model (Eq. (1), Q, the adsorption capacity of a soil, depends on the specific surface area, surface charge characteristics, etc., and thus on clay content, clay mineralogy, organic matter content, etc. For example, Berkheiser et al. (1980) have presented statistical relationships between Q and soil properties for phosphate adsorption in soils. The distribution coefficient K_L is a measure of the adsorption energy or the steepness of the adsorption isotherm. For example, when the product of C, the solution concentration, and K_L, the distribution coefficient (K_LC), equals unity, half the adsorption sites will be filled (half-Q adsorption). Thus, for small values of K_L, half-Q adsorption occurs at large solution concentrations (Small slope or gradient), and for large K_L values, half-Q adsorption occurs at very small solution concentrations. Therefore, K_L may be considered an affinity or preference parameter. In the Freundlich model, the power coefficient M is a measure of nonlinearity; when M is unity, the isotherm is linear. Several solute-soil interactions conform to Freundlich-type models. Whereas Langmuir-type models assume homogeneous adsorption energy for all adsorption sites, a Freundlich-type model can be derived, for heterogeneous adsorption energies, by assuming the adsorption surfaces to be composed of a series of different homogeneous adsorption energy sites, each following Langmuir-type interaction (Sheindorf et al. 1981). The Freundlich distribution coefficient K_F may also be considered as a measure of affinity. These model parameters can be readily estimated from experimental isotherm data, using linearized forms of the adsorption models.

The Langmuir model can be linearized in several different ways (e.g., Eqs. (3a) and (3b)).

Linearized Langmuir models

$$\frac{C}{S} = \frac{1}{KQ} + \frac{C}{Q} \quad \{C/S \text{ vs. } C \text{ plot}\} \qquad (3a)$$

$$\frac{1}{S} = \frac{1}{Q} + \frac{1}{KCQ} \quad \{1/S \text{ vs. } 1/C \text{ plot}\} \qquad (3b)$$

Under ideal conditions both approaches are identical, but in the presence of experimental errors—random, concentration-dependent, adsorption-dependent, etc.—different forms could yield slightly different values for model param-

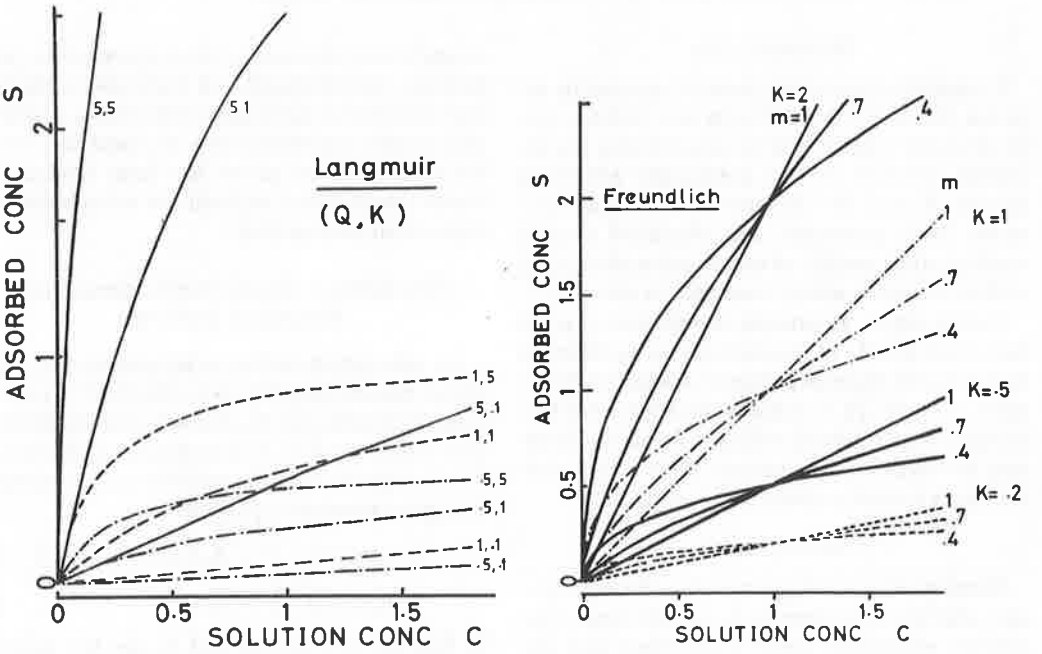

FIG. 1. Single-species equilibrium adsorption isotherms: (a) Langmuir isotherms; (b) Freundlich isotherms.

In Fig. 2a, the curves are competitive isotherms for species 1 [i.e., S_1 (C_1) for different fixed values of T_2]. Compared with single-species isotherms of species 1 (curve 0), curves A, B, and C show small, moderate, and large reductions in adsorbed phase concentration, respectively, at any given C_1, over the entire range of solution concentration. Figure 2b shows the effect of C_1 on the adsorption of S_2, for the three fixed totals of species 2 in the system (curves A, B, and C of Fig. 2b correspond to the same conditions as for curves A, B, and C of Fig. 2a). Note that in the absence of competition, curves A, B, and C of Fig. 2b would be parallel to the x-axis, because T_2 is constant for a given curve. Thus the decrease in S_2 with increasing C_1 is due to competitive adsorption, and the slope of the curve is a measure of competition or the preference the soil has for species 2, in relation to species 1. If $K_1 > K_2$, the slopes would be greater. The relative rate of change $[(1/S_2)\cdot(\partial S_2/\partial C_1)]$ is dependent on the total concentration (T_2) of species 2. Over the range from 0 to 4 for C_1, the relative rate of decrease for curves A, B, and C of Fig. 2b was 0.5, 0.39, and 0.27, respectively. This indicates that competitive effects on species 2 were of most consequence at lower amounts.

Under the same conditions as Figs. 2a and 2b, the relationship between S_1 and S_2 (corresponding to curve C) was essentially linear (Fig. 2c). This linear relationship between S_1 and S_2, when T_2 is constant, is particularly true at lower values of S_1.

It can be readily shown that in Langmuir competition the equilibrium adsorption isotherm of species 1, when C_2 is maintained constant, can be described by a single-species Langmuir isotherm. The effective distribution coefficient would depend on K_1, K_2, and C_2 [$K_1^* = K_1/(1 + K_2C_2)$, where K_1^* is the effective distribution coefficient of species 1, when C_2 is constant]. Thus the experimental competitive isotherm could appear to be of single-species Langmuir form, provided C_2 is approximately constant. This would be true over a narrow range of C_1.

Simulation 3: Relationship between cumulative adsorption and cumulative solution concentrations

There is some experimental evidence in the literature (e.g., Karim 1967; Martin and Al-Bahrani 1977) to suggest that simple Langmuir-type relationships exist between the cumulative

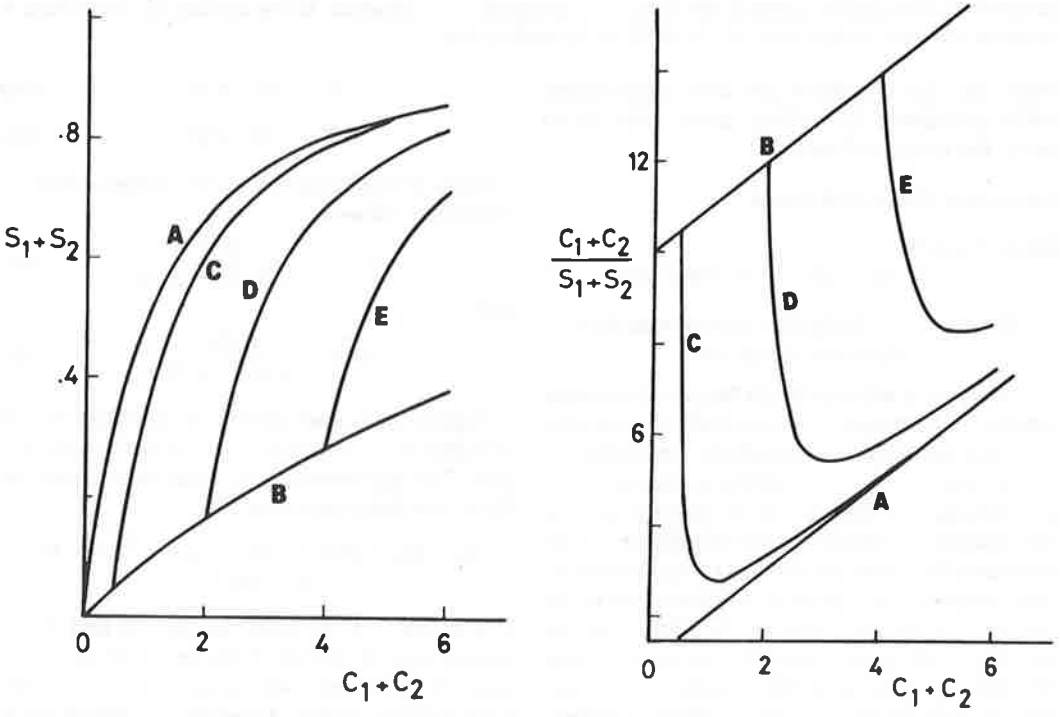

FIG. 3. Total isotherms (equilibrium relationship between total adsorbed and total solution concentration) based on Langmuir-type competition: (a) isotherm plot; (b) linearized plot.

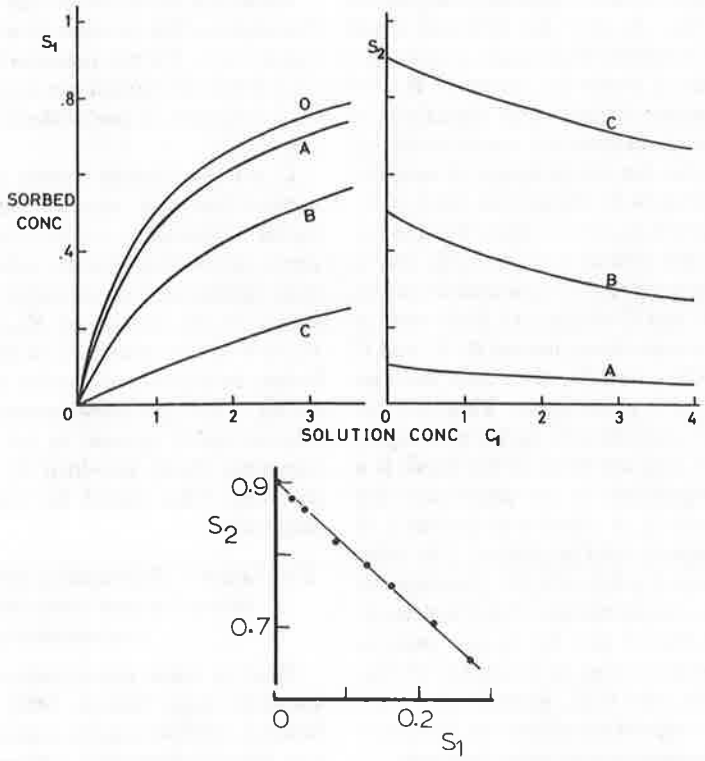

FIG. 2. Effect of Langmuir-type competition on the equilibrium distributions, in a binary system: (a) competitive isotherms of species 1; (b) S_2 vs. C_1 relationship (T_2 is constant. In the absence of competition, S_2 would be constant, independent of C_2); (c) S_2 vs. S_1 relationship.

eters. Similar problems are also encountered while estimating Freundlich model parameters using the linearized form.

Linearized Freundlich model

$$\log S = \log K + M \log C \quad \{\log S \text{ vs. } \log C \text{ plot}\} \quad (4)$$

Simulation 2: Langmuir-type competitive adsorption isotherms

Competitive adsorption for binary systems are usually determined experimentally by varying the total (solution plus adsorbed) concentration of one species and maintaining a constant total concentration of the second (competing) species. Adsorption isotherms for binary mixtures were computed for these conditions using Langmuir-type competition. The total concentration in the system, for the two species, is related to the adsorbed and the solution phase concentrations, through Eqs. (5a) and (5b), where β and θ are the soil bulk density and water content, respectively

$$T_1 = \beta S_1 + \theta C_1 \quad (5a)$$

$$T_2 = \beta S_2 + \theta C_2 \quad (5b)$$

Langmuir equations for binary systems may be written as follows

$$S_1 = \frac{K_1 C_1 Q}{1 + K_1 C_1 + K_2 C_2} \quad (6a)$$

and

$$S_2 = \frac{K_2 C_2 O}{1 + K_1 C_1 + K_2 C_2} \quad (6b)$$

Figures 2a, b, and c show the simulated effects of binary competition for Langmuir type adsorption. The parameters and other values used for these computations were

$$K_1 = K_2 = Q = 1;\ \beta = 1.5\ (\text{g cm}^{-3});\ \theta = 0.4\ (\text{cm}^3\text{cm}^{-3})$$

For curves 0, A, B, and C in Figs. 2a and 2b, T_2 values were 0, 0.1944, 1.15, and 4.95 (g cm^{-3}), respectively. These correspond to 0, 0.1, 0.5, and 0.9 surface coverage of species 2 in the absence of competition, i.e., in a single-species system.

adsorption ($S_T = S_1 + S_2$) and solution $C_T = C_1 + C_2$) phase concentrations. However, such results are not always observed.

The existence or the nonexistence of simple Langmuir-type relationships would become evident from isotherms [$S_T(C_T)$] and linearized Langmuir plots of the form C_T/S_T vs. C_T. Results of the simulations of the relationship between C_T and S_T are plotted in Figs. 3a and 3b. The parameter values used were $K_1 = K_2 = Q = 1$. Curves A and B correspond to $C_2 = 0$, and $C_1 = 0$, respectively, i.e., the single-species isotherms. Curves C, D, and E are for binary mixtures corresponding to fixed C_2 values of 0.5, 2, and 4, respectively. If simple Langmuir-type relationships were to hold, we should find a unique isotherm or single straight line in the linearized Langmuir plot. The results in Figs. 3a and 3b, however, indicate the nonuniqueness of $S_T(C_T)$ relationships, in both linear and isotherm plots. This suggests that even if Langmuir-type models closely describe competitive adsorption in soils, the observation of a unique relationship of $S_T(C_T)$ is not universally valid. It can be demonstrated however (see Appendix) that under some circumstances, Langmuir-type competition can yield simple Langmuir-type relationships between S_T and C_T. Thus it is not surprising that some workers have found unique relationships between S_T and C_T, while others have not.

Simulation 4: Langmuir-type competition involving adsorption of a species on to a soil initially saturated with a competing species; effect of solution-to-solid ratio on the equilibrium isotherms

During competitive adsorption in soils, a previously adsorbed species can, on desorption, compete for adsorption sites. The significance of such competition was simulated by solving the adsorption equations for appropriate initial conditions (Eq. (7))

$$t \leq 0,\ C_1 = T_1,\ S_1 = 0,\ C_2 = 0,\ S_2 = Q \quad (7)$$

The adsorption parameters used were

$$K_1 = K_2 = Q = 1$$

Six cases, A to F, for β values 0.025, 0.1, 0.25, 0.5, 1, and 1.5, were simulated by solving Eqs. (5a), (5b), (6a), and (6b). The water content (θ) was related to β, through particle density (= 2.5, assumed); thus $\theta = 1 - \beta/2.5$. The range of β values used covers most experimental conditions. A bulk density of 1.5 (g/cm^3) is typical of field situations for a loamy soil, and $\beta = 1$ simulates a swollen clay soil. $\beta = 0.5$, 0.25, 0.1, and 0.025, correspond to solution-to-solid ratios ranging from approximately 1.5 to 40.

Figure 4a shows the effect of β on simulated equilibrium adsorption isotherms of species 1, when the adsorption sites of the soil are initially saturated with the competing species 2. Most adsorption experiments are performed by equilibrating known quantities of dry soil with solutions of different concentrations of the adsorbing species under study. Thus, the total amount of species 2 in the system depends on the solution-to-solid ratio, or β. Since, at $t \leq 0$, $S_2 = Q = 1$, T_2 equals β from Eq. (5b). Figure 4a demonstrates that if a soil had a potentially competing species already adsorbed (e.g., Ca-saturated soil in Zn adsorption studies; phosphate-rich soil in sulfate, selenite, or molybdate adsorption studies) prior to the experiment, "single-species" adsorption studies would yield different equilibrium isotherms for different solution-to-solid ratios. Further, the isotherms so determined at high solution-to-solid ratios would be vastly different from those at realistic bulk densities (e.g., $\beta = 1.5$). Most of such isotherms may have Langmuir-shape. Figure 4b shows linearized Langmuir plots (C_1/S_2 vs C_1) for different β values. Note that the results could be approximated to straight lines. If they were perfect straight lines, which they would be if they were truly Langmuir-type, statistical regression would yield R^2 values of 1.00. However, the R^2 values obtained from these simulated data were less than unity (Table 1). At realistic bulk density (β) values, R^2 was about 0.9 and increased with increasing solution-to-solid ratio (or decreasing β) to 0.97 at $\beta = 0.025$. The parameter (K_1 and Q) values estimated from the linearized Langmuir plots of Fig. 4b were different at different solution-to-solid ratios. The K_1 values estimated varied between 1.5 for $\beta = 0.025$ to 0.8 for $\beta = 1.5$, when the value used in the simulation was 1.0. Thus, such adsorption experiments can yield K values either smaller or larger than the actual values. The value of the adsorption capacity Q estimated from Fig. 4b ranged from 0.91, for $\beta = 0.025$, to 0.67, for $\beta = 1.5$, while the value used to generate the data was $Q = 1.0$. Thus, at high solution-to-solid ratios, one may obtain better estimates of Q than at low values, even by ignoring competition, but the distribution coefficients (K) could be overestimated by up to 50% of more.

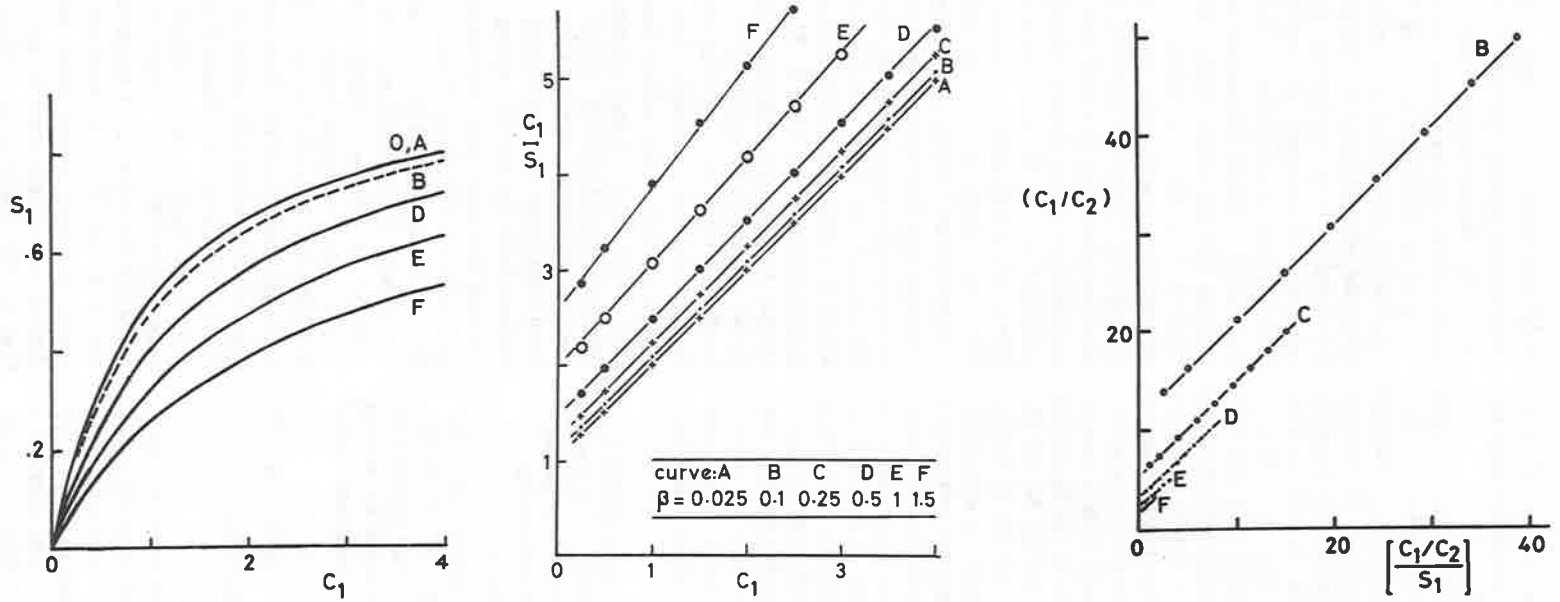

FIG. 4. Effect of solution-to-solid ratio on equilbrium adsorption in a binary Langmuir-type competition: (a) isotherms plots; (b) linearized plots (C_1/S_1 vs. C_1) that ignore competition; (c) linerized plots $\{(C_1/C_2)/S_1$ vs. $(C_1/C_2)\}$ that partly account for competition. Curves A to E correspond to β values of 0.025, 0.1, 0.25, 1, and 1.5 (In Fig. 4c, the computed data points for curve A were outside the range).

TABLE 1

Estimates of K_1 *and* Q *from different methods when desorbed species compete in adsorption*[a]

Case	A	B	C	D	E	F	Expected values
β	0.025	0.1	0.25	0.5	1.0	1.5	
Method 1							
R^2	0.97	0.96	0.95	0.94	0.92	0.89	1.00
K_1	1.51	1.42	1.29	1.13	0.93	0.79	1.00
Q	0.91	0.90	0.88	0.85	0.77	0.67	1.00
Method 2							
R^2	0.98	0.98	0.97	0.95	0.91	0.86	1.00
K_1	0.04	0.14	0.27	0.52	0.72	1.23	1.00
Q	0.91	0.90	0.90	0.88	0.83	0.76	1.00
Method 3							
Fitted perfectly, with $R^2 = 1.00$, and yielded $K_1 = Q = 1.00$							

[a] Method 1: Ignores competition, i.e., single-species approach. K_1 and Q were estimated by fitting equation: $C_1/S_1 = 1/(K_1Q) + C_1/Q$.

Method 2: Accounts for competition. Special case where total surface coverage or high solution concentrations are assumed. K_1 and Q were estimated by fitting equation

$$\frac{C_1/C_2}{S_1} = \frac{1}{(K_1/K_2)\cdot Q} + \frac{(C_1/C_2)}{Q}$$

and using the known $K_2 = 1$.

Method 3: No simplifying assumptions involved. K_1 and Q were estimated by fitting multiple linear regression equation of the form

$$\frac{1}{S_1} = \frac{1}{Q} + \frac{1}{K_1Q}\cdot\frac{1}{C_1} + \frac{1}{(K_1/K_2)\cdot Q}\cdot\frac{1}{(C_1/C_2)}$$

A different way of estimating Langmuir isotherm parameters, in the presence of desorption of a competing species, at high solution concentrations (or near total surface coverage) is by using plots of (C_1/C_2) vs. $(C_1/C_2)/S_1$. The data of Fig. 4a are plotted in this manner in Fig. 4c. If the assumption of high solution concentration is realistic, one would expect a single straight line for all β values. Figure 4c, however, shows that all the generated data do not fall on one single straight line, but forms different straight lines for different β values. Again, the lines are not perfectly straight, and R^2 values are smaller than unity. At low β values (or high solution-to-solid ratios), for example $\beta = 0.025$ and 0.1, R^2 was 0.98, but decreased with increasing β, to 0.86 at $\beta = 1.5$. Thus, replacing (C_1/C_2) for C in simple Langmuir plots, to account for competition, can result in Langmuir-type isotherms. However, the model parameters so estimated are quite different from those used ($Q = K_1 = 1$) in generating the data. For example, K_1 estimated from the plots of Fig. 4c (Method 2 of Table 1) range from 0.04 to 1.23 for β values of 0.025 to 1.5. Q values estimated are about 0.9 for β values of 0.025 to 0.25, but decrease to 0.76 for $\beta = 1.5$. Thus, despite the Langmuir-type appearance, the simplified approach to account for competition can yield unrealistic values of the adsorption parameters.

The same data as in Figs. 4a, b, and c were analyzed by a third method, which does not use simplifying assumptions and which accounts for Langmuir-type competition (Method 3 of Table 1). As would be expected, the generated data fitted perfectly, yielding $R^2 = 1.00$, and $K_1 = Q = 1.00$, the values used to generate the data.

This simulation thus indicates the need for caution when estimating equilibrium adsorption isotherms for a species; competition can be easily overlooked if proper precautions are not taken. The statistical significance of linearized Langmuir plots is not adequate proof that competition is absent or, more importantly, that competition can be accurately accounted for by simplified approaches. These simulations suggest that adsorption isotherms are better estimated from experiments at different solution-to-solid ratios and by analyzing the solution phase for all possible competing species. In the

absence of competition, however, all solution-to-solid ratios would yield the same isotherm. In Method 2, at high solution-to-solid ratios (approximately 40), the estimated value of K_1 was very much smaller than the real value (0.04 against 1.0), while in Method 1, it was higher (1.51 compared to 1.0. In binary competition, multiple regression (Method 3 of Table 1) appears to be better than using simplified linear forms.

Simulation 5: Adsorption dynamics in binary Langmuir-type competition

The effects of the dynamic nature of adsorption on the adsorption process and the approach to equilibrium conditions were simulated using Eqs. (8a) and (8b)

$$\frac{\partial S_1}{\partial t} = k_{a1}C_1[Q - S_1 - S_2] - k_{d1}S_1 \quad (8a)$$

$$\frac{\partial S_2}{\partial t} = k_{a2}C_2[Q - S_1 - S_2] - k_{d2}S_2 \quad (8b)$$

Because most adsorption studies use closed systems, mass balance equations (Eqs. (5a) and (5b)) were coupled with Eqs. (8a) and (8b). The initial conditions used conform to mixing a known mass of soil, which has no residual adsorption, with a finite volume of a solution containing a binary mixture of two competing species. The solution phase is assumed to be uniformly mixed at all times. The initial conditions and parameter values were

$$t = 0;\ C_1 = T_1,\ S_1 = 0,\ C_2 = T_2,\ S_2 = 0$$

$$k_1 = k_{a1} = k_{a2} = Q = 1$$

$$K_2 = k_{a2}/k_{d2} = 5$$

$$T_1 = 1.8,\ T_2 = 1.02$$

$$\beta = 1.5,\ \theta = 0.4$$

These simulations are presented in Fig. 5a for species 1 and Fig. 5b for species 2. Different curves correspond to different k_{a2} values, 0 (corresponding to the no-competition case), 0.1, 0.5, and 2. Simulations presented here and elsewhere indicate that adsorption vs. time curves in binary competition can be of two types. The first type is that typified by the single-species curve (0) of Fig. 5a. In this case adsorption increases rapidly with time at the beginning, then slows to reach a plateau without any maxima or peaks. The second type exhibits a distinct peak, i.e., adsorption increases with time, reaches a maximum (in excess of equilbrium value), then drops, rapidly at first and then gradually, to reach the equilibrium value. This case is typified by curves for $k_{a2} = 0.1$, 0.5, and 2. The peak value reached and the time corresponding to peak adsorption appear to depend on the adsorption rate characteristics of the competing species. Figure 5b shows the adsorption vs. time relationship for species 2. Different curves correspond to different adsorption rate coefficients of species 2, but identical equilibrium coefficients. In these figures (5a and 5b), the time axis has been plotted on the log-scale to accentuate the differences at small and large times. Figure 5b shows the effect of k_{a2} on adsorption of species 2. Increasing k_{a2} from 0.1 to 0.5 and then to 2 had a significant effect on the adsorption dynamics. For example, the time taken to reach an adsorption value of 0.3 decreased from nearly 7 units of time (e.g., hours, days) for $k_{a2} = 0.1$, to about 1 unit of time for $k_{a2} = 0.5$, and approximately 0.1 unit of time for $k_{a2} = 2$.

Simulation 6: Equilibrium adsorption isotherms with Freundlich-type competition

Freundlich-type competition may be presented by equations of the form

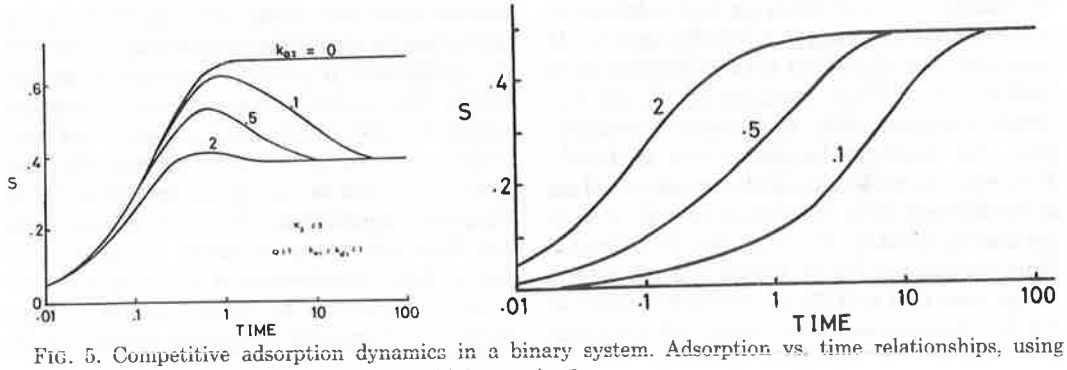

FIG. 5. Competitive adsorption dynamics in a binary system. Adsorption vs. time relationships, using Langmuir-type equations: (a) for species 1; (b) for species 2.

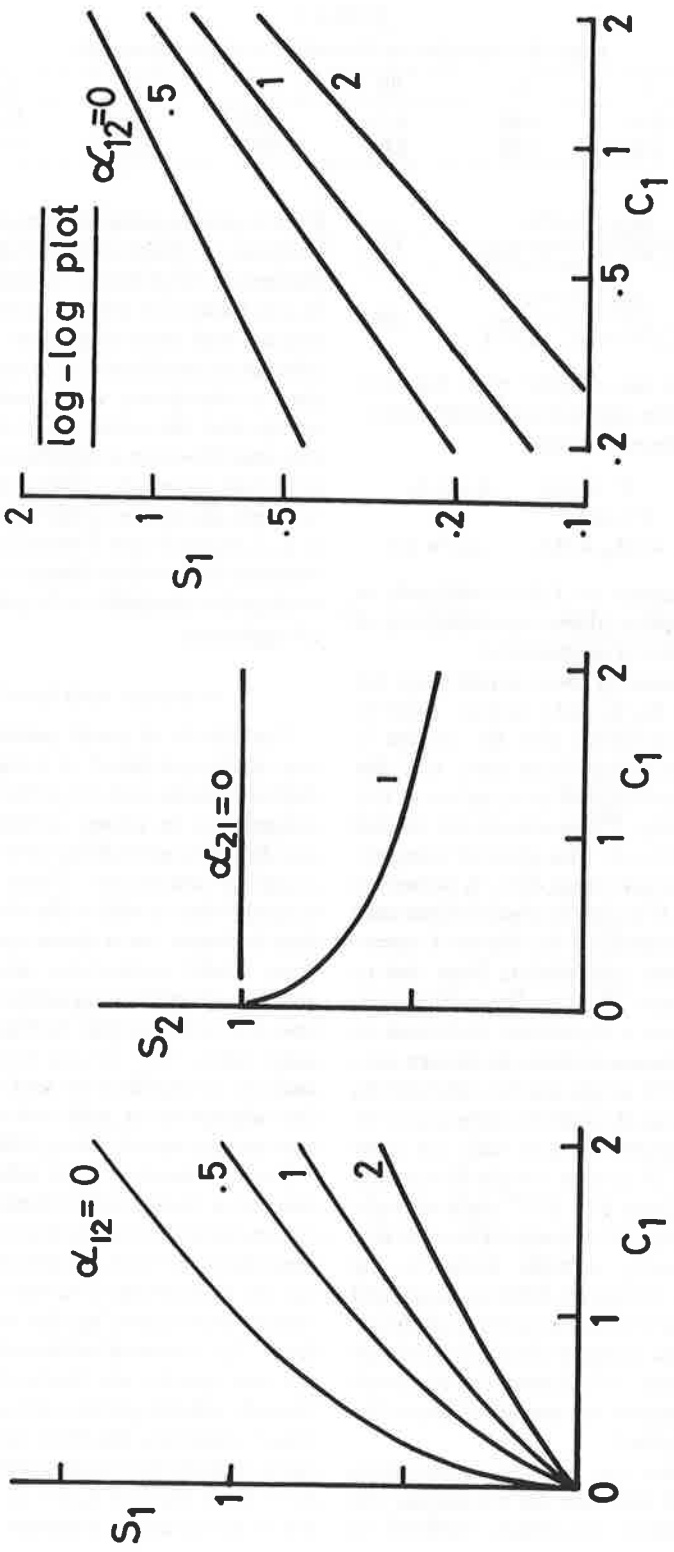

FIG. 6. Freundlich-type competition in a binary system: (a) isotherm plots, for species 1 (numbers on curves correspond to α_{12} values); (b) S_2 vs. C_1 relationship (in the absence of competition $\alpha_{21} = 0$); (c) log-log plots (data same as in (a)).

TABLE 2

Effect of competition on Freundlich isotherm parameters

α_{12} =	0	0.1	0.5	0.8	1.0	1.5	2.0
K	0.50	0.56	0.71	0.77	0.80	0.85	0.89
M	1.00	0.90	0.64	0.53	0.48	0.38	0.32

$$S_1 = \frac{K_1 C_1^{(M_1+M_{11})}}{[C_1^{M_{11}} + \alpha_{12} \cdot C_2^{M_{12}}]} \quad (9a)$$

$$S_2 = \frac{K_2 C_2^{(M_2+M_{22})}}{[C_2^{M_{22}} + \alpha_{21} \cdot C_1^{M_{21}}]} \quad (9b)$$

These equations are coupled with material balance equations (5a, 5b) and solved for $S_1(C_1)$. The model parameters used were

$$K_1 = K_2 = 1, \qquad T_2 = 1.9, \qquad \beta = 1.5,$$
$$\theta = 0.4$$
$$M_1 = M_2 = M_{11} = M_{22} = 0.5, \qquad \alpha_{21} = 1.0$$

The value of T_2 chosen (= 1.9) corresponds to solution and adsorption phase concentrations of unity, in the absence of competition.

The results of some of these simulations are presented in Figs. 6a, b, and c and in Table 2. Figure 6a is the isotherm plot for species 1. Curve 0 is the no-competition case, and the remaining curves correspond to α_{21} values of 0.5, 1, and 2, respectively. These curves are plotted over a C_1 range of 0 to 2. The effect of competition on species 2, in this range of C_1, is presented in Fig. 6b. Curve 0 is the no-competition case and hence independent of C_1. Curve 1 corresponds to the binary competition. Note that in both figures, 6a and 6b, the Freundlich-type competition predicts a significant reduction in adsorbed phase concentrations in binary systems compared with single-species adsorption, over the entire group of solution concentrations. Figure 6c is the double-log plot with the same data as in Fig. 6a. Note that simple Freundlich isotherms of the form $S = KC^M$ yield straight lines on a log-log plot. The competitive case also yielded approximately straight lines (in the range of 0.2 to 2), though of different slope and intercept compared with the noncompetitive situation. Thus, in the example simulation, binary competition affected both K and M. The extent of the effect, estimated by statistical curve-fitting, is given in Table 2.

Other simulations (not presented here) show that the empirical approach for computing the effects of competitive adsorption outlined in Part 1, yields results that are equivalent for most purposes to those obtained using the previous theoretical treatments. Adsorption of species 1, at any particular solution concentration C_1, decreased with increasing value of the preferential adsorption coefficient of species 2. This reduction is adsorption as a result of competition occurs over the entire range of solution concentrations. However, a significant advantage of the empirical approach is that it allows competition between adsorption isotherms of different types (e.g., Langmuir and Freundlich) to be handled, whereas the previous theoretical approaches are confined to competition between the same type of isotherms.

SUMMARY AND CONCLUSIONS

The effects of model parameters on adsorption isotherms based on Langmuir and Freundlich equations and, in particular, the effects of competition in binary systems on equilibrium and dynamic adsorption have been examined by computer simulation. These simulations illustrate the way in which the shape of the adsorption isotherm for a given species may depend upon model parameters, such as the affinity factors, adsorption capacities, relative concentrations, nonlinearity coefficients, solution-to-solid ratios, etc. To our knowledge simulated analyses of equilibrium and dynamic competitive adsorption in soils and related substances have not previously been published.

During Langmuir-type adsorption, the presence of a fixed total (solution plus adsorbed) concentration of a second competing species has been shown to have a marked effect in depressing the adsorption isotherm of species 1 to an extent determined by the relative concentrations. The adsorbed concentrations S_1 and S_2 of the two species are inversely, and essentially linearly, related, particularly at low values of S_1. Total isotherms $\{S_T(C_T)\}$ and their linearized plots indicate that unique relationships between $S_T(= S_1 + S_2)$ and $C_T(= C_1 + C_2)$ are usually not to be expected, although simple Langmuir-

type relationships are possible in certain circumstances.

With a competing species already adsorbed on a soil, changes in the solution-to-solid ratio can significantly influence the shape of the equilibrium isotherm. In these circumstances, ignoring competition or only partly accounting for it can result in estimates of model parameters for a given species that change from one set of experimental conditions to another.

Simulations taking into account adsorption dynamics during binary Langmuir-type competition demonstrate that adsorption values in excess of the equilibrium value could occur during some stages with such time-dependent processes.

It is significant that the shapes of the isotherms in competitive binary systems of either Langmuir or Freundlich type may resemble those expected for single-species systems. Thus, with limited experimental data, the presence of competitive adsorption may easily be overlooked, even when it has a significant influence on the equilibrium adsorption isotherms. In these circumstances the adsorption parameters estimated can change from one set of experimental conditions to another, if the effects of competition are ignored. Accounting for competition should allow the correct parameters to be estimated independently of the experimental conditions.

APPENDIX

If simple Langmuir-type relationships were to exist, we might write

$$S_T = S_1 + S_2 \tag{A1}$$

or

$$\frac{K_T C_T Q}{1 + K_T C_T} = \frac{(K_1 C_1 + K_2 C_2) Q}{1 + K_1 C_1 + K_2 C_2} \tag{A2}$$

Equation A2 would be true when:

1. $K_T = K_1 = K_2$
2. $C_1/C_2 = \text{constant} = C_r$ (say). Then $K_T = (K_1 C_r + K_2)/(1 + C_r)$
3. $K_1 C_1 + K_2 C_2 \gg 1$ or $K_1 C_1 + K_2 C_2 \simeq K_1 C_1 + K_2 C_2$

Here, however, we have $S_T = Q$, or total surface coverage. Isotherm plots $[(S_T(C_1)]$ would have experimental points on the plateau only, and C_T/S_T vs. C_T plots would be linear, because S_T is a constant $(= Q)$.

Thus, under certain limited circumstances, even Langmuir-type competition can result in simple Langmuir isotherms for $S_T(C_T)$ relationship.

REFERENCES

Berkheiser, V. E., J. J. Street, P. S. C. Rao, and T. L. Yuan. 1980. Partitioning of inorganic orthophosphate in soil-water systems. CRC Crit. Rev. Environ. Control 10:179–224.

Karim, M. 1967. Physico-chemical factors affecting the leaching of fertiliser sulphate. Ph.D. thesis, University of Western Australia, Australia.

Martin, R. J., and K. S. Al-Bahrani. 1977. Adsorption studies using gas-liquid chromatography: 2. Competitive adsorption. Water Res. 11:991–999.

Murali, V., and L. A. G. Aylmore. 1983. Competitive adsorption during solute transport in soils: 1. Mathematical models. Soil Sci. 135:143–150.

Sheindorf, C. H., M. Rebhum, and M. Sheintuch. 1981. A Freundlich-type multicomponent isotherm. J. Colloid Interface Sci. 79:136–142.

0038-075X/83/1365-0279$02.00/0
SOIL SCIENCE
November 1983
Vol. 136, No. 5
Printed in U.S.A.

COMPETITIVE ADSORPTION DURING SOLUTE TRANSPORT IN SOILS: 3. A REVIEW OF EXPERIMENTAL EVIDENCE OF COMPETITIVE ADSORPTION AND AN EVALUATION OF SIMPLE COMPETITION MODELS

V. MURALI AND L. A. G. AYLMORE

Department of Soil Science and Plant Nutrition, University of Western Australia, Nedlands, W.A. 6009, Australia

Received for publication 23 September 1981; revised 29 June 1982

ABSTRACT

Experimental evidence from the literature is presented to demonstrate that adsorption of chemical substances in soils and related materials is significantly influenced by competition from other adsorbing chemicals. Both organic and inorganic ions are capable of competing for adsorption sites on soils. Potential competing chemical species include: phosphate, sulfate, selenite, molybdate, arsenate, bicarbonate, oxalate, citrate, different phenols, and polygalacturonate among anions, and calcium, lead, magnesium, sodium, and zinc among cations. Competitive adsorption occurs on a wide variety of soils, on such clay minerals as kaolinite, montmorillonite, haematite, goethite, gibbsite, pseudoboehmite, etc., and on such other materials as activated carbon. Although the diversity of experimental conditions and methods to study competitive adsorption is great, competition is clearly influenced by factors such as pH, solution concentration, and nature of the competing species.

Results of some experimental studies on the effects of competition on the ion distributions between the solution and solid (adsorbed) phases are qualitatively similar to those expected from theoretical models and simulations presented in previous papers. The evaluation of the models was incomplete because the adsorption data for all the competing species were not available. Several quantitative comparisons between experimental isotherms and the theoretical predictions showed that the competitive adsorption models satisfactorily describe competition.

INTRODUCTION

Mathematical models of competitive adsorption and multispecies solute transport in soils and some simulations of competitive adsorption were presented in earlier papers (Murali and Aylmore 1983*a* and *b*). These simulations predicted that competition between species for adsorption sites could markedly influence the adsorption of a given species and demonstrated the ways in which equilibrium adsorption varied with the nature of the species involved. In the present paper we briefly review the experimental work on equilibrium and rate studies of competitive adsorption in soils and related materials to demonstrate the occurrence, the extent, and the diversity of competitive adsorption in soils. Because Langmuir and Freundlich-type adsorption isotherms are invariably used to describe equilibrium adsorption in soils, experimental data from the literature have been used to evaluate competitive adsorption models and simulations using these isotherms.

This review is not exhaustive, particularly of the studies on activated carbon. Multispecies adsorption by activated carbon is included

1. to demonstrate its similarity to adsorption in soils
2. to show the effects of competition on adsorption dynamics and
3. to examine Freundlich-type competition models

The results from activated carbon studies may not be directly applicable to soils, but could help in identifying gaps in the soils' literature, e.g., the importance of studying adsorption dynamics in systems of several competing species using soils.

TABLE I

Summary of experimental conditions used by different workers in studying competitive adsorption

S. no.	Authors	Competing species	Soils/clays etc.	Solution/ solid ratio	Shaking period	pH	Background electrolyte	Other information
1	Kamprath et al. 1956	Sulphate × phosphate	Three soils of N. Carolina, and H-Al-bentonite	10 and 5	30 min shaking, left overnight then analysis of filtrate	4,5,6	Acetic acid	Soils were initially leached with pH 4.8 sodium acetate-acetic acid buffer prior to adsorption experiments
2	Karim 1967	Sulfate × phosphate	Kaolinite, haematite and pseudoboehmite	25		4.6		
3	Nagarajah et al. 1968	Phosphate × citrate, bicarbonate	Kaolinite	400	24 and 43 h	6.3	0.04 M KCl	Binary systems. (a) Adsorption from mixtures—24 h equil. (b) Adsorption of Isospecies + 24 h equil. followed by 2nd species + 24 h equil
4	Gorlach et al. 1969	Molybdate × phosphate, sulfate	Three soils of Poland	10	1 h shaking, 24 h no shaking, 1 h shaking	5.7	0.1 M KCl	<0.25 mm fraction used in the study. Binary mixtures
5	Nagarajah et al. 1970	Phosphate × citrate, tartrate, oxalate, malate, succinate, malonate, lactate, acetate, polygalacturonate, α-D-galacturonate	Kaolinite, gibbsite and goethite	400 for kaolinite, 500 for oxides	24 h	Variable	0.01 M KCl	Binary mixtures
6	Hingston et al. 1971	Phosphate × arsenate, selenite	Goethite and gibbsite	Approx. 250 for goethite, approx. 500 for gibbsite		Variable	0.1 M NaCl	Binary mixtures
7	Bailey 1973	Sulfate × phosphate	One soil of New Zealand			5.6 to 5.9	–	Allophane and kaolin were present in soil. Extraction with pH 4, 0.01 M $CaCl_2$ at 20:1 solution-to-solid ratio
8	Gary and Gissel-Nielsen 1973	Selenate, selenite × nitrate, sulfate and phosphate	Two soils. Jefferson county, Oregon and Tomkins county, N.Y., U.S.A.	0.25 and 0.28	Variable	Not available	–	Extraction, following equilibration through 5 min shaking of soil at solution-to-soil ratio of 5, using 0.01 M $CaCl_2$. Binary competition
9	Barrow 1974*a*,*b*	Phosphate × arsenate; molybdate × phosphate and hydroxide	4 soils (unfertilized sites). 3 from Western Australia and 1 from New South Wales, Australia	Incubation-type expts. Water content variable & close to field capacity	Incubation period was 18 days and variable	Different for different soils: 4.2 to 6.2. Also variable	–	For extraction: 10:1 solution-to-soil ratio. Shaking period—48 h. Extraction solutions—0.1 M NaOH, 0.275 M ammonium oxalate, 0.1 M phosphate solution, 0.5 M sodium arsenate. Binary competition

10	Griffin and Au 1977	Lead × calcium	Smectite (montmorillonite) bentonite clay	50 to 1000 (variable)	Equilibrated till pH change in 24 h was less than 0.02.	5		Distilled water and 0.1 M calcium perchlorate
11	Harter and Baker 1977	Zinc × desorbed species	7 soil samples from 4 profiles, U.S.A.	100	Not available	Not available		Distilled water
12	Martin and Al-Bahrani 1977	Pyridine, 2-methylpyridine, 0-cresol, 2-chlorphenol, nitrobenzene, 0-methylphenol and quinaldine	Activated charcoal	Variable	100 h oscillatory shaking for isotherms. Variable for adsorption rate studies	Not available		Distilled water	Studies mixtures of 2, 3 and 5 solutes
13	Metson and Blakemore 1978	Sulfate × phosphate	33 soil samples from 11 profiles, New Zealand			4.6		Sodium acetate acetic acid buffer	2 g of soil leached with 25 ml solution
14	Earl et al. 1979	Phosphate × acetate, citrate and oxalate	2 soils of New Zealand, Fe, gel and Al gel	40 for soils, and 1000 for oxide gels	40 h, end-to-end shaking	6		0.1 M sodium perchlorate	Binary mixtures
15	Fritz and Schlunder 1981	*p*-nitrophenol × *p*-chlorphenol, benzoic acid and phenol. *p*-chlorphenol × phenyl acetic acids	Activated carbon	Variable	3 to 4 days for isotherms. Variable for rate studies	Not available		Distilled water	Binary mixtures

Although in many instances there is inadequate information available in the literature to provide absolute confirmation of the validity of the models previously outlined (Murali and Aylmore 1983*a*), the qualitative comparisons provided suggest that such simple approaches may be adequate to describe the majority of competitive situations.

COMPETITIVE ADSORPTION

The existence of competition among adsorbing ions for adsorption sites of soils and related materials has been recognized for some time. For example, the extraction of "available" phosphate in soils by organic and inorganic anions, such as citrate, oxalate, bicarbonate and fluoride, has been well documented (e.g., Swenson et al. 1949; Struthers and Sieling 1950).

There is conclusive evidence in the literature to show that competition between adsorbing and exchanging ions occurs widely in soils and that competition can be of major significance. Table 1 summarizes the materials and experimental conditions used and emphasizes the diversity of experimental conditions under which competition has been observed. A wide range of organic and inorganic ions appear to compete for adsorption sites of soils, clay minerals, and activated carbon.

Most experiments involved high solution-to-solid ratios and shaking or agitaton to obtain equilibration (dilute-shaking). Among the few exceptions are Barrow (1974 *a,b*) and Cary and Gissel-Nielsen (1973), who used more realistic water contents during equilibration but employed the dilute-shaking technique for extraction. However, it seems self-evident that adsorption studies should be performed under conditions close to those encountered in the field, viz., realistic water contents with no shaking or agitation, if these results are to be related to solute transport models.In the following sections the evidence for competitive adsorption and its nature are first discussed, and the ability of simple competition models to predict the effects observed is evaluated.

Qualitative evidence from simple experiments

There is considerable evidence in the literature to show that in binary systems, the adsorption of one species is reduced by the presence of a second species. Kamprath et al. (1956), for example, demonstrated that sulfate adsorption

in soils was significantly reduced by competition from phosphate, when both species were present at the same time. Phosphate was the stronger of the two competitors, and even small quantities of phosphate were adequate to substantially reduce sulfate adsorption, making the latter in many instances an effectively nonadsorbing species. In phosphate-molybdate and suflate-molybdate systems (Fig. 1) Gorlach et al. (1969) found the increasing the total concentration of phosphate or sulfate decreased molybdenum retention by soils, but phosphate had a substantially greater competing power than sulfate.

Hingston et al. (1971) showed the existence of competition in phosphate-selenite and phosphate-arsenate systems. Their results show that, in a system consisting of a fixed amount (~ 1 mmol) of selenite or arsenate, an increase in total phosphate resulted in an increase in adsorbed P and decreased in the adsorption of selenite and arsenate. Adsorbed phosphate concentrations were linearly related to adsorbed concentrations of selenite and arsenate, particularly at low phosphate levels. Figure 2 gives an example of phosphate-selenite competition. From a given total phosphate, goethite adsorbed more phosphate in the presence of selenite than in the presence of arsenate (both Se and As at ~ 1 mmol), indicating that arsenate is a stronger competitor than selenite against phosphate for adsorption on goethite. This point will be discussed later.

Cary and Gissel-Nielsen (1973) demonstrated that the presence of phosphate in soil enhanced the solubility (in 0.01 *M* $CaCl_2$) of native and applied selenite, but that sulfate and nitrate had no influence. Similarly, incubation studies by

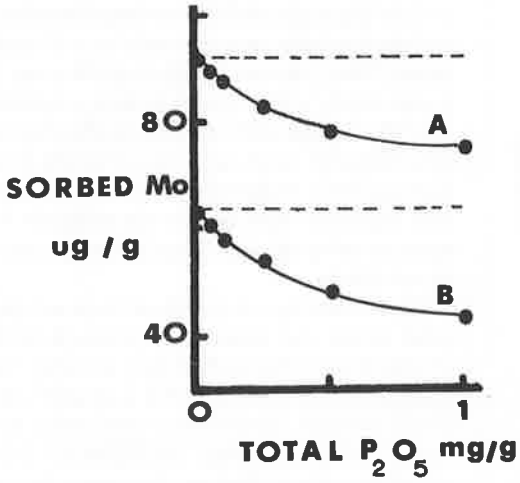

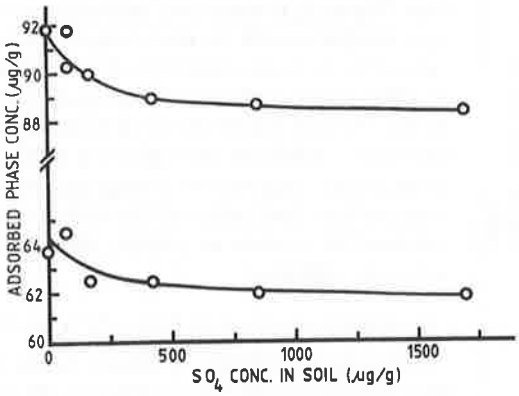

FIG. 1. Effect of competitive adsorption on Mo retention by Polish soils: top, molybdate-phosphate system; bottom, molybdate-sulfate system (*after Gorlach et al. 1969*).

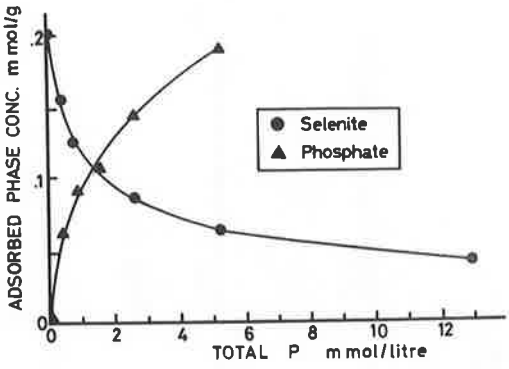

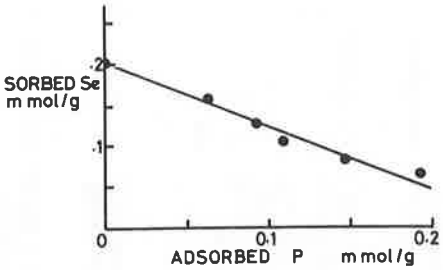

FIG. 2. Phosphate-selenite competition: top, effect of total P in the system on adsorbed phase concentrations of phosphate and selenite; bottom, relationship between adsorbed phase Se and P (*replotted from Hingston et al. 1971*).

Barrow (1974*a*) demonstrated that phosphate can displace soil molybdate and arsenate can desorb the adsorbed phosphate. A field investigation by Bailey (1974) showed that applied fertilizer phosphate can be responsible for greater downward movement of native sulfate in soils. Using leaching-type laboratory experiments, Metson and Blakemore (1978) demonstrated that the presence of phosphate decreased the sulfate retention power of soils. They also observed that in potentially high sulfate-retaining soils, the presence of sulfate can reduce phosphate sorption. Singh et al. (1981) also showed that selenite and selenate could compete with phosphate and sulfate for adsorption on soils.

Competition is not restricted to anions alone. Cation exchange and greater preference by some soils and clays for some cations over others, e.g., divalent vs. monovalent, are well documented (e.g., Russell 1961; Thomas 1977; Bolt and Bruggenwert 1976). The work of Griffin and Shimp (1976) and Lai et al. (1978) demonstrated the existence of competition among cations, such as sodium, calcium, magnesium, and lead.

However, competition may not always occur. For example, Hingston et al. (1971) were of the opinion that certain adsorption sites were selective to only one of the competing ions, phosphate, selenite, and arsenite. The existence of such selective sites for selenite and selenate were also observed by Singh et al. (1981) in soils. Similarly, Bingham and Page (1971) showed that adsorption of boron was unaffected by the presence of anions such as phosphate and sulfate.

Competitive adsorption has been shown to occur in materials other than soils and clays, such as activated carbon, textile fibers, and synthetic resins (Fritz and Schlunder 1981; Sheindorf et al. 1981; Jossens et al. 1978; Martin and Al-Bahrani 1977; Fritz and Schlunder 1974; Ott and Rys 1973). Competitive adsorption studies with activated carbon have been directed toward an understanding of the performance of adsorbents in water and in waste water treatment. A complete discussion of these aspects is beyond the scope of this paper, but a few selected examples are worth mention. Martin and Al-Bahrani (1977) studied competitive adsorption, with activated carbon, in systems containing up to five different adsorbing organic compounds. In a five-species system, they found that individual adsorption isotherms were of an inverted U shape. In general, their results indicate that, in multispecies systems, cumulative adsorption exceeds the adsorption of individual species in the single-species system, at any particular solution concentration of a given competing species. However, adsorption of individual species in the multispecies system was lower than its adsorption in the single-species system. Competitive reduction in the adsorption of any given species increased with increasing number of competing species.

There is evidence that in some cases cumulative isotherms, the relations between total adsorption and total solution concentration of all competing species, are similar to those for single-species isotherms (e.g., Aylmore and Karim 1967, unpublished data; Martin and Al-Bahrani, 1977). However, in general such relationships are not observed.

The papers previously cited demonstrate clearly that competition between a wide range of adsorbing species occurs with a wide variety of adsorbing surfaces and involves considerable complexity.

Effect of pH on competitive adsorption

Most soils are well buffered with respect to pH, and it may be expected that under normal conditions pH changes are small. However, experiments conducted in the laboratory, where conditions were altered, demonstrate that pH has a considerable influence on sorption and competition. For example, the work of Gorlach et al. (1969) showed that molybdenum retention and competitive reduction in adsorbed Mo due to phosphate, were pH-dependent in some Polish soils (Fig. 3). Phosphate-molybdate competition was most prominent around pH 6 to 7.

Nagarajah et al. (1970) demonstrated that a wide range of organic anions are potentially capable of competing with and reducing phosphate adsorption on the surface of kaolinite, goethite, and gibbsite (Table 2 and Fig. 4). The relative effectiveness of different organic anions in their competition with phosphate (for adsorption) was assessed using a parameter, R, defined as

$$R = (S_{P0} - S_P)/S_P$$

where S_{P0} is the amount of phosphate adsorbed in the absence of competition from a known amount of phosphate added to the system, and

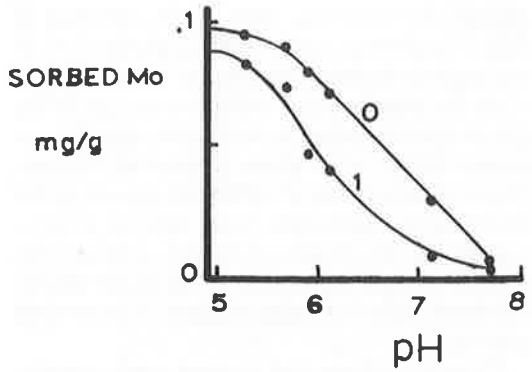

FIG. 3. Effect of pH on sorbed Mo in a Polish soil. Curve 0 refers to the no-competition case, and curve 1 is in the presence of phosphate.

S_P is the phosphate adsorbed in the presence of a competing species. Their results showed that the R value depended on pH and the concentration of the competing ion, and that citrate and oxalate were very effective in reducing phosphate adsorption on kaolinite and gibbsite. Malonate, tartrate, and malate were moderately effective, and acetate, succinate, and lactate had little effect on phosphate adsorption.

Hingston et al. (1971), in their studies on competition in phosphate-selenite and phospate-arsenate systems, used the selectivity coefficient ($K_{1,2}$), which is the ratio (K_1/K_2) of the individual single-species equilibrium Langmuir distribution coefficients as a measure of the relative preference in a binary competition (among species 1 and 2). At pH 7, goethite was found to possess almost equal preference for the three species—phosphate, selenite, and arsenate ($K_{P,As} = 0.94$; $K_{P,Se} = 1.1$), whereas at lower pH values the ordering of preference was: selenite>arsenate>phosphate. For example, at pH 3, $K_{P,As}$ was 0.62, and $K_{P,Se}$ was 0.16. Gibbsite, however, appeared to prefer phosphate to arsenate at most pH values, as indicated by $K_{P,As} = 3$ at pH 9, and 5 at pH 4, 5, and 7.

There is an apparent discrepancy in this work in the interpretation as to which of the two competing species is more preferred. The interpretation clearly depends on whether one assumes that all adsorption sites are equally avail-

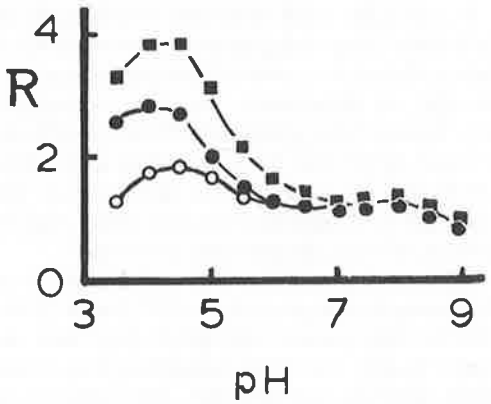

FIG. 4. Effect of pH on the competitive ability factor, R (defined in the text), for polygalacturonate (PGA)-phosphate system. The top, middle, and bottom curves are for 0.01, 0.1, and 1 mg PGA/L (*extracted from Nagarajah et al. 1971*).

TABLE 2

R_{max} *values for competition between organic anions and phosphate for adsorption onto clay and oxide surfaces (after Nagarajah et al. 1970)*[a]

Anion	pK_1	pK_2	Kaolinite		Gibbsite		Goethite	
			R_{max}	pH at R_{max}	R_{max}	pH at R_{max}	R_{max}	pH at R_{max}
Citrate	3.13	4.76	4.3	4.8	6.0	5.25	0.23	4.25
Tartrate	3.03	4.37	1.5	4.3	0.9	5.25	0.1	4.0
Oxalate	1.25	4.28	7.0	4.0	2.0	5.75	0.1	4.0
Malate	3.46	5.05	1.2	4.5	1.0	5.0	0.1	4.0
Succinate	4.21	5.64	0.2	No max	0.2	5.5	–	–
Malonate	2.85	5.7	1.9	4.5	0.6	5.75	–	–
Lactate	3.86	–	0.2	No max	0.2	No max	–	–
Acetate	4.76	–	0.2	No max	0.2	No max	–	–
PGA (0.1%)	3–5		4.0	4.25	1.4	4.0	0.4	4.0
α-D-GA	3.48	–	0.5	4.5	0.8	7.0	–	–

[a] Total (solution + sorbed) conc. Organic anion: 1.6×10^{-5} M (except PGA – 4×10^{-5} M, α-D-GA = 5×10^{-3} M); P = 6.45×10^{-5} M.

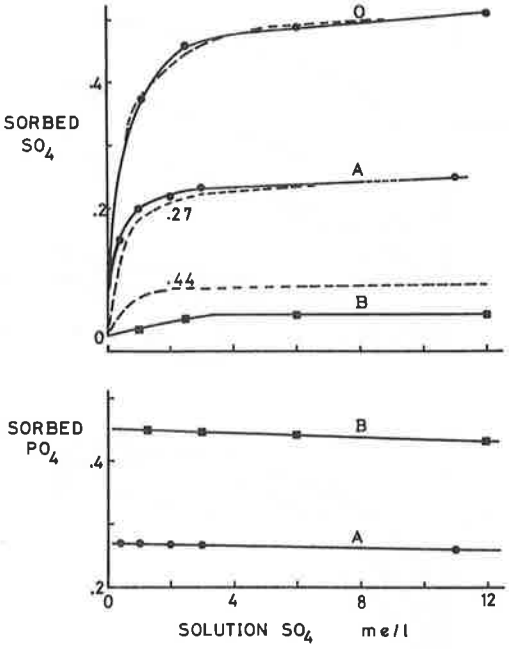

FIG. 5. Effect of competitive adsorption on the equilibrium distributions in sulfate-phosphate system for Clackline kaolinite. Top, sulfate equilibrium isotherms in the presence of zero (0), 0.45 (A), and 1.5 meq/L (B) of phosphate. Bottom, effect of sulfate solution concentration on the adsorbed phosphate. Total phosphate in the system was 0.45 meq/L for curve A and 1.5 meq/L for B. Broken lines (top) are predicted isotherms (refer to text and Table 3 for details). Numbers on predicted curves are the S_2 values used (*after Aylmore and Karim 1967, unpublished data*).

able for competitive adsorption or whether these are effectively compartmentalized, with only a portion of the total sites being involved in competition. In the models previously discussed (Murali and Aylmore 1983*a*,*b*) it was considered that all adsorption sites of soils show competition. However, this feature can be readily incorporated in the models where necessary.

Barrow (1974*a*) found that the increase in Mo extracted from soils due to the presence of P was largest around pH 7. Clearly pH is an important factor influencing adsorption processes in multispecies soil systems.

Competitive isotherms

Although the previous comparisons have been largely qualitative, in some cases a quantitative assessment of the effects of competition on the equilibrium adsorption isotherms is possible. Aylmore and Karim (1967; unpublished data) studied the competition between sulfate and phosphate adsorption on a kaolinite and two oxide (pseudoboehmite and hematite) samples. Equilibrium distributions of sulfate and phosphate between solution and adsorbed phases were measured in systems composed of different amounts of sulfate and fixed amounts of total phosphate. Figure 5 shows the effect of different amounts of total P on sulfate adsorption isotherms for Clackline kaolinite. Curves O, A, and B (continuous lines) are the sulfate isotherms in the presence of 0, 0.45, and 1.5 meq P/L, respectively. There was a reduction in sulfate adsorption, due to phosphate in the system, over the entire range of solution concentration. The competitive reduction in sulfate adsorption at any particular sulfate solution concentration increased with increasing phosphate level. The corresponding effect on phosphate adsorption, due to an increase in solution sulfate concentration, is plotted in Fig. 5 (bottom). Note that, in the absence of competition, the curve would be parallel to the x axis, because the total phosphate in the system (for a given curve) was constant. However, due to competition from sulfate, the phosphate adsorption slightly decreased with increasing sulfate concentration for both low and high phosphate levels. This decrease is much smaller than in the case of sulfate adsorption. Because the single-species sulfate isotherm was of the Langmuir form, equilibrium Langmuir adsorption parameters (Table 3) were estimated from the data of curve A in Fig. 5 (top). Further, because phosphate adsorption changed very little for a given curve (A, B of Fig. 5 (bottom)), it was assumed that S_2, the phosphate adsorbed, was constant (0.27 and 0.44 for curves A and B). The predicted binary sulfate

TABLE 3

Adsorption parameters (K_1, Q) *for the predicted curves*[a]

Fig. no.	K_1	Q	Source of data
5 (top)	2.25	0.527	Karim 1967
6 (top)	4.4	0.228	Nagarajah et al.
6 (bottom)	4.5	0.204	1968
7 (left)	67	0.062	Earl et al.
7 (right)	36	1.55	1979

[a] Numbers on the predicted (broken) curves are S_2 values in Fig. 5 (top)c and K_2C_2 values in Figs. 6 and 7.

isotherms were computed using the equation

$$S_1 = \frac{K_1 C_1 (Q - S_2)}{1 + K_1 C_1}$$

Comparing the theoretical (broken) and experimental (continuous) isotherms, it can be concluded that the Langmuir model is a good representation of sulfate adsorption by kaolinite, and that the trend of competition predicted by the Langmuir-type approach closely follows the experimental results. Due to specific adsorption of phosphate, pH and thus Q of the system may change, particularly at high phosphate levels (Murrmann and Peech 1969). This is not included in the model and is perhaps the reason for difference in the predicted and experimental sulfate isotherms at high P level.

Nagarajah et al. (1968) presented evidence for competition in phosphate-citrate and phosphate-bicarbonate systems (Fig. 6). These experiments were carried out in two ways. The first involved equilibration, through shaking, of the clay-solution suspensions for 24 h with the required amounts of the two competing species. The second involved two equilibrations, first with the required amounts of phosphate and then a second equilibration, after adding the required quantity of the competing species, e.g., citrate or bicarbonate. Curve A of Fig. 6 (top) represents the phosphate adsorption isotherm in the absence of competition, and curves C and E are phosphate adsorption isotherms for mixtures (Case 1) in the presence of low (1.25×10^{-5} M) and high (2.5×10^{-3} M) levels of citrate. Curves B and D are the phosphate isotherms at the same low and high levels of citrate, when citrate was added after an initial phosphate equilibration. Thus, the second case involves desorption of adsorbed phosphate due to competition from citrate. The effect of competition was greater when both the competing species, phosphate and citrate, were added together. The competitive reduction in phosphate adsorption occurred over the entire range of solution concentrations. The smaller reductions due to competition when phosphate desorption was involved might be indicative of a slower rate of equilibration during desorption or the presence of a separate interaction mechanism, such as irreversible solid phase reaction. Curve A of Fig. 6 (bottom) represents the single-species phosphate adsorption isotherm, and curve C is the phosphate isotherm when bicarbonate and phosphate were added together. Curve B is the adsorption isotherm when phosphate was first equilibrated and bicarbonate added later. However, when kaolinite was first equilibrated with bicarbonate and phosphate was subsequently added, the isotherm was essentially similar to C, i.e., adsorption from mixture. (This final case does not involve phosphate desorption.)

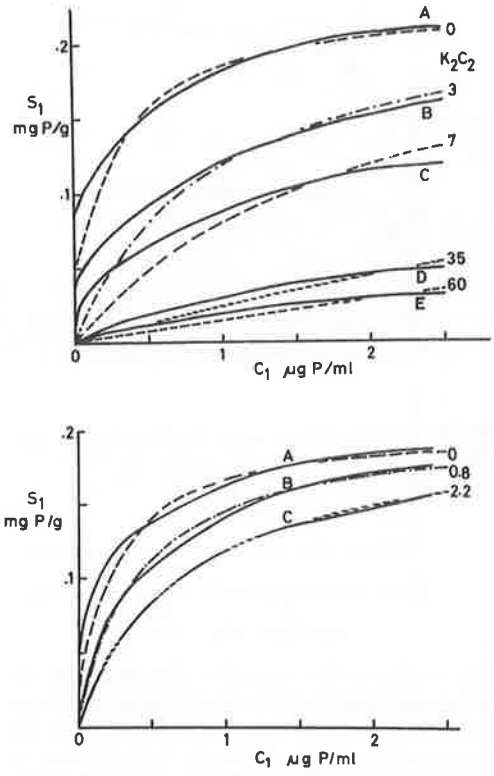

FIG. 6. Equilibrium phosphate isotherms in binary systems for kaolinite: top, phosphate-citrate system; bottom, phosphate-bicarbonate system. Curves A are in absence of competition, and the others are in the presence of competition. Numbers on the predicted (broken) curves refer to K_2C_2 values assumed in the predictions (*after Nagarajah et al. 1968*).

Earl et al. (1979) investigated the effects of acetate, tartrate, and citrate on phosphate adsorption by two contrasting soils—Egmont black loam developed from andesitic tephra, and Okaihau gravelly clay developed from deeply weathered olivine basalt—and two synthetic gels, of iron and aluminium oxides. Some of their results are presented in Fig. 7. Figure 7 (left) shows the equilibrium phosphate adsorption isotherms, in single and binary systems, for Okai-

hau soil, and Fig. 7 (right) is for iron gel. Curves A, B, and C are for phosphate adsorption in the absence of competition, in the presence of tartrate (1 mmol) and citrate (1 mmol), respectively. The equilibrium phosphate isotherm in the presence of acetate was practically similar to curve A. In all cases acetate had little or no effect on phosphate adsorption. In iron-rich materials, citrate had a more pronounced (reducing) effect on phosphate adsorption, whereas, in aluminium-rich materials, both citrate and tartrate had a similar effect. Even though the actual amount of phosphate sorption was different for the solids used (about 23 times more phosphate was adsorbed by iron oxide gel then Okaihau soil, at 0.2 mM solution phosphate concentration), the relative proportionate reductions due to the presence of competing ions were comparable. For example, at 0.2 mM phosphate solution concentration, acetate, tartrate, and citrate caused 1, 19, and 51% reduction in phosphate adsorbed by Okaihau soil. The corresponding reduction in phosphate adsorbed by iron oxide gel was 1, 24, and 60%, respectively. Aluminium-rich Egmont soil and aluminium oxide gel behaved in a similar manner.

The results of Nagarajah et al. (1968) and Earl et al. (1979) are in qualitative agreement with the theory, in that competition lowered the equilibrium phosphate isotherms and influenced adsorption over the entire range of solution phosphate concentrations. In Fig. 6 we compared these results quantitatively with Langmuir-type competition model predictions because the single-species phosphate isotherms were of the Langmuir type. In the absence of some of the necessary details (e.g., values of K_2, C_2, etc.) a few simplifying assumptions have been made. Consequently, this exercise is not a complete evaluation of the competition model used. An estimation of the order of magnitude of the model parameters was, however, possible.

Single-species isotherms (curves A of Figs. 6 and 7) were used to estimate Langmuir model parameters for phosphate adsorption (considered species 1), K_1 and Q. Because solution phase concentration C_2 of the competing species (e.g., citrate, oxalate, bicarbonate, etc.) was not known, it was assumed constant, such that for a given binary isotherm K_2C_2 is the only unknown in the equation

$$S_1 = \frac{K_1 C_1 Q}{1 + K_1 C_1 + K_2 C_2}$$

The model parameters K_1 and Q are given in Table 3, and the K_2C_2 values used for the predicted (broken) curves are given as numbers in the figures. Note that the magnitudes of K_1 and Q depend on the units of C_1 and S_1, respectively. K_1 has units reciprocal to those of C_1, and Q has the same units as S_1. Thus K_1 and Q may appear large or small depending on the units and also depending on whether they are based on unit mass (g), on molar or equivalents. It is, however, interesting to note that a high phosphate ad-

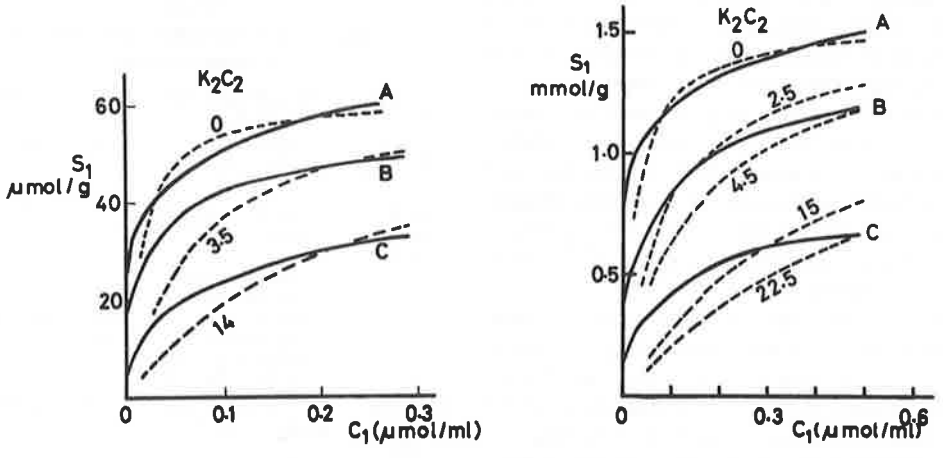

FIG. 7. Equilibrium phosphate isotherms for a soil (left) and for a synthetic iron oxide gel (right). Curves A are single-species (no-competition) isotherms, B are phosphate-tartrate system, and C are phosphate-citrate system.

sorption capacity substance, iron oxide gel (Q = 1.55) had a lower distribution coefficient (K_1 = 36) compared with a low adsorption soil capacity (Q = 0.062; K = 67).Thus, a larger potential for adsorption may not necessarily mean a stronger adsorption (or a greater preference).

Griffin and Au (1977) studied the adsorption of lead (from pure lead nitrate solutions and in the presence of excess calcium) by calcium-saturated montmorillonite clay (<2 μm) using four different solid-to-solution ratios. Their results indicate that, in the presence of excess calcium, lead adsorption was independent of the solid-to-solution ratio, whereas lead absorption depended on the solid-to-solution ratio when the amount of calcium in the system was limited. Further, lead adsorption from pure lead nitrate solution was highest when the solid-to-solution ratio was smallest, and it decreased with increasing clay in the suspension. Using a simplified form of the linearized Langmuir-type plot for binary competition, they found that the adsorption data for all the solid-to-solution ratios could be described by a single line and concluded that the lead-calcium system might be treated as simple Langmuir-type competition.

Harter and Baker (1977) analyzed the experimental results of zinc adsorption, for several soils, using a binary competitive Langmuir equation. They were of the opinion that adsorption isotherms sometimes need not be split into two (or more) simple Langmuirs, but, instead, the process could be considered as adsorption of the ion in question (e.g., zinc) with competition from the consequently desorbed ions. They concluded that the nonlinearity in the relationship of C/S vs. C (C is the solution phase concentration, and S is the adsorbed phase concentration) might not necessarily be the result of multiple adsorption mechanisms, but could be due to the neglect of the effect of competition from the desorbed species. In an earlier paper in this series (Murali and Aylmore 1983*a*), we showed that for single-species Langmuir-type adsorption, C/S vs. C plots would be linear.

There is some experimental evidence, from activated carbon studies, supporting the use of Freundlich-type competition models for certain species. Sheindorf et al. (1981) used some of the published work on adsorption from binary systems consisting of acetone-propionitrite, PNP^--BS^-, PNP°-PBP° and found that the Freundlich-type model was capable of describing equilibrium adsorption in binary systems (Table 4). Independent measurements of the preference parameters (α_{12} and α_{21}) shoed that, as expected from theory, α_{21} was (very nearly) equal to $1/\alpha_{12}$. They had also stated that their Freundlich-type competition model adequately described adsorptions in the binary systems of phenol-PBP, phenol-BS, PBP-BS in activated carbon. Freundlich-type adsorption models in multi-species systems have also been used effectively by Fritz and Schlunder (1980), Jossens et al. (1978), and others to describe and compute multispecies adsorption in activated carbon. The previous comparisons thus suggest that under equilibrium conditions at least, simple models of competition can be reasonably successful.

Dynamics of competitive adsorption

The experimental results of Martin and Al-Bahrani (1977) (Fig. 8) show that adsorption vs. time curves in competitive situations are generally of two shapes. The first is the most common type where the amount of adsorption increases with time, such that the rate of increase decreases with increasing time until an equilibrium adsorption value (plateau) is reached. The second type is characterized by an adsorption peak, i.e., the amount of adsorption increases with time to a maximum value, then decreases until the equilibrium plateau is eventually reached. These two types of adsorption vs. time curves (without peaks and with distinct peaks) and their intermediates have been observed ex-

TABLE 4

Evaluation of a Freundlich-type competitive adsorption model

Data source	Competing species (1 & 2)	Preference parameters α_{12}	α_{21}	$1/\alpha_{12}$
Radke & Prausnitz 1972	1. Acetone 2. Proprionitrile	0.75	1.30	1.33
Jaine & Snoeyink 1973	1. Anionic benzen-sulfonate (BS^-) 2. Anionic *p*-nitro-phenol (PNP^-)	17.25	0.054	0.58
	1. Neutral *p*-nitro-phenol (PNP°) 2. Neutral *p*-brom-ophenol (PBP°)	1.0 to 1.09	1.12 to 1.13	0.92 to 1
Sheindorf et al. 1981	All three binary combinations of a. Phenol b. PBP c. BS	Not available		

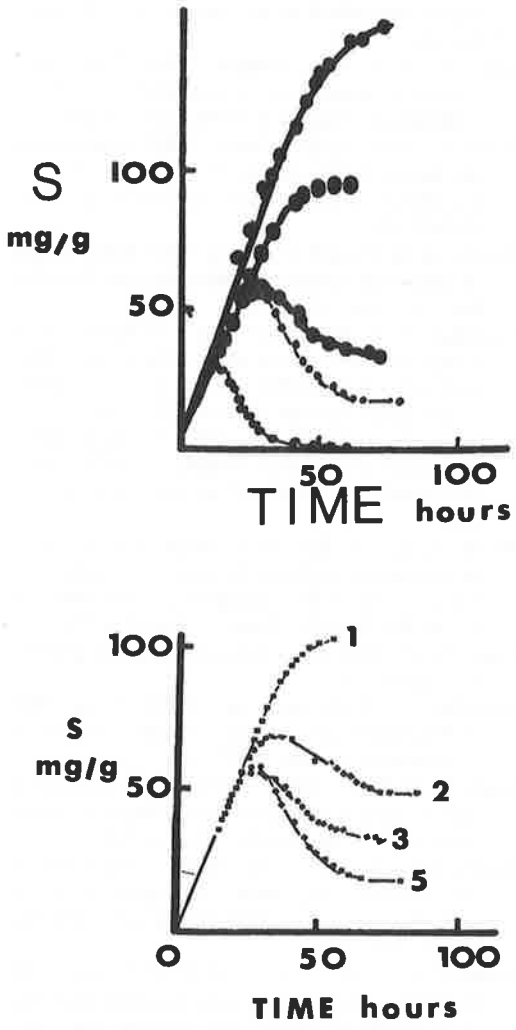

FIG. 8. Adsorption dynamics (adsorption vs. time relationships) in competitive systems for activated carbon: top, adsorption of individual species from 3 and 5 solute mixtures; bottom, adsorption of 2-methyl pyridine from systems 1, 2, 3, and 5 solutes.

perimentally (Martin and Al-Bahrani 1977) and agree with dynamic models of competitive adsorption (Fig. 5, Murali and Aylmore 1983*b*).

CONCLUSIONS

Competitive adsorption in soils is a common occurrence and has considerable significance. It is thus essential to include competitive adsorption in solute transport theories of soils.

Most studies of competitive adsorption seem to be the batch-type experiments involving dilute shaking. Some workers have used realistic water contents during equilibrium, but resorted to dilute shaking during the extraction stage. We believe that adsorption in soils should be studied under experimental conditions more closely representing those in field soil and at realistic water contents.

Competitive adsorption is influenced by such factors as pH, solution concentration, the nature of the competing species, and experimental conditions. Both organic and inorganic ions compete for adsorption sites of soils. However, there is evidence that selective adsorption sites occur and that in some circumstances particular chemical species may not be subject to competition.

Most experimental observations from the literature are in qualitative agreement with simple competitive adsorption models and simulations. In several comparisons between experimental and calculated equilibrium isotherms, these adsorption models were shown to satisfactorily describe competition.

Later papers will examine experimental and theoretical aspects of the effects of competitive adsorption on solute transport in soils and to plant roots.

REFERENCES

Barrow, N. J. 1974*a*. On the displacement of adsorbed anions from soils: 1. Displacement of molybdate by phosphate. Soil Sci. 116:423–431.

Barrow, N. J. 1974*b*. On the displacement of adsorbed anions from soils: 2. Displacement of phosphate by arsenate. Soil Sci. 117:28–33.

Bailey, J. M. 1974. Changes in the adsorbed sulphate status of a yellow-brown earth after phosphate fertilization and legume growth. N.Z. J. Agric. Res. 17:257–265.

Bingham, F. T., and A. L. Page. 1971. Specific character of B adsorption by an amorphous soil. Soil Sci. Soc. Am. Proc. 35:892–893.

Bolt, G. H., and M. G. M. Bruggenwert. 1976. Soil chemistry: A. Basic elements. Elsevier, Amsterdam.

Cary, E. E., and G. Gissel-Nielsen. 1973. Effect of fertiliser anions on the solubility of native and applied selenium in soil. Soil Sci. Soc. Am. Proc. 37:590–593.

Earl, K. D., J. K. Syers, and J. R. McLaughlin. 1979. Origin of the effect of citrate, tartrate and acetate on phosphate sorption by soils and synthetic gels. Soil Sci. Soc. Am. J. 43:674–678.

Fritz, W., and E. U. Schlunder. 1974. Simultaneous adsorption equilibria of organic solutes in dilute aqueous solutions on activated carbon. Chem. Eng. Sci. 29:1279–1282.

Fritz, W., and E. U. Schlunder. 1981. Competitive adsorption of two dissolved organics onto activated carbon: 1. Adsorption equilibria. Chem. Eng. Sci. 36:721–729.

Gissel-Nielsen, G., and B. Bisbjerg. 1970. The uptake of applied selenium by agricultural plants: 2. Utilisation of various selenium compounds. Plant Soil 32:382–396.

Gorlach, E., K. Gorlach, and A. Compala. 1969. The effect of phosphates on the sorption and desorption of molybdates in the soil. Agrochimica 13(6):506–511.

Griffin, R. A., and N. F. Shimp. 1976. Effect of pH on exchange adsorption or precipitation of lead from landfill leachates by clay minerals. Environ. Sci. Technol. 10:1256–1261.

Griffin, R. A., and A. K. Au. 1977. Lead adsorption by montmorillonite using a competitive Langmuir equation. Soil Sci. Soc. Am. J. 41:880–882.

Harter, R. D., and D. E. Baker. 1977. Applications and misapplications of the Langmuir equation to soil adsorption phenomena. Soil Sci. Soc. Am. J. 41:1077–1080.

Hingston, F. J., A. M. Posner and J. P. Quirk, 1971. Competitive adsorption of negatively charged ligands on oxide surfaces. Disc. Faraday Soc. 52:334–342.

Jossens, L., J. M. Prausnitz, W. Fritz, E. U. Schlunder, and A. L. Myers. 1978. Thermodynamics of multisolute adsorption from dilute aqueous solutions. Chem. Eng. Sci. 33:1097–1106.

Kamprath, E. J., W. L. Nelson, and J. W. Fitts. 1956. The effect of pH, sulphate and phosphate concentration on the adsorption of sulphate by soils. Soil Sci. Soc. Am. Proc. 20:463–466.

Lai, S. H., J. J. Jurinak, and R. J. Wagenet. 1978. Multicomponent cation adsorption during convective-dispersive flow through soils: Experimental study. Soil Sci. Soc. Am. J. 42:240–243.

Martin, R. J., and K. S. Al-Bahrani. 1977. Adsorption studies using gas-liquid chromatography: 2. Competitive adsorption. Water Res. 11:991–999.

Metson, A. J., and L. C. Blakemore, 1978. Sulphate retention by New Zealand soils in relation to the competitive effect of phosphate. N.Z. J. Agric. Res. 21:243–253.

Murali, V., and L. A. G. Aylmore. 1983*a*. Competitive adsorption during solute transport in soils: 1. Mathematical models. Soil Sci. 135:143–150.

Murali, V., and L. A. G. Aylmore. 1983*b*. Competitive adsorption during solute transport in soils: 2. Simulations of competitive adsorption. Soil Sci. 135:203–213.

Murrmann, R. P., and M. Peech. 1969. Effect of pH on labile and soluble phosphate in soils. Soil Sci. Soc. Am. Proc. 33:205–210.

Nagarajah, S., A. M. Posner, and J. P. Quirk. 1970. Competitive adsorption of phosphate with polygalacturonate and other organic anions on kaolinite and oxide surfaces. Nature 228:83–85.

Nagarajah, S., A. M. Posner, and J. P. Quirk. 1968. Desorption of phosphate from kaolinite by citrate and bicarbonate. Soil Sci. Soc. Am. Proc. 32:507–510.

Ott, R. J., and P. Rys. 1973. Sorption-diffusion in heterogeneous systems: 6: General behaviour of diffusion controlled competitive processes. J. Chem. Soc. Faraday Trans. 1 69:1705–1710.

Russel, E. W. 1961. Soil condition and plant growth. Longmans, U.K.

Sheindorf, C., M. Rebhum, and M. Sheintuch. 1981. A Freundlich-type multicomponent isotherm. J. Colloid Interface Sci. 79:136–142.

Singh, M., N. Singh, and P. S. Relan. 1981. Adsorption and desorption of selenite and selenate selenium on different soils. Soil Sci. 132:134–141.

Struthers, P. H., and D. H. Sieling. 1950. Effect of organic anions on phosphate precipitation by iron and aluminium an influenced by pH. Soil Sci. 69:205–213.

Swenson, R. M., C. V. Cole, and D. H. Sieling. 1949. Fixation of phosphate by iron and aluminium and replacement by organic and inorganic ions. Soil Sci. 67:3–22.

Thomas, G. W. 1977. Historical developments in soil chemistry: Ion exchange. Soil Sci. Soc. Am. J. 41:230–238.

Aust. J. Soil Res., 1983, **21**, 435–43

The Use of Computer-assisted Tomography to Determine Spatial Distribution of Soil Water Content

J. M. Hainsworth and L. A. G. Aylmore

Department of Soil Science and Plant Nutrition,
University of Western Australia, Nedlands, W.A. 6009.

Abstract

To date no experimental technique has been capable of directly and repetitively measuring spatial distributions of soil water content in a non-destructive manner. The potential of computer assisted tomography (CAT) to overcome this problem has been examined in this paper.

The results obtained from a commercially-produced X-ray CAT scanner and a conventional gamma scanner suggest that CAT scanning can be used to determine spatial changes in soil water content with adequate resolution for soil–plant studies. The technique can clearly be used to resolve spatial changes in soil water content with time. Application of the technique to water uptake by a single plant root shows that CAT scanning presents an extremely exciting possibility for studies of soil–plant water relations.

Introduction

A serious difficulty encountered in attempts to relate soil water to plant response is the fact that the water content in a plant root zone varies markedly in both time and space. The importance of the soil–plant interface is described by Slatyer's (1967) statement that the soil water potential at the root–soil interface appears to be the main soil characteristic controlling the availability of soil water to plant growth. Its value depends on both the soil water potential of the bulk soil, and the potential gradient from the bulk soil to the root surface which develops as a result of the removal of water by the root.

Unfortunately, progress in this area has been hindered largely because of the difficulties associated with direct experimental measurement of soil water content at the root–soil interface and in the soil immediately around the root (So *et al.* 1976). Furthermore, although the soil-water tension or matric suction at a given depth in the root zone may correlate well with plant response in some circumstances and provide a useful basis for irrigation, a clearer understanding of water availability to plants requires some means of resolving changes in soil suction or water content over the entire root zone. Existing techniques for the direct measurement of soil water content or potential are either destructive and hence lack continuity, perturb the sensitive balance being examined, are too slow in their response time, or simply lack the dimensional resolution necessary for meaningful definitions of water content distributions (So *et al.* 1976). Consequently, questions as to the relative magnitude of soil and plant resistance to water movement under different conditions of soil water potential and transpiration demand, and the

0004-9573/83/040435$02.00

extent to which root–soil contact resistance, solute concentration etc. influence water availability, remain largely unresolved and, in some cases, the subject of considerable controversy (Newman 1969*a*, 1969*b*; Passioura 1980).

The ideal technique for monitoring soil water content and soil density distributions in single-root studies and across whole-root networks, should clearly be non-destructive, sufficiently sensitive to follow the relatively rapid changes which occur, and able to resolve differences in water content of less than 0·2% over distances of the order of a few millimetres, particularly in studies of the drawdown associated with single-root systems.

Until 1970 similar problems existed in diagnostic radiology in seeking to obtain non-destructive three-dimensional representations of the human brain. This problem has been essentially overcome by Hounsfield (1972), who developed the technique known as computer-assisted tomography. Computer-assisted tomography (CAT) determines the distribution of the linear attenuation coefficients (μ) of X-rays in a slice which has been scanned linearly at 1–10° intervals for 180° using a collimated radiation source and detector. Commercially available X-ray CAT scanners are capable of detecting differences in attenuation as low as 0·1%, and recently a X-ray CAT scanner has been used by Petrovic *et al.* (1982) to determine spatial changes in soil bulk density. However, such equipment is extremely expensive and unlikely to be generally available for studies of soil–plant systems.

As the change in attenuation of gamma radiation has frequently been used to determine soil water contents (Groenevelt *et al.* 1969; Ryhiner and Pankow 1969) it should be equally possible to apply the CAT scanning technique using considerably cheaper gamma systems to determine the spatial variation in soil water content. This paper presents a preliminary examination of the possibility of using CAT scanning to examine spatial changes in soil water content using both a commercial X-ray scanner and a modified gamma scanner.

Theory

In computer-assisted tomography (CAT) a slice of the object under examination is divided into a M × M matrix consisting of small squares called pixels. The purpose of CAT is to determine the densities of each pixel. A cartesian (x, y) coordinate system is used to describe points in the slice under examination (Fig. 1). The purpose of the scanning process is to determine the attenuation coefficient $\mu(x, y)$ for each point in the slice. As the slice is scanned, ray paths through the slice can be defined by the angle (ϕ) of the ray with respect to the y axis and r, its distance from the origin (Fig. 1). The position on any ray path is given by the coordinate s.

The attenuation of the ray (r, ϕ) with initial intensity I_0 and transmitted intensity I is given by

$$I = I_0 \exp\left| -\int \mu(x, y)\, ds \right| \tag{1}$$

and the integral of $\mu(x, y)$ along the ray is defined by

$$p(r, \phi) = \int_{r,\phi} \mu(x, y)\, ds, \tag{2}$$

where $p(r, \phi)$ is the ray projection. By combining equations (1) and (2)

$$p(r, \phi) = \ln(I_0/I). \tag{3}$$

In the scanning process, values of $p(r, \phi)$ are determined using equation (3) for each family of parallel lines. In theory if $p(r, \phi)$ is known for every line of width ω passing through a small square (pixel) of dimension ω then $\mu(x, y)$ can be determined if equation (2) can be inverted (Panton 1981). Bracewell (1956) was the first to devise a numerical reconstruction technique for determining $\mu(x, y)$ from equation (2), given $p(r, \phi)$, and with subsequent advances there are now 13 different methods of reconstructing $\mu(x, y)$ (Budinger and Gullberg 1974). However, it is

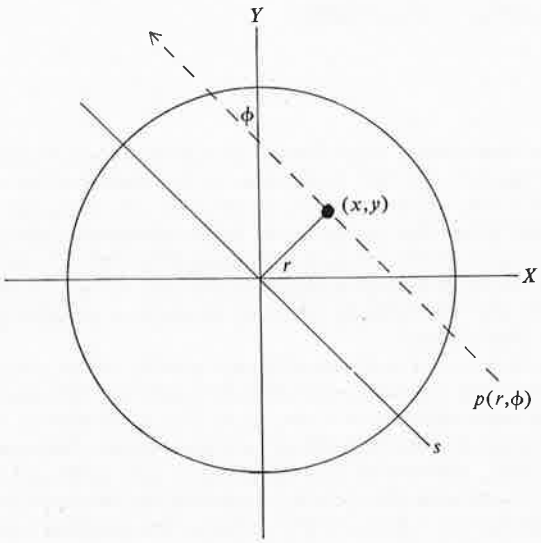

Fig. 1. Coordinate system for calculation of net attenuation of transmission in a given pixel. Rays are specified by their angle (ϕ) with the Y-axis their distance from the origin (r).

possible to clarify the approaches broadly into three methods: (i) back-projection, (ii) iterative reconstruction and (iii) analytical reconstruction (Brooks and Di Chiro 1975, 1976). Of the three methods, analytical reconstruction is the most commonly used, and is considered to be the most accurate (Panton 1981). The basis of the analytical methods involves a fundamental relationship between the Fourier transform of the linear attenuation function $\mu(x, y)$ and the projection function $p(r, \phi)$. Such a relationship filters the projection accounting for the portions of the projection which may pass outside a given pixel. The filtered projection is then back-projected using the following equation:

$$\mu(x, y) = \sum_{j=1}^{m} p(x \cos\phi_j + y \sin\phi_j, \phi_j)\Delta\phi. \tag{4}$$

The result of image reconstruction is initially to produce an array of numbers representing the values of μ for each pixel. However, in commercial CAT scanners it has been found to be more convenient to express the values of μ as Hounsfield units (H) which are defined by the equation

$$H = \frac{\mu - \mu_{\text{water}}}{\mu_{\text{water}}} \times 1000. \tag{5}$$

For the case of wet soil the μ term can be expanded to

$$\mu_{\text{wet}} = \mu_s \rho_s + \mu_w \theta_v, \tag{6}$$

where μ_s and μ_w are the mass attenuation coefficients of soil and water and ρ_s and

θ_v the soil bulk density and volumetric water content respectively. When the soil is dry $\theta_v = 0$ and

$$\mu_{dry} = \mu_s \rho_s. \quad (7)$$

Thus θ_v can be calculated from a combination of equations (6) and (7) to give

$$\theta_v = (\mu_{wet} - \mu_{dry})/\mu_w \quad (8)$$

or for Hounsfield units

$$\theta_v = (H_{wet} - H_{dry})/1000. \quad (9)$$

Materials and Methods

Instrumentation

An EMI CT 1007 scanner was used for these studies. This scanner is an early model which employs two X-ray tubes and NaI detectors, enabling two 1 cm slices of the object to be examined at the same time. During a scan time of approximately 1 min, 160 measurements are taken for each linear scan and 60 linear scans through 180° are completed. From these measurements linear attenuation coefficients, expressed as Hounsfield units, are mapped into a 160 by 160 pixel array using filtered back-projection. The size of each pixel is 1·5 by 1·5 mm. In all the present studies the X-ray tube voltage was set at 120 kV. At this voltage μ_{water} equals 0·191 cm^{-1} (McCullough 1975) and the standard deviation in H is approximately 4 units (Brooks and Di Chiro 1976).

In the concentric ring experiment (described later), a conventional gamma scanning system was used. This scanner utilized a 2 mm wide by 5 mm long collimated americium–241 source and NaI detector, giving a pixel size of 2 mm by 2 mm, and a slice thickness of 5 mm. As the source and detector were fixed, the concentric ring pot was moved across the beam and scanned at 2 mm intervals. This resulted in 35 points in the linear scan. At each point, twenty-seven 10 s measurements were taken and then averaged. As the pot had circular symmetry, the mean data for the 35 points of the linear scan could be back-projected using filtered back-projection for a given number of angles. The minimum number of angles required is given by $n\pi/4$, where n is the number of points in the linear scan (Panton 1981). Thus, the data for the linear scan were back-projected at $35\pi/4 = 27$ times at 6·667° intervals through 180°. Whilst back-projecting the data fewer times at larger intervals was also tried, this approach was discontinued as the resultant images were clearly inaccurate. Once the 27 back-projections had been completed, the linear absorption coefficients were then mapped onto a 35 by 35 pixel array.

Experimental

In all the experiments, a surface sandy loam from Bakers Hill, W.A., was used. The three experiments conducted were as follows:

Concentric ring pot

Three 7 cm tall concentric acrylic rings with diameters 7·0, 5·0 and 1·5 cm respectively were uniformly packed with soil. Each ring was then equilibrated at a given water content, the outside ring having the highest water content and the inner ring the lowest (Table 1). As the pot had to be horizontally placed in the EMI scanner, the top of the pot was packed with plasticene to keep the soil in place. When the EMI scanner was used, the inner ring was kept dry and θ_v of the two other rings determined by using the mean Hounsfield units in each ring and equation (9). However, when the experiment was repeated using the gamma scanning system, the concentric ring pot was first scanned with the soil in the rings dry and then rescanned after water had been added and allowed to equilibrate. Water content for each pixel was then obtained using equation (8). The water content of the soil in each ring after wetting was determined gravimetrically by taking a series of 2 g samples after the scanning process had been completed.

Artificial root (alundum tube) experiment

A 7 cm diameter, 12 cm tall Perspex pot was packed with soil. A length of alundum tubing, 1·5 mm outer diameter and 0·6 mm inner diameter, was inserted through the centre of the pot. Each end of the alundum tubing was connected to plastic tubing which passed through small holes in the ends

of the pot. The pot was then placed in the horizontal position and inserted into the EMI scanner, and a single slice scanned. One end of the plastic tubing was then connected to a water reservoir, the level of which was approximately 50 cm above the alundum tubing, with the other end sealed. As water flowed into the alundum tubing and then into the soil, scans of the same slice were made at 1, 10, 15 and 20 min after watering commenced. The water content of each pixel at each time was then determined using equation (8).

Water uptake by a single root

A radish seed was planted in a 7 cm diameter, 12 cm tall pot, packed with soil. Seven days after germination, the pot was watered to field capacity, the surface packed with plasticene and a slice 4 cm from the top of the pot scanned using the EMI scanner. The same slice was rescanned 7 and 20 days later. On these days, transpirational losses were measured by changes in weight of the pot. Root diameter was determined to be 0·1 cm and the root length involved in water uptake approximately 12 cm on day 20. Changes in water content around the plant root could be calculated using the expression

$$\text{Decrease in } \theta_v \text{ from field capacity} = (H_{\text{field cap.}} - H_o)/1000,$$

where H_o is the Hounsfield number at day 7 or 20. As the water content at field capacity was known, the water content of each pixel could be determined.

Results and Discussion

The results of the concentric ring experiment are presented in Table 1 and Fig. 2. The differences in the water content for the soil within different rings could be readily observed using both the EMI scanner and the gamma scanner (Fig. 2). The attenuation of the acrylic tubing is vastly different to that of the soil–water system and hence has been eliminated from Fig. 2. The standard deviations cited in Table 1 refer to the actual variation in water content measured within each ring and not those associated with errors in determination. Detectable differences in attenuation of 0·1% would represent measurable differences in water content of 0·006 g/cm^3, and would thus be comparable with the accuracy of gravimetric determinations.

Table 1. A comparison between calculated θ_v using CAT and θ_v determined gravimetrically for both the X-ray CAT scanner and the gamma scanner in the concentric ring experiment[A]

Scanner	Ring	Water content (g/cm^3) θ_v (CAT)	θ_v (Grav.)
X-ray	Outer	0·180 ± 0·065	0·175 ± 0·041
	Middle	0·063 ± 0·060	0·075 ± 0·022
	Inner	0·000 ± 0·020	0·000 ± 0·001
Gamma ray	Outer	0·350 ± 0·040	0·325 ± 0·045
	Middle	0·142 ± 0·040	0·150 ± 0·020
	Inner	0·000 ± 0·060	0·001 ± 0·001

[A] The standard deviations cited refer to the actual variation in water content measured within each ring and not those associated with errors in determination.

Whilst the calculated values of θ_v are comparable to the measured values (Table 1), examination of the results shows that in both cases the calculated values of θ_v are higher than the measured values for the outer ring and lower for the middle ring. This was originally thought to arise from what is known as the Gibbs phenomenon, where large changes in μ from high density to low density areas cause the calculated values in the low density area to be less than the actual μ in that region (Brooks and Di Chiro 1976). Such an effect could lead to the underestimation of μ and hence θ_v in the middle ring, and also the overestimation of μ and θ_v in the outer ring, since

the attenuation of the beam is measured after passing through both rings. However, subsequent examination of the data suggests that the limiting of the spatial frequencies in the Fourier transform of the projection functions may be responsible for this effect rather than the Gibbs phenomenon, which usually only occurs over the width of a few pixels. The combined effects of the Gibbs phenomenon and spatial limiting of the Fourier transformation arise from the stepped nature of θ_v in the concentric ring experiment. This results in a doming effect within each ring (see in particular the inner ring in Fig. 2), and consequently a large standard deviation in θ_v. However, in soil-plant systems, changes in θ_v are unlikely to be discontinuous but of a more gradual nature, and such difficulties should not arise in normal experimentation. The standard deviation in θ_v in the artificial root experiment described later is, for example, 0·006 g/cm^3. Furthermore, both the problems of limiting of spatial frequencies and the Gibbs phenomenon can be overcome by appropriate techniques (Bracewell 1965; Brooks and Di Chiro 1976).

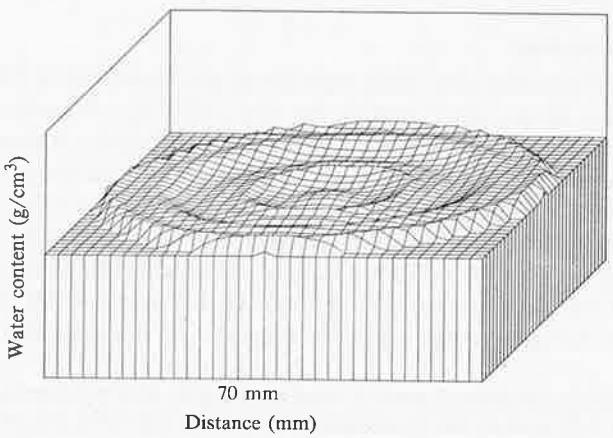

Fig. 2. Three-dimensional plot showing different water contents in soil packed in three concentric acrylic rings obtained by application of CAT to gamma scanning measurements.

A further problem encountered with the EMI scanner was the large (20*H*) standard deviation in each ring which corresponds to a standard deviation in calculated θ_v of 0·02 g/cm^3. However, Petrovic *et al.* (1982) found similar variations in H for dry soil. Thus, calculated water contents using this scanner would have been more uniform if the pot had been scanned dry first, enabling the natural variation in H dry to be accounted for. This concentric ring experiment clearly demonstrates the potential of computer-assisted tomography in measuring changes in water content within soil systems. However, the examination of water uptake by plant roots also requires the resolution of spatial changes in θ_v with time.

The spatial changes in θ_v with time for the alundum tube experiment can be seen in Figs 3*a–d*. As expected, the zone into which water has infiltrated increases with time and is readily mapped by the CAT approach. It is interesting to note the persistence and reproducible location by the CAT scanning technique, of a depression in the infiltration zone in Figs 3*a–d*, which presumably arises as a result of an air pocket. Outside the zone of infiltration θ_v should be uniform and equal to zero. At t = 20 min, the calculated values of θ_v in the outer zone were however

$0{\cdot}002 \pm 0{\cdot}006$. This non-conformity can be explained by the standard deviation of $4H$ for each pixel. As θ_v is calculated by the difference between two Hounsfield numbers, ideally the standard deviation of θ_v should be $(\sqrt{2} \times 4)/1000$, which is equal to the calculated standard deviation. An increase in H due to compaction of the dry soil caused by swelling of the wet soil in the middle of the pot may explain why $\bar{\theta}_v$ is greater than zero. In swelling soils increased accuracy could be obtained by using the dual source method of Bridge (1971). Despite this relatively minor problem the alundum tube experiment demonstrated that spatial changes in θ_v with time of the order of $0{\cdot}006$ g/cm^3 can be readily resolved using CAT. Clearly there is no reason why the reverse phenomenon of water uptake by plant roots using this technique should not be equally amenable to this approach.

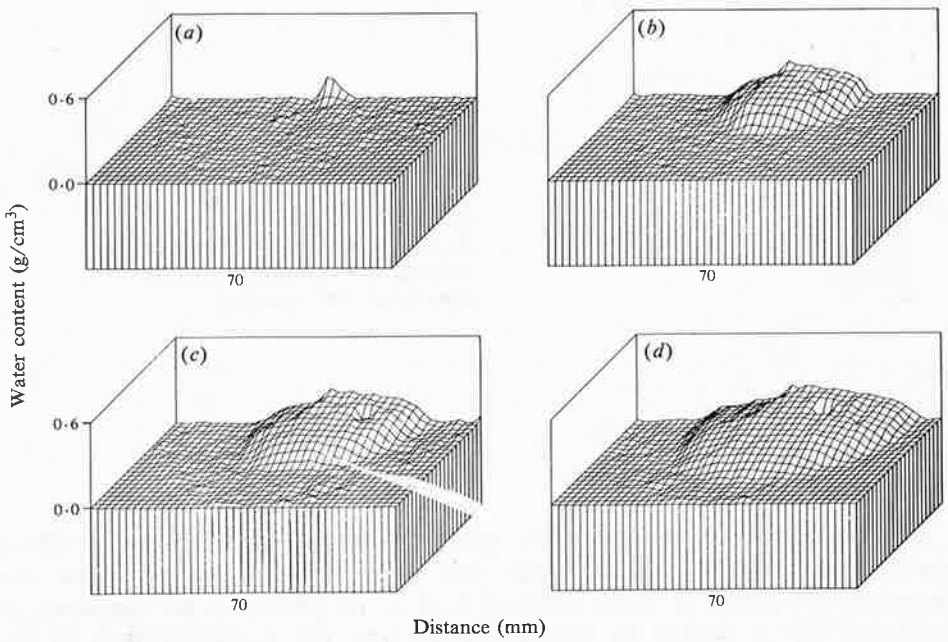

Fig. 3. Half-slice three-dimensional plots showing changes in soil-water content with time due to the infiltration of water into a soil column from an artificial root (alundum tube). Representations at (*a*) 1 min, (*b*) 10 min, (*c*) 15 min and (*d*) 20 min infiltration are illustrated.

Fig. 4 shows the spatial distribution of water content from a radish root to bulk soil at day 7 and day 20 respectively. The change in the drawdown with time is clearly shown and readily resolved over distances of $1{\cdot}5$ mm.

Transpiration rates at days 7 and 20 were calculated to be $0{\cdot}1$ and $0{\cdot}02$ cm^2/h respectively. For the drawdown curves presented to correspond to the predictions of Gardner's (1960) model, soil water diffusivities at the outside edge of the pot would have to be approximately $0{\cdot}35$ cm^2/h at day 7 and $0{\cdot}09$ cm^2/h at day 20. These calculated diffusivities are at least one order of magnitude smaller than the diffusivities of $2{\cdot}32$ and $1{\cdot}84$ cm^2/h determined by the method of Bruce and Klute (1956). However, the calculated diffusivities are of the same order of magnitude as the measured diffusivities for the water contents of the pixel adjacent to the plant root of $0{\cdot}13$ cm^2/h at day 7 and $0{\cdot}08$ cm^2/h at day 20. These results highlight the disparity between theoretical and experimentally determined drawdowns.

Gamma scanning systems are considerably cheaper to construct than commercially available X-ray systems and are likely to be more accessible to workers in this field. The ideal source should show essentially linear attenuation and be of an energy level to provide maximum sensitivity to changes in water content. Caesium–137 sources, which are valuable for measuring bulk water content changes, were found less suitable for the present application due to relative insensitivity to small changes in water content over small distances, and difficulties in achieving a linear attenuation coefficient with soil column thickness as counting losses from double peaks and electronic dead time which may occur with high-power caesium–137 sources (Bridge 1971).

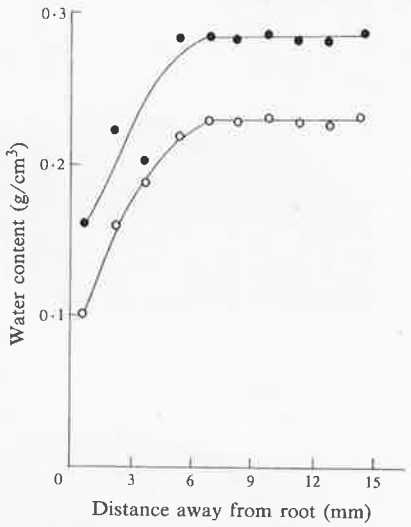

Fig. 4. Drawdowns of soil water content in proximity to a radish root after (*a*) 7 days' (●) and (*b*) 20 days' (○) transpiration following watering to field capacity measured using X-ray CAT scanning.

An americium–241 source, while suitable with respect to both the above requirements, has the disadvantage that the maximum output from the americium–241 source is of the order of $5{\cdot}57 \times 10^7$ photons/s per steradian, as americium–241 is limited by self absorption and has a narrow peak in the scintillation detector. Consequently a single measurement, for example, on the plant root system, would involve a total counting time of some 90 min, thus precluding the following of rapid changes in soil water content associated with plant water uptake. However, the authors are currently examining the use of a 1 Ci ytterbium–169 source, since the available output can be increased to approximately 6×10^8 photons/s per steradian, and counting times for each scan should then be reduced to approximately 5 min. The energy levels of the gamma radiation from a ytterbium source (0·063 MeV) are similar to that of the americium (0·06 MeV) isotope and should provide a similar sensitivity to changes in water content. Its major disadvantage will be its relatively short half-life of 31 days, which would provide a working life of only some 2 months compared with the many years use of an americium source.

Despite the above difficulties, these experiments indicate that the application of CAT to soil–plant studies possesses an extremely exciting potential. With refinements such as additional filtering to eliminate the Gibbs phenomenon, there seems no real reason why this technique will not ultimately become a major

research tool for studies of soil–plant water relations. It seems equally likely that the measurement of sequences of overlapping tomographs should enable accurate three-dimensional representations of soil structural configurations to be constructed, and this possibility is currently being examined by the authors.

Acknowledgments

The authors gratefully acknowledge the assistance of Dr John Glancy and the staff of the Radiology Department at the Sir Charles Gairdner Hospital, and the advice of Mr L. Munslow-Davies of the Radiation Protection Office at the Queen Elizabeth II Medical Centre and Dr C. J. Barnes of this department.

References

Bracewell, R. M. (1956). Strip integration in radio astronomy. *Aust. J. Phys.* **9**, 198–217.

Bracewell, R. M. (1965). 'The Fourier Transform and its Application.' p. 193. (McGraw-Hill: New York.)

Bridge, B. J. (1971). The effect of ground surface conditions on water movement and storage in cracking clay soils. Ph.D. Thesis, University of Sydney.

Brooks, R. A., and Di Chiro, G. (1975). Theory of image reconstruction in computed tomography. *Radiology* **117**, 561–72.

Brooks, R. A., and Di Chiro, G. (1976). Principles of computer-assisted tomography (CAT) in radiographic and radioisotopic imaging. *Phys. Med. Biol.* **21**, 689–732.

Bruce, R. R., and Klute, A. (1956). The measurement of soil water diffusivity. *Soil Sci. Am. Proc.* **20**, 458–62.

Budinger, T. F., and Gullberg, G. T. (1974). Three dimensional reconstruction in nuclear medicine emission imaging. *IEEE Trans. Nucl. Sci.* NS-**21**, 2–20.

Gardner, W. R. (1960). Dynamic aspects of water availability to plants. *Soil Sci.* **89**, 63–73.

Groenevelt, P. H., de Swart, J. G., and Cirler, J. (1969). Water content measurement with 60 keV gamma ray attenuation. *Bull. Int. Assoc. Sci. Hydrol.* **14**(2), 67–78.

Hounsfield, G. N. (1972). A method of and apparatus for examination of a body by radiation such as X- or gamma-radiation. Brit. Pat. No. 1283915, London.

McCullough, E. C. (1975). Photon attenuation in computed tomography. *Med. Phys.* **2**, 307–20.

Newman, E. I. (1969*a*). Resistance to water flow in soil and plant. I. Soil resistance in relation to amounts of root: theoretical estimation. *J. Appl. Ecol.* **6**, 1–12.

Newman, E. I. (1969*b*). Resistance to water flow in soil and plant. II. A review of experimental evidence on the rhizosphere resistance. *J. Appl. Ecol.* **6**, 261–72.

Panton, D. M. (1981). Mathematical reconstruction techniques in computer axial tomography. *Math. Sci.* **6**, 87–102.

Passioura, J. B. (1980). Transport of water from soil to shoot in wheat seedling. *J. Exp. Bot.* **31**, 333–45.

Petrovic, A. M., Siebert, J. E., and Lieke, P. E. (1982). Soil bulk density analysis in three dimensions by computed tomographic scanning. *Soil Sci. Soc. Am. J.* **46**, 445–50.

Ryhiner, A. H., and Pankow, J. (1969). Soil moisture measurement by the gamma transmission method. *J. Hydrol.* **9**, 194–205.

Slatyer, R. O. (1967). 'Plant–Water Relationships.' (Academic Press: London.)

So, H. B., Aylmore, L. A. G., and Quirk, J. P. (1976). Measurement of water fluxes in a single root system. I. The tensiometer–potometer system. *Plant Soil* **45**, 577–94.

Manuscript received 1 March 1983, accepted 24 May 1983

Aust. J. Soil Res., 1984, **22**, 31–41

A Theoretical Treatment of the Effects of Ionic and Non-Ionic Competitive Adsorption during Solute Transport in Soils

C. J. Barnes[A,B] *and L. A. G. Aylmore*[A]

[A] Department of Soil Science and Plant Nutrition,
University of Western Australia, Nedlands, W.A. 6009.
[B] Present address: Division of Water and Land Resources, CSIRO, P.O. Box 1666, Canberra, A.C.T. 2601.

Abstract

The method of characteristics is used to analyse multi-species solute movement through a non-linearly reactive soil taking dispersion into account. Both ionic and non-ionic solutes are considered, and it is shown that the shape of a solute front depends on the shape of the adsorption isotherms. At large times, overall solute movement is effected by a series of solute fronts moving independently. The composition of each front, and hence individual solute concentrations within the front, are determined by the degree of competition reflected in the adsorption isotherms.

Varying water contents are considered explicitly, although the detailed analysis is restricted to uniform water contents for simplicity.

Introduction

In recent publications, Murali and Aylmore have indicated the importance of non-linearity in the adsorption isotherms (Aylmore and Murali 1981; Murali and Aylmore 1981*a*), and of competitive adsorption (Murali and Aylmore 1981*b*, 1982*a*, 1982*b*, 1983). They reported both experimental evidence and numerical simulations in support of their arguments. The simulations were performed using 'brute force' techniques involving finite difference schemes to solve the non-linear equations numerically. Consequently, while they obtained qualitative similarity between experimental and theoretical results, each simulation is strictly only valid for the particular conditions assumed for the simulation, and this approach is not capable, without much repetitive calculation, of indicating the general effect of a particular assumption on the shape of the solute profiles or breakthrough curves (BTC's).

In this paper we consider the process of competitive solute transport from the more general theoretical standpoint of Charbeneau (1981), and the general features of both the experimental results and simulations are explained. The present work is not restricted to uniform water contents, so that it applies also to the recently published work of several other authors (Bond *et al.* 1982; Smiles and Gardiner 1982; Laryea *et al.* 1982). The general shape of the solute front is seen to depend on a small number of parameters, including the convexity or otherwise of the adsorption isotherm, and for competitive adsorption, on the extent of the competition.

0004-9573/84/010031$02.00

Single Component Adsorption

In this section certain aspects of single component adsorption are reviewed in order to demonstrate some theoretical consequences of non-linear adsorption, and also to enable use to be made of these results in the next section on competitive adsorption. While few of these results are novel, being inherent in much of the early chromatography literature, for example, their application to solute movement in soils does not appear to be well known.

The equation for solute transport may be written

$$\partial(\theta c + \rho s)/\partial t = D_s \partial^2 c/\partial x^2 - \partial(Vc)/\partial x, \tag{1}$$

where x and t are the space and time variables respectively, c is the solute concentration in the soil liquid, ρ is the soil bulk density, s the specific adsorption and D_s the apparent diffusion coefficient of the solute in the soil water at the convective velocity V.

Assuming a homogeneous porous medium and a uniform convective velocity V, dimensionless variables

$$x' = Vx/D_s \quad \text{and} \quad t' = V^2 t/D_s$$

can be defined. If an instaneous adsorption isotherm of the form $s = s(c)$ is also assumed, equation (1) can be rewritten

$$(\theta + \rho \mathrm{d}s/\mathrm{d}c)\, \partial c/\partial t' = \partial^2 c/\partial x'^2 - \partial c/\partial x'. \tag{2}$$

Replacing c by x' as the dependent variable, and assuming $\partial c/\partial x' \neq 0$, equation (2) may be recast in the form

$$\partial x'/\partial t' = (\theta + \rho \mathrm{d}s/\mathrm{d}c)^{-1}\{ 1 - \partial(\partial c/\partial x')/\partial c \} \tag{3}$$

(cf. Philip 1969, equation (85)).

Under appropriate boundary and initial conditions, this equation can be solved by the same methods as used by Philip, in the above reference, for the infiltration equation. However, such a solution is only appropriate for short times, although the radius of convergence of the resulting solution (possibly infinite) is not known. Bear (1972, p. 607) implies that for Peclet numbers in the range 1–10 or greater, the characteristic length D_s/V is of the order of the mean grain size of the porous medium, so that $x' >> 1$ or equivalently, $t' >> 1$ except for points very close to the surface, or at very early times. The consequence is that (particularly for BTC's) the influence of initial conditions may be expected to be small, and for constant boundary conditions we may expect the solute front to exhibit a 'profile at infinity' (Philip 1957).

Following Philip (1957) we note that there are really only two possibilities for a given solute 'profile at infinity' — either it will spread out so that the profile becomes progressively more diffuse, or it will tend to a fixed shape which will then be convected unchanged down the profile. In the first case, note that the second term on the right-hand side of equation (3) becomes arbitrarily small, so that the region of a given concentration c is convected with speed $(\theta + \rho \mathrm{d}s/\mathrm{d}c)^{-1}$ down the profile.

Consider the boundary conditions

$$c = c_0 \text{ at } x' = 0, \text{ and } c = c_\infty \text{ at } x' = \infty;$$

and assume the concentration c is in a region where the absorption isotherm is convex ($\mathrm{d}^2 s/\mathrm{d}c^2 < 0$). Then higher concentrations will travel at greater speed,

tending to contract the front if $c_0 > c_\infty$. As a result, in convex regions of the absorption isotherm the solute front will remain sharp, the tendency of the profile to contract in the above manner being balanced by the diffusing effect of dispersion under these conditions.

Following Charbeneau (1981) or otherwise, we can show that if the region of convexity is $c_1 < c < c_2$, concentrations in that range will advance in a relatively sharp front with velocity down the profile of

$$\partial x'/\partial t' = \left(\theta + \rho \frac{s_2 - s_1}{c_2 - c_1}\right)^{-1}. \tag{4}$$

Conversely, for concave regions the solute front will be diffuse, individual concentrations being convected with velocity down the profile of

$$\partial x'/\partial t' = (\theta + \rho \mathrm{d}s/\mathrm{d}c)^{-1} \tag{5}$$

which tends to diffuse the front still further. We note that in both cases the speeds at which individual concentrations are transported are bounded by the quantities

$$\left(\theta + \rho \mathrm{d}s/\mathrm{d}c|_{c=c_1}\right)^{-1} \text{ and } \left(\theta + \rho \mathrm{d}s/\mathrm{d}c|_{c=c_2}\right)^{-1},$$

so that predictions from linear isotherms of corresponding slopes would give upper and lower bounds on solute displacement.

Alternatively, for $c_0 < c_\infty$ the same sort of analysis shows that the roles of convex and concave regions of the isotherm are reversed. The consequence of this is that the breakthrough and breakback curves (low to high, and high to low concentrations, respectively) for a particular solute will not be symmetric for non-linear isotherms, in contrast to the behaviour of linear isotherms. So, for example, a pulse of solute having a convex isotherm travelling down a long column will exhibit a sharp leading edge combined with a diffuse trailing edge. By examining the large time behaviour of equation (3), it can be shown that the width of the diffuse interface will grow linearly with time, whereas for a linear isotherm the rate of growth is slower, proportional to $t^{1/2}$.

It is interesting to note that under the assumption of a constant convective velocity the solute flux can be written as proportional to the gradient of a solute 'potential'. As a result of this there is a one-to-one correspondence between the infiltration equation (e.g. Philip 1969) and the above equations for solute movement. This correspondence is accomplished by identifying water content and soil water potential with total salt and the logarithm of concentration respectively. Then the above equations correspond to the special case of the infiltration equation where the hydraulic conductivity is an exponential function of the soil water potential. The correspondence extends to the phenomenon of hysteresis; hysteresis in the soil water potential–water content relationship is equivalent to hysteresis in the adsorption–concentration relationship.

As a result, methods developed earlier to deal with infiltration of water may be immediately transferred to solute movement in reactive systems. For example, the results of Philip (1969) imply that in two and three dimensions solute movement from a line or point source respectively leads to stationary profiles, where the region in which the solute concentration varies appreciably from the initial one is finite. However, because the length scale is small, of the order of the mean grain size as discussed above, for normal convective velocities convection always dominates diffusion, and the solute profiles are effectively vertical (cf. Figs 11 and 12 of Philip 1969).

Finally, in this section we must indicate the criteria under which these asymptotic features of equation (3) will apply. Generally we may expect that under mildly non-linear or nearly linear conditions the reduced tendency of the interface to contract will allow a much greater spread of the interface due to diffusion, so that much greater times will be required in these cases before the effects of non-linearity become apparent. This suggests that the condition of large time should be replaced more formally by a condition reflecting the degree of non-linearity. For example, such a condition for convex isotherms is

$$t' >> \{\partial x'/\partial t' \left(\theta + \rho \frac{s - s_1}{c - c_1}\right) - 1\}^{-1}$$

where $\partial x'/\partial t'$ is given by equation (4).

Multi-Component Adsorption

Charbeneau (1981) has presented an analysis of multi-species solute movement applicable to any number of solutes, under the assumption that dispersion is negligible. Since only the shape and not the position of the solute front (i.e. the velocity of propagation) depends on the dispersion term at large times, this analysis gives a fairly accurate qualitative understanding of the process for non-linear adsorption.

This work should also be placed in the context of the earlier work of Wilson and Gelhar (1981). They used the method of characteristics to investigate the case of single component adsorption under non-steady and unsaturated conditions, including the effect of dispersion by considering it as a perturbation on the process of convection. The present work is more general than theirs, considering more than one solute species; but their consideration of the effects of water movement goes beyond the present treatment.

Here we shall be considering competitive adsorption between only two species, while generalizing Charbeneau's work to include more general adsorption isotherms, and including non-ionic competition. Two-component adsorption will be the most important practically; in addition the general features of competitive adsorption are illustrated with the minimum degree of complexity.

Assuming again that adsorption is effectively instantaneous, but that isotherms depend on the concentrations of both species, under the same assumptions as for equation (2) the transport equations are

$$(\theta + \rho\partial s_1/\partial c_1)\,\partial c_1/\partial t' + \rho\partial s_1/\partial c_2 \partial c_2/\partial t' = \partial^2 c_1/\partial x'^2 - \partial c_1/\partial x' \qquad (6a)$$

$$\rho\partial s_2/\partial c_1 . \partial c_1/\partial t' + (\theta + \rho\partial s_2/\partial c_2)\partial c_2/\partial t' = D_2 \partial^2 c_2/\partial x'^2 - \partial c_2/\partial x', \qquad (6b)$$

where the dispersion coefficient of species 1 has been used to define the dimensionless distance and time variables x' and t' (cf. the previous section) and D_2 is the ratio of the two dispersion coefficients.

Following Charbeneau, we find that equation (6) may be rewritten in terms of the characteristics q_1 and q_2 as

$$\lambda_1 \partial q_1/\partial t' = -\partial q_1/\partial x' + \beta\{S_{21}\partial^2 c_1/\partial x'^2 - \tfrac{1}{2}S_-(1+k)D_2\partial^2 c_2/\partial x'^2\} \qquad (7a)$$

$$\lambda_2 \partial q_2/\partial t' = -\partial q_2/\partial x' + \gamma\{\tfrac{1}{2}S_-(1+k)\partial^2 c_1/\partial x'^2 + S_{12}D_2\partial^2 c_2/\partial x'^2\}, \qquad (7b)$$

where

$$\lambda_1 = \theta + \rho s_{11} - \tfrac{1}{2}\rho S_-(1-K) \qquad (8a)$$

$$\lambda_2 = \theta + \rho s_{22} + \tfrac{1}{2}\rho S_-(1-K) \tag{8b}$$

$$K^2 = 1 + 4S_{12}S_{21}/S_-^2$$

$$S_- = S_{11} - S_{22}, \quad \text{and} \quad S_{ij} = \partial s_i/\partial c_j$$

and β and γ are integrating factors for the differential equations

$$\mathrm{d}q_1/\beta = S_{21}\mathrm{d}c_1 - \tfrac{1}{2}S_-(1+k)\mathrm{d}c_2 \tag{9a}$$

$$\mathrm{d}q_2/\gamma = \tfrac{1}{2}S_-(1+k)\mathrm{d}c_1 + S_{12}\mathrm{d}c_2. \tag{9b}$$

By changing the dependent variable, equations (7) may be written

$$\lambda_1(\partial x'/\partial t')\big|_{q_1} = 1 - \beta\{S_{21}\partial/\partial \mathrm{q}_1(\partial c_1/\partial x')_{t'} - \tfrac{1}{2}S_-(1+k)D_2\partial/\partial q_1(\partial c_2/\partial x')t'\} \tag{10a}$$

$$\lambda_2(\partial x'/\partial t')\big|_{q_2} = 1 - \gamma\{\tfrac{1}{2}S_-(1+k)\partial/\partial q_2(\partial c_1/\partial x')\big|_{t'} + S_{12}\partial/\partial q_2(\partial c_2/\partial x')\big|_{t'}\}. \tag{10b}$$

In equation (10a) the independent variables are q_1 and t', whereas in equation (10b) they are q_2 and t'. The notation is intended to indicate that differentiation on the left-hand side of equations (10a) and (10b) is for fixed q_1 and q_2 respectively, whereas on the right-hand side t is kept constant.

Equations (10) are the result needed for the subsequent discussion in this paper, but they appear rather daunting in form. The second term on the right-hand side of these equations in clearly due to dispersion, being the sum of terms involving the product of a diffusivity and a concentration gradient. If this term is ignored for the moment, we see that the rate of movement of a particular value of q_1 or q_2 down the profile is simply given by λ_1^{-1} or λ_2^{-1} respectively, *independent of each other*. Since λ_1 and λ_2 will not be equal in general, after a sufficient time the region in which q_1 is varying will be in a region in which q_2 is constant, and vice versa.

Inclusion of the dispersion terms does not alter this picture, so that for large times the second term on the right-hand side of equation (10a) represents the dispersion of q_1 about a front, for instance. The shape of the front will depend on whether λ_1 is an increasing or decreasing function of q_1 for the particular (constant) value of q_2, by analogy with the single component analysis. In this region c_1 and c_2 do not vary independently, but are restricted by the condition that q_2 is constant. Similar remarks apply to the region in which q_1 is constant, but q_2 varies. As these two 'fronts' move apart, they will be separated by a growing region in which both q_1 and q_2 (and hence c_1 and c_2) are constant. A breakthrough curve for this situation is shown schematically in Fig. 1. In the two frontal regions variations in c_1 and c_2 are connected by the equations

$$q_1(c_1, c_2) = \text{const. or } q_2(c_1, c_2) = \text{const.}$$

So for the case where $S_{11} > S_{22}$ ($S_- > 0$), $\lambda_1 > \lambda_2$ and the q_2-front will proceed faster than the q_1-front; after a time the profile will consist of:

Region I

$$q_1 = q_1^\infty; \qquad q_2 = q_2^\infty \qquad (c_1 = c_1^\infty,\ c_2 = c_2^\infty).$$

Region II

$q_1 = q_1^\infty$, q_2 lies between q_2^0 and q_2^∞, changing monotonically between these two limits. Values of c_1 and c_2 lie between the limits c_1^∞ and c_1^*, and c_2^∞ and c_2^* respectively, where c_1^* and c_2^* are fixed values discussed below. Changes in c_1 and c_2 are related by the equation

$$dc_1/dc_2 = -2S_{12}/[S_-(1+K)], \tag{11}$$

which can be integrated to give the required variation of c_1 and c_2 in this region.

Region III

$$q_1 = q_1^\infty,\ q_2 = q_2^\circ; \qquad (c_1 = c_1^*,\ c_2 = c_2^*).$$

Region IV

q_1 varies monotonically between the limits q_1° and q_1^∞, while $q_2 = q_2^\circ$. Variations in c_1 and c_2 are related by

$$dc_2/dc_1 = 2S_{21}/[S_-(1 + K)], \tag{12}$$

with c_1 and c_2 varying between c_1^* and c_1^∞, and c_2^* and c_2^∞ respectively. Values of c_1^* and c_2^* are determined by the intersection of the relationship derived from equation (11) with starting values c_1^∞ and c_2^∞, and the relationship derived from equation (12) with starting values c_1° and c_2°.

Region V

$$q_1 = q_1^\circ,\ q_2 = q_2^\circ; \qquad (c_1 = c_1^\circ,\ c_2 = c_2^\circ).$$

The values of c_1^* and c_2^* depend on the form of the adsorption isotherms, and in particular the degree of competition between the solutes for the adsorption sites, measured by the cross terms S_{12} and S_{21}. For example, it is possible for one or other of these values (in Region III) to be higher or lower than both the boundary and initial values (in Regions I and V). This is seen more clearly in the following example.

Example: $S_{21} = 0$

This is the example considered explicitly by Charbeneau for ionic competition; unfortunately, as we shall see in the next section, the model is not strictly applicable in his case. If the adsorption of species 2 is assumed to be independent of the concentration of species 1, the analysis is greatly simplified. Let us assume that $S_{22} > S_{11}$, and that a solution with concentrations c_1° and c_2° is displacing a solution with initial concentrations c_1^∞ and $c_2 = 0$. Then the characteristic $q_2 = c_2$, and the front for solute 2 moves down the column independently of concentration c_1.

The other characteristic is given by

$$dq_1 = (S_{11} - S_{22})dc_1 + S_{12}dc_2 = dS_1 - S_{22}dc_1. \tag{13}$$

By the assumption that $S_{11} < S_{22}$, $\lambda_1(= \theta + \rho S_{11}) < \lambda_2(= \theta + \rho S_{22})$, so that the q_1-front is transported at a faster rate than the c_2-front. After sufficient time, variations in q_1 occur at $c_2 = 0$; i.e. the q_1-front is just a c_1-front, whose shape is determined by the convexity of S_1. On the other hand, the region of varying q_2 is a region of constant q_1. Then from equation (11)

$$dc_1/dc_2 = -S_{12}/(S_{11} - S_{22}). \tag{14}$$

Since S_{12} is generally negative, dc_1/dc_2 is negative, and c_1 and c_2 vary reciprocally in this region, the degree of variation in c_1 depending on the competition term S_{12}. Thus the concentration c_1 rises ahead of the c_2-front to a plateau value c_2^* determined by $q_1(c_1^*, 0) = q_1(c_1^\circ, c_2^\circ)$. The height of the plateau value depends on the

degree of competition, measured by S_{12}, but under the present assumptions it will always be greater than the boundary value c_1^o, provided that c_1^o is non-zero (the 'snow plough' effect; Starr and Parlange 1979). Furthermore, the sign of $\partial c_1/\partial x'$ at the leading edge of the solute front depends on the relative magnitudes of c_1^* and c_1^∞ — if c_1^∞ is greater than c_1^* it will be negative, and conversely.

Ionic Competition

A soil with a net surface charge will adsorb ionic species from solution and, strictly speaking, competition will always arise because of the presence of hydrogen and hydroxyl ions in aqueous solutions. However, provided soil solutions are approximately neutral, and the pH does not vary greatly, neglect of these species can frequently be justified. In cases where they cannot be neglected, two more species must be included in the analysis, though one may be eliminated by using the constant value of the ion product for water. Even if such effects can be ignored, the presence of more than one solute species is of practical interest, as this is the rule rather than the exception in soil solutions.

For simplicity, negatively charged surfaces and a single anion (designated by subscript o) are considered, together with two competing cations (subscript 1 and 2). The reverse case of two anions and a single cation relies on virtually identical analysis. In addition, we assume instantaneous and reversible adsorption, so that the results are not valid without modification for species like phosphate, which appears to have a time dependent isotherm which is partly irreversible (e.g. Aylmore and Murali 1981).

The novel feature of ionic adsorption in the present context is that the concentrations and the adsorption isotherms are not independent, even considering only the cations. This is because requirements of electroneutrality must be met, both in the bulk solution and in the adsorbed phase (defined relative to a Gibbs dividing surface which makes the adsorption of water zero). In the bulk solution therefore

$$c_o = c_1 + c_2, \tag{15}$$

whereas in the adsorbed phase

$$s_1 + s_2 = s_o - \sigma. \tag{16}$$

For a negatively charged surface the anion adsorption s_o will be negative, but for dilute solutions will depend mainly on the total ionic strength (measured by c_o), and only weakly on the individual cation concentrations.

Using the same terminology as in the previous section, equation (6) will describe cation transport, while anion movement is governed by

$$\partial/\partial t'(\theta c_o + \rho s_o) = \partial/\partial x'(D_o \partial c_o/\partial x') - \partial c_o/\partial x'. \tag{17}$$

Anion Dynamics

Even if we assume that anion adsorption depends only on total ionic strength, so that

$$s_o = s_o(c_o), \tag{18}$$

equation (17) cannot strictly be decoupled from the equations for cation movement because the dispersion coefficient D_o is not constant, but is a concentration

weighted average of the cation dispersion coefficients. Corresponding to equation (10) we can write

$$\lambda_o \partial x'/\partial t'|_{c_o} = 1 - \partial/\partial c_o (D_o \partial c_o/\partial x'|_{t'})|_{t'}; \qquad \lambda_o = (\theta + \rho S_{oo}), \tag{19}$$

and we observe from this that the velocity of propagation at large times is independent of the individual cation concentrations (although the shape of the anion front is not).

Since the number of anions excluded from the double layers in the vicinity of the charged surfaces increases with ionic strength (though the region of exclusion becomes smaller as the double layer contracts), S_{oo} is generally negative and the speed of propagation λ_o^{-1} is larger than it would be in the absence of anion exclusion. Similar considerations suggest that d^2S_o/dc_o^2 is positive, so that the adsorption isotherm is concave, and an anion pulse may be expected to have a diffuse leading edge and a sharp trailing edge. Both these will in general be travelling faster than the accompanying water front, as measured by an effectively non-adsorbing species such as tritium. This is just the excluded volume effect discussed by other authors; assuming a constant value for the excluded volume is equivalent to assuming a linear adsorption isotherm for the anion. Bond *et al.* (1982) (Figs 1 and 2) compare experimental results with theoretical predictions in which the importance of the excluded volume term was incorrectly assessed. The evidently wider spread of their experimental anion front may be for this reason, while the lack of agreement for the tritium profile is probably due to neglecting the effects of tortuosity.

Cation Dynamics

For cation movement, the two dispersivities may be assumed independent, and equations (15) and (16) used to eliminate the anion. However, because concentrations are constrained to be non-negative, the cation adsorptions are not independent. The assumption inherent in equation (18) implies, on differentiating equation (16),

$$S_{11} + S_{21} = S_{oo} = S_{12} + S_{22}. \tag{20}$$

Assuming that species 2 is more strongly adsorbed, so that S_- is negative, and substituting in equations (8) and (9), the characteristics are given by

$$dq_1 \propto dS_1 - S_{oo} dc_1 \tag{21a}$$

$$q_2 = c_1 + c_2 = c_o \tag{21b}$$

with $\lambda_1 \left(= \theta + \rho \partial s_1/\partial c_1|_{c_o}\right) > \lambda_2 = \lambda_o$.

The description of the general behaviour at large times follows that of the previous section, with regions of constant concentration alternating with regions in which one or other of the characteristics, but not the concentrations, is constant.

In the first transition region $c_o = c_1 + c_2$ is constant, so that in this region changes in c_1 are matched by equal and opposite changes in c_2. In the second transition region, c_o changes from c_o^o to c_o^∞, and changes in c_1 and c_2 are governed by the requirement that $q_1 = q_1^\infty$ in this region.

For example, if the excluded volume is assumed constant, then

$$q_1 = s_1 + k_o c_1; \qquad k_o = -S_{oo} \tag{23}$$

and c_1^* and c_2^* $(= c_o^o - c_1^*)$ are determined by the intersection of the curves

$$y = s_1^\infty + k_o(c_1 - c_1^\infty) \text{ and } y = s_1(c_o^o, c_1).$$

Numerical Simulation

As a concrete example of this analysis, Fig. 1 shows breakthrough curves calculated for the isotherms

$$s_1 = -kc_1 - \alpha c_1 c_2 - \sigma c_1/c_0; \qquad s_2 = -kc_2 + \alpha c_1 c_2 - \sigma c_2/c_0; \qquad s_0 = -kc_0, \quad (24)$$

which, while being comparatively simple, are capable of exhibiting the main features of ionic competition in dilute solutions. The effect of anion exclusion is modelled by the use of the parameter k, while cation competition enters through the parameter α. The assumed values of the various parameters are given in the figure.

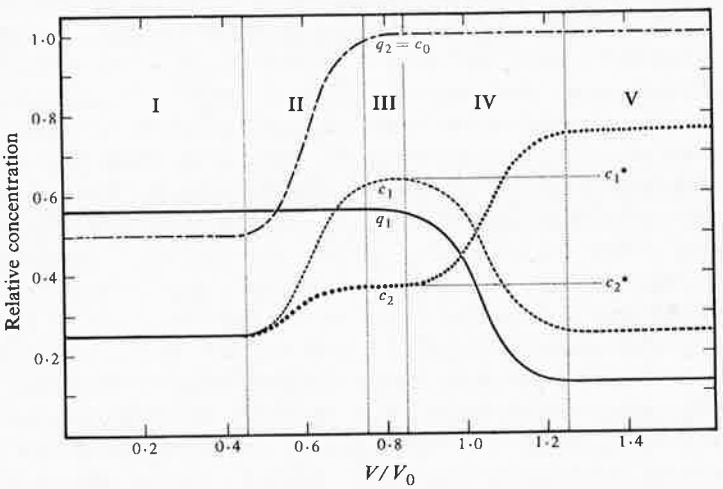

Fig. 1. Theoretical breakthrough curves of concentrations and characteristics calculated for the competitive adsorption isotherms given in the text. The non-dimensional length of the column was $x = 150$; other parameters were $\theta = 0{\cdot}25$, $k\rho = 0{\cdot}1$, $k/\alpha = 1$, $\sigma/\alpha = -1{\cdot}25$. Initial relative concentrations were $c_0 = 0{\cdot}5$, $c_1 = c_2 = 0{\cdot}25$; input relative concentrations were $c_0 = 1$, $c_1 = 0{\cdot}25$, $c_2 = 0{\cdot}75$. The Roman numerals are explained in the text.

Region III has been shown slightly exaggerated, as the length of the given column is the smallest for which this region will exist; the region will increase for a longer column proportionately to the extra length. For longer columns region II will remain the same length, due to the shape of the isotherms, whereas regions I, III and IV will increase linearly and region V will decrease.

The characteristics q_1 and $q_2 = c_0$ are also shown, and the calculations have been made under the assumption that the regions in which the characteristics vary are disjoint, which can be seen to be just valid. As a result, these profiles could be determined analytically; for shorter columns with both characteristics varying together the calculation of the profiles is more difficult.

Unsteady Flow

Although the foregoing analysis has assumed a uniform water content for simplicity, the analysis is not complicated much further by dropping this assumption, as in the work of Charbeneau (1981). In order to define the dimensionless variables x' and t', some fixed velocity V_0 characteristic of the

system, such as the saturated hydraulic conductivity or the convective velocity at a given time at $x' = 0$, must be used. Then if $v = v(x', t')$ is the dimensionless ratio of the convective velocity to V_o, equation (3) for example is replaced by

$$\partial x'/\partial t' = (\theta + \rho ds/dc)^{-1}\{v - \partial/\partial c(\partial c/\partial x')\}. \quad (25)$$

The movement of a solute front under conditions of varying water content is altered in two ways by varying water content:

(i) The velocity of the front varies with the convective water flux, and (ii) the solute front velocity varies in an inverse manner with the water content, due to the factor $(\theta + \rho ds/dc)^{-1}$. Because of the second of these two effects, the concentration at any particular water content may change in time, even in an unreactive system, becoming more concentrated with decreasing water contents. In reactive soils, positively adsorbed species will tend to minimize this effect through increased adsorption at the higher concentrations; however, negatively adsorbed species may show a quite dramatic response to decreasing water contents, the above effect being enhanced with increasing concentration (cf. Bond *et al.* 1983; Figs 2 and 5).

For a plurality of species similar considerations apply. The velocities of the characteristics rather than the individual concentrations now are proportional to v. On the other hand, the equations for the characteristics (equations (9)) are unchanged, and the effect of varying water content is seen through its effect on the λ_i (equation (8)) and by replacing 1 by v on the right-hand side of equation (10). Consequently, the foregoing analysis is easily extended in principle to account for varying water content, although clearly detailed features of solute profiles or breakthrough curves may be modified considerably by unsteady conditions. The shape of the solute front which depends on the convexity of the adsorption isotherm will not normally be qualitatively different; and the relative relationships between concentrations in a given region, which are governed by the characteristics, will be the same, so that conclusions based on considerations of these factors will be unchanged under conditions of varying water content.

A further effect of unsteady flow is due to the dependence of the dispersion coefficient on the convective velocity. Although this complicates quantitative calculations of the exact shape of the solute front (though not the general form as shown above), it is often quite permissible to assume a constant value for this coefficient, if the region in which the solute concentration is varying rapidly corresponds to a region in which the convective velocity is changing relatively slowly, or under the same conditions for which the soil-water diffusivity can be approximated by a 'delta-function diffusivity', because most of the flux occurs at the highest water content.

The case of intermittent flow should also be mentioned, because of its importance in natural systems. If periods of flow alternate with periods of no flow, the effects of dispersion will be more evident than otherwise, though the movement of the solute front is similar to that described above when considering varying water content.

Conclusion

This work shows that one-dimensional multi-component solute movement in reactive soils is similar in some respects to non-competitive solute movement. After an initial period, solute fronts consisting of certain well-defined combinations of concentrations (as distinct from individual concentrations in the non-competitive

case) move through the soil column independently, at well-defined velocities. The particular combinations which behave in this way are determined by the form of the competitive adsorption isotherms only, and are not affected by the water content or convective velocity changing.

During the initial period before the solute fronts separate, there is some interaction between the different solute combinations due to dispersion, with the result that the shape of the solute fronts during this time are perturbed by adjacent solute combinations.

The effect of time dependence and hysteresis of the adsorption isotherms on solute movement has not been considered. However, the present work should make it possible to separate such effects unambiguously from those described here, and so provide the basis of a more comprehensive theoretical treatment embracing both effects. Experimental work aimed at testing the assumptions and limitations of the present theory is necessary in order to guide further development of the competitive solute movement model.

References

Aylmore, L. A. G., and Murali, V. (1981). A convective-dispersive-adsorptive flow model for solute transport in soils. II. Evaluation of single and two-component adsorption models for phosphate movement in soils. *Aust. J. Soils Res.* **19**, 287–98.

Bear, J. (1972). 'Dynamics of Fluids in Porous Media.' (American Elsevier: New York.)

Bond, W. J., Gardiner, B. N., and Smiles, D. E. (1982). Constant flux adsorption of a tritiated $CaCl_2$ solution by a clay soil with anion exclusion. *Soil Sci. Soc. Am. J.* (in press).

Bond, W. J., Gardiner, B. N., and Smiles, D. E. (1984). Movement of $CaCl_2$ solutions in an unsaturated clay soil: the effect of solution concentration. *Aust. J. Soil Res.* **22**, 43–58.

Charbeneau, R. J. (1981). Groundwater contaminant transport with absorption and ion exchange chemistry: method of characteristics for the case without dispersion. *Water Resour. Res.* **17**, 705–13.

Laryea, K. B., Elrick, D. E., and Robin, M. J. L. (1982). Hydrodynamic dispersion involving cationic adsorption during unsaturated transient water flow in soil. *Soil Sci. Soc. Am. J.* **46**, 667–71.

Murali, V., and Aylmore, L. A. G. (1981*a*). A convective-dispersive-adsorptive flow model for solute transport in soils. I. Model description and some simulations. *Aust. J. Soil Res.* **19**, 23–39.

Murali, V., and Aylmore, L. A. G. (1981*b*). Competitive adsorption: its importance in ionic transport in soils. *Search* **12**, 133–5.

Murali, V., and Aylmore, L. A. G. (1982*a*). Competitive adsorption during solute transport in soils. I. Mathematical models. *Soil Sci.* **134** (in press).

Murali, V., and Aylmore, L. A. G. (1982*b*). Competitive adsorption during solute transport in soils. II. Simulations of competitive adsorption. *Soil Sci.* **134** (in press).

Murali, V., and Aylmore, L. A. G. (1983). Competitive adsorption during solute transport in soils. III. A review of experimental evidence of competitive adsorption and an evaluation of simple competitive models. *Soil Sci.* **135** (in press).

Philip, J. R. (1957). The theory of infiltration: 2. The profile at infinity. *Soil Sci.* **83**, 435–48.

Philip, J. R. (1969). Theory of infiltration. *Adv. Hydrosci.* **5**, 215–96.

Smiles, D. E., and Gardiner, B. N. (1982). Hydrodynamic dispersion during unsteady, unsaturated water flow in a clay soil. *Soil Sci. Soc. Am. J.* **46**, 9–14.

Starr, J. L., and Parlange, J.-Y. (1979). Dispersion in soil columns: the snow plough effect. *Soil Sci. Soc. Am. J.* **43**, 448–50.

Wilson, J. L., and Gelhar, L. W. (1981). Analysis of longitudinal dispersion in unsaturated flow: I. the analytical method. *Water Resour. Res.* **17**, 122–30.

Manuscript received 28 February, accepted 2 August 1983

Soil Biol. Biochem. Vol. 16, No. 4, pp. 299–304, 1984
Printed in Great Britain.

0038-0717/84 $3.00 + 0.00

SPECIFIC ACTIVITY OF PHOSPHORUS IN MYCORRHIZAL AND NON-MYCORRHIZAL PLANTS IN RELATION TO THE AVAILABILITY OF PHOSPHORUS TO PLANTS

N. S. BOLAN, A. D. ROBSON, N. J. BARROW[1] and L. A. G. AYLMORE
Department of Soil Science and Plant Nutrition, University of Western Australia, Nedlands, Western Australia 6009
[1]Division of Animal Production, C.S.I.R.O., Underwood Avenue, Floreat Park, Western Australia 6014

(*Accepted* 24 *November* 1983)

Summary—Phosphate was allowed to react with a soil to which iron hydroxide had been added. The P was then labelled by a subsequent addition of ^{32}P. Soil P was extracted by 10 mM $CaCl_2$, 0.5 M $NaHCO_3$, and acid NH_4F solutions and the specific activity of P in the extracts was measured. Subterranean clover plants were grown both with and without a mycorrhizal fungus. Phosphorus contents and the specific activities of P in the plant shoots were determined.

For mycorrhizal plants, adding iron hydroxide had no effect on the amount of P taken up, but for non-mycorrhizal plants it decreased the uptake. However there was no effect of iron hydroxide or of mycorrhizal infection on the specific activity of P in the plants. Adding iron hydroxide had no effect on the amount of P extracted by acid NH_4F, but decreased the P extracted by 10 mM $CaCl_2$ and by 0.5 M $NaHCO_3$. The specific activity of P in the extracts was not affected by the addition of iron hydroxide and was the same for the three extractants. Further, the specific activity of P in all extractants was similar to that of P in both mycorrhizal and non-mycorrhizal plants. Thus differences in the availability of soil P to mycorrhizal and non-mycorrhizal plants and to the extractants were not reflected by differences in labelling. It therefore follows that lack of difference in specific activity between mycorrhizal and non-mycorrhizal plants does not eliminate the possibility that mycorrhizal plants can obtain P that was unavailable to non-mycorrhizal plants.

INTRODUCTION

When the phosphorus supply in soil limits growth, plants infected with vesicular–arbuscular mycorrhizal fungi are able to take up more P from soil and grow better than uninfected plants (Mosse, 1973; Tinker, 1978; Abbott and Robson, 1982). Radioactive P(^{32}P) has been used to test the possibility that mycorrhizal plants can obtain P from soil which is not accessible to ^{32}P (Sanders and Tinker, 1971). This involves labelling the soil with ^{32}P and then comparing the specific activity of P absorbed by mycorrhizal and non-mycorrhizal plants. A lower value of specific activity of P in the mycorrhizal plants would indicate that the mycorrhizal fungus helped the plants to take up P that was not labelled by the added ^{32}P. In most such experiments (Table 1), similar specific activities have been observed for both mycorrhizal and non-mycorrhizal plants. The only conclusion that can be drawn from these observations is that both mycorrhizal and non-mycorrhizal plants absorb similarly labelled P (called "labile" P by Tinker, 1975) from soil. However, such results have led to further conclusions such as that both mycorrhizal and non-mycorrhizal plants obtain their P requirement from the same "sources" (Hayman and Mosse, 1972), "fractions" (Mosse *et al.*, 1973), "pools" (Owusu-Bennoah and Wild, 1980), or "forms" (Powell, 1975) of P from the soil.

There are difficulties in the use of ^{32}P for making such conclusions. Firstly, isotopic exchange is a continuing process (McAuliffe *et al.*, 1947; Barrow and Shaw, 1975) and it has been observed that added ^{32}P exchanges with even the "slowly exchangeable" P (Nye and Foster, 1958). Secondly, Olsen and Watanabe (1970) suggested that there may be P in soil which is accessible to ^{32}P but not to plants and hence the use of ^{32}P does not necessarily distinguish between forms of P which differ in their availability to plants. Thus the possibility exists that there may be differences in availability of P to mycorrhizal and non-mycorrhizal plants, which are not reflected by differences in labelling with ^{32}P.

In this experiment we examine the effect of a mycorrhizal fungus on the uptake of P which has reacted with soil amended with iron hydroxide and which was subsequently labelled with ^{32}P. We show that within the treated soil, there was P which was accessible to ^{32}P and to mycorrhizal plants, but not to non-mycorrhizal plants.

MATERIALS AND METHODS

Sub-soil samples (15–30 cm) which were free of indigenous mycorrhizal fungi were collected from a virgin forest of *Eucalyptus marginata* Donn ex Sm. near Jarrahdale, Western Australia. The soil is a red earth (Uc 5.22 Northcote *et al.*, 1975) with the following properties: pH 5.3 in 10 mM $CaCl_2$; clay content 28%; total Fe_2O_3 7.28%; total P 35 $\mu g\,g^{-1}$ (Black, 1967); $NaHCO_3$ extractable P 0.16 $\mu g\,g^{-1}$ (Colwell, 1963). We chose a soil with a low level of native P so that we could examine the effect of iron hydroxide addition on the proportion of the added P that became labelled by ^{32}P ("labile" P—Tinker, 1975) and the difference in the availability within the labelled P between mycorrhizal and non-mycorrhizal

Table 1. Comparisons of specific activities (SA) of phosphorus in mycorrhizal (+M) and non-mycorrhizal (−M) plants

Host plant	Growth conditions	Observations	Conclusions	Ref.
Allium cepa	4 weeks P incubation; 8 weeks growth; 1 endophyte	SA same for +M & −M plants	Same sources of P	1
Paspalam notatum *Melinus minutiflora* *Centrosema pubens*	4 weeks P incubation; 8 weeks growth; 2 endophytes	For *Melinis* SA same for +M & −M; for *Paspalum* & *Centrosema* −M took up no P	Same fractions of P; +M has lower threshold P	2
Allium cepa	P not completely mixed; 3 weeks growth; 1 endophyte	SA for +M less than −M plants	+M took up more P	3
Allium cepa *Trifolium pratense* *Lactuca sativa*	4 weeks P incubation; 6 weeks growth; 1 endophyte	SA same for +M & −M plants	Same pools of P	4
	2 weeks P incubation	SA for +M less than −M plants	P solubilized	
Agrostis sp.	13 weeks growth; 3 harvests; 1 endophyte	SA same for +M & −M; SA decreased with time	Same pools of P	5
Allium cepa *Trifolium pratense*	4 weeks P incubation; 10 weeks growth 7 endophtyes	SA same for +M & −M; SA decreased with time	Same forms of P	6
Allium cepa	5 weeks growth 4 harvests; 1 endophyte	SA same for +M & −M; SA decreased with time	Similarly labelled P	7

(1) Hayman and Mosse (1972); (2) Mosse *et al.* (1973); (3) Owusu-Bennoah and Wild (1979); (4) Owusu-Bennoah and Wild (1980); (5) Pichot and Binh (1976); (6) Powell (1975); (7) Sanders and Tinker (1971).

plants. Larsen (1967) suggested that within the "labile" P there exist different categories such as rapidly labile and slowly labile. That is the reason we did not use the term "labile" P; instead we simply called the P labelled by ^{32}P as labelled P. Samples of 200 g soil were placed in small cups and 0, 20 or 40 g of freshly-precipitated iron hydroxide were mixed thoroughly with the soil. Seven levels of phosphate (0, 100, 200, 400, 600, 800 and 1000 mg P) were then added as KH_2PO_4 in 50 ml solutions and the soil was incubated for 3 weeks at 20°C. Carrier-free ^{32}P was then added at the rate of 74 kBq mg^{-1} of P added, for levels of P of 200 mg and above, and incubated for a further 3 weeks. Each of these samples was mixed with 2800 g of the original soil to which basal nutrients had been added in sufficient amounts to overcome all nutrient deficiencies (Bolan *et al.*, 1983). About 5 g of fresh roots of subterranean clover (*Trifolium subterraneum* L. cv. Seaton Park) infected with a vesicular–arbuscular mycorrhizal fungus, *Glomus fasciculatum* (Thaxter) Gerdemann and Trappe, was used for inoculation. Uninfected roots were added to the control (non-mycorrhizal) treatment. The procedures for producing mycorrhizal inoculum, for inoculating and for assessing mycorrhizal infection have been described by Abbott and Robson (1978). Subterranean clover plants (9 plants per pot) were grown and harvested 35 days after sowing. Shoots were dried in a forced draught oven at 70°C. Roots were used for assessing mycorrhizal infection.

Dried shoot materials were digested in a 1:4 nitric:perchloric acid mixture. Phosphorus concentration in the plant digests was measured by the molybdovanado–phosphoric acid method. The ^{32}P activity was measured by Cerenkov counting using an Isocap 300 liquid scintillation counter (Lauchli, 1969). For specific activity measurements, the ^{32}P activity in the shoots was plotted against the P content in the shoots for the various levels of iron hydroxide and phosphate application. The slope of the linear regression line gives the specific activity of P in the plants. Values for the P content of the seed were not subtracted from the P content of the shoots because the contribution of seed-P to the shoots varies with the amount of plant growth (Brookes, 1982).

Before planting, soil samples were taken from the pots and each were extracted with either 10 mM $CaCl_2$, 0.5 M $NaHCO_3$ (Colwell, 1963) or 30 mM NH_4F + 25 mM HCl (Bray and Kurtz, 1945). The P concentration in the extracts was measured by the method of Murphy and Riley (1972). The ^{32}P activity in the extracts and in the plant digests was measured at the same time for direct comparison of the specific activity in the extracts and in the plants. At the time of the measurement of the ^{32}P activity of the soil extracts and plant digests, if all the ^{32}P had mixed uniformly with the added P, the specific activity of the added phosphate would have been 1.61 counts min^{-1} μg^{-1} P.

RESULTS

Phosphate uptake by plants

When inoculated with a mycorrhizal fungus, the

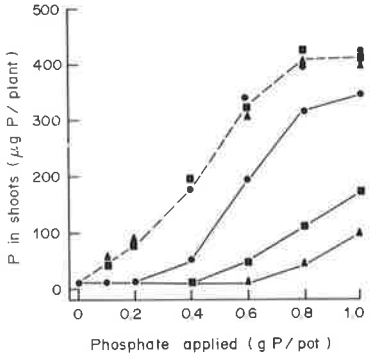

Fig. 1. Effects of the addition of phosphate and of iron hydroxide (●, 0, ■, 20 and ▲, 40 g per pot) on the phosphorus contents in the mycorrhizal (– – –) and non-mycorrhizal (——) plants.

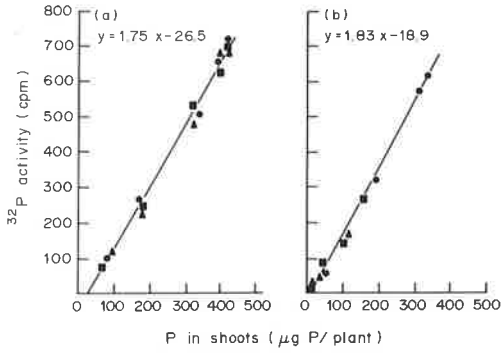

Fig. 2. Regression relationship between the P content and the ^{32}P activity in the shoots of mycorrhizal (a) and of non-mycorrhizal (b) plants; (levels of iron hydroxide are as in Fig. 1).

roots of subterranean clover plants were heavily infected; control plants were uninfected. Mycorrhizal plants took up more P than did non-mycorrhizal plants at all levels of addition of iron hydroxide and of phosphate (Fig. 1). For mycorrhizal plants addition of iron hydroxide had little effect on the amount of P in the shoots. In contrast, for non-mycorrhizal plants, adding iron hydroxide decreased the amount of P in the shoots. For these plants there was no increase in the P content in the shoots until large amounts of phosphate had been added. The phosphate level below which there was little uptake of P increased with the level of iron hydroxide added. There was no effect of adding iron hydroxide on the specific activity of P in either mycorrhizal or non-mycorrhizal plants. The specific activity of P in the mycorrhizal and the non-mycorrhizal plants did not differ significantly ($P < 0.05$) and the regression estimates were 1.75 and 1.83 respectively. The regression lines relating P content in the shoots and the ^{32}P activity (Fig. 2) did not pass through the origin probably because the P content in the shoots were not corrected for seed-P. The intercepts of the regression lines on the x-axis give the regression estimate of the seed-P contributed to the shoots.

Extraction of soil phosphorus

At all levels of addition of iron hydroxide and phosphate the acid NH_4F solution extracted more P from the soil than did the 10 mM $CaCl_2$ or the 0.5 M $NaHCO_3$ solutions. Adding iron hydroxide had little effect on the amount of P extracted by the acid NH_4F solution, but decreased the amount of P extracted by both 10 mM $CaCl_2$ and 0.5 M $NaHCO_3$ (Fig. 3). However, adding iron hydroxide had little effect on the specific activity of P extracted by any of the solutions. Moreover the specific activities of P extracted by the three solutions did not differ significantly ($P < 0.05$). The values were 1.84, 1.74 and 1.96 for acid NH_4F, 0.5 M $NaHCO_3$ and 10 mM $CaCl_2$ solutions respectively (Fig. 4). The specific activity values were obtained from the regression relationship between the amount of P extracted and the ^{32}P activity in the extracts. These relationships were found to be linear. This indicates that the proportion of the added P that exchanged with the added ^{32}P was independent of the level of addition—as was observed by Barrow and Shaw (1975). The values for specific activity of both the soil extracts and the plant digests were only slightly greater than the values of specific activity that would have been obtained if all the ^{32}P had uniformly mixed with the added P. This indicates that more than 85% of the added P became labelled with the ^{32}P added.

DISCUSSION

We found, adding iron hydroxide did not affect the

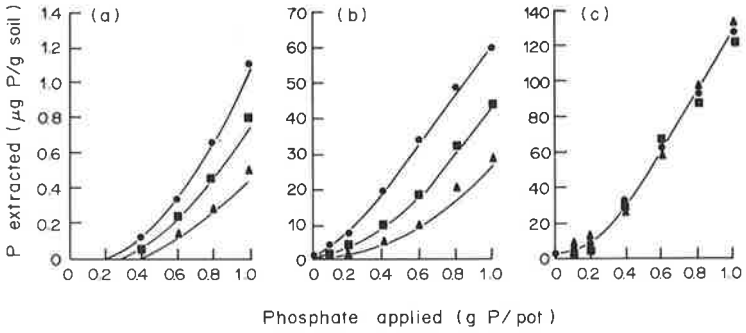

Fig. 3. Effects of the addition of iron hydroxide and of phosphate on the amounts of P extracted by 10 mM $CaCl_2$ (a), 0.5 M $NaHCO_3$ (b), and 30 mM NH_4F + 25 mM HCl (c); (levels of iron hydroxide are as in Fig. 1).

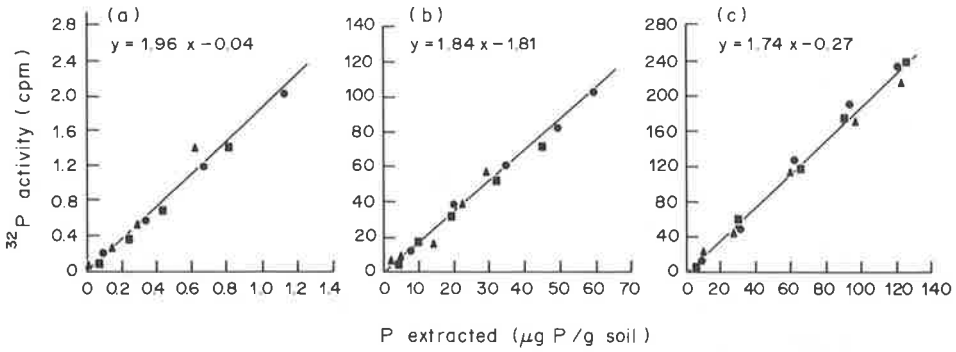

Fig. 4. Regression relationship between the ^{32}P activity and the amount of P extracted by 10 mM $CaCl_2$ (a), 0.5 M $NaHCO_3$ (b), and 30 mM NH_4F + 25 mM HCl (c); (levels of iron hydroxide are as in Fig. 1).

P extracted by NH_4F nor the P available to mycorrhizal plants, but decreased P extracted by both $NaHCO_3$ and $CaCl_2$ and the P available to non-mycorrhizal plants. Further, at high levels of addition of iron hydroxide, it was not until large amounts of phosphate had been added that non-mycorrhizal plants took up any P. Thus for these treatments, there was a category of P that was available to mycorrhizal plants but unavailable to non-mycorrhizal plants. Yet labelling the soil with ^{32}P failed to reflect this difference and the specific activity remained the same for both mycorrhizal and non-mycorrhizal plants and for the three extractants. In order to interpret these observations we need to understand the processes involved when P in the soil is labelled with ^{32}P, when P is extracted by reagents, and when P is taken up by mycorrhizal plants. Each of these processes will be dealt with in turn.

In soil, isotopic exchange is a continuing process (McAuliffe *et al.*, 1947; Barrow and Shaw, 1975). Rather than having a definite end point, the added ^{32}P exchanges at a decreasing rate with an increasing proportion of the soil P (Larsen, 1967; Jose and Krishnamoorthy, 1972). Evidence for this continuing exchange can also be seen from the observations that the specific activity of P in plants decreased with time even after having been corrected for isotopic decay (Sanders and Tinker, 1971; Powell, 1975; Pichot and Binh, 1976). The processes involved in this continuing exchange are similar to those involved in the continuing reactions when P is added to soil (Barrow, 1983)—although the kinetics may differ. Thus in our experiment, phosphate was added to the soil and permitted to react for 3 weeks. This would have allowed the added phosphate to react both with the soil and, where appropriate, with the added iron hydroxide. This reaction appears to be a solid-state diffusion into the particles onto which it is initially adsorbed (Barrow, 1983). Kinetic studies of phosphate have shown that a similar reaction seems to occur for iron hydroxide also (Bolan *et al.*, 1984). After the initial 3 weeks, ^{32}P was added and incubated for a further 3 weeks. The kinetics of tracer diffusion in the solid state differ from those of chemical diffusion because, for tracer diffusion, gradients of electrochemical potential are not involved (Manning, 1968). Nevertheless the added ^{32}P exchanged with a large proportion of the previously-added unlabelled P. Therefore the extent of this exchange will be similar for all of the P that has not yet penetrated deeply into soil particles and iron hydroxide by solid-state diffusion.

The 10 mM $CaCl_2$ solution extracted only a small amount of P added and the relationship between the amount of P added and the P extracted (recovery lines) were markedly curved. This reflects the curvilinear relationship between the concentration of P in the solution and the amount of P adsorbed in the absence of a competing anion. The 0.5 M $NaHCO_3$ solution extracted more P than did 10 mM $CaCl_2$ and the recovery lines were not as steeply curved as for 10 mM $CaCl_2$. This suggests that curvilinear adsorption still occurred in the presence of the weakly competing anion-HCO_3 (Barrow and Shaw, 1976). Because of this, the soil with the highest sorption (with 40 g of iron hydroxide) gave the lowest recoveries. The recovery lines for the acid NH_4F extractant were less curved. This reflects strong competition for adsorbed phosphate from the fluoride ion. It is consistent with this that there was no effect of iron hydroxide on the amount of P extracted by the acid NH_4F solution. Thus the acid NH_4F solution extracted a greater proportion of P reacted with the soil particles and the iron hydroxide. Chloride, bicarbonate and fluoride all displace different sections of the adsorbed phosphate, but all have the same specific activity. Extraction involves an induced desorption of some of the penetrated P. However the P most likely to be desorbed is that near the surface which has not penetrated too deeply. This may be the reason for the similar specific activity of the P extracted by the three extractants.

Various mechanisms have been suggested to account for the increased uptake of P by mycorrhizal plants. First there may be greater exploration of the soil associated with hyphae extending beyond the zone of depletion around non-mycorrhizal roots (Tinker, 1978). The mycorrhizal hyphae thus decrease the distance that ions must diffuse to roots (Rhodes and Gerdemann, 1975). Second mycorrhizal and non-mycorrhizal roots may differ in the absorption of phosphorus from solution. Mycorrhizal plants took up P from solution faster than did non-mycorrhizal plants (Bowen *et al.*, 1975; Cress *et al.*, 1979; Howeler *et al.*, 1982). Additionally there have been suggestions that mycorrhizal plants may have a lower threshold

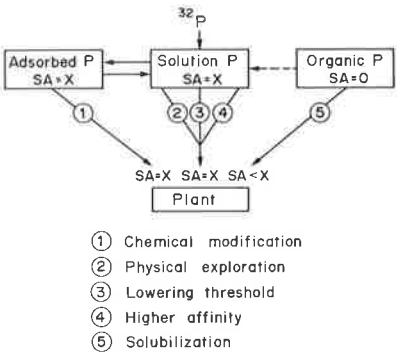

Fig. 5. Mechanisms for the increased uptake of P by mycorrhizal plants and their effects on specific activity (SA) of P in the plants.

concentration for absorption from solution than non-mycorrhizal plants (Mosse *et al.*, 1973; Howeler *et al.*, 1982). Third mycorrhizal plants may produce exudates which increase the amount of P available to plants (Tinker, 1975). Oxalate is produced by ecto-mycorrhizal fungi (Cromack *et al.*, 1979; Malajczuk and Cromack, 1982). Fourth differences between mycorrhizal and non-mycorrhizal plants in the absorption of anions and cations (Buwalda *et al.*, 1983) may lead to differences in rhizosphere pH. Such changes in rhizosphere pH may change the availability of adsorbed phosphate to plants (Hedley *et al.*, 1982). All of these processes involve desorption of phosphate from the soil particles, and in this case, from iron hydroxides. However all of the desorbed phosphate would be uniformly labelled and none of these mechanisms would lower the specific activity of P in the plants. Reduction in the specific activity can occur only when organic P which is not labelled by isotopic exchange is solubilized for example by the production of phosphatases (Fig. 5). There is no evidence for this mechanism in our results.

Acknowledgements—We thank Dr L. K. Abbott for providing mycorrhizal inoculum and advice on techniques for inoculation and assessing mycorrhizal infection. N.S.B. gratefully acknowledges the award of a University of Western Australia Research Studentship. Dr J. W. Bowden, Dr N. Malajczuk and Mr B. Whelan have made helpful comments on the manuscript.

REFERENCES

Abbott L. K. and Robson A. D. (1978) Growth of subterranean clover in relation to the formation of endomycorrhizas by introduced and indigenous fungi in a field soil. *New Phytologist* **81,** 575–585.

Abbott L. K. and Robson A. D. (1982) The role of vesicular-arbuscular mycorrhizal fungi in agriculture and the selection of fungi for inoculation. *Australian Journal of Agricultural Research* **33,** 389–408.

Barrow N. J. (1983) A mechanistic model for describing the sorption and desorption of phosphate by soil. *Journal of Soil Science* **34,** 733–750.

Barrow N. J. and Shaw T. C. (1975) The slow reactions between soil and anions: 3. The effect of time and temperature on the decrease in isotopically exchangeable phosphate. *Soil Science* **119,** 190–197.

Barrow N. J. and Shaw T. C. (1976) Sodium bicarbonate as an extractant for soil phosphate. I. Separation of the factors affecting the amount of phosphate displaced from soil from those affecting secondary adsorption. *Geoderma* **16,** 91–107.

Black C. A. (1967) *Methods of Soil Analysis.* American Society of Agronomy, Wisconsin.

Bolan N. S., Robson A. D. and Barrow N. J. (1983) Plant and soil factors including mycorrhizal infection causing sigmoidal response of plants to applied phosphorus. *Plant and Soil* **73,** 187–201.

Bolan N. S., Barrow N. J. and the late Posner A. M. (1984) Describing the effect of time on sorption of phosphate by iron and aluminium hydroxides. *Journal of Soil Science.* In press.

Bowen G. D., Bevege D. I. and Mosse B. (1975) Phosphate physiology of vesicular-arbuscular mycorrhizas. In *Endomycorrhizas* (F. E. Sanders, B. Mosse and P. B. Tinker, Eds), pp. 241–260. Academic Press, London.

Bray R. H. and Kurtz L. T. (1945) Determination of total, organic and available forms of phosphorus in soils. *Soil Science* **59,** 39–45.

Brookes P. C. (1982) Correction for seed-phosphorus effects in L-value determinations. *Journal of the Science of Food and Agriculture* **33,** 329–335.

Buwalda J. G., Stribley D. P. and Tinker P. B. (1983) Increased uptake of bromide and chloride by plants infected with vesicular-arbuscular mycorrhizas. *New Phytologist* **93,** 217–225.

Colwell J. D. (1963) The estimation of phosphorus fertilizer requirement of wheat in southern New South Wales by soil analysis. *Australian Journal of Experimental Agriculture and Animal Husbandry* **3,** 190–197.

Cress W. A., Throneberry G. O. and Lindsay D. L. (1979) Kinetics of phosphorus absorption by mycorrhizal and non-mycorrhizal tomato roots. *Plant Physiology* **64,** 484–487.

Cromack K. Jr, Sollins P., Graustein W. C., Speidel K., Todd W. A., Spycher G., Li C. Y. and Todd R. L. (1979) Calcium oxalate accumulation and soil weathering in mats of the hypogeous fungus *Hysterangium crassum. Soil Biology & Biochemistry* **11,** 463–468.

Hayman D. S. and Mosse B. (1972) Plant growth responses to vesicular-arbuscular mycorrhiza. III. Increased uptake of labile P from soil. *New Phytologist* **71,** 41–47.

Hedley M. J., White R. E. and Nye P. H. (1982) Plant-induced changes in the rhizosphere of rape (*Brassica napus* var *Emerald*) seedlings. II. Origin of the pH changes. *New Phytologist* **91,** 31–44.

Howeler R. H., Asher C. J. and Edwards D. G. (1982) Establishment of an effective mycorrhizal association on cassava in flowing solution culture and its effects on phosphorus nutrition. *New Phytologist* **90,** 229–238.

Jose A. I. and Krishnamoorthy K. K. (1972) Isotopic exchange of phosphate in soil: 'E' value. *Soils and Fertilizers* **35,** 620–627.

Larsen S. (1967) Soil phosphorus. *Advances in Agronomy* **19,** 151–210.

Lauchli A. (1969) Radio assay for β-emitters on biological material using Cerenkov radiation. *International Journal of Applied Radiation and Isotopes* **20,** 265–269.

Malajczuk N. and Cromack K. Jr (1982) Accumulation of calcium oxalate in the mantle of ectomycorrhizal roots of *Pinus radiata* and *Eucalyptus marginata. New Phytologist* **92,** 527–531.

Manning J. R. (1968) *Diffusion Kinetics for Atoms in Crystals.* Van Nostrand, Princeton, NJ.

McAuliffe C. D., Hall N. S., Dean L. A. and Hendricks S. B. (1947) Exchange reactions between phosphates and soils: hydroxylic surfaces of soil minerals. *Soil Science Society of America Journal* **12,** 119–123.

Mosse B. (1973) Advances in the study of vesicular-arbuscular mycorrhiza. *Annual Review of Phytopathology* **11,** 171–196.

Mosse B., Hayman D. S. and Arnold D. J. (1973) Plant growth responses to vesicular-arbuscular mycorrhiza. V. Phosphate uptake by three plant species from P deficient soils labelled with ^{32}P. *New Phytologist* **72,** 809–815.

Murphy J. and Riley J. P. (1962) A modified single solution method for the determination of phosphorus in natural waters. *Analytica Chimica Acta* **27,** 31–36.

Northcote K. H., Hubble G. D., Isbell R. F., Thompson C. H. and Bettenay E. (1975) *A Description of Australian Soils*. CSIRO, Australia, 20 pp.

Nye P. H. and Foster W. H. M. (1958) A study of mechanism of soil phosphate uptake in relation to plant species. *Plant and Soil* **9,** 338–342.

Olsen S. R. and Watanabe F. S. (1970) Diffusive supply of phosphorus in relation to soil textural variations. *Soil Science* **110,** 318–329.

Owusu-Bennoah E. and Wild A. (1979) Autoradiography of the depleted zone of phosphate around onion roots in the presence of vesicular-arbuscular mycorrhiza. *New Phytologist* **82,** 133–140.

Owusu-Bennoah E. and Wild A. (1980) Effects of vesicular-arbuscular mycorrhiza on the size of the labile pool of soil phosphate. *Plant and Soil* **54,** 233–242.

Pichot J. and Binh T. (1976) Action of endomycorrhizae on growth and phosphorus nutrition of *Agrostis* in pots and on isotopically exchangeable phosphorus in soil. *Agronomie Tropical* **31,** 375–378.

Powell C. Ll. (1975) Plant growth responses to vesicular-arbuscular mycorrhiza. VII. Uptake of P by onion and clover infected with different *Endogone* spore types in ^{32}P labelled soils. *New Phytologist* **75,** 563–566.

Rhodes L. H. and Gerdemann J. W. (1975) Phosphate uptake zones of mycorrhizal and non-mycorrhizal onions. *New Phytologist* **75,** 555–561.

Sanders F. E. and Tinker P. B. (1971) Mechanism of absorption of phosphate from soil by *Endogone* mycorrhizas. *Nature* **233,** 278–279.

Tinker P. B. (1975) Soil chemistry of phosphorus and mycorrhizal effects on plant growth. In *Endomycorrhizas* (F. E. Sanders, B. Mosse and P. B. Tinker, Eds), pp. 353–371. Academic Press, London.

Tinker P. B. (1978) Effects of vesicular-arbuscular mycorrhizas in plant nutrition and plant growth. *Physiologie Vegetale* **16,** 743–751.

Reprinted from the *Soil Science Society of America Journal*
Volume 50, no. 4, July–August 1986
677 South Segoe Rd., Madison, WI 53711 USA

Water Extraction by Single Plant Roots[1]

J. M. HAINSWORTH AND L. A. G. AYLMORE[2]

ABSTRACT

Application of computer assisted tomography to x-ray attenuation measurements has been used to study the drawdowns in soil-water content associated with single plant roots. Drawdowns have been measured at different depths along radish (*Raphanus sativus* cv long scarlet) roots growing in soil at two different initial water contents while the plants were subjected to either a high or low transpirational demand. This novel approach has provided the most detailed observations of this type yet obtained, particularly by a nondestructive technique. Soil resistance to water flow is clearly of significance even at the high soil-water potentials used since it has been observed to markedly influence water uptake. Comparisons between these experimentally determined drawdowns and those predicted by an analytical approach indicate that this model does not adequately describe the extraction process. In particular, the assumption that a plant root acts as a uniform absorbing cylinder along its length is clearly erroneous. While a numerical model gives a closer fit to the experimental data, it is clear that improvements in the physical concepts on which this is based are necessary to accurately describe the position and shape of the drawdowns.

Additional Index Words: **computer tomography, analytical, numerical models, root-soil interface, soil hydraulic resistance.**

Hainsworth, J.M., and L.A.G. Aylmore. 1986. Water extraction by single plant roots. Soil Sci. Soc. Am. J. 50:841–848.

IN RECENT YEARS numerous models aimed at a quantitative formulation and prediction of the processes involved in the movement of soil water and its extraction by plant roots have been developed (Hillel, 1982). Not only do these models differ in aim and level of detail, but also in approach. Two alternative approaches have generally been taken in modeling water uptake by plant roots. The first can be described as the macroscale or whole root system approach in which the soil-root system is assumed to be a continuum and water movement essentially a one-dimen-

[1] Contribution from Soil Science and Plant Nutrition, School of Agriculture, Univ. of Western Australia, Nedlands, Western Australia, 6009. Received 23 May 1985.

[2] Research Officer and Associate Professor of Soil Science, respectively.

sional flow, for example Ogata et al. (1960), Molz and Remson (1970; 1971), Nimah and Hanks (1973), and Hillel et al. (1976). Absorption of water by the root is treated as a sink term that is distributed in a certain pattern throughout the soil. The major disadvantage of the macroscopic approach in understanding mechanisms is that it is based on spatial averaging of soil-water content or potential and thus does not quantitatively describe the magnitude of the gradient from bulk soil to individual plant root.

The alternative approach is the microscale or single root approach based on the radial flow of water to a cylindrical sink. Solutions to this approach have been attempted by both analytical means (Gardner, 1960; Cowan, 1965), usually requiring restrictive assumptions (Hillel, 1982), and by numerical means (Molz and Remson, 1970; Hillel et al., 1975). However, such models have differed widely in their quantitative prediction of water extraction. These conflicting approaches have resulted in some workers concluding that root resistances predominate in determining water uptake (Newman, 1969), whilst others conclude that soil resistance predominates (Carbon, 1973). Thus, as pointed out by Hillel (1982), there are numerous theoretical models, lacking in consensus, which remain largely untested and, hence, unproven. It has become easier to formulate models of water extraction by plant roots than to validate them (Belmans et al., 1979).

A major problem in validating single plant root models has been the inability to directly and repetitively measure soil-water content or potential distributions in a nondestructive manner (So et al., 1976). Whilst So et al. (1976) were able to determine water potential at the root surface by extrapolation, using a collar tensiometer-potometer system, there has until recently been no system capable of directly and repetitively measuring soil-water content distributions from plant root to bulk soil in a nondestructive manner. However, in a recent paper, Hainsworth and Aylmore (1983) have demonstrated that the application of computer assisted tomography (CAT) to x-ray attenuation measurement is capable of resolving changes in soil-water contents of the order of 0.006 g/cm^3 over distances of some 1.5 mm. This is more than adequate to describe the drawdown in soil-water content associated with water uptake by plant roots. Thus it is clear that the CAT technique has considerable potential to elucidate the mechanisms of water uptake by plant roots and to provide vital experimental data for the testing of both single root models and models of whole root systems.

In this paper, the effects of transpiration rate, initial soil-water content, and root age on water uptake by single radish (*Raphanus sativus* cv long scarlet) roots have been examined using the CAT technique.

Computer Assisted Tomography (CAT)

Whilst the theory and use of the CAT technique for medical purposes have been reviewed in some detail (Brooks and DiChiro, 1975; 1976; Panton, 1981), a brief introduction to its application to the determination of soil-water content distributions will be necessary for most soil scientists.

In CAT, a slice of the object under examination is divided into a M × M matrix consisting of small squares called pixels. The purpose of CAT is to determine the density or water content of each pixel. This is achieved by scanning across the object linearly at 1 to 10° intervals for 180° using a collimated radiation source and detector. Each linear scan consists of M equally spaced beams of radiation passing through the object. The attenuation coefficient of each beam is determined by measuring the transmitted and incident intensities of the beam and employing Beer's law. Each attenuation coefficient is then modified using a Fourier transform to allow for portions of the beam that may pass outside a given pixel and, conversely, portions of a pixel that may lie outside the beam path, and then divided by the number of pixels through which the beam passed. This modified attenuation coefficient is then assigned to each pixel through which the beam passed. By summing the contributions of all beams passing through a given pixel the linear attenuation coefficient (μ) is determined for the pixel (Brooks and DiChiro, 1976). As μ is the product of the mass attenuation coefficient (μ_m) and the density of the pixel, the density and water content of the pixel can be determined if μ_m is known. In the case of wet soil μ becomes equal to

$$\mu_{\text{wet soil}} = \mu_{\text{soil}}\,\rho_{\text{soil}} + \mu_{\text{water}}\theta_v \qquad [1]$$

where μ_{soil} and μ_{water} are the mass attenuation coefficients of soil and water, respectively, and ρ_{soil} and θ_v the soil bulk density and volumetric water content, respectively.

When the soil is dry, θ_v equals zero and Eq. [1] becomes

$$\mu_{\text{dry soil}} = \mu_{\text{soil}}\,\rho_{\text{soil}}\,. \qquad [2]$$

By substracting Eq. [2] from Eq. [1] the volumetric water content of a pixel can be determined from

$$\theta_v = (\mu_{\text{wet soil}} - \mu_{\text{dry soil}})/\,\mu_{\text{water}}\,. \qquad [3]$$

In practice, the water content of a pixel is determined by scanning the soil column when dry and rescanning it in the same position when the soil is wet (Hainsworth and Aylmore, 1983).

MATERIALS AND METHODS

Instrumentation

An EMI CT 1007 scanner was used in these studies. The scanner employs a 120-kV x-ray tube and NaI detector. During a scan time of approximately 1 min, the scanner makes 160 measurements per linear scan and completes 60 linear scans at 3° intervals through 180°. Pixel size is 1.5 by 1.5 mm, and slice thickness 1 cm. McCullough (1975) has shown μ_{water} is 0.191 cm^{-1} for the scanner operating at 120 kV.

Experimental

A total of 16, 9-d-old single root radishes were used in a factorial experiment consisting of two transpiration rates by two initial water contents by four root depths.

Sixteen, 4.2-cm diam, 12-cm tall acrylic columns were uniformly packed with an oven-dry soil mix consisting of 85% Bassendean sand and 15% Clackline kaolinite from Western Australia. A first set of four columns was placed horizontally in the scanner and scanned at 4, 5, 6, and 8 cm, respectively, from the top of the pot. The pots were then wetted to a water content of 0.30 g/cm^3 (soil-water potential of −0.034 MPa) and a single radish planted in each. The radishes were grown in a laboratory under lights from two 60-W fluorescent tubes for 16 h/d and darkness for 8 h/d. Temperatures rose to an average of 19.5°C during the day and fell to approximately 11.7°C during the night. Relative humidity remained approximately constant at 21%. After 8 d the columns were rewatered (reaching 0.299 g/cm^3) and kept in darkness for 24 h, allowing the water content in the columns to equilibrate. The pots were then placed under

lights for 10 h and rescanned in the same positions as when dry. The water content of each pixel was then determined using Eq. [3], thus allowing the water loss from each slice scanned to be calculated. Equation [3] assumes that ρ_{soil} remains constant. It is possible that some compaction of the soil immediately surrounding the root occurs as the root grows through the soil. This would lead to an increase in bulk density, an increased attenuation of the x-radiation, and, hence, an overestimate of the water content close to the root surface. This effect would clearly reduce the measured drawdowns and, as will be discussed later, there was some evidence that this may have occurred to a slight extent. At the end of each scan, drawdowns were calculated using the mean of four pixels equidistant from the root on four traverses at right angles to each other (Hainsworth and Aylmore, 1983). In each slice under examination, root diameter, total root length, and total water loss by weight were also measured.

A second set of four columns were subjected to the same treatment except that during the 10 h preceding the rescan, a high evaporative demand was produced by subjecting the radishes to air flow from a 1200-W fan placed 1 m away from the plants. These experiments were then repeated with the remaining eight columns, using an initial water content of 0.24 g/cm^3 (soil-water potential of -0.047 MPa). The drawdowns obtained from the scanning procedure were then compared with the analytical model of Cowan (1965) and a numerical model conceptually the same as that of Hillel et al. (1975). These models were computed on the basis of water extraction from the slice under consideration and using diffusivities determined by the method of Bruce and Klute (1956). Water retention and diffusivity functions for the relevant range of water contents are shown in Fig. 1.

A further, two 4.2-cm diam by 12-cm tall columns were packed uniformly with the soil mix and scanned down the entire length of the column. The two columns were then watered to 0.30 g/cm^3 and a radish planted in each. The radishes were grown under the same condition as previously described. After 8 d the columns were rewatered to 0.30 g/cm^3 and kept in darkness for 24 h to allow the water content to equilibrate. One radish was then subjected to low evaporative demand (lights only) and the other to high evaporative demand (lights plus fan) for 10 h. The columns were rescanned and water loss, minimum and maximum water content, the number of pixels between minimum and maximum water content, and root diameter for each slice along the column determined.

RESULTS AND DISCUSSION

In Fig. 2 to 5 the drawdowns obtained by the scanning procedure are compared with the predictions of Cowan's (1965) and Hillel et al.'s (1975) models. Cowan's (1965) is an analytical model in which water is uniformly supplied from within a soil cylinder in order to maintain a steady-rate flow to the plant root, given by the following equation

$$Q = 2\pi D\Delta\theta/\ln(b/1.65a) \quad [4]$$

in which Q is uptake of water per centimeter of root, D the diffusivity at b, the radius to the outside edge of the soil cylinder, and $\Delta\theta$ the change in water content from bulk soil at b to a root having radius a.

The numerical model is essentially similar to that of Hillel et al. (1975), consisting of a series of concentric rings surrounding a cylindrical sink representing the root. The sink extracts a constant flux of water from the innermost ring of soil, which is replenished from the ring outside it, and so on. The movement of water from ring to ring is governed by the gradients of water content and diffusivities of the rings. The major advantage of the numerical model is that it has few restrictive assumptions in comparison to analytical models.

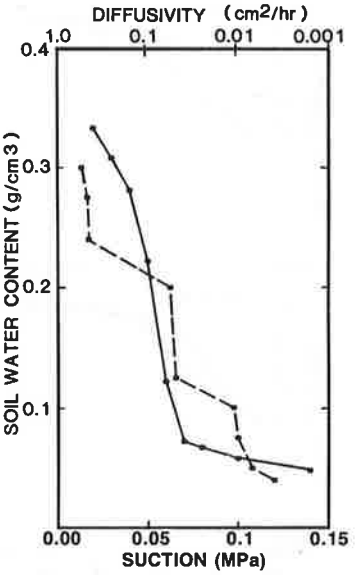

Fig. 1. Water retention (——) and diffusivity (---) functions for the range of water contents used in plant experiments.

The results presented in Fig. 2 to 5 clearly show the ability of the CAT technique to resolve in some detail, the changes in drawdowns resulting from differences in evaporative demand and initial water content. These experimentally-determined drawdowns show several significant and sometimes surprising trends. Of particular interest is the contrast in the results obtained with high and low initial water contents. First, for both the high and low evaporative demands, total water uptake from layers of equivalent depth were always less for the low initial water content than for the high

Table 1. Average uptake per unit root length and uptake from individual layers along single radish roots.

Treatment imposed	Layer depth	Avg uptake/ unit root length	Uptake in layer	Δθ†	Root radius
	cm	cm³/cm			mm
		High transpiration			
High initial water content (0.3 g/cm³)	4	0.200	0.235	0.255	0.25
	5	0.201	0.225	0.243	0.21
	6	0.200	0.221	0.241	0.19
	8	0.201	0.197	0.220	0.18
Low initial water content (0.24 g/cm³)	4	0.115	0.128	0.145	0.24
	5	0.116	0.124	0.139	0.22
	6	0.116	0.121	0.138	0.20
	8	0.116	0.115	0.128	0.19
		Low transpiration			
High initial water content (0.3 g/cm³)	4	0.146	0.161	0.170	0.25
	5	0.145	0.157	0.165	0.23
	6	0.147	0.151	0.156	0.20
	8	0.146	0.140	0.141	0.18
Low initial water content (0.24 g/cm³)	4	0.081	0.077	0.098	0.26
	5	0.081	0.075	0.090	0.21
	6	0.080	0.072	0.085	0.19
	8	0.080	0.065	0.081	0.17

† Difference in soil-water content between bulk soil and root surface.

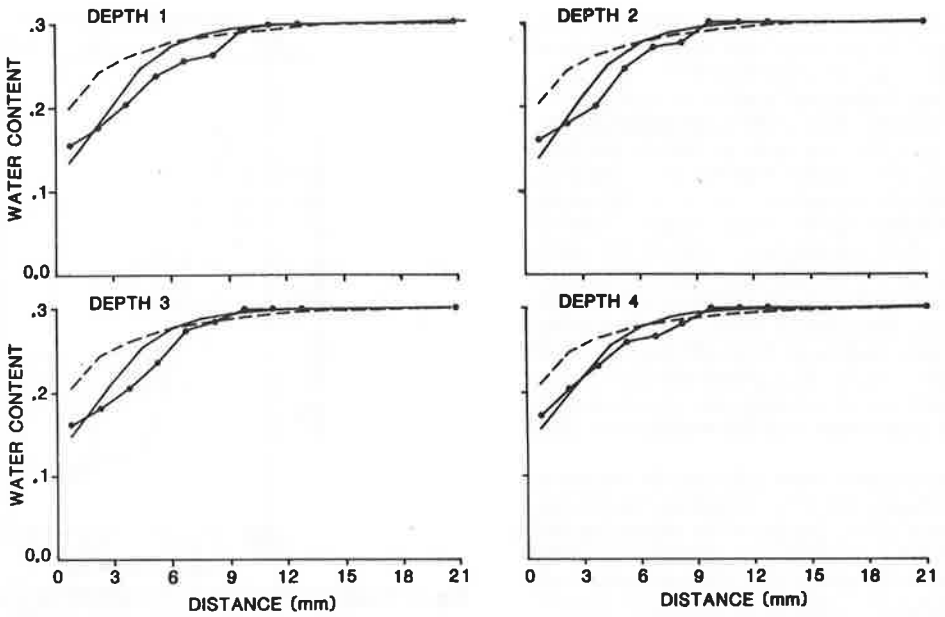

Fig. 2. Drawdowns in soil-water content from high initial water content (0.3 g/cm³) at 4, 5, 6, and 8 cm distances, respectively, from soil surface, associated with single radish roots following low transpirational demand. (-----Cowan model, ———— Hillel model, — • — experimental).

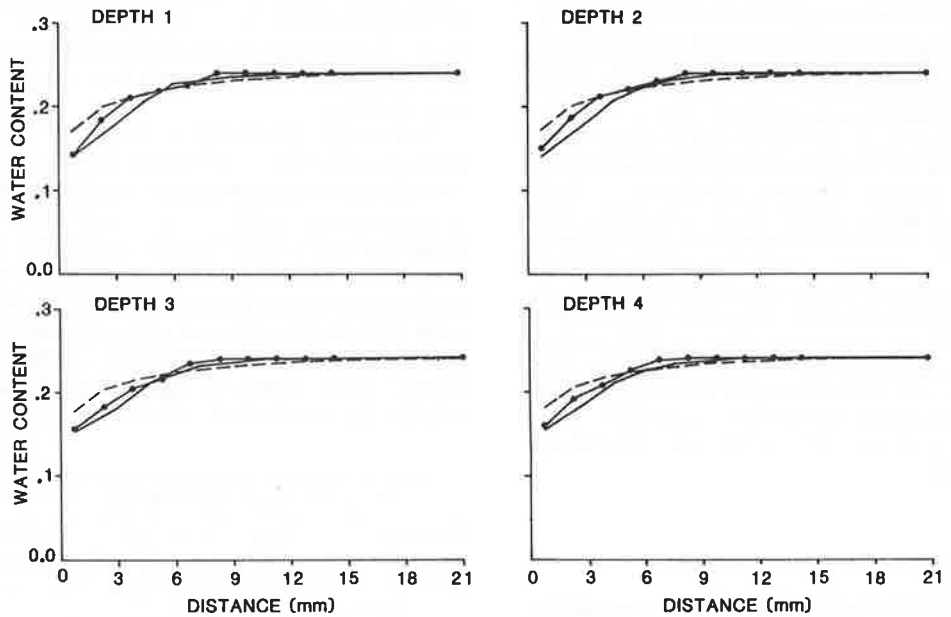

Fig. 3. Drawdowns in soil-water content from low initial water content (0.24 g/cm³) at 4, 5, 6, and 8 cm distances, respectively, from soil surface, associated with single radish roots following low transpirational demand. (------Cowan model, ———— Hillel model, — • —— — experimental).

initial water content (see Table 1). This could be anticipated in view of the slightly lower potential gradient across the soil-plant–atmosphere continuum. Also, in the case of the low evaporative demand, uptake could be reduced as a result of the lower water content and, hence, lower diffusivity at the root surface (see Fig. 2 and 3) restricting uptake. This implies an increased soil resistance and would be consistent with the suggestion of Slatyer (1967) that the soil-water potential at the root surface is the major factor controlling water availability to plants. However, the latter suggestion appears to be contradicted by the results obtained under the high evaporative demand. Surprisingly, the water content at the root surface following transpiration was higher at any given depth for the lower initial water content column (Fig. 5), and thus soil resistance near the root surface should be less limiting than for the high initial water content treatment (Fig. 4). This observation held for all cases of high transpiration and may reflect partial closure of stomata at the lower soil-water potential.

Second, for both high and low evaporative demand the distances over which the drawdown occurred were less for the lower initial water content treatments than for the high initial water content treatments (Table 2). The experimental results also show that for the same

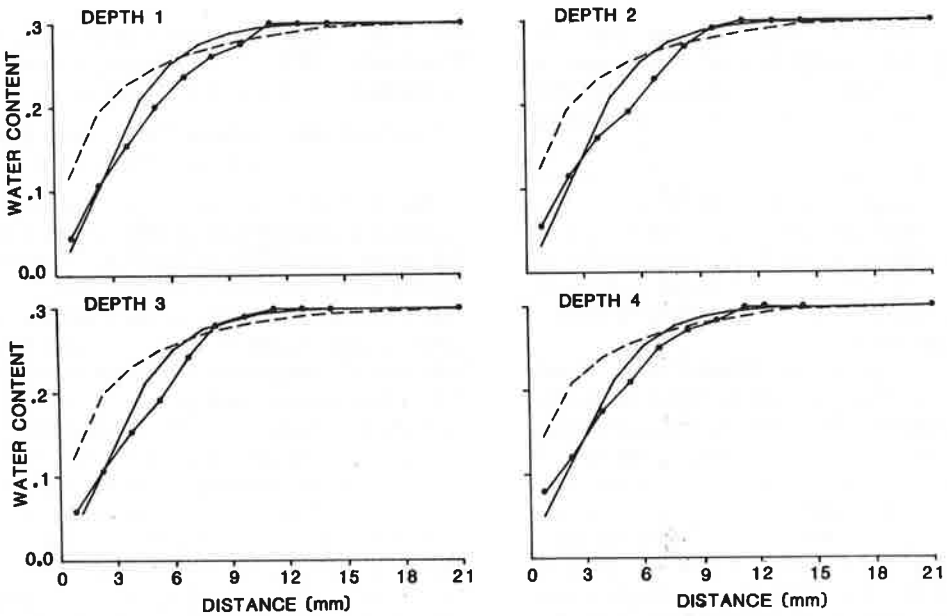

Fig. 4. Drawdowns in soil-water content from high initial water content (0.3 g/cm³) at 4, 5, 6, and 8 cm distances, respectively, from soil surface, associated with single radish roots following high transpirational demand. (-----Cowan model, ——— Hillel model, —— • ——— experimental).

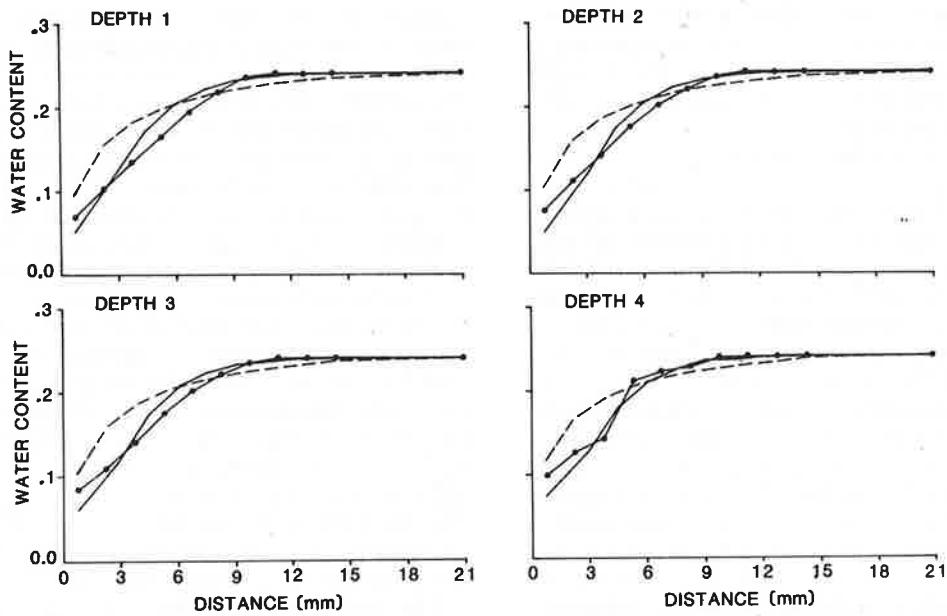

Fig. 5. Drawdowns in soil-water content from low initial water content (0.24 g/cm³) at 4, 5, 6, and 8 cm distances, respectively, from soil surface, associated with single radish roots following high transpirational demand. (-----Cowan model, ——— Hillel model, —— • ——— experimental).

evaporative demand the drawdown distance is always less for the low initial water content than for the high initial water content. Such results are consistent with the suggestion of Gardner (1960) that the distance over which the drawdown occurs is a function of time and the diffusivity of the bulk soil. A consequence of Garner's (1960) relationship is that the drawdown distance is diminished if the diffusivity is reduced. Such a relationship could account for the differences observed between the high and low initial water contents, with differing diffusivity at the same evaporative demand. However, it does not explain why the drawdown distance under low evaporative demand is less than that for the high evaporative demand when both water content and diffusivity of the bulk soil are

Table 2. Extent of soil-water content drawdown from single radish roots under differing transpirational demand and initial soil-water content.

Initial soil-water content, g/cm³	Drawdown distance, mm	
	High transpirational demand	Low transpirational demand
0.299	11.25	9.75
0.240	9.75	8.25

the same (Table 2). Thus it would appear that the distance over which the drawdown occurs is also a function of extraction rate. This suggests that the modeling functions used by Gardner (1960) involving time and diffusivity and by Cowan (1965) involving root density should be modified to include a function whereby drawdown distance is dependent on extraction rate. The rate at which the distance increases could be controlled by the diffusivity and the extraction rate until the outer limit prescribed by Cowan (1965) is reached, after which no subsequent increase in drawdown distance should occur.

Third, for a given evaporative demand and initial water content, the rate of extraction appears to be dependant on root diameter. The roots in the upper layers where the root diameters were larger, extracted more water than those of smaller diameter roots further down the columns (see Table 1). For a given treatment, however, the total extraction, averaged per unit length of root, remained the same for all four plants, and Table 3 showing data for uptake along single roots confirms that uptake clearly decreases with root diameter. Presumably this reduction in uptake occurs because the larger diameter sections of the root have a larger surface area and consequently have a greater root–soil-water contact or surface area over which water flow takes place. That is, they have a lower resistance to water movement. Of course the resistance will also be influenced by the rate of transfer through the xylem channels and these may be significantly narrower further along the root.

It is not possible on the basis of the present data to make a direct comparison between the relative contributions of soil and plant resistances to water uptake since detailed and continuous measurement of leaf water potentials were not possible during CAT scanning with the system used. However, it seems clear from the previous discussion that soil resistance to water movement does play a significant part in controlling water uptake by the plant root even at the high water potentials applicable in these measurements. This result contradicts to some extent the conclusions reached in several recent reviews (Newman, 1969; Molz, 1981), that soil resistance only becomes significant at very low water potentials under field conditions. In part, this disagreement may be explained by the fact that root densities during these experiments were appreciably lower and transpiration rates slightly higher than those encountered under field conditions. This would result in the drawdown gradients and, hence, soil resistances measured, being somewhat more severe than those encountered under field conditions.

The evidence of reduced water uptake with decrease in cross-sectional area for flow as root diameter decreases confirms that root resistance is likely to be a major controlling factor. Recent work (Oosterhuis, 1981) suggests that the axial resistance is negligible and that the seat of root resistance lies in the radial pathways. More comprehensive studies of the soil-plant–atmosphere continuum using the CAT technique to monitor soil-water distributions in conjunction with detailed plant water potential measurements are planned and will undoubtedly elucidate this question. Similarly, the evidence for contact resistance between root and soil (Herkelrath et al., 1977; Faiz and Weatherly, 1977; 1978) should be equally amenable to resolution by the CAT technique.

Comparisons between Theoretical Predictions and Experimental Data

The comparisons between experimental data and theoretical drawdowns given in Fig. 2 to 5 suggest that the measured diffusivities (Fig. 1) are of sufficient accuracy since integrated water extractions from the initial soil-water content in each slice conform to those determined experimentally. However, comparisons between the predictions of Cowan's (1965) model and the experimental data (Fig. 2–5) show two major discrepancies. First, Cowan's (1965) model predicts that the drawdown distance is a constant 21 mm. This arises from the assumption that water is supplied from within a soil cylinder of radius $(1/\pi L)^{1/2}$ where L is root density in centimeters of root per cubic centimeter of soil. As there was a constant 1 cm of root in each slice, cylinder radius remains constant. On the other hand, the experimental drawdowns occur over a much shorter distance (see Table 2).

A second major discrepancy is that the model always underestimates the magnitude of the gradient in water content from bulk soil to plant root. Consequently, the decrease in water content in close proximity to the root is underestimated and that further out in the bulk, soil is overestimated (see Fig. 2–5). Presumably this discrepancy arises for two reasons. First, the model requires that water is moved from a greater distance away from the plant root and, thus, less water needs to be removed in close proximity to the plant root. Second, the model assumes a constant diffusivity. Whilst this is reasonable if water content remains essentially constant, it is invalid if water content is changing rapidly (Passioura and Cowan, 1968), as would have occurred at the root surface. Furthermore, the assumption of constant diffusivity implies that for a given uptake the water content in the bulk soil must change according to $1/\ln(b/a)$ (see Eq. [4]). However, in reality water content from plant root to bulk soil will change as a function of the changing diffusivities along the path of flow as water is extracted. Clearly the model of Cowan (1965) does not adequately describe the drawdowns associated with water uptake by a single plant root.

The predictions of the numerical model understandably give a closer fit to the experimental data than does Cowan's model (see Fig. 2–5). A major difference between predicted and experimental results is that in most cases the experimental results show that more water is extracted from the soil in the range 4 to 12 mm away from the root. The numerical model slightly overestimates the amount of water extracted at the root surface and, hence, overestimates the gradient in water content from bulk soil to plant root. This discrepancy may arise through the absence of any contact resistance term in the numerical model. It is also interesting to note that whilst both the numerical and Cowan's (1965) model show smooth, continuous curves of water content vs. distance away from the root, the experimental data shows a stepped nature over the distance 3 to 12 mm from the root (for ex-

ample, see Fig. 2). The stepped nature of the experimental drawdowns is of particular interest, but is difficult to explain. It occurs in virtually all cases, but it cannot be attributed to errors in the calculation of soil-water contents for pixels in each slice by the CAT technique. A possible explanation is that it arises from some slight redistribution of water in the column during preparations for scanning, or alternatively from some slight compaction of the soil as the root grows through it. Further examination of this phenomenon is continuing.

Both the previous models assume the roots to be a hollow cylinder having a uniform absorption along its length, allowing uptake to be simplified to essentially a one-dimensional flow to the root. Table 3 clearly shows that this is not so; both uptake and water content gradients decrease with root depth, presumably as a result of decreasing root surface area. Furthermore, Table 3 shows that the differential drawdowns along the root result in a slight vertical water content gradient at the root surface. Undoubtedly such a gradient should result in a vertical flux of water from the bottom to the top of the root (see Table 3). Thus, single root models that entail essentially a one-dimensional flow to the root (Gardner, 1960; Cowan, 1965; Whistler et al., 1970; Molz and Remson, 1970; Hillel et al., 1975) will be inadequate as they suffer from spatial averaging of uptake and, consequently, water content gradients, and generally omit the possibility of a vertical flux arising from differential drawdowns along the root by not including an extraction function. For adequate descriptions of practical systems there is clearly a need to formulate a conceptual model in which uptake along the root need not be uniform and vertical flow may occur. The authors are currently devising a simulation model to take these factors into account. Examination of the gradients in water potential does, however, suggest that the effect of vertical flow is likely to be a minor perturbation.

Table 3. Soil-water content at root surface, distance to bulk soil-water content, and uptake from individual layers along a single radish root.

Depth	θ_v at root surface	Distance to bulk soil θ_v	Uptake from layer	Root radius
cm	g/cm³	mm	g	mm
		High transpiration		
2	0.054	9.75	0.220	0.28
3	0.056	9.75	0.220	0.26
4	0.057	9.75	0.201	0.25
5	0.061	9.75	0.193	0.22
6	0.076	11.25	0.189	0.20
7	0.128	11.25	0.181	0.17
8	0.178	9.75	0.104	0.15
9	0.216	9.75	0.072	0.05
10	0.290	8.25	0.040	0.02
		Low transpiration		
2	0.059	9.75	0.201	0.27
3	0.061	8.25	0.190	0.25
4	0.066	8.25	0.176	0.24
5	0.090	8.25	0.139	0.23
6	0.110	8.25	0.133	0.19
7	0.145	8.25	0.124	0.17
8	0.181	8.25	0.090	0.15
9	0.261	9.75	0.071	0.07
10	0.298	6.75	0.055	0.05

CONCLUSIONS

The application of computer assisted tomography to x-ray attenuation measurements is an exciting new approach that clearly has the potential to resolve the major controversies surrounding the extraction of soil water by plant roots. The present measurements of the drawdowns in soil-water content associated with a single root provide the most detailed descriptions yet obtained, particularly by a nondestructive technique. Soil resistance to water flow is clearly of significance even at these high soil-water potentials since it has been shown to markedly influence water uptake. Analytical methods are unlikely to provide satisfactory descriptions of such drawdowns due to the restrictive assumptions required for their solution. In particular, the assumption that a plant root acts as a uniform absorbing cylinder along its length is clearly erroneous. Although numerical methods are capable of providing a reasonable approximation to the position and shape of the measured drawdowns, significant improvements in the physical concepts on which these are based are clearly still required.

Studies of this type need to be extended to a wide range of plant species under different environmental conditions and in a range of soil types at different water contents. With this intent, the authors have successfully applied CAT to γ-ray attenuation measurements of soil-water content and have adapted (Hainsworth and Aylmore, in preparation) a conventional dual source gamma scanning system to enable continuous long-term studies of this nature (including whole root systems) to be undertaken. Such systems are infinitely less expensive, more suitably designed, and considerably more accessible to soil and plant scientists than commercially available x-ray CAT scanners developed for medical purposes.

ACKNOWLEDGMENTS

This research was funded by grants from the Australian Research Grants Scheme and the Australian Water Resources Council; their support is gratefully acknowledged.

REFERENCES

Belmans, C., J. Feyen, and D. Hillel. 1979. An attempt at experimental validation of macroscopic-scale models of soil moisture extraction by roots. Soil Sci. 127:174–186.

Brooks, R.A., and G. DiChiro. 1975. Theory of image reconstruction in computed tomography. Radiology 117:561–572.

Brooks, R.A., and G. DiChiro. 1976. Principles of computer assisted tomography (CAT) in radiographic and radioisotopic imaging. Phys. Med. Biol. 21:689–732.

Bruce, R.R., and A. Klute. 1956. The measurement of soil-water diffusivity. Soil Sci. Soc. Am. Proc. 20:458–562.

Carbon, B.A. 1973. Water stress in plants on a coarse soil. Aust. J. Soil Res. 11:33–42.

Cowan, I.R. 1965. Transport of water in the soil-plant-atmosphere system. J. Appl. Ecol. 2:221–239.

Faiz, S.M.A., and P.E. Weatherley. 1977. The location of the resistance to water movement in the soil supplying roots of transpiring plants. New Phytol. 78:337–347.

Faiz, S.M.A., and P.E. Weatherley. 1978. Further investigations into the location and magnitude of the hydraulic resistances in the soil: plant system. New Phytol. 81:19–28.

Gardner, W.R. 1960. Dynamic aspects of water availability to plants. Soil Sci. 89:63–73.

Hainsworth, J.M., and L.A.G. Aylmore. 1983. The use of computer assisted tomography to determine spatial distribution of soil water content. Aust. J. Soil Res. 21:435–443.

Herkelrath, W.N., E.E. Miller, and W.R. Gardner. 1977. Water up-

take by plants: II. The root contact model. Soil Sci. Soc. Am. J. 41:1043–1049.
Hillel, D. 1982. Application of soil physics. Academic Press, New York.
Hillel, D., C. van Beek, and H. Talpaz. 1975. A microscopic-scale model of soil water uptake and salt movement to plant roots. Soil Sci. 120:385–399.
Hillel, D., H. Talpaz, and H. van Keulen. 1976. A macroscopic model of water uptake by a non-uniform root system and of water and salt movement in the soil profile. Soil Sci. 121:242–255.
McCullough, E.C. 1975. Photon attenuation in computed tomography. Med. Phys. 2:307–320.
Molz, F.J. 1981. Models of water transport in the soil-plant system: A review. Water Resour. Res. 17:1245–1260.
Molz, F.J., and I. Remson. 1970. Extraction term models of soil moisture use by transpiring plant. Water Resour. Res. 6:1346–1356.
Molz, F.J., and I. Remson. 1971. Application of an extraction term model to the study of moisture flow to plant roots. Agron. J. 63:72–77.
Newman, E.I. 1969. Resistance to water flow in soil and plant. I. Soil resistance in relation to amounts of root: theoretical estimates. J. Appl. Ecol. 6:1–12.
Nimah, M.N., and R.J. Hanks. 1973. Model for estimating soil, water, plant and atmosphere interactions: I. Description and sensitivity. Soil Sci. Soc. Am. Proc. 37:522–527.
Ogata, G., L.A. Richards, and W.R. Gardner. 1960. Transpiration of alfalfa determined from soil water content changes. Soil Sci. 89:179–182.
Oosterhuis, D.M. 1981. Hydraulic conductivity and drought acclimation of cotton root systems. Ph.D. thesis, Utah State Univ., Logan.
Panton, D.M. 1981. Mathematical reconstruction techniques in computer axial tomography. Math. Sci. 6:87–102.
Passioura, J.B., and I.R. Cowan. 1968. On solving the non-linear diffusion equation for the radial flow of water to roots. Agric. Meterorol. 5:129–134.
Slatyer, R.O. 1967. Plant-water relationships. Academic Press, London.
So, H.B., L.A.G. Aylmore, and J.P. Quirk. 1976. Measurement of water fluxes in single root system. I. The tensiometer-potometer system. Plant Soil 45:577–594.
Whistler, F.D., A. Klute, and R.J. Millington. 1970. Analysis of radial steady state solution and solute flow. Soil Sci. Soc. Am. Proc. 34:382–387.

Predicting Structural Amelioration and Crop Response on Hard Setting Soils.

Proc. N.Z./Aust. Soil Sci. Soc. Conf., Rotorua, N.Z., (1986),49-54.

L.A.G. Aylmore and H.R. Cochrane

PREDICTING STRUCTURAL AMELIORATION AND CROP RESPONSE ON HARD SETTING SOILS

L.A.G. Aylmore and H.R. Cochrane
Soil Science and Plant Nutrition,
University of Western Australia, Nedlands, W.A. 6009

ABSTRACT

Plant growth on problem structured soils from the Western Australian wheatbelt has been shown to have a strong negative correlation with soil structural stability as measured by the Modulus of Rupture (MOR) technique. Consequently, measurements of MOR and of the way in which MOR changes with change in exchangeable sodium percentage (ESP), termed the sodium sensitivity, provide a useful method for predicting the structural amelioration and crop response to be derived from the application of gypsum. The sodium sensitivity parameter has been shown to correlate well with the percentage increase in grain yield achieved as a result of the application of 5 tonnes/hectare of gypsum to these soils.

INTRODUCTION

An essential prerequisite to the evaluation and realization of the full productive potential of a soil in terms of its physical constitution (i.e. the minimization of soil physical constraints to productivity) is the ability to quantitatively characterize its physical status at any given time. Soil physical fertility involves considerations of a multiplicity of factors, and in general a range of measurements are necessary to provide an adequate description of soil physical status. In specific circumstances, however, measurement of one particular physical parameter may serve as a sufficient criteria to quantitatively characterize and monitor changes in the physical status of surface soils associated with their management.

In this respect there have been a number of useful developments in recent years. Simple dispersion tests (Emerson, 1967; Loveday and Pyle, 1973), based essentially on the dependence of soil stability on exchangeable cation and electrolyte concentrations (Quirk and Schofield, 1955), have received considerable attention. Rengesamy et al. (1984) have, for instance, demonstrated that a classification of red-brown earths on the basis of their dispersion behaviour, provides a useful basis for the formulation of appropriate management strategies for the manipulation of the surface structure of these soils. Similarly, Lloyd and Collis-George (1982) have developed the torsional shear box as as a method of monitoring the 'in situ' surface strength of agricultural soils.

Studies carried out on a wide range of problem structured soils from the Western Australian and Victorian wheatbelts indicate that characterization on the basis of dispersive behaviour alone does not explain nor satisfactorily predict the field behaviour of these soils (Cochrane and Aylmore, unpublished data). On the other hand, the Modulus of Rupture-Exchangeable Sodium Percentage (MOR-ESP) technique (Aylmore and Sills, 1982) has proved a reliable indicator of the behaviour of these soils in the field (e.g. response to gypsum, tillage and pasture rotations). This is largely because the developemnt of dry strength in soils subjected to this testing technique is dependent on the same mechanisms within the soil as are responsible for the strength characteristics of hard setting soils in the field.

The ultimate test of any method for the characterization of soil structured status, and in particular of soil physical conditions for plant

growth, lies in its ability to correlate with or predict the suitability of the soil for plant growth. In this paper the relationship between the susceptibility of wheatbelt soils to structural amelioration by gypsum application as measured by the MOR-ESP technique, and plant growth improvement in response to gypsum application, has been examined.

MATERIALS AND METHODS

Soils which, in the view of the farmer, posed significant management problems because of poor structural stability leading to restricted trafficability when wet and hard setting on drying, were collected from a wide area of the Western Australian wheatbelt over the period from 1982-1985.

These problem structured soils typically show considerable spatial variability in physical behaviour both horizontally and down the profile. At the more intensively monitored sites considerable variability was also found to occur within the season. The influence of this inherent variability on the usefulness of results obtained has, where possible, been minimized by using data derived from soils collected from the surface 7 cm in late autumn/early winter.

Soils were air dried, gently crushed and sieved to pass through 2 mm, then thoroughly mixed. Soil constituents and modulus of rupture were determined as described by Aylmore and Sills (1982) and mechanically dispersed clay followed the method of Rengesamy et al. (1984). Soil modification for determination of sodium sensitivity and baseline MOR was as described by Aylmore and Sills, with the exception that leaching was carried out using 1.2 litres of sodium/calcium chloride solutions at an ionic strength of 93 mmol dm^{-3} followed by the same quantity of solution at 23 mmol dm^{-3} per 200 g soil. This procedure produced modified soils of equal chemical potential at each SAR level, and permitted the leaching process to be completed within 10 hours for all but the least permeable soils.

The emergence percentage with time of sub-clover seedlings grown in pots maintained at 20°C, watered daily to a moisture content equivalent to a matrix potential of -0.1 MPa using pregerminated seed, was measured for two soils. Apart from the natural soils, each soil was also modified to have an ESP of approximately 1 and 20 respectively, thus giving a range of levels of soil strength.

Field trials to determine the efficacy of gypsum application in ameliorating soil physical conditions and in improving crop growth, were set up at a number of the sites from which soil samples had been taken. Trial design was not uniform, varieties, fertilizer rates and seeding density being chosen on the basis of local recommendations. All trials, however, incorporated a five tonne per hectare broadcast treatment, and comparisons of gypsum response are reported at this application rate although this is not necessarily the optimum rate tested in each trial.

RESULTS AND DISCUSSION

The Modulus of Rupture-Exchangeable Sodium Percentage relationships presented in Figure 1 illustrate the type of behaviour commonly exhibited by sandy-loam soils of the Western Australian wheatbelt. The criteria used to designate soils which farmers consider hard-setting is a MOR value for

the natural soil of some 60 kPA. This is of course a somewhat arbitrary distinction as there is no abrupt change in soil behaviour at this value.

For most soils the relationship between MOR and ESP is essentially linear, and two useful parameters can be determined from the line of best fit. Baseline MOR or soil strength when ESP is zero, provides an assessment of the structural stability under calcium saturated conditions, i.e. close to structurally optimum exchangeable cation composition. On the other hand, the sodium sensitivity or slope of the line (measured in kPa/% increase in ESP) estimates the disruptive effects of the sodium ion on soil structure, i.e. the ability of the soil to resist structural breakdown. In this sense the effects of varying ESP on swelling pressure has been turned to advantage as a means of subjecting the soil matrix to a range of internal disruptive forces and hence as a measure of the inherent stability of the soil matrix to the wetting process.

In general, a harder setting soil (e.g. Lake Grace) exhibits a higher baseline MOR and significantly higher sodium sensitivity than those classified as non-hard setting (e.g. Greenhills) (Fig. 1). The value of the MOR-ESP method of assessing the structural status of these soils has been demonstrated (Aylmore and Sills, 1982) by its ability to differentiate clearly between the structural status of soils subjected to different management techniques, even in the short term, and in particular the susceptibility of the soil to structural amelioration by gypsum application.

The sodium sensitivity obtained from the MOR-ESP test reflects, amongst other things, the susceptibility to dispersion of the soil colloids to the nature of the exchangeable cations and to electrolyte concentration. It thus logically provides a means for estimating probable gypsum responsiveness at least in terms of soil structural status, since gypsum application acts to replace a portion of the undesirable monovalent cations on the exchange complex with calcium and to significantly increase soil solution concentration.

The significance of soil strength as measured by the MOR technique in relation to seedling emergence is illustrated in Figure 2. The trend towards slower, less complete emergence on the harder soils is very marked and the influence that soil strength had on the effort required by the seedlings to get their cotelydons through the soil surfce could clearly be observed. Seedlings growing on the harder soils not only had to push aside larger chunks of soil, but also had to exert a greater pressure to initially crack the more coherent soils.

The eventual level of emergence attained under field conditions on these soils may not vary greatly with soil strength if there are frequent, light rains and low evaporative demand during the emergence period, but the time taken for seedlings to emerge is always greater in the harder setting soils, leaving seedlings vulnerable to unfavourable conditions for a longer period.

The influence of such factors is clearly evident in the increases in percentage seedling emergence observed in the field trials with the application of 5 tonnes gypsum/hectare. Reductions in MOR values for soil strength as a result of gypsum application correlated very strongly ($r^2 = 0.9$) with the MOR of the untreated soil (Fig. 3). In turn, and despite the variability arising from variations in trial design, climatic conditions etc., percentage increase in wheat seedling emergence as a

result of that application of 5 tonnes/hectare shows a good correlation ($r^2 = 0.6$) with the MOR of the soils before treatment.

Figure 4 shows the relationship between percentage increase in wheat grain yield following a 5 tonne/hectare gypsum application and sodium sensitivity of the surface soil for 32 sites on which gypsum trials had been conducted betweeen 1982 and 1985. Despite large variations in climatic conditions, seeding rates, cultivars, nutritional status, tillage conditions and weed competition, the relationship accounts for 60% of the variation between trials. This may be compared with a coefficient of determination of 0.10 in the linear relationships between percentage increase in grain yield and mechanically dispersible clay for the same group of soils (Cochrane and Aylmore, unpublished data).

Under field conditions a crop is responding to a multiplicity of environmental factors. The best parameter for producing useful quantitative relationships with crop productivity on those soils where physical conditions are most limiting for productive capacity, will be one which is most representative of the mechanisms by which soil physical conditions limit growth, i.e. one which integrates the effects of soil physical processes on plant productivity. While measurements of mechanically dispersible clay have been shown to be a reliable basis for asssessing the gypsum requirement of red brown earths in Victoria (Rengesamy et al., 1984), it is clearly a considerably less efficient means than the MOR-based tests for discriminating in a quantitatively useful way between the heterogeneous group of soils examined in this study.

There is considerable scope for improving the utility of the MOR-based testing methods in predicting crop response. For example, the sodium sensitivity parameter does not currently reflect the ameliorative effects of the increase in electrolyte concentration following gypsum application. However, bearing in mind the variations introduced by other factors such as subsoil physical characteristics, variations in regional and seasonal climate, intensity of tillage, nutrient treatment and weed control, the trends apparent in the previous group of trials are extremely encouraging.

REFERENCES

Aylmore, L.A.G. and Sills, I.D. (1982). Characterization of soil strucutre and stability using Modulus of Rupture-Exchangeable Sodium Percentage relationships. Aust. J. Soil Res. 20, 213-214.

Emerson, W.W. (1967). A classification of soil aggregates based on their coherence in water. Aust. J. Soil Res. 5, 47-57.

Lloyd, J.E. and Collis-George, N. (1982). A torsional shear box for determining the shear strength of agricultural soils. Aust. J. Soil Res. 20, 203-211.

Loveday, J. and Pyle, J. (1973). The Emerson dispersion test and its relationship to hydraulic conductivity. Division of Soils Tech. Paper 15, CSIRO, Australia.

Quirk, J.P. and Schofield, R.K. (1955). The effect of electrolyte concentration on soil permeability. J. Soil Sci. 6, 163-178.

Rengesamy, P., Greene, R.J.B., Ford, G.W. and Mikanni, G.H. (1984). Identification of dispersive behaviour and the management of red-brown earths. Aust. J. Soil Res. 3, 493-497.

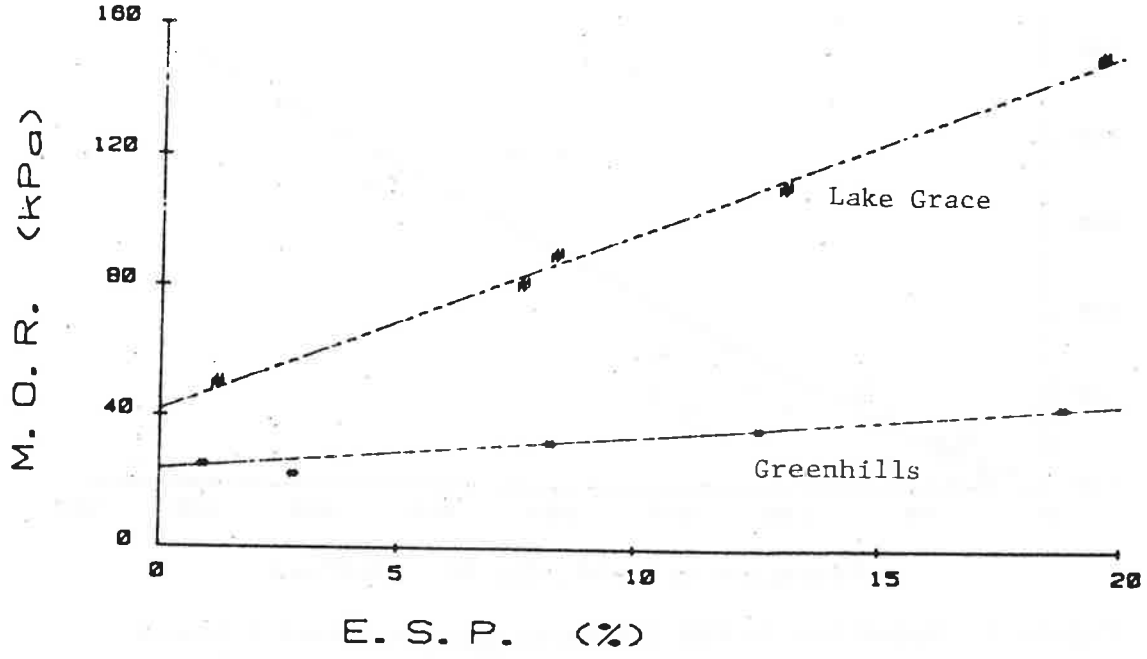

Figure 1. Modulus of Rupture versus exchangeable sodium percentage for a hard-setting soil (Lake Grace) and non-hard-setting soil (Greenhills).

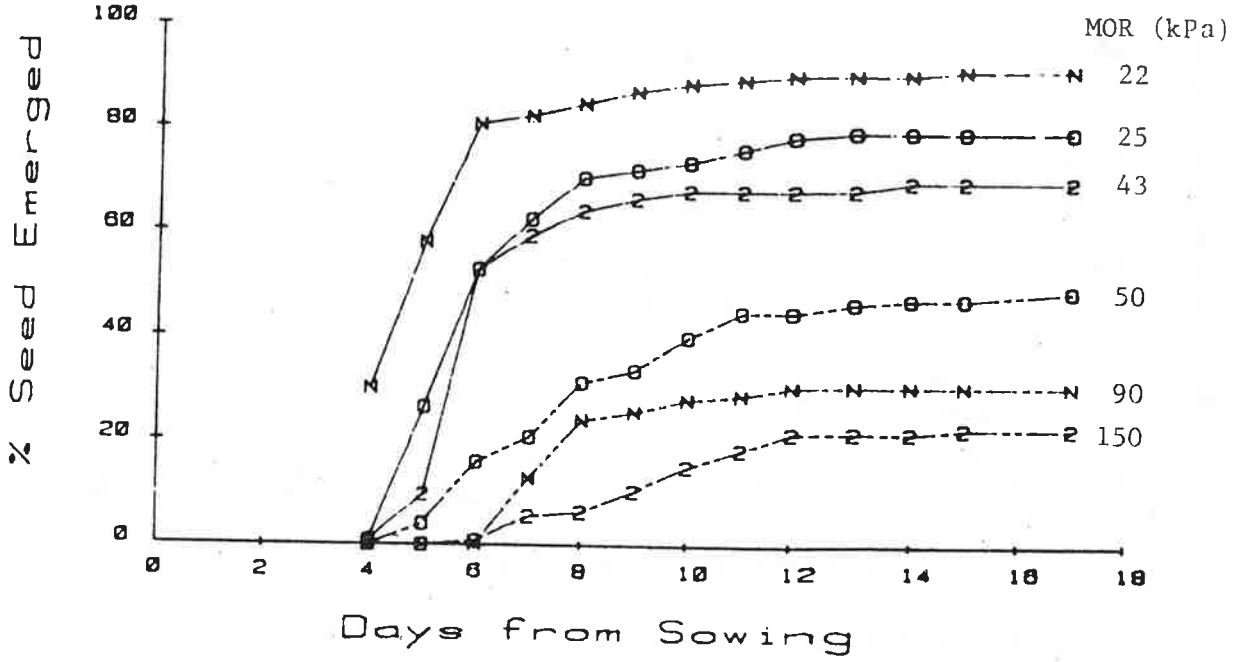

Figure 2. Percentage seedling emergence with time on soils with different Modulus of Rupture ____ Greenhills, ---- Lake Grace, N natural, 0 SAR zero, 2 SAR 20.

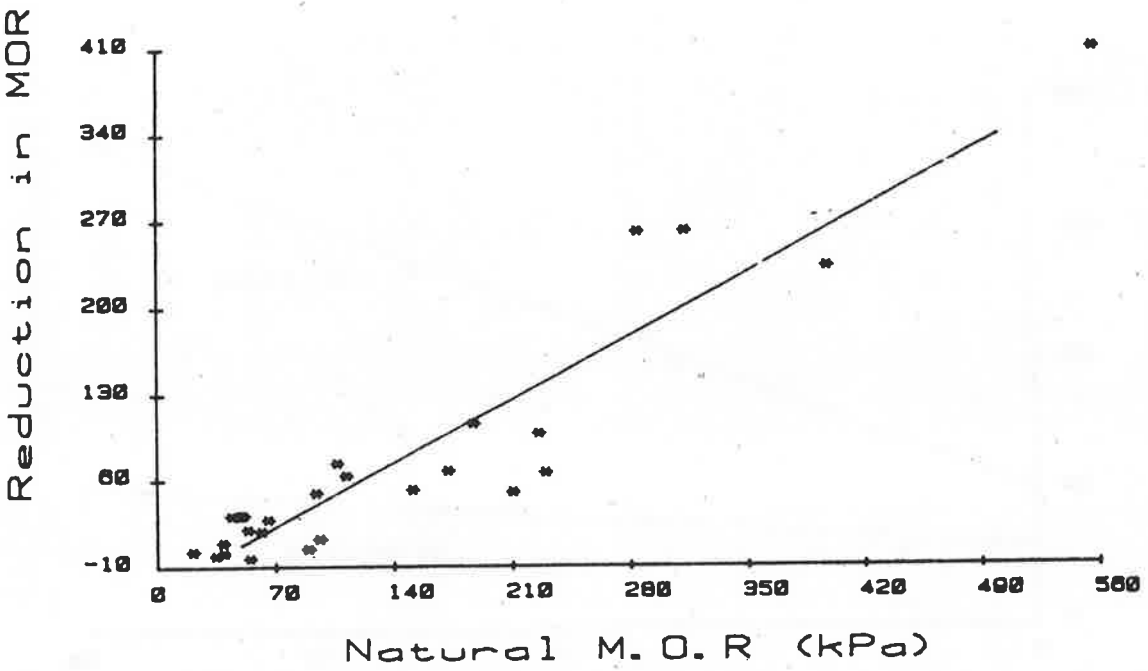

Figure 3. Reduction in MOR following application of 5 tonnes gypsum per hectare versus MOR of natural soils.

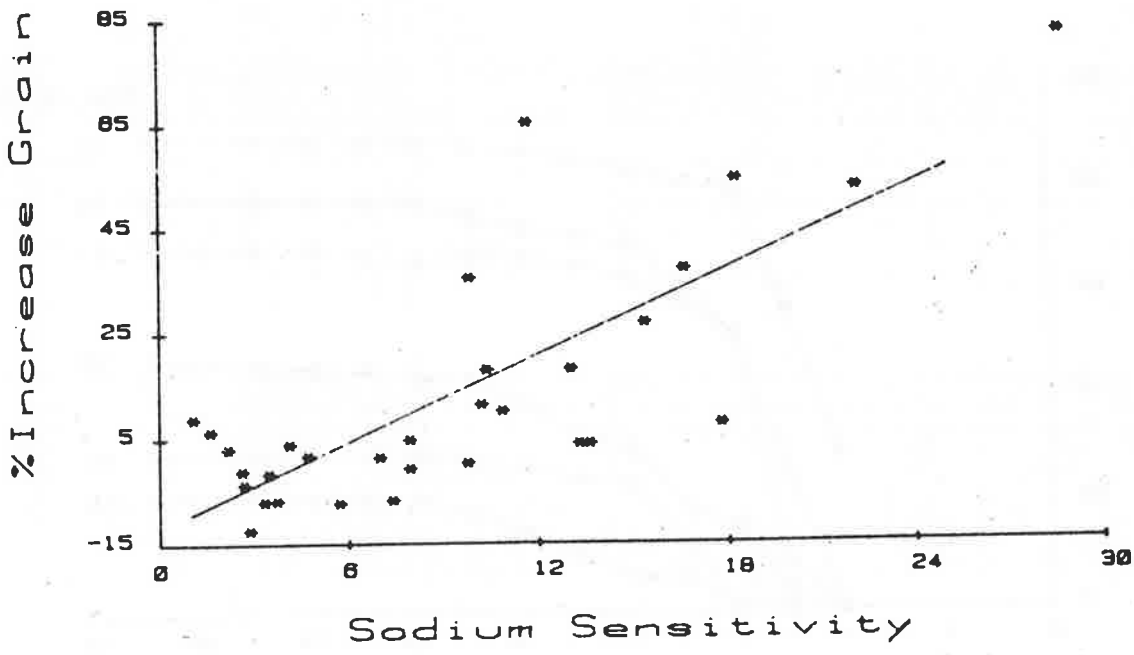

Figure 4. Percentage increase in grain yield following application of 5 tonnes gypsum per hectare versus sodium sensitivity of natural soils.